SYNTHESIS, CHARACTERIZATION, AND APPLICATION
OF CHIRAL SCHIFF-BASE COMPLEXES

by

KAYODE OSHIN

B.S., Emporia State University, 2006

AN ABSTRACT OF A DISSERTATION

submitted in partial fulfillment of the requirements for the degree

DOCTOR OF PHILOSOPHY

Department of Chemistry
College of Arts and Sciences

KANSAS STATE UNIVERSITY
Manhattan, Kansas

2011

Abstract

This work examines the synthesis of novel chiral Schiff-base complexes derived from (1*R*,2*R*)-cyclohexanediamine and (*R*)-[1,1'-binaphthalene]-2-2'-diamine structural backbones with quinoline, isopropyl-quinoline, and benzoquinoline structural side-arms. We incorporated some degree of flexibility in the ligands and complexes so they can accommodate the sterics of different substrates during a catalytic reaction. We successfully achieved this by reducing the imine bond in the ligands to the corresponding amine bond. Therefore, the successful reduction and metallation of some of these ligands to give structures of different symmetries is reported. We had difficulty reducing ligands with the binaphthalene backbone but were able to partially reduce the ligand through a one-pot reaction with a zinc(II) salt and $NaBH_4$.

The complete ^1H NMR assignments of the complexes reported in this thesis serve as a valuable tool for use in the characterization of future complexes. The complete NMR characterization of compounds reported is a complex process because they are polycyclic aromatic systems and the coupling network similarity in different parts of the molecule usually results in severe overlap of their ^1H resonances. To overcome this impediment, we took advantage of various 2D-NMR techniques (COSY, NOESY, ROSEY, HSQC, and HMBC) along with other 1D-NMR experiments (^1H HOMODEC, ^1H, and ^{13}C) to completely assign the desired complexes. Subsequently we also studied the coordination chemistry of several meal cations with our ligand system with the goal of obtaining single stranded monhelices.

The potential use of some of the complexes in the area of NMR discrimination and kinetic resolution of racemic mixtures was examined and shown to be promising. Several NMR experiments were conducted using the racemic olefins 3-buten-2-ol and 1-penten-3-ol to demonstrate the discriminating power of our silver(I) complexes. We discovered that sterics play an important role in this resolution experiment and the bulky nature of our complexes affect the overall efficiency of the NMR discriminatory process as it diminishes the contact between the reactive metal center and the olefins involved. Temperature also plays a vital role in the chiral recognition of racemic olefins as we examined the ideal temperature needed to reduce the various dynamic processes that take place in solution at room temperature.

SYNTHESIS, CHARACTERIZATION, AND APPLICATION
OF CHIRAL SCHIFF-BASE COMPLEXES

by

KAYODE OSHIN

B.S., Emporia State University, 2006

A DISSERTATION

submitted in partial fulfillment of the requirements for the degree

DOCTOR OF PHILOSOPHY

Department of Chemistry
College of Arts and Sciences

KANSAS STATE UNIVERSITY
Manhattan, Kansas

2011

Approved by:

Major Professor
Dr. Christopher J. Levy

Abstract

This work examines the synthesis of novel chiral Schiff-base complexes derived from (1*R*,2*R*)-cyclohexanediamine and (*R*)-[1,1'-binaphthalene]-2-2'-diamine structural backbones with quinoline, isopropyl-quinoline, and benzoquinoline structural side-arms. We incorporated some degree of flexibility in the ligands and complexes so they can accommodate the sterics of different substrates during a catalytic reaction. We successfully achieved this by reducing the imine bond in the ligands to the corresponding amine bond. Therefore, the successful reduction and metallation of some of these ligands to give structures of different symmetries is reported. We had difficulty reducing ligands with the binaphthalene backbone but were able to partially reduce the ligand through a one-pot reaction with a zinc(II) salt and NaBH$_4$.

The complete ^{1}H NMR assignments of the complexes reported in this thesis serve as a valuable tool for use in the characterization of future complexes. The complete NMR characterization of compounds reported is a complex process because they are polycyclic aromatic systems and the coupling network similarity in different parts of the molecule usually results in severe overlap of their ^{1}H resonances. To overcome this impediment, we took advantage of various 2D-NMR techniques (COSY, NOESY, ROSEY, HSQC, and HMBC) along with other 1D-NMR experiments (^{1}H HOMODEC, ^{1}H, and ^{13}C) to completely assign the desired complexes. Subsequently we also studied the coordination chemistry of several meal cations with our ligand system with the goal of obtaining single stranded monhelices.

The potential use of some of the complexes in the area of NMR discrimination and kinetic resolution of racemic mixtures was examined and shown to be promising. Several NMR experiments were conducted using the racemic olefins 3-buten-2-ol and 1-penten-3-ol to demonstrate the discriminating power of our silver(I) complexes. We discovered that sterics play an important role in this resolution experiment and the bulky nature of our complexes affect the overall efficiency of the NMR discriminatory process as it diminishes the contact between the reactive metal center and the olefins involved. Temperature also plays a vital role in the chiral recognition of racemic olefins as we examined the ideal temperature needed to reduce the various dynamic processes that take place in solution at room temperature.

Table of Contents

List of Figures

List of Tables

Acknowledgements

First of all, I would like to thank my major professor, Dr. Christopher Levy for his advice, support, and encouragement, while a member of his research group. You created a research environment that fostered growth and supported independent work; that made me a better chemist. I would like to express my gratitude to my graduate committee, Dr. Eric Maatta, Dr. Stefan Bossmann, Dr. Kenneth Klabunde, and Dr. Prakash Om for their continuous advice and support. Also deserving of praise are the support staff of the chemistry department, Mr. Ron Jackson, Mr. Tobe Eggers, Dr. John Desper, and Mr. Jim Hodgson. Special thanks go to Dr. Leila Maurmann; thank you for taking the time to teaching me a lot of what I now know about Nuclear Magnetic Resonance. I would also like to thank my co-workers and other graduate students at Kansas State University who have made my time and experience a positive one. Finally, I would like to thank my family for their love, support, and motivation throughout the years. None of this would be possible without them.

Dedication

To my lovely wife, for her undying love and support, thank you!

CHAPTER 1

Introduction

1.1 Synopsis

Stereochemistry plays a very important role in the chemical interactions that dominate several fields of chemistry such as petrochemical, pharmaceutical, biological, and materials chemistry. Consequently, there is high demand to design practical synthetic methods for chiral compounds as single enantiomers. The thought of controlling the stereochemistry of reaction products, on a consistent basis, has captured the imagination of many scientists over the years. This led to the development of the field now generally refer to as asymmetric synthesis. In 2001, the Royal Swedish Academy of Sciences awarded the Nobel Prize in chemistry to William S. Knowles, Barry Sharpless, and Ryoji Noyori for their pioneering work in this field. They played an intricate role in the development of asymmetric catalysis, which is the application of enantioenriched catalysts to transform prochiral and racemic substances into valuable enantioenriched synthetic building blocks.[1]

Over the years, a number of organometallic catalysts have been synthesized for application in asymmetric catalysis.[2-6] Unfortunately, only a few of them result in the catalytic asymmetric transformations desired. The ideal catalytic asymmetric transformation would proceed in 100% yield, and would provide complete chemocontrol, regiocontrol, and stereocontrol (diastereoselectivity and enantioselectivity). It would be conducted with a minimum of solvent and additives, generate no wasteful by-products, and employ an inexpensive recoverable catalyst at low loadings.[7] The active conformation of the catalyst during the chemical reaction plays a significant role on the observed stereoselectivities. Studies show that a wide variety of chiral transition metal and organocatalysts (catalysts without a reactive metal component) exhibit substantial conformational mobility contributing to the poor efficiency observed in many asymmetric reactions.[8] Therefore, controlling this mobility is critical to developing practical asymmetric catalysts that meet the desired results mentioned above.

1.2 Catalyst Design

Our approach to restricting the conformational flux observed is to introduce a secondary structure that restricts the range of motion. We plan on achieving this by designing the catalyst to employ a helical motif. This helicity not only locks the structure in place, restricting its motion, but also amplifies any existing chiral elements within the structure. We utilize a simple blueprint in the design of our catalysts made up of two parts; a chiral backbone and polyaromatic sidearms that can overlap to achieve the desired restricted conformation (Figure 1.1).
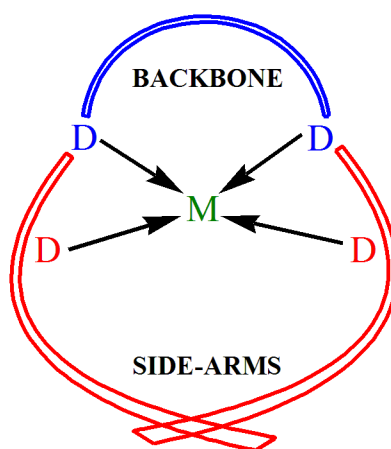
Figure 1.1: Catalyst Design Blueprint

It is important to note that we do not want these catalysts to be completely immobile as some degree of flexibility is desirable to accommodate the sterics of different substrates during a reaction. We achieve this by incorporating a flexible *trans*-substituted ethylene bridge into the backbone of the structure. This allows the catalyst to be flexible in the right location (backbone) while drastically reducing the substantial conformational mobility observed in previous studies caused by "unlocked" sidearms. Hence, this thesis details the ongoing work on the synthesis and characterization of novel chiral tetradentate complexes with the goal of designing new catalysts that show improved efficiency in the area of asymmetric catalysis. Emphasis will be placed on Nuclear Magnetic Resonance (NMR) studies and the intriguing application of select complexes in the area of NMR discrimination and resolution of racemic olefins.

1.3 Design Considerations

Extensive work has been done by our group on the synthesis and application of metallo-salen type complexes.[9-10] This report expands on that work by exploring the synthesis of tetradentate nitrogen complexes which maintain the number of donor atoms present (four) as their salen counterparts. The nitrogen atoms have comparable electronegativity values to the oxygen donor atoms utilized in the metallo-salen complexes making them applicable to study in a comparative manner (Figure 1.2).
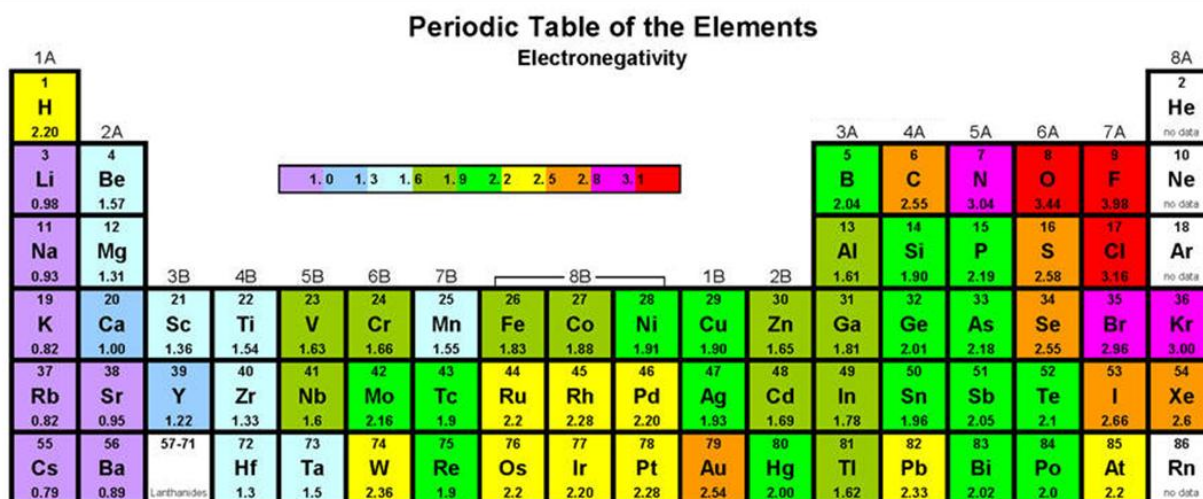
Figure 1.2: Electronegativity Comparison of Oxygen and Nitrogen Atoms

The presence of the four nitrogen donor atoms in the ligands usually results in the formation of a helicate structure after complexation with a metal salt.[11-12] We are interested in the formation of single stranded monohelical complexes as they are highly attractive in asymmetric catalysis due to their well defined reaction centers. Research done by Luigi Fabbrizi and Lorenzo Mosca show that the formation of mononuclear or dinuclear single stranded helicates is usually a fast process, in which the thermodynamics equilibrium is reached over a period of ranging from seconds to minutes.[13] However monohelices or double helicates of higher nuclearity, especially in the presence of bulky substituents on the ligand backbone, may reach the thermodynamic equilibrium over a period of hours and days.[14] They explain that the helical

structure of these complexes results from the fine balance between; (*i*) the coordinative geometrical preferences of the metal center and (*ii*) the steric constraints present in the linear ligand, which may contrast the formation of a mononuclear complex.[15]

Further research carried out by Luca Prodi and Nelsi Zaccheroni show that double helical metal complexes are frequently obtained when metal cations preferring tetrahedral coordination are used, provided that the fragment separating the two bidentate units is rigid and short enough to prevent the wrapping of a single ligand around a single metal cation according to a tetrahedral geometry.[16] They observe that when reactions were carried out with Cu^I salts, they form the stable dinuclear double-stand helicate $[Cu_2^I(\mathbf{L})_2]^{2+}$ as shown in Figure 1.3. This study has prompted many researchers to investigate the reaction conditions that lead to the formation of single stranded monohelical complexes as opposed to double stranded helicates, such as the role the choice of metal ion plays in the structural outcome of the complex.[17]
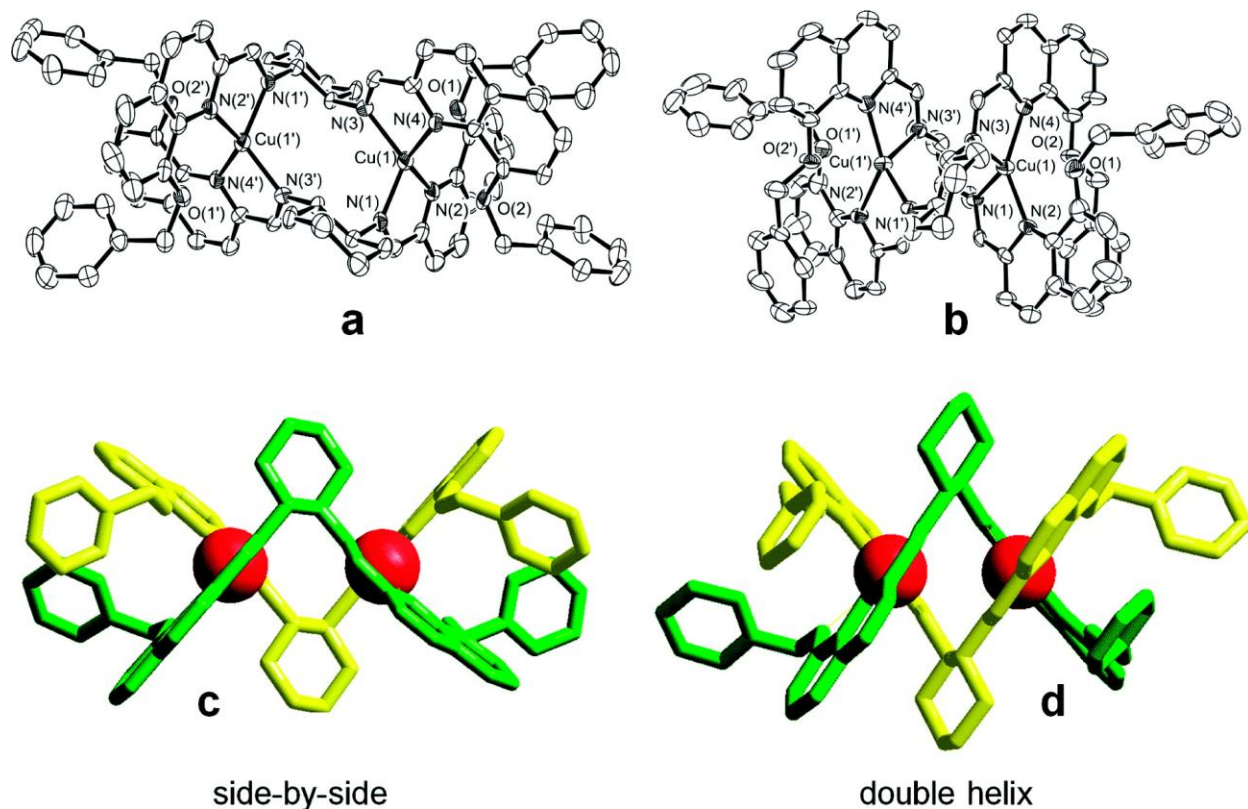
Figure 1.3: (a) & (b) ORTEP Diagrams for $[Cu_2^I(L)_2]^{2+}$, (c) & (d) Ball & Stick Models[16]

1.4 Choice of Metal Ion Incorporated

The choice of metal atom incorporated in the reactive center of a catalyst plays a major role in the overall structure and activity of the catalyst. Several factors affect the way a given ligand will bind to the metal center, such as the atomic radius, the overall charge of the metal, and the preferred geometry of the metal ion. Coordination research done with copper(I) ions shows that the d^9 cation prefers to be five- or six-coordinated with tetradentate ligands arranging in a more or less distorted square disposition around the cation, with one or two solvent molecules completing the coordination sphere.[18] Reactions with silver(I) shows that it is extensively employed as a tetradentate cation in the formation of classical polypyridine and imino-pyridine helicates.[19-22] Zinc(II) cations prefer coordinating with ligands **tcp**(trans) and **ccp**(cis) in numbers ranging from four to six and is rarely observed in the form of a double or triple helical complex (Figure 1.4).[23] Research carried out by Miquel Costas, Lawrence Que, and

tcp (trans, *RR* form)   **ccp** (*cis*, meso form)
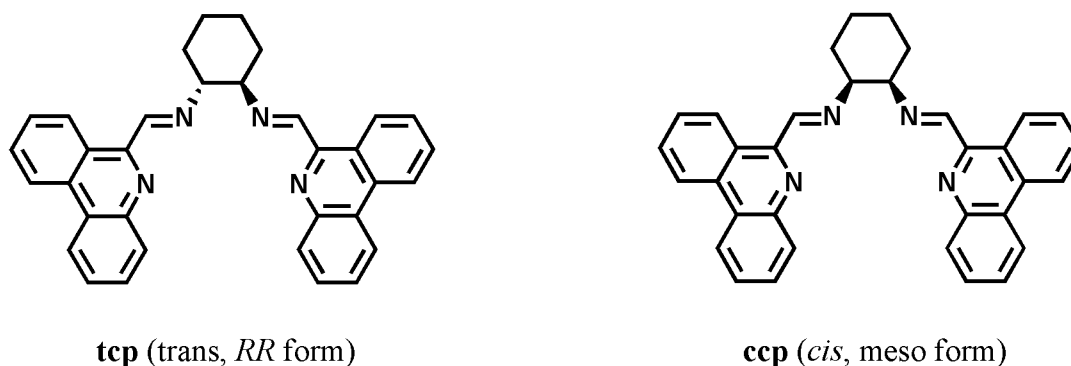
Figure 1.4: Tetradentate Ligands **tcp** and **ccp** used by the Hannon Group

Anna Company report on the structure of non-heme iron complexation with the Fe(II) metal center preferentially binding in a distorted octahedral fashion having a tetradentate ligand and two triflate anions coordinated *cis* to each other.[24]

It is, from the numerous examples mentioned above, apparent that the choice of metal salt used to form the desired complex affects the solid state geometry of the complex. Kiyoshi Sawanda and Keiichi Satoh studied the effect of changing the central metal ion on the ^{1}H NMR

results obtained for various complexes.[25] This solution study focused on lanthanum (La^{3+}), lutetium (Lu^{3+}), and yttrium (Y^{3+}) size effects on ternary complexes. They observed that there is a decrease in the number of coordinated oxygen atoms in the 3,6,9,12,15,18-hexaoxatriacontana-1-ol ligand used for the respective complexes as we progress from La^{3+} to Lu^{3+} and finally to Y^{3+}. This reduction is due to the decreasing size of the metal center and results in a downfield shift in the observed methylene proton signals of the corresponding complexes.

1.5 Spin-Spin Coupling in Polycyclic Aromatic Systems

All ligands and complexes examined in this thesis are polycyclic aromatic systems. We employ Nuclear Magnetic Resonance (NMR) as the dominant characterization technique used to analyze all compounds in this work. In NMR spectroscopy, spin-spin interactions between the same or different nuclear species of a system can reveal a variety of structural information about the compound and is second in importance only to the phenomenon of the chemical shift.[26] A detailed discussion of spin-spin coupling is outside the scope of this report but is detailed extensively in available texts.[27-31] A brief definition of spin-spin coupling is the phenomenon which causes small change of the energy levels in the spin states of magnetic nuclei owing to the presence in their immediate neighborhood of other magnetic nuclei which may be in their various quantized spin states.[32] Most of the NMR information obtained for various compounds is based on the interpretation of spin-spin interactions between protons separated by two or three bonds; coupling across more than three bonds is referred to as long-range coupling.

Many examples of long-range proton-proton couplings have been reported and the existence of a 'through-space' contribution to some of them was first suggested by Davis *et al*.[33] At a proton-proton distance of less than 220 pm, the interaction of two C–H bond orbitals can lead to through-space coupling.[34-35] Long-range couplings of protons that are further apart than 220 pm have also been detected and in some cases, transmission of coupling information via the lone-pair orbitals of an oxygen[36] or a sulphur[37] atom to the second proton has been observed.[38] Proton-proton couplings over more than three bonds are usually too small to easily detect. However, there are a number of important scenarios where such couplings are present and can provide useful structural information on the compounds analyzed.[39] Coupling across π-systems

are the most encountered ^{4}J couplings with the meta coupling in aromatic compounds and the 4-bond allylic, propargylic and allenic couplings.[39] Research done by the Reich group at the University of Wisconsin show that 4-bond couplings across saturated carbons (sp^3) or heteroatoms are rarer, and are usually seen only when there is a favorable geometric alignment along the H–C–C–H chain ("W-Coupling"). Figure 1.5 displays some of the common ^4J and ^5J couplings discussed above for some aromatic and aliphatic systems.

	Allylic	Propargylic	Allenic	W-Coupling
^{4}J = 2 to 3 Hz	^{4}J = -3 to +3 Hz	^{4}J = 2 to 4 Hz	^{4}J = 6 to 7 Hz	^{4}J = -1 to +3 Hz

	Homoallylic	Homopropargylic	Homoallenic
	^{5}J = 0 to 8 Hz	^{5}J = 2 to 4 Hz	^{5}J = 3 to 6 Hz
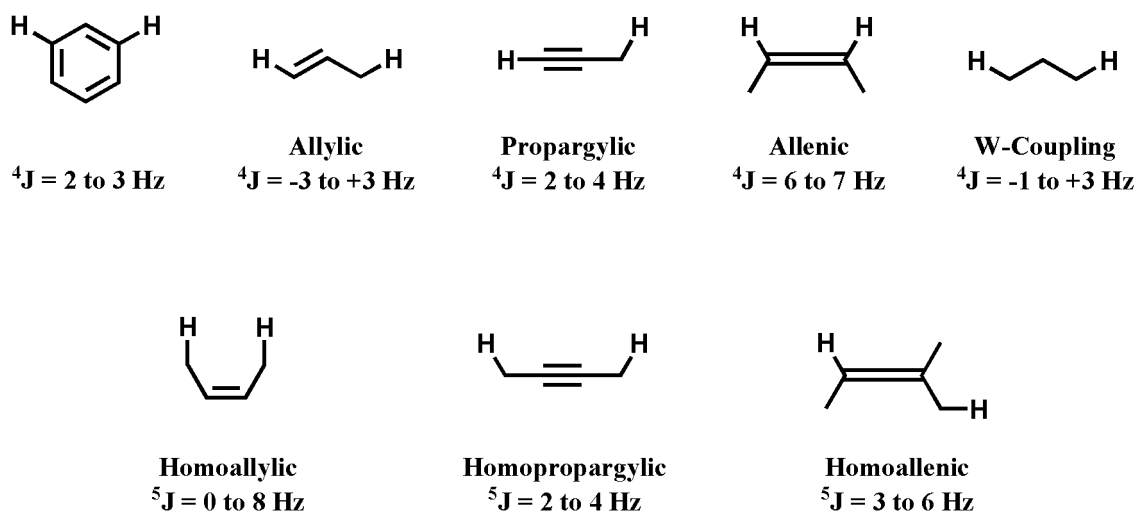
Figure 1.5: Common ^{4}J and ^{5}J Couplings for Aromatic and Aliphatic Systems

Research carried out by Ronald Harvey and Bongsup Cho on the complete ^{1}H and ^{13}C NMR assignment of polycyclic aromatic fluoratenes by long-range optimized homo- and hetero-nuclear correlation spectroscopy showed that protons in a polycyclic system can couple to each other through four modes; epi, peri, para, and through-space.[40] These modes can be observed in the compound indeno[1,2,3-hi]chrysene as shown in Figure 1.6. This long range coupling of protons can be observed as cross peaks in Correlation Spectroscopy (COSY) experiments but does not allow for the measurement of the magnitude of couplings with reasonable accuracy. Nevertheless, delayed COSY spectra were used by the Platzer group to observe long-range couplings in rigid polyaromatic systems such as terpenes and steroids.[41] They observed the presence of through-space couplings between the methyl groups and the hydrogen atoms close enough in space but not connected by a zig-zag path. Much weaker couplings were later found in

the COSY spectra obtained by the Paryzek group through four and five bonds away. More recently, the Strongin group at Louisiana State University reported and unusual seven bond proton-proton spin coupling while analyzing the compound tiliacorinine.[42] They observed the coupling between the resonances of two aromatic protons located on two different benzene rings that were formally separated by two sp^3 carbon atoms. They attribute this unusual coupling, seven bonds away, to the close special proximity of the protons. Indeed, this seems to be the predominant explanation for unusual long range couplings observed in polyaromatic systems as detailed in the research done by the Haslinger group.[43] They go on to further explain that a certain stereospecific arrangement between the coupling nuclei is important for the existence of long range coupling. The stereospecific criteria is fulfilled if the C–H bonds of interest are not parallel to each other and if the distance between the coupled protons is shorter than 225 pm. It has been suggested that overlap between two proximate hydrogen orbitals and overlap of the back lobes of the C–H bonds which are close in space lead to the transmission of the coupling information between protons.[44-46]

epi

peri

through-space

para
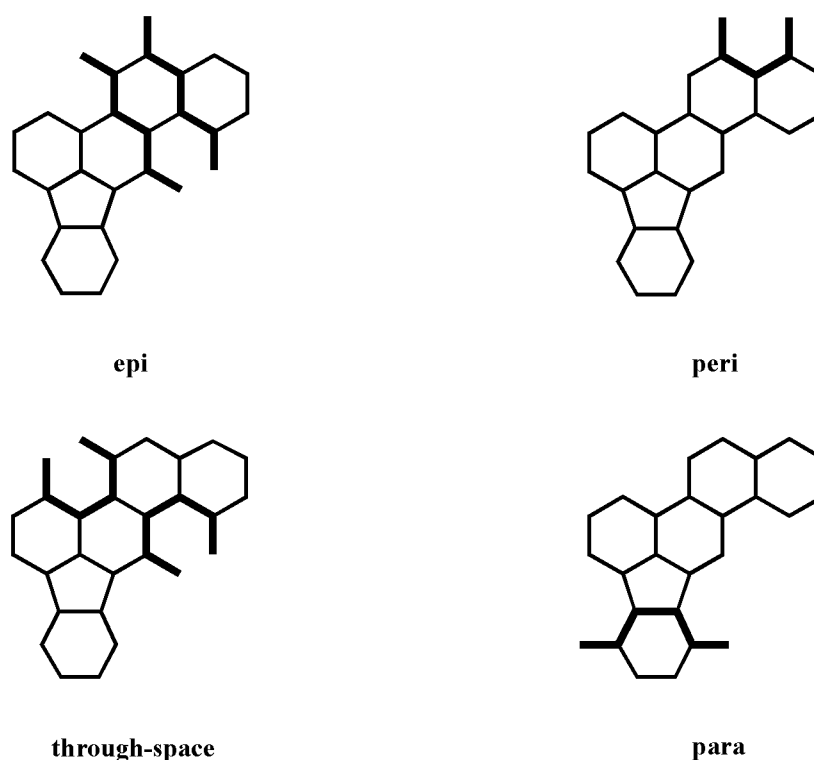
Figure 1.6: Modes of Long Range Coupling for Indeno[1,2,3-hi]chrysene

1.6 Research Objectives

Taking all factors discussed in this chapter into consideration, we therefore set out to synthesize a diverse library of novel chiral complexes incorporating various metal centers. The choice of metal counter ion used for the chelation reactions largely depends on ligating ability and on the electronic influence the strong or weak coordination has on the metal center. The counter-ions; Cl⁻, I⁻, OTf⁻, and acetate, are predominantly used in this report. Chirality is incorporated into our complexes through the two separate C_2 symmetric backbone precursors used in their design. The cyclohexyl backbone (1R,2R)-diaminocyclohexane) and the binaphthyl backbone ((R)-1,1'-binaphthyl-2,2'-diamine) used are shown in Figure 1.7. Incorporating the cyclohexyl backbone increases the probability of forming monohelix complexes as the relatively small ring forces the donor atoms to be close to one another. The binaphthyl backbone typically exists as a highly twisted moiety and increases the probability for forming only one helical conformer after complexation. This observed twist helps direct the ligand side-arms to be in close proximity to one another, increasing the probability of all four nitrogen donor atoms in the ligand system binding to the same metal center.

**Cyclohexyl
Backbone**

**Binaphthyl
Backbone**

Figure 1.7: (1R,2R)-diaminocyclohexane & (R)-1,1'-binaphthyl-2,2'-diamine Backbones

The side-arms used to complete the complex design are polyaromatic ring systems as they increase the probability of obtaining a 'locked' complex after metallation. The use of saturated ring systems to design the side-arms may result in increased flexibility and conformational mobility which is not a desired characteristic. Also, the use of unsaturated polyaromatic cyclic side-arms improves the helix stabilizing interaction and reduces the steric

clashes as they are able to stack on top of one another utilizing π–π stacking or σ–π stacking interactions.[47] With this in mind, we chose to incorporate quinoline, isopropyl-quinoline, and benzo-quinoline as the side-arms of choice (Figure 1.8).

Quinoline

Isopropyl-Quinoline

Benzo-Quinoline
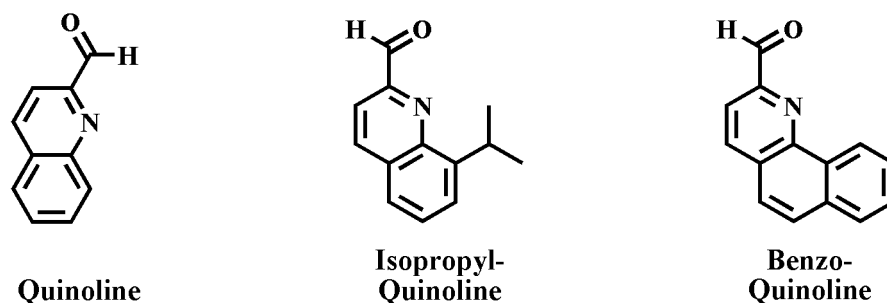
Figure 1.8: Unsaturated Polyaromatic Side-arms used in Complex Design

The following chapters of this thesis will focus on the design of various ligands incorporating the backbones and side-arms discussed in this chapter with the hope of synthesizing single-stranded mononuclear helical transition metal complexes. We will explore the reduction of select ligands in our library with the hope of improving the flexibility of the eventual complexes so they can accommodate bulkier substrates during asymmetric catalysis reactions. The desired ligand library is shown in Figure 1.9 and displays both the unreduced and reduced ligands of interest (**1**, **2**, **3**, **4**, **5**, **11**, and **12**). Select chapters will also detail the intricate complete ^{1}H NMR assignments of select ligands and complexes through the use of select 1D NMR techniques and various 2D NMR experiments (COSY, NOESY, ROESY, HSQC, HMBC). This characterization helps us track the effect of the metal ion as we transition from ligand to complex. Finally, we explore the potential use of select complexes in the area of NMR discrimination and kinetic resolution of racemic mixtures of olefins. The role of sterics and temperature in the chiral recognition experiments will also be examined.
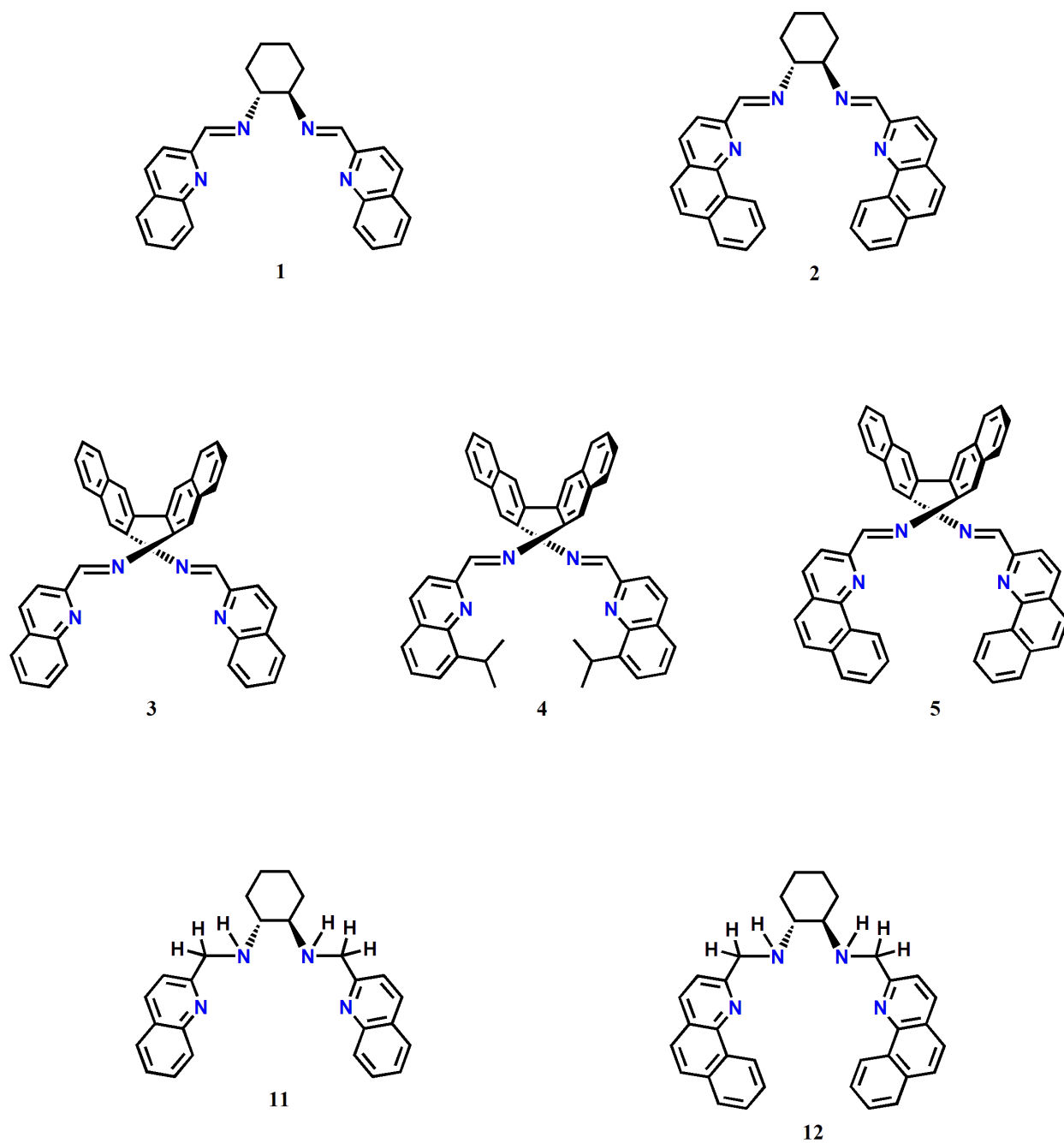
Figure 1.9: Desired Ligand Library Incorporating Cyclohexyl and Binaphthalene Backbones

CHAPTER 2

Synthesis, Characterization and Reduction of
Tetradentate Nitrogen Ligands

2.1 Synthesis of Ligand Precursors

The preparation of ligands **1 – 5** involves a simple condensation of the desired diamine backbone with the appropriate aldehyde sidearm (Figure 2.1). The synthesis procedure for the backbones and sidearms has been established by previous members of this group and will be included in this report for clarity purposes. The aldehydes, although seemingly simple, are quite complex and had to be synthesized using a combination of literature preparations. The chiral diamine backbones, (1*R*,2*R*)-1,2-cyclohexanediamine (*R*,*R*)-**6** and (*R*)-(1,1'-binapthalene) -2,2'- diamine (*R*)-**7** are commercially available but their high cost and the need for multi-gram quantities made their syntheses in the laboratory necessary.

(*R*,*R*)-**6**   (*R*)-**7**

8   **9**   **10**
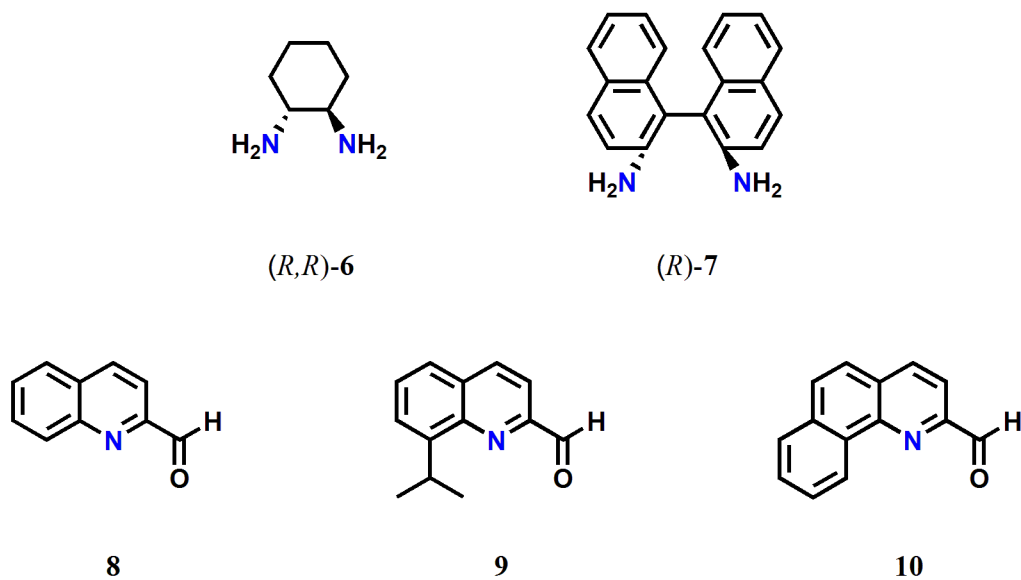
Figure 2.1: List of Backbones and Sidearm Precursors

The diamine backbone (*R*)-**7** can be synthesized using known methods in the literature[48] and (*R,R*)-**6** can be prepared via the Jacobsen procedure.[49] Therefore, no further synthetic discussion on those precursors will be made in this report. To generate aldehyde **8**, commercially purchased quinaldine was oxidized with selenium dioxide for 3 hours. The product obtained was then run through a plug of silica gel to remove the colloidal orange-red selenium.
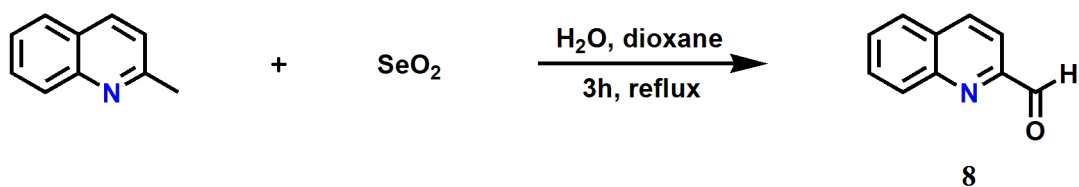
Figure 2.2: Synthesis of Aldehyde Precursor **8**

Aldehyde **9** was made using a two step procedure. In step one, 2-isopropylaniline and crotonaldehyde were reacted under strongly acidic oxidative conditions, via a modified Skraup's procedure, to yield the dialkyl substituted quinoline.[50] Crotonaldehyde was used in excess because of its low stability and rapid self-polymerization in acidic media. This process afforded the *bis*-pyridyl imine product in 58% yield. The second step was the oxidation of 8-isopropyl-2-quinoline moiety as described in precursor **8** to generate aldehyde **9**. The product was run through a short plug of silica gel to give the purified product in 84% yield.[51]
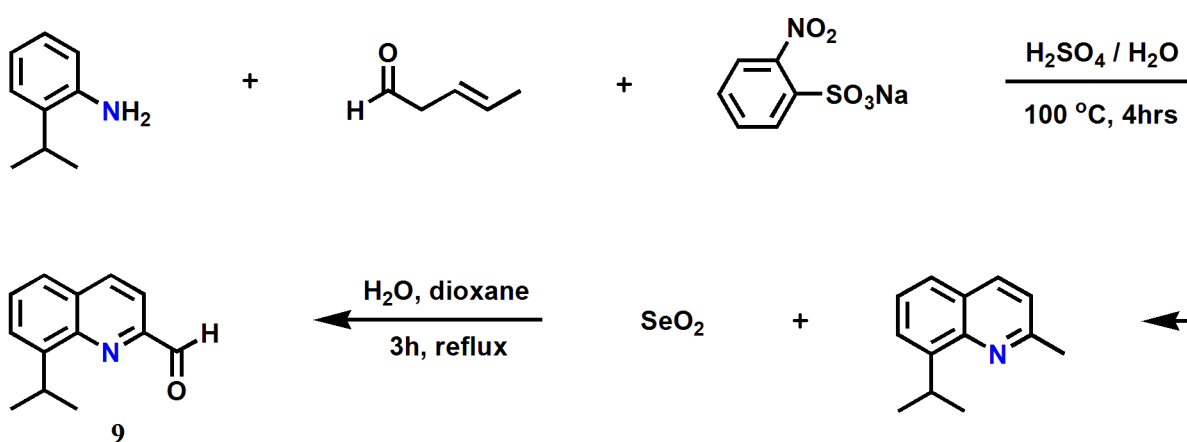
Figure 2.3: Synthesis of Aldehyde Precursor **9**

The final aldehyde (**10**) was synthesized using 1-amino naphthalene as the starting compound. Reaction with crotonaldehyde was carried out in acidic conditions as described in the synthesis of aldehyde **9** above. Once again, crotonaldehyde was used in excess because of its low stability and rapid self-polymerization in acidic media. The quinaldine by-product formed from this reaction was obtained in 25% yield and oxidized with selenium dioxide to afford aldehyde **10**. The brownish-red colored product obtained was run through a short plug of silica gel to give the purified aldehyde product in 38% yield.[51]
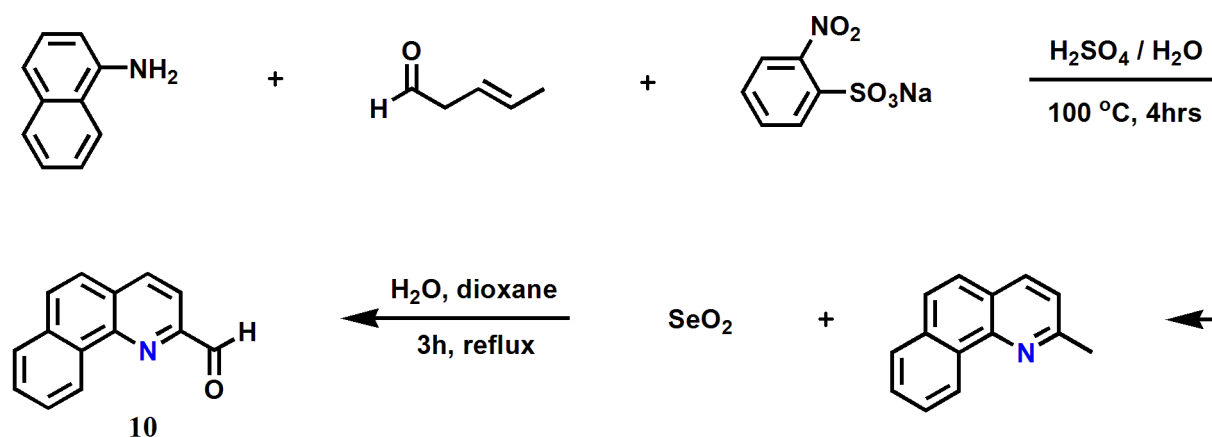
Figure 2.4: Synthesis of Aldehyde Precursor **10**

2.2 Synthesis of Ligands

The desired bis(imine-quinoline) ligands were all generated from the Schiff-base condensation of the corresponding chiral diamine backbone with the preferred aldehyde sidearm precursor. Condensation was achieved by refluxing the backbone and sidearm in dry ethanol with molecular sieves added in some cases (reactions with the binaphthalene backbone) to remove water and drive the reaction towards the product. Dry solvents were used in these reactions since the ligands are susceptible to hydrolysis, which reforms the aldehyde and diamine. As solids, the ligands are stable to decomposition from atmospheric moisture. Syntheses of ligands **1** and **2** are shown is shown in Figure 2.5.
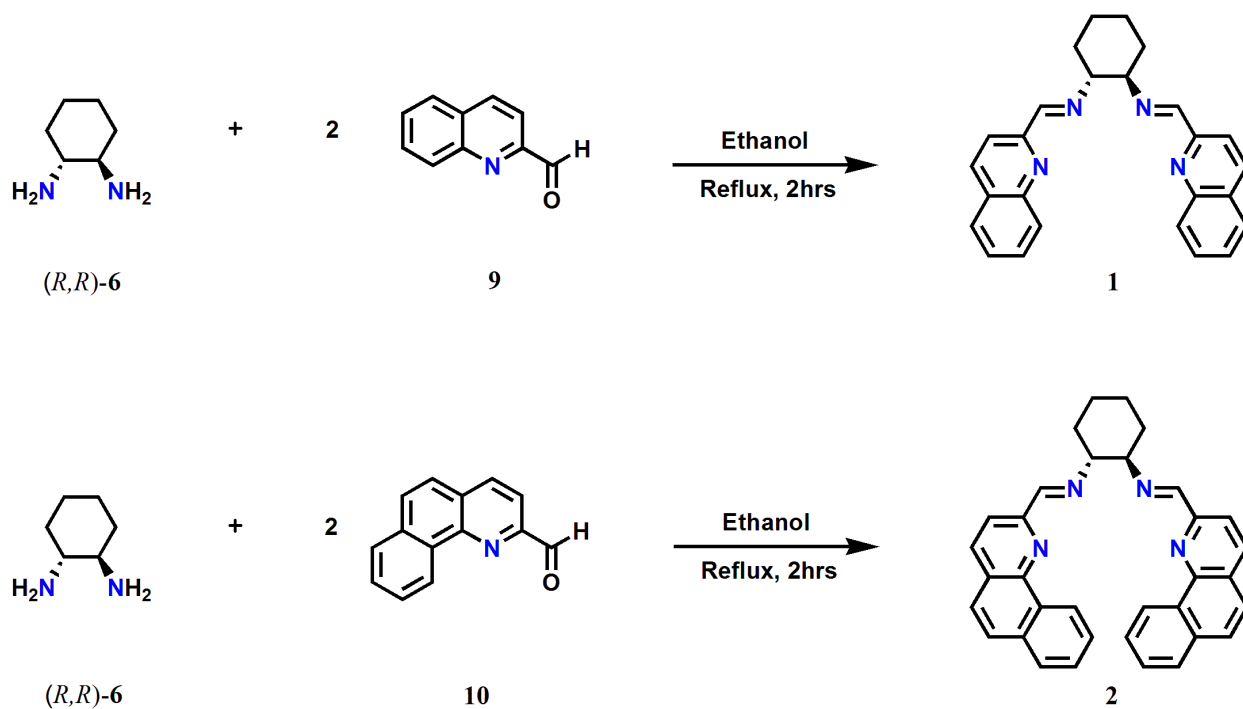
Figure 2.5: Synthesis of Ligands **1** and **2**

Ligands **3**, **4**, and **5** are more prone to hydrolysis given the electron withdrawing character of the binaphthalene backbone used in their design, ^{1}H NMR is shown in Figure 2.6.
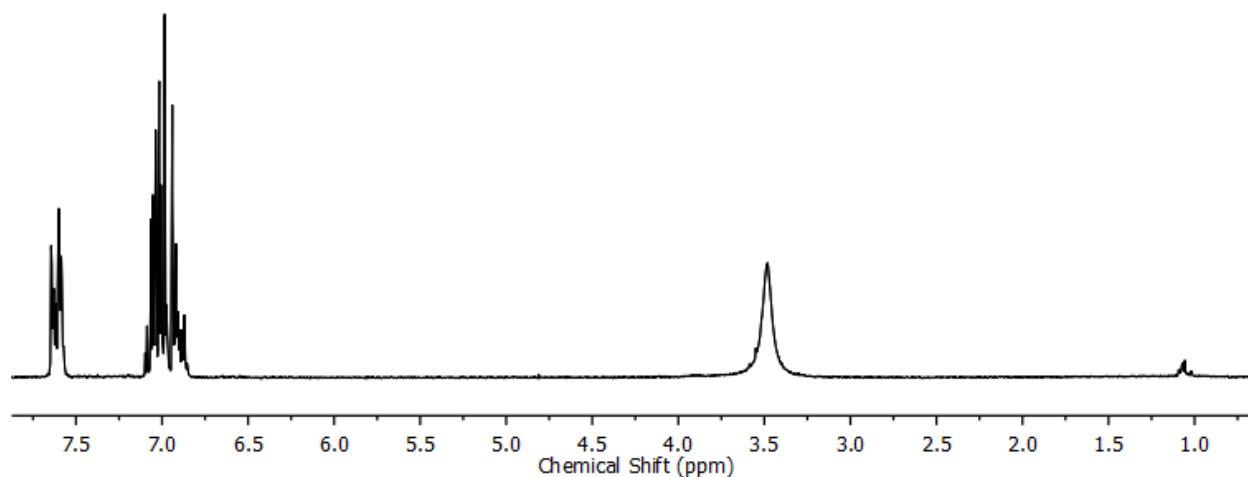
Figure 2.6: 400 MHz ^{1}H NMR Spectrum of (**R**)-**7** Backbone Precursor (CDCl$_3$)

15

Therefore, condensation reactions done with the binaphthalene backbone were carried out with molecular sieves present in the reaction vessel. The synthetic steps for ligands **3** - **5** were carried out under the same reaction conditions as described for ligands **1** and **2** and are shown below in Figure 2.7. The yields and purity are generally high because the reactants involved are completely soluble in ethanol while the products are not.
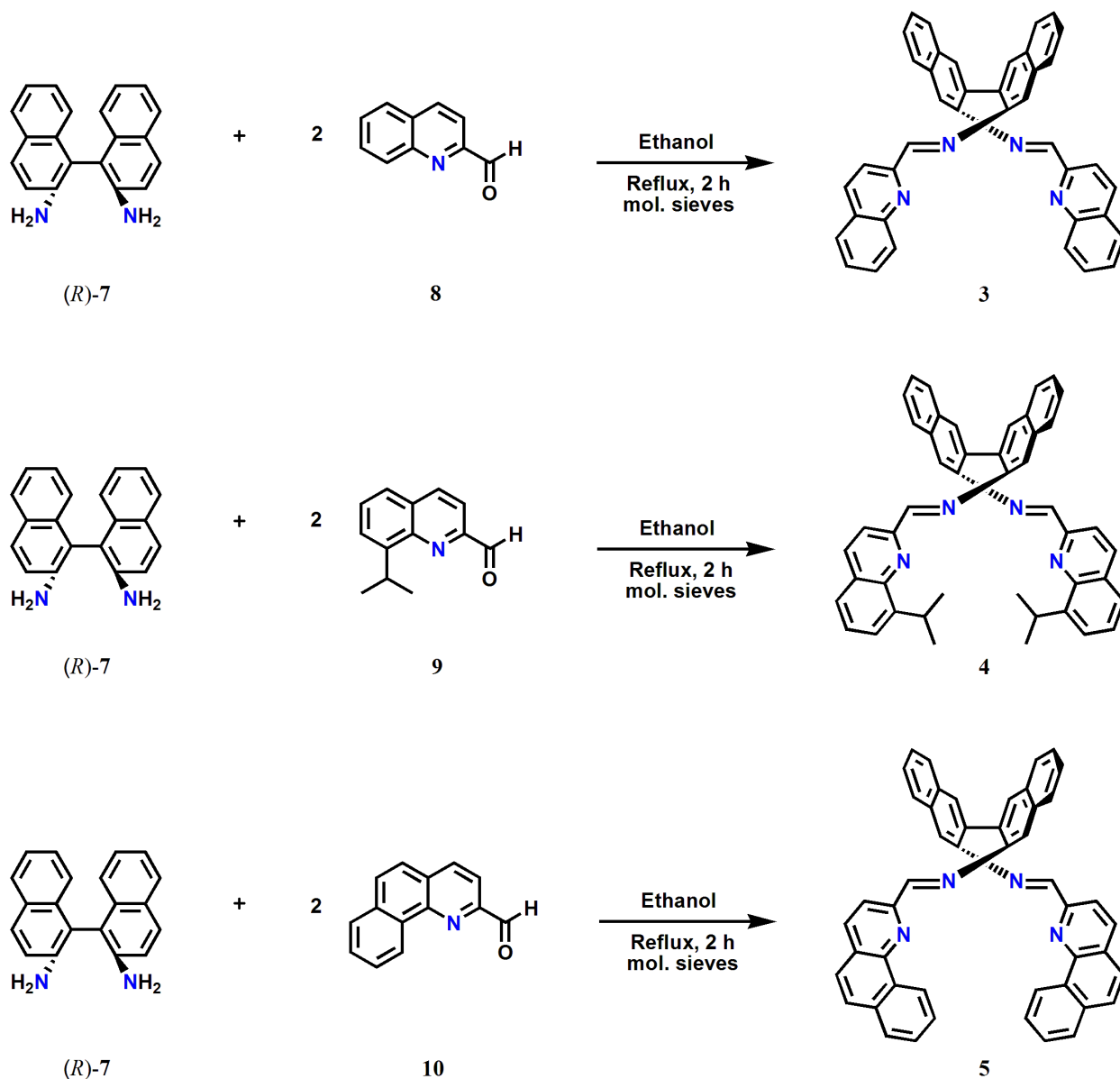
Figure 2.7: Synthesis of Ligands **3**, **4** and **5**

2.3 Complete NMR Assignment of Ligands

The ligands described in this thesis are synthesized to serve as building blocks in the design of chiral catalysts. Their future reaction with various metal-salts to make the desired catalysts will also result in a change to the physical and chemical properties of the ligands. Consequently, it is important to characterize the ligands so that this change can be monitored. A great technique to use is Nuclear Magnetic Resonance (NMR) as the position (frequency) of protons on the ligands can be deciphered and monitored as we transition from ligand to complex. NMR characterization is a complex process because the ligands are polycyclic aromatic systems and the coupling network similarity in different parts of the molecule usually results in the severe overlap of their ^{1}H resonances. To overcome this impediment, we took advantage of various 2D-NMR techniques (COSY, NOESY, ROSEY, HSQC, and HMBC) and were successful in resolving the complete NMR assignment of ligands **1 – 5**.

The ^{1}H NMR spectrum for ligand **1** is shown in Figure 2.8. It is the simplest structure of the five ligands showing well resolved peaks but still exhibits an overlap of protons around 8.00 ppm. The characteristic imine proton appears as a singlet at 8.50 ppm and the distinct triplets for the molecule appear at 7.64 ppm and 7.48 ppm. To clarify the overlap at 8.00 ppm and decipher the number of protons present in that region, a Heteronuclear Single Quantum Coherence (HSQC)
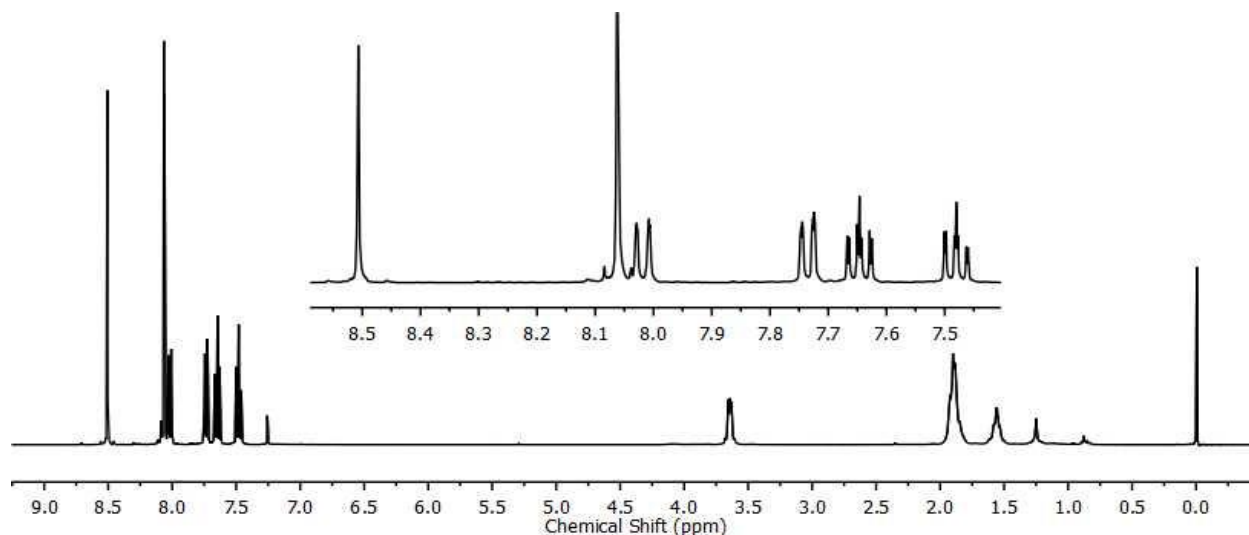
Figure 2.8: 400MHz ^{1}H NMR Spectrum of Ligand **1** (CDCl$_3$)

17

experiment was conducted (Figure 2.9). The spectrum displayed the expected number of proton to carbon coupling for the molecule (12) and confirmed the presence of three protons in the overlapped region. The contours also show the difference between methine and methylene protons with methine displayed as red contours and methylene displayed as blue contours. This allowed us to assign eight protons as methine and four protons as methylene.
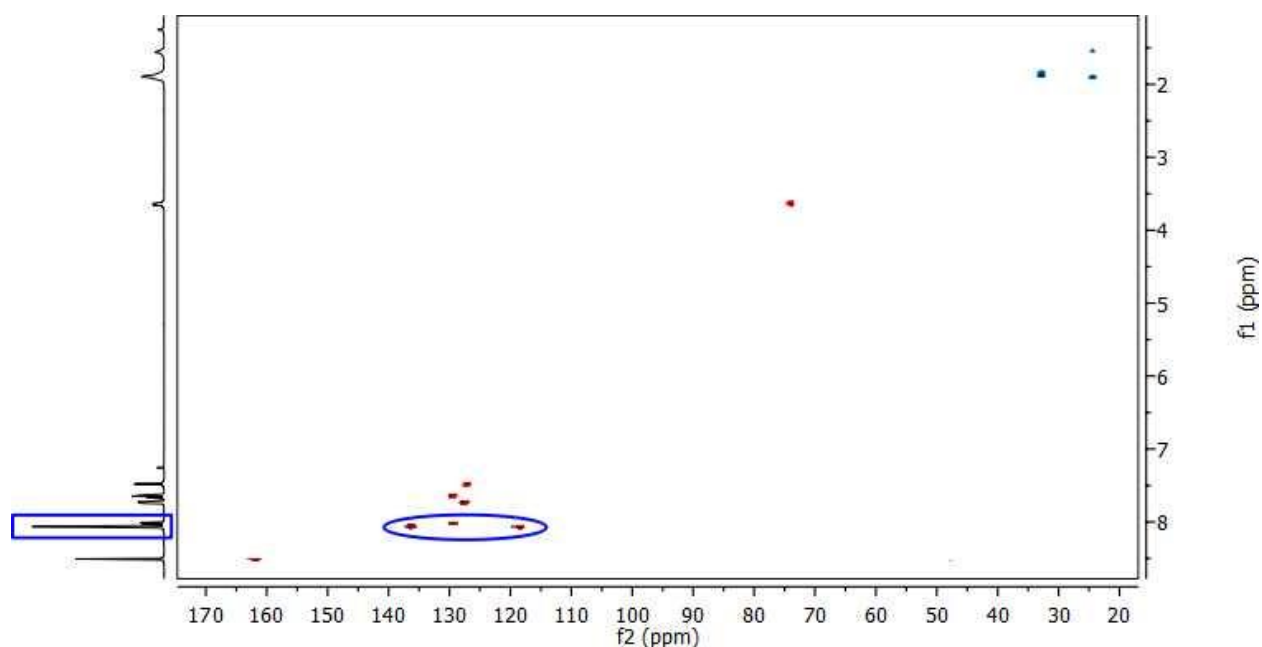
Figure 2.9: 400 MHz HSQC Spectrum of Ligand **1** (CDCl$_3$)

To understand the proton to proton coupling and ultimately solve the complete ^{1}H assignment of ligand **1**, a Correlation Spectroscopy (COSY) experiment was conducted and is shown in Figure 2.10. As expected, the imine proton is not coupled to any other proton on the quinoline arm. The triplet that appears at 7.64 ppm shows strong coupling to the neighboring triplet (7.48 ppm) and doublet (8.00 ppm) but also shows the weak coupling to the distant doublet (7.73 ppm) on the same ring. The COSY experiment typically displays proton coupling one carbon away but because of the conjugated ring system present in ligand **1**, we were able to observe this coupling two carbons away. We deciphered the complicated coupling network present in the region where the three protons overlap (8.00 ppm), and were able to solve the complete ^{1}H NMR assignment for ligand **1** shown in Figure 2.11.
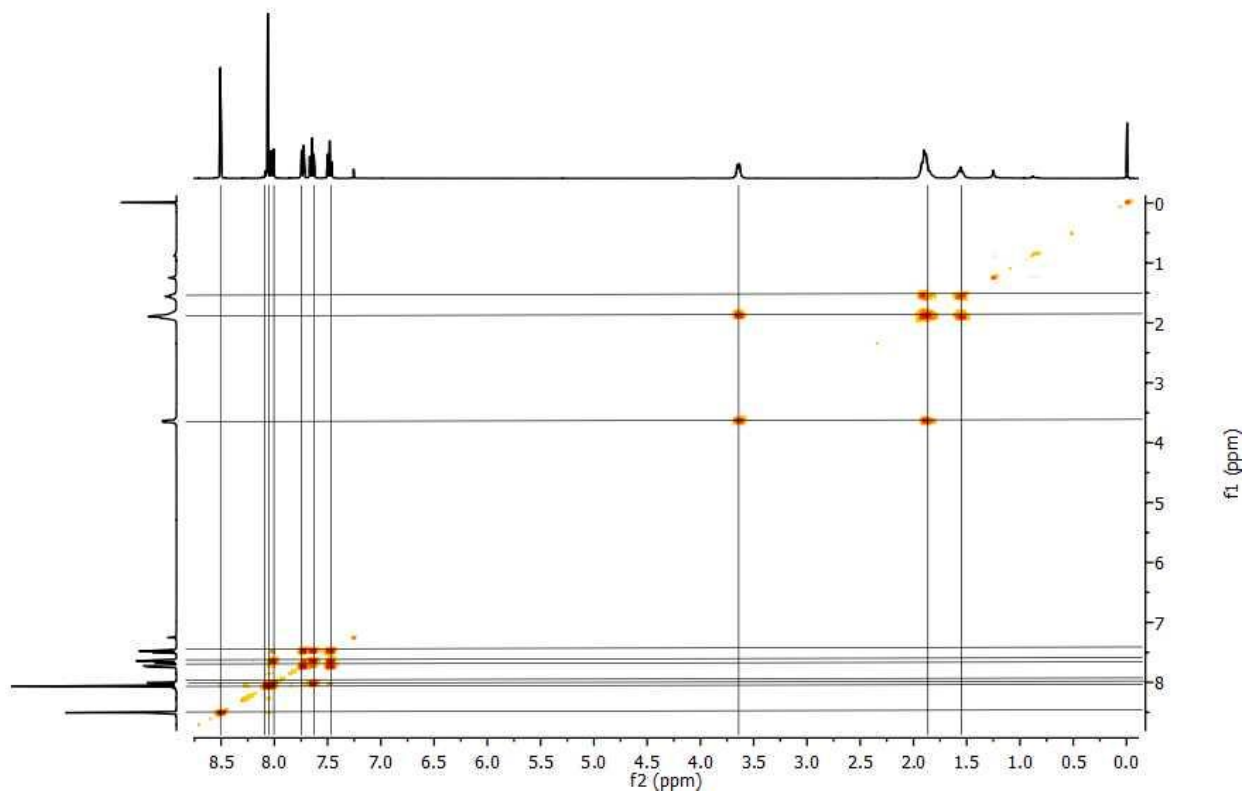
Figure 2.10: 400 MHz COSY Spectrum of Ligand **1** (CDCl$_3$)

1,2 (1.63/1.99 ppm)

3,4 (1.99 ppm)

5   (3.73 ppm)

6   (8.50 ppm)

7   (8.07 ppm)

8   (8.04 ppm)

9   (8.00 ppm)

10   (7.64 ppm)

11   (7.48 ppm)

12   (7.73 ppm)
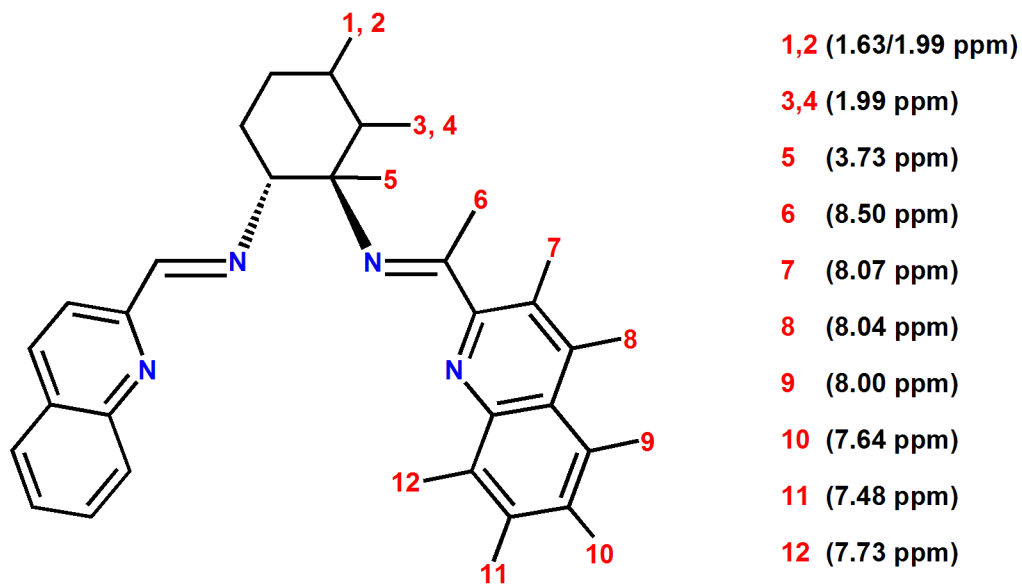
Figure 2.11: Complete 400 MHz ^{1}H NMR Assignment of Ligand **1** (CDCl$_3$)

The complete ^{1}H NMR for ligand **2** was previously resolved using the magnetic field of an 800 MHz NMR spectrometer (Figure 2.12), leading to the assignment shown in Figure 2.13.
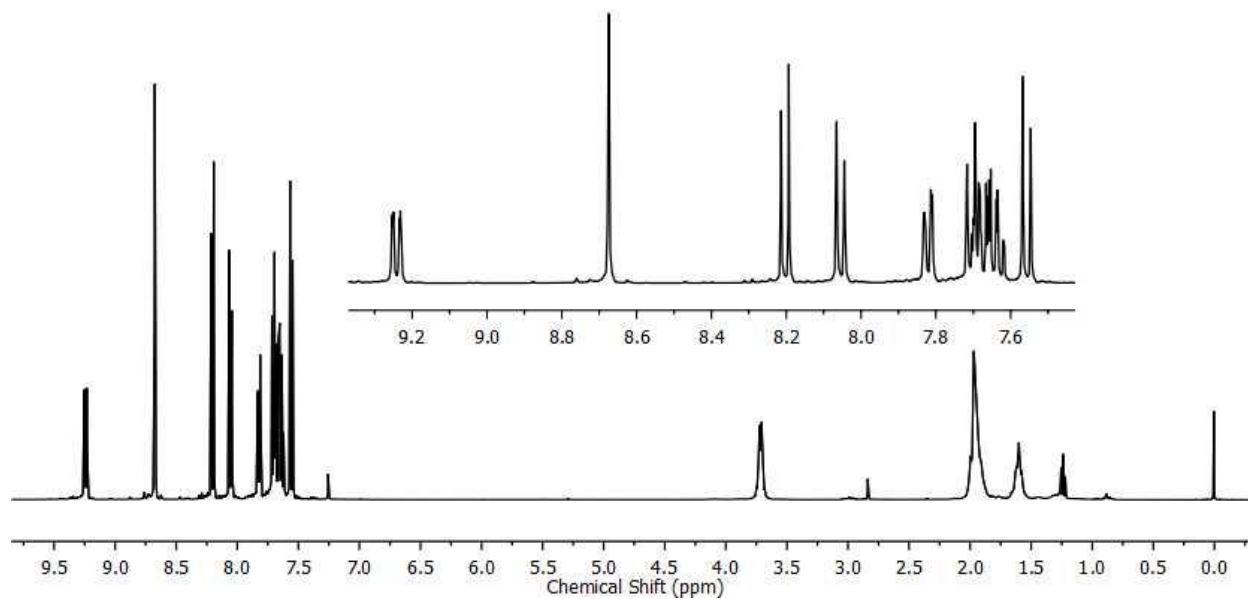
Figure 2.12: 800 MHz ^{1}H NMR Spectrum of Ligand **2** (CDCl$_3$)

1,2 (1.63/1.99 ppm)
3,4 (1.99 ppm)
5   (3.73 ppm)
6   (8.69 ppm)
7   (8.22 ppm)
8   (8.07 ppm)
9   (7.57 ppm)
10 (7.72 ppm)
11 (7.84 ppm)
12 (7.66 ppm)
13 (7.70 ppm)
14 (9.26 ppm)
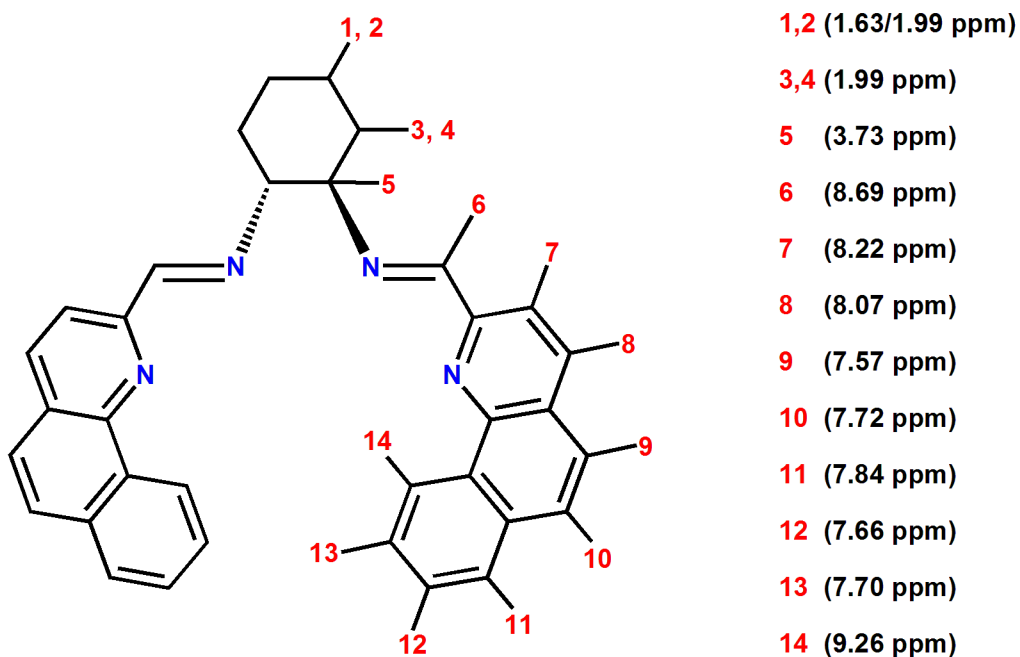
Figure 2.13: Complete 400 MHz ^{1}H NMR Assignment of Ligand **2** (CDCl$_3$)

Ligand **3** incorporates the more complex binaphthalene backbone and the ^{1}H NMR spectrum is shown below in Figure 2.14. We observe the correct number of resonance signals
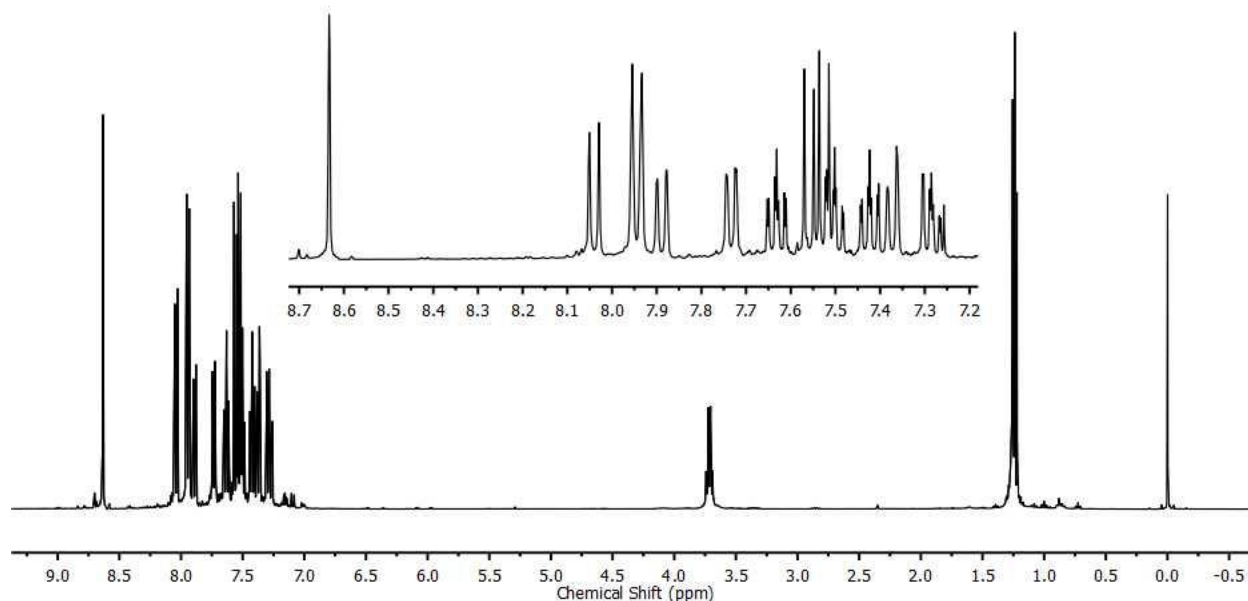
Figure 2.14: 400 MHz ^{1}H NMR Spectrum of Ligand **3** (CDCl$_3$)

consisting of the distinct imine singlet at 8.62 ppm, eight doublet resonance signals that span from 8.05 to 7.37 ppm, and four doublet of doublets peaks that appear at 7.63 ppm, 7.50 ppm, 7.42 ppm, and 7.28 ppm. These resonance signals amount to a total of thirteen for ligand **3** with the aromatic proton peaks centered between 8.62 and 7.26 ppm. A COSY experiment was conducted to simplify the resonance overlap observed in the ^{1}H NMR spectrum and is shown in Figure 2.15. We observe the expected ^{3}J coupling between protons (1→2, 2→3, 3→4, 5→6, 8→9, 10→11, 11→12, and 12→13). Examining similar polyaromatic systems in the literature revealed that long range coupling of protons in an epi, para, peri, or through-space fashion can sometimes be observed in a COSY spectrum.[52-54] We observe these long range couplings in ligand **3** for the following protons; (1→3{meta}, 1→4{para}, 1→5{epi}, 6→7{through-space}, 7→8{through-space}, 9→10{peri}, 13→9{epi}, 13→10 {para}, and 13→11{meta}). These long range couplings occur because of the highly conjugated system present in the molecule.
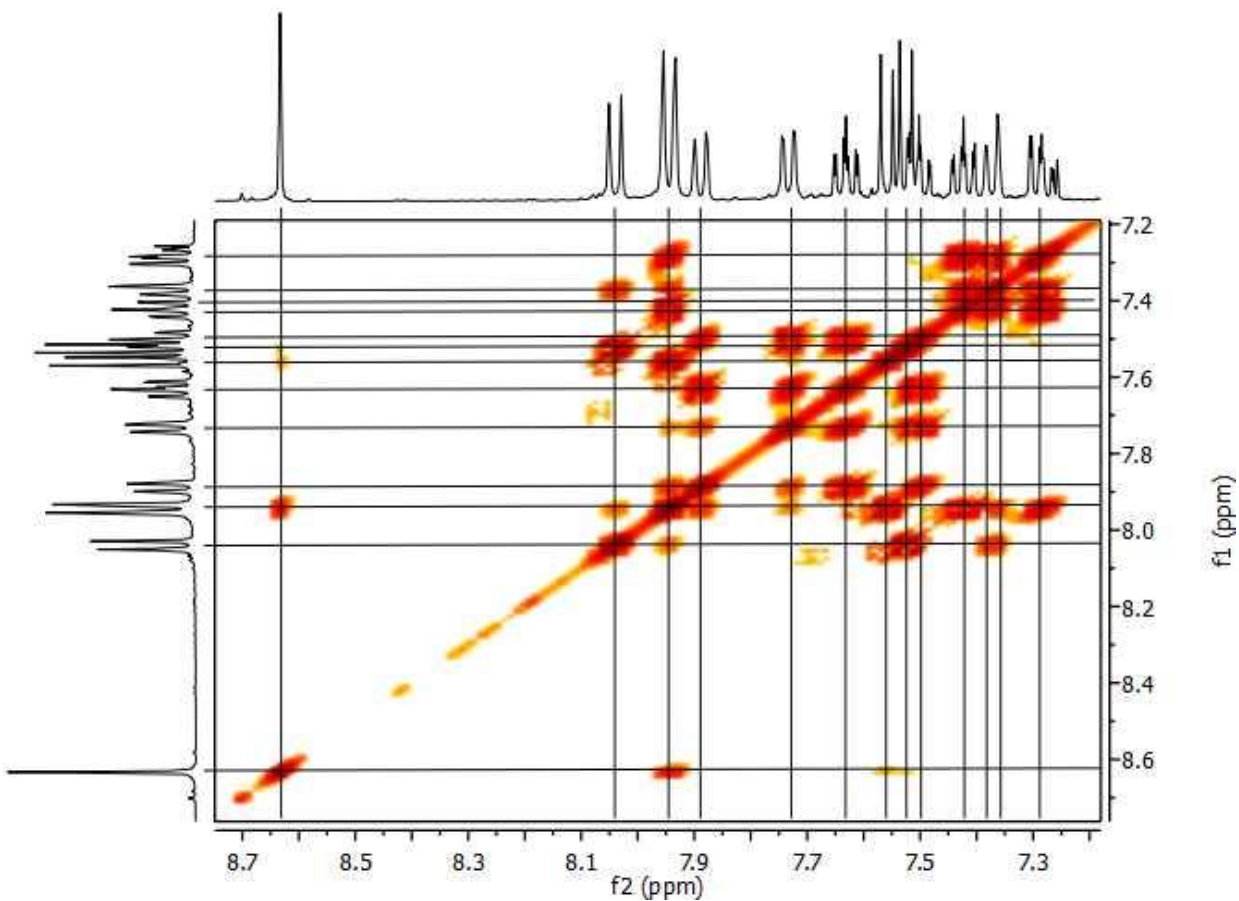
Figure 2.15: 400 MHz COSY Spectrum of Ligand **3** (CDCl$_3$)

An HSQC experiment (Figure 2.16) was conducted to confirm the number of protons present at 7.52 ppm. We observe that there are two aromatic methine protons present in that region, a doublet at 7.52 ppm and a doublet of doublet at 7.50 ppm. Since all the contours displayed in the spectrum are due to methine protons, the spectrum also helps differentiate the quaternary carbons from the tertiary carbons displayed in the ^{13}C NMR on the x-axis of the HSQC spectrum. This was of use when interpreting the Heteronuclear Multiple Bond Coherence (HMBC) spectrum conducted for ligand **3** (Appendix I). From the HSQC experiment, we observe that the carbon atom associated with the imine proton is shifted downfield because of its conjugation with the nitrogen group in the imine bond. These 2D NMR experiments allowed for the complete ^{1}H NMR assignment for ligand **3** shown in Figure 2.17.
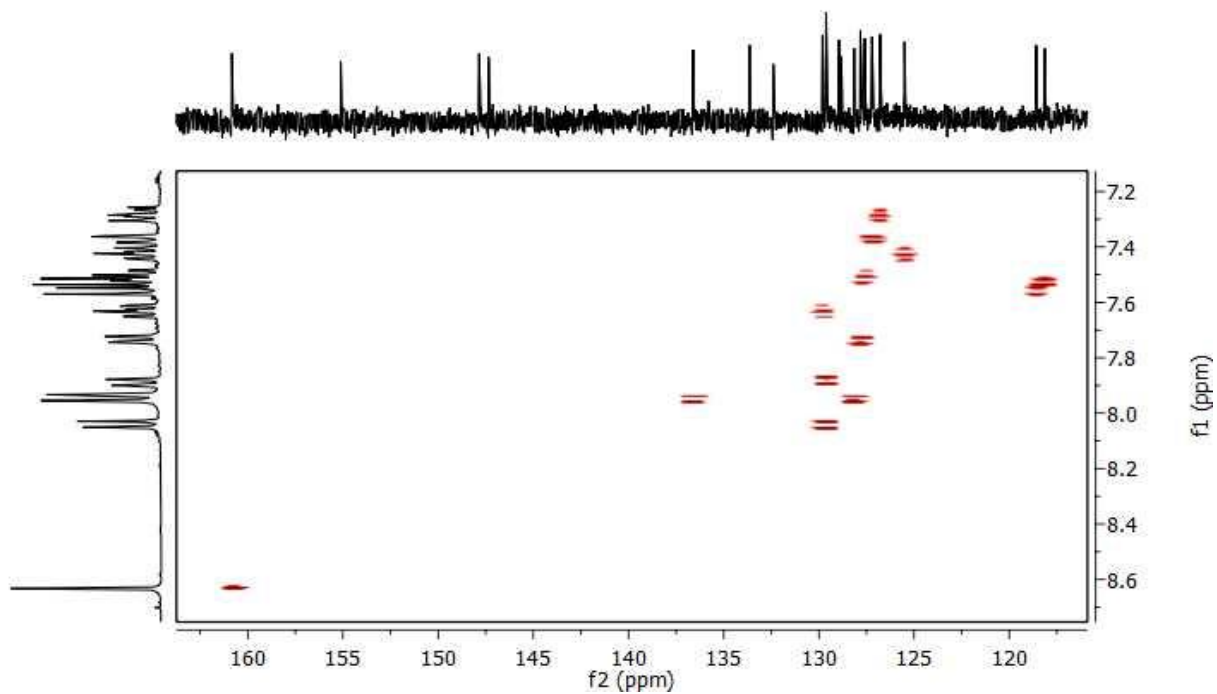
Figure 2.16: 400 MHz HSQC Spectrum of Ligand **3** (CDCl$_3$)

1	**(6.43 ppm)**
2	**(6.88 ppm)**
3	**(6.78 ppm)**
4	**(6.41 ppm)**
5	**(6.47 ppm)**
6	**(7.97 ppm)**
7	**(9.35 ppm)**
8	**(8.49 ppm)**
9	**(8.59 ppm)**
10	**(7.82 ppm)**
11	**(7.27 ppm)**
12	**(6.40 ppm)**
13	**(5.88 ppm)**
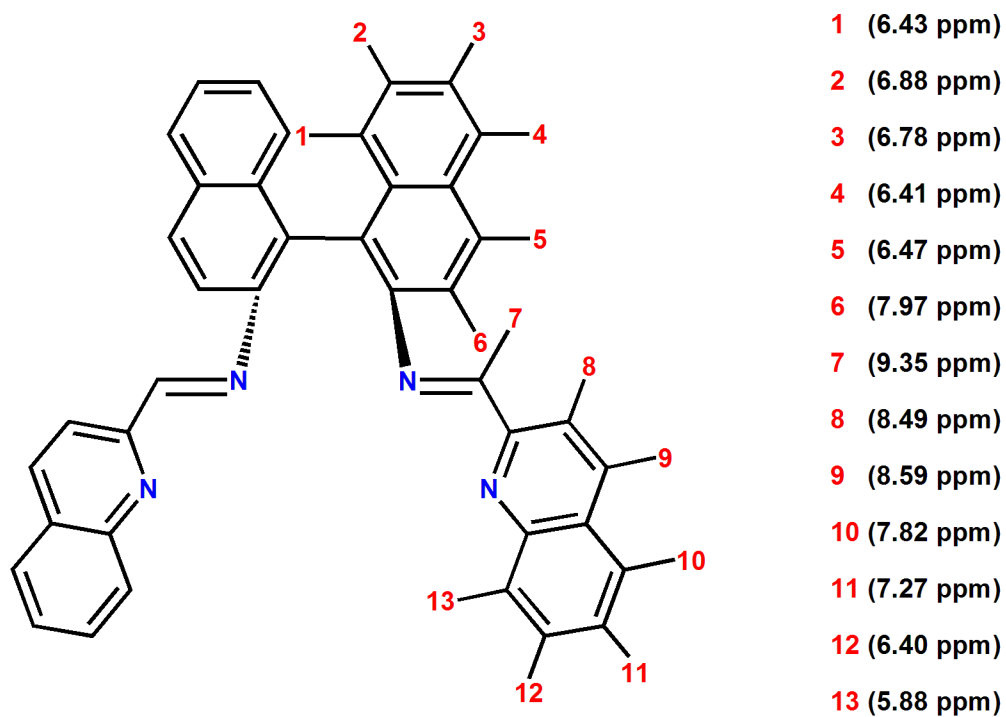
Figure 2.17: Complete 400 MHz ^{1}H NMR Assignment of Ligand **3** (CDCl$_3$)

Ligand **4** incorporates an isopropyl unit on the quinoline ring and the ^{1}H NMR spectrum is shown in Figure 2.18. The aliphatic protons that correspond to the isopropyl unit are centered upfield in the spectrum. Here the isopropyl methine peak is centered at 4.09 ppm and appears as a septet because of the six neighboring methyl protons. The isopropyl methyl peaks are located at 1.08 and 1.24 ppm and show up as doublet of doublets due to the neighboring methine proton. Once again, the characteristic imine peak is observed as a singlet at 8.59 ppm. The aromatic peaks are centered between 7.27 ppm and 8.59 ppm, once again displaying the complicated resonance overlap characteristic of polyaromatic cyclic structures.
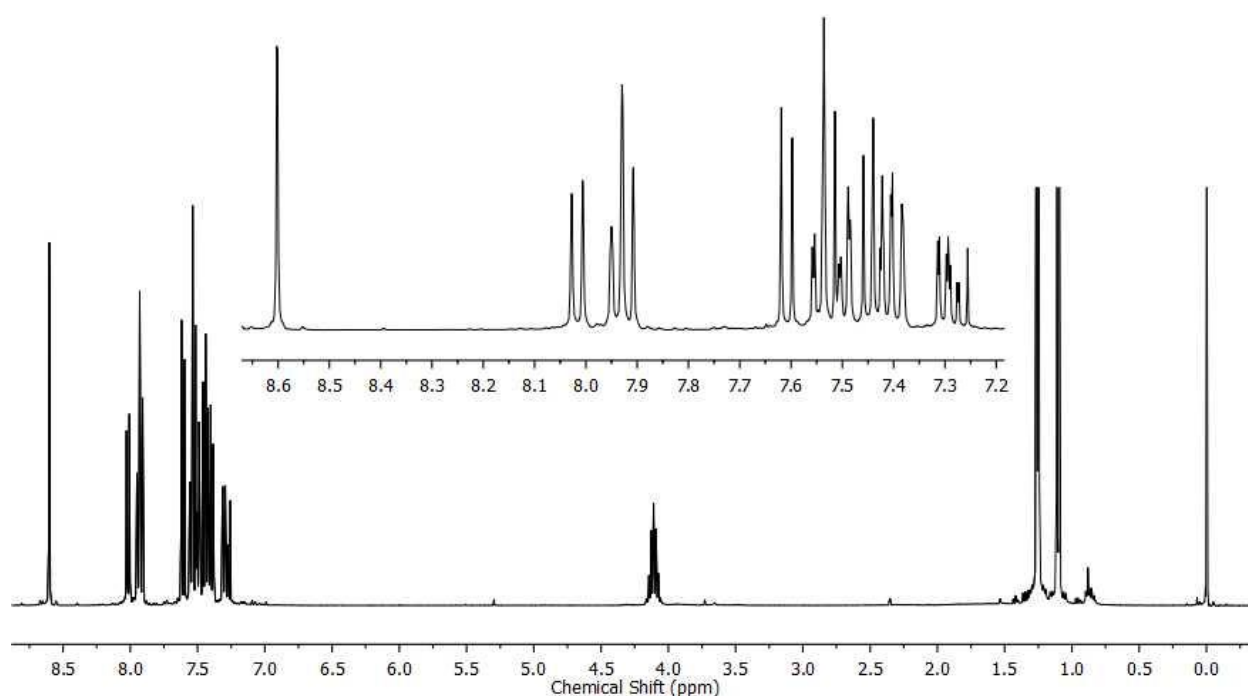
Figure 2.18: 400 MHz ^{1}H NMR Spectrum of Ligand **4** (CDCl$_3$)

The COSY NMR spectrum obtained for ligand **4** is shown in Figure 2.19 (aromatic region) and Figure 2.20 (aliphatic region) displaying the expected [3]J coupling between protons (1→2, 2→3, 3→4, 5→6, 8→9, 10→11, 11→12, and 13→14). It also exhibits the long range couplings discussed earlier in Ligand **3**; (1→3{meta}, 1→4{para}, 1→5{epi}, 6→7{through-space}, 7→8{through-space}, 9→10{peri}, 10→12{meta}, and 12→13{meta}). Some of these

couplings are 4 bonds away, (1→3) and in some instances up to 5 bonds away, (1→5). As discussed earlier in chapter 1, these unusual long-range couplings have been observed in COSY experiments carried out on other similar polyaromatic cyclic systems. The research done on those systems show that the spatial arrangement of the protons on the aromatic rings involved in the couplings contributes to the interactions observed in the COSY spectra. An interesting observation in the COSY spectrum obtained for ligand **4** is the coupling of the imine proton (7) with proton (8) from the isopropyl quinoline side-arm. This is unusual because the imine proton is not part of the aromatic conjugation of the side-arm but still displays coupling to proton (8). This may be due to the presence of stable conformations (as a result of the lone pair of electrons on the nitrogen donor atoms and the imine double bond) that allows the noteworthy coupling of proton (7) and proton (8) to occur in ligand **4**.
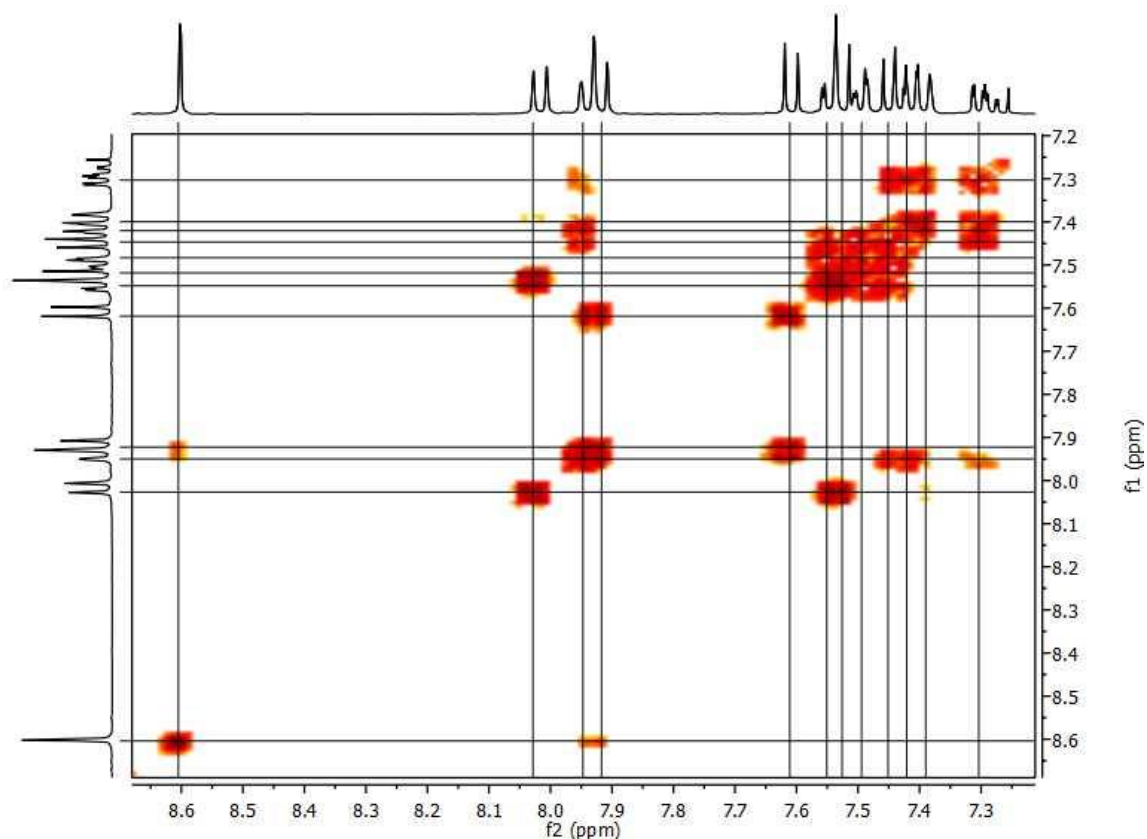
Figure 2.19: 400 MHz COSY Spectrum of Aromatic Region in Ligand **4** (CDCl$_3$)

25
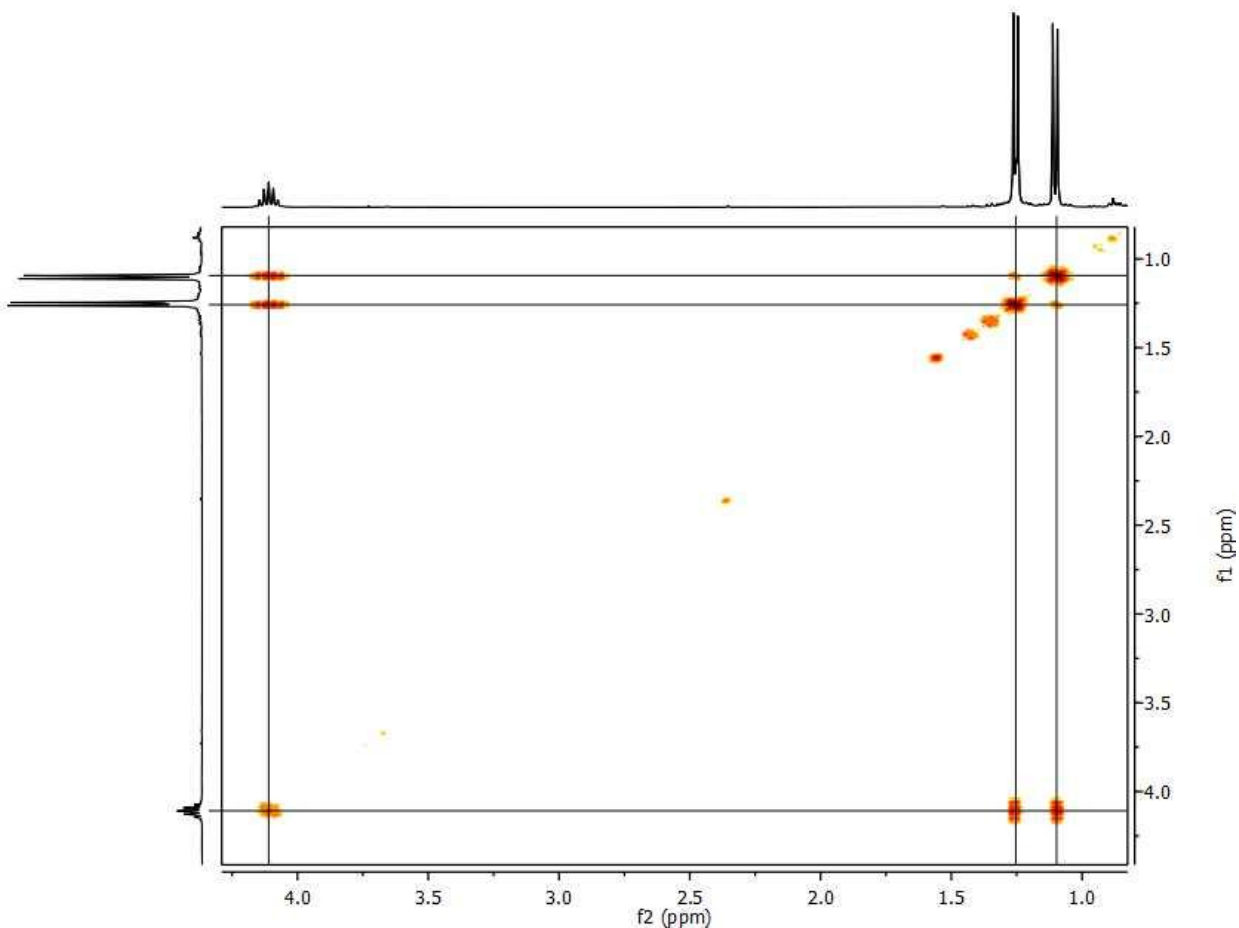
Figure 2.20: 400 MHz COSY Spectrum of Aliphatic Region in Ligand **4** (CDCl₃)

We obtained the right number of aromatic cross peaks in the HSQC experiment, which was conducted to simplify proton overlaps and also helped to differentiate the quaternary carbons from tertiary carbons (Figure 2.21). This separation was beneficial when analyzing the HMBC spectrum obtained for ligand **4** (Appendix I). We observe that the carbon attached to the imine proton displays a solitary downfield contour position in the HSQC spectrum. This is most likely due to the electron withdrawing nature of the nitrogen atom in the imine bond. The imine proton and imine carbon signals are unique in that they are the only ones attached to an electron withdrawing nitrogen atom. The combination of these 2D NMR experiments and subsequent 1D NMR experiments allowed us to be able to navigate the complex resonance overlap of ligand **4** and eventually led to the complete ^{1}H assignment shown in Figure 2.22.

26
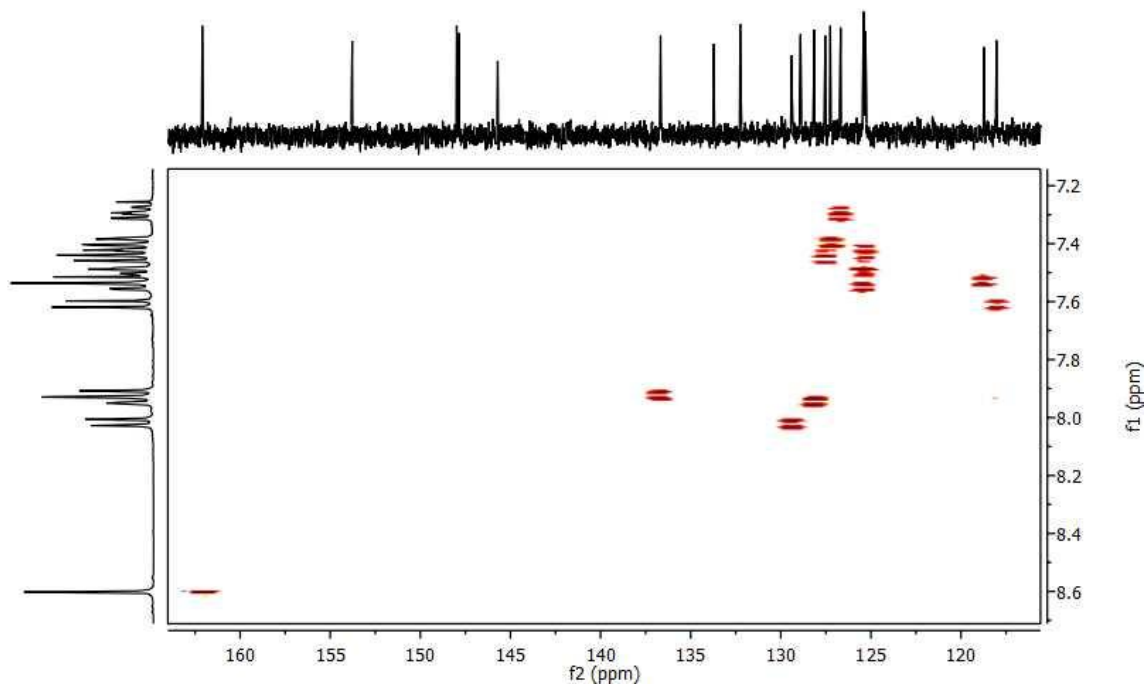
Figure 2.21: 400 MHz HSQC Spectrum of Ligand **4** (CDCl$_3$)

1 (7.92 ppm)

2 (7.39 ppm)

3 (7.28 ppm)

4 (7.41 ppm)

5 (8.00 ppm)

6 (7.59 ppm)

7 (8.59 ppm)

8 (7.90 ppm)

9 (7.43 ppm)

10 (7.52 ppm)

11 (7.54 ppm)

12 (7.40 ppm)

13 (4.09 ppm)

14 (1.08/1.24 ppm)

15 (1.08/1.24 ppm)
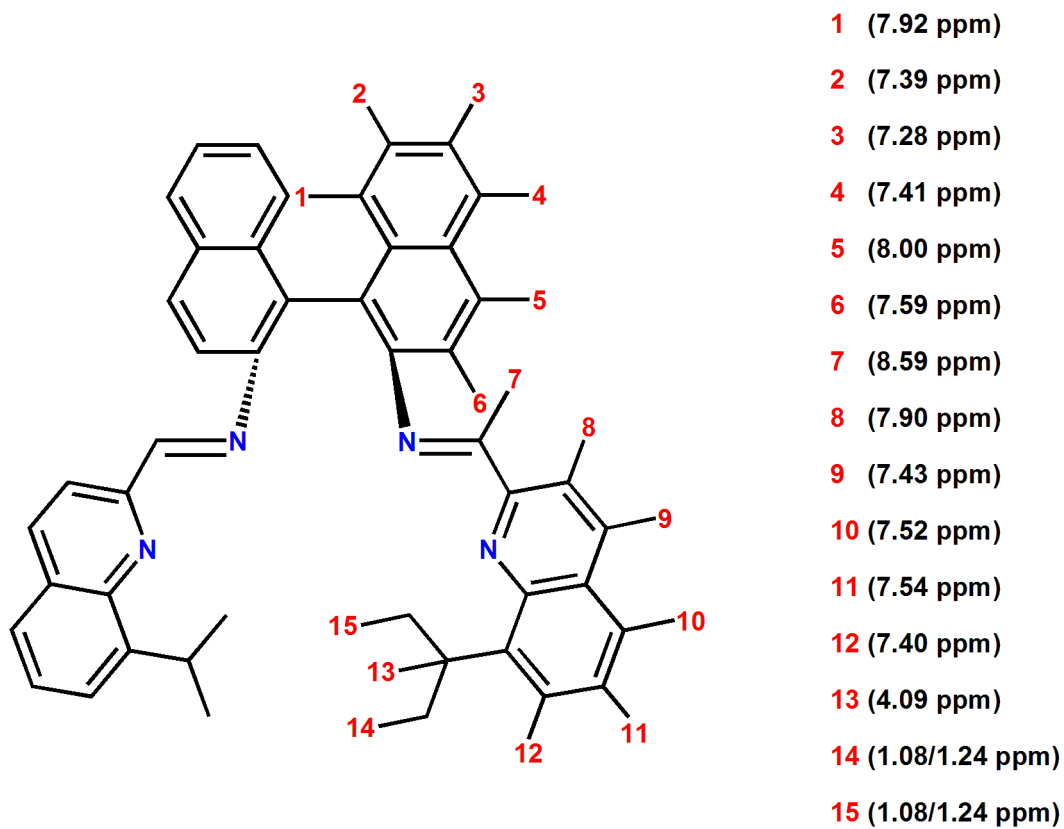
Figure 2.22: Complete 400 MHz ^{1}H Assignment of Ligand **4** (CDCl$_3$)

27

The last ligand (**5**) is structurally the biggest and most complex. The ^{1}H NMR spectrum obtained for ligand **5** is shown in Figure 2.23 and consists of fifteen aromatic protons that range from 7.26 ppm to 8.80 ppm. The polyaromatic resonance sets are made up of ten doublets, four doublet of doublets and the distinct imine singlet that appears at 8.65 ppm.
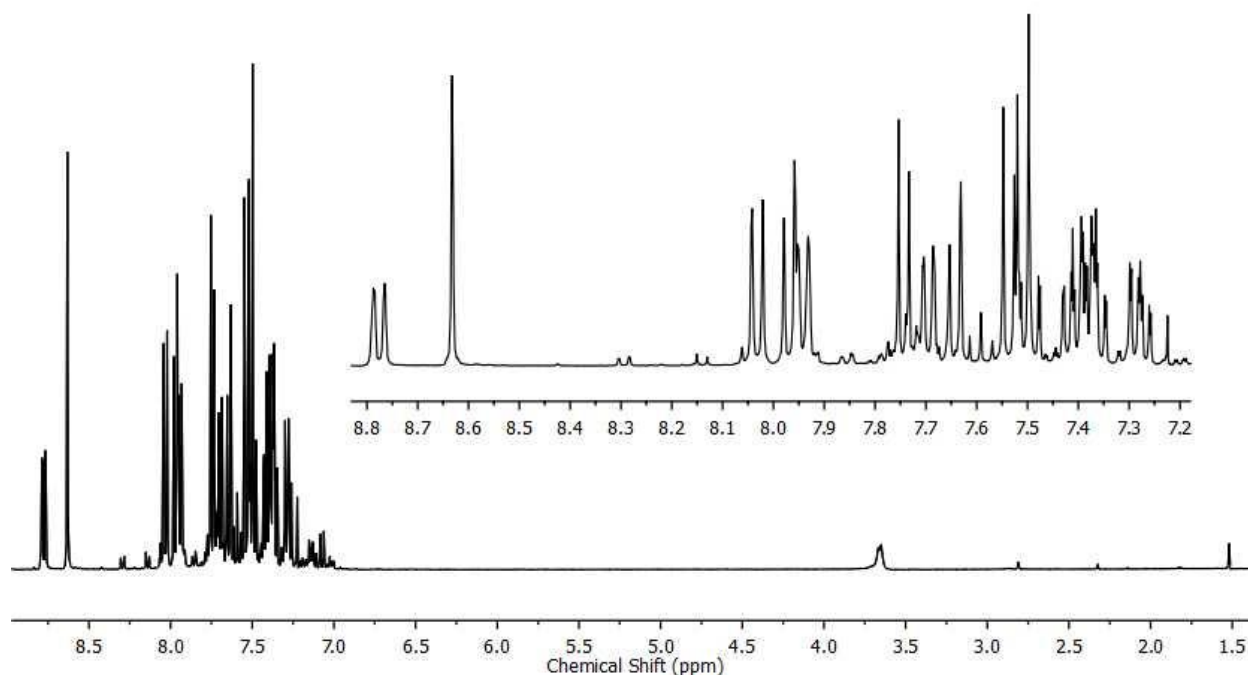
Figure 2.23: 400 MHz ^{1}H NMR Spectrum of Ligand **5** (CDCl$_3$)

The COSY experiment shown in Figure 2.24 demonstrates just how complex the coupling is between the protons in ligand **5**. Once again, we observe the expected ^{3}J coupling between protons (1→2, 2→3, 3→4, 5→6, 8→9, 10→11, 11→12, 12→13, and 13→14). We also observe the para, peri, epi, and through-spce long range couplings reflected in our previous systems (1→3 {meta}, 1→4{para}, 1→5{epi}, 6→7{through-space}, 7→8{through-space}, 11→12{peri}, 15→13{meta}, 15→12{para}, and 15→11{epi}). The unusual coupling of the imine proton (7) beyond the imine bond is observed in this ligand as well but this time, the imine proton (7) couples to protons both on the benzoquinoline side-arm (8) and the binaphthalene backbone (6). The coupling of proton (7) to proton (6) in the binaphthalene backbone may be

28

due to a common twist of the backbone bringing the two protons spatially close in proximity to experience coupling. We are also able to observe both strong and weak couplings in the COSY due to the unique conjugation characteristic of the ligand.
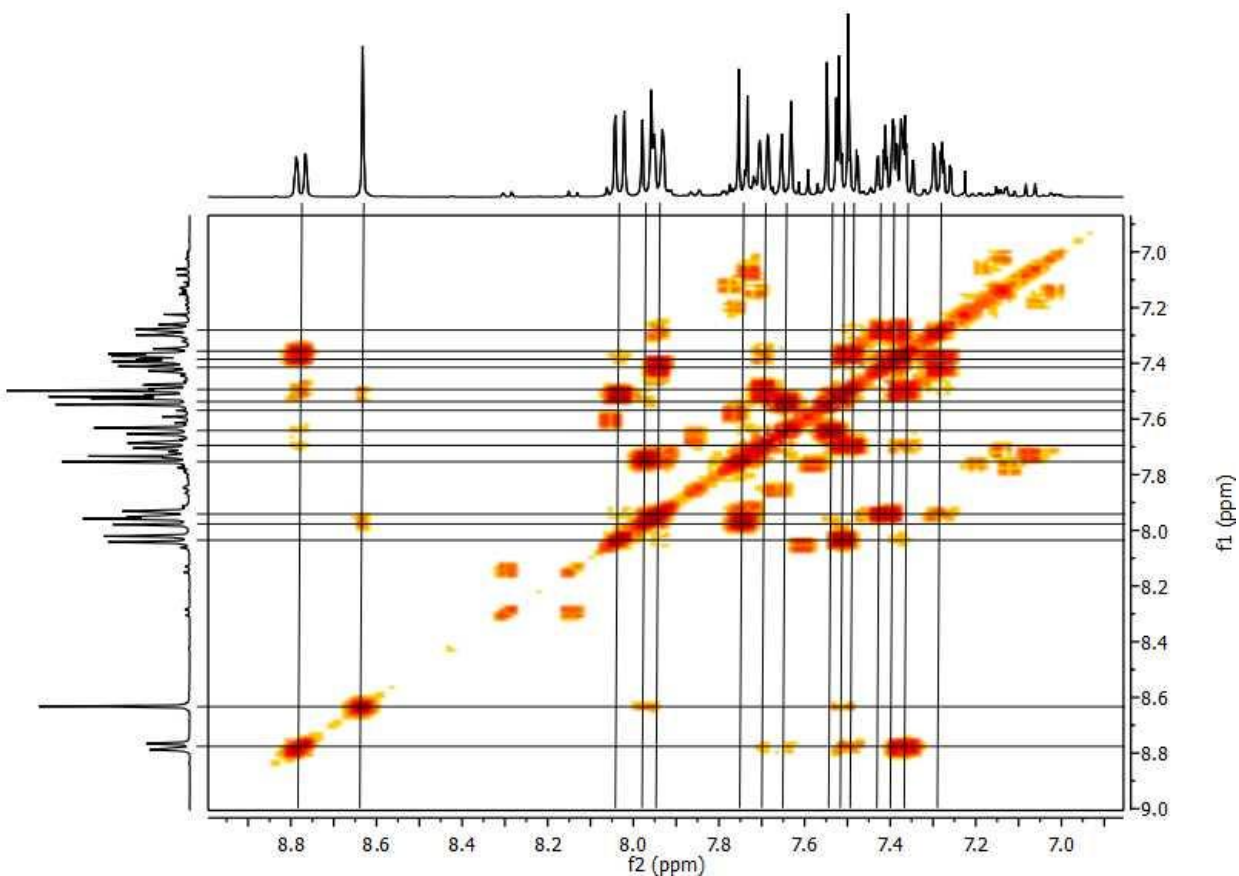
Figure 2.24: 400 MHz COSY Spectrum of Ligand **5** (CDCl$_3$)

To analyze the considerable resonance overlap at 7.40 ppm, a HSQC experiment was conducted (Figure 2.25). From the cross-peaks obtained in the HSQC, we clearly see that there are three separate proton peaks present in that region. The peak position of the imine carbon on the ^{13}C spectrum from the x-axis of the HSQC once again shows the effect the imine nitrogen atom has on the carbon atom, moving it significantly downfield compared to other tertiary carbons. The careful analysis of these 2D NMR experiments allowed us to solve the complete ^{1}H assignment for ligand **5** shown in Figure 2.26.
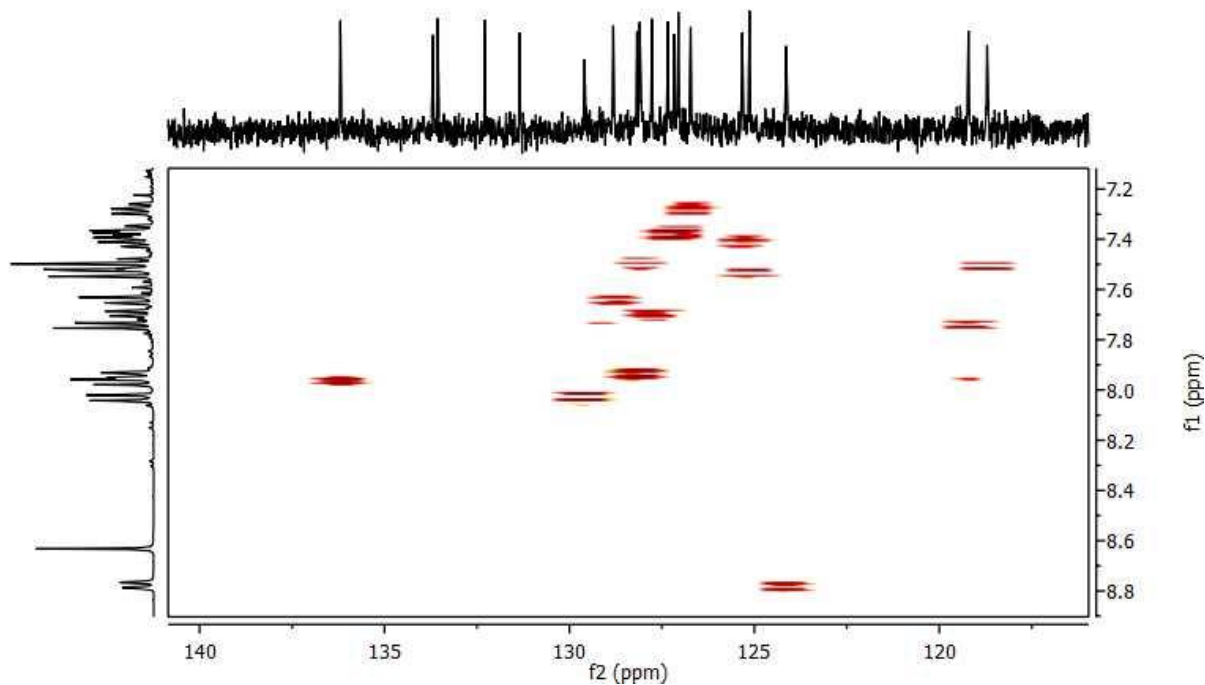
Figure 2.25: 400 MHz HSQC Spectrum of Ligand **5** (CDCl$_3$)

1 (7.40 ppm)
2 (7.29 ppm)
3 (7.43 ppm)
4 (7.96 ppm)
5 (8.05 ppm)
6 (7.52 ppm)
7 (8.65 ppm)
8 (7.98 ppm)
9 (7.76 ppm)
10 (7.55 ppm)
11 (7.66 ppm)
12 (7.71 ppm)
13 (7.51 ppm)
14 (7.38 ppm)
15 (8.79 ppm)
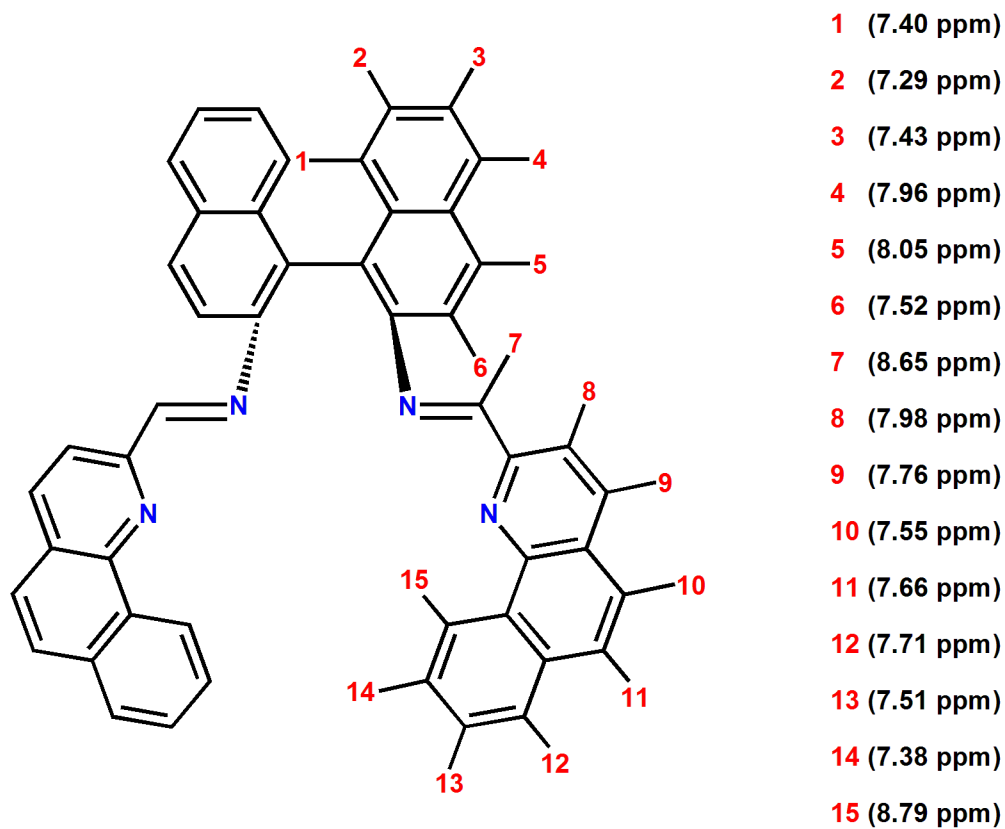
Figure 2.26: Complete 400 MHz ^{1}H Assignment of Ligand **5** (CDCl$_3$)

30

2.4 Reduction of Ligands

Many factors contribute to the efficiency of a catalyst during a reaction, for example; type of metal incorporated, presence or absence of electronic donating or withdrawing groups in the structure, number of chiral centers present, and the capability to regenerate itself at the end of the catalytic cycle. One universal factor that has to be addressed is how accessible the active metal center of the catalyst is to the substrates involved in the reaction. If the catalyst is designed with bulky groups present that lead to steric hindrance of the active site, the enantiomeric excess (ee) values and yields will be significantly reduced for that catalytic reaction. If the active center is not hindered, we now have to consider the size if the substrates involved and how that can affect their ability to access the metal center. Many studies have been done on the mechanism of catalytic reactions[55-57] leading to the general understanding that the substrate approaches the metal center through the least hindered quadrant. This is further demonstrated in the mechanistic study of homogeneous asymmetric hydrogenations of C=O bonds conducted by Dr. Sam French incorporating [(*S*)-XyIBINAP-RuH$_2$-(*S,S*)-DPEN] as the chiral catalyst (Figure 2.27).[58]
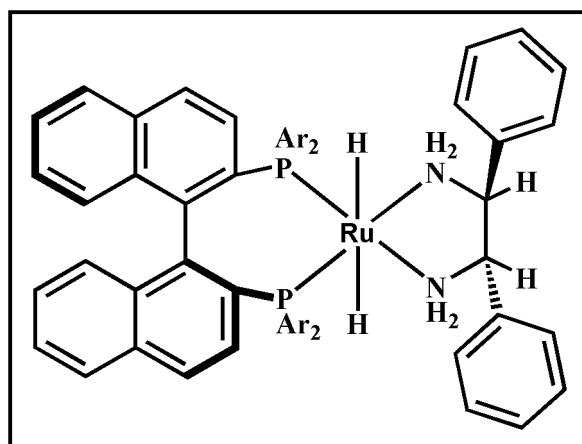
Figure 2.27: Structure of [(*S*)-XyIBINAP-RuH$_2$-(*S,S*)-DPEN] Catalyst

Using the four quadrant technique[59], the study examined the trajectory path of acetophenone as it approached the active site of the catalyst (Figure 2.28). They conclude that the substrate must first push into the pocket of the chiral catalyst before arriving at the desired

alignment with the C=O bond of the ketone and the Ru–N bond of the catalyst parallel to each other thereby maximizing orbital overlap for hydrogen transfer. The highest energy barrier to overcome as the substrate approaches the active site is when the phenyl ring of the ketone interacts with ligands of the catalyst, with this steric interaction increasing as the ketone is pulled down onto the active site. To accommodate this constraint, there is a conformational change in the substrate as the phenyl ring tilts so that so that all the carbons of the ring are now no longer in the plane of the other atomic centers of the ketone. The catalyst also experiences a slight structural change as the backbone stretches out to accommodate the approaching ketone.
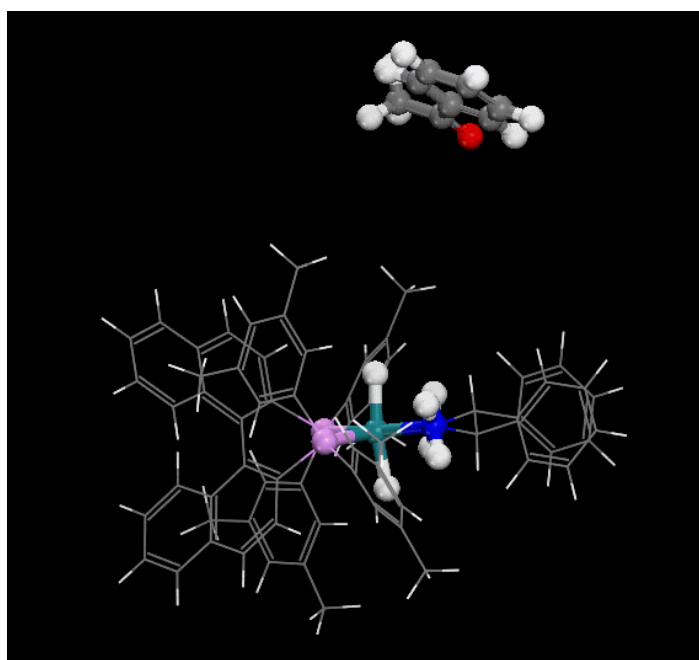
Figure 2.28: Molecular Model Showing Catalyst and Acetophenone Orientation

This hydrogenation reaction is successful because of the conformational changes made by the substrate and catalyst. The enantiomeric excess and yield of this reaction, and many similar to this, can be increased if the ligand structure of the catalyst is designed to be more flexible in the right area. This will significantly improve the interaction between substrate and catalyst active site and now make the catalyst more accommodating to bulkier substrates, further improving its efficiency. This idea of improved flexibility is already present is some of nature's

own catalysts, biological enzymes. Here the unique enzyme has a flexible active site unlike the typical 'lock and key' model many common enzymes have allowing it to shape its active site to accommodate bulkier substrates (Figure 2.29), improving its efficiency as an enzyme.
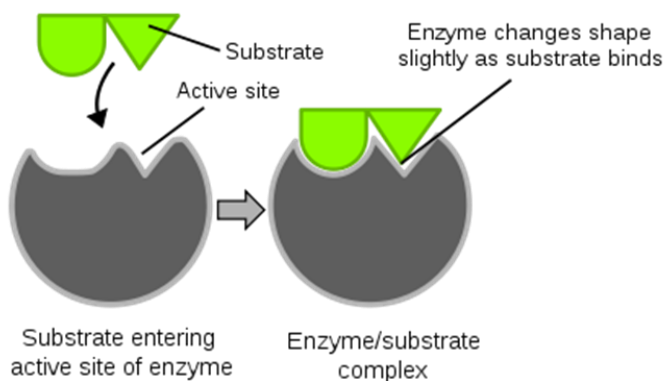
Figure 2.29: Flexibility of Enzyme at Active Site

To incorporate this flexibility in catalyst systems, care must be taken to increase the conformational mobility of the complex in the right location as substantial conformational mobility leads to poor efficiency of the catalyst as described in chapter one. In our ligand systems, the right area to improve flexibility is the imine bridge of the backbones. This ensures that the side-arms of the future complex will still remain in a locked confirmation, limiting mobility, while making the backbone flexible enough for the active center to accommodate bulkier substrates. We therefore set off to improve the flexibility in the imine bridge of our ligands by reducing the imine bond to give the corresponding amine. Eliminating the double bond in this area will remove the pi-bond formed by the carbon and nitrogen p_z orbitals and allows rotation around the central sp^2 sigma bond making it flexible.

To achieve the selective reduction of the imine bond, we decided to use sodium borohydride ($NaBH_4$) as our reducing reagent. We chose this reagent because it is inexpensive, nontoxic and is considered a soft reducing agent. This provides the control we require to reduce a select location of the ligand unlike the hard metal hydride compounds (LAH) that are not as selective. The delocalization of electrons in the imine bond with the lone pair on the nitrogen atom creates a partial positive charge on the carbon atom allowing for the nucleophilic attack of

the hydride from $NaBH_4$ on that electrophilic center. This creates a net negative charge on the nitrogen atom allowing the $NaBH_3^+$ to coordinate and upon hydrolysis; another hydrogen atom is attached to the nitrogen atom converting it from an imine to an amine. This is shown below in the reduction of ligand **1** to form ligand **11** (Figure 2.30). This reduction, leads to the creation of a second order AB spin system which can be observed in NMR experiments as the two protons
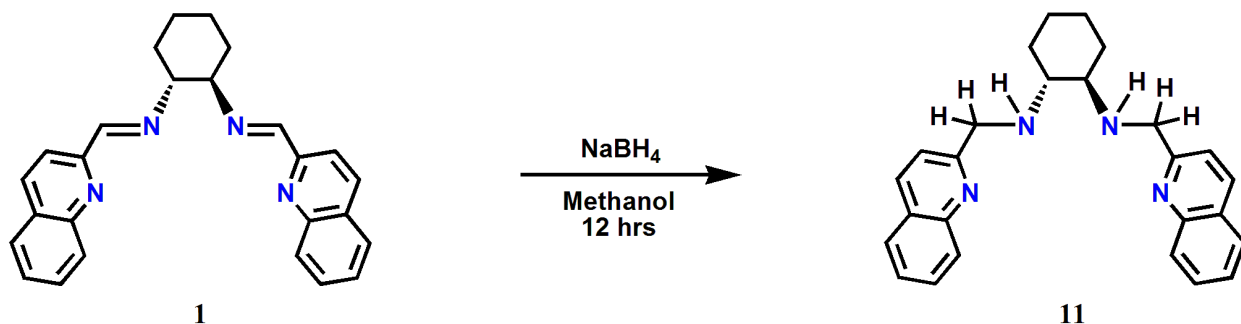
Figure 2.30: Reduction of Ligand **1** to Ligand **11**

on the amine carbon are in different environments making them non-equivalent. The predicted AB pattern in shown in Figure 2.31 and is characterized by a unique 'roofing effect' where the coupled signals lean towards each other creating the impression of a roof. We monitored the appearance of this pattern and the disappearance of the distinct imine singlet to confirm the
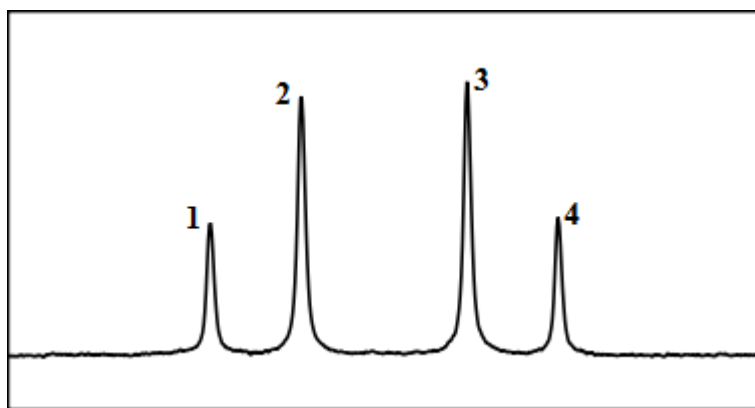
Figure 2.31: Predicted Signals of Second Order Spin System (AB)

34

successful reduction of our ligands and noticed that the reaction time played an important role in the reaction. The reduction of ligand 1 took 12 hours to reach completion with the AB pattern observed at 4.05 ppm (Figure 2.32). If the reaction is stopped before 12 hours, we observe an
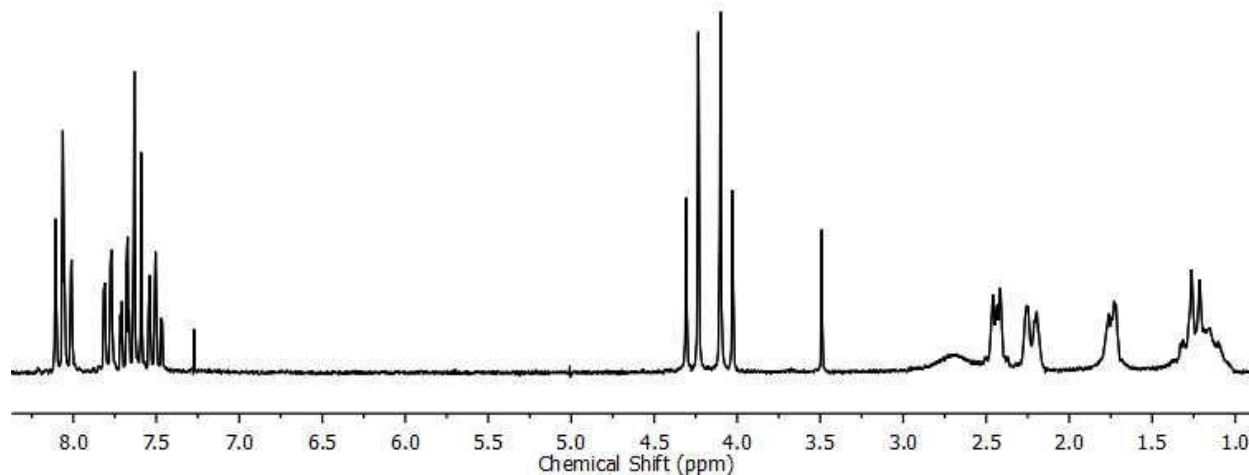
Figure 2.32: 400 MHz ^{1}H NMR Spectrum for Complete Reduction of Ligand **1** (CDCl$_3$)

incomplete reduction of the imine bond to give the NMR pattern shown in Figure 2.33. This is indicative of the presence of pure ligand, partially reduced ligands and completely reduced ligands in the NMR sample. If the reaction is allowed to proceed beyond 12 hours, we observe
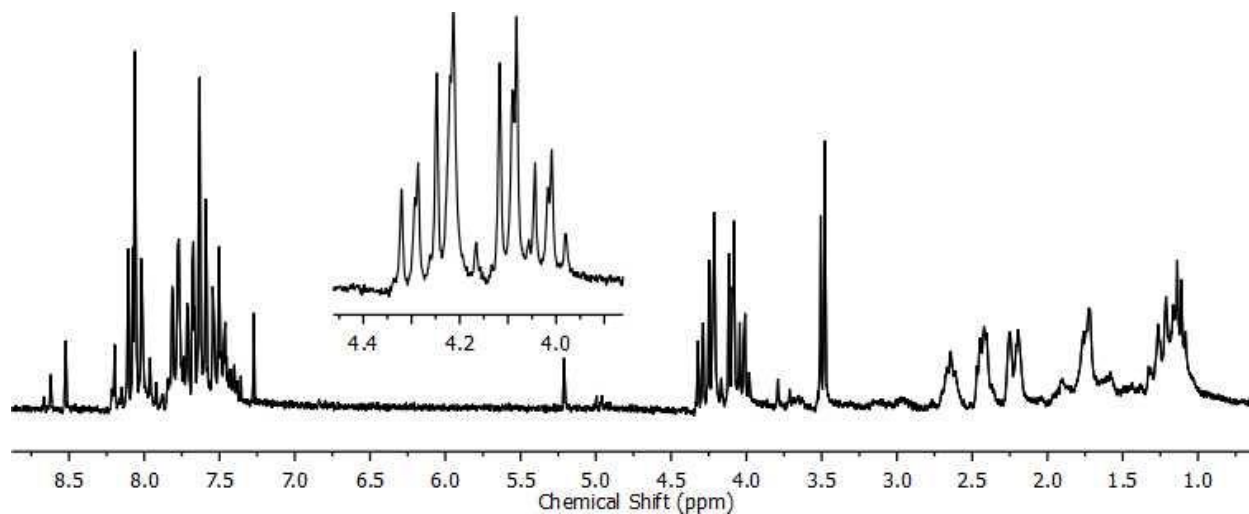
Figure 2.33: 400 MHz ^{1}H NMR Spectrum for Partial Reduction of Ligand **1** (CDCl$_3$)

the complete reduction of the imine proton but start to see changes in the aromatic protons as the sodium borohydride now reacts with the next available double bond in the ligand. The reduction of ligand **2** was carried out under similar reaction conditions but only took 6 hours to reach
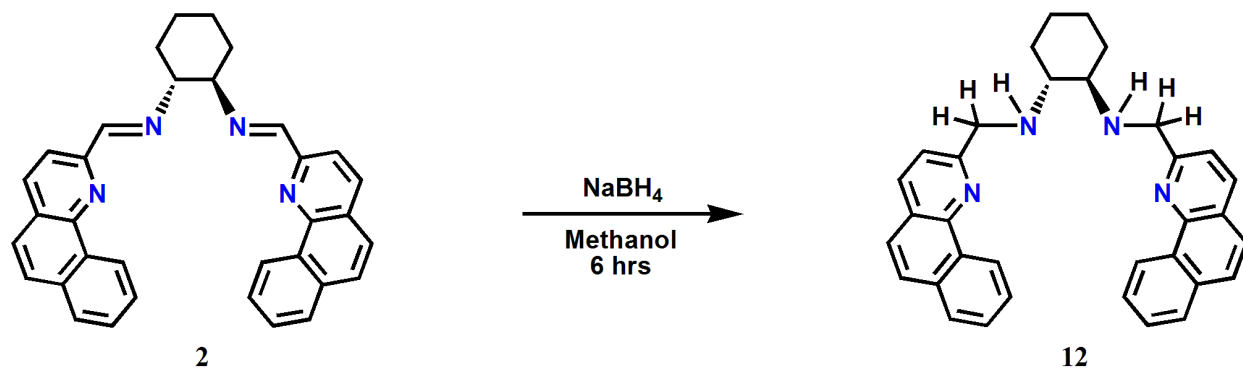
Figure 2.34: Reduction of Ligand **2** to Ligand **12**

completion (Figure 2.34). We observe the disappearance of the distinct imine singlet and the appearance of the distinct AB pattern at 4.25 ppm in the ^{1}H NMR spectrum for ligand **12** (Figure 2.35). We propose that the reaction for ligand **2** does not take as long to reach completion, compared to ligand **1**, because it incorporates two more phenyl rings in its structure introducing
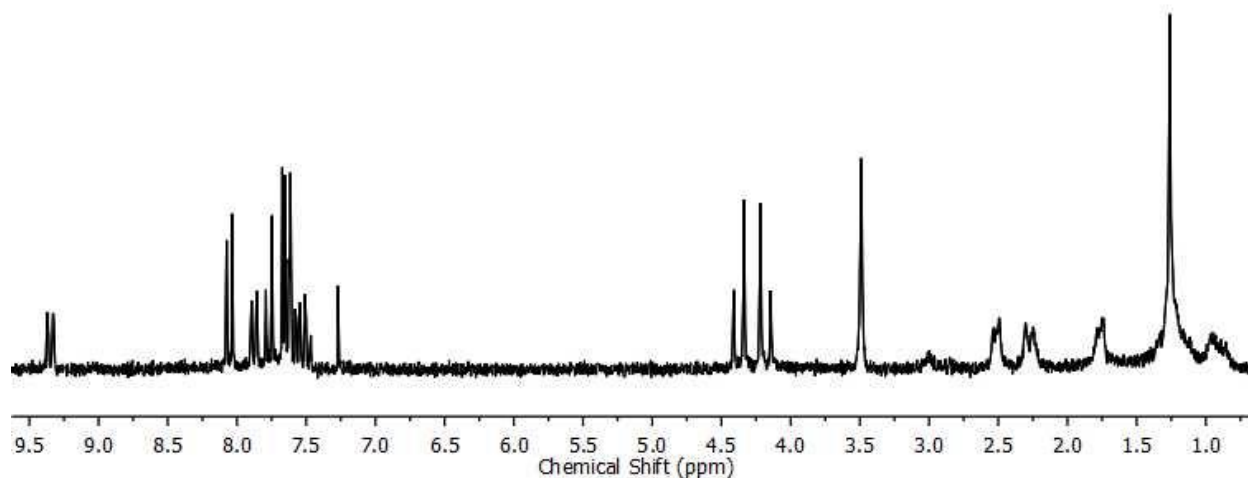
Figure 2.35: 400 MHz ^{1}H NMR Spectrum for Complete Reduction of Ligand **2** (CDCl$_3$)

more susceptible double bonds into the system therefore making the ligand more sensitive to the reaction with $NaBH_4$. As observed with ligand **1**, if the reaction is terminated before 6 hours, we observe the presence of a pattern indicative of a mixture of pure ligand, partially reduced ligands and completely reduced ligands (Figure 2.36). Reaction longer than 6 hours led to the reducing agent attacking the phenyl rings and breaking up the ligand structure.
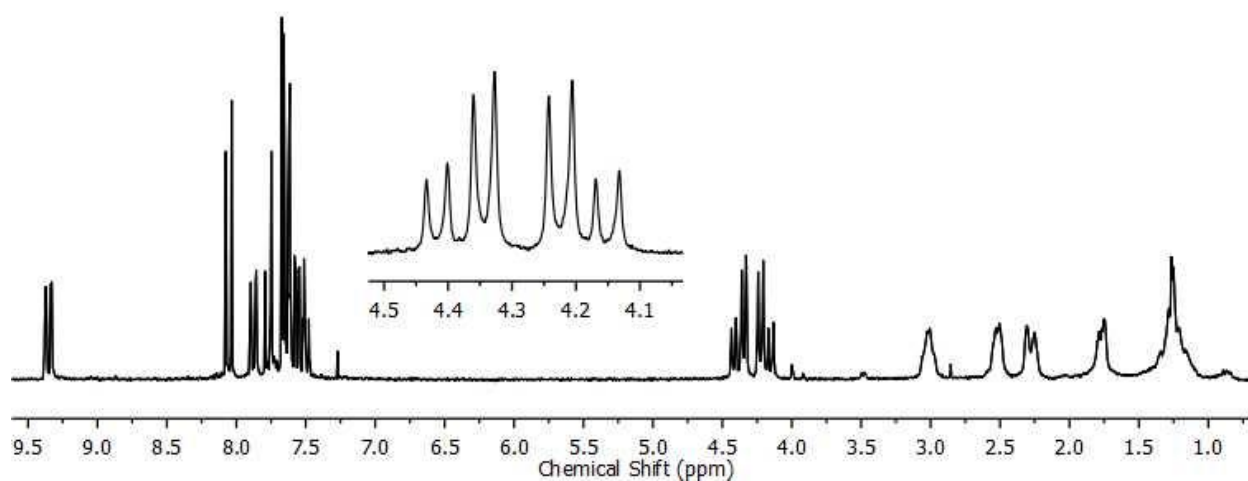
Figure 2.36: 400 MHz ^{1}H NMR Spectrum for Partial Reduction of Ligand **2** ($CDCl_3$)

Multiple attempts were made to reduce the ligands incorporating binaphthalene as their backbone (**3** − **5**) mimicking the successful reduction conditions of ligands **1** and **2** to no avail. The following changes were then made to the reaction conditions to find a suitable combination for the successful reduction of ligands **3**, **4**, and **5**.

(i)   Reaction time with $NaBH_4$ was increased from 6 hours to 24, 36, 48, and 72 hours.

(ii) Mole ratio of $NaBH_4$ added was increased from 1:1 to 1:1.5, 1:2 and finally to 1:4.

(iii) Solvent was changed from methanol to ethanol, dichloromethane, and tetrahydrofuran.

(iv) Heat was introduced as the reaction mixture was refluxed for varying time frames.

(v) $NaBH_4$ was pumped down on using a vacuum line to remove any traces of water present.

(vi) Finally, a more powerful reducing agent, lithium aluminum hydride (LAH) was used to react with the ligands with reaction conditions varying as described above in (i) to (iv).

The changes made did not lead to the synthesis of the desired products but a series of unreacted ligands and in most cases, products whose conjugated ring system had been disrupted due to attack from the reducing agent. Figure 2.37 shows the ^{1}H NMR spectrum of the product from the attempted reduction of ligand **5** using sodium borohydride and methanol for 24 hours.
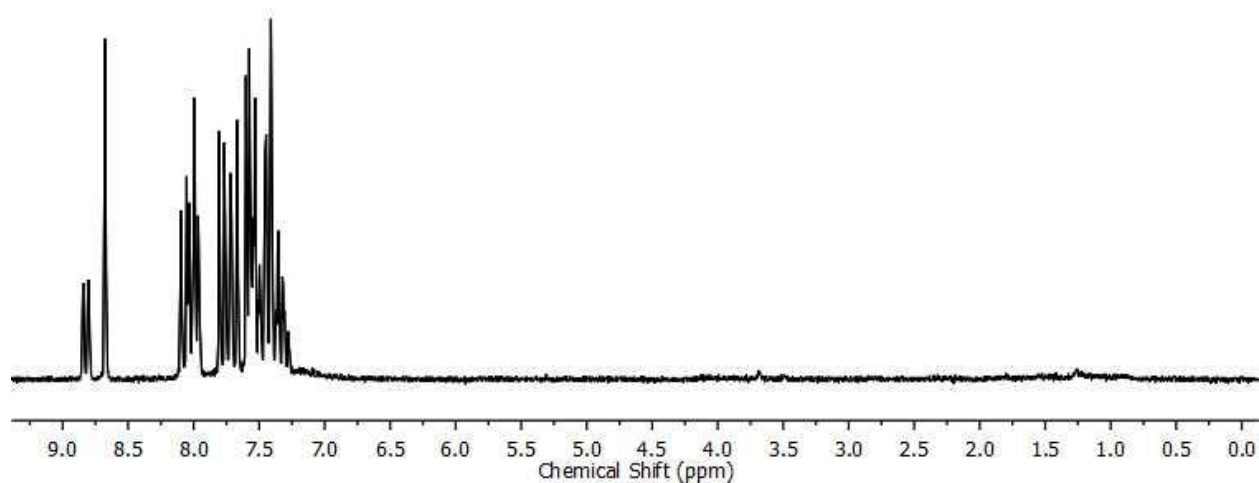
Figure 2.37: Attempted Reduction of Ligand **5** Using NaBH$_4$

Both ligand and NaBH$_4$ completely dissolved in the solvent but no reaction occurred after the given time frame. When the more powerful reducing agent (lithium aluminum hydride) was reacted with the same ligand (**5**), the ^{1}H NMR of the product obtained is shown in Figure 2.38.
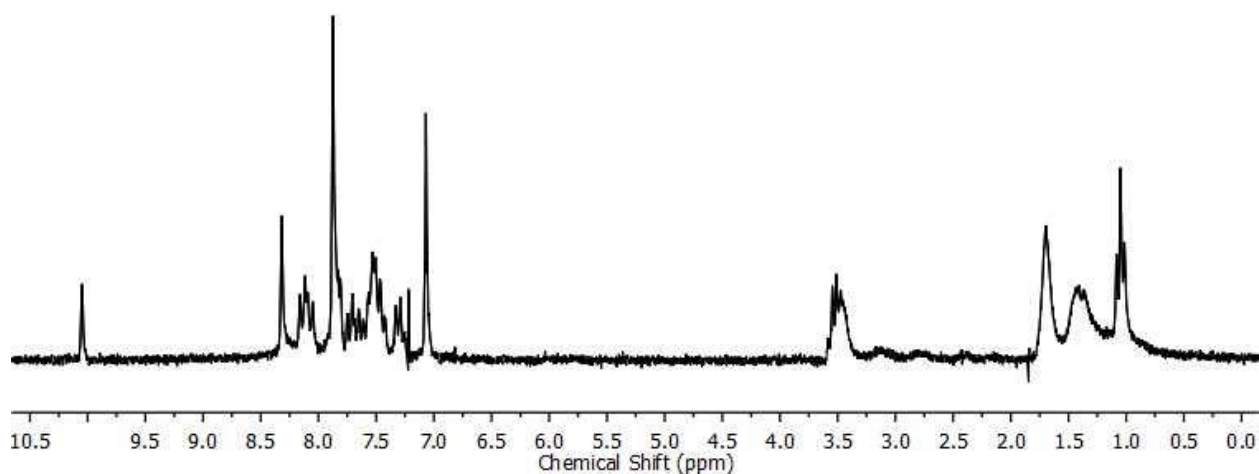
Figure 2.38: Attempted Reduction of Ligand **5** Using LAH

38

The reaction was carried out without any heat for 6 hours using methanol as the solvent. It is clear from the ^{1}H NMR that the ligand had degraded from the attack of LAH on the conjugated ring systems present in the compound. Subsequently, all straight forward reduction reactions on ligands **3**, **4**, and **5** were stopped. Since these ligands are going to be reacted with metal salts in the future to make new complexes, we decided to attempt a one-pot reduction reaction with the ligand, a metal salt, and a reducing agent all present at the same time.

The one-pot reaction of ligand **5** with slight excess of $NaBH_4$ (1:1.5) and $ZnCl_2$ refluxed in toluene for 12 hours gave an orange product whose ^{1}H NMR could not be interpreted and was considered unsuccessful. The counter-ion of the salt and the solvent used were later changed to the triflate ion and a combination of ethanol and tetrahydrofuran to observe the effect this may have on the success of the reaction. The new one-pot reaction was refluxed for 15 hours at 80 ^{o}C to afford a bright orange colored solution which was filtered and vacuum dried. The predicted reaction scheme is shown below in Figure 2.39 but the ^{1}H NMR obtained for the product did not reflect the desired product (Figure 2.40). First impression of the spectrum is that of an impure product but upon closer examination of the proton peaks, we observe a pattern that is characteristic of a pure complex with broken symmetry. The distinctive AB pattern typical of reduced imine bonds, which we observed in ligands **11** and **12**, is present at 4.55 ppm leading us to believe that only one arm of the ligand got reduced breaking the C_2 symmetry of the complex. The broken symmetry results in the appearance of 32 proton peaks in the ^{1}H NMR spectrum
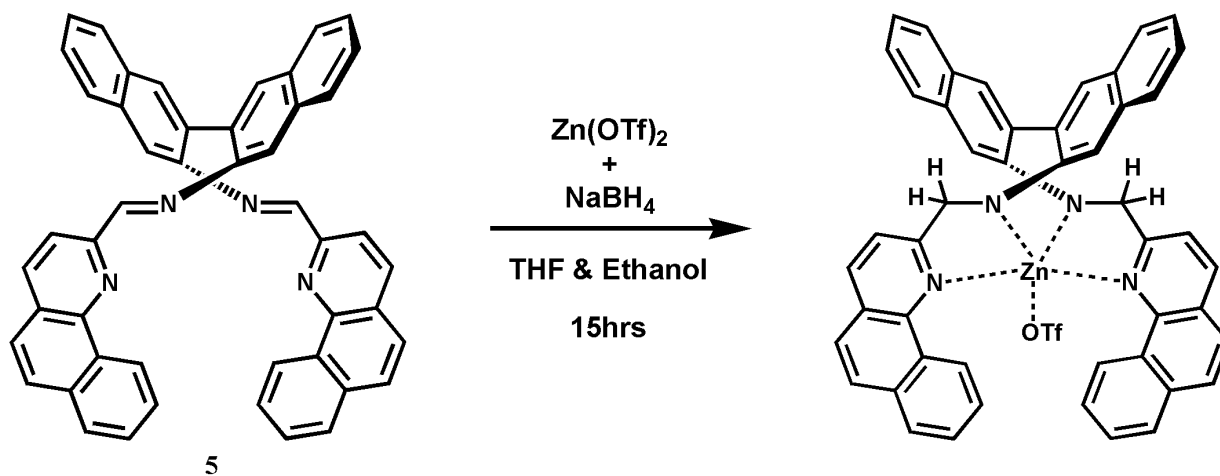
Figure 2.39: Proposed One-Pot Reduction and Complexation Scheme for Ligand **5**

(1 singlet, 23 doublets, and 8 doublet of doublets), the singlet located at 9.81 ppm is most likely due to the imine proton on the side-arm that did not get reduced. This peak is highly shifted
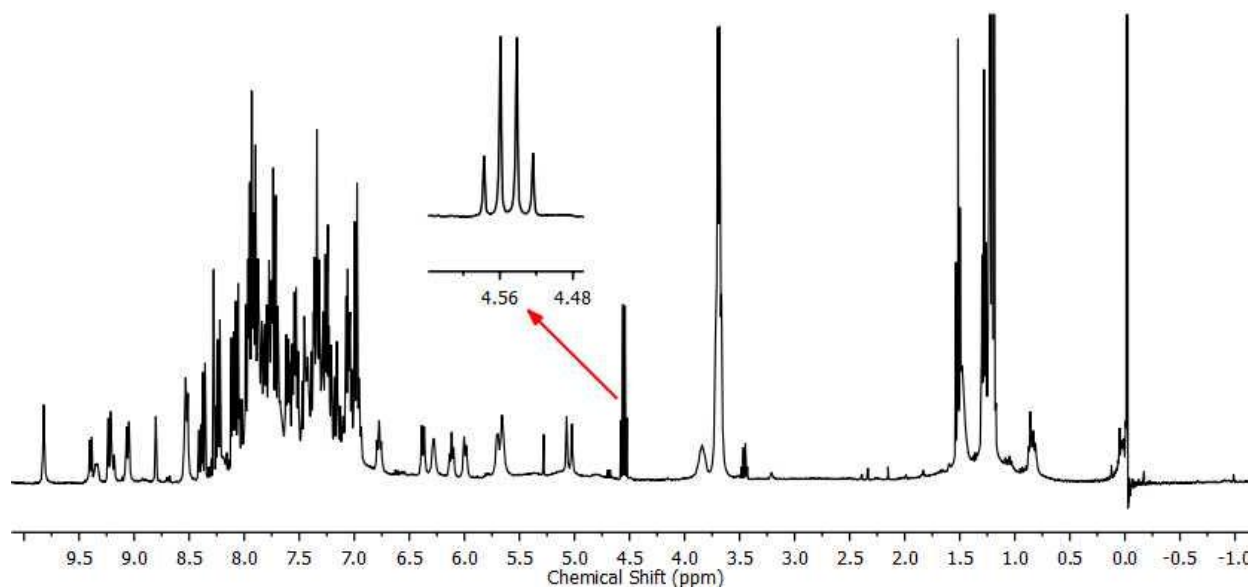
Figure 2.40: 400 MHz ^{1}H NMR Spectrum of Complex **13** (CDCl$_3$)

because of its proximity to the metal center and the conjugation present in the molecule. The information obtained from the ^{1}H NMR spectrum provided us with enough evidence to change our initial reaction scheme to what is now displayed in Figure 2.41. The large number of proton
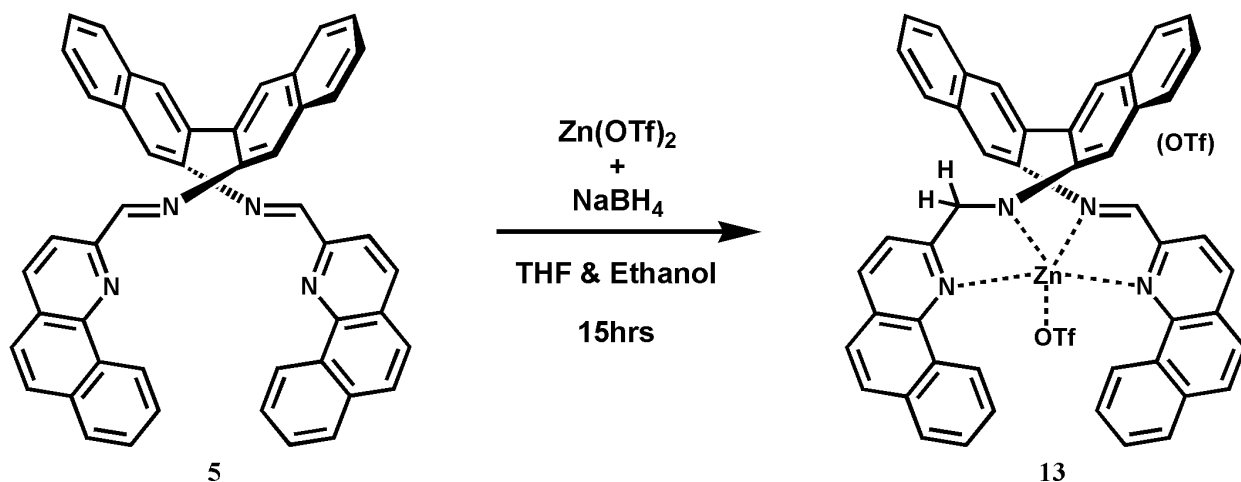
Figure 2.41: Observed Reduction and Complexation Scheme for Ligand **5**

40

resonances leads to very complex coupling which is observed in the COSY spectrum obtained for complex **13** (Figure 2.42). The resonance overlap is too severe preventing us from solving the complete ^{1}H assignment of complex **13**. Nevertheless, we were successful in the partial reduction of the compound using a 'one-pot' reaction approach achieving our goal of increased flexibility.
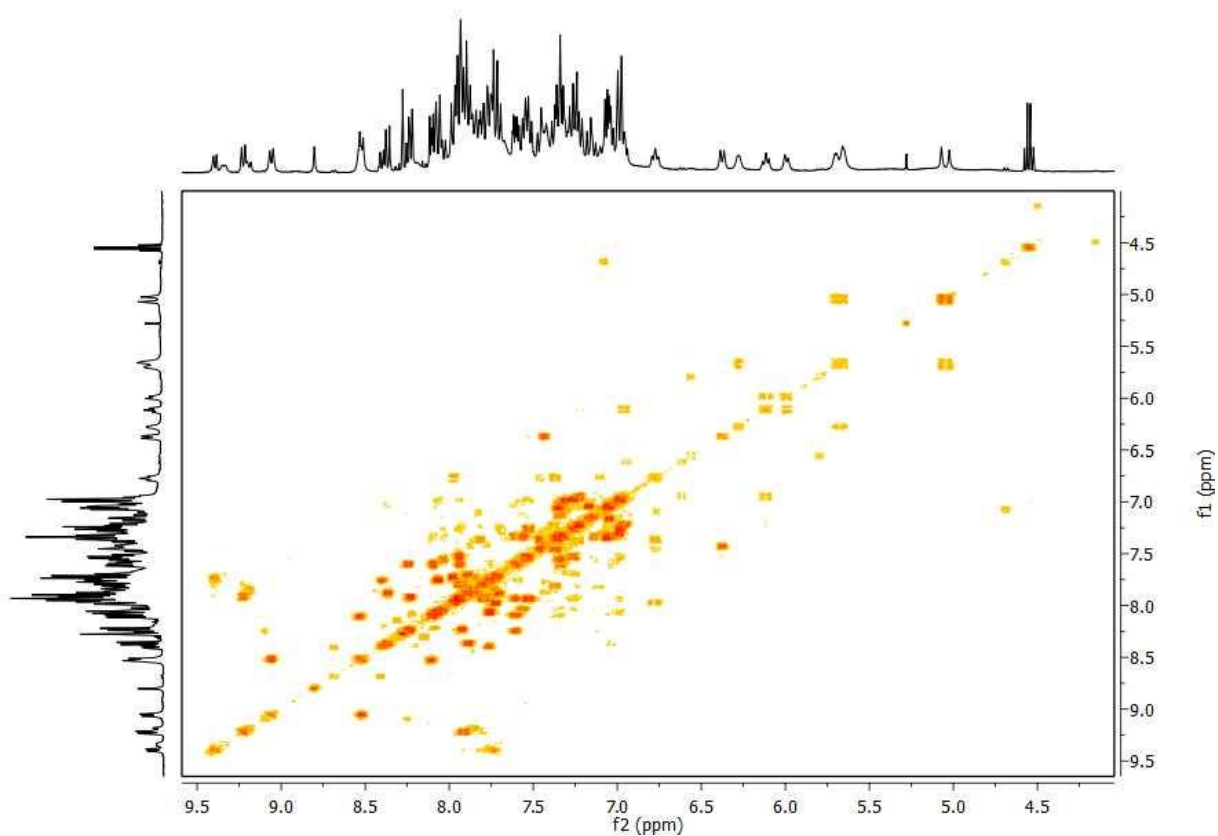
Figure 2.42: 400 MHz COSY Spectrum for Complex **13** (CDCl$_3$)

To support the results obtained from the 1D and 2D NMR experiments, single crystals of complex **13** that were suitable for X-ray analysis were grown. We utilized the solvent diffusion method using tetrahydrofuran as our base solvent with hexane layered on top. X-ray analysis revealed a desired monohelical structure with π-π and/or σ-π interactions between the locked side-arms of the complex. This may be due to the triflate counter-ion of the metal salt as they are known, in most cases, to minimize anion coordination and allow exclusive coordination of the ligand to the metal center. Looking at the space filling model for complex **13** (Figure 2.44), we

observe that one triflate anion remains coordinated to the zinc metal center while the other is present in the outer coordination sphere. The Zn^{II} cation appears to be coordinated to the four nitrogen donor atoms and the triflate anion in a distorted square pyramidal fashion. This type of coordination could be a result of the corporative effect of the increased flexibility in complex **13**, due to the reduced imine bond, and the metal cation preferring coordination numbers ranging from four to six.[60] We also observe that the complex arranges itself in the *P*-helimer form alone, this is unusual because salen complexes synthesized with the (*R*)-binapthyl backbone produce exclusively *M* helices.[61] The ball and stick model for complex **13** (Figure 2.43) shows the reduction of one imine double bond as the C–N bond length of the unreduced imine is 1.296 Å and the C–N bond length of the reduced imine is 1.471 Å. We also observed the effect of the reduction in the torsion angle as the amine side (C54-C53-N53-C25) is -161.3^o while the torsion angle for the imine side (C64-C63-N63-C32) is -81.8^o. The reduction of the imine bond also affects the bond distance of the zinc metal center with the nitrogen donor atoms on the imine bond. Due to the flexibility of the amine side, we observe a longer bond length for the Zn–N bond (2.222 Å) compared to a shorter Zn–N bond length with the more rigid imine nitrogen atom (2.044 Å). The space filling model indicates that the aromatic rings of the side-arms are slightly offset and do not lie directly on top of each other. Typical distances for aromatic ring π–π interactions are approximately 3.5 Å. In comparison, the distances between the two benzoquinoline side-arms in complex **13**, calculated by measuring the centroid of an aromatic ring in one side-arm to the closest carbon in the opposite side-arm, ranges from 3.278 Å to 3.533Å. Due to complexation, the binaphthalene backbone now experiences a twist to a degree of 76.54^o. Select bond distances, bond angles, and torsion angles are for complex **13** are displayed in Table 2.1, with complete crystal and refinement data for complex **13** available in Appendix II. It should be noted that complex **13** had be previously synthesized in the Levy group by refluxing a mixture of Ligand **5** and zinc(II) triflate in ethanol. Toluene was subsequently added to the mixture and the solution then heated for 48 hours.[61] Complex **13** was obtained with those reaction conditions and without the presence of a reducing agent, it was suggested that the reduction of one imine double bond was due to hydrogen transfer from the ethanol solvent used in the first step. Further efforts to synthesize complex **13** based on those reaction conditions proved futile and attention was shifted to the use of reducing agents as described in this chapter.
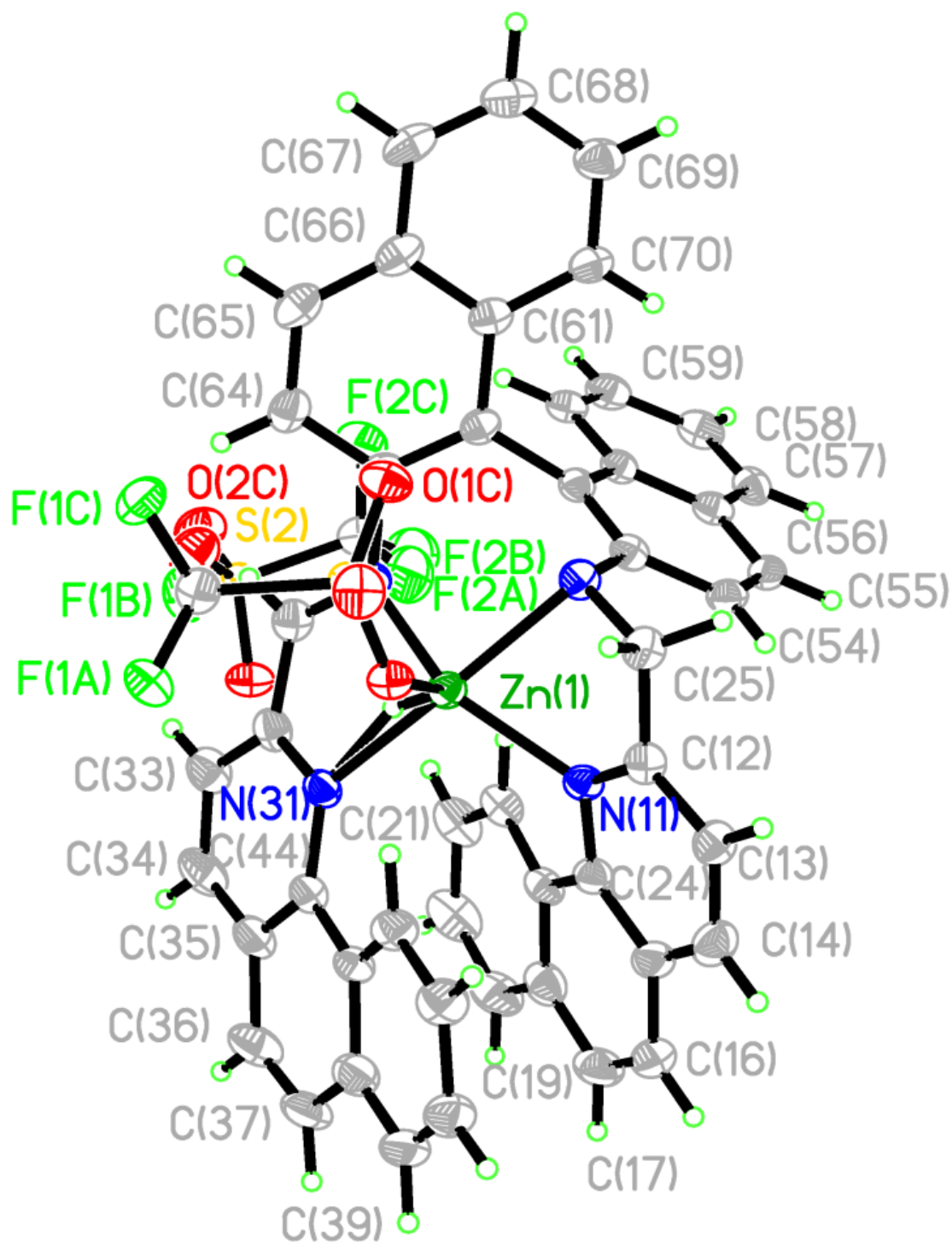
Figure 2.43: Thermal Ellipsoid Crystal Model for Complex **13**
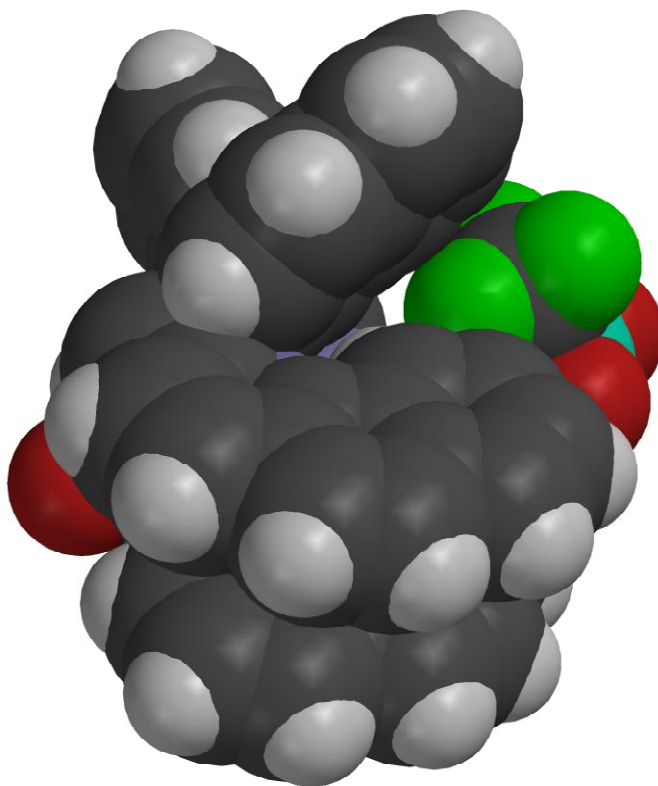
Figure 2.44: Space Filling Crystal Model for Complex **13**

Bond Length	Zn_1-N_{63}	2.044(3)	Zn_1-O_1	1.961(2)
	Zn_1-N_{11}	2.067(2)	C_{25}-N_{53}	1.471(4)
	Zn_1-N_{31}	2.167(2)	C_{65}-N_{31}	1.291(7)
	Zn_1-N_{53}	2.222(3)	C_{45}-N_{63}	1.296(4)
Bond Angles	N_{63}-Zn_1-N_{11}	139.48(9)	N_{63}-Zn_1-N_{53}	93.86(10)
	N_{63}-Zn_1-N_{31}	82.09(10)	O_1-Zn_1-N_{11}	109.29(12)
	N_{11}-Zn_1-N_{31}	104.25(10)	O_1-Zn_1-N_{31}	90.3(7)
Torsion Angles	C_{64}-C_{63}-N_{63}-C_{32}	-81.6(6)	C_{54}-C_{53}-N_{53}-C_{25}	-161.3(5)

Table 2.1 Selected Bond Lengths (Å), Bond Angles, and Torsion Angles for Complex **13**

CHAPTER 3

Metallation of Ligands

One of the most important goals in asymmetric catalysis is the rational design of new catalysts. It is now clear that the choice of ligand used, degree of flexibility in the ligand, and type of metal-salt incorporated, all play a major role in the design and function of a catalyst.[62] Therefore, this chapter examines the synthesis of novel catalysts using an assortment of our ligands with varying flexibilities (**2**, **5**, and **11**) chelated with different metal salts. Given the tetradentate nature of the ligands involved, we expect an increased probability for the formation of single-stranded monohelical motifs in complexes to be synthesized. This is due to the four nitrogen donor atoms present in the ligands that increase the likelihood of the ligand binding to the central metal ion with the coordination strength increasing with every bound nitrogen atom. The successful binding of all four nitrogen donor atoms should lead to formation of desired single-stranded monohelices. These are uncommon and highly attractive in asymmetric catalysis due to their well defined reaction centers and highly twisted conformations. Configurations of helical chiral compounds are assigned using the (*P*)- and (*M*)- descriptors which denote plus (+) and minus (-) respectively. If the helical turn is clockwise, the (*P*) configuration is assigned and if the turn is counterclockwise, the configuration (*M*) is assigned (Figure 3.1).

M (minus)   *P* (plus)
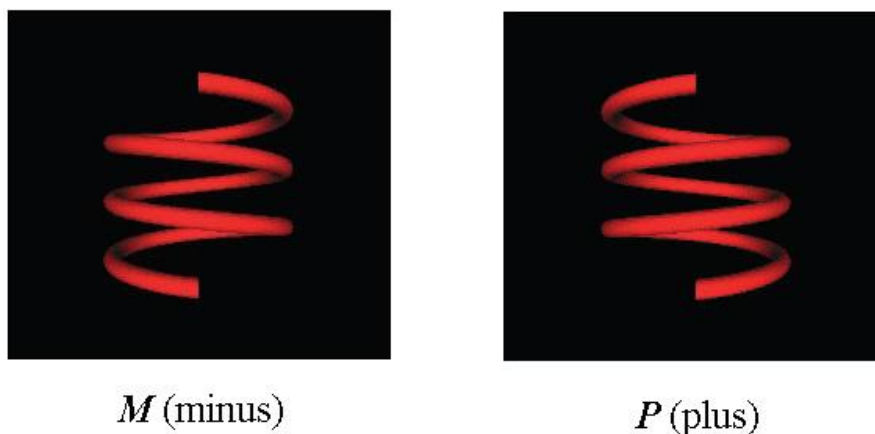
Figure 3.1: Helical Configurations *M* (Counterclockwise) and *P* (Clockwise)

The most common forms of helical transition metal complexes are the double and triple stranded dihelicates which are produced when ligands with two chelating sections coordinate to two metal centers (Figure 3.2).[63-64] These di-helicates form because of the stabilization that occurs in the multiple interactions and/or bonds that are present in the structure (Figure 3.3).

Double stranded   Triple stranded
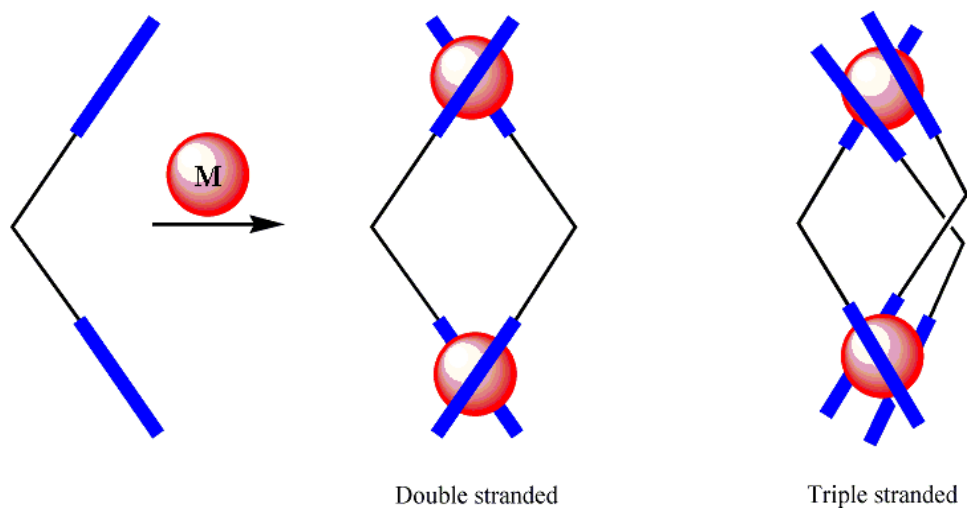
Figure 3.2: Structural Examples of Double and Triple Stranded Helicates
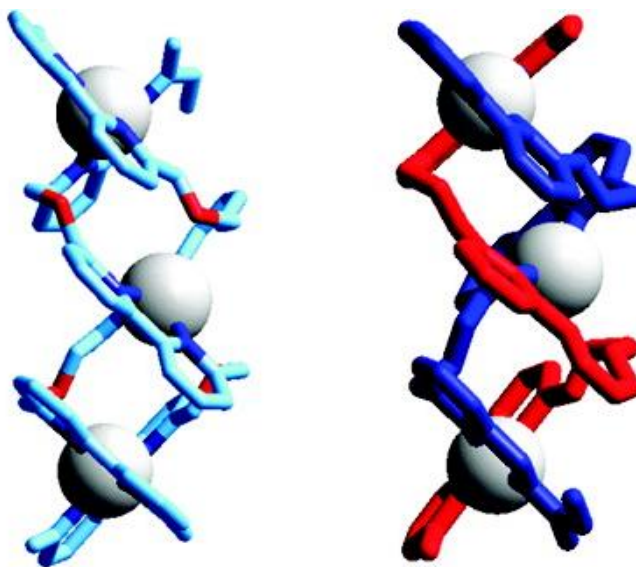
Figure 3.3: Stabilization in Double and Triple Stranded Di-helicates

The tendency to form di-helicates in the presence of two metal centers was demonstrated by Luigi Fabbrizzi and Lorenzo Mosca as they examined the helicate formation of octahedral copper(II) and tetrahedral copper(I) salts.[65] They observed that their ligand of choice, (1*R*,2*R*)-*N*,*N'*-bis-[1-(8-benzyloxyquinolin-2-yl)methylidene]cycloexane-1,2-diamine behaves as a bis-bidentate ligand when it with copper(I), which adopts a distorted tetrahedral geometry through the coordination by four *sp*2 hybridized nitrogen atoms. The same ligand behaves as a bis-terdentate ligand when it reacts with copper(II) salts to reveal a distorted octahedral coordination to the metal center. They obtain double stranded helicate complexes with copper(II) cations containing two Cu^{II} octahedral centers (Figure 3.4) as the complex is stabilized in the solid state by an intricate system of π–π interactions between aromatic subunits, just as we observed in the crystal structure of complex **13**.
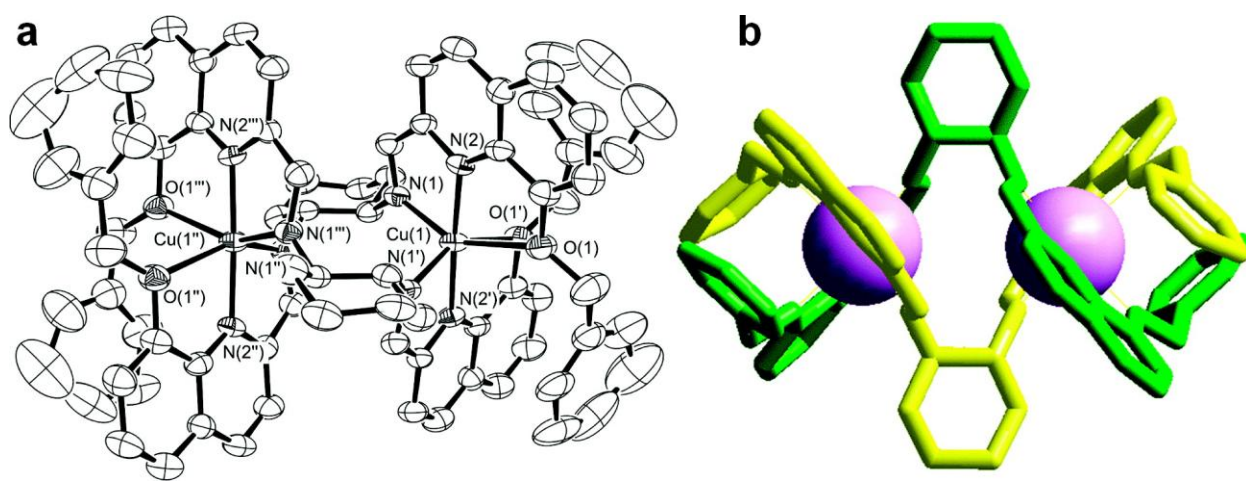
Figure 3.4: (a) ORTEP Diagram for *P*,*P*-[Cu$_2$^{II}(^{RR}**5**)$_2$]$^{4+}$ and (b) Tube Representation

A similar double helicate structure was obtained by Hannon et al. as they studied the reaction of silver(I) acetate with (*S*),(–)-1,1'-binaphthalene-2,2'-diamine (**L^S**) and (*R*),(+)-1,1'-binapththalene-2,2'-diamine (**L^R**).[66] X-ray results revealed the coordination of two **L^R** ligands around two silver(I) tetradentate ions forming a *P*-double helix and the formation a *M*-double helix with coordination to two **L^S** ligands (Figure 3.5). The two silver(I) centers within the helical structures are separated by 3.61Å – 3.78 Å.
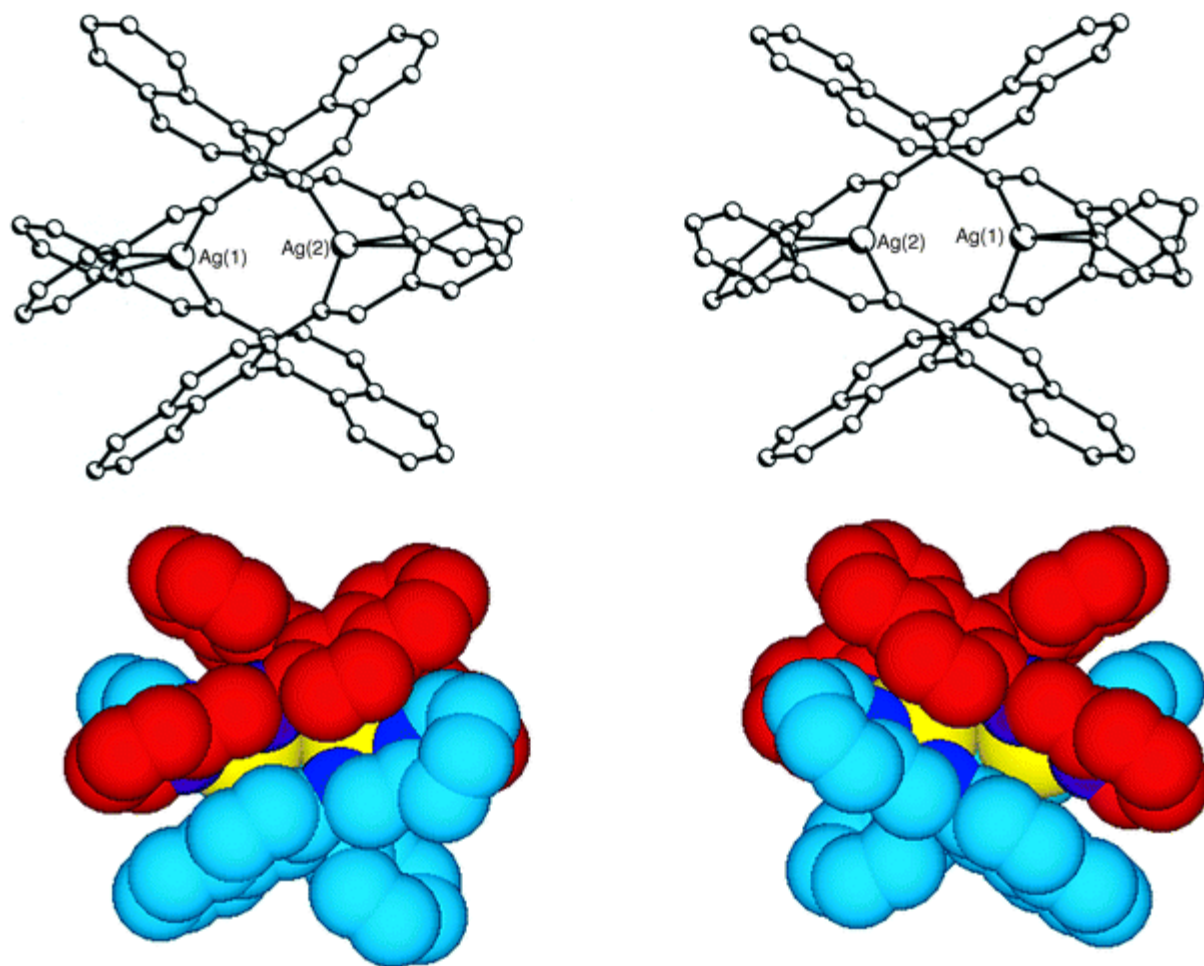
Figure 3.5: Crystal Structures Confirming the Formation of Dihelicate Ag(I) Complexes

However, in order to serve as a well defined and effective catalyst, any complex formed in or complexation reactions should exist as a single helical type (*M* or *P*). This is because single stranded monohelices usually have well defined reaction centers and highly twisted conformations that typically result in higher enantiomeric excess (ee) obtained during a catalytic asymmetric reaction. In order to achieve a mono helical structure, the ligand incorporated must have some degree of flexibility or have its chelating groups carefully placed to fit the geometry of the metal ion integrated.[67] The ligands used for complexation in this report have backbones that direct the side-arms to be close to one another increasing the probability of binding to only one metal center, this in turn increases the possibility of forming single stranded mono-helicates.

The complexes made in this chapter exhibit helical chirality around their metal center due to the chiral nature of their ligand backbones. The axial chirality of the backbone controls the position and orientation of the phenyl substituents forming helical structures. This feature in the design of our catalysts results in the complexes having a C_2 symmetry axis which plays a vital role in the way they transmit asymmetry in enantioselective reactions. Studies show that in many cases, asymmetric catalysts often transmit asymmetry by binding and reacting preferentially with one of the prochiral faces of the substrate while others bind the substrate and shield one of the prochiral faces, thus impeding reaction at that face.[68] Research done on the transmission of asymmetry during reactions with C_2 symmetric catalysts showed that they were more enantioselective because of the presence of a C_2 axis compared to those made from non C_2 symmetric ligands.[69-70] This selectivity is proposed to result from the smaller number of metal-substrate adducts and transition sites available to the C_2 symmetric catalysts during the chemical reaction as opposed to their non C_2 symmetric counterparts.

This principle is illustrated in the asymmetric palladium catalyzed allylation reaction of olefins using a C_2 symmetric P–P ligand and a non-C_2-symmetric P–N ligand to make the catalyst (Figure 3.6). The most common mode of nucleophilic attack on the η^3-allyl is on the face opposite the bulky palladium center.[71] The catalyst containing the P–N ligands can bind either of the two prochiral faces of the allyl group therefore, attack of the nucleophile can occur *pseudotrans* to phosphorous or *pseudotrans* to nitrogen in intermediates **A** and **C**, respectively, to generate the (*R*)-product (Figure 3.6, top). The same is observed during attack on diastereomers **B** and **D**, giving rise to the (*S*)-product. This happens because the two modes of attack are both sterically inequivalent and electronically distinct due to the *trans* effect.[72] In contrast, when a C_2 symmetric catalyst is used, the transition states for attack on intermediates **A'**, **B'**, **C'**, and **D'** are equivalent reducing the number of competing diastereomeric transition states. This is a key design advantage for C_2 symmetric catalysts and although many catalysts lacking C_2 symmetry exhibit high levels of enantioselectivity, those containing C_2 symmetry compromise one of the most important and selective classes of catalysts.[70]

We therefore set out to synthesize a library of C_2 symmetric complexes that can be used as catalysts utilizing an array of metal salts. The ligands synthesized and analyzed in chapter 2 all have C_2 symmetry that should be preserved during metallation reactions to form the desired

complexes. Symmetry can be broken during the chelation reaction if the conjugation of the imine bond is disrupted on one side of the ligand alone as describe in section 2.4. Any atypical loss of the C_2 symmetry does not translate into a failed complexation but rather a catalyst with a more complex reaction mechanism leading to a more difficult analysis. Catalysts with certain metal centers have been shown to be more applicable in select areas given the unique electronic properties of the metal atom.[73] With this in mind, we plan to use different metal salts with size, charge and geometry differences to observe how such changes can affect the structure of the complexes produced. We desire three goals during the complexation reactions;

(i)   The metal atom should coordinate to the four nitrogen donor atoms present on the ligand.
(ii) After coordination, the side-arms of the ligand should overlap and be held in a locked position, forming a chiral helicate motif of either (*M*) conformer or (*P*) conformer.
(iii) The reduced ligands (**11** and **12**) should remain reduced after the complexation reaction.
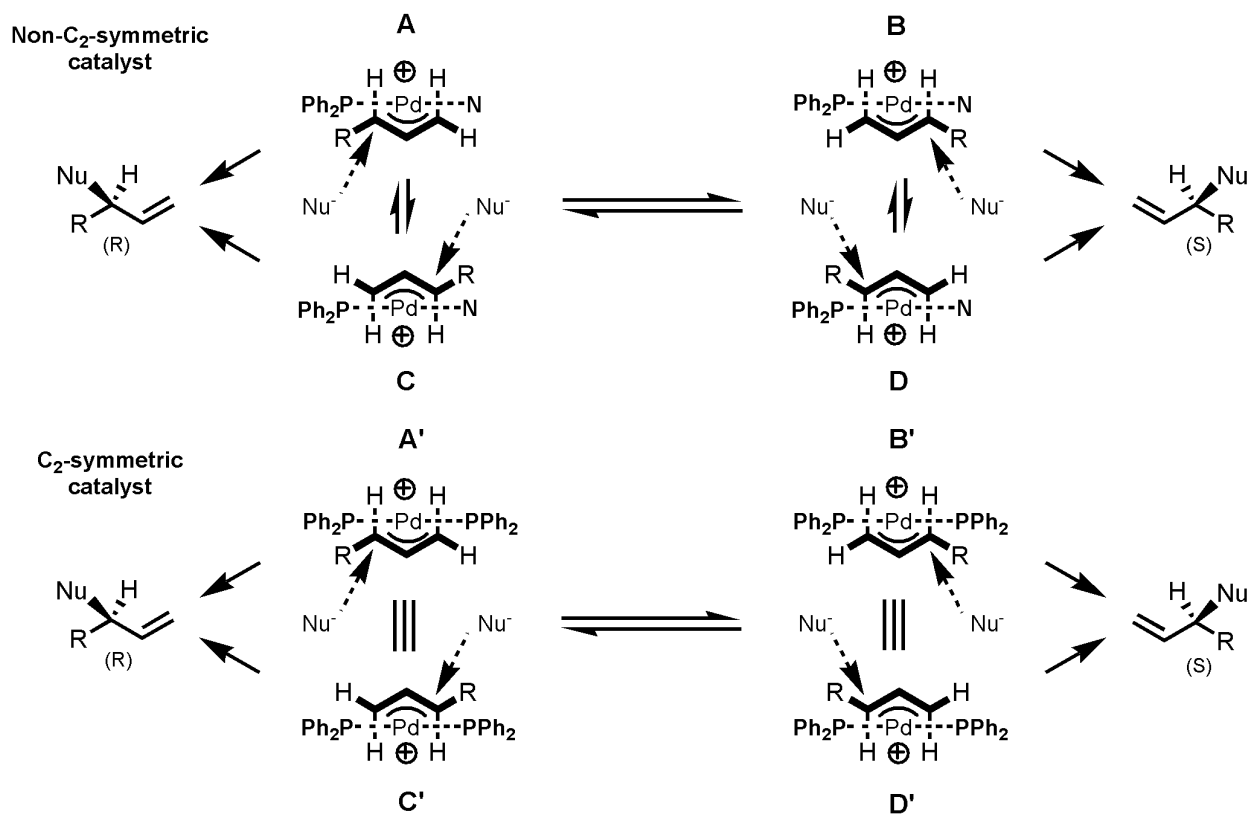
Figure 3.6: Asymmetric Palladium Catalyzed Allylation Reaction of Olefins

50

3.1 Complexation with ZnCl₂
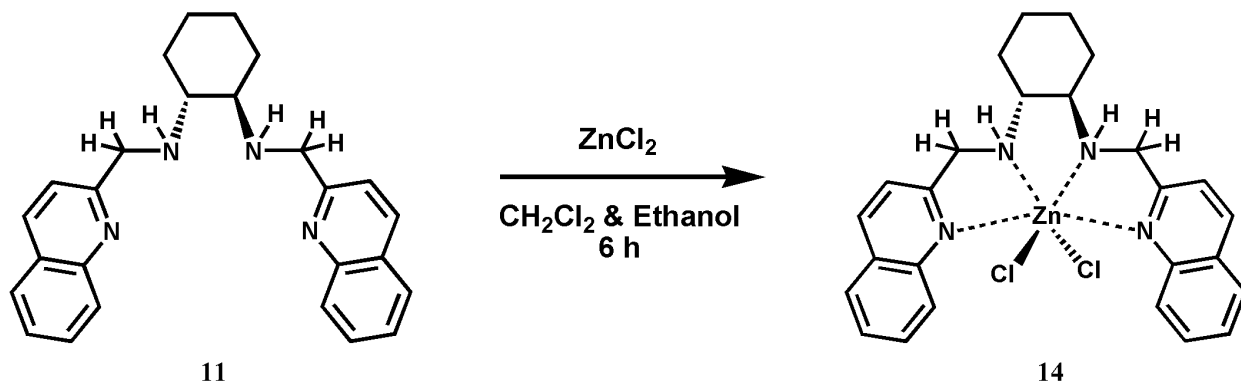
Figure 3.7: Proposed Reaction Scheme for Ligand **11** with ZnCl₂

Catalysts that incorporate zinc metal in the reactive center have been long studied[74-75] with increased interest in that area after the discovery of important biological enzymes that also integrate zinc metal in their centers.[76] We chose to use ZnCl₂ as the metal source because of its high solubility and availability. However, zinc chloride is hygroscopic and deliquescent and was handled in the glove box to prevent exposure to water vapor in the air. Zinc(II) complexes have a Zn^{2+} ionic radius of 81 ± 3 pm and are diamagnetic in character as the cation has a $3d^{10}$ electronic configuration . The reaction of ligand **11** with ZnCl₂ was carried out in a 1:1 ratio to yield an orange colored product in 74.2 % yield after six hours. The ^{1}H NMR of the product obtained is shown in Figure 3.8 and reflects the diamagnetic nature of the complex as there are no broad signals observed in the spectrum. This is due to all the electrons in the *d*-shell orbital being paired up ($3d^{10}$). We observe that the integrity of the reduced imine bond is maintained during complexation and the distinctive second order AB pattern is observed at 4.20 ppm. Peaks in the aromatic region have shifted positions compared to the ^{1}H NMR of corresponding ligand **11** and is indicative of a complex being formed during the reaction.

The arrangement of the metal center and the orientation of the complex as a result of the metallation are important structural factors; therefore we set out to obtain a crystal structure for complex **14**. Several attempts were made at growing single crystals using the solvent diffusion method with methylene chloride and tetrahydrofuran as base our solvents layered with ethanol,
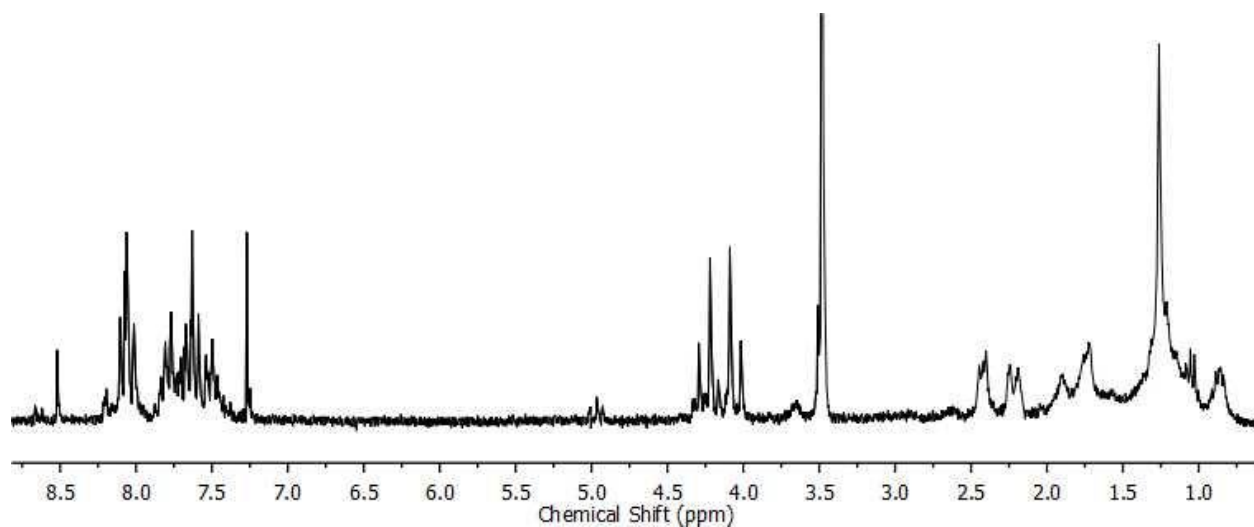
Figure 3.8: 400 MHz ^{1}H NMR Spectrum for Complex **14** (CDCl$_3$)

methanol, ether, and chloroform to no avail. We were finally successful in obtaining crystals suitable for X-ray analysis using a methylene chloride, hexane solvent combination with the thermal ellipsoid structure shown in Figure 3.10. We observe that the ligand does not bind to the zinc metal center with all four nitrogen donor atoms; instead we have one nitrogen atom on the quinoline side-arm free causing the complex to not completely wrap. This revelation prompted us to change the reaction scheme to what is shown below in Figure 3.9.
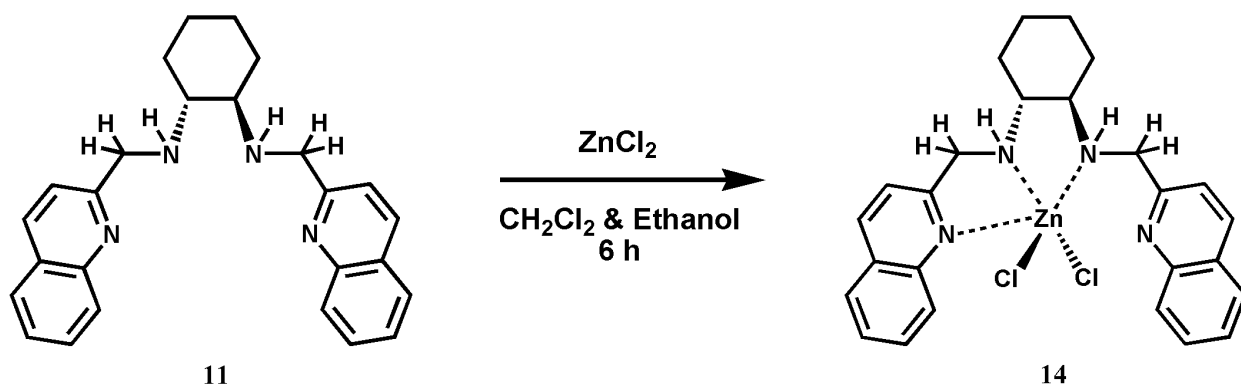
Figure 3.9: Observed Reaction Scheme for Ligand **11** with ZnCl$_2$

The thermal ellipsoid structure obtained shows the presence of one methylene chloride molecule in the coordination sphere of the complex. This is from the base solvent used in the solvent diffusion method used to grow the crystal. The metal center coordinates to the three nitrogen donor atoms and two chlorine ligands with trigonal bipyramidal geometry. We clearly see that one of the side-arms orients itself so as to twist outwards from the center of the complex. This is reflected in the torsion angle as we progress from the quinoline side-arm to the cyclohexyl backbone: C42-N41-C52-C53 (-57.04°) and C41-N41-C52-C53 (179.9°). We have observed similar N_3-coordination in the Levy group with previous metallation reactions of similar ligands with nickel salts. Similar zinc(II) reaction complexations with tetradentate ligands carried out by the Zema report the formation of a complex with the ligand arranged in a square disposition around the metal cation and two solvent molecules completing the coordination sphere in the apical position to give the metal center a distorted octahedral geometry.[74] This is what we would expect of our complex if the last nitrogen donor atom were bound to the metal center with the two chloride ligands in the apical position.
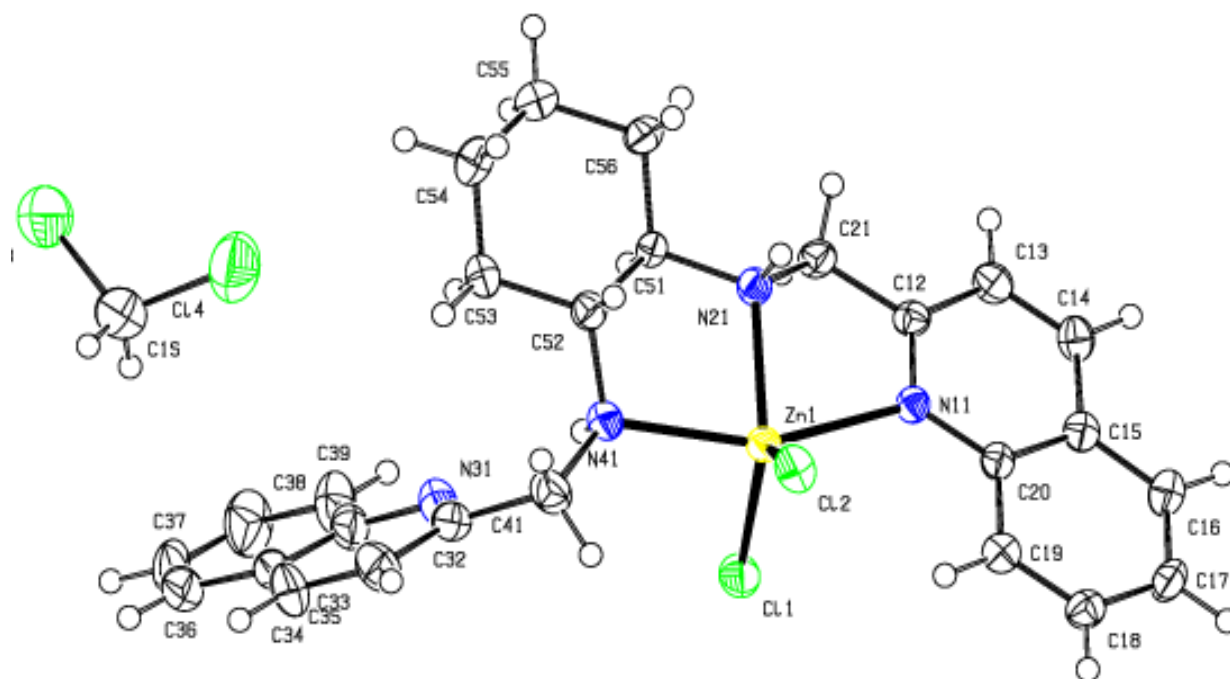
Figure 3.10: Thermal Ellipsoid Crystal Structure for Complex **14**

53

The crystal structure of complex **14** shows that the two chloride ligands are attached to the zinc metal center and this may prevent the second quinoline arm from coordinating to the metal center due to their steric effect. It is a possibility that once in solution, conditions may be favorable to result in the last donor atom binding. Even though the crystal structure shows only three donor atoms bound, breaking the symmetry of the complex, the ^{1}H NMR result obtained is not reflective of a non-symmetric compound. This may be due to the $ZnCl_2$ unit rapidly "hopping" around the pocket and binding to all four donor atoms but with only three at one time resulting in an average NMR signal (Figure 3.11).
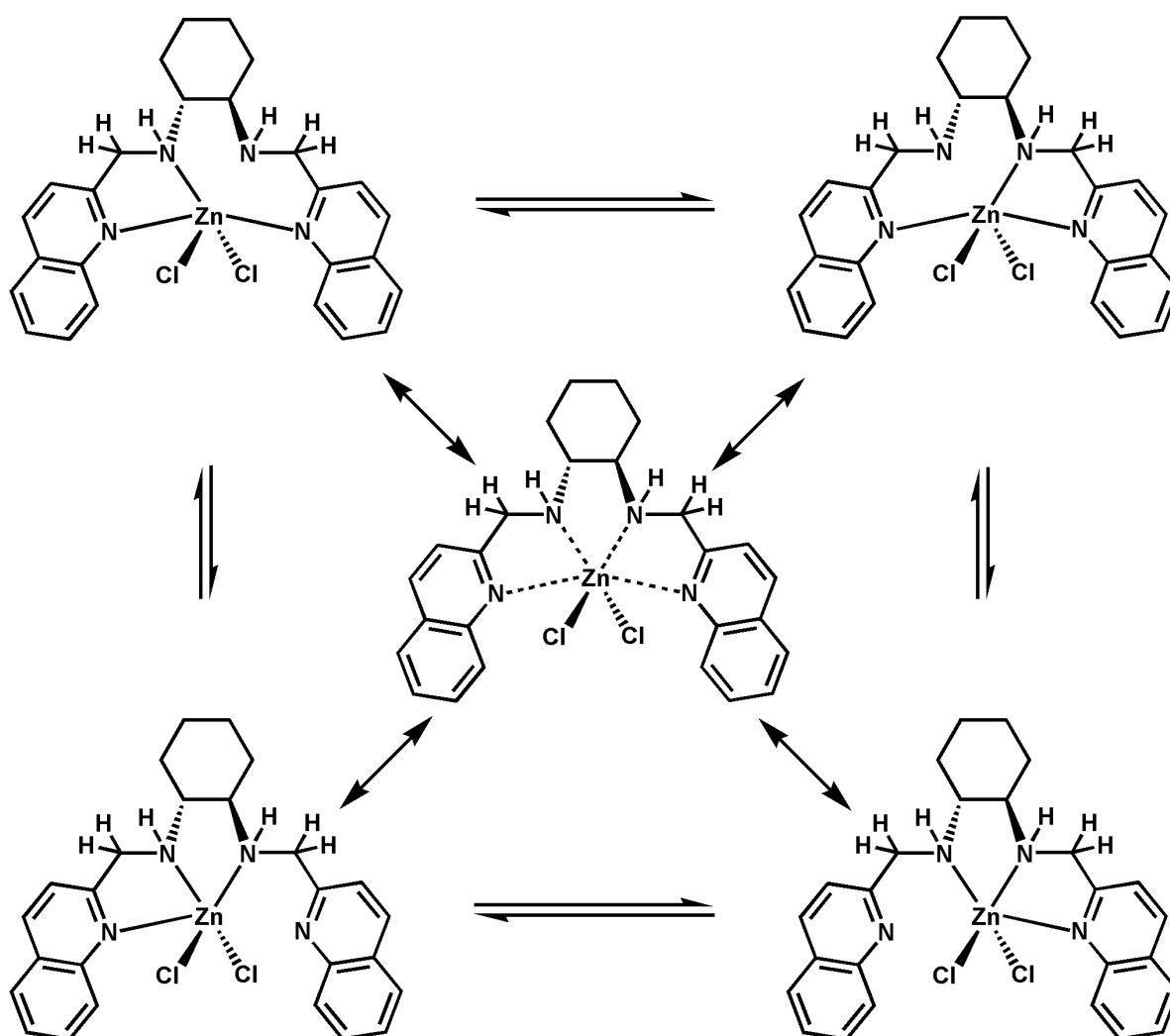
Figure 3.11: Fluxional Coordination Possibilities for Complex **14**
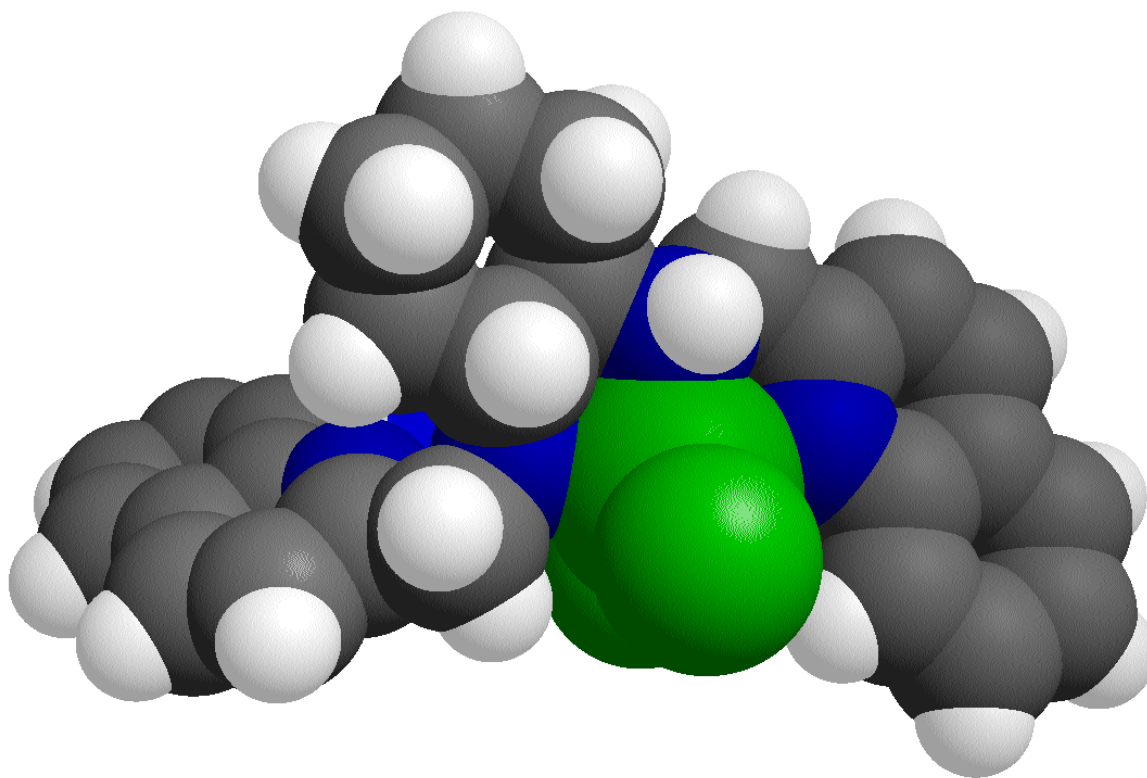
Figure 3.12: Space Filling Crystal Structure for Complex **14**

Bond Length				
Bond Length	Zn_1-N_{21}	2.098(3)	Zn_1-Cl_2	2.257(8)
	Zn_1-N_{41}	2.181(3)	C_{21}-N_{21}	1.458(4)
	Zn_1-N_{11}	2.235(3)	C_{41}-N_{41}	1.458(4)
	Zn_1Cl_1	2.264(9)	C_{12}-N_{11}	1.324(4)
Bond Angles	N_{21}-Zn_1-N_{41}	79.51(10)	N_{21}-Zn_1-Cl_2	108.79(8)
	N_{21}-Zn_1-N_{11}	76.31(9)	N_{41}-Zn_1-Cl_2	96.72(8)
	N_{41}-Zn_1-N_{11}	153.20(9)	Cl_2-Zn_1-Cl_1	122.80(3)
Torsion Angles	N_{21}-Zn_1-N_{11}-C_{12}	-21.2(2)	N_{41}-Zn_1-N_{11}-C_{12}	4.94(4)

Table 3.1 Selected Bond Lengths (Å), Bond Angles, and Torsion Angles for Complex **14**

3.2 Complexation with Zn(OTf)₂
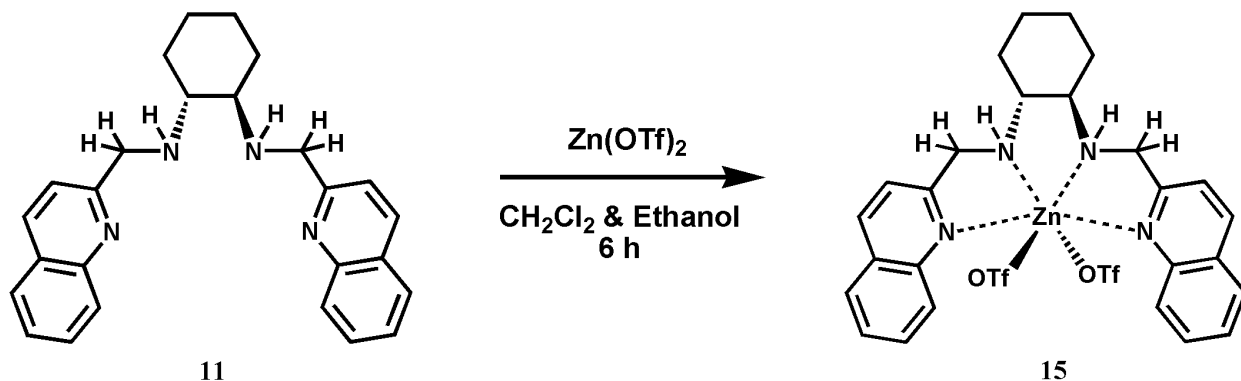
Figure 3.13: Proposed Reaction Scheme for Ligand **11** with Zn(OTf)$_2$

After the successful reaction with ZnCl$_2$ and in an attempt to obtain complete wrapping, we carried out the same reaction with a different counter-ion (trifluoromethanesulfonate). We chose the triflate counter-ion to try and minimize the anion coordination and achieve exclusive coordination of the ligand to the metal center. The reaction was carried out with a 1:1 ration of ligand to metal salt and we obtain an orange colored product in 81.3 % yield. Several attempts to grow crystals suitable for X-ray analysis using the slow diffusion method and the heating and cooling method proved futile. The ^{1}H NMR obtained for this reaction is shown in Figure 3.14 and once again we obtain a sharp spectrum due to the diamagnetic nature of the bound zinc metal cation. We observe upfield and downfield shifts when the spectrum is compared to that of the ligand (**11**) and the previous zinc(II) complex (**14**). For example, the two doublet peaks located at 8.09 ppm in the corresponding ligand (**11**) have separated and moved upfield to 8.40 ppm and 8.48 ppm. The distinct AB pattern corresponding to the amine protons have shifted downfield from 4.05 ppm in ligand **11** to 3.82 ppm in complex **15**. Close examination of the ^{1}H NMR spectrum reveals a pattern similar to the second order AB pattern at 3.46 ppm. This was considered to be due to the presence of a different zinc complex but the aromatic region does not reflect the formation of two separate complexes. Therefore, the second order AB pattern observed at 3.46 ppm may be due to the presence of impurities in the product obtained the after the complexation reaction. We observe a slight shift of peaks located in the aliphatic region as
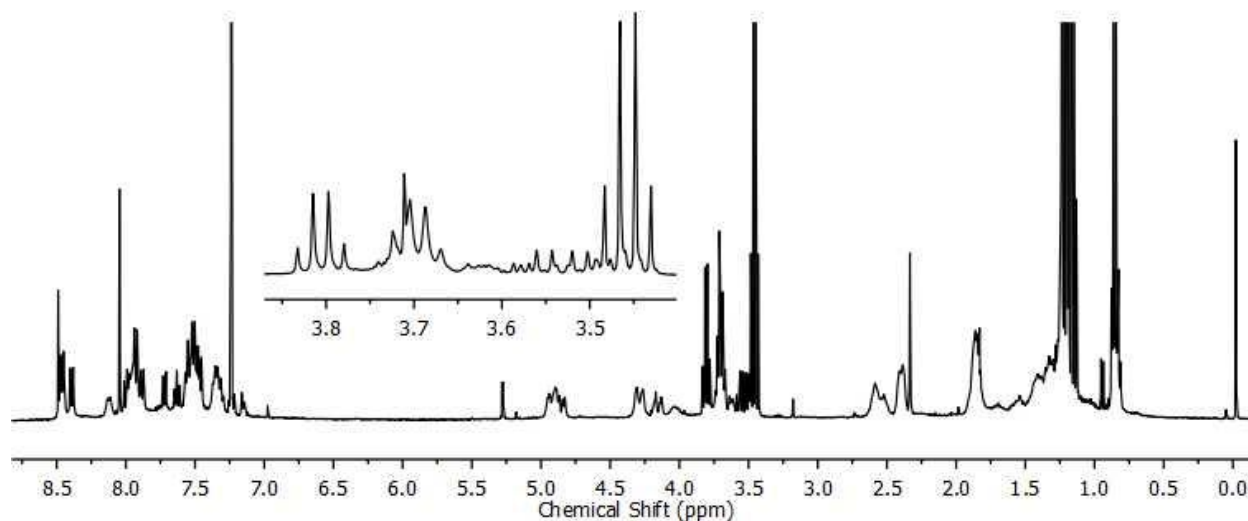
Figure 3.14: 400 MHz ^{1}H NMR Spectrum for Complex **15** (CDCl$_3$)

the broad peak at 2.48 ppm in ligand **11** is now at 2.60 ppm in complex **15**. When we compare the ^{1}H NMR spectrum of complex **15** with complex **14**, we observe slight changes in peaks located in the aromatic region and the distinct second order AB pattern as observed when comparing with ligand **11**.

Since we were not able to obtain single crystals suitable for X-ray analysis, we carried out electro-spray ionization mass spectrometry on complex **15** to detect the presence of the desired complex. The mass spectrum obtained (Appendix I) shows the presence of two ions corresponding to the desired complex minus one triflate counter-ion [C$_{26}$H$_{28}$N$_4$Zn(CF$_3$SO$_3$)]$^+$ and the desired complex minus both triflate counter-ions [C$_{26}$H$_{28}$N$_4$Zn]$^{2+}$. These results help confirm the synthesis of a complex with the right mass as our desired compound but until the successful growth of single crystals for complex **15**, we cannot confirm the arrangement of the metal center and if we managed to bind all four nitrogen donors to the zinc(II) cation to form a single stranded helicate. The ^{1}H NMR spectrum obtained suggests the formation of a C_2 symmetric complex with all four nitrogen donor atoms bound but as we discovered in complex **14**, we may be observing an average NMR signal due to the Zn(OTf)$_2$ unit hopping around in the pocket, subsequently binding with all four nitrogen atoms in solution but doing so through binding with three nitrogen atoms at one time.

3.3 Complexation with Ni(OTf)$_2$
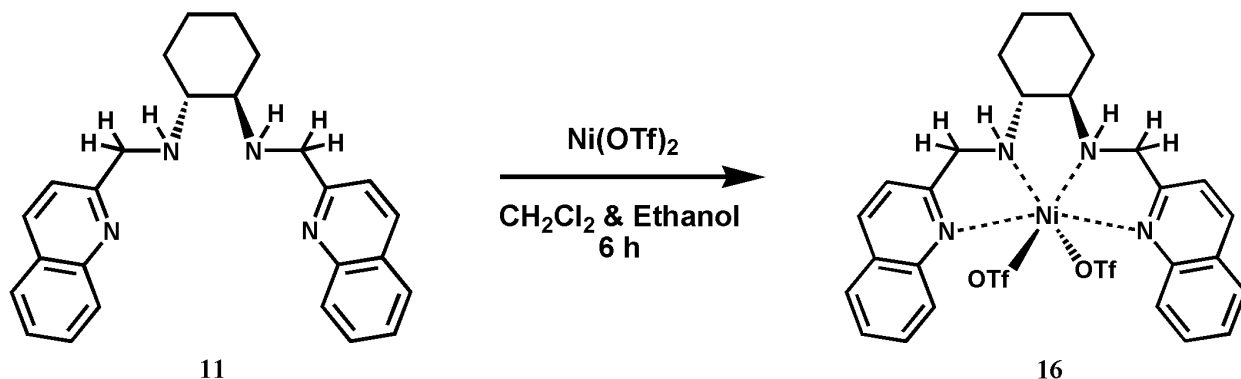
Figure 3.15: Proposed Reaction Scheme for Ligand **11** with Ni(OTf)$_2$

After the reaction with Zn(OTf)$_2$, we decided to explore the reaction of ligand **11** with a metal that had a smaller ionic radius with the proposal that a smaller metal center should improve the chances of all four nitrogen donor atoms binding to the metal cation resulting in the formation of a single stranded helix. Nickel(II) cation has a smaller ionic radius (75 ± 5 pm) compared to its zinc(II) counterpart. The complexation reaction was carried out with a 1:1 ration of ligand to metal salt and the triflate counter-ion was used to minimize coordination of the anion. We obtain a brown colored product from the reaction in 79.2 % yield. Nickel(II) complexes have a $3d^8$ electronic configuration and result in the formation of a paramagnetic complex when bound in a octahedral or tetrahedral geometry due to the presence of two unpaired electrons. On the other hand, when nickel(II) cation is bound in a square planar geometry, it results in the formation of a diamagnetic complex because all electrons are paired. The final complex possibility is the formation of a 5-coordinate nickel(II) complex. In this case, the nature of the ligand will determine if the complex will be high-spin or low-spin.[61] Therefore, there is a possibility for such 5-coordinate complexes to be either paramagnetic or diamagnetic. With this in mind, we hope to form square planar complexes with our ligands so the diamagnetic complexes obtained can be interpreted using nuclear magnetic resonance. The ^{1}H NMR spectrum obtained for complex **16** is shown in Figure 3.16 and clearly indicates that the complex is paramagnetic as we observed highly broadened peaks.
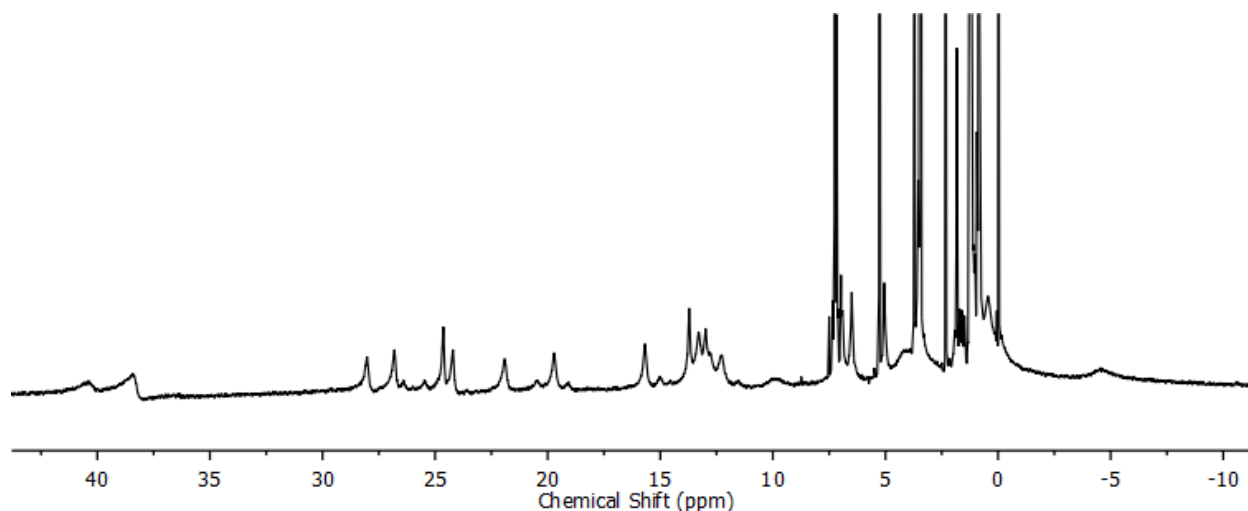
Figure 3.16: 400MHz ^{1}H NMR Spectrum for Complex **16** (CDCl$_3$)

Given the difficulty in interpreting paramagnetic spectra, we were still able to obtain some valuable information from the spectra. It clearly shows the formation of a complex as the ^{1}H NMR character has shifted from sharp signals in ligand **11** to highly broadened signals in complex **16**. There are proton resonances present in the normal aromatic and aliphatic regions of the spectrum and there are also resonances present outside the normal diamagnetic chemical shift range. These are most likely due to the proton signals that are close in proximity to the nickel metal center. We expect that protons present on the quinoline side-arm will experience a greater paramagnetic shift compared to the protons present on the cyclohexyl back bone. The ^{1}H NMR spectrum also indicates that the symmetry is broken in complex **16** and we did not obtain a C_2 symmetric complex as desired. The other scenario that could explain the large number of resonance peaks is the presence of two distinct complexes. Several attempts to grow single crystals of complex **16** suitable for X-ray analysis either by solvent diffusion of heating and cooling were unsuccessful. To support the ^{1}H NMR results that a complex was formed during the reaction, we conducted electro-spray mass spectrometry on complex **16**. The spectrum obtained (Appendix I) confirms the formation of ions that correspond to the desired complex minus a triflate counter-ion $[C_{26}H_{28}N_4Ni(CF_3SO_3)]^+$. Given this information, the nickel cation may be bound to three nitrogen donor atoms and one triflate counter ion (through the oxygen atom) breaking the symmetry of the complex explaining the ^{1}H NMR results obtained.

59

3.4 Complexation with NiI$_2$
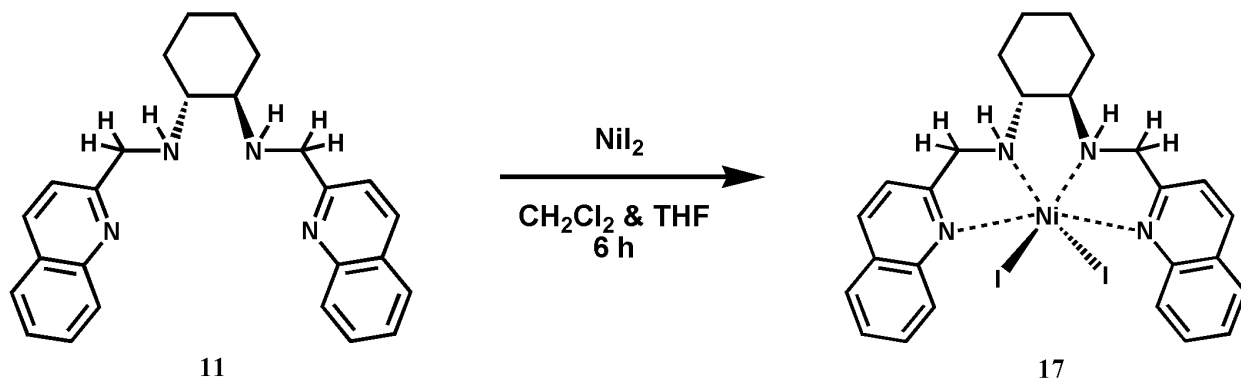
Figure 3.17: Proposed Reaction Scheme for Ligand **11** with NiI$_2$

To increase our chances of obtaining a solid state structure using our ligand and a nickel(II) cation, we attempted to use a different counter-ion and explored the complexation of ligand **11** with NiI$_2$. The reaction produced a black-brown colored product in 82.7 % yield. The ^{1}H NMR obtained for complex **17** is shown in Figure 3.18 and displays the formation of a paramagnetic compound once again as we observe resonances outside the normal diamagnetic chemical shift range. The reaction with NiI$_2$ looks to have produced a pure complex compared to the reaction carried out with Ni(OTf)$_2$ as the number of peaks observed in the ^{1}H NMR spectrum is less than what was present for complex **16**. Closer examination of the spectrum reveals that there might be unreacted ligand (**11**) left after the reaction as we observed sharp peaks in the normal aromatic region of the spectrum. This paramagnetic spectrum clearly indicates the presence of unpaired electrons eliminating the possibility of the formation of a square planar complex with NiI$_2$. The proton resonances obtained are highly broadened and range from -0.3 ppm to 36.92 ppm. Surprisingly, the broad signals that appear outside of the normal diamagnetic chemical shift range are well defined in their position and correspond to six protons. They are located at 10.81, 13.34, 14.01, 24.00, 26.95, and 36.92 ppm. Once again, we were not successful in obtaining crystals of complex **17** suitable for X-ray analysis. Electro-spray mass spectrometry results obtained for complex **16** shows the presence of ions corresponding to the desired complex minus one iodide counter ion [C$_{26}$H$_{28}$N$_4$NiI]$^+$ shown in Figure 3.19.

60
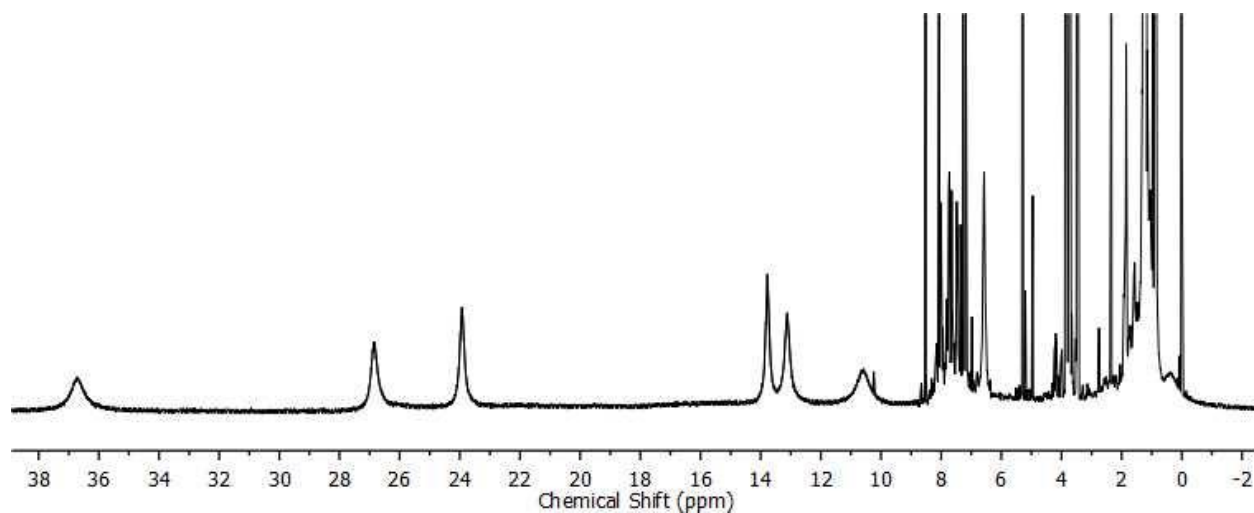
Figure 3.18: 400 MHz ^{1}H NMR Spectrum for Complex **17** (CDCl$_3$)
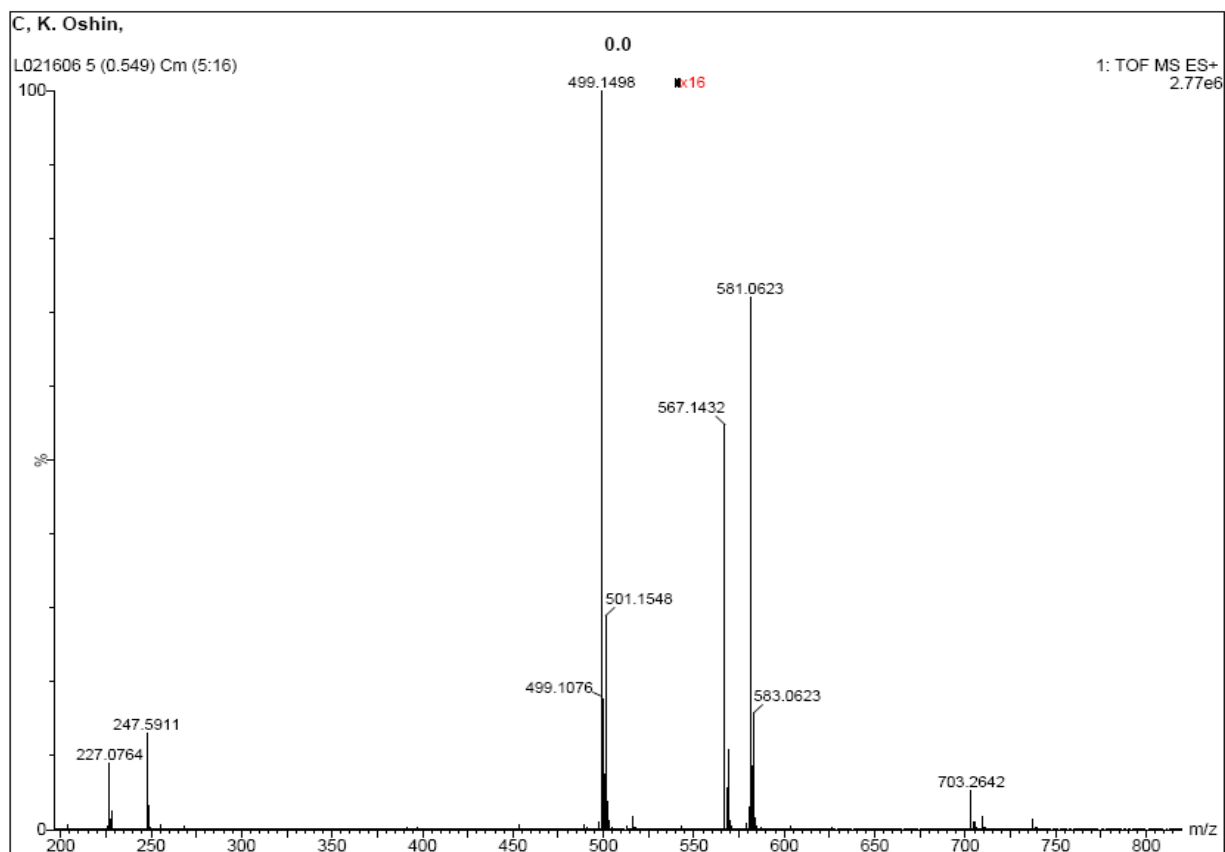
Figure 3.19: Electro-Spray Mass Spectrum for Complex **17**

3.5 Complexation with FeCl$_2$
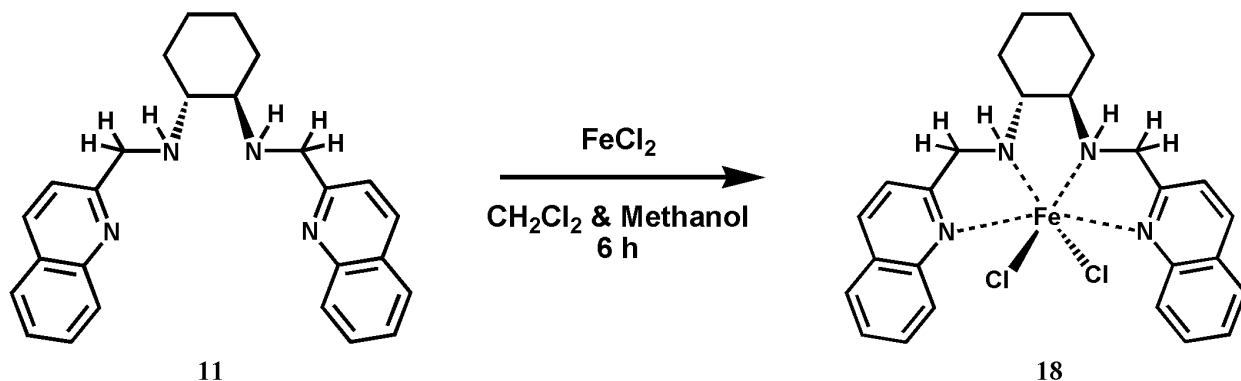
Figure 3.20: Proposed Reaction Scheme for Ligand **11** with FeCl$_2$

The unsuccessful crystallization results we obtained using nickel(II) salts prompted us to try the metallation reaction of ligand **11** using a different metal with comparable ionic radius. Iron(II) chloride was selected because of its availability and ionic radius size of 74 ± 5 pm, which is similar to nickel with 75 ± 5 pm. Numerous chelation reactions have been carried out with iron(II) salts and this continues to be an area of growing interest ever since the discovery of non-heme iron enzymes, such as methane monooxygenase and Riske dioxygenases as catalysts for alkane oxidation.[75] Much recently, exceptional non-heme iron catalysts have been synthesized by the likes of Costas[76], Chen[77], Britovsek[78], and Mekmouche[79] utilizing similar tetradentate N$_4$ ligands belonging to the tripodal **TPA** and linear **BPMEN** ligand family that can perform efficient stereo-specific alkane hydroxylation using H$_2$O$_2$ as the oxidant. As a result, these bioinspired iron catalysts have provided key insights into the mechanisms by which alkanes are oxidized by enzymes in nature.

The reaction of ligand **11** with FeCl$_2$ was carried out in the usual 1:1 ratio to give a tan colored product that crashed out of solution after six hours in 84.3 % yield. The dry product was isolated by filtering and pumping down on the resulting solution using a vacuum line. The ^{1}H NMR obtained for this product is shown in Figure 3.21 and indicates the presence of a paramagnetic compound. Iron(II) cations have $3d^6$ electronic configurations and can be high-spin or low-spin depending on the nature of the ligand. The high-spin conformation typically results

in the formation of a paramagnetic compound as we have four unpaired electrons present and the low-spin conformation usually results in a diamagnetic compound as we have all electrons paired up. Unpaired electrons affect the NMR linewidth and result in broad signals in the ^{1}H NMR spectrum. The degree of line broadening for paramagnetic molecules predominantly depends on the electronic relaxation time, which for the unpaired spin states of high-spin Fe(II) is relatively short.[80] Complete assignment of the spectra was not attempted due to the difficulty in interpreting highly broadened spectra. None the less, the ^{1}H NMR spectrum provided valuable information in that metallation did occur and a complex was formed. We observe seven proton resonance peaks present outside the normal diamagnetic chemical shift range. They are located at -32.03, -25.04, -19.34, -10.02, 24.26, and 75.00 ppm. The spectrum appears to be of a pure complex as we do not observe an unusual high number of proton signals.
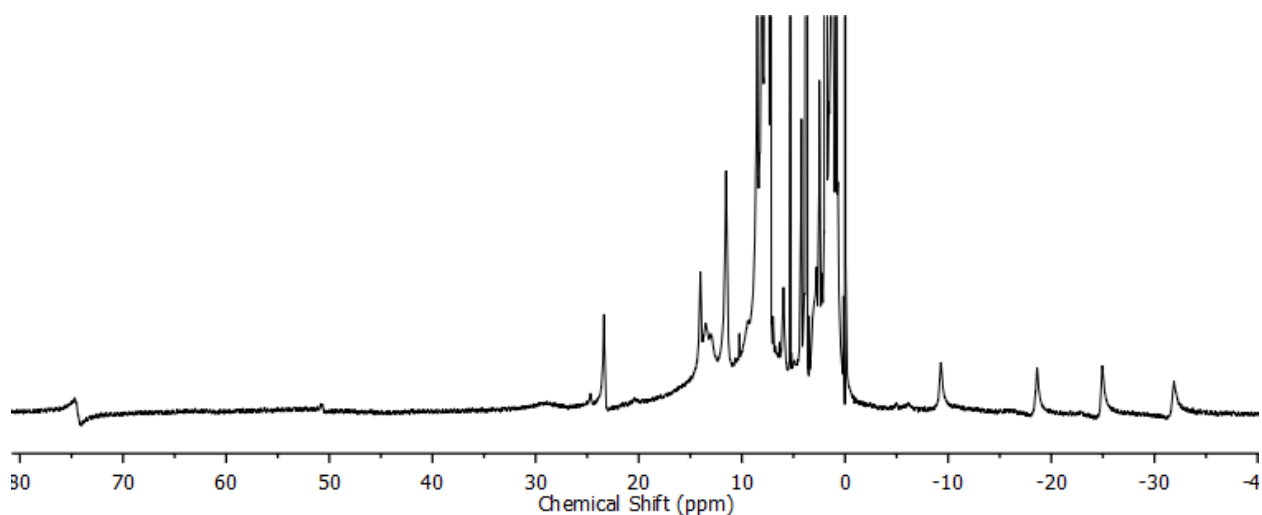
Figure 3.21: 400 MHz ^{1}H NMR Spectrum for Complex **18** (CDCl$_3$)

Using the solvent diffusion method, we were able to grow single crystals of complex **18** suitable for X-ray analysis. The thermal ellipsoid structure obtained for complex **18** is shown in Figure 3.24 and displays the iron metal center bound to the four nitrogen donor atoms, a chloro ligand and an oxo bridge connected to a second iron cation with three chloro ligands coordinated to it. It is a unique structure because both complexation and crystallization reactions were carried out under oxygen free conditions. A possible source of the oxygen atom could be traces of water

present in the "dry" solvents used during crystallization. The presence of this oxygen atom also changes the oxidation states of the two iron centers as they appear to now be both Fe(III) cations. This would be the scenario that explains the paramagnetic ^{1}H NMR spectrum obtained for complex **18**. The other coordination possibility is the very rare high Fe(IV) oxidation state for the iron center bound to the three chlorine atoms with the second iron center staying as Fe(II). In an attempt to understand the oxidation state on the metal centers, we performed EPR spectroscopy on complex **18**. Figure 3.22 shows the perpendicular and parallel mode X-band EPR spectrum for the complex at 20 K. In the perpendicular mode spectrum, the large signal at g = 4.22 is consistent with high spin ferric iron ion. We also note the presence of another small signal at g = 9.69 and g = 2.01. The former signal is also associated with ferric iron while the latter cannot be identified at the present time. The parallel mode EPR spectrum displays small signals that could not be interpreted. Review of the literature on similar iron(III) complexes reveals that a phenomenon known as antiferromagnetic exchange could in a molecule that had two iron(III) centers and an oxo bridging ligand.[81] A bond could be formed in the Fe$_2$O unit by delocalizing one of the oxygen p_x electron into the d_{x2-y2} orbital of the metal. Using the Pauli principle, this transferred electron is required to point down forcing one of the Fe(III) $5d$ electrons to point in the opposite direction. The spin of the two-iron system becomes zero and we have a molecular diamagnet causing no signal to be observed in an EPR experiment. This may be the reason we do not observe any noteworthy signals in the parallel mode EPR spectrum
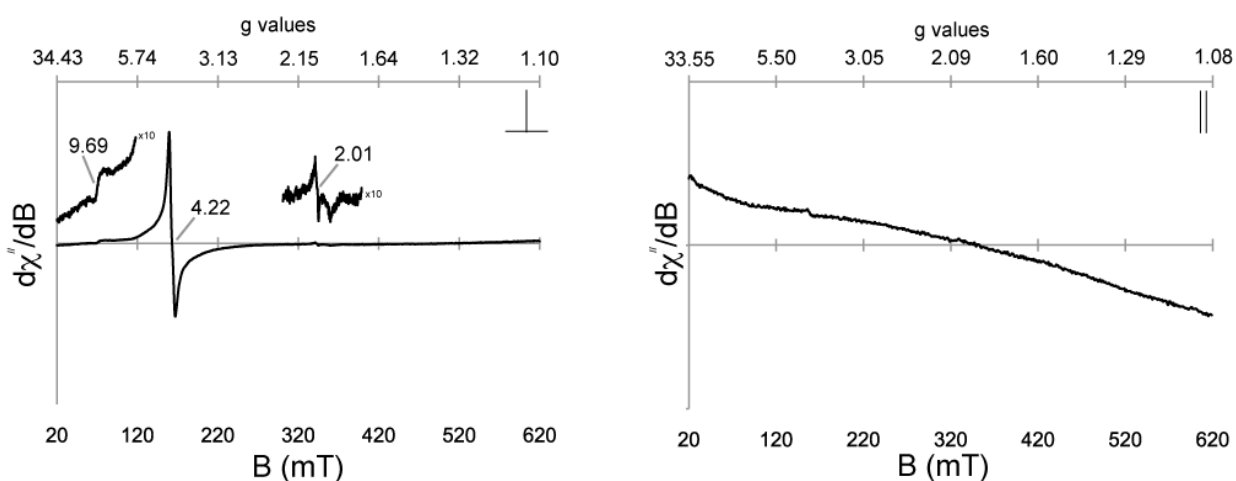
Figure 3.22: EPR Spectrum for Complex **18** (CH$_2$Cl$_2$)

We observe that we were successful in getting the complex to completely wrap around the metal center by binding to the four nitrogen donor atoms and also maintain the integrity of the reduced imine bond forming a complex that meets all our goal requirements set out on page 50. After obtaining the crystal structure for complex **18**, we now know that the reaction scheme for ligand **11** with $FeCl_2$ occurs as shown in Figure 3.23.
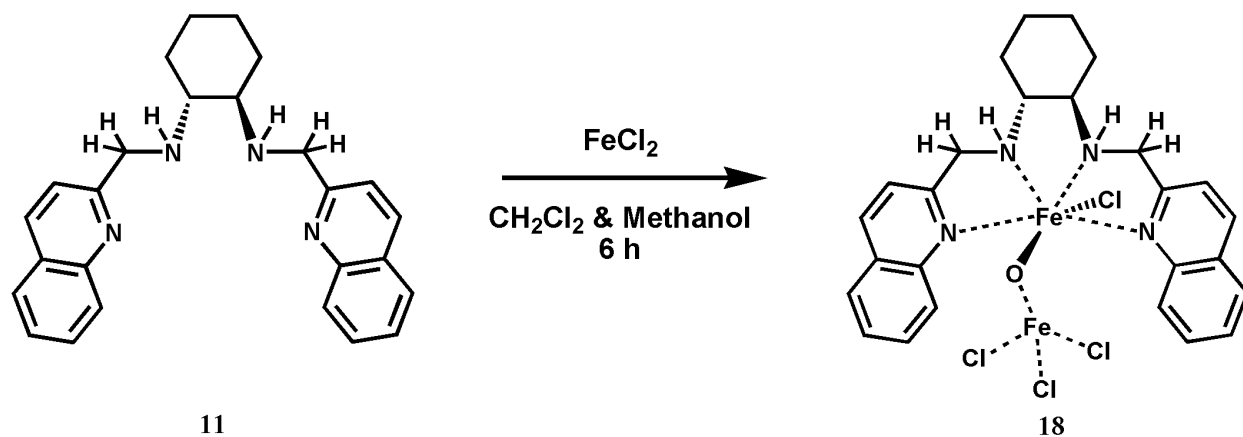
Figure 3.23: Observed Reaction Scheme for Ligand **11** with $FeCl_2$

The thermal ellipsoid structure obtained shows that the iron metal bound to the four nitrogen donor atoms is coordinated in a distorted octahedral fashion while the iron metal bound to the three chloro ligands and bridging oxygen is coordinated in a tetrahedral fashion. The bond lengths of the iron cation bound to the two nitrogen donor atoms in the amine bond show a slight difference with Fe1-N52 as 2.159 Å and Fe1-N53 as 2.172 Å. We observe slightly longer bond lengths between the iron cation and the nitrogen donor groups on the quinoline arms with Fe1-N11 as 2.243 Å and Fe1-N31 as 2.221 Å. The iron center is bound to a chloro ligand with a bond length of 2.356 Å for Fe1-Cl1 and a much shorter bond length to the bridging oxo group with Fe1-O1 as 1.807 Å. The oxo ligand then binds to the second iron cation with a shorter bond length of 1.756 Å. The second iron center is bound to three chloro ligands with varying bond lengths of 2.2198 Å for Fe2-Cl3, 2.2328 Å for Fe2-Cl4, and 2.2427 Å for Fe2-Cl2. We notice that the average bond length for the second iron cation with the chloro ligands is shorter than the bond length of the first iron center with the last chloro ligand. This is most likely due to the steric

interaction caused by the two quinoline arms wrapping about the metal center and stacking on top of each other. The ligand itself experiences slight changes as we observe the amine bond lengths to be 1.474 Å for C21-N51 and 1.465 Å for C41-N52. These will be compared to future complexation reactions made with ligand **11** that successfully wrap. In comparison with the imine bond from complex **13** of 1.293 Å, we can conclude that the longer amine bond increases the chances of the ligand wrapping around a metal center and the longer bond lengths observed with complex **18** contributed to the complete wrapping observed.

The bond angles of complex **18** also give us some important information on how the compound packs in the crystal lattice. We observe that the structure has a space group of P2(1)2(1)2(1) and an orthorhombic crystal system. The bridging oxo ligand is held at an angle almost perpendicular to the iron cation bound to the four nitrogen donor atoms with bond angles of 97.47^o for O1-Fe1-N52, 97.25^o for O1-Fe1-N51, 90.55^o for O1-Fe1-N31, and 85.42^o for O1-Fe1-N11. The bond angles in the tetrahedral FeCl$_3$ unit are 112.06^o for O1-Fe2-Cl3, 107.22^o for O1-Fe2-Cl4, and 107.85^o for O1-Fe2-Cl2. Of interest is the bond angle of the di-iron μ-oxo core and we observe an angle of 150.28^o for Fe2-O1-Fe1. We examine the twist of the quinoline side-arm by looking at the angle formed between the iron metal bound to the nitrogen donor atom on the quinoline side-arm to the carbon atom located on the same phenyl ring. We observe this angle to be 126.2^o for C40-N31-Fe1 and 127.7^o for C20-N11-Fe1. The torsion angles describe the twist present in parts of the structure and we observe an angle of -2.4^o for N52-Fe1-O1-Fe2, -80.5^o for N51-Fe1-O1-Fe2, 71.2^o for N32-Fe1-O1-Fe2, and -154.7^o for N11-Fe1-O1-Fe2. The torsion angles about the chloro ligands are worth noting and they are -50.9^o for Cl1-Fe1-N53-C41, 75.1^o for Cl1-Fe1-N11-C20, 71.2^o for Cl1-Fe1-N31-C32, and -98.3^o for Cl1-Fe1-N31-C40. The space filling model structure obtained for complex **18** is shown in Figure 3.25 and displays the presence of a single stranded monohelix as desired. We observe that complex **18** is present only as the *M* (left-handed) conformer. The space filling model also suggests that there are π–π and/or σ-π interactions present between the phenyl rings at the ends of the quinoline side-arms. The aromatic rings do not lie directly on top of each other but are slightly offset creating an ideal alignment that fosters a π-π interaction or σ-π interaction. Table 3.2 shows other bond distances, bond angles, and torsion angles for complex **18**. Complete crystal data and structure refinement information for complex **18** can be found in Appendix II.
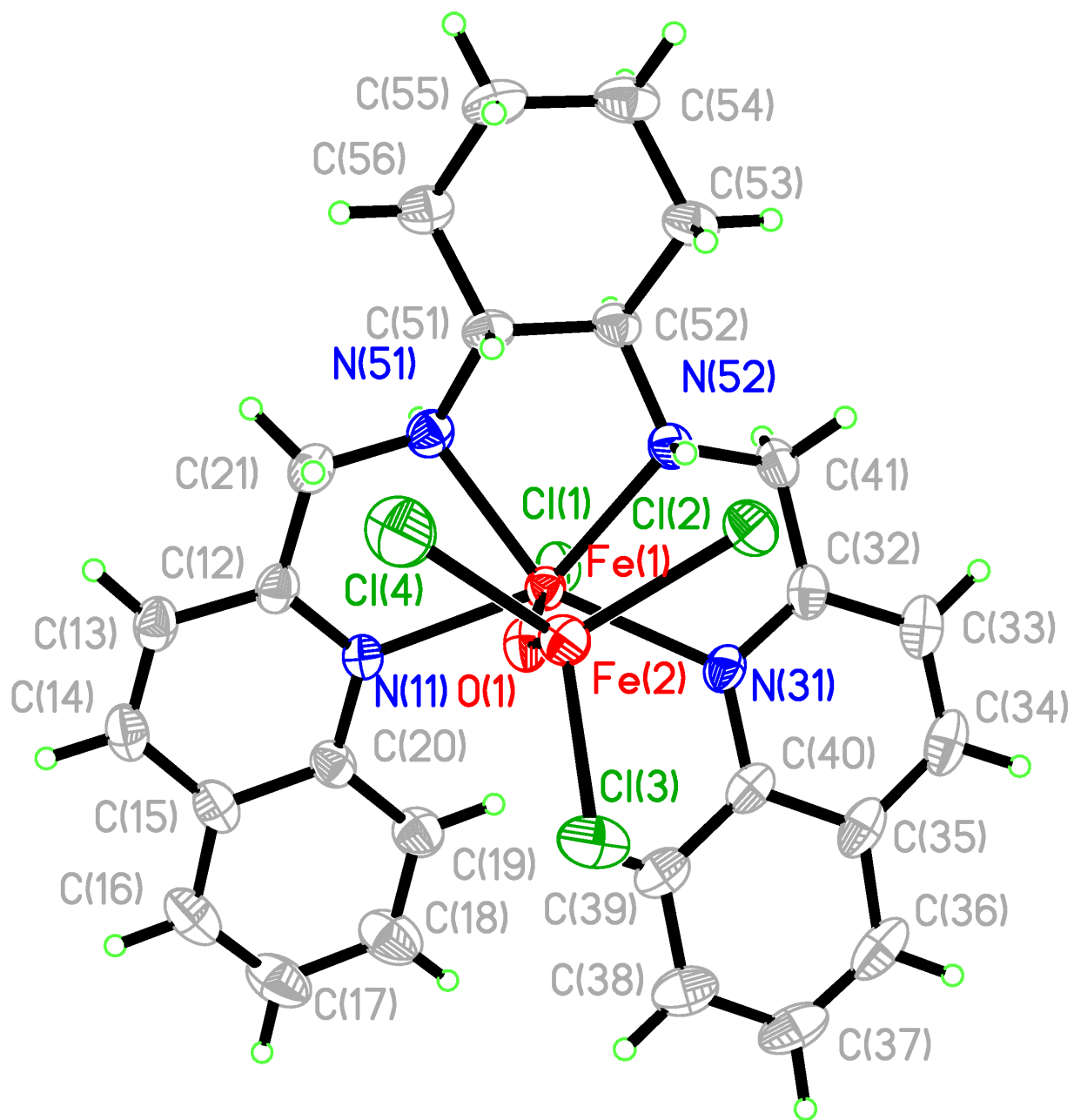
Figure 3.24: Thermal ellipsoid Crystal Structure for Complex **18**
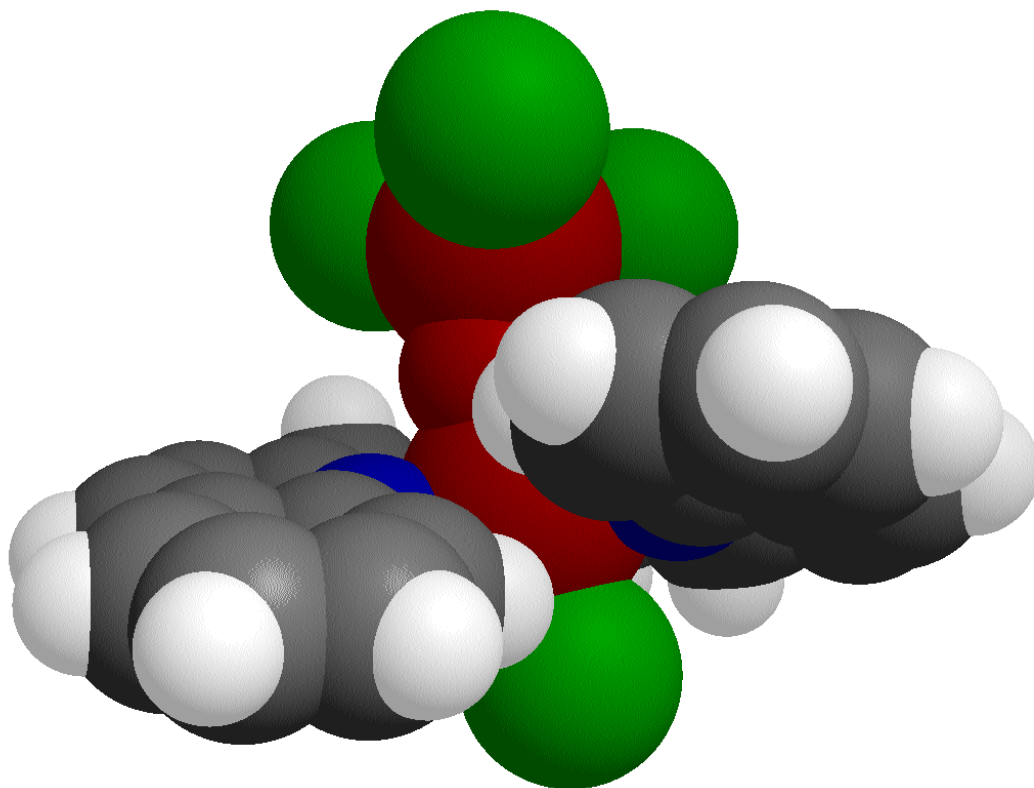
Figure 3.25: Ball & Stick and Space-Filling Crystal Structure for Complex **18**

Bond Length	Fe_1-O_1	1.807(2)	Fe_1-N_{11}	2.243(3)
	Fe_1-N_{52}	2.159(3)	Fe_1-Cl_1	2.356(9)
	Fe_1-N_{51}	2.172(3)	O_1-Fe_2	1.756(2)
	Fe_1-N_{31}	2.221(3)	Fe_2-Cl_3	2.219(10)
Bond Angles	O_1-Fe_1-N_{52}	97.47(11)	O_1-Fe_1-N_{31}	90.55(1)
	O_1-Fe_1-N_{51}	97.25(12)	N_{52}-Fe_1-N_{31}	73.63(10)
	N_{52}-Fe_1-N_{51}	77.30(11)	N_{51}-Fe_1-N_{31}	150.64(11)
Torsion Angles	N_{52}-Fe_1-O_1-Fe_2	-2.4(3)	N_{51}-Fe_1-O_1-Fe_2	-80.5(3)

Table 3.2 Selected Bond Lengths (Å), Bond Angles, and Torsion Angles for Complex **18**

3.6 Complexation with RuCl$_2$(COD)
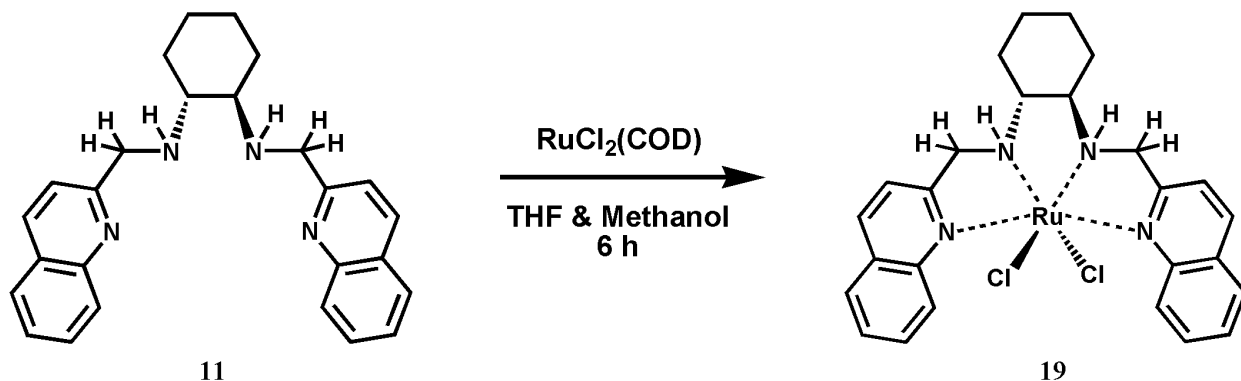
Figure 3.26: Proposed Reaction Scheme for Ligand **11** with RuCl$_2$(COD)

After the successful chelation reaction of ligand **11** with FeCl$_2$, we decided to try a complexation reaction with an inert metal and chose ruthenium(II). Because the coordination environment around the central metal ion directs the chemical and physical properties of the complex, metallation reactions using ligands of different types and ruthenium salts have been of significant importance.[82] Ruthenium complexes have become more attractive over the years because of their potential use as catalysts in the area of photovoltaics.[83] Complexes of this type are of high interest from both a fundamental point of view where the dynamics of excited state electron and energy transfer are under investigation and from a practical point of view where photochemical devices related to light-to-energy conversion have been proposed or devised.[84-85] Other experimental studies carried out by the Gross group focused on the successful use of ruthenium(II) porphyrin complexes as oxidation catalysts in the asymmetric epoxidations of non-activetaed olefins.[86] Further catalytic activities of ruthenium(II) complexes in the oxidation of alcohols using *N*-methylmorpholine-*N*-oxide as the co-oxidant have been studied by Reimers[87], Kureshy[88], El-Hendawy[89], and Bhowon[90]. We therefore set out to synthesize novel ruthenium(II) complexes using ligand **11** to be used as catalysts in future reactions.

Ligand **11** was reacted with dichloro-1,5-cyclooctadiene ruthenium(II) in the same 1:1 ratio as previous reactions in this chapter to produce a navy blue colored product in 92.4 % yield. The ^{1}H NMR obtained for complex **19** is shown in Figure 3.27 and reveled proton peak patterns

that were very similar to the unreduced ligand, **1**. We also observe the disappearance of the second order AB pattern suggesting a loss of the reduced imine bond to form the original ligand (**1**) again. The reaction was repeated three times giving the same ^{1}H NMR results. During the reaction, the amine bond is converted back to the imine bond in the absence of any oxidizing agents. The only source of protons for this transformation is the 1,5-cyclooctadiene (COD) present in the metal salt. The COD is eventually removed at the end of the reaction when the product is pumped down on using the vacuum line but is present during the reaction phase to provide the complex with hydrogen atoms. We have witnessed the ability of solvents, such as ethanol, to affect the reduction state of the imine bond[61] but never as part of the metal salt affecting the reduction outcome of the imine bond. The ^{1}H NMR spectrum obtained also shows no significant shift in the aromatic or aliphatic proton signals to signal the formation of a complex. This is unusual given other solution studies that have been carried out by Pazderski[91], Natarajan[92], and Ludi[93], all showing shifts in the proton signals obtained for their respective ruthenium complexes. Analysis of the complex [Ru(bpy)$_2$(dcbpy-H)](PF$_6$) by the Rillema group at Wichita State University show that the proton next to the nitrogen donor atom bound to the ruthenium metal center experiences the greatest shift upon coordination.[94] This is due to significant shielding of the nitrogen adjacent protons by the ruthenium metal.
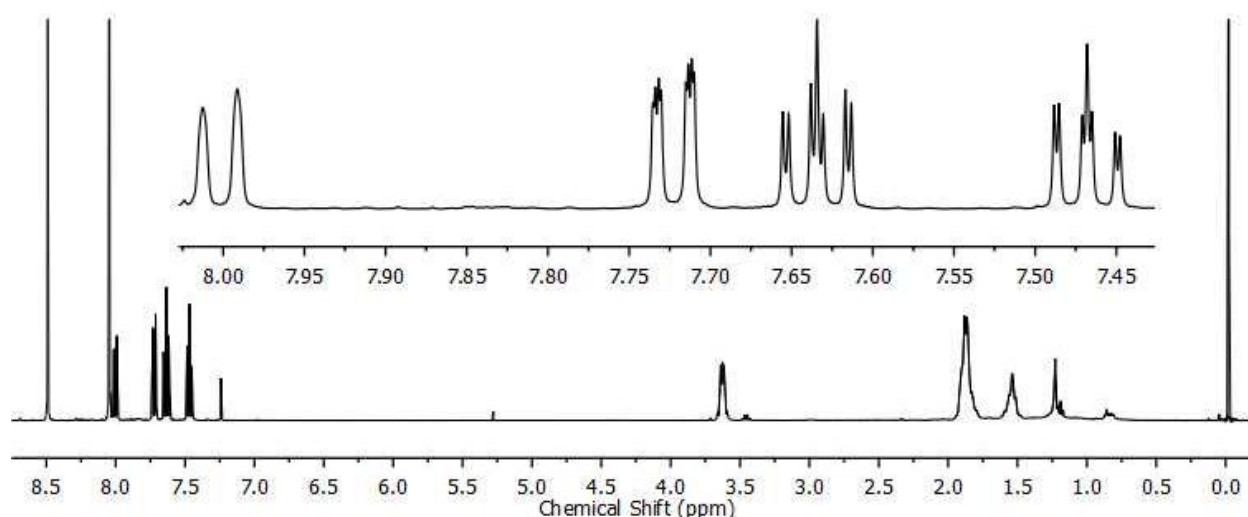
Figure 3.27: 400 MHz ^{1}H NMR Spectrum for Complex **19** (CDCl$_3$)

Subsequently, we conducted a HSQC experiment on complex **19** to see if we obtain the right number of proton to carbon coupling (Figure 3.28). Analysis of the spectrum obtained reveals seven proton to carbon correlations which is the right number of contour points expected for complex **19**. The analysis is the same as that obtained for the HSQC spectrum of pure unreduced ligand **1**. Once again, we observe the characteristic imine carbon peak isolated at 162.79 ppm due to the electron withdrawing nature of the nitrogen atom in the imine bond. The other six contour peaks are centered from 116.21 ppm to 137.72 ppm. The sharp proton signal at 8.08 ppm reveals the presence of two proton to carbon correlation points with the other four contour points well separated for analysis. This similarity in the HSQC spectra of ligand **1** and complex **19** suggests that no metallation occurred as there should be observable shifts in the contour peaks of the pure ligand and the chelated ruthenium(II) complex.
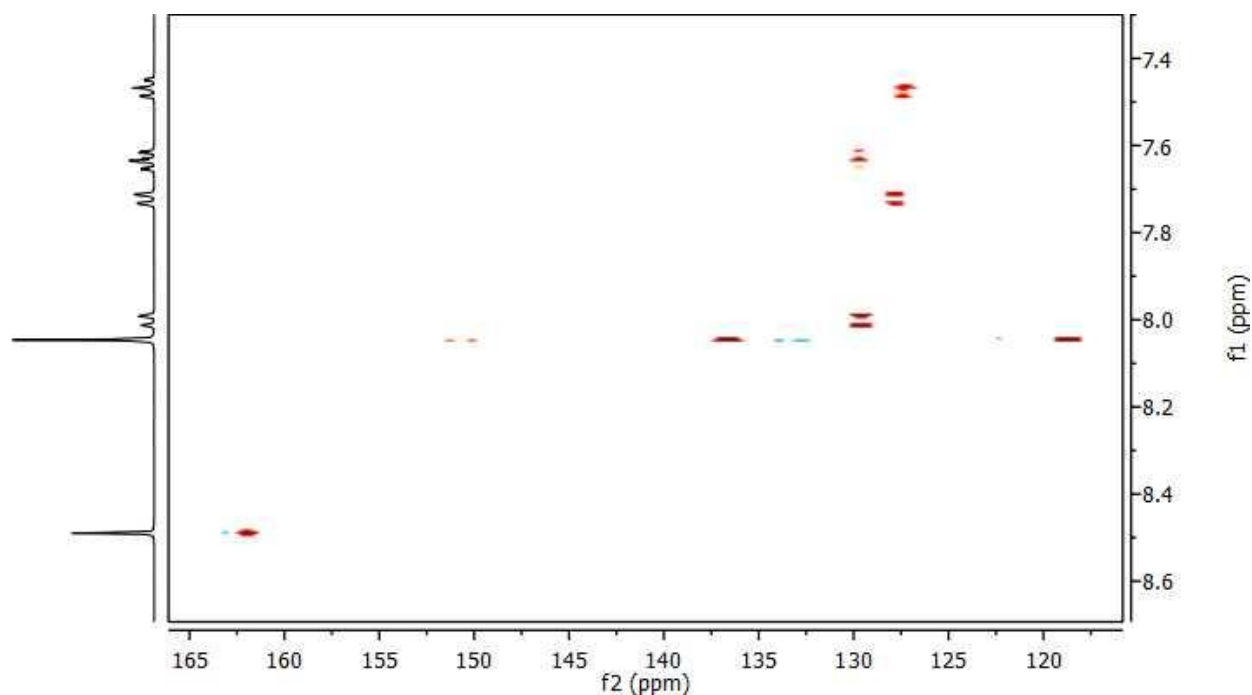
Figure 3.28: 400 MHz HSQC Spectrum for Complex **19** (CDCl₃)

The HSQC results prompted us to conduct a COSY experiment and observe any notable differences between ligand **1** and complex **19** (Figure 3.29). The coupling pattern obtained is similar to what was obtained for pure ligand **1** as shown in chapter two. Once again, we observe the expected ^{3}J coupling between protons and long range coupling of the imine proton to the quinoline side-arm but not to the cyclohexyl backbone. This coupling is attributed to the conjugation in the imine C=N bond allowing resonance conformers to carry on the observed conjugation. Two protons are located in the large peak at 8.06 ppm and we observe conjugation between the both of them. Both doublet of doublet peaks located at 7.47 ppm and 7.63 ppm show the expected ^{3}J coupling to their respective neighboring protons but also show one long range coupling to the last proton in the conjugated system.
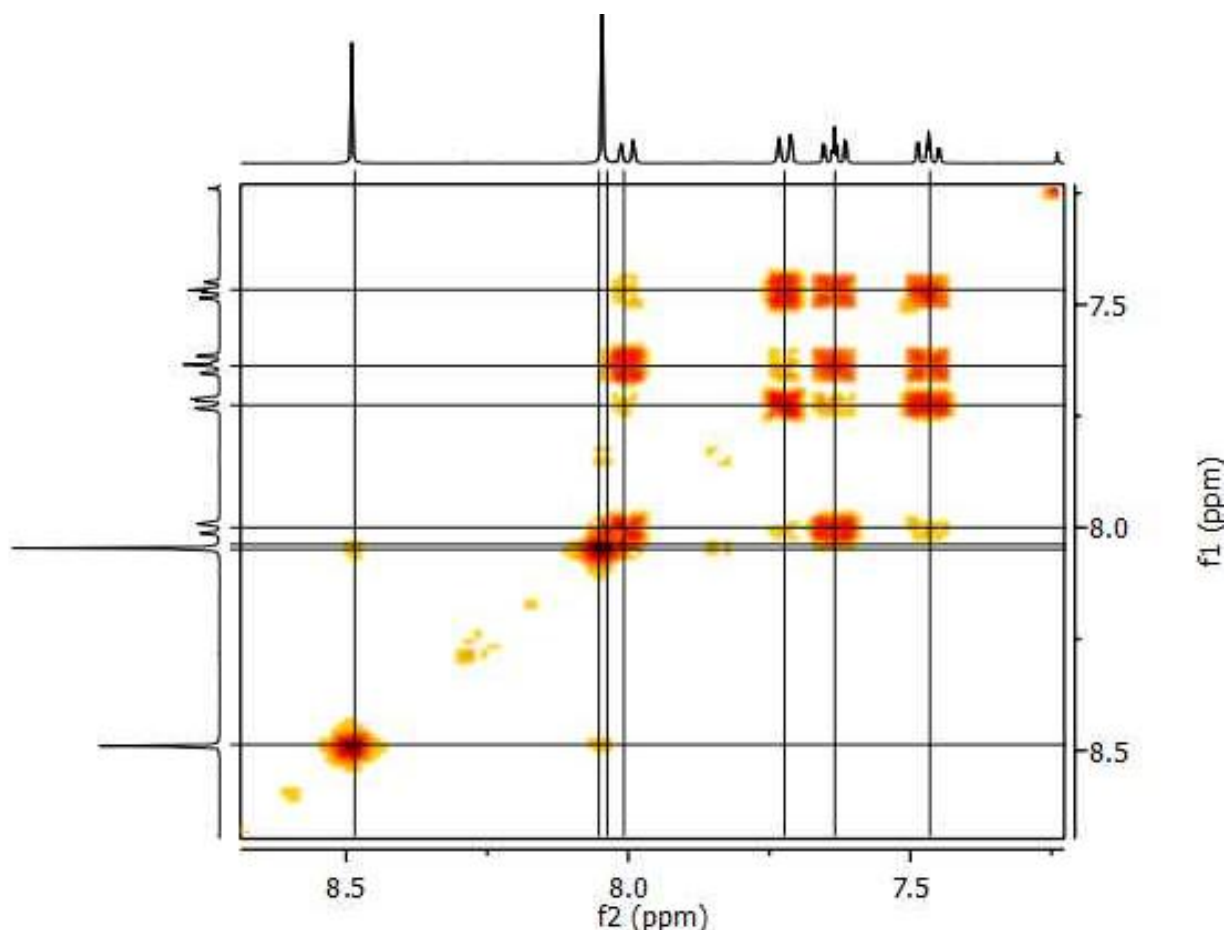
Figure 3.29: 400 MHz COSY Spectrum for Complex **19** (CDCl$_3$)

All experiments carried out so far, suggest the oxidation of ligand **11** back to ligand **1** with 1,5-octadiene as the possible source of protons for this transformation. The puzzling thing this about the ruthenium(II) reaction that does not agree with the 1D and 2D NMR analysis is the blue color of the product obtained. If pure ligand **1** was truly the synthesized product, then the product should have had a yellowish-brown color to it. To understand what happened during the reaction and what product was obtained, crystals suitable for X-ray analysis were grown using the solvent diffusion method with tetrahydrofuran as the base solvent and hexane layered on top. We obtained deep blue colored crystals and the thermal ellipsoid structure for complex **19** is shown in Figure 3.31. We observe that the ruthenium(II) cation binds to the ligand through all four nitrogen donor atoms causing the ligand to completely wrap around the metal center. We achieved part of our goal set forth on page 50 with the complete wrapping of the ligand but notice, as suggested in the various 1D and 2D NMR spectra obtained, the oxidation of the amine bond. As expected, we do not observe the presence of any 1,5-cyclooctadiene molecules in the coordination sphere as they were removed when complex **19** was pumped down on to remove solvent using the vacuum line. The crystal size for complex **19** is 0.22 x 0.14 x 0.08 mm^3 and is present as a monoclinic crystal system with a space group of C2. The two chloride cations from the ruthenium salt are attached as chloro ligands to the ruthenium(II) metal center in the structure. We observe a C_2 symmetric complex which is also confirmed in the ^{1}H NMR spectra obtained for complex **19**. The coordination information obtained from the crystal structure allowed us to modify the proposed reaction scheme to what is shown in Figure 3.30.
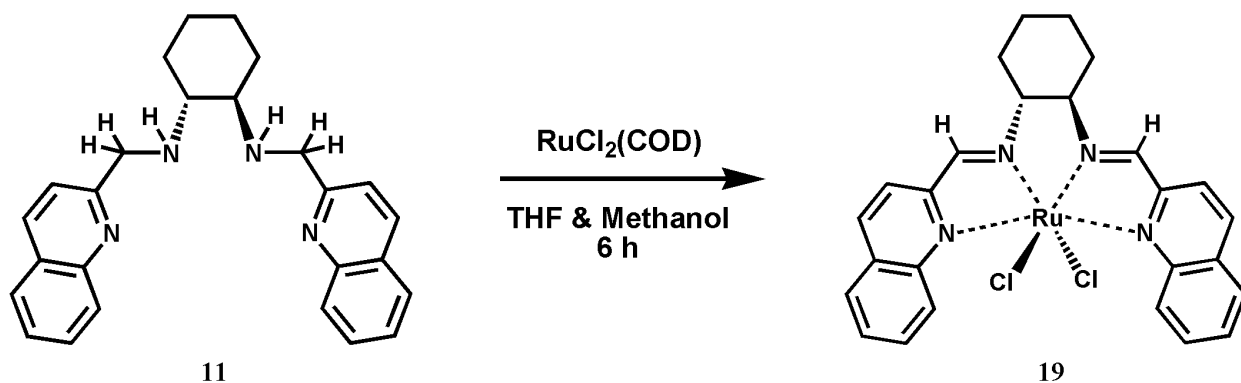
Figure 3.30: Observed Reaction Scheme for Ligand **11** with RuCl$_2$(COD)

The coordination geometry of the $4d^6$ ruthenium metal center is that of a distorted octahedron with a RuN_4Cl_2 core. The overall charge of the monoclinic complex is neutral. The bond lengths between the ruthenium metal center and nitrogen donor atoms in the imine bridge are shorter that the bond lengths between the ruthenium cation and the nitrogen donor atoms in the quinoline side-arm: 1.912 Å for Ru1-N212, 1.950 Å for Ru1-N211, 2.155 Å for Ru1-N111, and 2.204 Å for Ru1-N112. This may be due to the steric of the chloro ligands pushing the quinoline side-arms further apart. The bond length between the ruthenium metal and the chloro ligands are slightly off from each other with Ru1-Cl2 as 2.376 Å and Ru1-Cl1 as 2.413 Å. The cyclohexyl backbone is held in a chair form arrangement and it is worth noting the similar bond length of the imine nitrogen to the cyclohexyl carbon atoms. They are 1.50 Å for N211-C311 and 1.52 Å for N212-C312. The odd transformation of ligand **11** back to ligand **1** results in the following bond lengths for the imine bridge: 1.306 Å for C212-N212 and 1.275 Å for C211-N211. This is comparable to the average imine bond length of 1.293 Å observed in complex **13** and much shorter than the average amine C–N bond length of 1.473 Å.

The crystal structure provided us with some valuable information on important bond angles. The ruthenium metal center is coordinated to the four nitrogen donor atoms at the following angles: 76.8° for N211-Ru1-N111, 77.5° for N212-Ru1-N112, 88.8° for N212-Ru1-N211, 164.8° for N212-Ru1-N111, 165.16° for N211-Ru1-N112, and 117.3° for N111-Ru1-N112. The chloro ligands are held in an almost perpendicular manner with respect to the ruthenium metal center with the following angles: 90.2° for N112-Ru1-Cl2, 89.6° for N111-Ru1-Cl1, 88.0° for N112-Ru1-Cl1, and 87.6° for N212-Ru1-Cl1. The thermal ellipsoid model for complex **19** shown in Figure 3.32 displays the presence of two single stranded monohelices as desired. We observe that complex **18** is present in a ratio of 1:1mixture of *M* (left-handed) conformer and *P* (right-handed) conformer that have the same orientation relative to each other. The core difference lies in the orientation of their quinoline side-arms. The space filling model suggests that there are π–π and/or σ-π interactions present between the phenyl rings at the ends of the quinoline side-arms. The aromatic rings do not lie directly on top of each other but are slightly offset creating an ideal alignment that fosters a π-π interaction or σ-π interaction. Table 3.3 shows other bond distances, bond angles, and torsion angles for complex **19**. Complete crystal data and structure refinement information for complex **19** can be found in Appendix II.
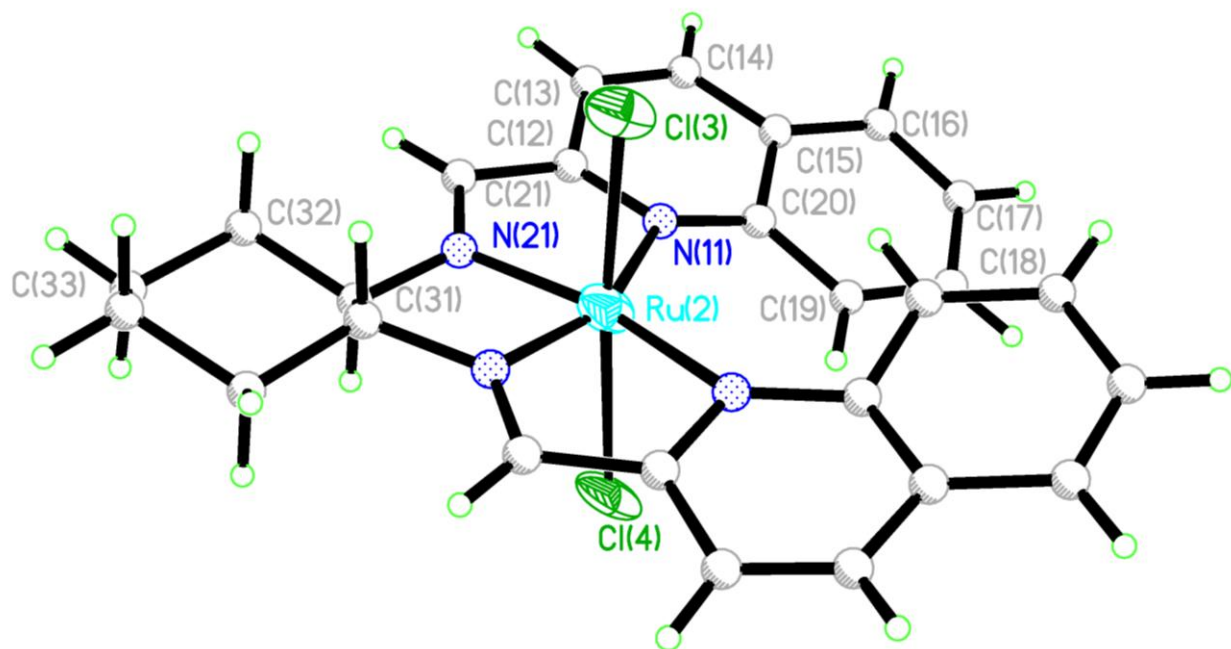
Figure 3.31: Thermal Ellipsoid Crystal Structure for Complex **19**
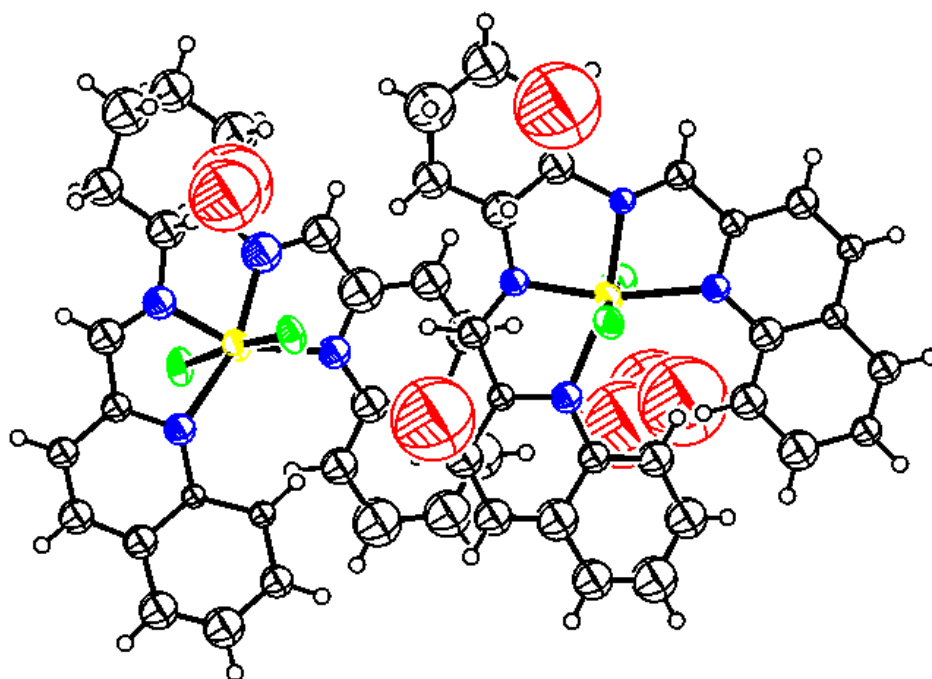
Figure 3.32: ORTEP Diagram for Complex **19** Showing 1:1 Mixture of *P*- and *M*- Helimers
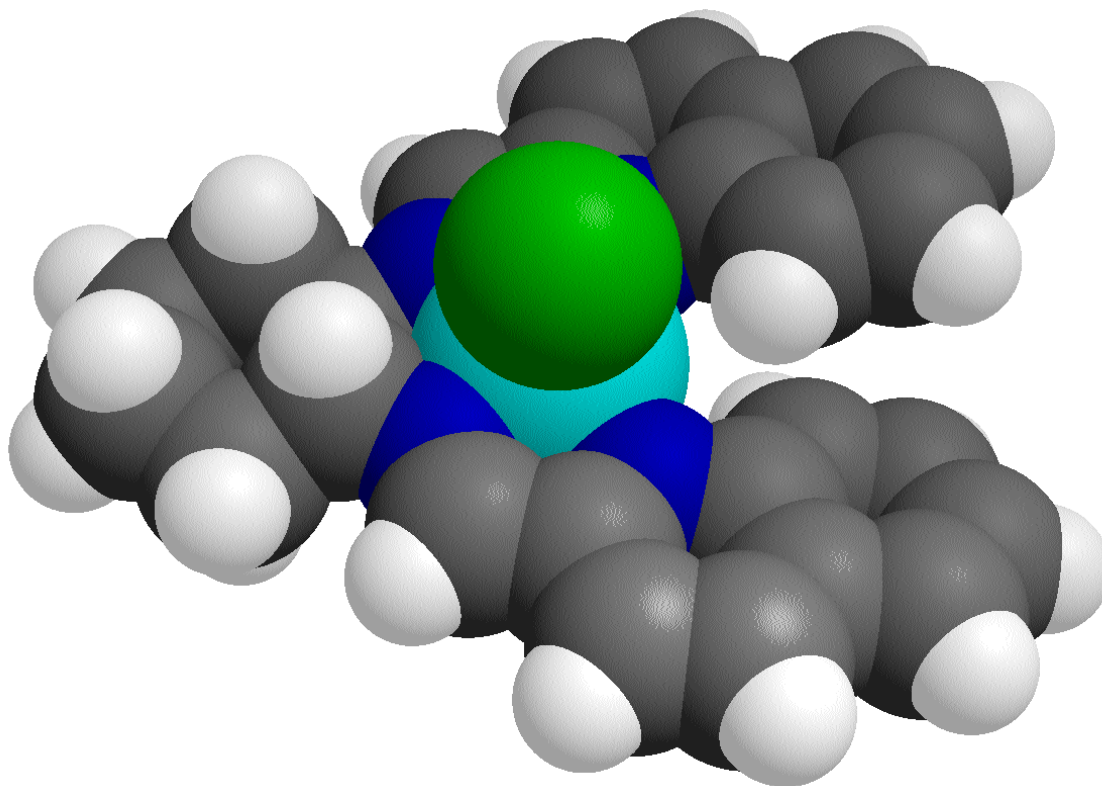
Figure 3.33: Space Filling Model Crystal Structure for Complex **19**

Bond Length	Ru$_1$-N$_{212}$	1.912(19)	Ru$_1$-Cl$_1$	2.413(10)
	Ru$_1$-N$_{211}$	1.950(16)	Ru$_1$-Cl$_2$	2.376(10)
	Ru$_1$-N$_{111}$	2.155(14)	Ru$_1$-N$_{214}$	1.894(19)
	Ru$_1$-N$_{112}$	2.204(15)	Ru$_1$-N$_{213}$	1.96(3)
Bond Angles	N$_{212}$-Ru$_1$-N$_{211}$	88.8(6)	N$_{212}$-Ru$_1$-N$_{112}$	77.5(6)
	N$_{212}$-Ru$_1$-N$_{111}$	164.8(6)	N$_{212}$-Ru$_1$-Cl$_2$	98.3(8)
	N$_{211}$-Ru$_1$-N$_{111}$	76.8(5)	N$_{211}$-Ru$_1$-Cl$_2$	86.0(6)
Torsion Angles	N$_{21}$-Ru$_1$-N$_{11}$-C$_{12}$	-30.0(4)	N$_{21}$-Ru$_1$-N$_{11}$-C$_{12}$	-11.8(17)

Table 3.3 Selected Bond Lengths (Å), Bond Angles, and Torsion Angles for Complex **19**

3.7 Complexation with Ni(OTf)$_2$
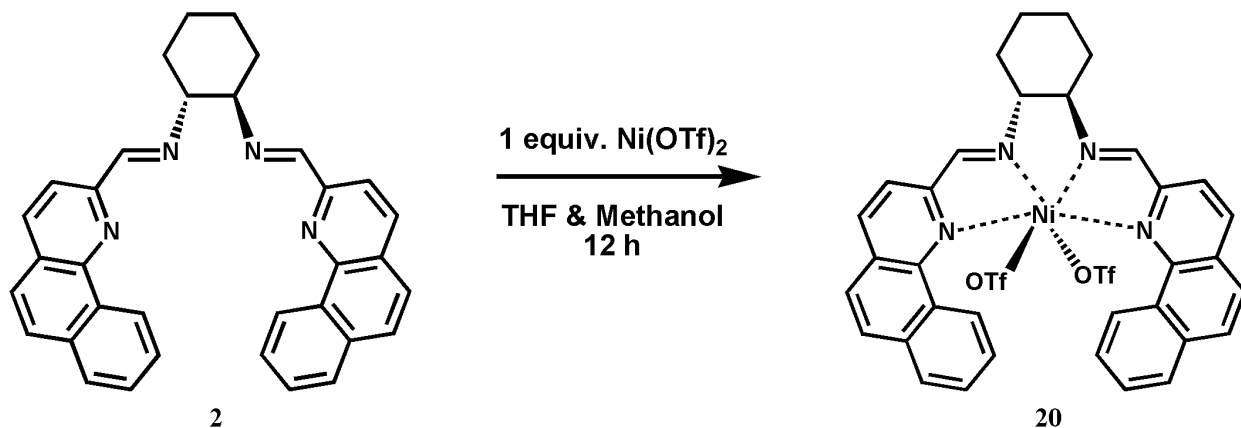
Figure 3.34: Proposed 1:1 Reaction Scheme for Ligand **2** with Ni(OTf)$_2$

The successful complexation reactions we achieved with ligand **11** encouraged us to investigate metallation reactions with the bigger, less flexible ligand **2**. We began with the 1:1 reaction with of ligand **2** with Ni(OTf)$_2$ to produced a yellowish-brown colored solid in 78.4 % yield. The ^{1}H NMR obtained for complex **20** is shown in Figure 3.35 and displays the formation of a paramagnetic compound as we observe resonances outside the normal diamagnetic chemical shift range. This is similar to the ^{1}H NMR results we obtained from the reaction of ligand **11** with nickel(II) salts. The reaction with Ni(OTf)$_2$ looks to have produced a impure complex as the number of peaks observed in the ^{1}H NMR spectrum is not as well defined as the reaction to produce complex **17**. Closer examination of the spectrum reveals that there might be unreacted ligand (**11**) left after the reaction as we observed sharp peaks in the normal aromatic region of the spectrum. This paramagnetic spectrum clearly indicates the presence of unpaired electrons eliminating the possibility of the formation of a square planar complex with NiI$_2$ but it does indicate that a nickel(II) complex, while impure, was formed during the reaction. Several attempts were made to obtain single crystals suitable for X-ray analysis using the solvent diffusion method and heating and cooling method to no avail. Electro-spray mass spectrometry conducted on complex **20** (Appendix II) did not indicate the presence of any of the following desired ions: $[C_{36}H_{28}N_4Ni(CF_3SO_3)]^+$, or $[C_{36}H_{28}N_4Ni]^{2+}$.
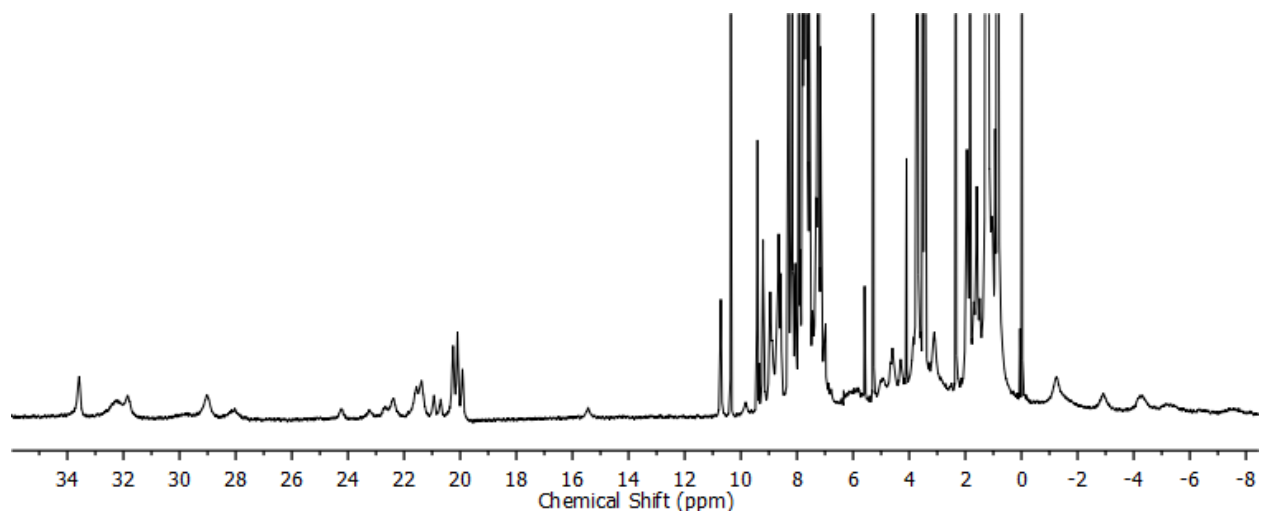
Figure 3.35: 400 MHz ^{1}H NMR Spectrum for Complex **20** (CDCl$_3$)

Given the unsuccessful reaction with one equivalent of nickel(II) triflate, the reaction was attempted with a 1:2 ratio of ligand to metal salt to give a brown colored product in 76.2 % yield, complex **21**. We carried out the reaction with two equivalents of nickel(II) salt as the ligand may prefer to bind to nickel in a dinuclear fashion. This could explain why the reaction with one equivalent of nickel salt produced a impure product with possible unreacted ligand as observed in Figure 3.35. The ^{1}H NMR obtained for the product is shown in Figure 3.37. Once again, we observe the presence of a paramagnetic compound with broad peaks and chemical shifts outside
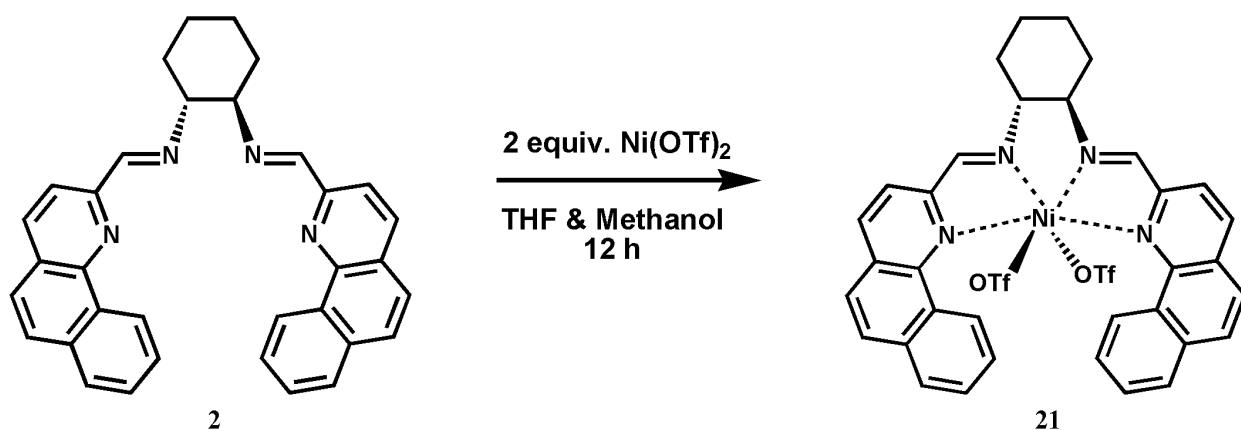
Figure 3.36: Proposed 1:2 Reaction Scheme for Ligand **2** with Ni(OTf)$_2$

78
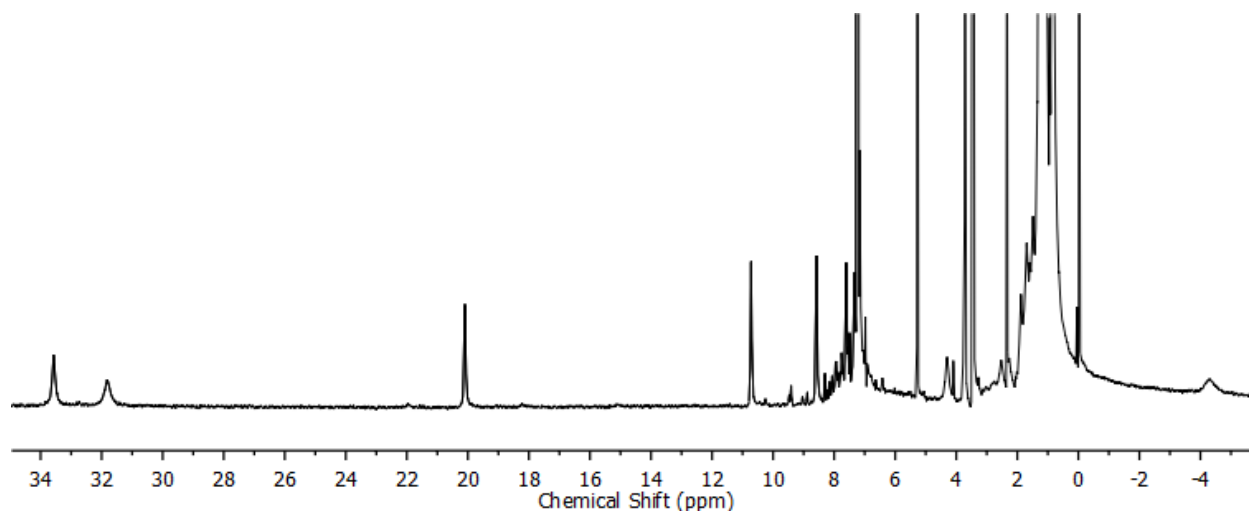
Figure 3.37: 400 MHz ^{1}H NMR Spectrum for Complex **21** (CDCl$_3$)

the normal diamagnetic chemical shift range. The spectrum obtained displays the synthesis of a pure complex compared to the ^{1}H NMR spectrum obtained for the one equivalent reaction. This could be due to the ligand binding with two nickel cations to form a dinuclear complex as proposed. We observe five peaks outside the normal diamagnetic chemical shift range at -4.01, 11.03, 20.08, 31.97, and 33.90 ppm. These are most likely due to the proton signals that are close in proximity to the nickel(II) metal center. Complete assignment of the ^{1}H NMR spectrum was not attempted due to the difficulty in interpreting highly broadened spectra. Several attempts were made at growing crystals using the solvent diffusion method with methylene chloride and tetrahydrofuran as base solvents layered with ethanol, methanol, ether, and chloroform with no success. The product might have to be further purified either by recrystallization methods or by running through a short silica plug to obtain a compound that can easily be crystallized using the solvent diffusion or heating and cooling method. Electro-spray mass spectrometry was conducted on complex **21** (Appendix II) and we did not observe the presence of any of the following desired ions: $[C_{36}H_{28}N_4Ni2(CF_3SO_3)_3]^+$, or $[C_{36}H_{28}N_4Ni2(CF_3SO_3)_2]^{2+}$. Reactions carried out by previous members of the Levy group indicate that complexation of nickel(II) triflate with our tetradentate ligands is possible and although complicated paramagnetic ^{1}H NMR spectra were also obtained, single crystals were grown that displays the tetradentate ligand binding to the nickel metal center forming a distinct double stranded helical complex.[61]
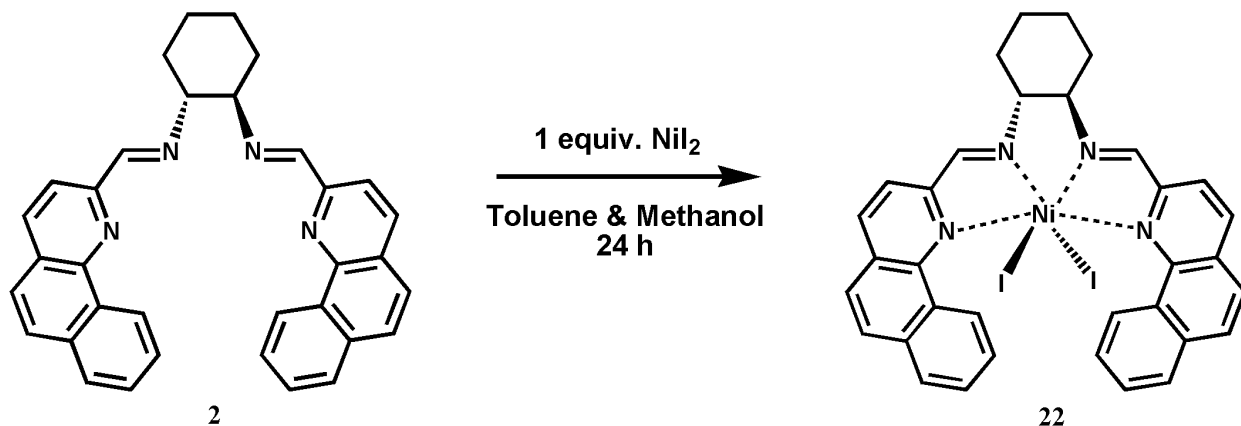
Figure 3.38: Proposed 1:1 Reaction Scheme for Ligand **2** with NiI$_2$

To improve the chances of obtaining a crystal structure of a nickel complex with ligand **2**, the counter-ion for the nickel metal was changed to iodide. Even though the iodide is a more coordinating counter-ion compared to the triflate counter-ion, many successful complexations have been achieved using nickel(II) triflate both in the literature[95] and with previous members of the Levy group.[61] Prior reactions with nickel(II) iodide resulted in 5-coordinate complexes that were unfortunately not single stranded monohelices. It is our goal here to improve on this work and synthesize a single stranded complex with all four nitrogen donor atoms bound to the metal center. The reaction of ligand **2** and NiI$_2$ was initially carried out with one equivalent of nickel salt to produce a dark blue colored product in 76.4 % yield, complex **22**. The ^{1}H NMR obtained for complex **22** is shown in Figure 3.39 and displays a spectrum that is not paramagnetic in character but consistent with the formation of an impure product or the result of an incomplete reaction. We were not able to analyze the spectrum as the proton signals were not well defined to assign any coupling present. Subsequent reactions conducted using the same reaction conditions, yielded the same poor ^{1}H NMR spectrum leading us to abandon the one equivalent reaction and attempt a reaction with two equivalents of metal salt. The idea is the same as what was proposed for the two equivalent reaction with NiI$_2$, the ligand may prefer to bind with two metal cations in the center and result in the formation of a dinuclear complex.
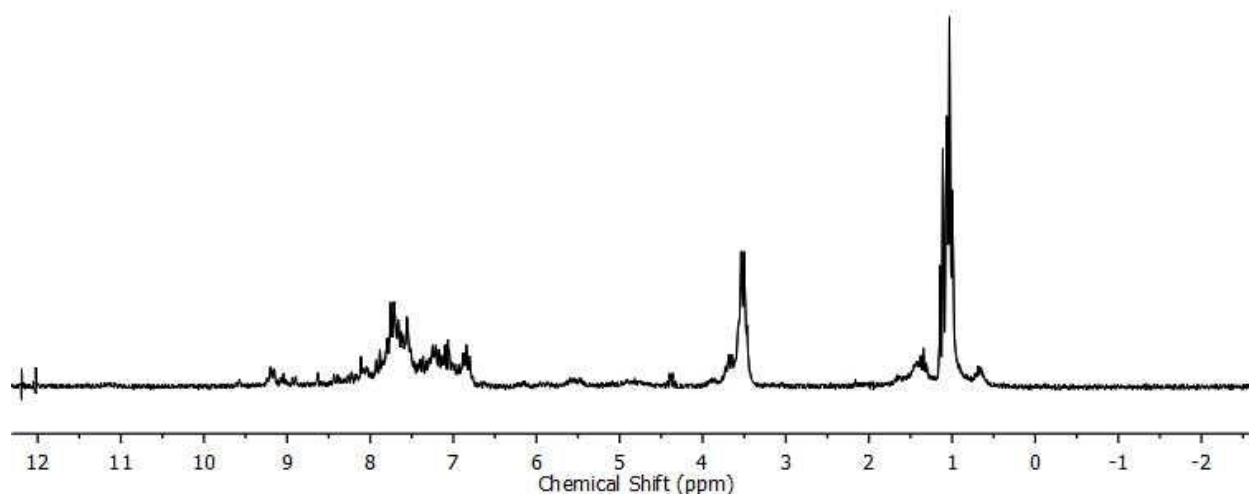
Figure 3.39: 400 MHz ^{1}H NMR Spectrum for Complex **22** (CDCl$_3$)

When the reaction was carried out with a 2 equivalents of metal salt, a green colored solution was obtained with a sand-brown precipitate present in the solution. The solution was subsequently filtered and vacuum dried to give both green colored solids in 48.2 % yield and sand-brown colored solids in 18.7 % yield. ^{1}H NMR was experiments were conducted on the two solids with the green solid spectrum shown in Figure 3.41 and the sand-brown colored solid spectrum shown in Figure 3.42. We obtain two different looking ^{1}H NMR spectra for the two colored solids with the green colored solid spectrum indicating the presence of more than one
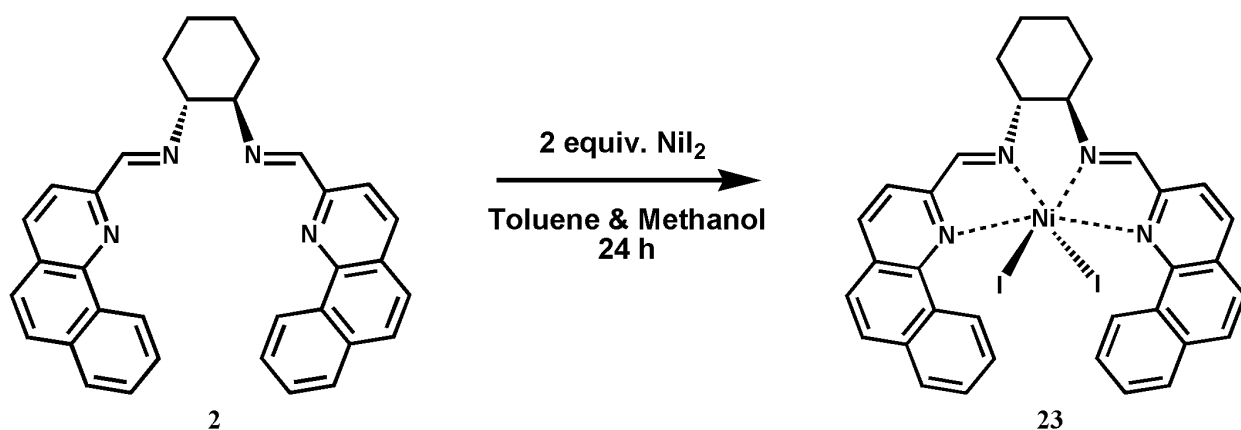
Figure 3.40: Proposed 1:2 Reaction Scheme for Ligand **2** with NiI$_2$

81
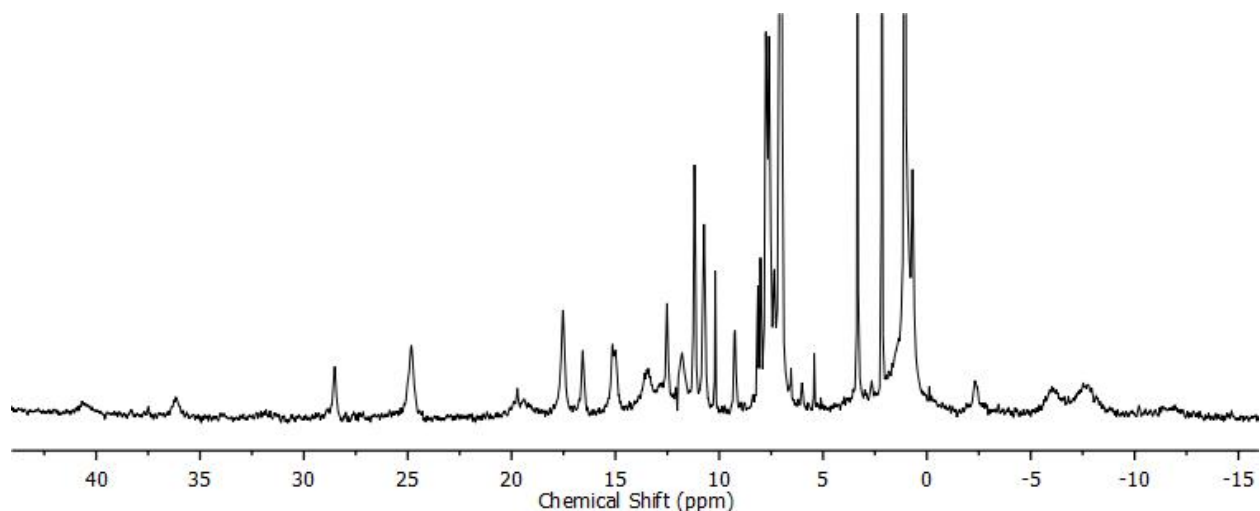
Figure 3.41: 400 MHz ^{1}H NMR of Green Colored Complex (CDCl$_3$)

complex in the product or the formation of a complex with broken symmetry. We clearly see more broad peaks present in the ^{1}H NMR spectrum of the green colored solid compared to the sand-brown colored solid. In comparison, the sand-brown colored solid show only six peaks that are outside the normal diamagnetic chemical shift range. This spectrum is also similar to previous ^{1}H NMR spectra obtained by other members of the Levy group during the reaction of nickel(II) iodide with tetradentate ligands. We observe similar peaks of the sand-brown solid in
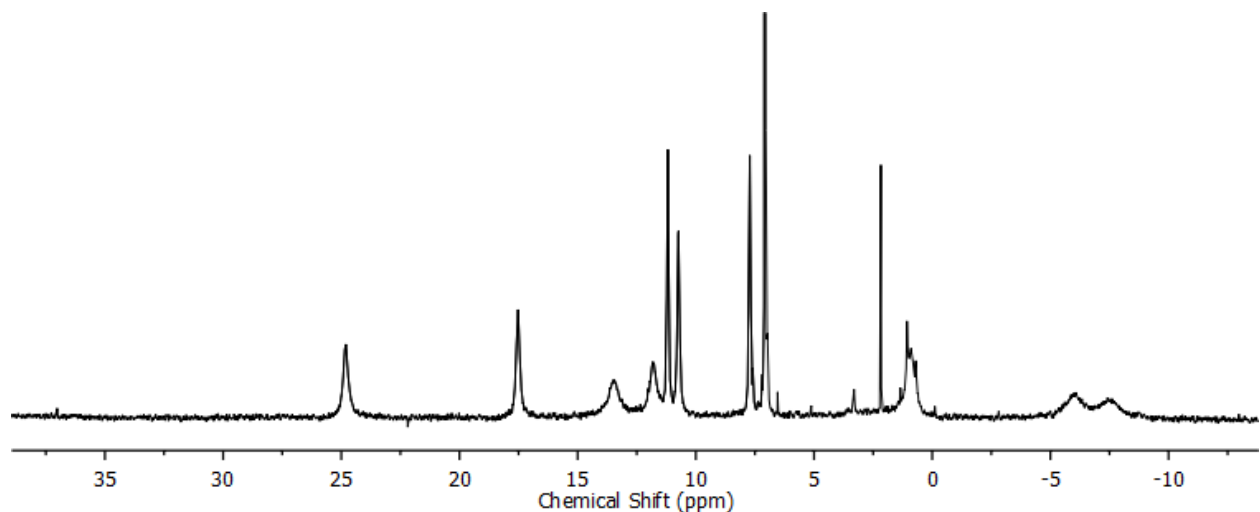
Figure 3.42: ^{1}H NMR of Sand-Brown Colored Complex (CDCl$_3$)

82

the ^{1}H NMR of the dark-green solid leading us to postulate that what we are occurring in the green-colored solution is the incomplete chelation of nickel(II) by ligand **2** , most likely bound to only three nitrogen donor atoms, to give a non-symmetric complex and as the reaction goes on, the metal binds to the last nitrogen donor atom and forms a C_2-symmetric complex that precipitates out of the solution as a sand-brown colored product.

Electro-spray mass spectrometry was carried out on the two colored complexes and we observe that the green colored complex exhibits the presence of the following species in ionic form: pure ligand **2** $[C_{36}H_{28}N_4]^+$, a complex with one nickel metal center and no iodide ligands $[C_{36}H_{28}N_4Ni]^{2+}$, a complex with one metal center and one iodide ligand $[C_{36}H_{28}N_4NiI]^+$, and a complex with one nickel(II) metal center and two iodide ligands $[C_{36}H_{28}N_4NiI^2]^+$ (Figure 3.43).
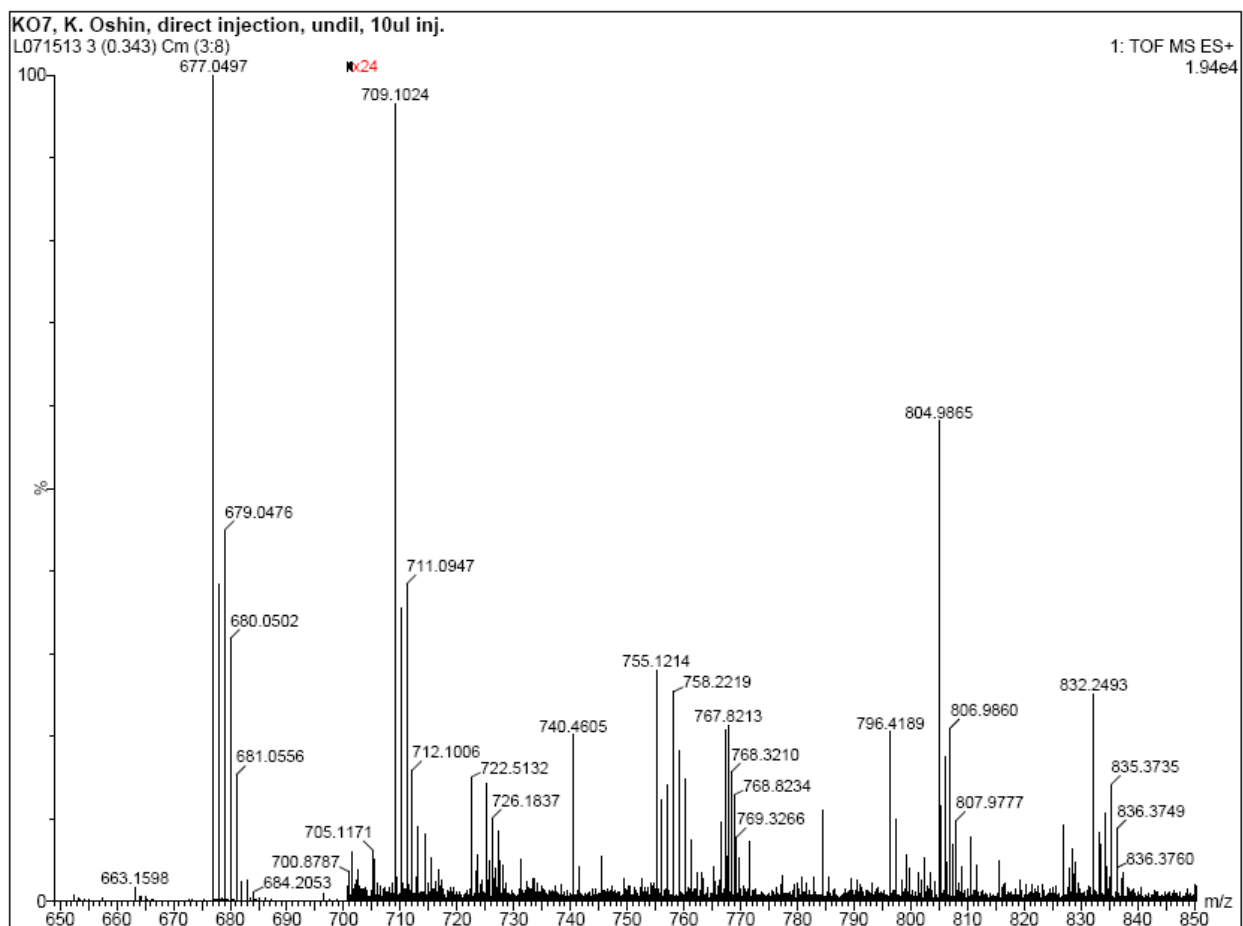
Figure 3.43: Electro-Spray Mass Spectrum for Green Colored Complex

The sand brown colored complex also exhibits the presence of pure ligand **2** $[C_{36}H_{28}N_4]^+$, and the presence of only one ionic species: a complex with one nickel(II) metal center and one iodide ligand $[C_{36}H_{28}N_4NiI]^+$ (Figure 3.44). According to the results, the fundamental difference between the two colored complexes is the presence of a compound containing one iodide ligand and a compound containing two iodide ligands that is present in the in the green colored complex spectrum. This could explain why the ^{1}H NMR spectrum of the green colored complex looks more complicated compared to the ^{1}H NMR spectrum of the sand-brown colored solid. The results obtained here support the idea that the ^{1}H NMR spectrum of the green colored solid reflects the presence of multiple compounds while the ^{1}H NMR spectrum of the sand-brown colored solid suggests the presence of a single pure compound.
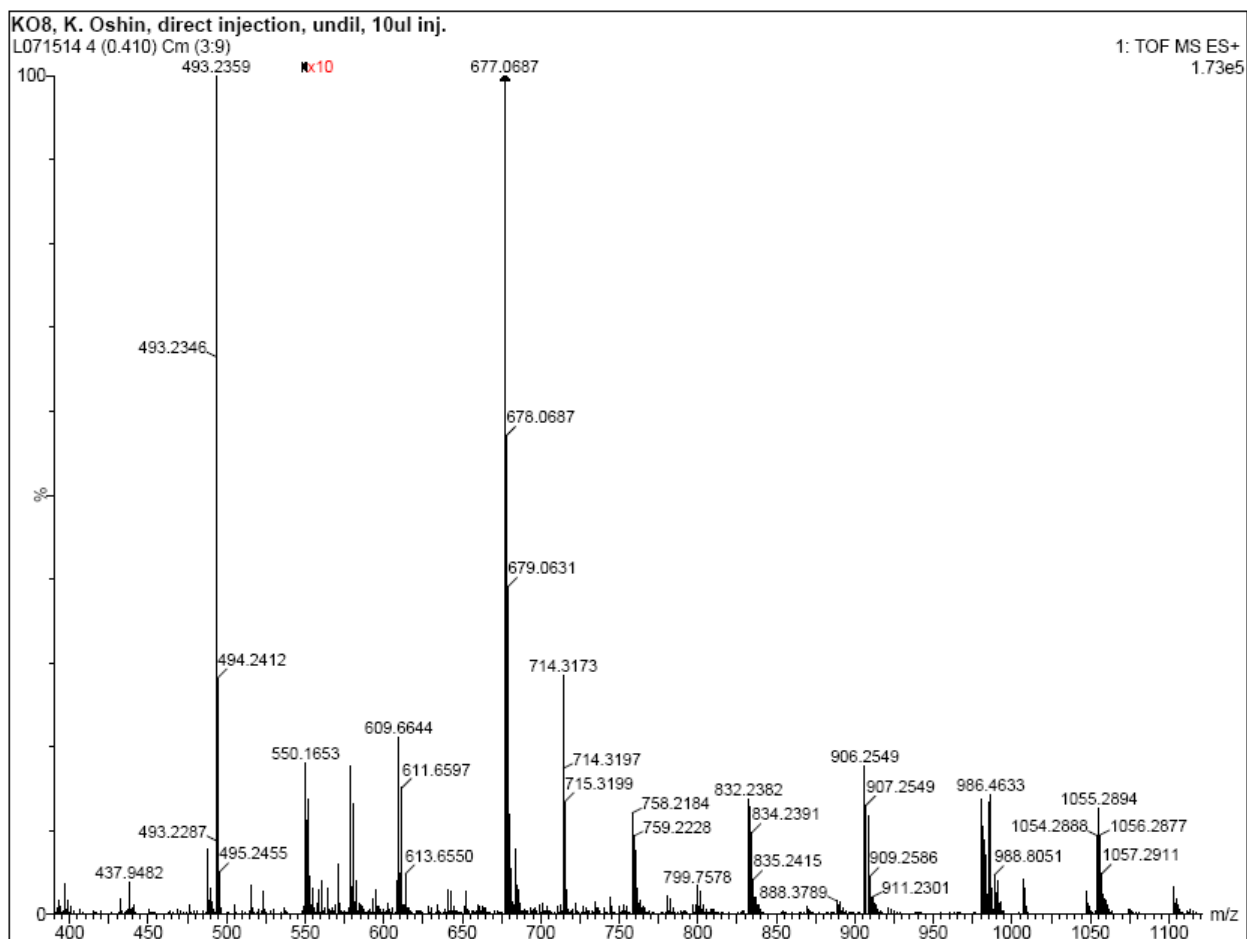
Figure 3.44: Electro-Spray Mass Spectrum for Sand-Brown Colored Complex

84

Single crystals were grown for both the green and sand-brown colored complexes with the green complex producing crystals of sufficient quality to conduct X-ray studies on. We obtained these crystals through the solvent diffusion method using methylene chloride as the base solvent with toluene layered on top. The crystals obtained for the sand-brown colored complex were also formed by the solvent diffusion method using methylene chloride layered with hexane. The sand-brown crystals were fine needle-like structures that decomposed when mounted for X-ray analysis. The green complex crystals on the other hand, produced the structure shown in figure 3.46. As observed with complex **14**, the metal center binds to only three nitrogen donor atoms leaving one benzoquinoline side-arm in an "unlocked" position. Two bound iodide ligands complete the coordination sphere and reveal a mononuclear 5-coordinate nickel complex. This may be due to the steric interactions from the iodide counter-ions but as seen with complex **18** and **19**, the side-arms can be made to wrap regardless of the counter-ions present on the metal center. The bulkier benzoquinoline side-arm in ligand **2** may therefore be the reason why complex **23** does not completely wrap.

The thermal ellipsoid structure displays a monoclinic crystal system with a P2(1) space group for complex **23**. The nickel(II) metal center coordinates to the three nitrogen donor atoms and two iodide ligands with trigonal bipyramidal geometry. We clearly see that one of the side-arms orients itself so as to twist outwards from the center of the complex to minimize the steric interaction of the two benzoquinoline side-arms. The bond lengths between the nickel(II) cation
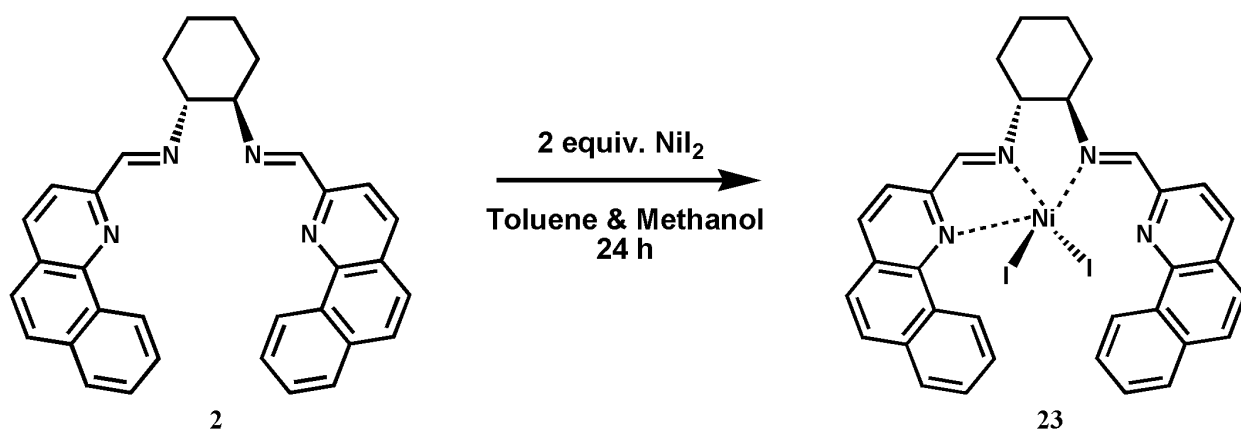
Figure 3.45: Observed Reaction Scheme for Green Colored Complex **23**

85

and the nitrogen donor atoms are as follows: 1.947 Å for Ni1-N25, 2.112 Å for Ni1-N45, and 2.202 Å for Ni1-N11. The bond lengths for the nickel(II) to the iodide ligands are comparably longer that those obtained for other complexes in this chapter and are as follows: 2.6402 Å for Ni1-I1 and 2.651 Å for Ni1-I2. The imine bond length of the bound benzoquinoline side-arm is 1.264 Å while that of the unbound side-arm is 1.265 Å. This is comparable to the C–N bond lengths obtained from other complexes in this chapter. The bond angle for the metal center with the two iodide ligands is 151.44^o, which is significantly greater that the angle obtained for the similar 5-coordinate zinc(II) complex **14** (122.8^o). Table 3.3 shows other important bond distances, bond angles, and torsion angles for complex **23**. Complete crystal data and structure refinement information for complex **23** can be found in Appendix II.
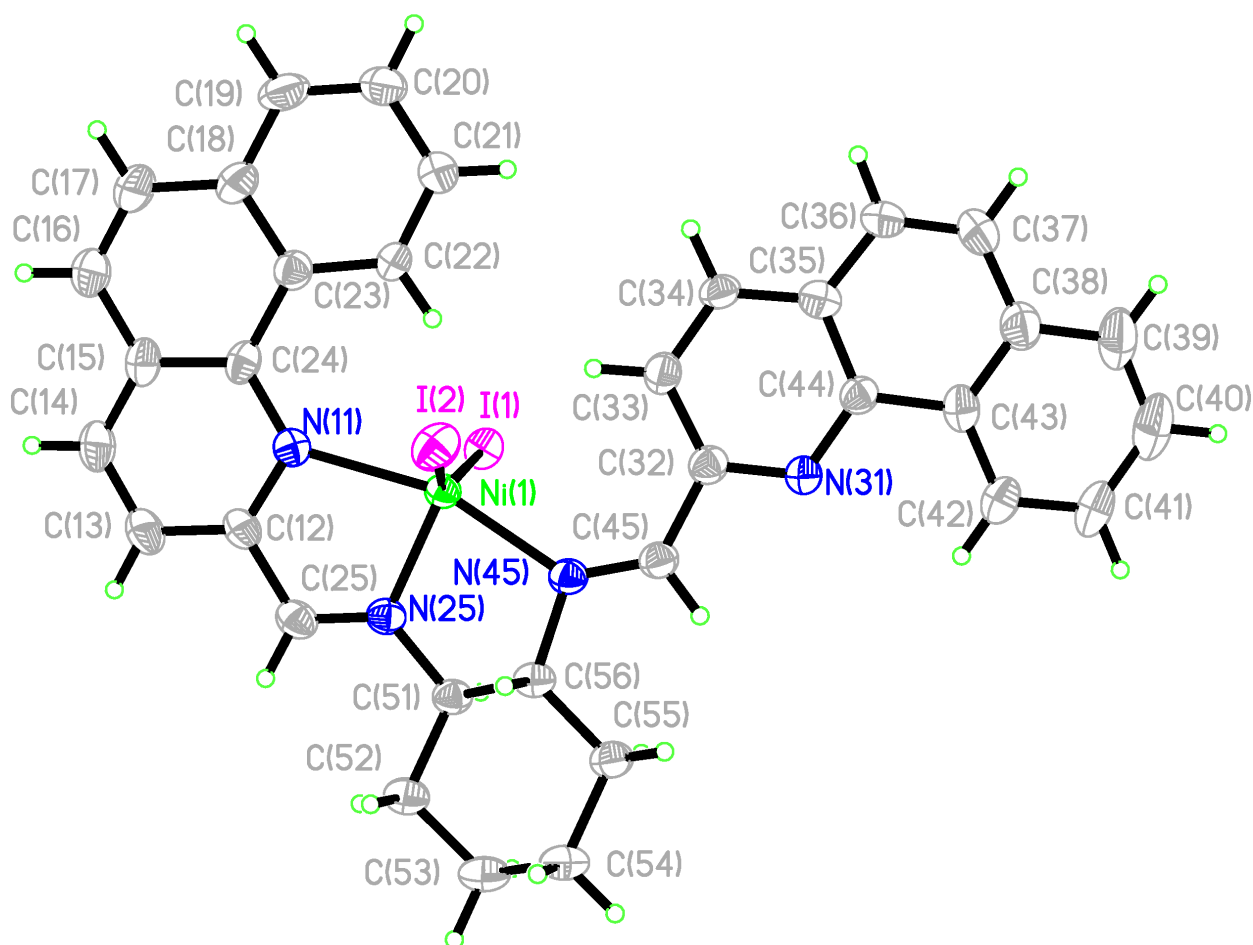
Figure 3.46: Thermal Ellipsoid Crystal Structure for Complex **23**
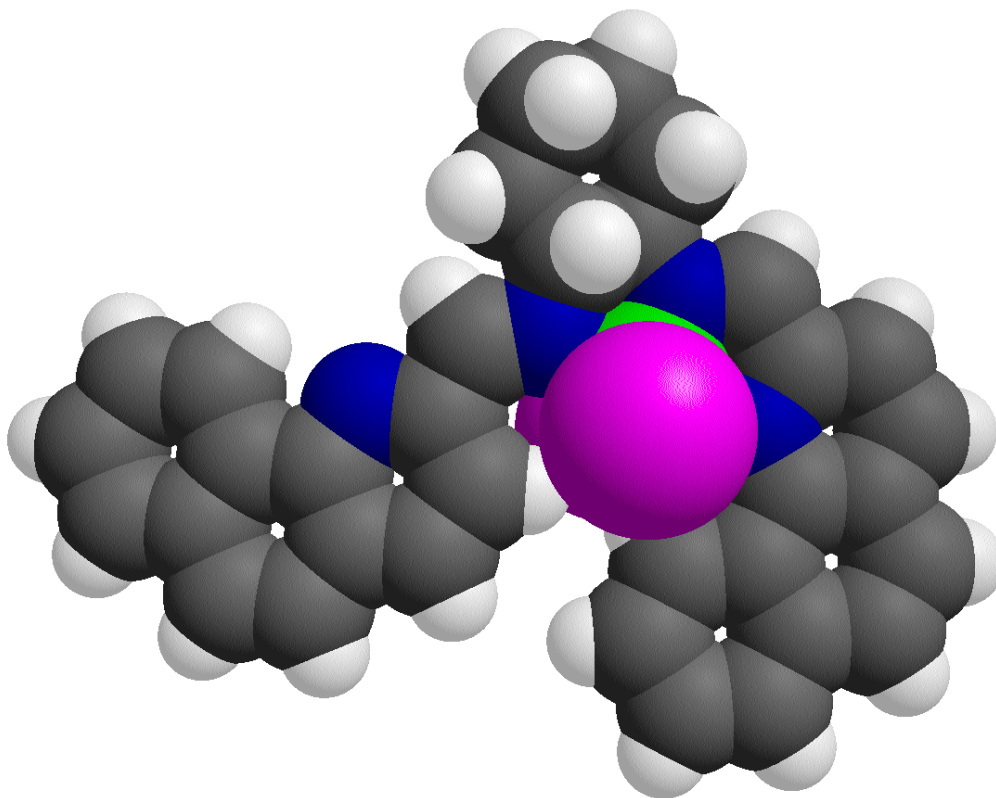
Figure 3.47: Ball & Stick and Space Filling Crystal Structures for Complex **23**

Bond Length	Ni_1-N_{25}	1.947(3)	Ni_1-I_2	2.652(5)
	Ni_1-N_{45}	2.112(3)	$C_{12}-N_{11}$	1.352(6)
	Ni_1-N_{11}	2.202(4)	$C_{24}-N_{11}$	1.362(6)
	Ni_1-I_1	2.640(6)	$C_{25}-N_{12}$	1.476(6)
Bond Angles	$N_{25}-Ni_1-N_{45}$	81.94(14)	$N_{25}-Ni_1-N_{11}$	97.77(9)
	$N_{25}-Ni_1-N_{11}$	80.60(14)	$I_1-Ni_1-I_2$	151.44(2)
	$N_{45}-Ni_1-N_{11}$	162.01(14)	$C_{24}-N_{11}-Ni_1$	124.4(4)
Torsion Angles	$N_{25}-Ni_1-N_{11}-C_{12}$	2.0(3)	$N_{45}-Ni_1-N_{11}-C_{12}$	-12.1(5)

Table 3.4 Selected Bond Lengths (Å), Bond Angles, and Torsion Angles for Complex **23**

The crystal structure obtained for complex **23** shows a non-symmetric compound but the ^{1}H NMR spectrum obtained in Figure 3.42 does not reflect this occurrence. It is possible that when in solution, complex **23** has enough mobility to completely wrap or the nickel metal center "hops" around different nitrogen donor atoms at different times and what we observe in the ^{1}H NMR spectrum is an average signal of this motion. This scenario has the nickel(II) cation bound to only three donor atoms as shown in the crystal structure but when in solution binds to all four nitrogen donor atoms but with only three at one time. Essentially we might be observing what is shown in Figure 3.48. The interesting thing about this model is that it provides a scenario where two of the possible fluxional structures have the benzoquinoline side-arms completely wrapped as the nickel(II) metal center binds to at least two of the nitrogen donor atoms from the two side-arms at once. The other two possible fluxional structures will have at least one of the benzoquinoline side-arms in an "un-locked" position.

To explore this fluxional possibility, a variable temperature NMR experiment was conducted on complex **23** with the goal of freezing out one the equilibrating complexes to cause a shift in the proton signals observed (Figure 3.49). If the nitrogen atom on one of the side-arms is unbound, then the spectrum should reflect a complex with broken symmetry and we would expect to double the number of proton resonances displayed in the ^{1}H NMR spectrum. As observed in the VT-NMR obtained, we do not see a doubling of the proton signals as we freeze the sample to 183 K, suggesting that we have a complex where the nickel(II) cation is bound to all four nitrogen donor atoms producing a C_2-symmetric complex. We observe that the complex losses some of its paramagnetic character as we slowly cool the sample. This is evident in the disappearance of the proton signals that are located outside the normal diamagnetic chemical shift range. Some peaks within the normal chemical shift range of 0.00 ppm to 14.00 ppm show changes during this experiment. For example, the peak located at 9.92 ppm progressively gets broader as we cool to 183 K and starts to split into multiple peaks at 248 K. This may be due to the severe overlap of protons in similar coupling environments finally being separated out as the temperature gets low enough to slow down their motion making them distinct. We also observe the sharp peaks at 13.00 ppm become more defined at 248 K with an extra peak separated out but as we cool down to 233 K, those well defined peaks coalesce into one broad peak at 14.00 ppm. As we continue to cool down the sample, the broad peak disappears at 193 K, this is also when

the peak at 9.92 ppm becomes broader. So we could be observing the motion of these broad paramagnetic peaks into the normal diamagnetic chemical shift range. If a non-symmetric complex is truly present in solution, another explanation for not obtaining a ^{1}H NMR spectrum with twice the number of peaks after cooling is that we were not able to freeze out the non-symmetric nickel(II) complex at the low end of our temperature range. We used deuterated methylene chloride as our NMR solvent which has a freezing point of -95 $^{\circ}$C and carried out the variable temperature experiment to a temperature of -90 $^{\circ}$C.
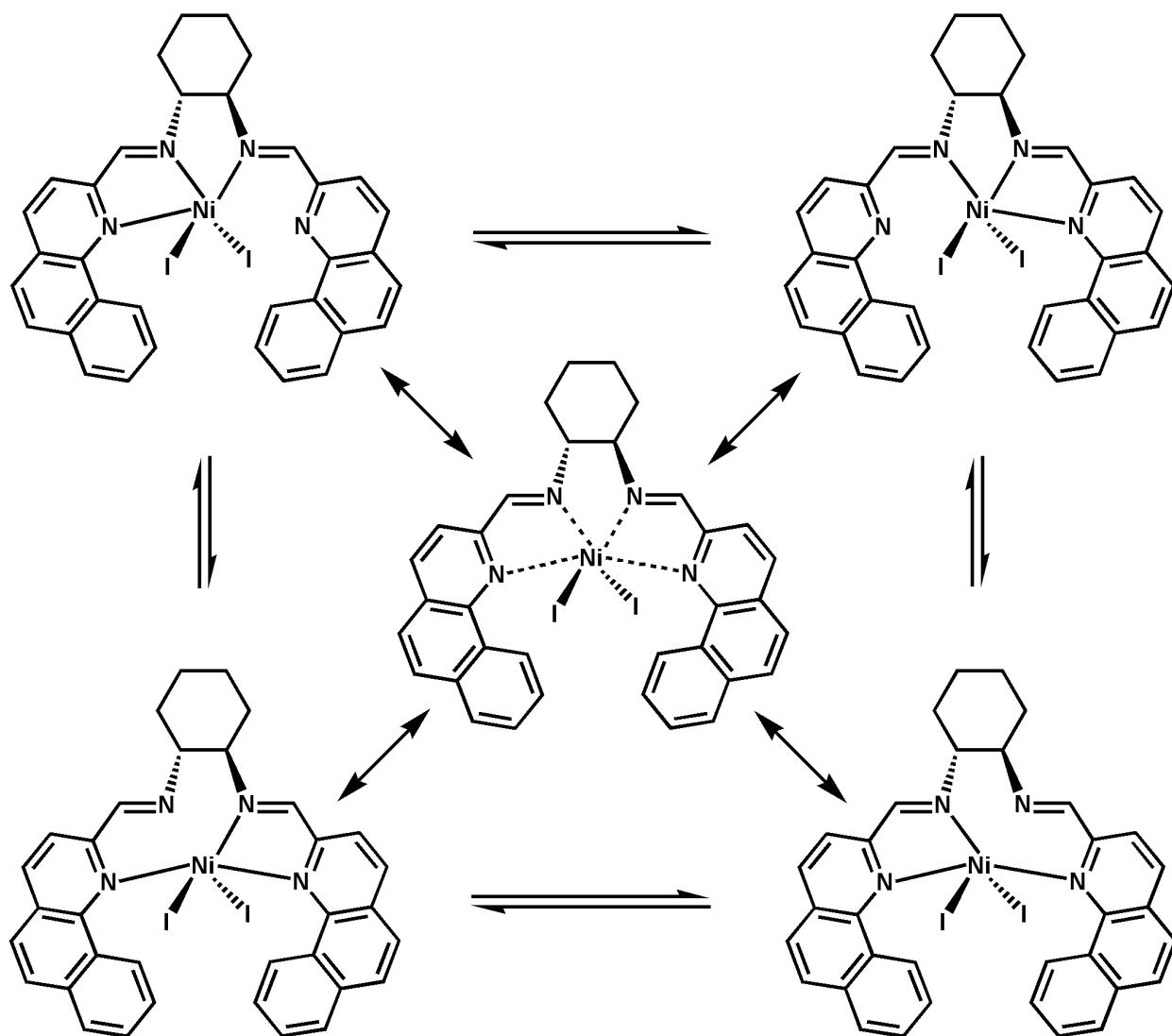
Figure 3.48: Fluxional Nickel(II) Coordination Possibilities for Complex **23**
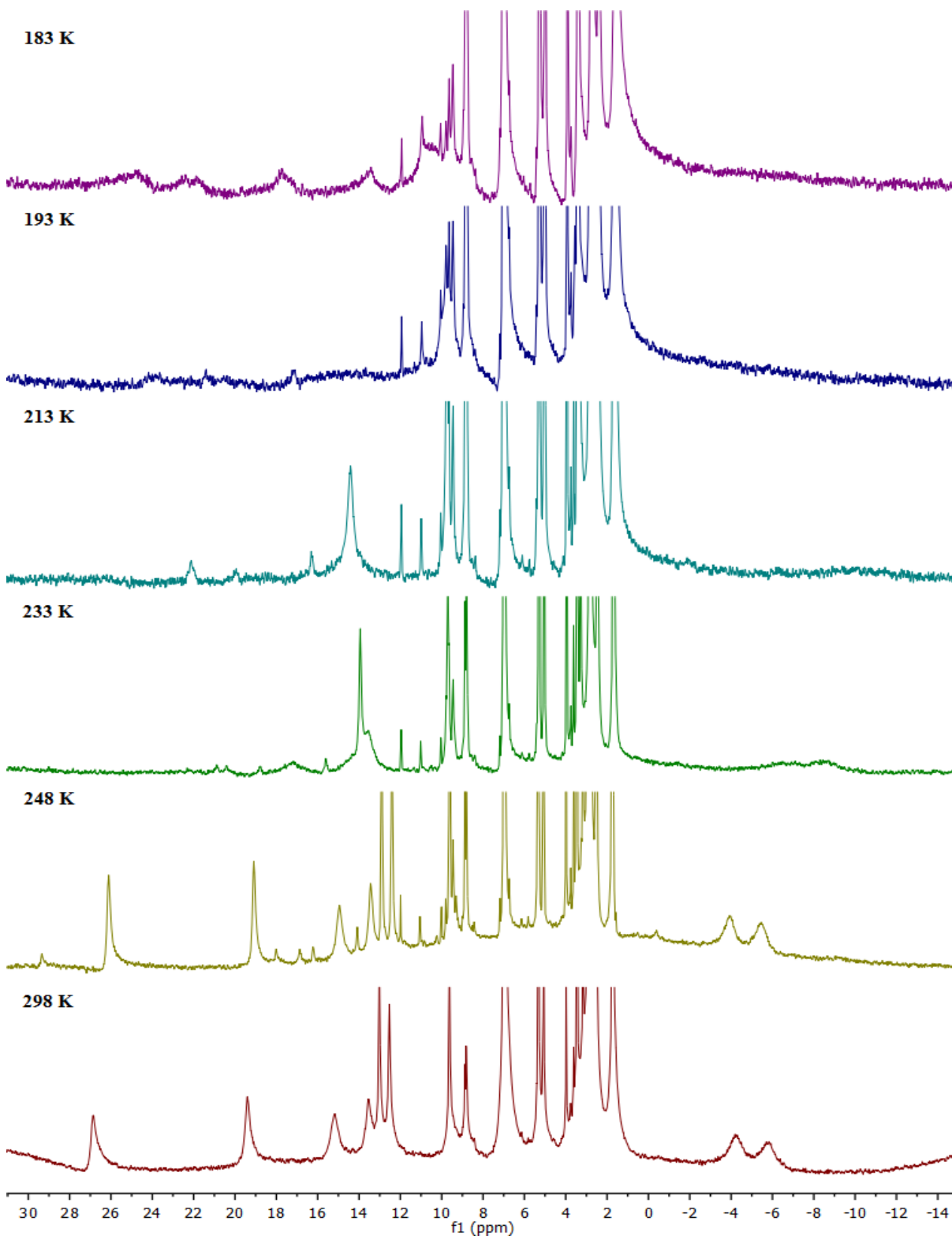
Figure 3.49: Variable Temperature Experiment Conducted on Complex **23** (CD_2Cl_2)

3.9 Complexation with AuCl$_3$
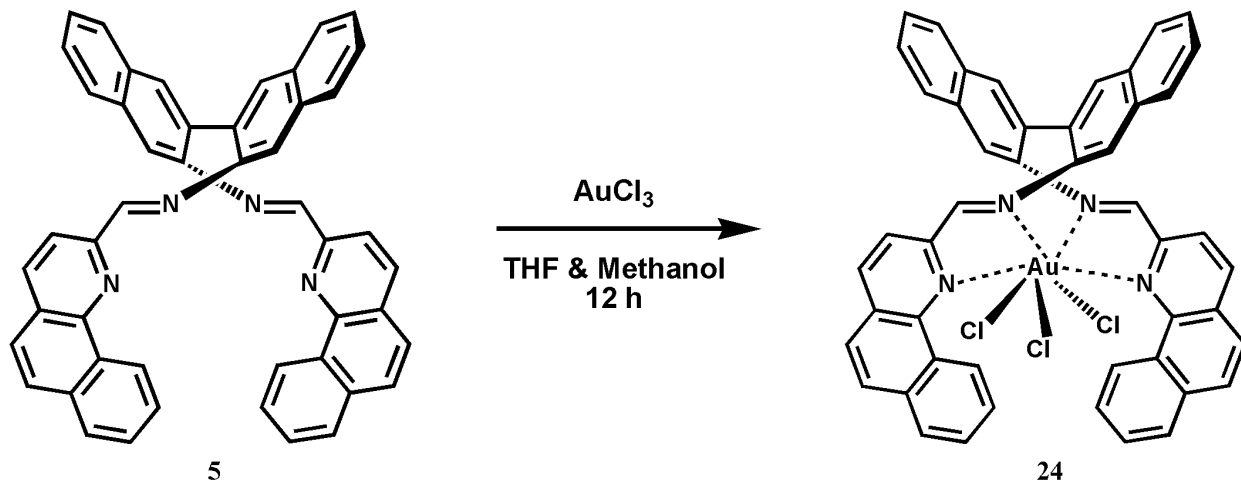
Figure 3.50: Proposed Reaction Scheme for Ligand **5** with AuCl$_3$

The last set of reactions will focus of the use of a C_2-symmetric ligand that incorporates a binaphthalene backbone in its structure. We hope to obtain a library of complexes that can be used as catalysts in various asymmetric reactions. This report will focus only on their synthesis and characterizations with catalytic reactions to be carried out at a later time. The reaction of ligand **5** with AuCl$_3$ produced a yellowish colored product in 68.2 % yield. The observed color change is a good indication that a complexation reaction occurred. The ^{1}H NMR spectrum obtained for complex **24** shows a drastic change to the aromatic peak region supporting the notion that a complexation reaction did occur (Figure 3.51). We observe the disappearance of the distinctive imine singlet peak that is present at 8.51 ppm in the ^{1}H NMR spectrum of the corresponding ligand **5**. Although a reaction did occur, we concluded that it is not of our desired complex but rather a new compound with significantly less polyaromatic conjugation than what we have present in the corresponding ligand **5**. We carried out a HSQC experiment to observe the proton to carbon correlations in complex **23** (Figure 3.52). We clearly see seven contour points in the spectrum, which is less than the fifteen contour points obtained in the HSQC spectrum for ligand **5**. The distinct contour point corresponding to the imine carbon, located at 135.00 ppm in ligand **5**, is also missing in the HSQC spectrum for complex **24**.
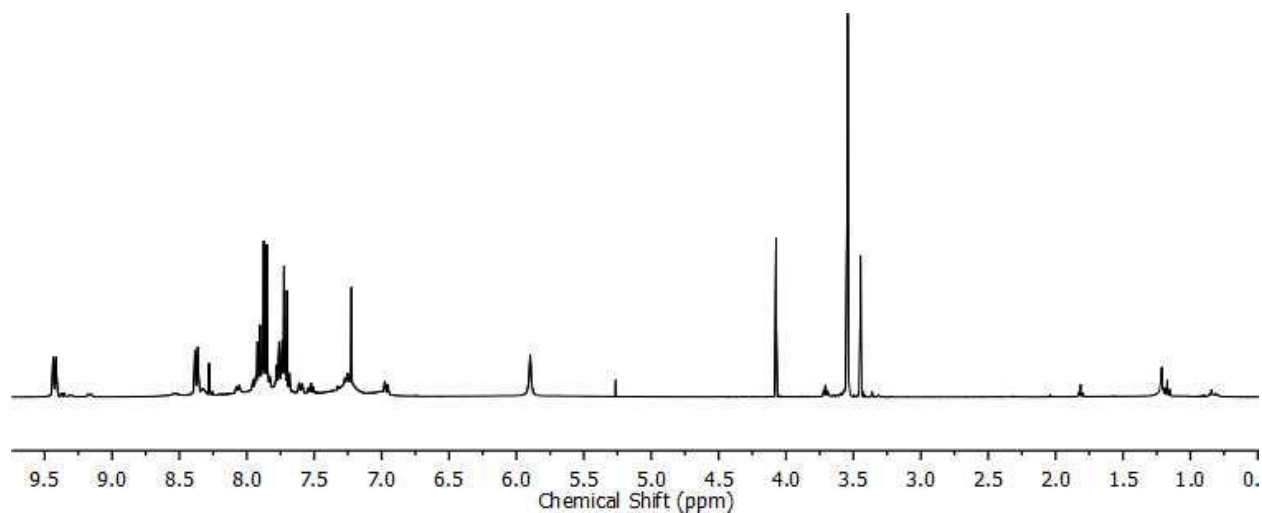
Figure 3.51: 400 MHz ^{1}H NMR Spectrum for Complex **24** (CDCl$_3$)

A COSY experiment was conducted for complex **24** and we observe significant coupling of the protons with each other (Figure 3.53). The coupling pattern obtained could not be use to solve the structure of complex **24**. When compared to the COSY spectrum obtained for ligand **5**,
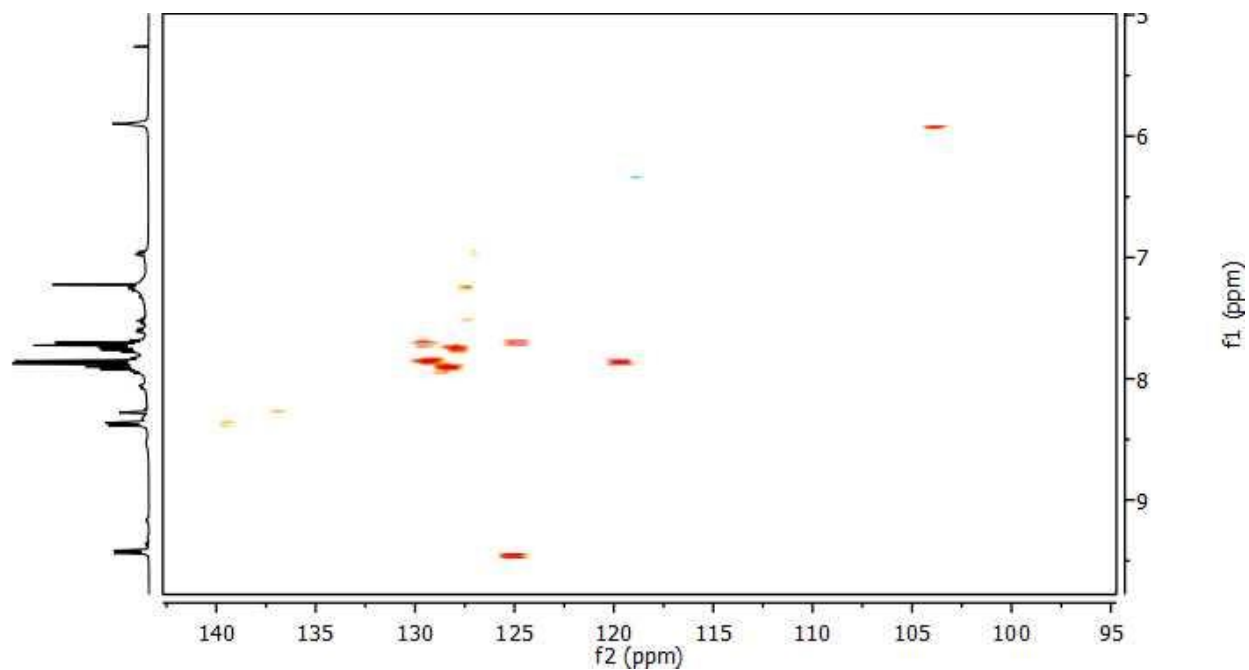
Figure 3.52: 400 MHz HSQC Spectrum for Complex **24** (CDCl$_3$)

92

we notice the loss of the observed ^3J coupling between protons ($1{\rightarrow}2$, $2{\rightarrow}3$, $3{\rightarrow}4$, $5{\rightarrow}6$, $8{\rightarrow}9$, $10{\rightarrow}11$, $11{\rightarrow}12$, $12{\rightarrow}13$, and $13{\rightarrow}14$) in ligand **5**. We also observe the presence of some para, peri, epi, and through-space long range couplings reflected in our previous systems in chapter two but do not observe the pattern displayed in ligand **5** for the following sets of protons ($1{\rightarrow}3$ {meta}, $1{\rightarrow}4$ {para}, $1{\rightarrow}5$ {epi}, $6{\rightarrow}7$ {through-space}, $7{\rightarrow}8$ {through-space}, $11{\rightarrow}12$ {peri}, $15{\rightarrow}13$ {meta}, $15{\rightarrow}12$ {para}, and $15{\rightarrow}11$ {epi}). Electro-spray mass spectrometry was carried out on complex **24** (shown in Appendix I) and we obtained a spectrum that did not indicate the presence of any of the following desired ions: $[C_{48}H_{30}N_4Au]^{3+}$, $[C_{48}H_{30}N_4AuCl]^{2+}$, $[C_{48}H_{30}N_4AuCl_2]^+$, and $[C_{48}H_{30}N_4AuCl_3]^+$
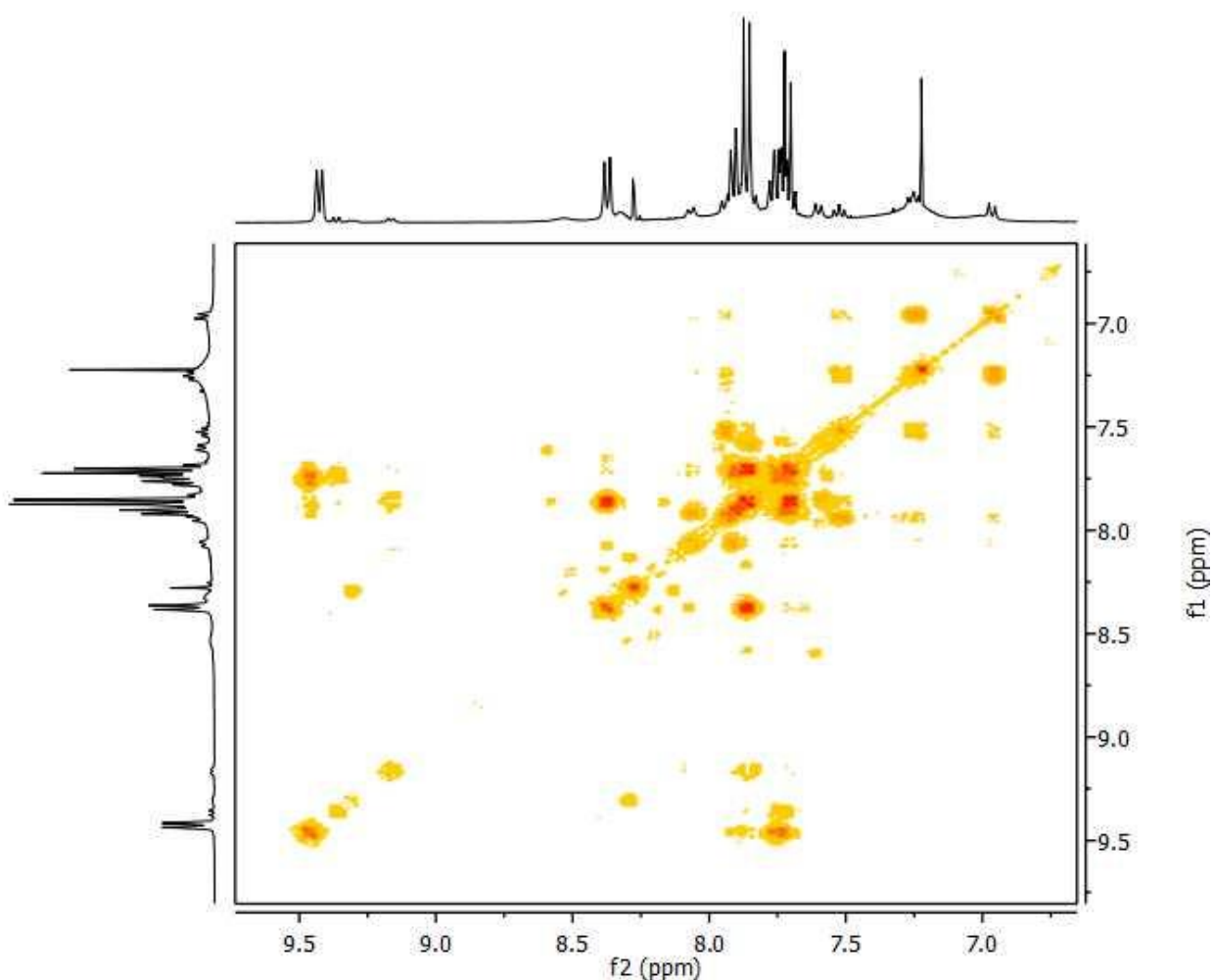
Figure 3.53: 400 MHz COSY Spectrum for Complex **24** (CDCl$_3$)

3.10 Complexation with HgBr$_2$
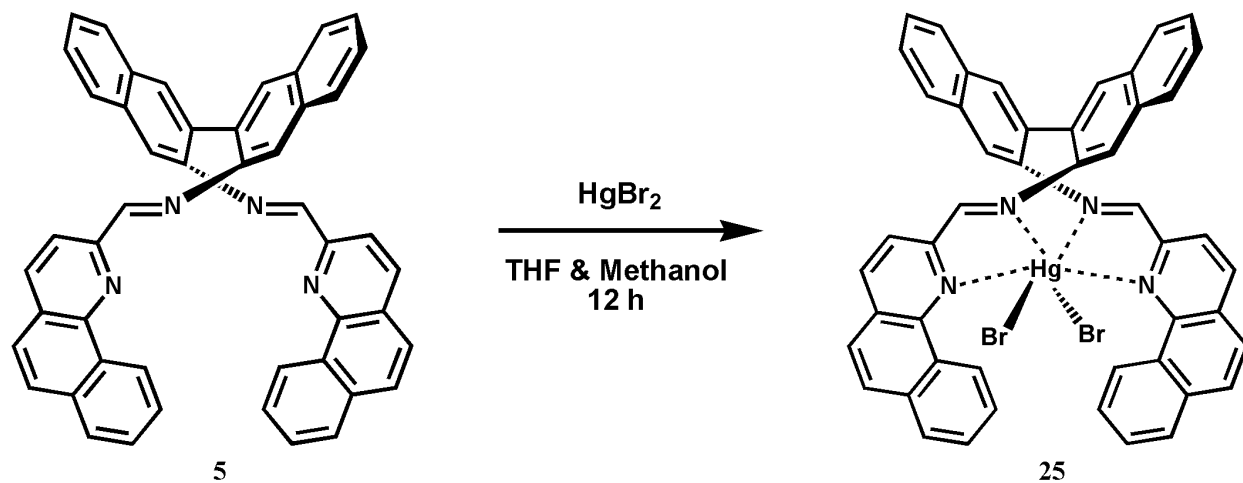
Figure 3.54: Proposed Reaction Scheme for Ligand **5** with HgBr$_2$

The reaction of ligand **5** with HgBr$_2$ gave a red colored product in 91.2 % yield. The ^{1}H NMR spectrum obtained for complex **25** is shown in Figure 3.55 and suggests the formation of a pure complex. The proton signals have shifted compared to their positions in the ^{1}H NMR of the corresponding ligand **5**. For example, the distinct imine proton is located at 8.51 ppm and is now
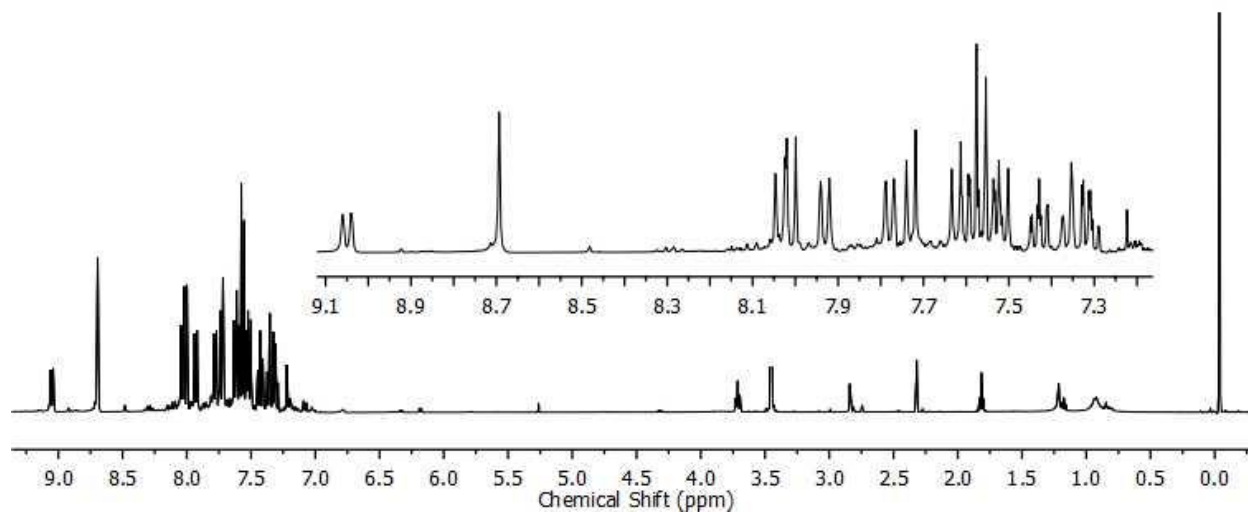
Figure 3.55: 400 MHz ^{1}H NMR Spectrum for Complex **25** (CDCl$_3$)

present at 8.72 ppm. We observe significant changes in peak positions at 8.03 ppm as we observe an overlap of doublet peaks that are separated in ligand **5** and at 7.75 ppm as we observe only two doublet peaks present compared to three doublet peaks in the ^{1}H NMR spectrum of ligand **5**. We obtain the correct number of total resonance signals expected for complex **25** (15). We carried out an HSQC experiment on complex **25** and obtained the spectrum shown below in Figure 3.56. We observe that there are fifteen proton to carbon coupling contour points, which is the right number expected. There is a slight shift observed for the HSQC contour points on the ^{13}C x-axis scale. The unique isolated C–N contour point is visible at 162.5 ppm but is present in the corresponding ligand **5** at 159 ppm. This is a shift could be attributed to the carbon atom's close proximity to the mercury(II) metal center just as we observe proton shifts in other complexes in this chapter. Several attempts to grow single crystals, using the solvent diffusion method and the heating and cooling method, suitable for X-ray analysis were unsuccessful so we conducted a COSY experiment to understand the coupling interactions of the protons present in complex **25**. The spectrum obtained is shown in Figure 3.57 and displays similar coupling
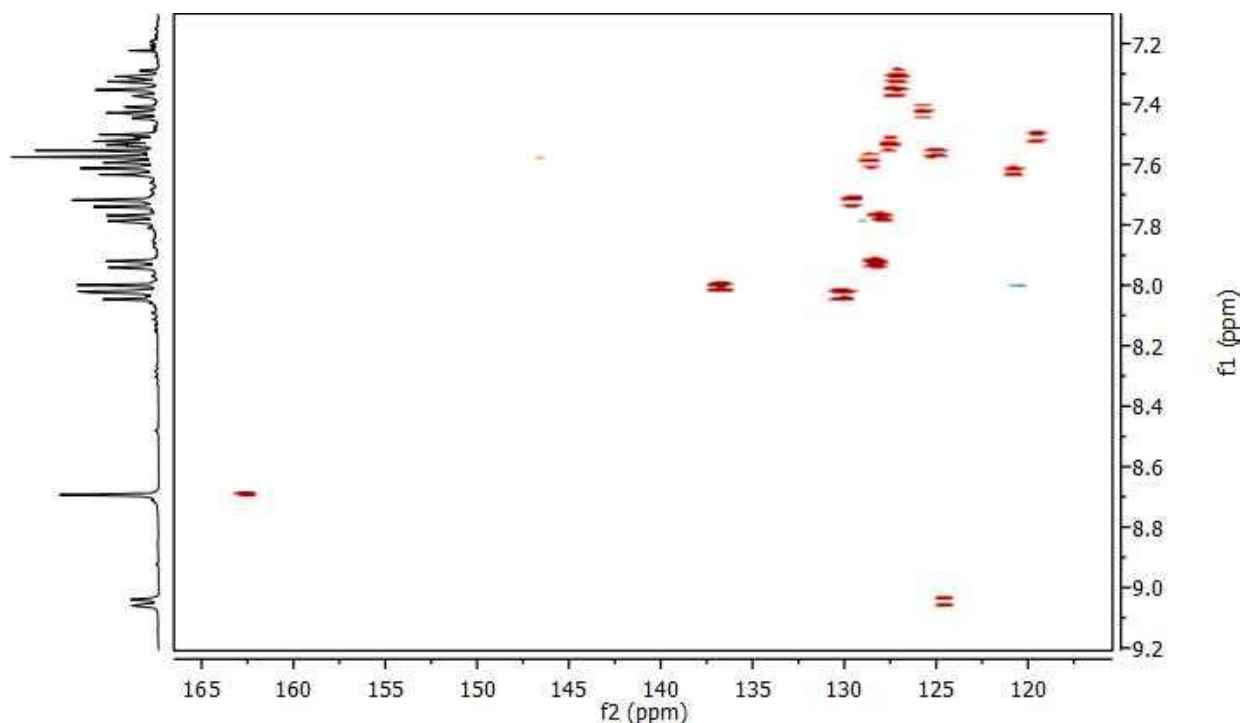
Figure 3.56: 400 MHz HSQC Spectrum for Complex **25** (CDCl$_3$)

patterns to the corresponding ligand **5**. We observe similar ^{3}J coupling as were observed between protons (1→2, 2→3, 3→4, 5→6, 8→9, 10→11, 11→12, 12→13, and 13→14) in ligand **5**. We also observe the presence of some para, peri, epi, and through-space long range couplings reflected in our previous ligand systems in chapter twofor the following sets of protons (1→3 {meta}, 1→4{para}, 1→5{epi}, 6→7{through-space}, 7→8{through-space}, 11→12{peri}, 15→13{meta}, 15→12{para}, and 15→11{epi}). Electro-spray mass spectrometry was carried out on complex **25** (Appendix I) and we obtained a spectrum that indicates the presence of the following desired ion: $[C_{48}H_{30}N_4HgBr]^+$.
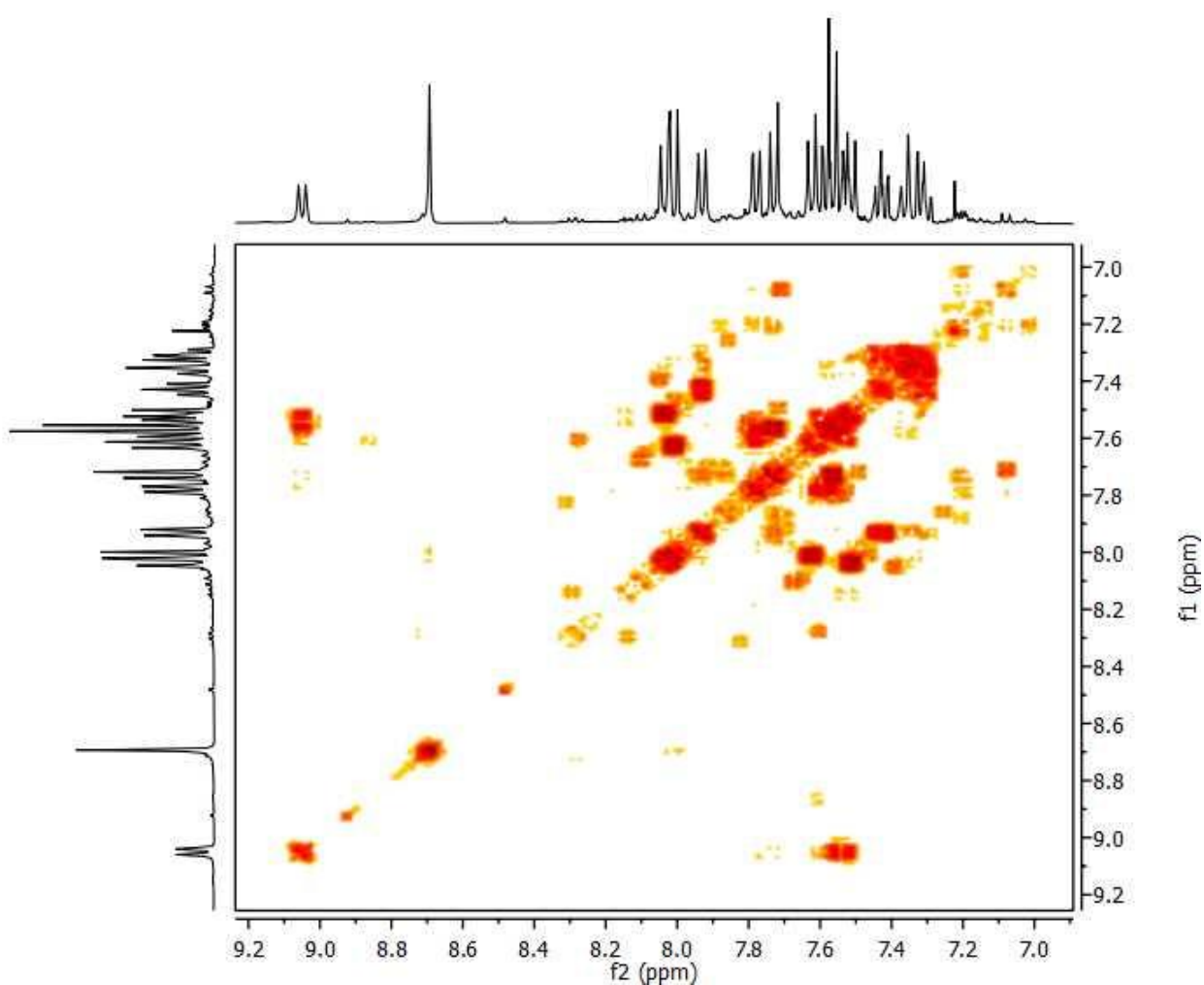
Figure 3.57: 400 MHz COSY Spectrum for Complex **25** (CDCl$_3$)

96

3.11 Complexation with Pd(C₄H₆O₄)
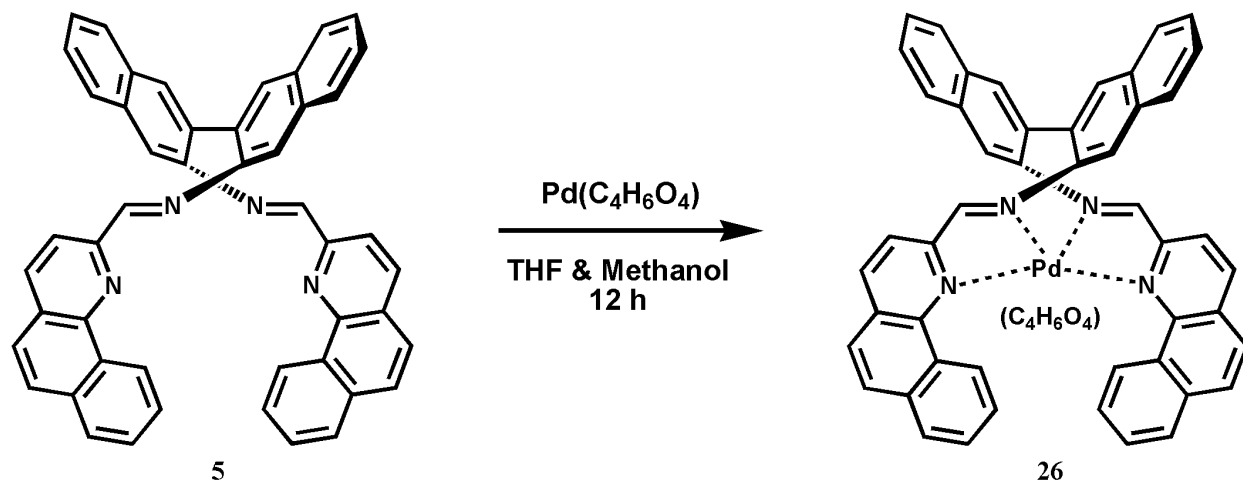
Figure 3.58: Proposed reaction Scheme for Ligand 5 with Pd(C₄H₆O₄)

The reaction of ligand **5** with Pd(C₄H₆O₄) resulted in the formation of a green colored product in 88.6 % yield. The ^{1}H NMR spectrum obtained for complex **26** indicates the formation of a pure C_2 symmetric complex. We maintain the integrity of the imine bond as we observe the
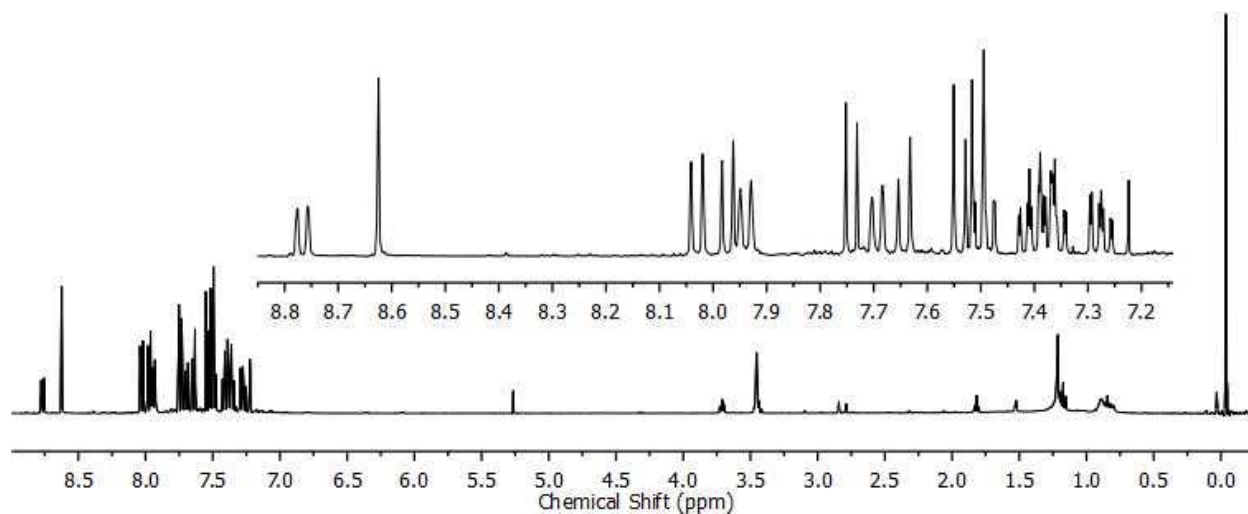
Figure 3.59: 400 MHz ^{1}H NMR Spectrum for Complex **26** (CDCl₃)

distinct singlet at 8.64 ppm. The right number of resonance signals (15) are obtained the ^{1}H NMR spectrum with slight shifts in their positions compared to the corresponding ligand **5**. The HSQC spectrum shown in Figure 3.61 displays fifteen contour points and we observe the characteristic imine carbon isolated at 165 ppm. We obtain the expected [3]J coupling and the unusual long range epi, meta, peri, and through-space couplings in the COSY spectrum of complex **26** (Figure 3.49). Electro-spray mass spectrometry was carried out on complex **25** (Figure 3.62) and the spectrum obtained indicates the presence of the following desired ion: $[C_{48}H_{30}N_4Pd]^+$. This suggests that the complex may be arranged with one acetate ligand bound as this gets removed to produce the ion in the mass spectrometry experiment.
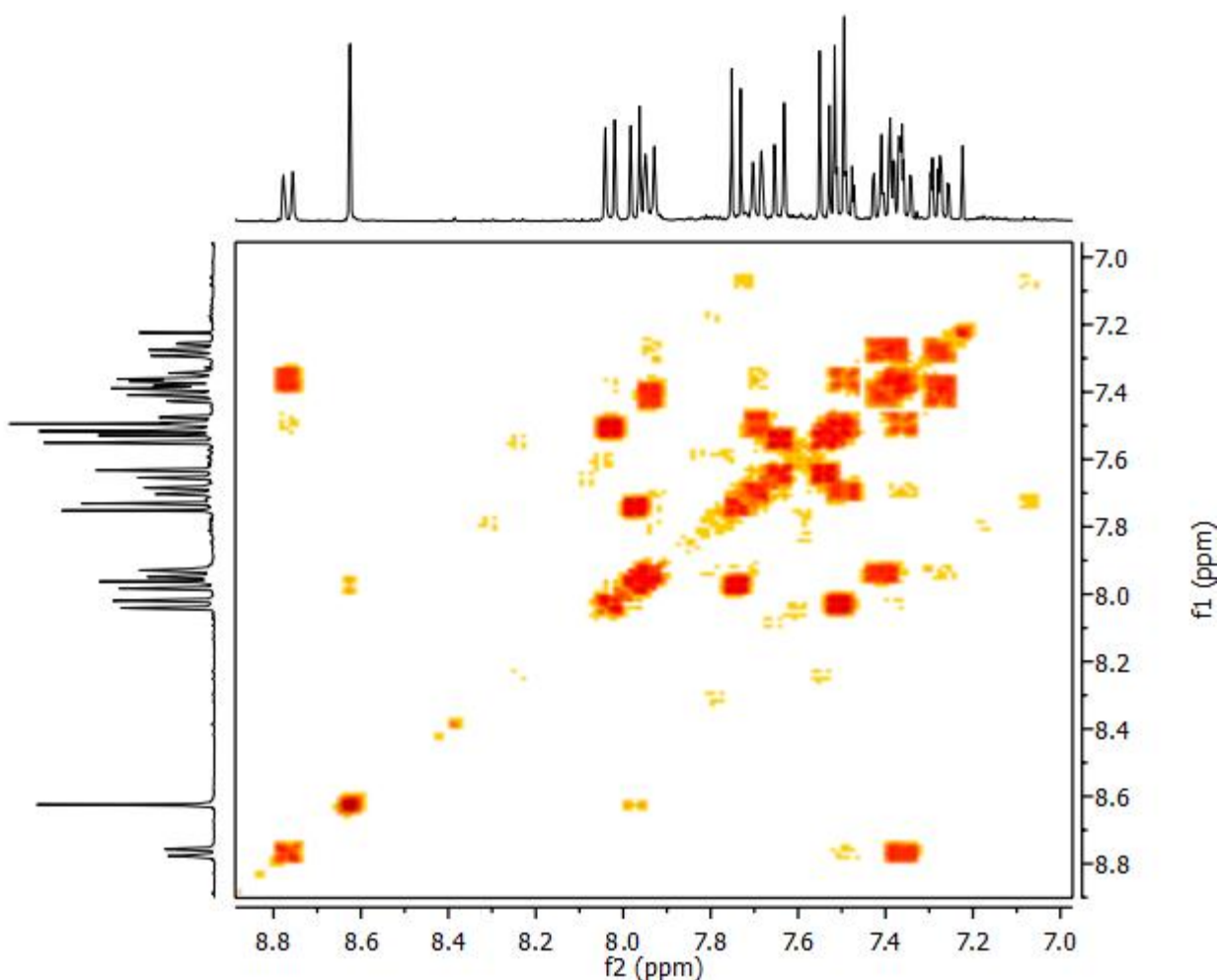
Figure 3.60: 400 MHz COSY Spectrum for Complex **26** (CDCl$_3$)

98
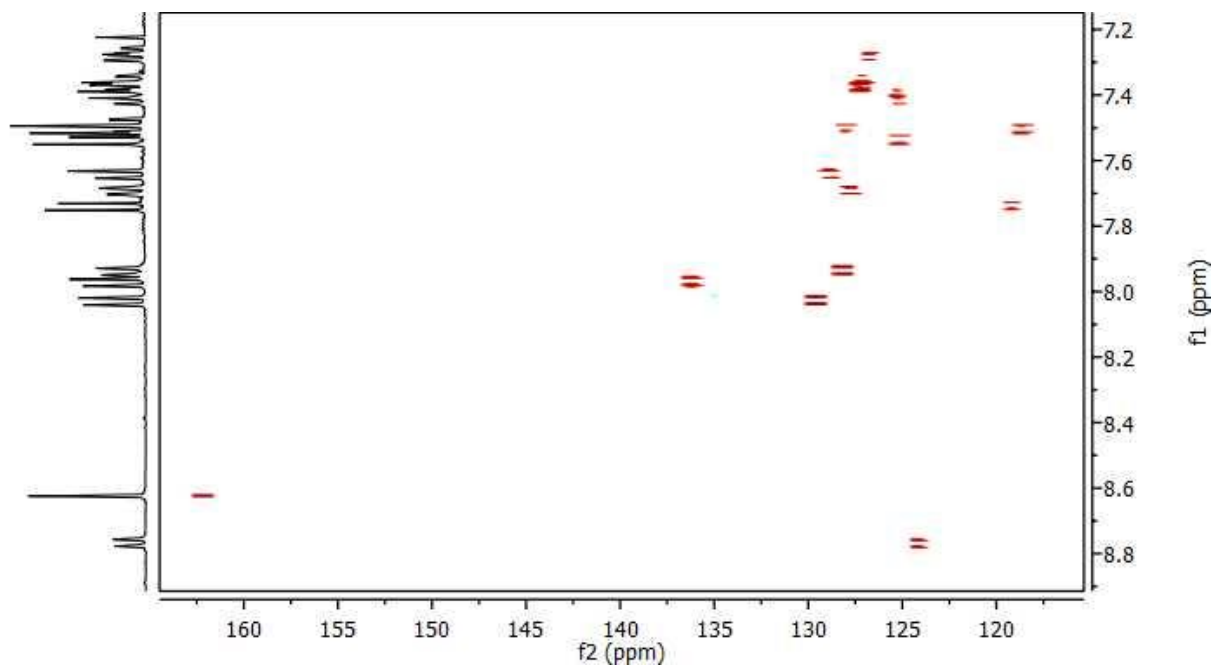
Figure 3.61: 400 MHz HSQC Spectrum for Complex **26** (CDCl$_3$)
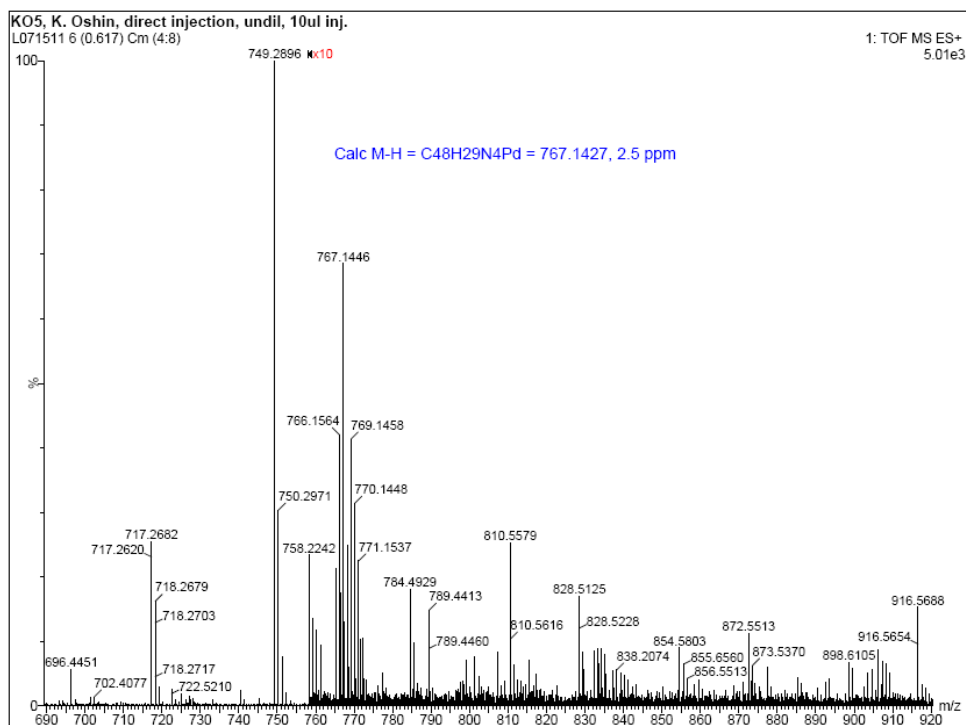
Figure 3.62: Electro-Spray Mass Spectrometry for Complex **26**

3.12 Complexation with CoCl₂
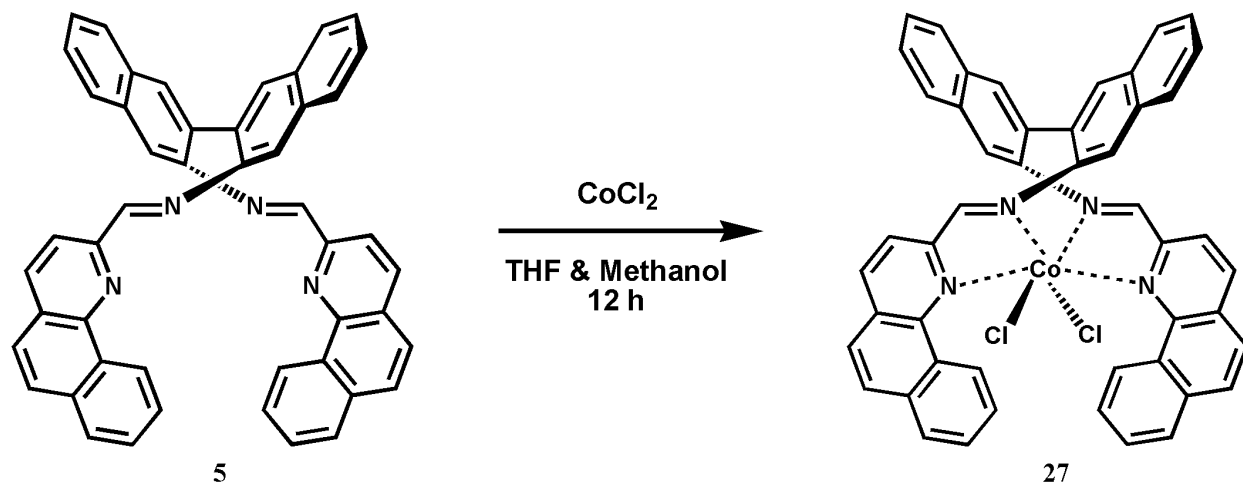
Figure 3.63: Proposed reaction Scheme for Ligand **5** with CoCl₂

The reaction of Ligand **5** with CoCl₂ produced a blue colored complex (**27**) in 84.7 % yield. The ¹H NMR spectrum obtained for this complex shows slight shifts in the aromatic region (compared to the corresponding ligand **5**) indicative of a successful complexation (Figure 3.64).
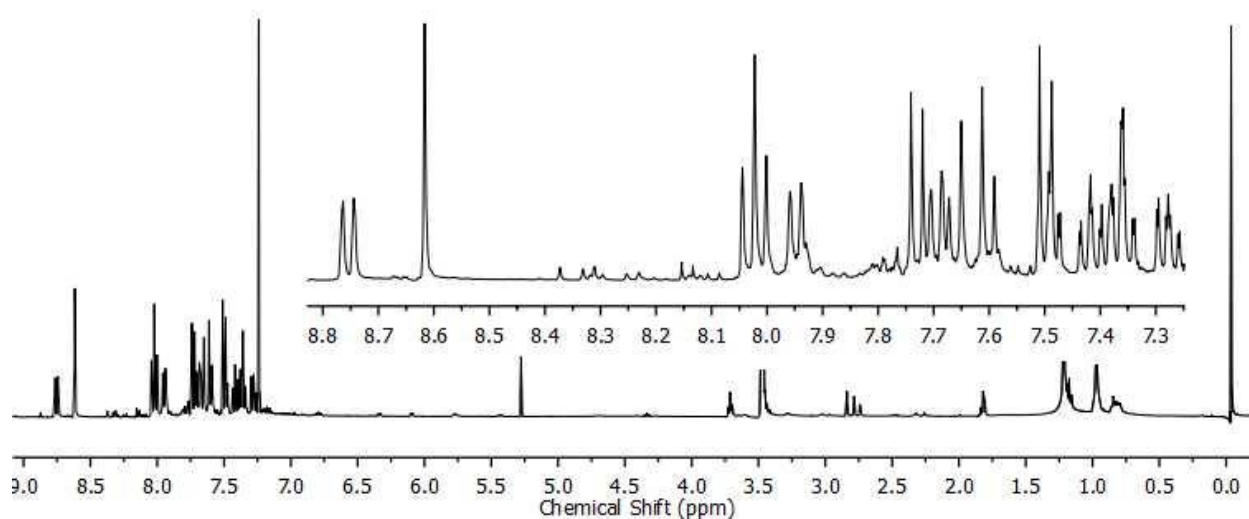
Figure 3.64: 400 MHz ¹H NMR Spectrum for Complex **27** (CDCl₃)

The HSQC experiment conducted on complex **27** shows the presence of fifteen proton to carbon resonance points. The contours are slightly shifted when compared to the HSQC spectrum of ligand **5**. The COSY spectrum obtained for complex **27** is shown in Figure 3.66 and displays patterns similar to the corresponding ligand **5**. We observe similar ^{3}J coupling as were observed between protons (1→2, 2→3, 3→4, 5→6, 8→9, 10→11, 11→12, 12→13, and 13→14) in ligand **5**. We also observe the presence of some para, peri, epi, and through-space long range couplings reflected in our previous ligand systems in chapter two for their coupling to the following sets of protons (1→3 {meta}, 1→4{para}, 1→5{epi}, 6→7{through-space}, 7→8{through-space}, 11→12{peri}, 15→13{meta}, 15→12{para}, and 15→11{epi}). We observe in complex **27** that the number of protons that experience long range coupling is much less that those in the corresponding ligand. That being said, we don't observe any long range coupling for the imine proton to the protons in the benzoquinoline side-arm or the binaphthalene backbone and this may be due to the presence of the cobalt(II) metal center. The complex may be bound in a particular orientation where the protons that usually experience long range coupling are no longer spatially in close proximity to each other.
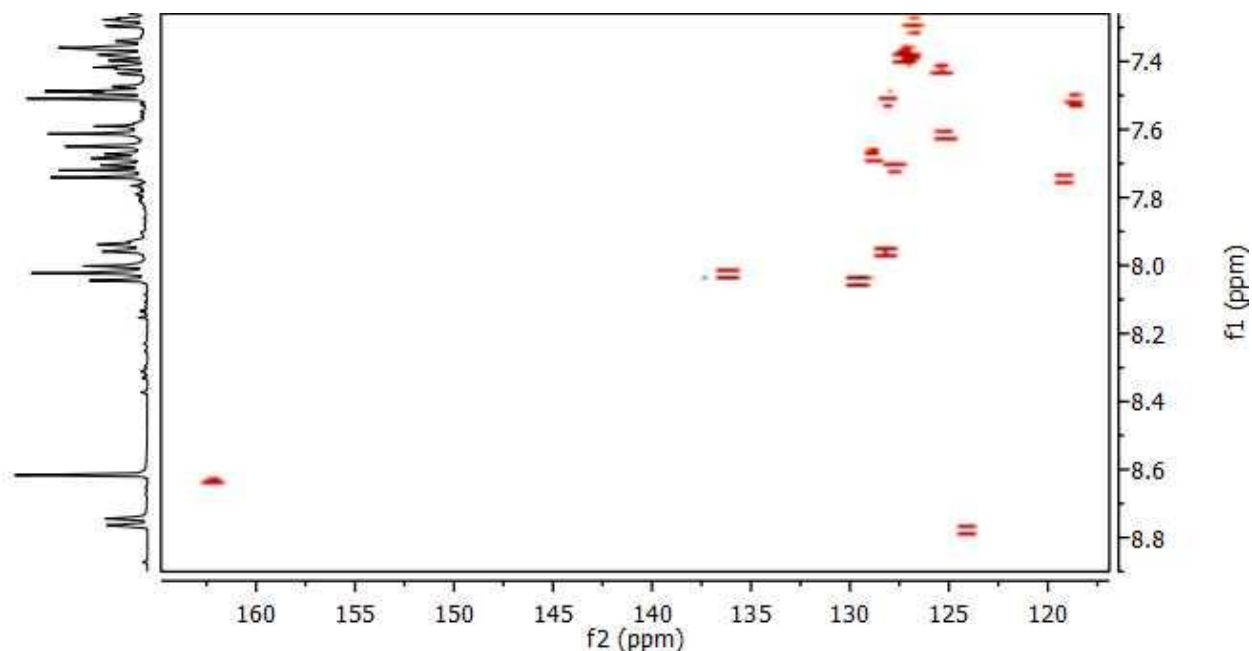
Figure 3.65: 400 MHz HSQC Spectrum for Complex **27** (CDCl$_3$)

Single crystals obtained for this complex using the solvent diffusion method were in the form of needle-like structures that degraded over time when mounted for X-ray analysis. Currently, we are attempting to change the solvents used for crystal growth to produce higher quality crystals that can be analyzed. Electro-spray mass spectrometry was carried out on complex **27** to obtain some more information on the structure present (Appendix I). The spectrum obtained indicates the presence of the following desired ions: a complex with one cobalt(II) metal bound and one chloro ligand coordinated $[C_{48}H_{30}N_4CoCl]^+$. The clean ^{1}H NMR spectrum obtained suggests that the cobalt(II) metal center in complex **27** is bound to all four nitrogen donor groups and results in a symmetric structure.
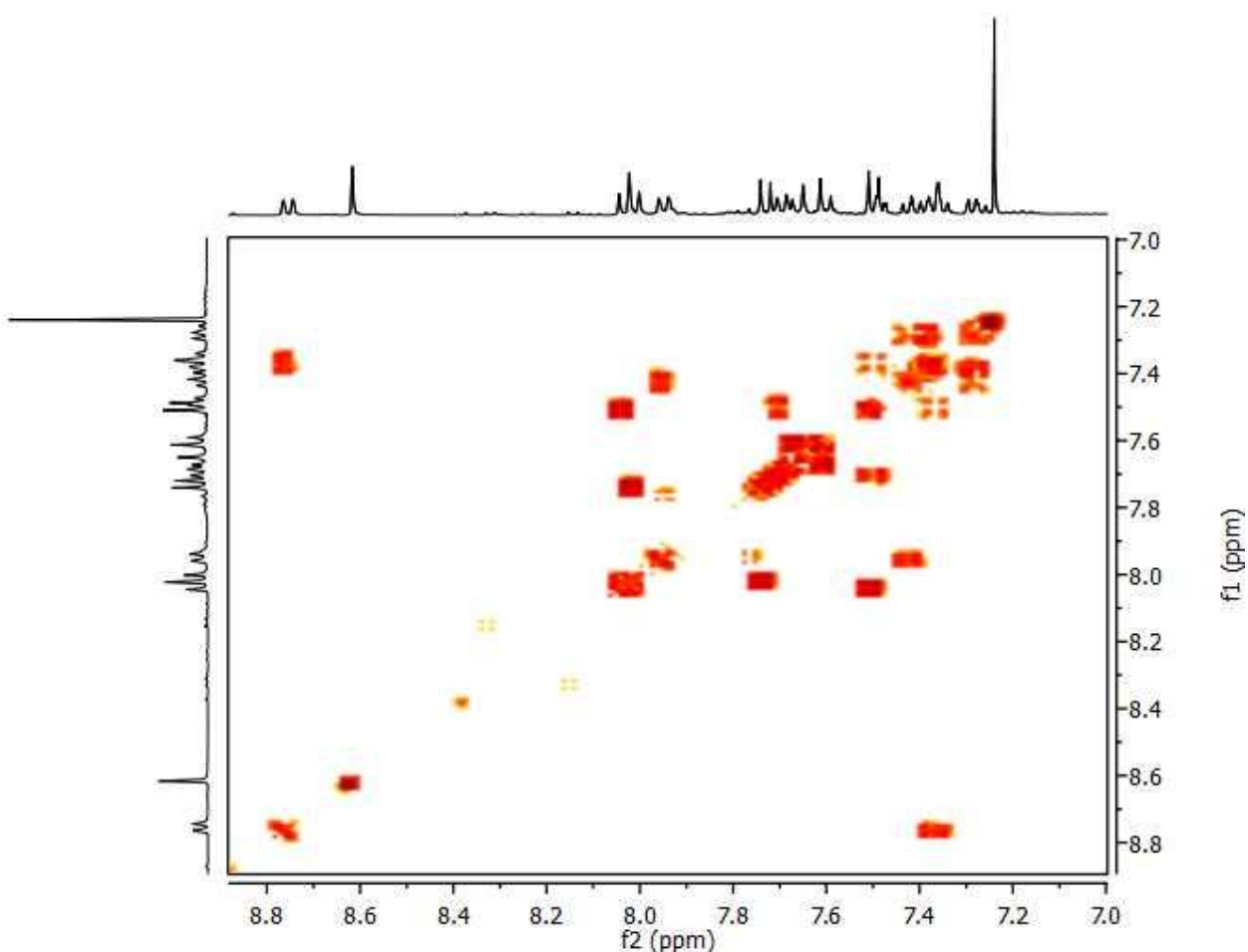
Figure 3.66: 400 MHz COSY Spectrum for Complex **27** (CDCl$_3$)

3.13 Complexation with Cu(OTf)₂
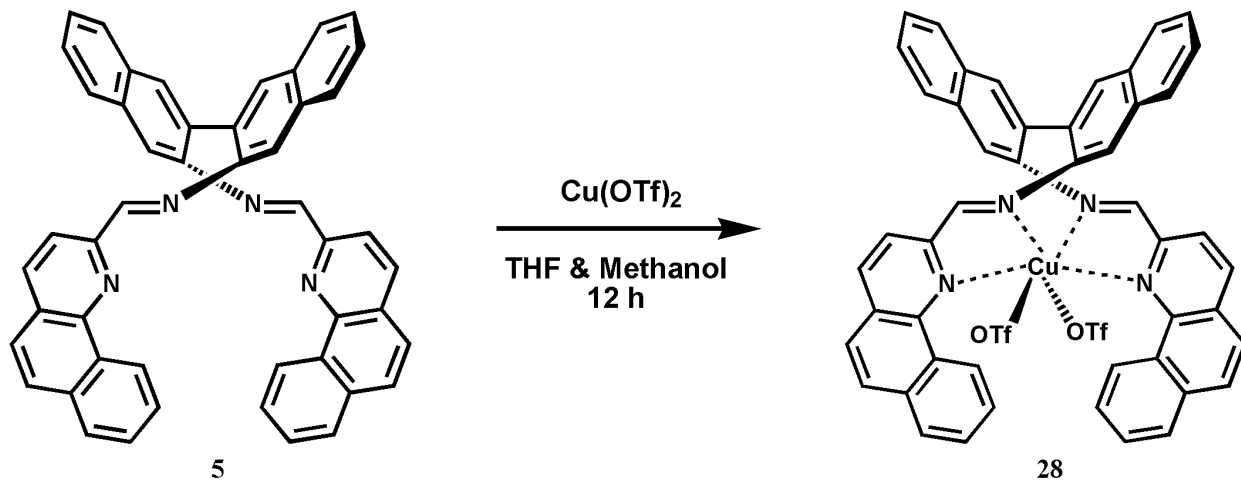
Figure 3.67: Proposed Reaction Scheme for Ligand **5** with Co(OTf)₂

The reaction of ligand **5** with one equivalent of Cu(OTf)₂ produced dark blue colored product in 68.3 % yield. The $3d^9$ copper(II) metal center has unpaired electrons present in it electronic configuration and these affect the NMR linewidth and give rise to paramagnetic shifts. We observe this in the ¹H NMR spectrum obtained for complex **28** (Figure 3.68). the complex appears to have maintained the integrity of the imine bond as we observe the distinctive singlet still present at 9.96 ppm. The paramagnetic nature of the complex detracted us from conducting further HSQC and COSY experiments as the complete analysis and assignment of protons in the complex would be impossible. Nonetheless, the ¹H NMR spectrum provided us with valuable information as it indicates a successful complexation reaction occurred to form a new product. Numerous attempts made at growing single crystals suitable for X-ray analysis using the solvent diffusion method and heating and cooling method proved unsuccessful. We turned our attention to electro-spray mass spectrometry to give us an idea of the complex that is present in this product. Analysis of the mass spectrum, shown in Figure 3.69, indicates the presence of the following desired ion: a complex with one copper(II) cation bound with no triflate ligands coordinated to the metal center $[C_{48}H_{30}N_4Cu]^{2+}$.
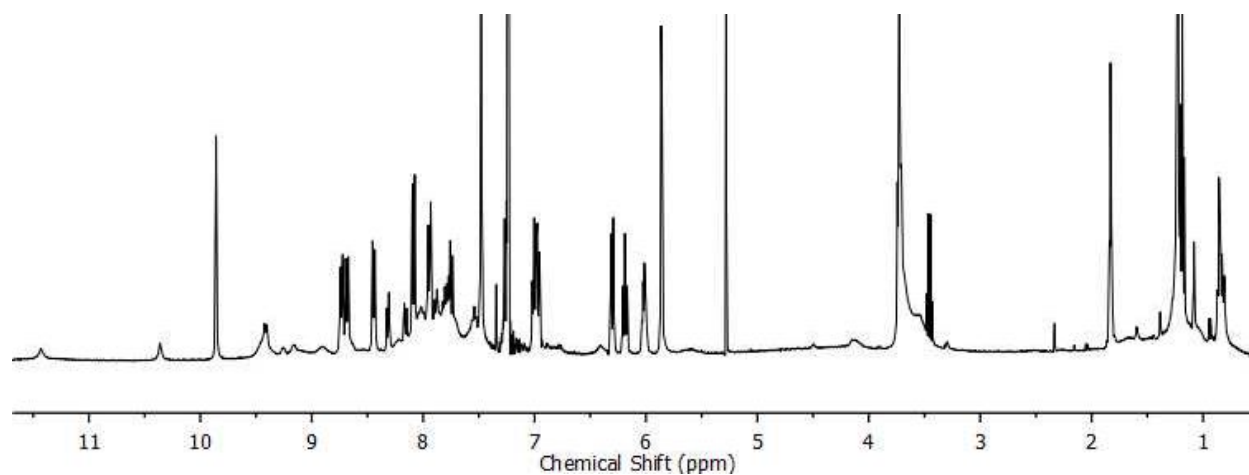
Figure 3.68: 400 MHz ^{1}H NMR Spectrum for Complex **28** (CDCl$_3$)
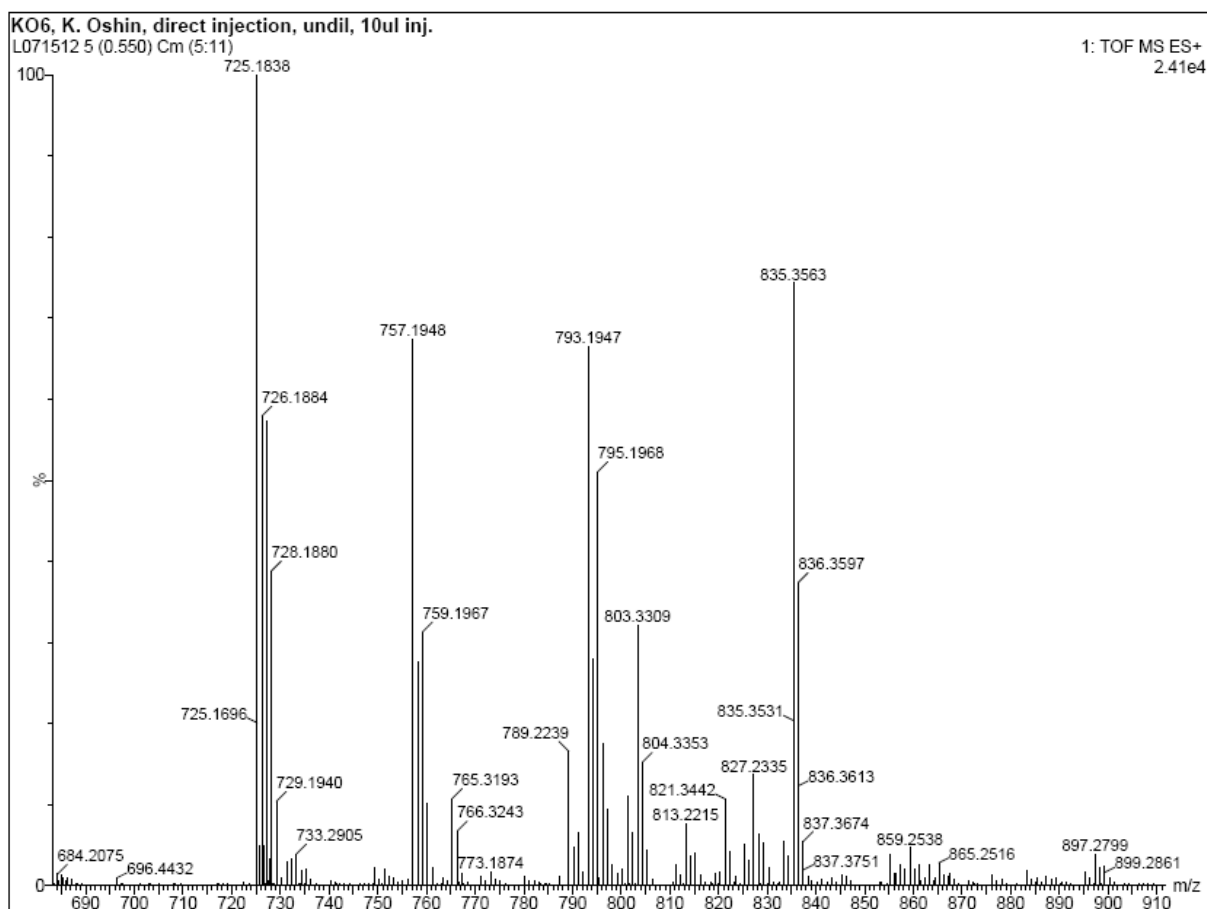
Figure 3.69: Electro-Spray Mass Spectrum for Complex **28**
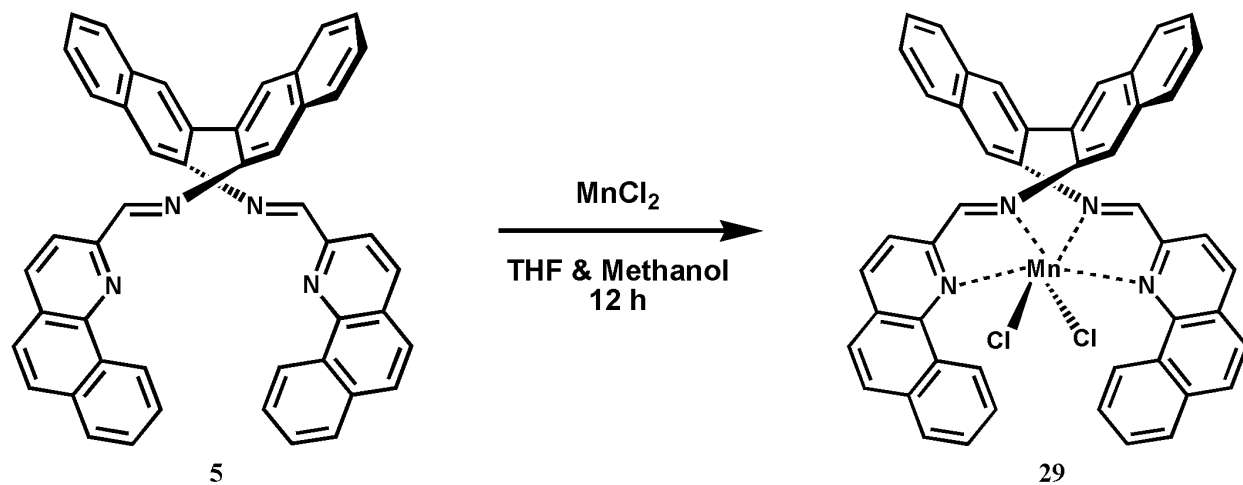
Figure 3.70: Proposed Reaction Scheme for Ligand **5** with MnCl₂

The reaction of Ligand **5** with MnCl₂ resulted in the formation of a bright yellow colored product in 94.1 % yield, complex **29**. The ^{1}H NMR spectrum obtained for complex **29** is shown below in Figure 3.71. We observe slight shifts in proton positions present in the aromatic region
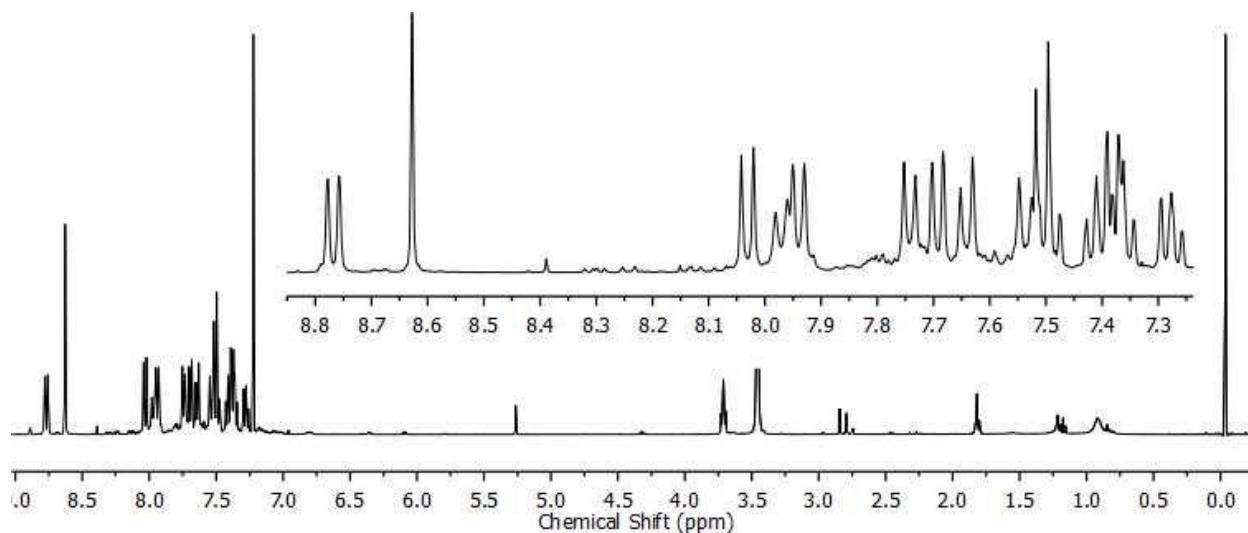
Figure 3.71: 400 MHz ^{1}H NMR Spectrum for Complex **29** (CDCl₃)

(compared to the corresponding ligand **5**) indicative of a successful complexation. The HSQC experiment conducted on complex **29** shows the presence of fifteen proton to carbon resonance points (Figure 3.72). The contours are slightly shifted when compared to the HSQC spectrum of ligand **5**. The COSY spectrum obtained for complex **29** is shown in Figure 3.73 and displays patterns similar to the corresponding ligand **5**. We observe similar ^{3}J coupling as were observed between protons (1→2, 2→3, 3→4, 5→6, 8→9, 10→11, 11→12, 12→13, and 13→14) in ligand **5**. We also observe the presence of some para, peri, epi, and through-space long range couplings reflected in our previous ligand systems in chapter two for their coupling to the following sets of protons (1→3 {meta}, 1→4{para}, 1→5{epi}, 6→7{through-space}, 7→8{through-space}, 11→12{peri}, 15→13{meta}, 15→12{para}, and 15→11{epi}). Once again, we don't observe any long range coupling for the imine proton to the protons in the benzoquinoline side-arm or the binaphthalene backbone and this may be due to the presence of the manganese(II) metal center. The complex may be bound in a particular orientation where the protons that usually experience long range coupling are no longer in close proximity spatially to each other.
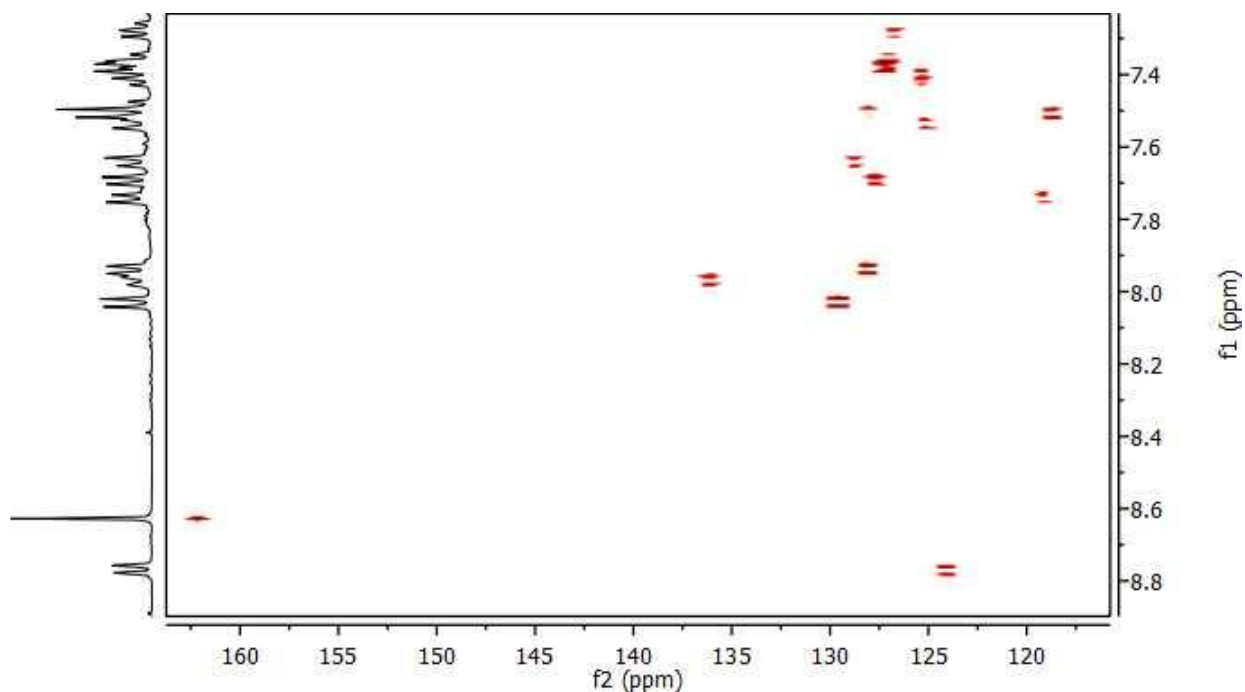
Figure 3.72: 400 MHz HSQC Spectrum for Complex **29** (CDCl$_3$)

Several attempts to grown single crystals suitable for X-ray analysis using the solvent diffusion method and heating and cooling method were unsuccessful. Currently, we are attempting to change the solvents used for crystal growth in the solvent diffusion method to produce crystals of higher quality that can be analyzed. Electro-spray mass spectrometry was carried out on complex **29** to obtain some more information on the manganese structure present (Appendix I). The spectrum obtained indicates the presence of the following desired ions: a complex with one manganese(II) metal bound to the ligand and one chloro ligand coordinated $[C_{48}H_{30}N_4MnCl]^+$ and a complex with one manganese(II) metal bound to the ligand with no chloro ligand coordinated $[C_{48}H_{30}N_4Mn]^{2+}$.
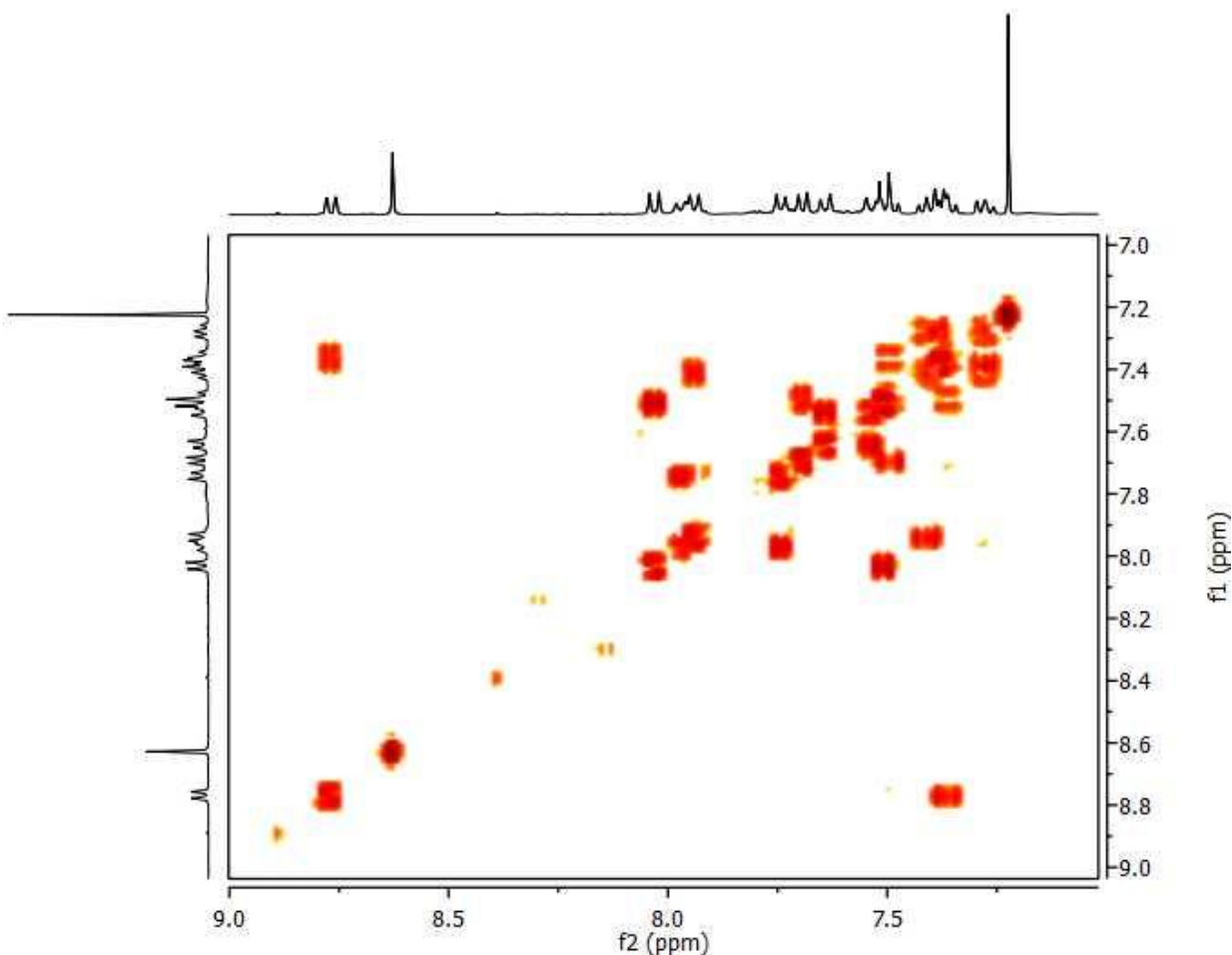
Figure 3.73: 400 MHz COSY Spectrum for Complex **29** (CDCl$_3$)

3.14 Complexation with CdCl₂
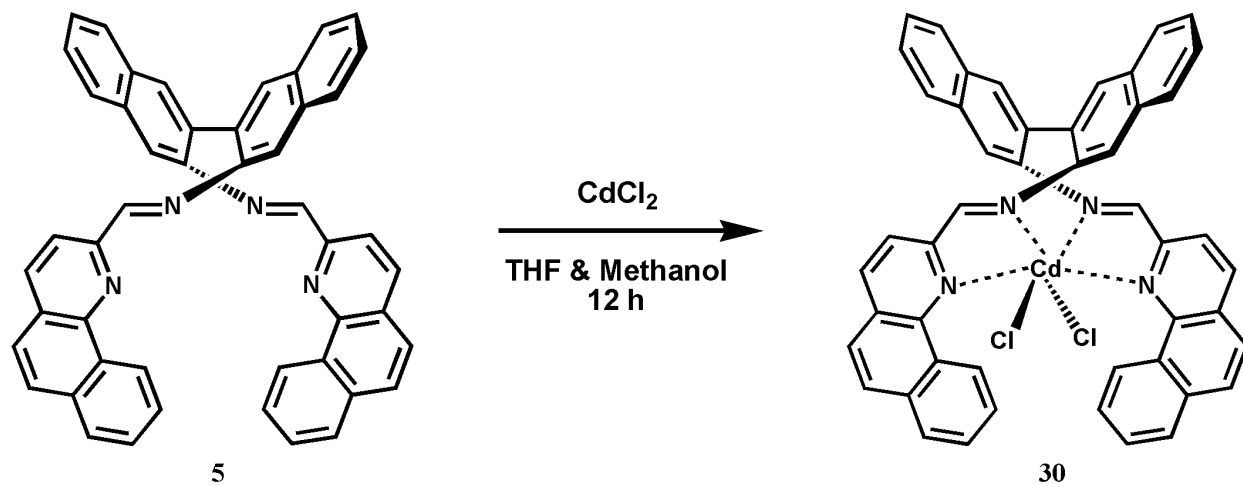
Figure 3.74: Proposed Reaction Scheme for Ligand **5** with CdCl₂

The reaction of ligand **5** with CdCl₂ produced a brown colored product, complex **30**. The ¹H NMR obtained shows the formation of a clean compound with the right number of resonance signals expected for complex **30**. The HSQC and COSY spectra obtained display the right number of contour points and short and long range couplings expected for complex **30**.
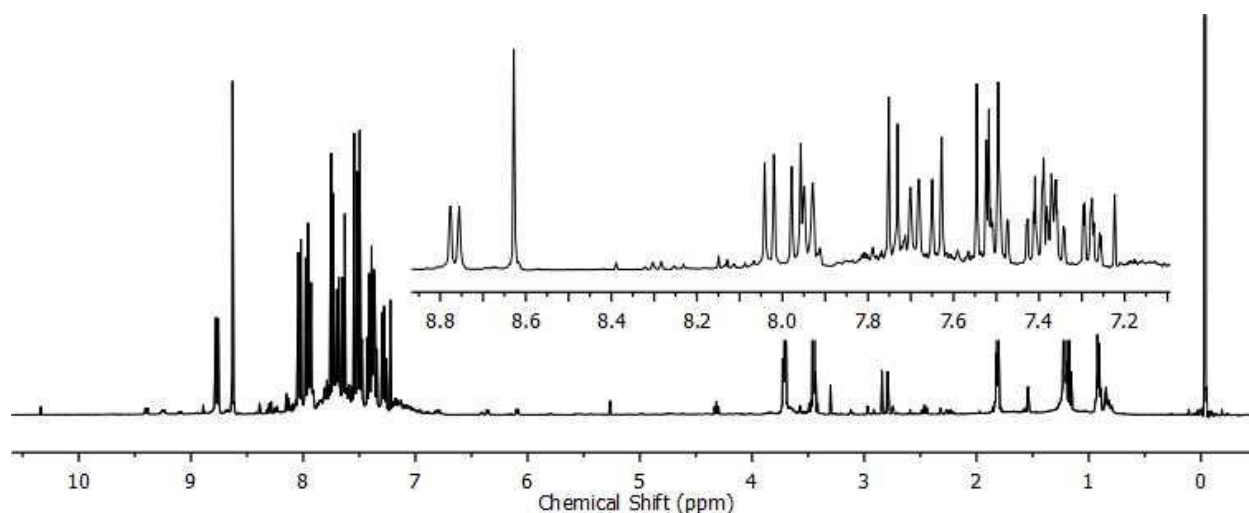
Figure 3.75: 400 MHz ¹H NMR Spectrum for Complex **30** (CDCl₃)
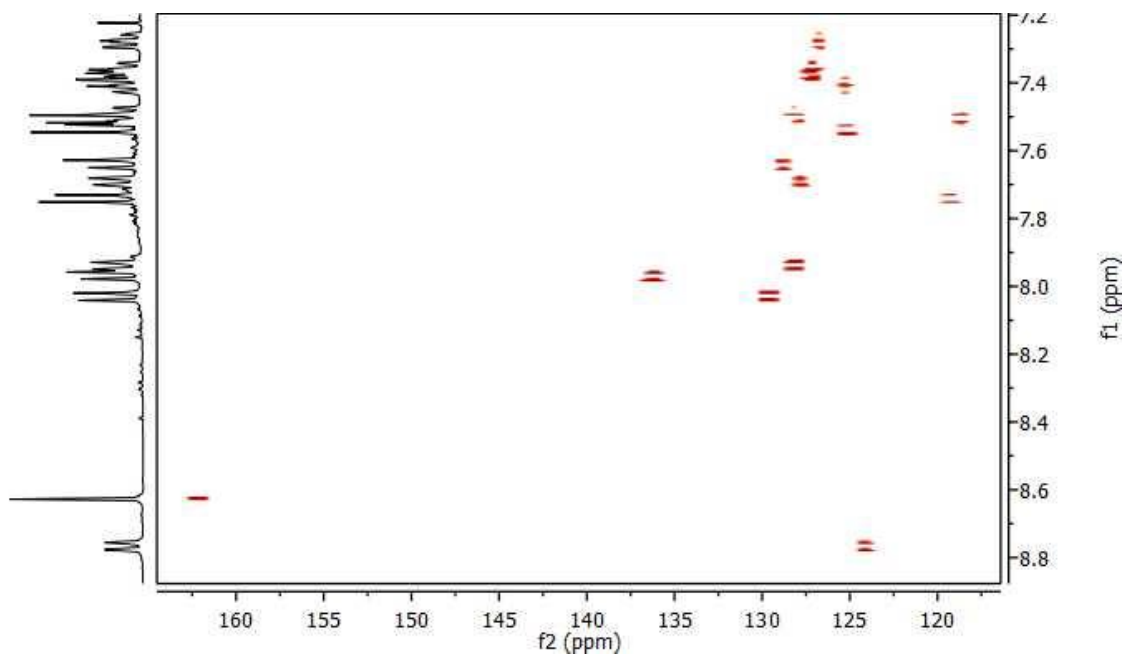
Figure 3.76: 400 MHz HSQC Spectrum for Complex **30** (CDCl$_3$)
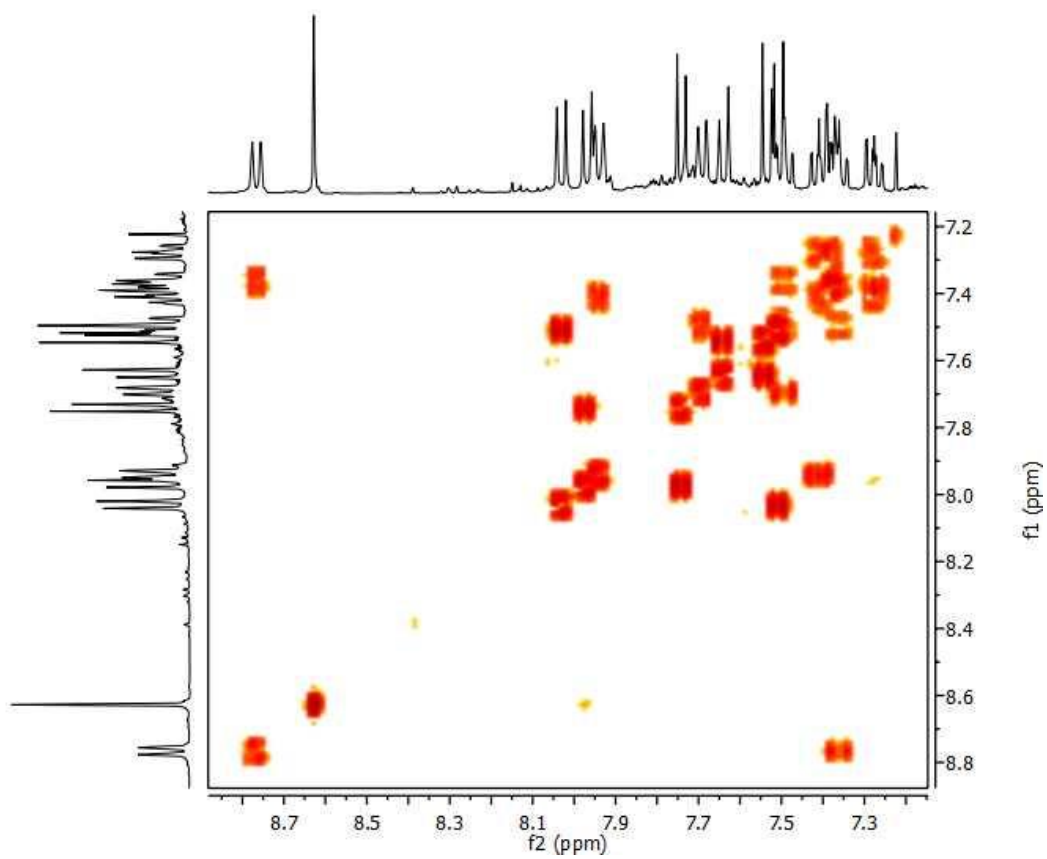
Figure 3.77: 400 MHz COSY Spectrum for Complex **30** (CDCl$_3$)

3.15 Complexation with AuClS(CH₃)₂
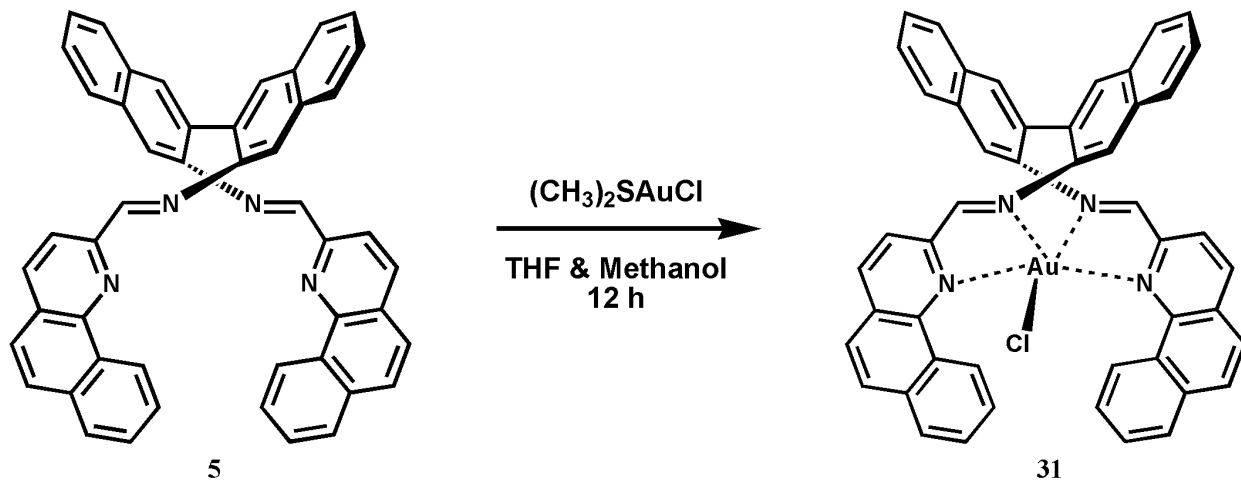
Figure 3.78: Proposed Reaction Scheme for Ligand **5** with $(CH_3)_2SAuCl$

The final reaction with Ligand **5** was carried out with $(CH_3)_2SAuCl$ to afford a brown colored product in 54.7 % yield. The ^{1}H NMR spectrum obtained for complex **31** shows a drastic change to the aromatic peak region as we observed with complex **24** supporting the notion that a complexation reaction did occur (Figure 3.79). We observe the disappearance of the distinctive imine singlet peak that is present at 8.51 ppm in the ^{1}H NMR spectrum of the corresponding ligand **5**. Although a reaction did occur, we concluded that it is not of our desired complex but rather a new compound with significantly less polyaromatic conjugation than what we have present in the corresponding ligand **5**. We carried out a HSQC experiment to observe the proton to carbon correlations in complex **31** (Figure 3.80). We clearly see eleven contour points in the spectrum, which is less than the fifteen contour points obtained in the HSQC spectrum for ligand **5**. The distinct contour point corresponding to the imine carbon, located at 165.00 ppm in ligand **5**, is also missing in the HSQC spectrum for complex **31**. This is probably due to the ligand breaking apart during the reaction to produce an unknown structure.

A COSY experiment was conducted for complex **31** and we observe significant coupling of the protons with each other (Figure 3.81). The coupling pattern obtained could not be use to solve the structure of complex **24**. When compared to the COSY spectrum obtained for ligand **5**,
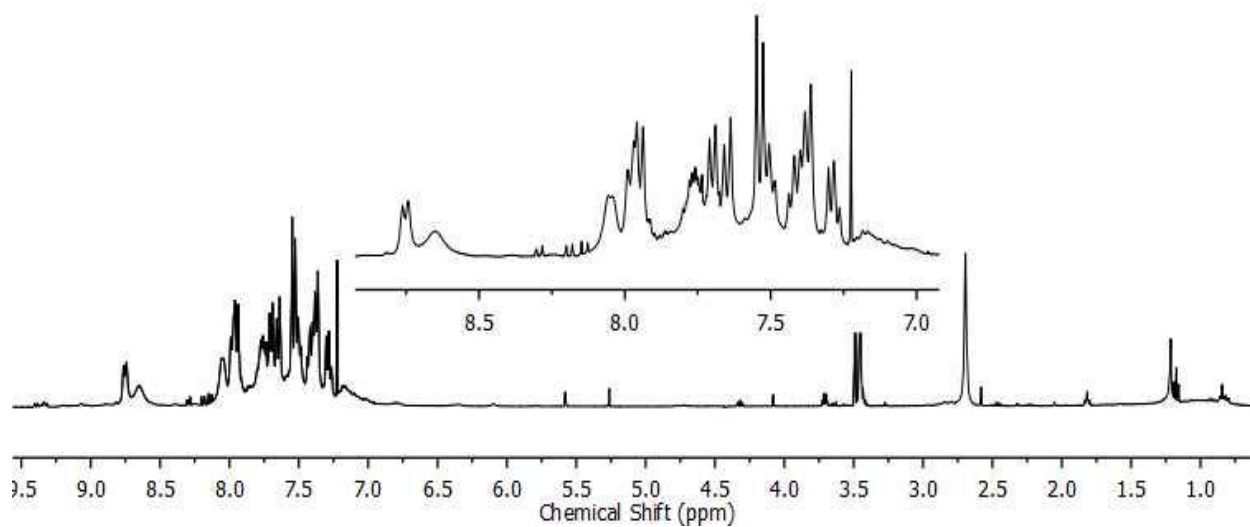
Figure 3.79: 400 MHz ^{1}H NMR Spectrum for Complex **31** (CDCl$_3$)
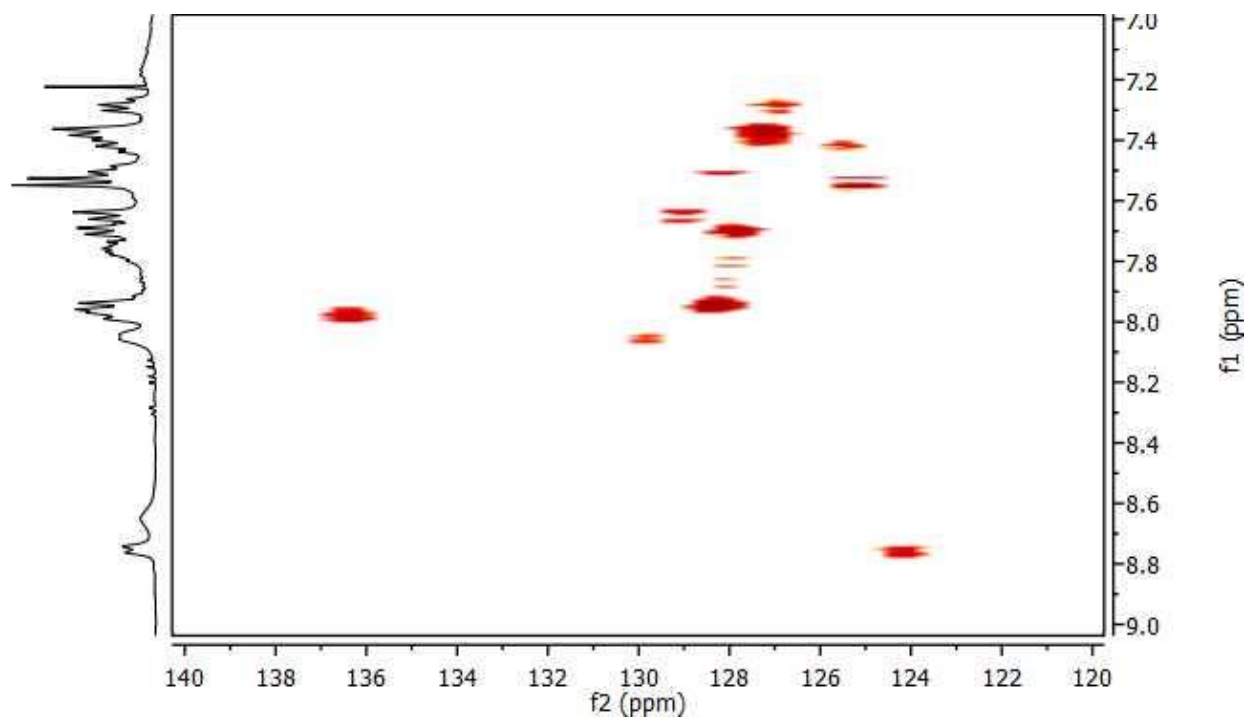
Figure 3.80: 400 MHz HSQC Spectrum for Complex **31** (CDCl$_3$)

111

we notice the loss of the observed ^3J coupling between protons (1→2, 2→3, 3→4, 5→6, 8→9, 10→11, 11→12, 12→13, and 13→14) in ligand **5**. We also observe the presence of some para, peri, epi, and through-space long range couplings reflected in our previous systems in chapter two but do not observe the pattern displayed in ligand **5** for the following sets of protons (1→3 {meta}, 1→4{para}, 1→5{epi}, 6→7{through-space}, 7→8{through-space}, 11→12{peri}, 15→13{meta}, 15→12{para}, and 15→11{epi}). Electro-spray mass spectrometry was carried out on complex **31** (shown in Appendix I) and we obtained a spectrum that surprisingly indicates the presence of the following desired ions: $[C_{48}H_{30}N_4AuSCl(CH_3)]^+$.
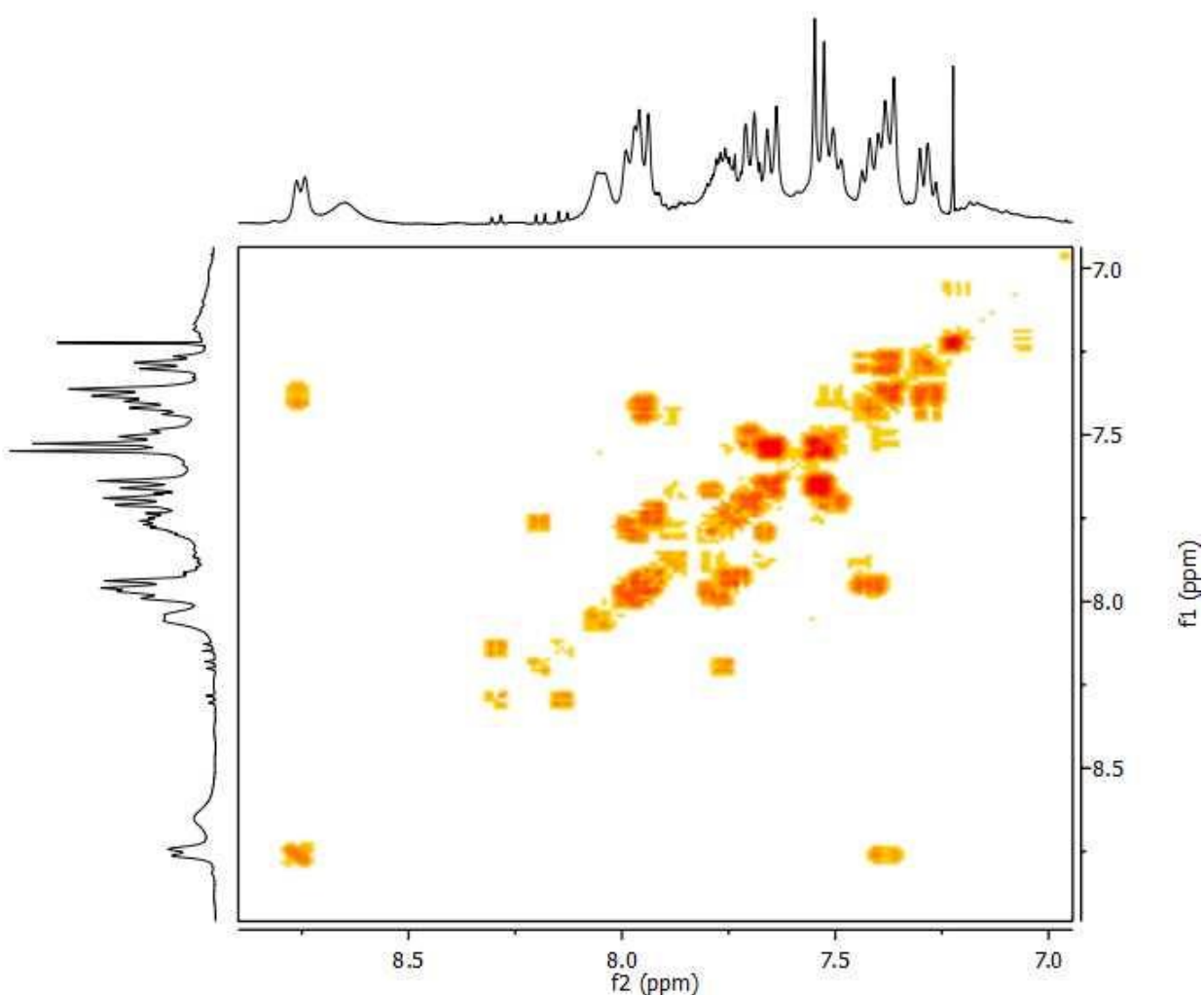
Figure 3.81: 400 MHz COSY Spectrum for Complex **31** (CDCl$_3$)

In summary, we were able to synthesize a diverse library of chiral complexes utilizing ligands **2**, **5**, and **11**. The ligands incorporated different degrees of flexibility with the reduced ligand, **11** being the most flexible about the amine bond. Ligand **2** is not as flexible as ligand **11** but does have a longer conjugated benzoquinoline side-arm which can increase the chances of completely wrapping around a metal center because of the possibility of π-π and σ-π interactions when the benzoquinoline side-arms stack up on each other. The last ligand (**5**) had a binaphthalene backbone incorporated in its design which can allow polyaromatic conjugation to be present throughout the complex thereby orienting itself in a stable conformer to improve the chances of a single stranded monohelix. No crystal structures were obtained from complexes made from ligand **5** but previous reactions carried out in the Levy group show that single crystals can be obtained with this ligand. The few that were grown using the solvent diffusion method were not suitable for use in X-ray analysis. Other characterizations carried out with 1D and 2D NMR experiments and electro-spray mass spectrometry provided us with enough information to deduce whether a complexation reaction occurred or not.

On the other hand, we obtained three solid state structures for complexes made with the reduced ligand **11**. The reaction with $ZnCl_2$ yielded a complex that did not completely wrap giving the metal center a trigonal bipyramidal geometry. The reaction with $FeCl_2$ produced a fascinating solid state structure with two iron centers and an oxo bridging ligand. We plan to use this complex in future hydroxylation reactions given the success of similar complexes for such catalytic reactions in the literature. The oxidation state of the metal centers remains elusive but information obtained from the ^{1}H NMR and EPR spectra suggest that both iron centers are of the +3 oxidation state. The final solid state structure obtained with ligand **11** was with $RuCl_2$(COD). We observe that the ligand gets oxidized back to ligand **1** but completely wraps about the metal center to give a distorted octahedral geometry for the $RuCl_2$ core. We obtained one solid state structure using ligand **2** with NiI_2. The reaction produced two distinct colored products that both ^{1}H NMR and electro-spray mass spectrometry indicate to be separate complexes. The structure obtained for the dark-green colored complex was for a complex that did not completely bind to the four nitrogen donor atoms resulting in a trigonal bipyramidal geometry for the NiI_2 core. For the two reactions that produced completely wrapped complexes, we obtained the M helicate for complex **18** and a 1:1 mixture of *M* and *P* helicates for complex **19**.

CHAPTER 4

Silver (I) Metallations

The synthesis of silver Schiff-base compounds has become more prevalent since their application in the heterogenous catalyzed epoxidation of ethylene to produce ethylene oxide was discovered.[95] This became one of the industrial methods used to satisfy the demand for the manufacture of ethlene glycol.[96] Silver based complexes have also been used in many useful reactions including amination of silyl enol ethers,[97] allylation of aldehydes,[98] nitroso-aldol type reactions,[99] the aziridination of alkenes,[100] and as NMR-shift reagents to determine the enantiomeric purity of alkenes.[101] The last application is of particular interest to this thesis as we were interested in the use of silver complexes as catalysts in various traditional asymmetric reactions (hydroxylations, epoxidations, and polymerizations), but also in bond activation reactions, where the silver complex does not take on the traditional catalytic role.

The two uses are interrelated as the enantioselective coordination of transition metals to unsaturated olefins is of significance in asymmetric catalysis. It is applicable in the area of chiral recognition and resolution of racemic mixtures of unsaturated compounds as the enantioselective binding of one multiple bond is often achieved by means of chiral organic ligands bound to a metal center.[102] Two different aspects of chiral recognition that should be considered are enantioface selectivity in the coordination of a prochiral olefin, which becomes diastereofaceselectivity in the case of a chiral olefin, and enantiomer selectivity in the coordination of a racemic chiral olefin.[103] The latter is relevant to the thermodynamic or kinetic resolution of racemic olefins.[104] The design and study of such complexes for selective coordination of olefins can be very difficult and time consuming leading to the limited research references available on that subject. To improve on this, we are interested in the use of our silver(I) Schiff-base complexes in the discrimination reaction of chiral olefins as this could become a great tool for chemists to use in analyzing products obtained from olefin synthesis. A simple NMR experiment with minimal amount of chiral silver(I) complex and olefin can help answer the unknown enantiomeric ratios of the product synthesized.

Given the wide use of these silver Schiff base complexes, their full characterization using various techniques is of vital importance in understanding their mechanism and to serve as a reference in future synthesis. Surprisingly, there is only a small amount of information available on the complete characterization of silver compounds, particularly in the area of nuclear magnetic resonance (NMR). A search through the literature reveals that the Pazderski group and the Lim group have successfully reported the complete NMR assignments of salen complexes incorporating cobalt(III), iron(II), osmium(II), and ruthenium(II) metal centers.[105] We now report on the complete 1D and 2D-NMR assignments of chiral silver(I) complexes using our C_2 symmetric ligands with the goal of utilizing them in the area of olefin resolution and in future traditional catalytic reactions. Silver(I) trifluoromethanesulfonate (triflate) was used as the source of metal ion to form subsequent complexes in this report. We chose to use the triflate counter-ion ($CF_3SO_3^-$) in order to minimize anion coordination and achieve exclusive coordination of the ligand to the silver metal center. Moreover, the triflate anion itself is very stable and as a result of its cylindrical structure and low dipole moment is very suitable when anion-cation complexes are desired.[106]

As observed in the ^{1}H NMR analysis of products obtained from the multiple complexation reactions carried out in chapter three and in the ^{1}H NMR analysis of our chiral tetradentate ligands in chapter two, most polyaromatic cyclic systems yield spectra that are difficult to evaluate and completely assign using traditional NMR methods. Justifiably, this is due to either the new electronic environment of the metal center disrupting the proton signals in the case of the complexes in chapter three or the similarity in coupling networks in different parts of the molecule leading to severe overlap of the ^{1}H resonances in the case of the ligands in chapter two. We observed that the reactions with silver(I) triflate generated complexes with a surprising expanded aromatic regions. Search of the literature for similar observations in other ligand system only led to the suggestion that the silver(I) salt may be acting as a NMR shift reagent as observed with binuclear lanthanide(III) complexes. Those studies also indicated that solvent plays an important role in the effectiveness of the shift reagent.[107]This unusual expansion made the complete complex ^{1}H NMR assignments relatively easy compared to the ligands. The difference in peak positions as we transition from ligand to complex is also examined in this chapter to understand the role the metal center plays in this transition.

4.1 Metallation of Ligand 3 with Silver(I) Triflate (Complex 32)
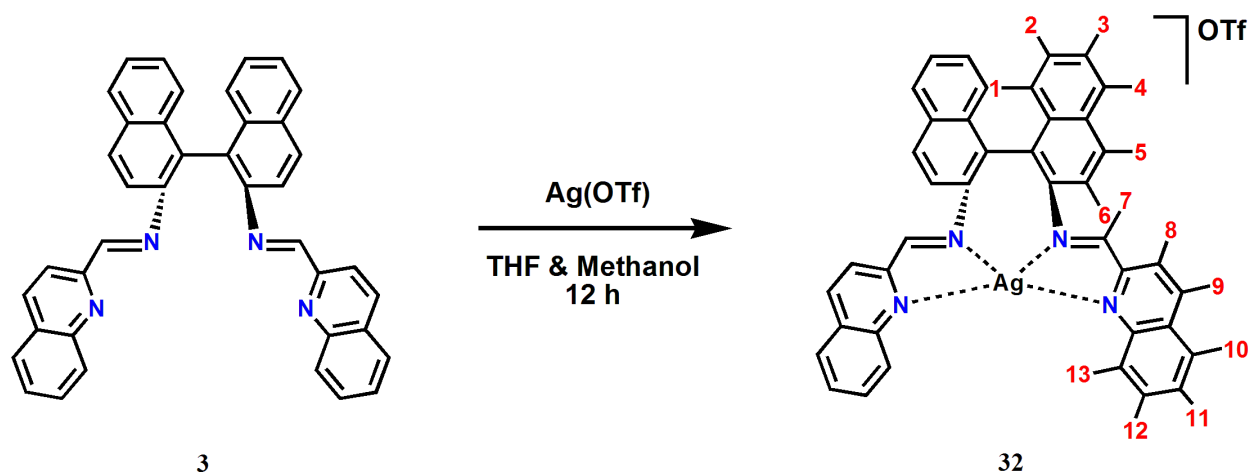
Figure 4.1: Proposed Reaction Scheme for Complex **32**

The reaction of ligand **3** with silver(I) triflate resulted in the ^{1}H NMR spectrum shown in Figure 4.2. We observe that once the ligand chelates with the silver cation to form complex **32**, the aromatic proton peaks spread out and occupy a new range from 5.88 ppm to 9.38 ppm. This is more than double the original aromatic region range present in ligand **3** and is attributed to the interaction of the silver metal atom with the protons of the ligand. Based on the integral values
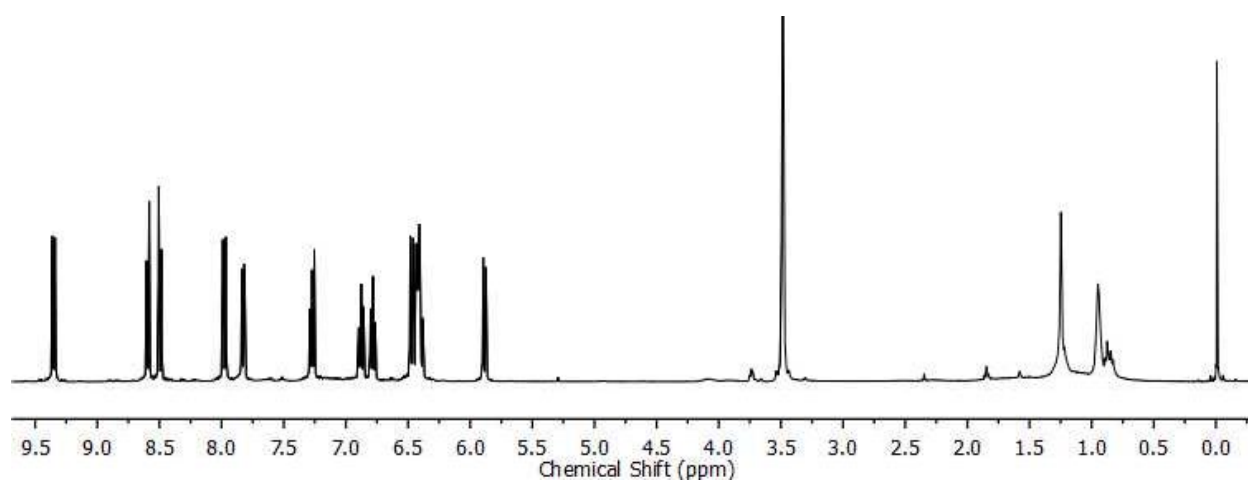
Figure 4.2: 400 MHz ^{1}H NMR Spectrum of Complex **32** (CDCl$_3$)

obtained from the peaks, the spectrum exhibits the right number of resonances (13) that should be obtained for complex **32**. Nine out of thirteen peaks can easily be deduced with substantial overlap observed for the last four signals located between 6.38 ppm and 6.49 ppm.

To interpret this overlapped region, a HSQC experiment was carried out and is shown in Figure 4.3. We observe that there are four cross-peaks in that area, confirming the presence of the last four proton resonances. Since all contours shown in the HSQC spectrum are due to methine protons, we were also able to differentiate the quaternary carbons from the tertiary carbons displayed in the ^{13}C NMR on the x-axis. This was helpful during the analysis and interpretation of the HMBC spectrum conducted for complex **32** (shown in Appendix I).
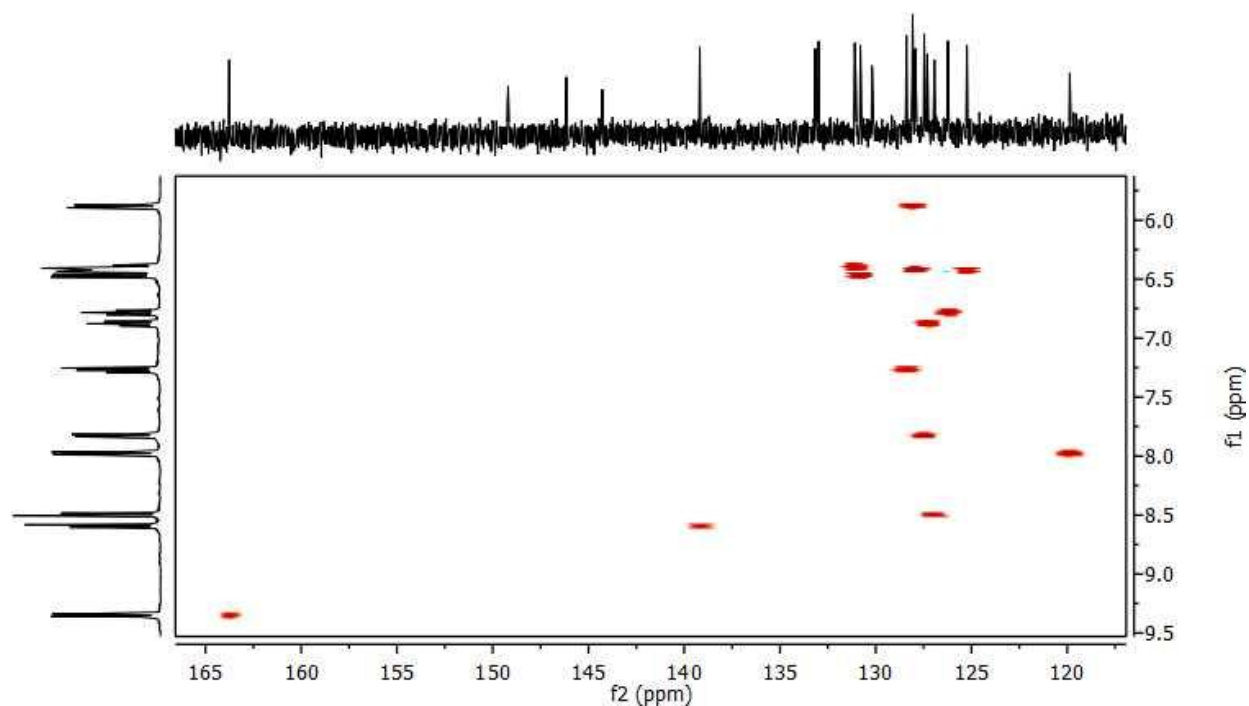
Figure 4.3: 400 MHz HSQC Spectrum of Complex **32** (CDCl$_3$)

An unusual observation in the ^{1}H NMR of complex **32** is the puzzling disappearance of the characteristic imine singlet peak observed at 8.62 ppm in the ^{1}H NMR of the corresponding ligand (**3**). Since complex **32** is symmetric and no reducing agents were added during the complexation reaction, the imine singlet peak should still be present after chelation. The ligand

was not reduced during the reaction as we do not observe the characteristic second order AB pattern in the spectrum as detailed in chapter two. A COSY experiment was conducted to determine how many proton peaks observed in the ^{1}H NMR display coupling and is shown in Figure 4.4. Based on its isolated position in the structure, we expect the characteristic imine proton to stand out as the only cross-peak not coupled to any other proton but we observed that all peaks exhibit coupling. The expected ^{3}J coupling was observed between protons 1→2, 2→3, 3→4, 5→6, 8→9, 10→11, 11→12, and 12→13. As observed in ligand **3**, there were also long range epi, para, peri, and through-space couplings as high as 5 bonds away in the COSY spectrum for the following protons (1→3 {meta}, 1→4 {para}, 1→5 {epi}, 6→7 {through-space}, 7→8 {through-space}, 9→10 {peri}, 13→9 {epi}, 13→10 {para}, and 13→11 {meta}).
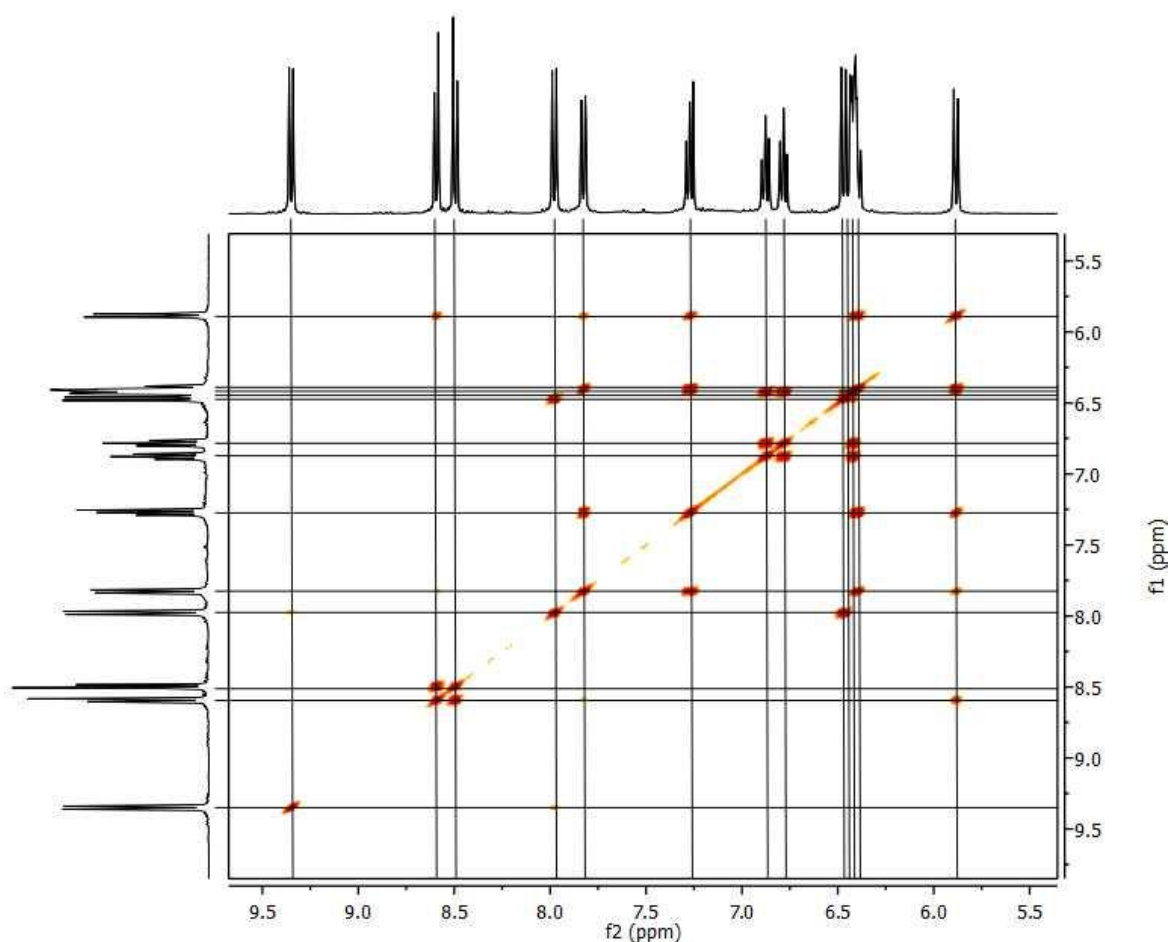
Figure 4.4: 400 MHz COSY Spectrum of Complex **32** (CDCl$_3$)

118

Another 2D NMR technique exploited to understand the proton coupling in complex **32** was the NOESY experiment. This typically shows the proton to proton through-space couplings that are two carbon atoms apart. The spectrum obtained from this experiment is shown in Figure 4.5 and displays the long range coupling between protons 4→5, 6→7, 7→8, and 9→10. The experiment also displays the long range couplings observed in the COSY experiment so care had to be taken when interpreting the results of the NOESY. As shown in the figure below, the proton couplings appear as blue contour points and the four cross-peaks circled in red are not present in the COSY spectrum. These are the proton to proton through-space couplings that are two carbons apart.
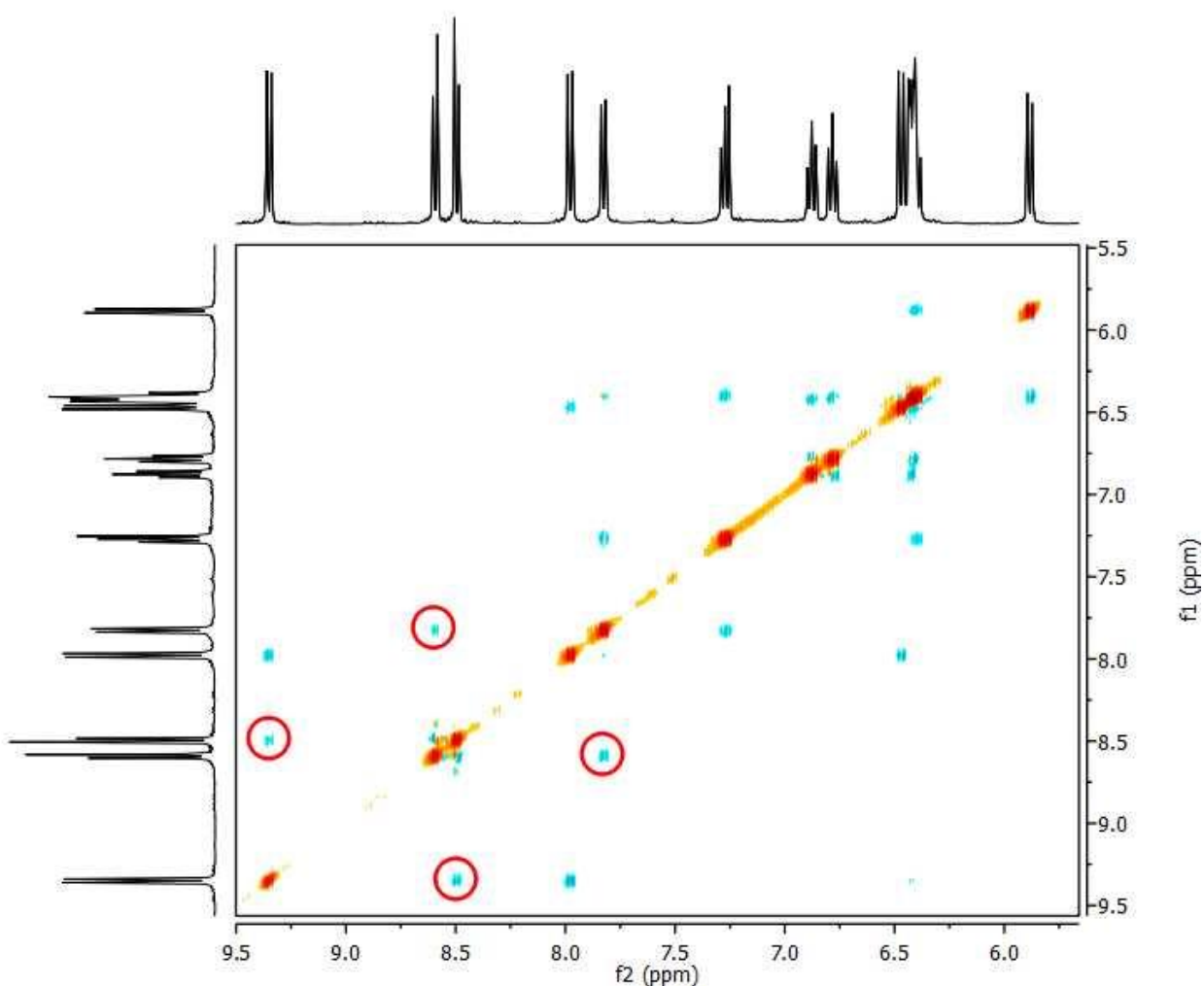
Figure 4.5: 400 MHz NOESY Spectrum of Complex **32** (CDCl$_3$)

119

A survey of other chelation experiments done with silver(I) ions provided an explanation for the disappearance of the imine proton singlet peak in the ^{1}H NMR of complex **32**. The literature shows that the presence of a $^3J(^1H–^{107,109}Ag)$ coupling can be responsible for the appearance of a doublet signal associated with the imine proton.[108-9] The nuclear spin of the metal plays a vital role in the appearance of the imine proton as either a doublet or a singlet. When a diamagnetic spin-half metal is present ($I = \frac{1}{2}$), the imine proton appears as a doublet but when a metal with a spin other than half is present, the imine proton generally appears as a singlet. This is evident in the experiment conducted where similar chiral ligand structures were reacted with silver(I) and copper(I) metal ions.[110] Silver(I) has a spin of half ($I = \frac{1}{2}$) and therefore resulted in a doublet signal for the imine proton in the ^{1}H NMR and copper(I), a quadrupolar nucleus with a spin of three-halves ($I = 3/2$) generated a singlet resonance signal for the imine proton.[110] This might not be a general trend as we observe the reaction of ligand **5** with $CdCl_2$ ($I = \frac{1}{2}$) in chapter three resulting in a singlet peak for the imine proton.

Understanding the role the nuclear spin of the metal plays and recognizing the electron withdrawing nature of the imine (N=C) bond, we proposed that the imine peak in complex **32** was the doublet located downfield at 9.35 ppm. To prove this, we carried out a ^{1}H Homonuclear Decoupling (HOMODEC) experiment on complex **32** (Figure 4.6). This experiment is advantageous because it allows us to isolate a particular frequency on the NMR scale and irradiate it with enough power that the signal essentially becomes lost. When this happens, any other protons neighboring the lost signal will lose the coupling they have with that proton and these changes will be displayed in the HOMODEC spectra obtained. Figure 4.6 shows the irradiated signals with red arrows and the affected resonances with blue arrows. We observe that when we irradiate the suspected imine signal at 9.35 ppm, no other resonance peaks were disrupted proving that the signal at 9.35 ppm is indeed the imine proton. When the doublet (proton #6) at 7.97 ppm was irradiated, we observe the change of the coupled doublet at 6.47 ppm (proton #5) to a singlet peak. Finally, we irradiated the doublet of doublet peak at 7.27 ppm (proton #11), we observe changes to two other coupled signals. The doublet at 7.82 ppm (proton #10) is now a singlet peak and the doublet of doublet signal at 6.40 ppm (proton #12) is now a doublet peak. The results obtained from the HOMODEC experiments also helped verify the proton peak positions obtained from the COSY experiment.
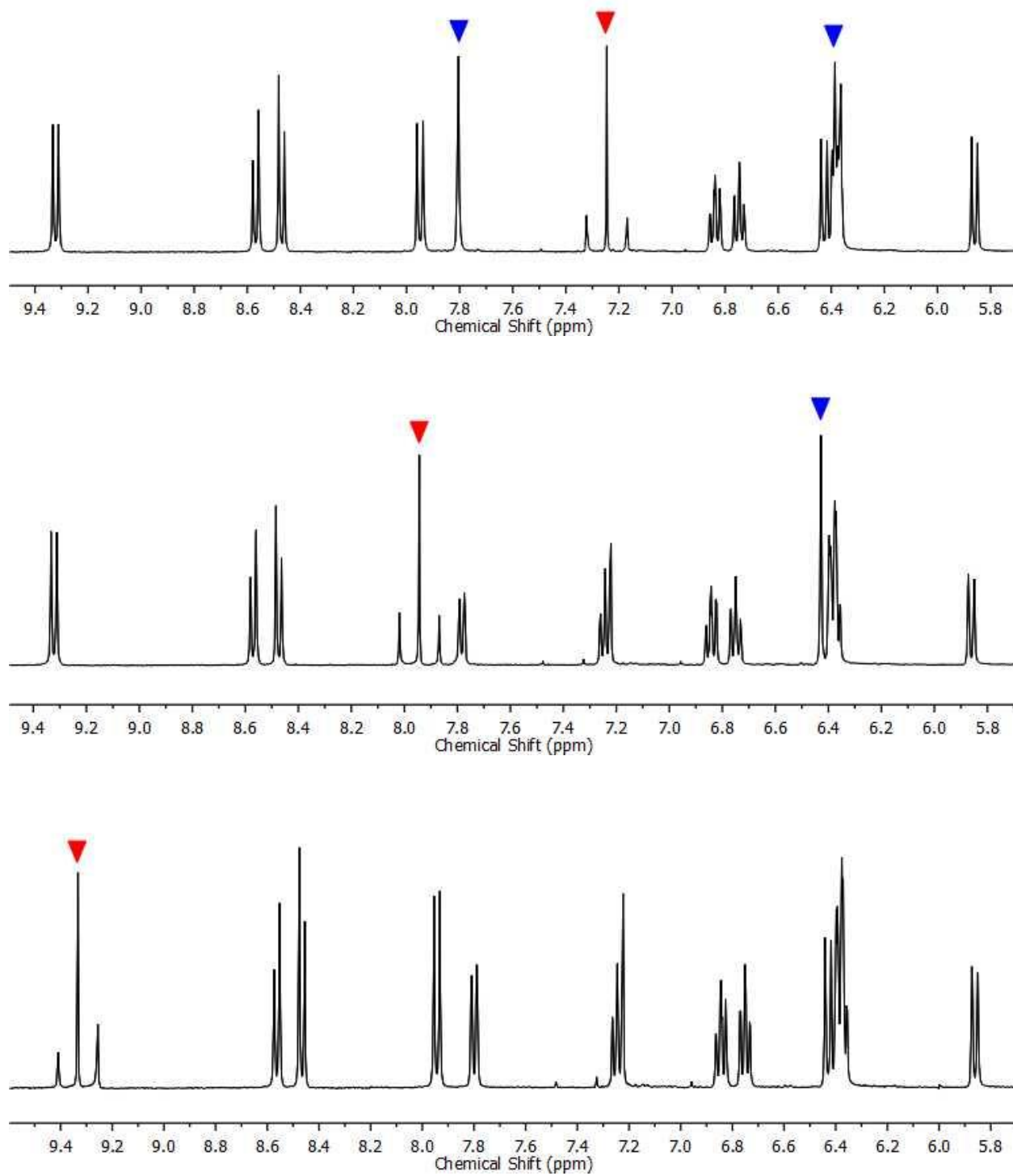
Figure 4.6: 400 MHz ^{1}H HOMODEC Spectrum of Complex **32** (CDCl$_3$)

Combining the results obtained from all 1D and 2D NMR experiments, we are now able to report the complete ^{1}H assignment of complex **32** shown in Figure 4.7. As reported earlier, the imine proton in this complex appears as a doublet peak in the ^{1}H NMR spectrum and is attributed to the presence of a ^{3}J(^{1}H-^{107,109}Ag) coupling with silver having a spin of half (I = ½). As indicated earlier, we believe this occurrence, is unique to the silver(I) metal ion and care should be taken to not generalize all metal centers with a spin of half and a ^{3}J(^{1}H-M) coupling as guaranteed conditions that will result in the coupled proton appearing as a doublet signal. Metallation reactions carried out with ligand **5** and HgBr$_2$, CdCl$_2$, and CoCl$_2$ (all spin half) in chapter three result in ^{1}H NMR spectrum that show the imine proton as a singlet peak. The mercury(II) salt also has an isotope (^{201}Hg) with a spin of 3/2 but ^{109}Hg (I = ½) has a 16.8 % natural abundance and is most likely what is observe in the ^{1}H NMR spectrum obtained for complex **25**. That being said, we move forward with our silver(I) reactions knowing that the imine proton may be observed as a doublet in ^{1}H NMR spectra.

1	(6.43 ppm)
2	(6.88 ppm)
3	(6.78 ppm)
4	(6.41 ppm)
5	(6.47 ppm)
6	(7.97 ppm)
7	(9.35 ppm)
8	(8.49 ppm)
9	(8.59 ppm)
10	(7.82 ppm)
11	(7.27 ppm)
12	(6.40 ppm)
13	(5.88 ppm)
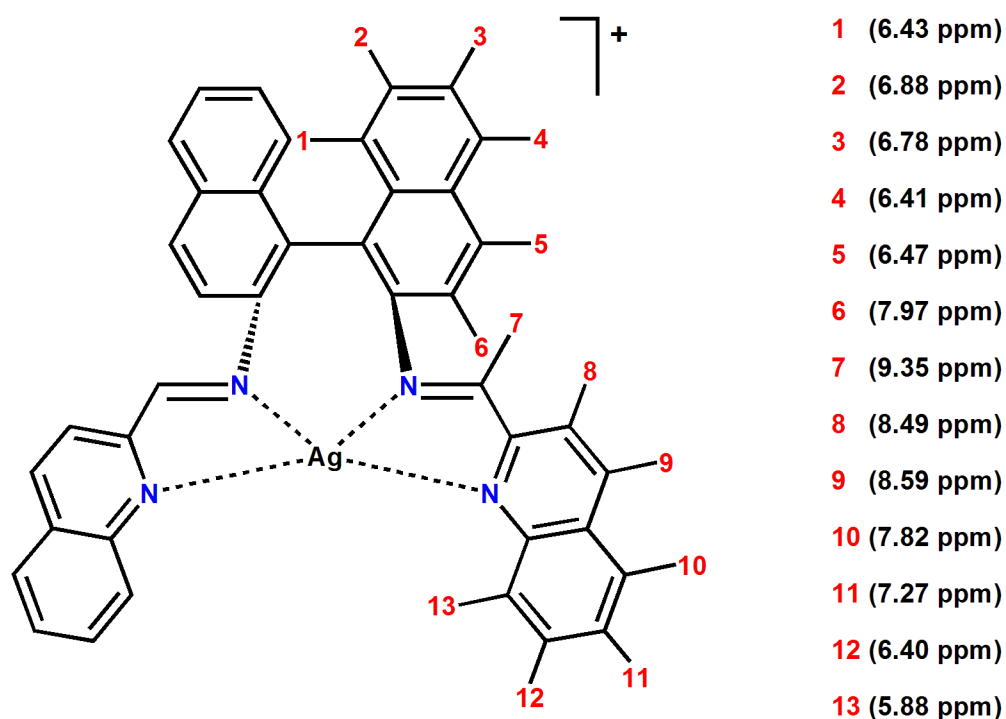
Figure 4.7: Complete ^{1}H Assignment of Complex **32**

122

4.2 Metallation of Ligand 4 with Silver(I) Triflate (Complex 33)
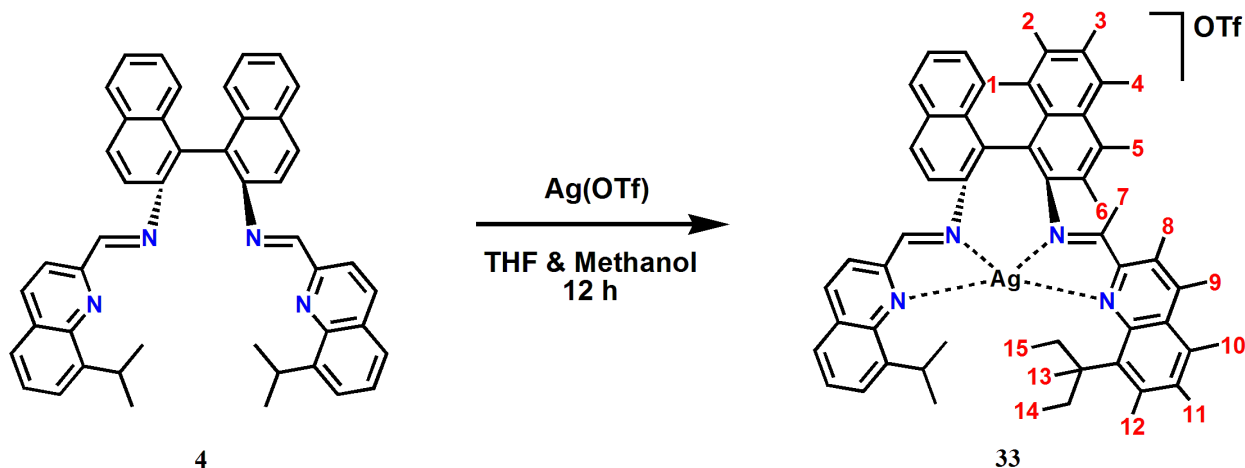
Figure 4.8: Proposed Reaction Scheme for Complex **33**

When ligand **4** was reacted with one equivalent of metal salt, there was an expansion in the aromatic region of the ^{1}H NMR obtained (Figure 4.9); as observed with complex **33**. However, this 1:1 reaction did not produce a pure product as evident in the spectrum obtained. Duplicate synthesis using the same reaction conditions yielded the same impure product. Close examination of the spectrum suggests the presence of two distinct compounds as similar overlapping peak patterns were observed. We propose that ligand **4** chelates more than one metal ion in the center pocket due to the bulky nature of the isopropyl groups on the side-arm. The bulky groups push the side-arms further away from the desired overlapping locked position, increasing the distance between the nitrogen donor atoms; essentially separating the donor groups into two sets. This increased distance therefore allows two silver atoms to fit into the chelating pocket. We have observed this preference for ligand **4** to react with two metal centers in previous reactions carried out using zinc(II) and nickel(II) salts.[61] The spectrum obtained from this reaction with silver(I) triflate reflects a product consisting of a mixture of half complex and half unreacted ligand. We conducted a COSY experiment on this product and the coupling results obtained also support the mixed product conclusion (Appendix I). No further reaction steps or analysis were carried out on this product.
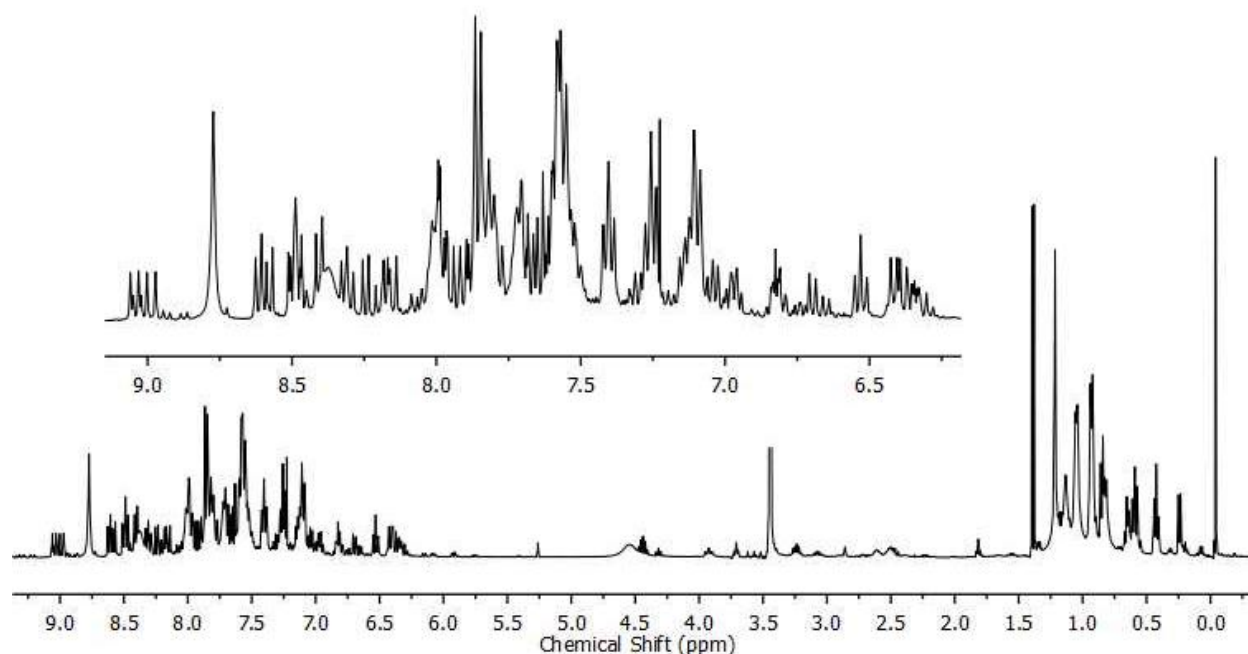
Figure 4.9: 400 MHz ^{1}H NMR Spectrum of Impure Complex **33** (CDCl$_3$)

To support the unreacted ligand hypothesis, ligand **4** was subsequently reacted with two equivalents of silver(I) triflate. The ^{1}H NMR spectrum obtained shows the formation of pure complex **33** (Figure 4.10). This suggests that ligand **4** requires more than one silver ion to form a complex. The reaction was also carried out with four equivalents of silver(I) triflate and resulted in the same clean ^{1}H NMR spectrum obtained when two equivalents of metal salt was used (Appendix I). A residual white precipitate was present at the end for the reaction, likely due to left over unreacted silver(I) triflate. While analyzing the spectra obtained for complex **33**, two interesting observations are apparent;

1. There is no expansion in the aromatic peak region as was observed in the ^{1}H NMR spectrum of complex **32**.
2. The characteristic imine singlet that appears at 8.59 ppm in ligand **4** is still present as a singlet at 8.92 ppm in complex **33**. As we recall, this singlet appeared as a doublet in the synthesis of complex **32** and was due to the presence of a $^3J(^1H-^{107,109}Ag)$ coupling.

124
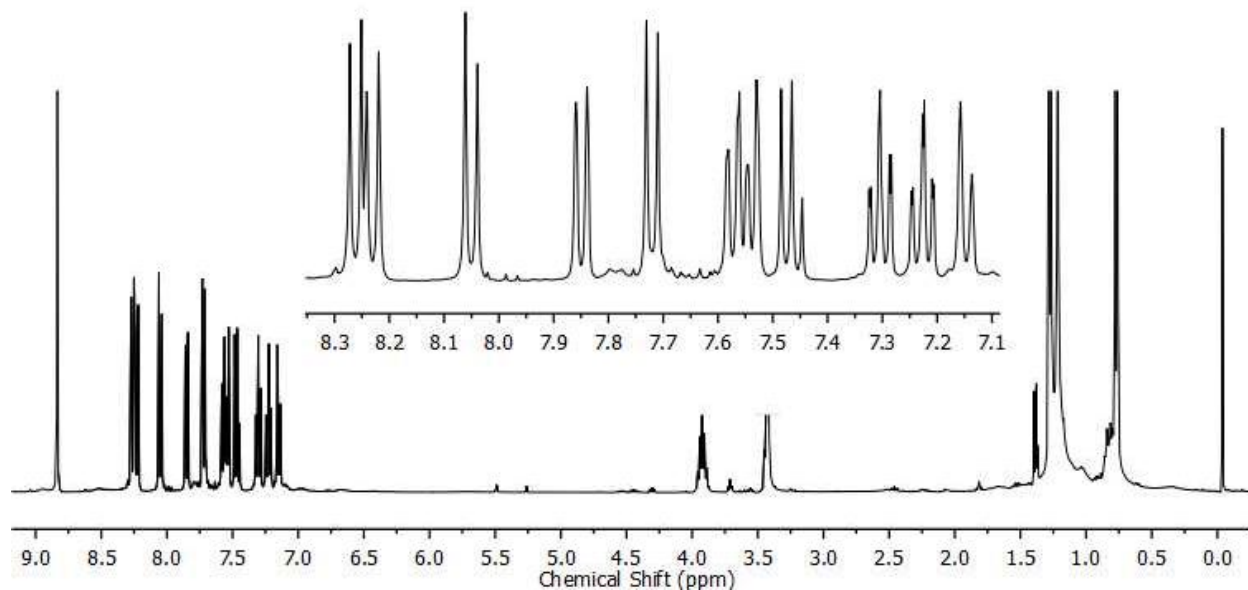
Figure 4.10: 400 MHz ^{1}H NMR Spectrum of Pure Complex **33** (CDCl$_3$)

The retention of the imine singlet resonance is most likely due to the fact that ligand **4** reacts with more than one equivalent of silver, altering the ^{3}J(^{1}H–^{107,109}Ag) coupling that would have otherwise occurred. We clearly see the expected number of resonance peaks (15) in the ^{1}H NMR for complex **33**. Three sets of doublet of doublet peaks appear at 7.31ppm, 7.39 ppm, and 7.65 ppm. The imine singlet appears at 8.92 ppm and the eight doublet peaks span from 7.45 to 8.28 ppm. The isopropyl methine peak is preserved as a septet at 4.01 ppm and the isopropyl methyl peaks are identified, with the aid of coupling constants, at 0.85 ppm and 1.36 ppm. Due to the free rotation of the methyl groups about the methine carbon, the observed doublet peaks cannot be assigned to the exact methyl groups. To observe the proton coupling, a COSY experiment was performed on complex **33** and is shown in Figure 4.11 and 4.12. The expected ^{3}J couplings are observed for protons (1→2, 2→3, 3→4, 5→6, 8→9, 10→11, 11→12, 13→14, and 13→15). The imine singlet once again experiences atypical long range coupling with proton 6 and proton 8. This is likely due to the imine double bond continuing the conjugation to the backbone and sidearms as the complex can form resonance structures. We do not observe the unusual coupling of proton 13 from the isopropyl unit with proton 12 in the quinoline ring as observed in the COSY spectrum for the corresponding ligand **4**.

125
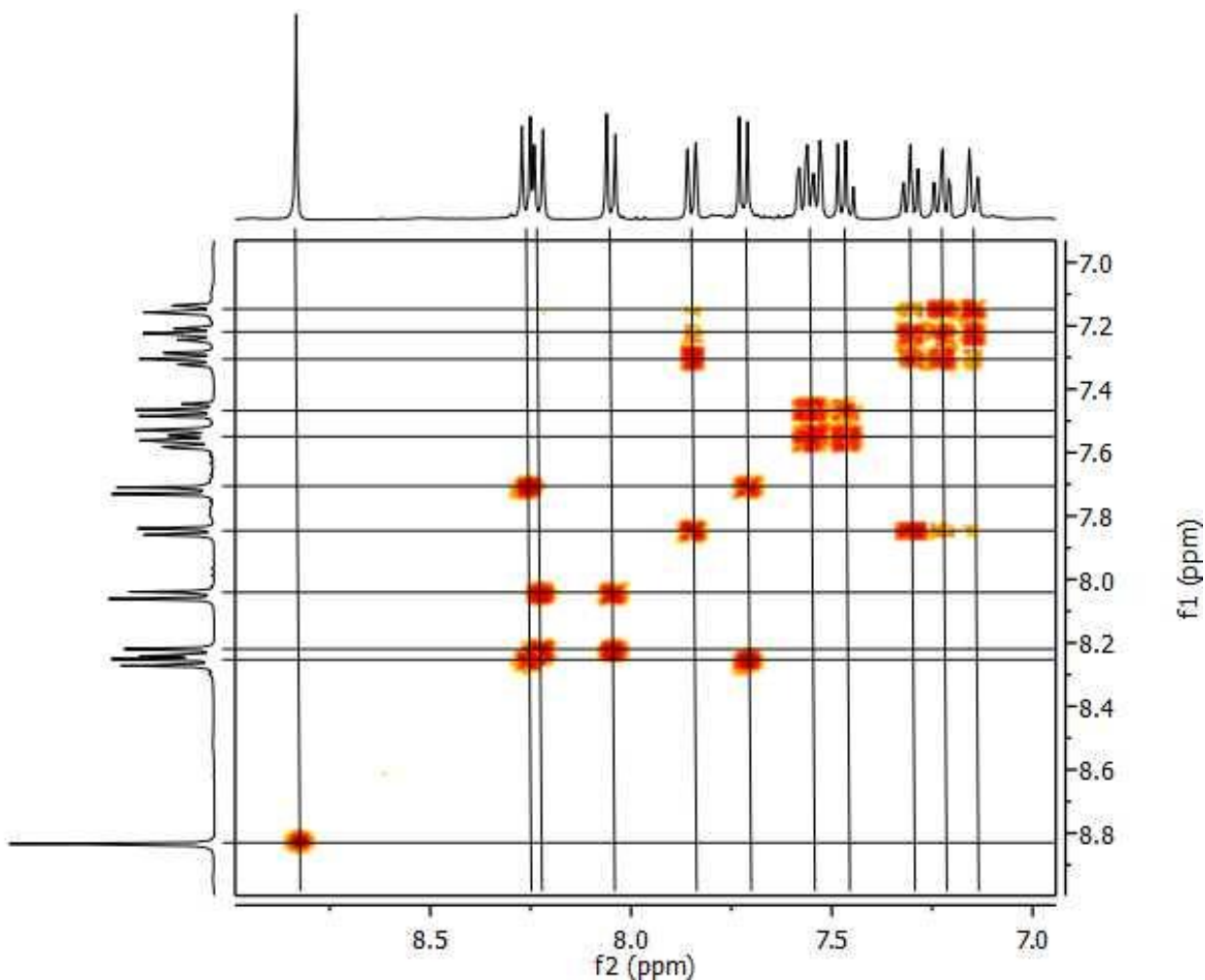
Figure 4.11: 400 MHz Aromatic Region COSY Spectrum of Complex **33** (CDCl₃)

Again, we observe long range epi, peri, para, and through-space coupling for protons (1→3 {meta}, 1→4 {para}, 1→5 {epi}, 6→7 {through-space}, 7→8 {through-space}, 9→10 {peri}, and 10→12 {meta}). These long range couplings are most likely due to the complex orienting itself with enough twist to bring those protons spatially close to interact with one another. The aliphatic region of the COSY experiment shows the expected coupling of proton 13 with protons 14 and 15 (Figure 4.12). As discussed in the analysis of Ligand **4**, there is free rotation of the methyl groups about the methine carbon so it is difficult to assign which methyl group belongs to the peak position at 0.85 ppm or at 1.36 ppm.
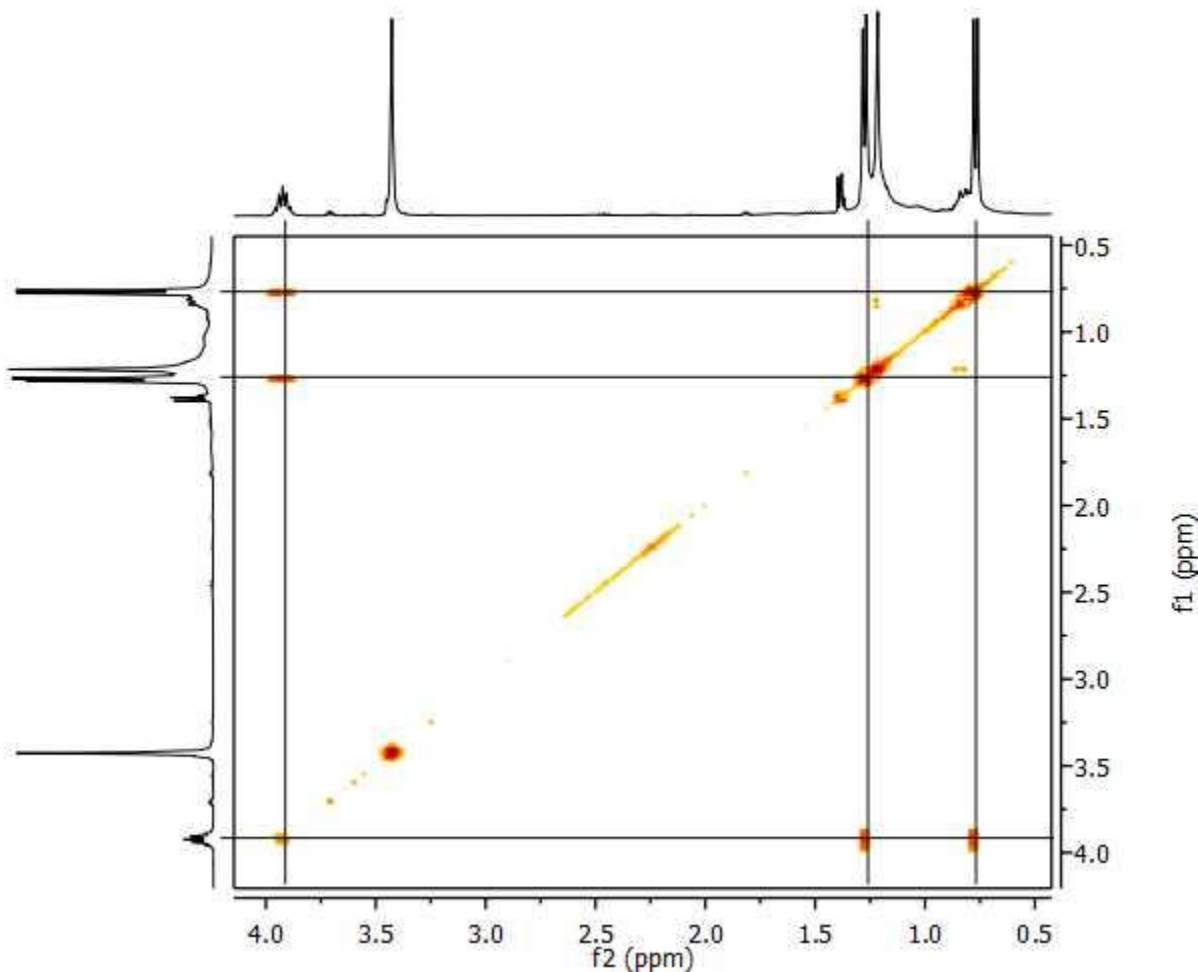
Figure 4.12: 400 MHz Aliphatic Region COSY Spectrum of Complex **33** (CDCl$_3$)

We conducted a HSQC experiment on complex **33** and the spectrum acquired is shown in Figure 4.13. We obtain the right number of contour peaks for the aromatic region (13) and the aliphatic region (3). We observe that the imine carbon has an isolated contour peak at 163 ppm and this is due to the electron withdrawing nature of the nitrogen atom in the imine bond. The ^{1}H NMR spectrum for complex **33** is well defined so there were no proton-carbon couplings to resolve in the HSQC experiment. That being said, the experiment helped us differentiate quaternary carbons from tertiary carbons on the x-axis ^{13}C spectrum which was beneficial in analyzing the HMBC spectrum obtained for complex **33** (Appendix I).
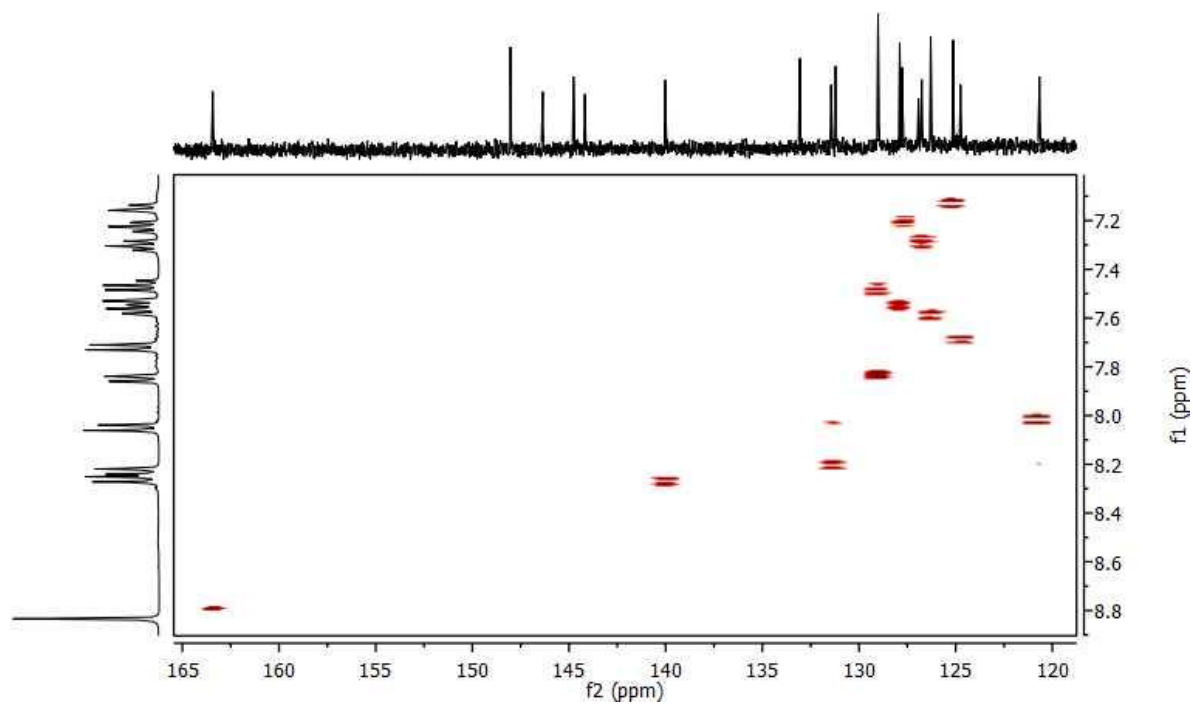
Figure 4.13: 400 MHz Aromatic Region HSQC Spectrum of Complex **33** (CDCl₃)
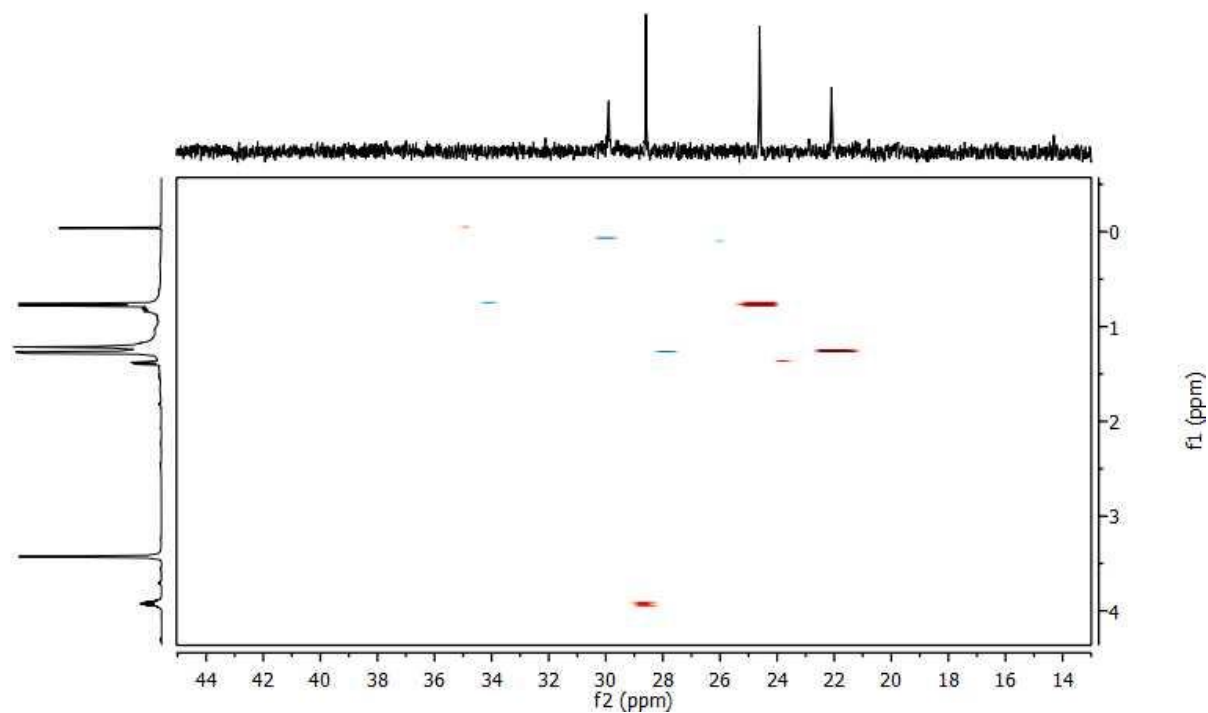
Figure 4.14: 400 MHz Aliphatic Region HSQC Spectrum of Complex **33** (CDCl₃)

To establish that the singlet observed at 8.92 ppm is due to the imine proton, we once again carried out a ^{1}H homonuclear decoupling experiment on complex **33** (Figure 4.15). When the selected imine singlet was irradiated, no other proton resonance peaks were affected proving that the singlet at 8.92 ppm is indeed the imine proton peak. This happens because there are no neighboring protons that experience coupling with the imine proton. When other selected proton peaks (red triangles) were irradiated in this experiment, their corresponding coupled peaks (blue triangles) were simultaneously affected. This experiment helped verify all the proton peak positions obtained from couplings in the COSY experiment. The combination of all 1D and 2D experiments allowed for the successful ^{1}H assignment of complex **33** (Figure 4.16).
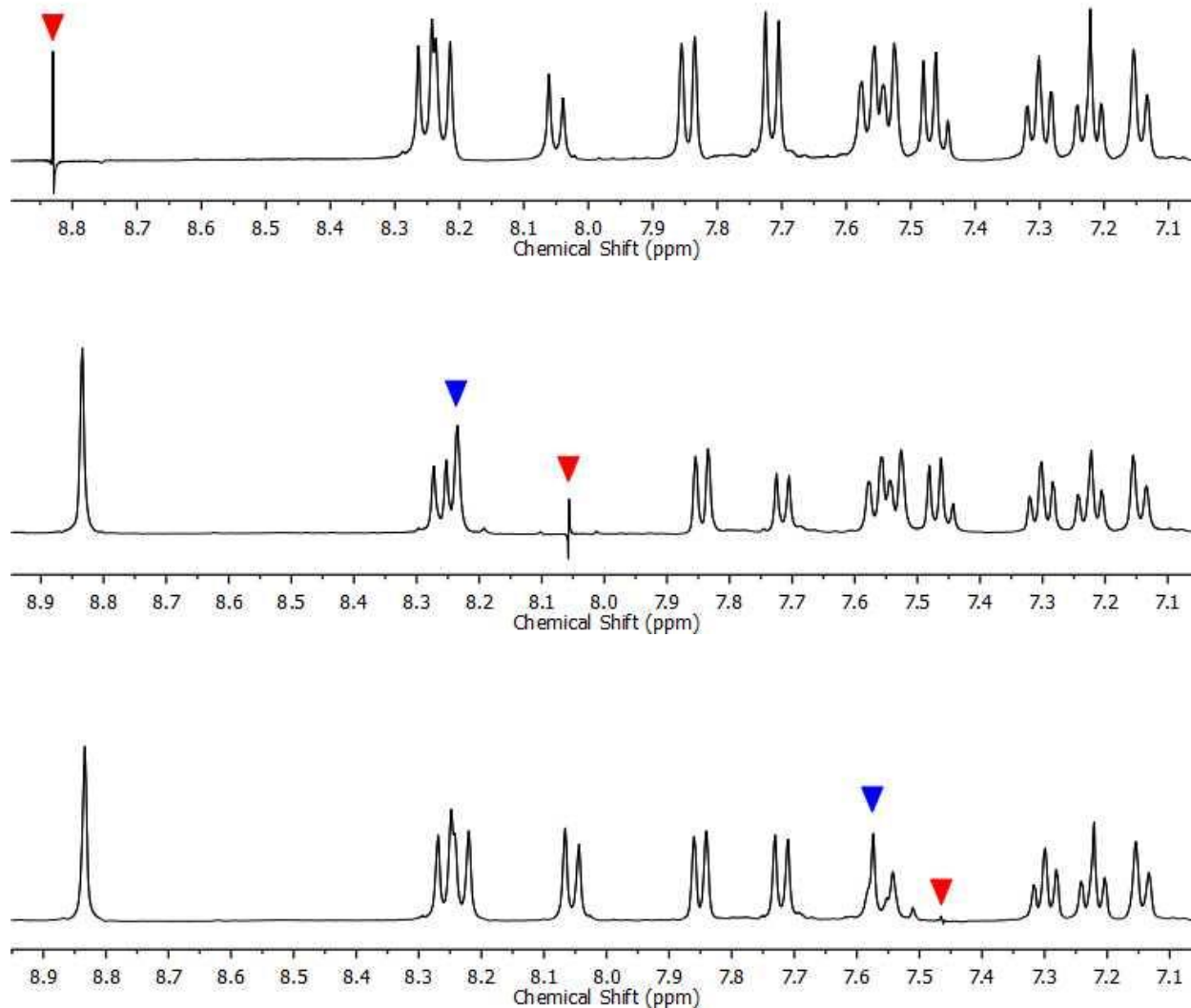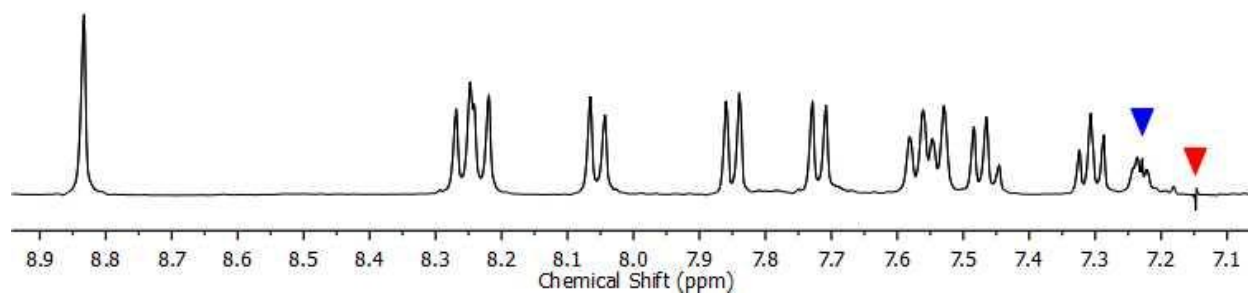
Figure 4.15: 400 MHz ^{1}H HOMODEC Experiment of Complex **33** (CDCl$_3$)

1	(7.93 ppm)
2	(7.39 ppm)
3	(7.31 ppm)
4	(7.23 ppm)
5	(8.31 ppm)
6	(8.13 ppm)
7	(8.92 ppm)
8	(7.80 ppm)
9	(8.34 ppm)
10	(7.62 ppm)
11	(7.65 ppm)
12	(7.55 ppm)
13	(4.01 ppm)
14	(0.85/1.36 ppm)
15	(0.85/1.36 ppm)
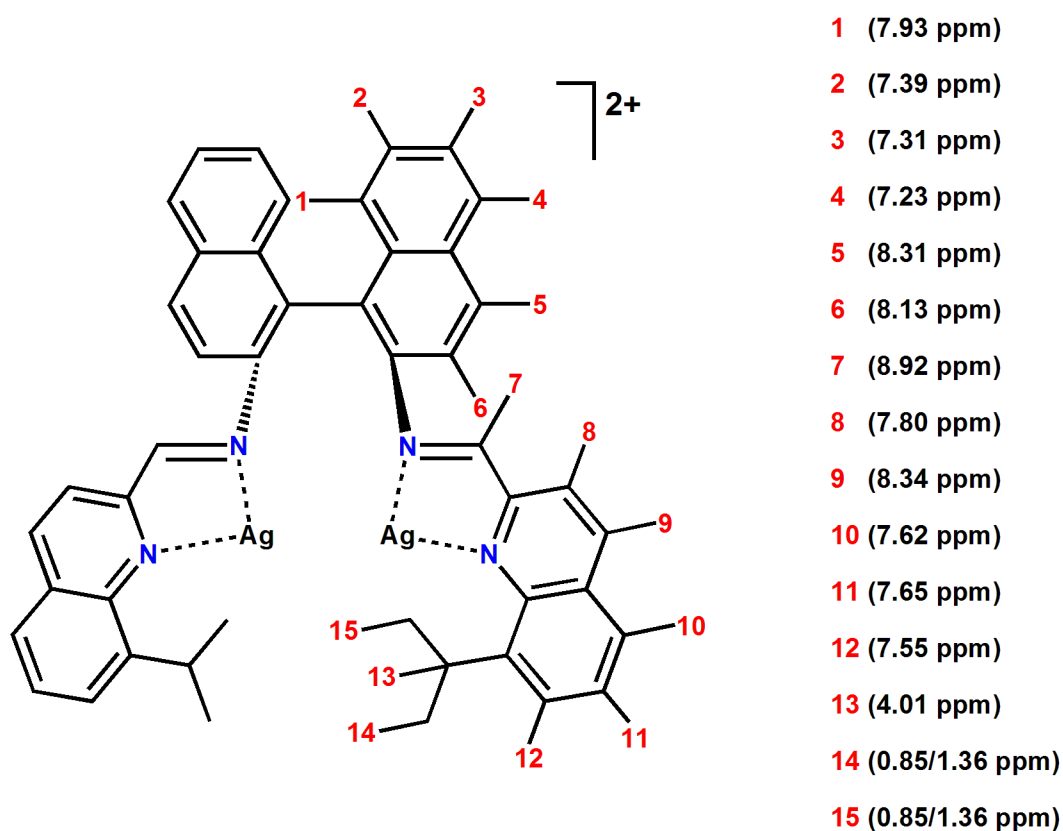
Figure 4.16: Complete ^{1}H Assignment of Complex 33

4.3 Metallation of Ligand 5 with Silver(I) Triflate (Complex 34)
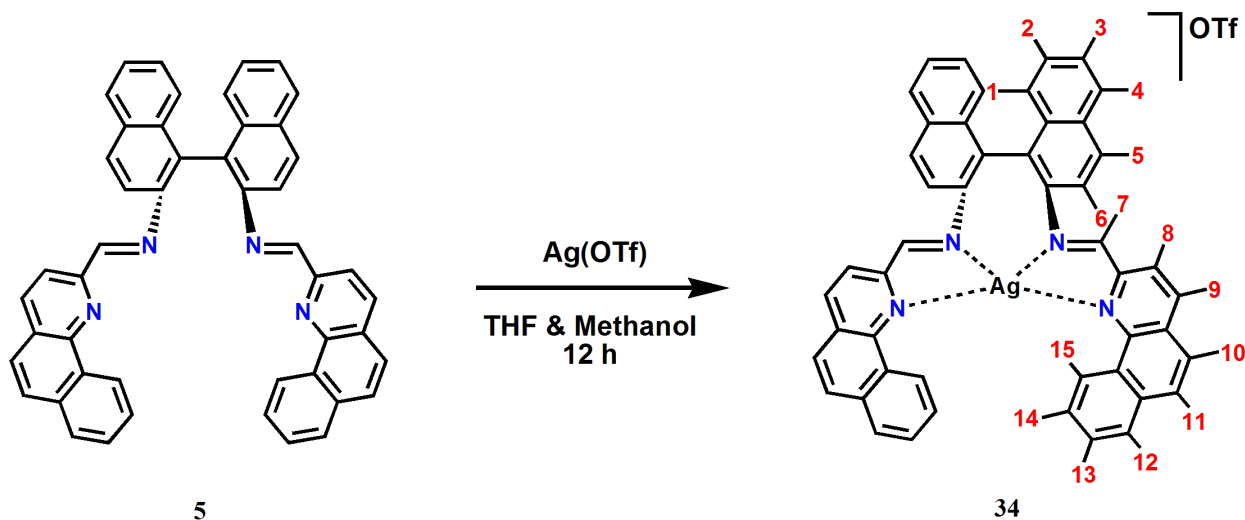
Figure 4.17: Proposed Reaction Scheme for Complex **34**

We obtain complex **34** from the reaction of ligand **5** with one equivalent of silver(I) triflate. The reaction produces a sand-brown colored product in 91.7 % yield. No further purification was carried out on the product. The product was stored in the glove box to prevent any exposure to atmospheric water vapor which may decompose the complex. Aluminum foil was also used to cover the storage vial to prevent the reduction of silver(I) to silver metal. The final complex further demonstrates the effect the silver ion has on the aromatic proton positions as evident in the ^{1}H NMR obtained in Figure 4.18. After complexation, the aromatic proton region expands to a range of three times what was originally observed in the corresponding ligand **5**. This expansion is not observed in any of our other complexation reactions that result in diamagnetic compounds as evident in the ^{1}H NMR spectra reported for all complexes synthesized in chapter three. Based on the integral values obtained from the peaks, the spectrum exhibits the expected number of resonance peaks for a C_2 symmetric complex (15). We clearly see thirteen signals in the aromatic region corresponding to ten doublets and three doublet of doublet peaks. There is a slight resonance overlap observed at 6.08 ppm which contains the last doublet and doublet of doublet signals.
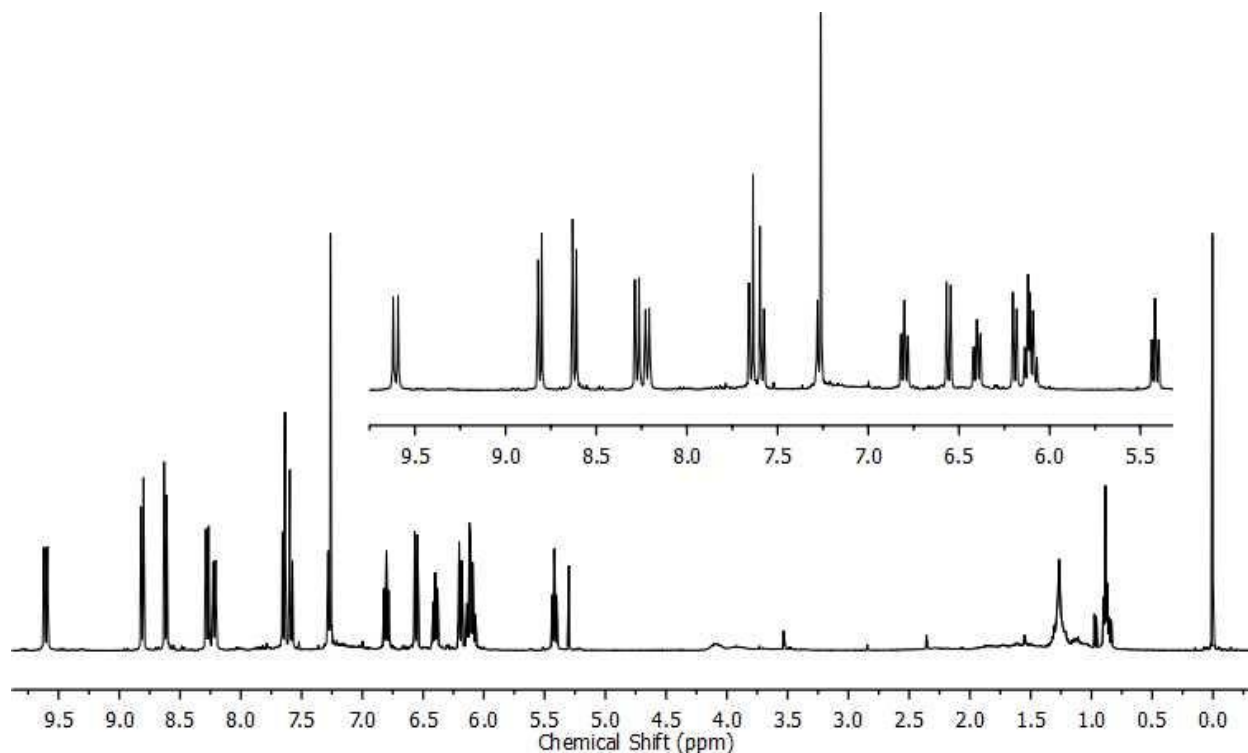
Figure 4.18: 400 MHz ^{1}H NMR Spectrum of Complex **34** (CDCl$_3$)

An HSQC experiment was carried to clarify the signal overlap observed at 6.08 ppm and is shown in Figure 4.19. It clearly shows two cross-peaks in that area and confirms that there are two carbon to proton correlations at 6.08 ppm. An observation worth noting is that the imine carbon peak again appears isolated but has shifted positions compared to both complex **32** and complex **33**. We observe this cross peak at 178.5 ppm for complex **34** which is a 14 ppm difference compared to the HSQC spectra for complexes **32** and **33**. The remaining aromatic peaks are centered between 132.5 ppm and 150 ppm as is similar to what we observe in the HSQC spectrum of complex **32** and complex **33**. This spectrum along with the Heteronuclear Multiple Quantum Coherence (HMBC) spectrum obtained for complex **34** (Appendix I) shows the remaining thirteen cross-peaks in the aromatic region and helped us distinguish the tertiary methine carbons from the quaternary ones in the x-axis ^{13}C NMR spectrum. The HMBC spectrum displayed long range proton to carbon couplings up to 4 bonds away.
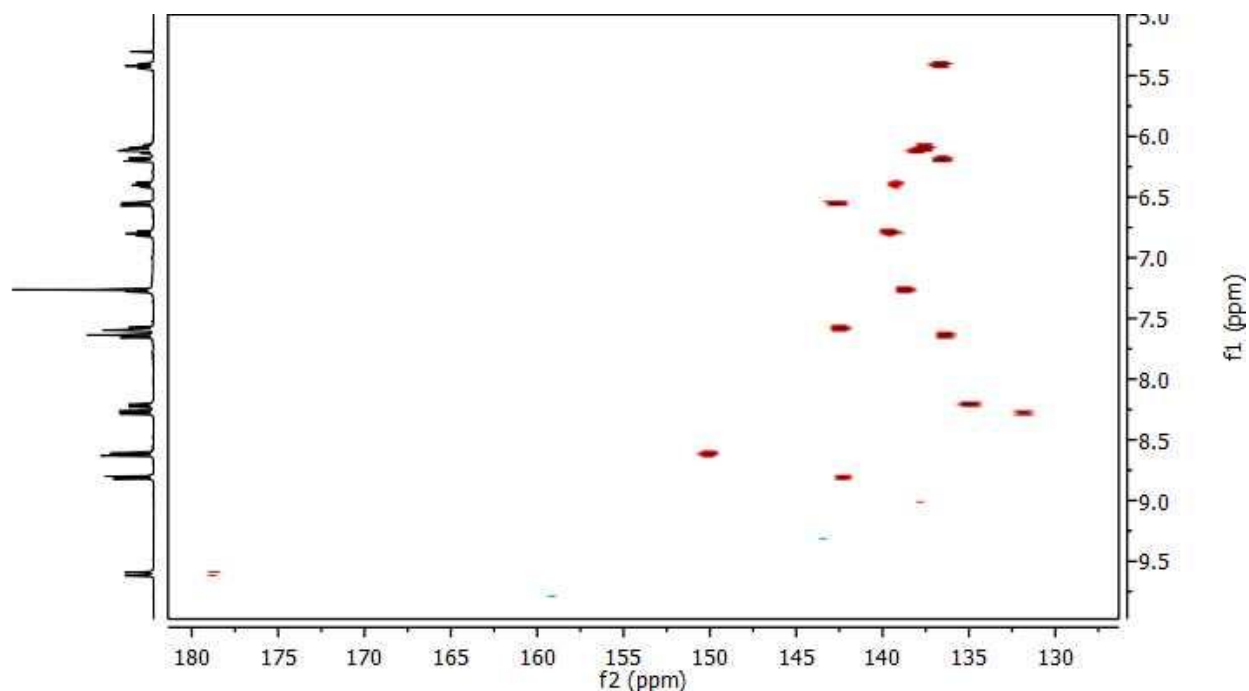
Figure 4.19: 400 MHz HSQC Spectrum of Complex **34** (CDCl$_3$)

Once again, we observe the transformation of the imine singlet peak into a doublet at 9.58 ppm as detected in the ^{1}H NMR of complex **32**. In this metallation reaction, the ligand chelates the silver ion in a 1:1 ratio preserving the unique ^{3}J(^{1}H–^{107,109}Ag) coupling that leads to that signal transformation. A COSY experiment was conducted to determine how many proton peaks observed in the ^{1}H NMR display coupling (Figure 4.20). Once again, based on its position in the structure, we expect the characteristic imine proton to stand out as the only cross-peak not coupled to another proton but we observed that all peaks exhibited some sort of coupling. The expected ^{3}J bond coupling was observed between protons 1→2, 2→3, 3→4, 5→6, 8→9, 10→11, 12→13, 13→14, and 14→15. And as observed in previous ligands and complexes, there were also long range epi, para, peri, and through-space couplings as high as 5 bonds away (1→3 {meta}, 1→4 {para}, 1→5 {epi}, 9→10 {para}, 11→12 {para}, 11→15 {epi}, and 12→14 {meta}). We do not observe the coupling of proton #7 with protons #6 and #8 as observed in the COSY of the corresponding ligand **5** suggesting that the twist in the structure of complex **34** is not large enough to bring those protons spatially close to each other.
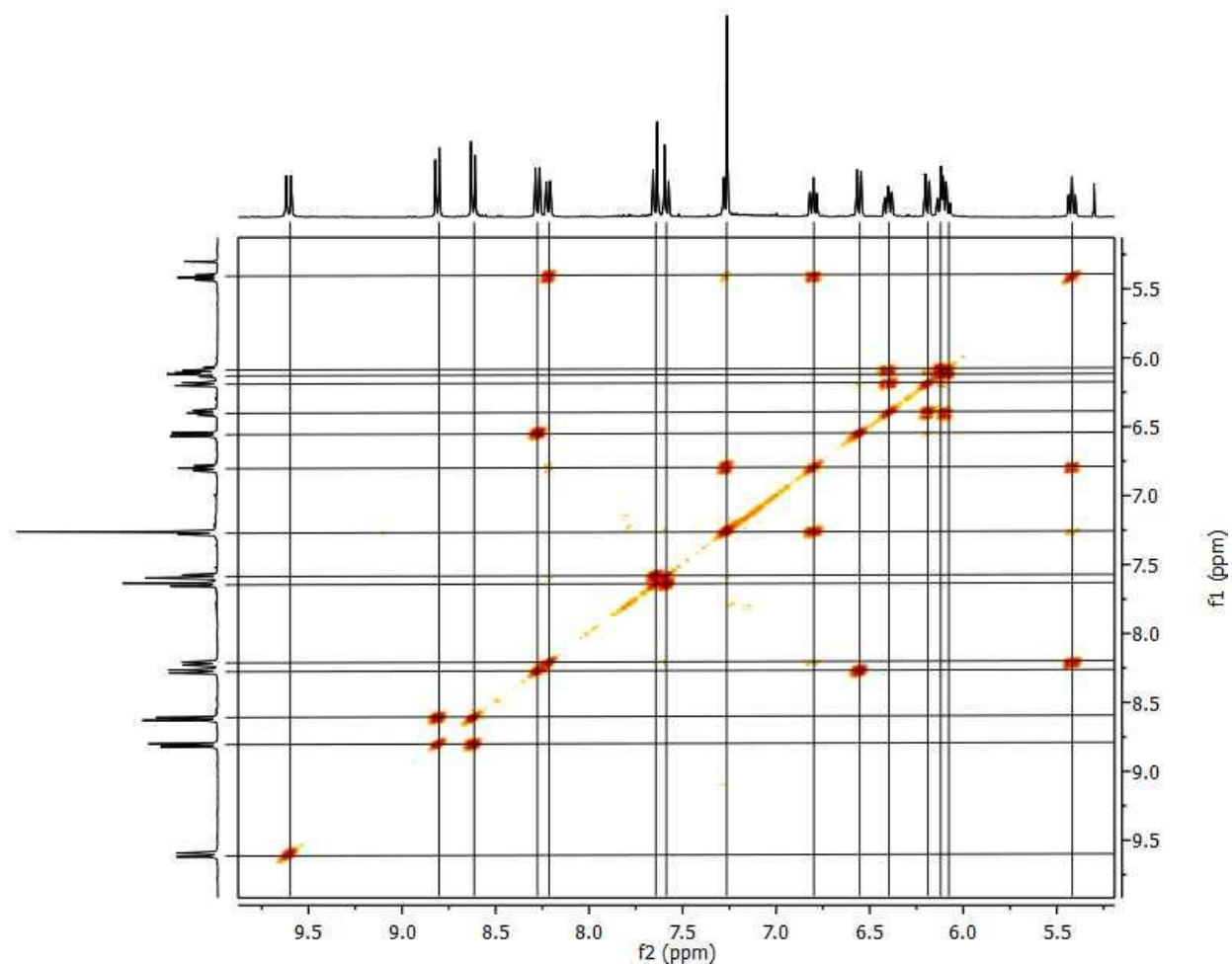
Figure 4.20: 400 MHz COSY Spectrum of Complex **34** (CDCl$_3$)

The NOESY experiment conducted on complex **34** is shown in Figure 4.21 and illustrates the proton to proton through-space correlation for protons 4→5, 6→7, 7→8, 9→10, and 11→12. These are typically cross-points that do not appear on a COSY spectrum as they are further than 3 bonds away. Looking at the proposed reaction scheme for complex **34** we expect to see five proton to proton couplings in the NOESY spectrum and that is what we observe. Here we observe the imine proton coupling to a proton in the binaphthalene backbone and a proton in the benzoquinoline side-arm. This suggests that a twist does exist in the complex due to the binaphthalene backbone the geometry of the silver(I) metal center to bring those protons spatially close together and was just not present in the COSY spectrum.
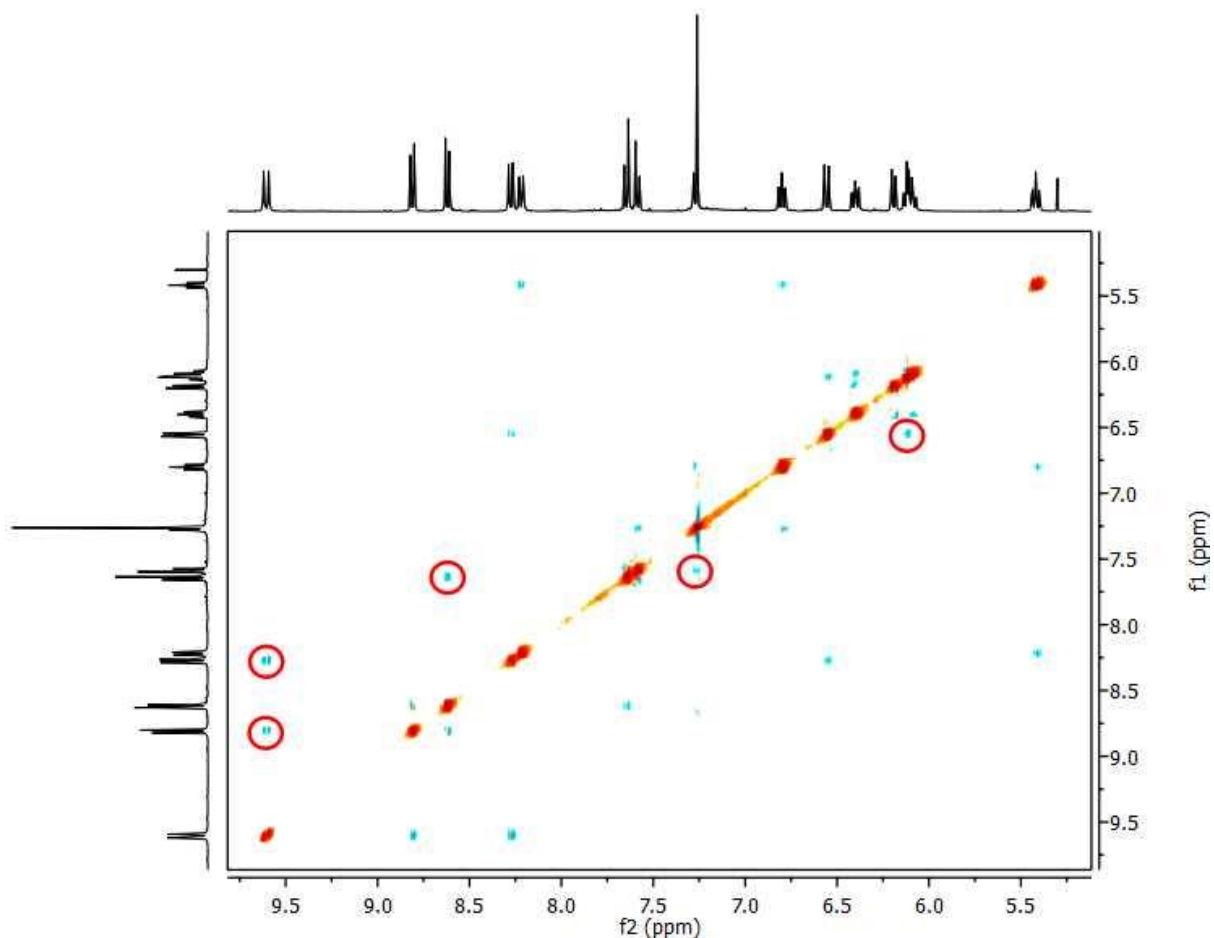
Figure 4.21: 400 MHz NOESY Spectrum of Complex **34** (CDCl$_3$)

As described in complex **34**, we predicted that the imine doublet peak is located at 9.58 ppm because the downfield shift can be explained by the electron withdrawing nature of N=C bonds. To prove this, we carried out a ^{1}H homonuclear decoupling experiment on the complex (Figure 4.22). When the selected doublet at 9.58 ppm was irradiated (red triangle), no other proton resonance peaks were affected in the experiment proving that the doublet at 9.58 ppm is indeed the imine proton. When the doublet at 8.78 ppm (proton #8) was irradiated, we observed the transformation of the doublet at 8.59 ppm (proton #9) into a singlet as they are coupled to each other. Finally, when the triplet at 5.40 ppm (proton #14) was irradiated, protons #15 and #13 were simultaneously affected. These results, once again, helped support the proton coupling results obtained in the COSY experiment for complex **34**.
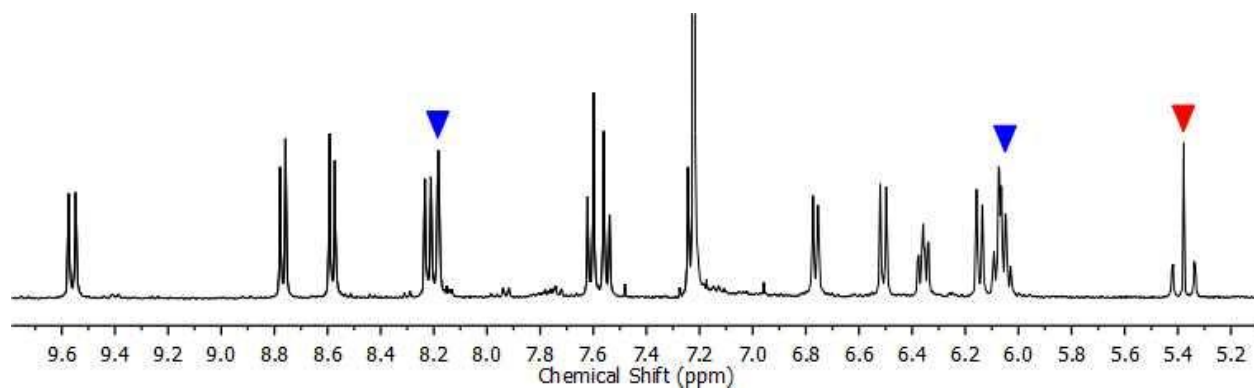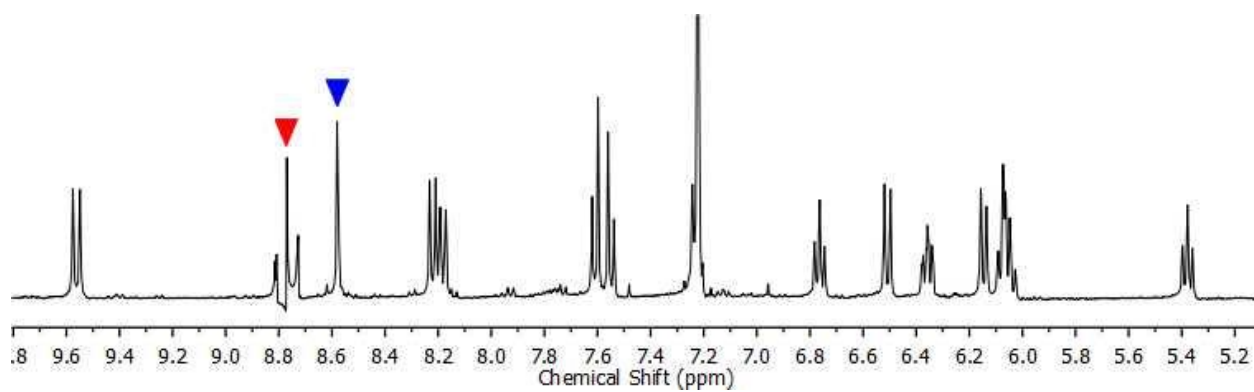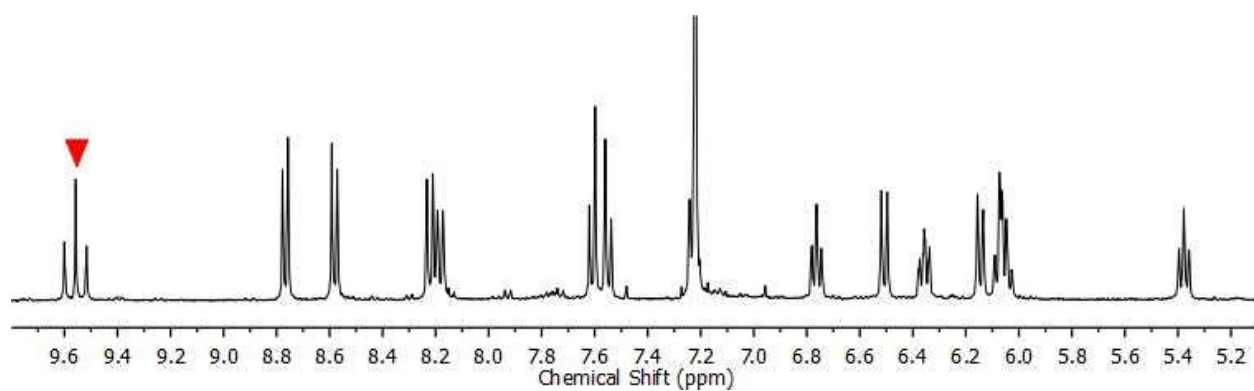
Figure 4.22: 400 MHz ^{1}H HOMODEC Experiments for Complex **34** (CDCl$_3$)

The HMBC spectrum obtained for complex **34** is shown in the supplementary material. This experiment, in concurrence with the COSY, HSQC, ^{13}C NMR, ^{1}H NMR and NOESY served as key tools that allowed us to solve the complete ^{1}H NMR assignment of the complex **34** (Figure 4.23). A quick glance at the proton peak positions show a similar pattern to what we obtained for complex **32** but is slightly different from the peak pattern obtained for complex **33**. This could be due to the observation that ligand **4** preferentially binds to two equivalents of silver(I) triflate interrupting the $^3J(^1H-^{107,109}Ag)$ coupling that would have otherwise occurred changing the shielding effect felt by the protons in the complex. A more detailed comparison of all three complexes as we transition from ligand to complex with silver(I) will be given towards the end of this chapter.

1	(6.17 ppm)
2	(6.38 ppm)
3	(6.09 ppm)
4	(6.06 ppm)
5	(6.53 ppm)
6	(8.25 ppm)
7	(9.58 ppm)
8	(8.78 ppm)
9	(8.59 ppm)
10	(7.62 ppm)
11	(7.56 ppm)
12	(7.25 ppm)
13	(6.78 ppm)
14	(5.40 ppm)
15	(8.19 ppm)
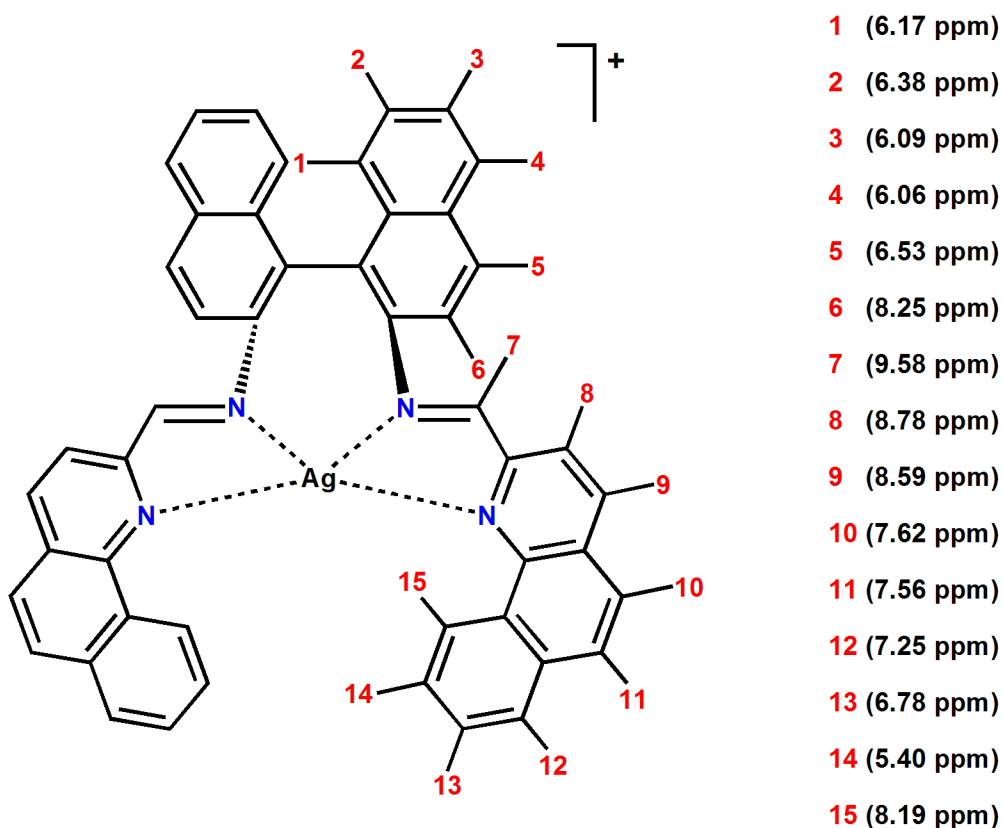
Figure 4.23: Complete [1]H Assignment of Complex **34**

We were successful in growing single crystals of complex **34** suitable for X-ray analysis using the solvent diffusion method. The thermal ellipsoid structure obtained is shown in Figure 4.24 and shows that complex **34** is a dinuclear compound. The binding occurs in a 1:1 ratio of ligand to silver(I) cation but the metal center binds to nitrogen donor atoms in the binaphthalene backbone and the nitrogen atoms the benzoquinoline side-arm of two separate ligands. Not all four nitrogen donor atoms are bound to the metal center with one silver cation adapting a trigonal planar geometry as it is bound to two nitrogen donor atoms from one ligand and one nitrogen donor atom from the benzoquinoline side-arm of the second ligand. The other silver metal center appears to bind to only two nitrogen donor atoms both form the binaphthalene backbone of different ligands taking on a bent or angular geometry. The ligands are arranged with the benzoquinoline side-arm of one ligand stacked with the binaphthalene backbone of the second ligand. This orientation suggests that π-π or σ-π interactions played a significant role in the orientation of complex **34** in the solid state. These interactions are more clearly seen in the space filling model structure for complex **34** shown in Figure 4.25.

The crystal arranges itself in a P2(1) space group and has a monoclinic crystal system. The bond lengths present in the structure give us valuable information about the complex. For the silver atom coordinated to the three nitrogen groups, we observe the following bond lengths: 2.051 Å for Ag2-N254, 2.157 Å for Ag2-N251, and 2.562 Å for Ag2-N111. We notice that the bond length is significantly longer for the metal cation bound to the lone nitrogen donor group from the benzoquinoline side-arm. The second metal center has the following bond lengths: 1.885 Å for Ag1-N252 and 2.594 Å for Ag1-N112. Once again the bond to the nitrogen donor atom on the benzoquinoline side-arm is significantly longer. We can observe the stretch in the ligands as the side-arms are pulled away from the binaphthalene backbones by noting their bond lengths. We have 1.4758 Å for N251-C121 and 1.390 Å for C351-C361. The imine bond lengths are the same for two bound silver(I) cations with 1.264 Å for C251-N251 and 1.264 Å for C252-N252. Complex **34** has a lot of twist incorporated in various parts of the structure so examining the bond angles of select areas will provide us with some valuable information. We observe the following bond angles for the silver cation bound to the three nitrogen donor atoms: 166.4^o for N254-Ag2-N251, 121.4^o for N252-Ag2-N111, and 68.9^o for N251-Ag2-N11. The second silver cation bound to only two nitrogen donor atoms has the following bond angles: 156.8^o for N252-

Ag1-N253 and 71.9° for N252-Ag1-N112. The torsion angles also provide us with valuable information on complex **34**. Some of the important ones are as follows: 151.6° for N254-Ag2-N111-C121, and -18.5° for N251-Ag2-N11-C121. Table 4.1 shows other important bond distances, bond angles, and torsion angles for complex **34**. Complete crystal data and structure refinement information for complex **34** can be found in Appendix II.
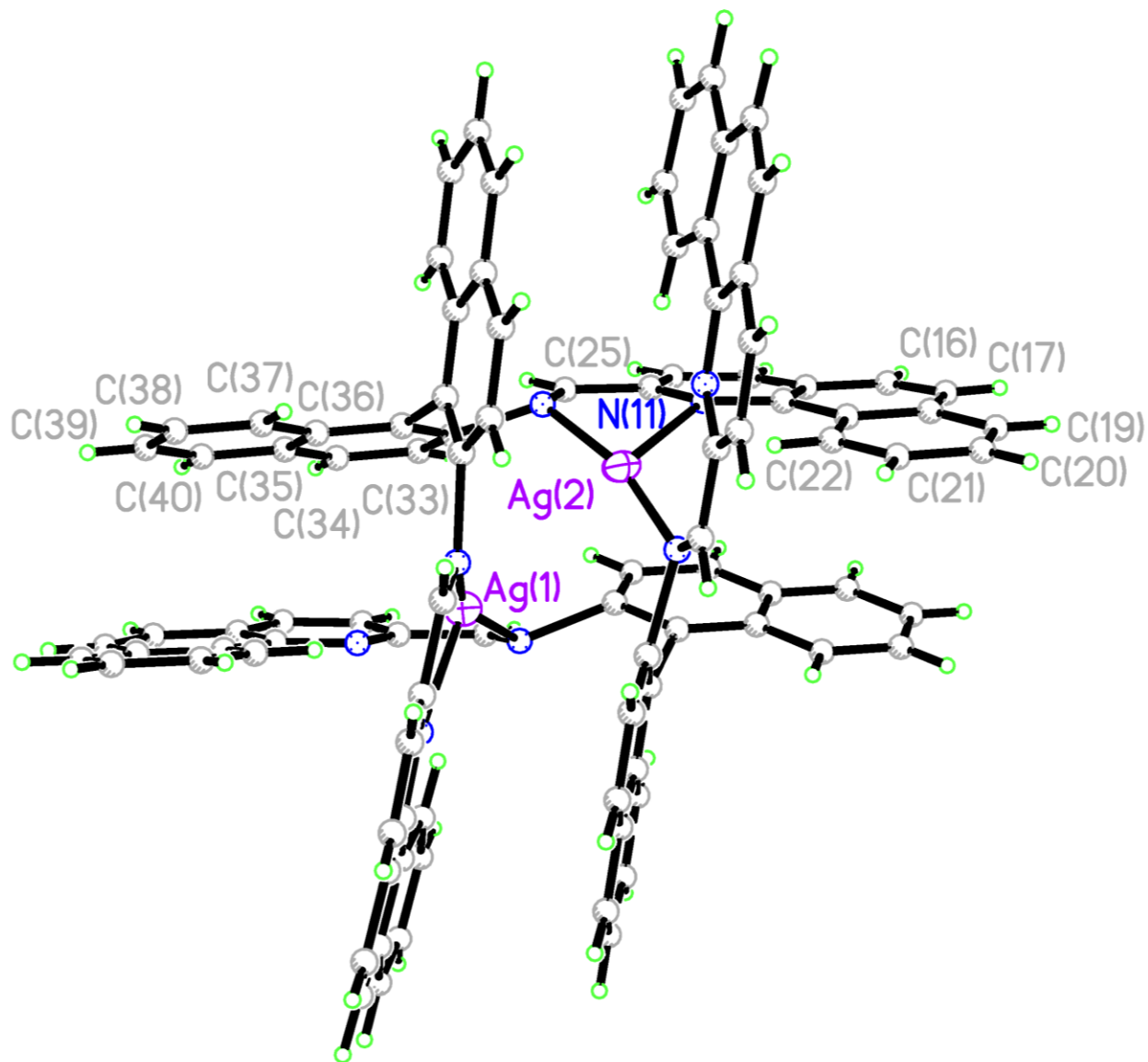
Figure 4.24: Thermal Ellipsoid Crystal Structure for Complex **34**
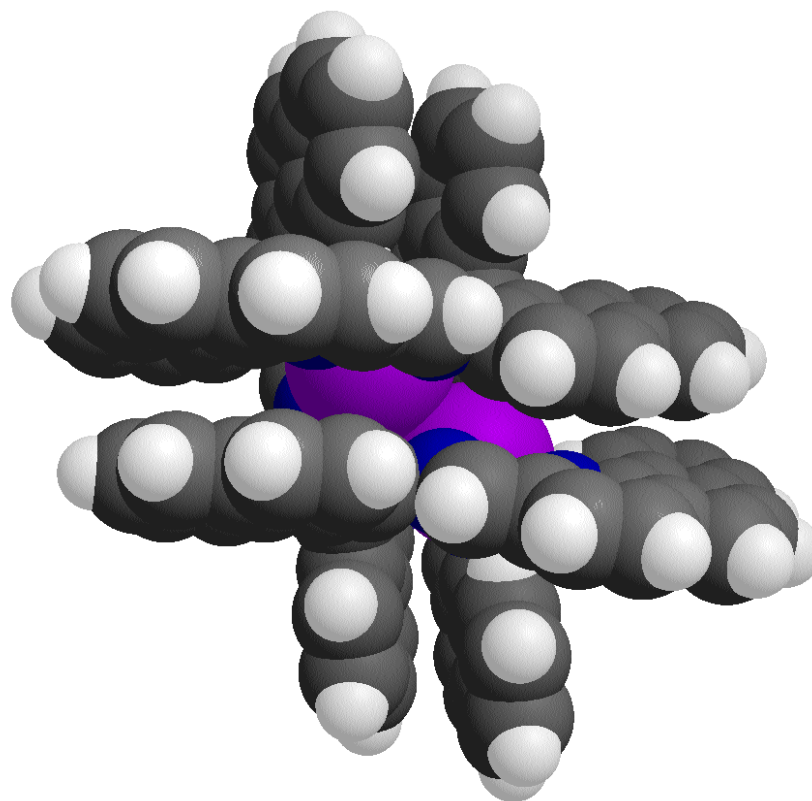
Figure 4.25: Space Filling Model for Complex **34**

Bond Length				
	Ag_2-N_{254}	2.051(16)	Ag_1-N_{112}	2.594(10)
	Ag_2-N_{251}	2.157(15)	$C_{251}-N_{251}$	1.264(2)
	Ag_2-N_{111}	2.562(10)	$C_{321}-N_{65}$	1.562(14)
	Ag_1-N_{252}	1.885(14)	$C_{122}-N_{112}$	1.351(6)
Bond Angles	$N_{252}-Ag_1-N_{253}$	156.8(5)	$N_{254}-Ag_2-N_{251}$	166.4(6)
	$N_{252}-Ag_1-N_{112}$	71.9(4)	$N_{254}-Ag_2-N_{111}$	121.4(6)
	$N_{253}-Ag_1-N_{112}$	118.4(5)	$N_{251}-Ag_1-N_{111}$	68.9(3)
Torsion Angles	$N_{25}-Ag_2-N_{11}-C_{12}$	151.6(5)	$C_{25}-Ag_2-N_{11}-C_{12}$	-18.5(6)

Table 4.1 Selected Bond Lengths (Å), Bond Angles, and Torsion Angles for Complex **34**

Other studies done by the Zema group on dinuclear silver(I) metal double helicates, made from cycloheyliminophenanthridine ligands to give the complex shown in Figure 4.26, showed that the complex retained its dinuclear form when in solution.[111] We therefore set out to investigate the possible solution form of complex **34** using a variety of techniques. First is to determine the molecular weight of the organometallic complex in solution and one of the most straightforward method of doing this is the molecular weight determination for non-volatile organometallic compounds developed by Signer.[112] It is centered around Raoult's Law and takes into account that the vapor pressure of an ideal solution is proportional to the concentration of the solute. This method works well for our complex because it does not require the use of any complicated instruments, requires small amounts of complex (~ 20 milligram), and does not expose the air-sensitive complex to water vapors in the atmosphere.
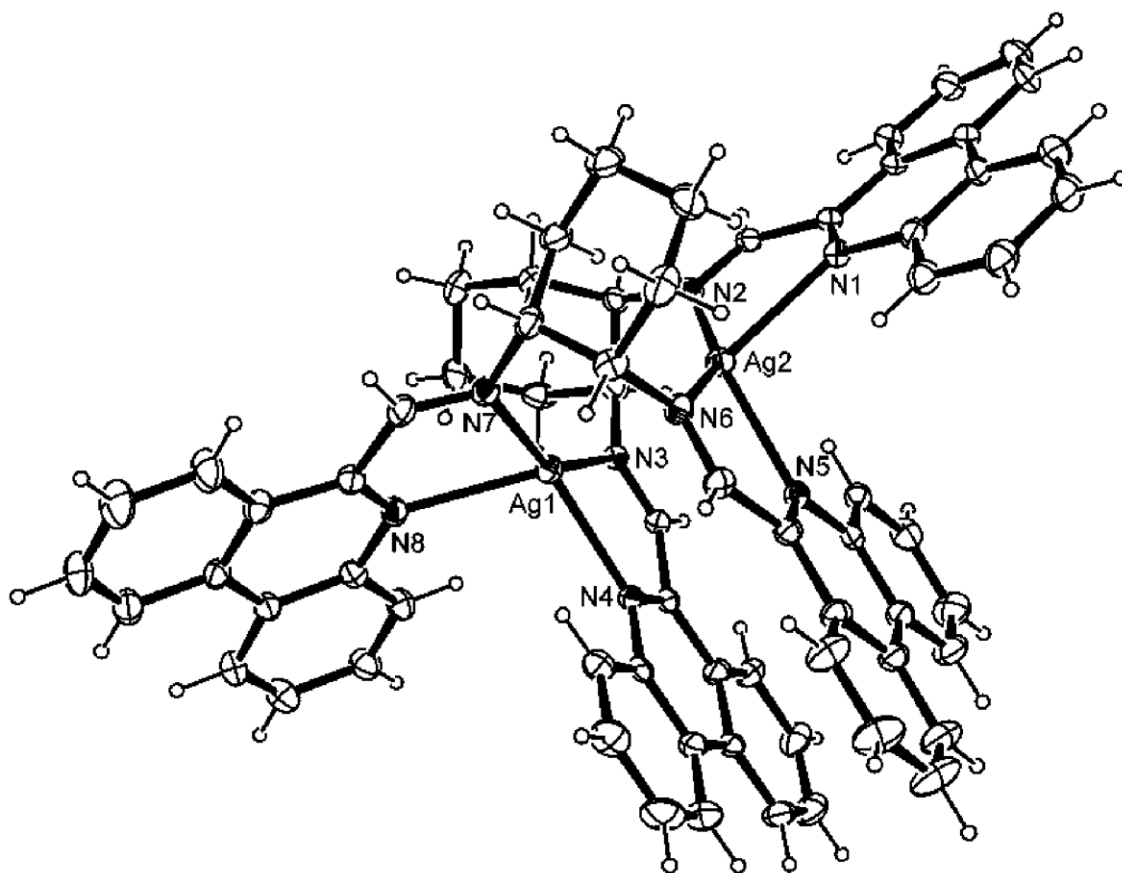
Figure 4.26: Zema Group Dinuclear Silver(I) Double Helicate Complex

141

The molecular weight of synthesized complexes can be calculated using the following equation;

$$MW_x = [(mg_x)(MW_s)(mL_s)] / [(mg_s)(mL_x)]$$

Where; mg_x = weight of complex

mg_s = weight of ferrocene

MW_x = molecular weight of complex

MW_s = molecular weight of standard

mL_x = volume of ferrocene solution

mL_s = volume of complex solution

Using the numbers we obtained from this molecular weight experiment carried out, we get;

$$MW_x = [(0.0100g)(186.04 \text{ g/mol})(0.81 \text{ mL})] / [(0.0045 \text{ g})(0.39 \text{ mL})] = 858.646 \pm 60 \text{ g/mol}$$

This is in line with the theoretical molecular weight expected for complex **34** (919.7304 g/mol). The percent error between the mass we obtained from the experiment and the theoretical mass is 6.64%. The result from this experiment supports the notion that complex **34** is a mononuclear compound in solution rather than a dinuclear complex which would have a theoretical molecular weight of 1541.32 g/mol. To gather further evidence on the species present in solution, electro-spray mass spectrometry was conducted on complex **34** (Figure 4.27). The spectrum obtained did not show any peaks patterns corresponding to the presence of the dinuclear complex $[C_{96}H_{60}N_8Ag_2(CF_3SO_3)]^+$, instead we observe a mass peak that corresponds to a mononuclear silver complex that has no triflate ligands bound to the metal center $[C_{48}H_{30}N_4Ag]^+$. The spectrum also showed the presence of pure ligand **5**, presumably the silver(I) cation gets kicked out off the coordination to the nitrogen donor atom during ionization.

There is still a possibility of a mononuclear to dinuclear equilibrium that may be present in solution for complex **34** so we conducted a variable temperature NMR experiment to look for any exchange that may be present in solution between those two conformations (Figure 4.28). Deuterated methylene chloride was used as the NMR solvent to be able to reach temperatures as

low as 193 K. The resulting spectrum obtained shows no evidence of exchange occurring between the protons in complex **34** leading us to conclude that the complex exist solely as a mononuclear complex in solution under the conditions examined. There is no significant peak movement and no coalescence is observed. Some viscosity broadening is observed at lower temperatures but is uniform across the spectrum. As the solution is cooled, we observe that the overlapped doublet peaks present at 8.20 ppm start to separate out and become more define as we reach 213 K. This is not surprising as the lower temperatures reduce the motion of the aromatic protons, in turn reducing the chances of observing averaged signals. We also observe the two doublets at 8.68 ppm and 8.77 ppm become less define as progress towards 193 K, that being said, there was no exchange observed between those protons.
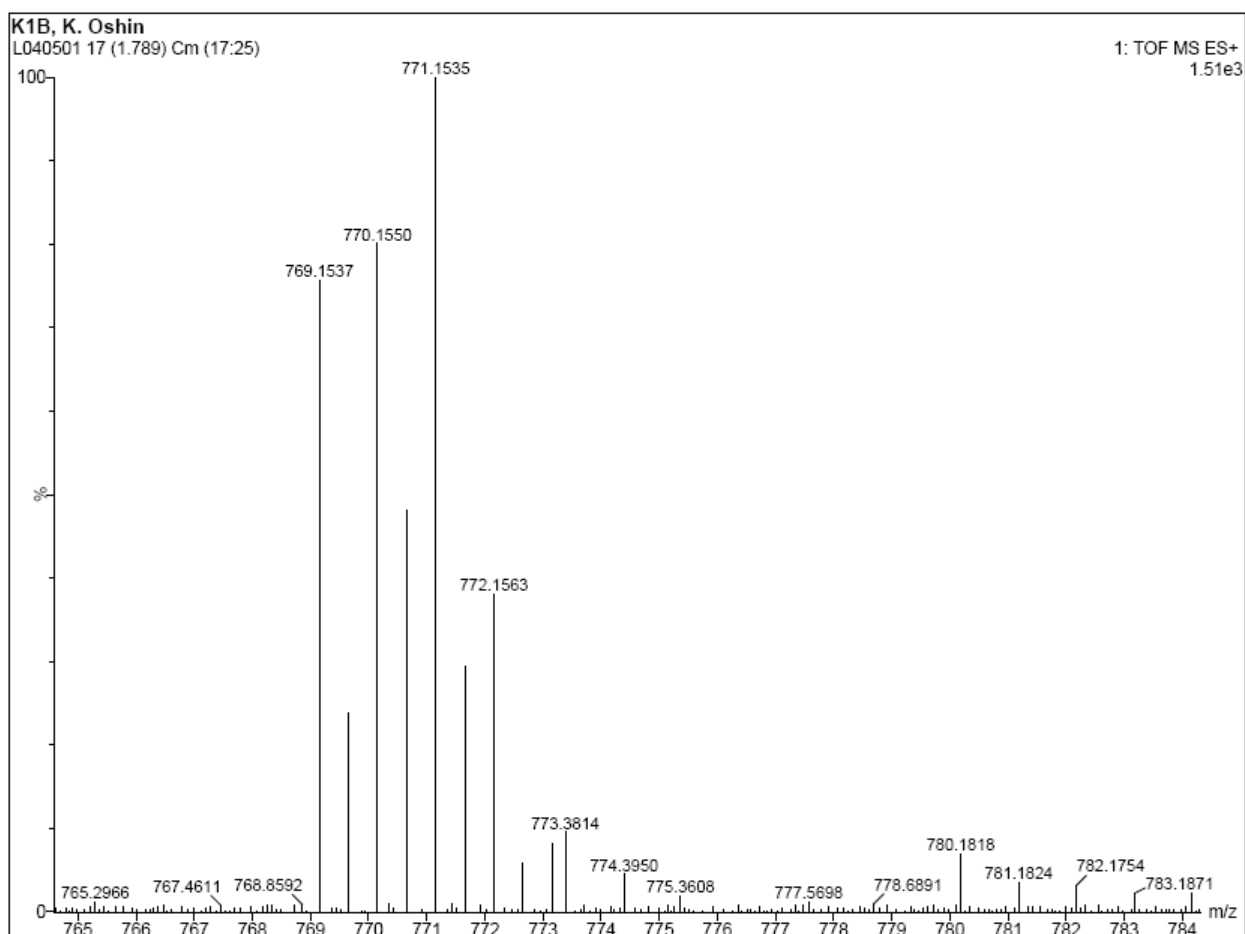
Figure 4.27: Electro-Spray Mass Spectrum of Complex **34**

143
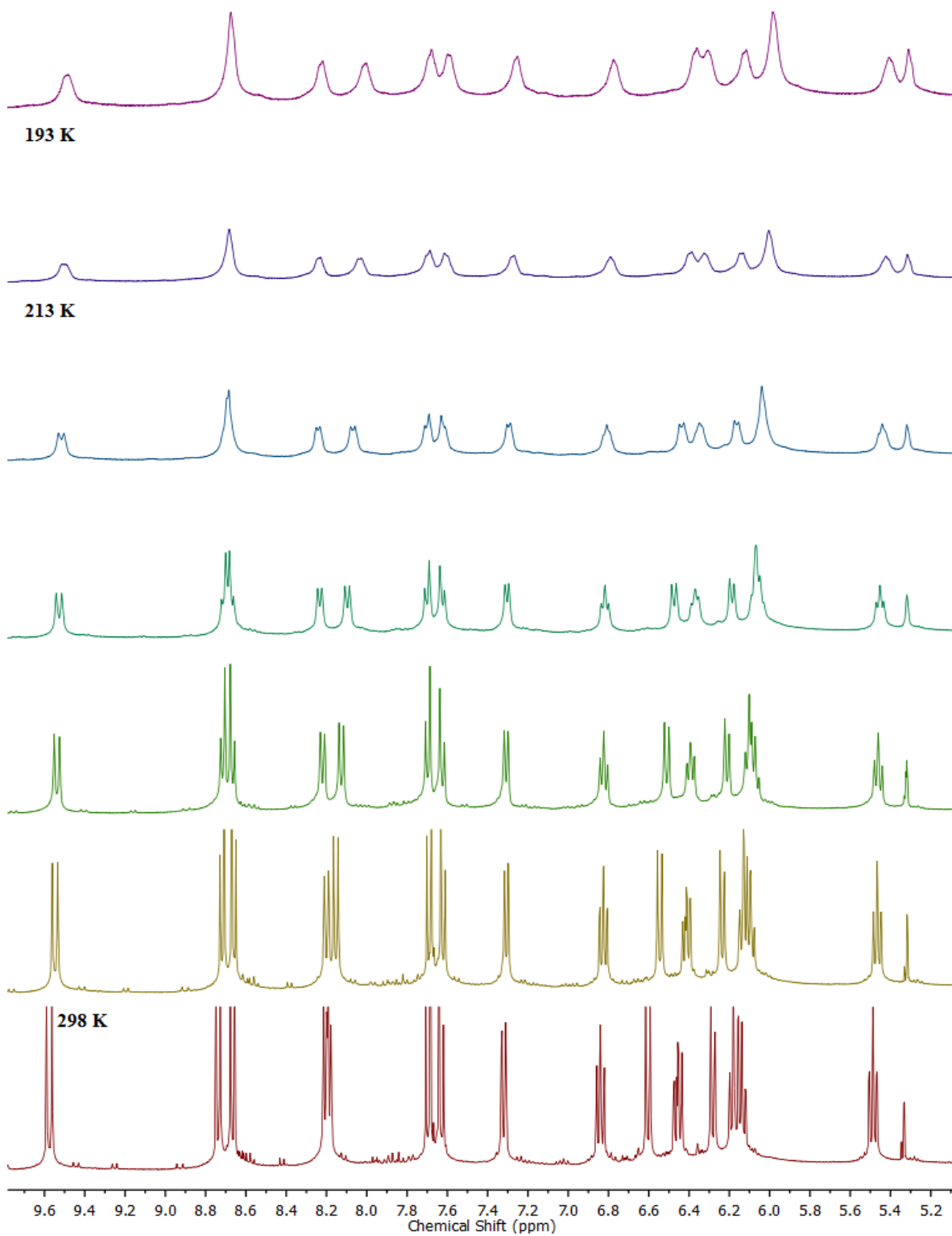
Figure 4.28: Variable Temperature NMR Spectrum of Complex **34** (CD$_2$Cl$_2$)

144

4.4 Metallation of Ligand 1 with Silver(I) Triflate (Complex 40)
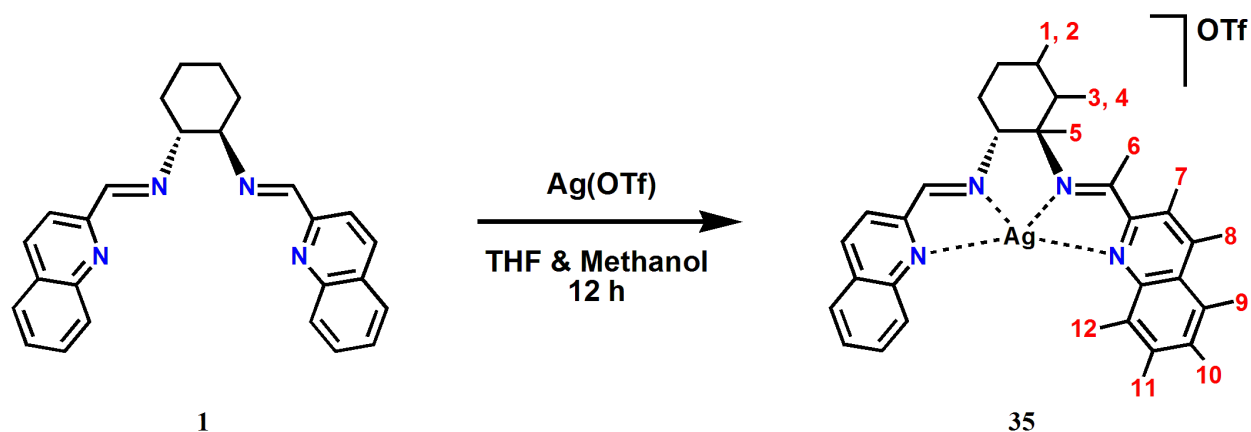
Figure 4.29: Proposed Reaction Scheme for Complex **35**

The successful silver(I) complexation reactions with the binaphthalene backbone ligands **3**, **4**, and **5**promted us to explore the same reaction with our cyclohexyl based ligands. What we observed was that unlike the ligands with binaphthalene backbones, when metallation was carried out with ligands **1** and **2**, the products obtained were impure. Ligand **1** was reacted with one equivalent of silver(I) triflate to give a solution that changed color over time from a yellow solution to a red solution, and finally to a black solution. After pumping down on the solution with the vacuum line, dark brown colored solids were obtained in 82.6 % yield. Once again, the product was stored in the glove box to prevent exposure to water vapor in the atmosphere and wrapped with aluminum foil to prevent the reduction of the silver cation to silver metal. The reaction carried out to produce complex **35** was repeated several times giving the same ^{1}H NMR spectrum shown in Figure 4.30. Analyzing the spectrum, we obtain the expected number of peaks for the aromatic region (7) but when the peaks are integrated, they amount to 8 protons being present in the aromatic region. We expect to see one singlet, four doublets, and two doublet of doublet peaks for complex **35**. Close examination of the ^{1}H NMR spectrum shows the presence of four doublets, no singlet, a multiplet at 7.01 ppm, and a broad peak at 7.52 ppm. The peak patterns observed could not interpreted to fit our proposed structure of complex **35** shown in Figure 4.29. All protons are accounted for in the aliphatic region of the spectrum.
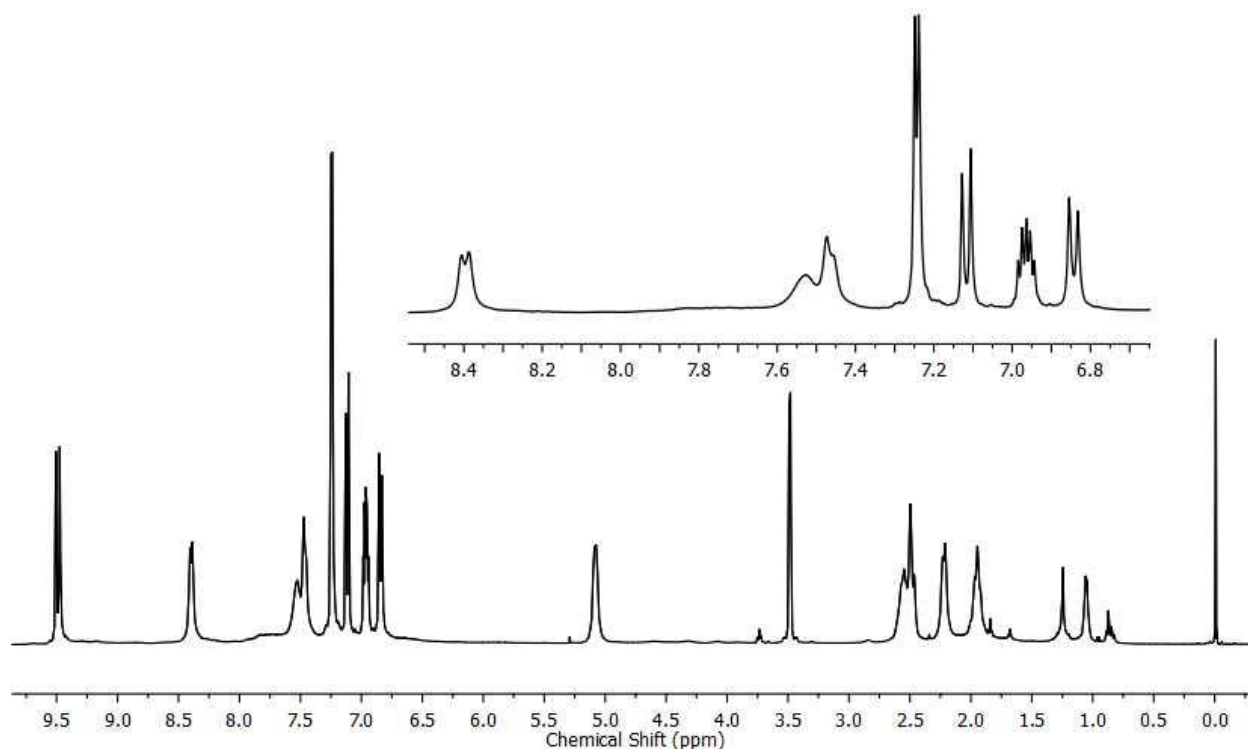
Figure 4.30: 400 MHz ^{1}H NMR Spectrum of Complex **35** (CDCl$_3$)

We conducted an HSQC experiment to verify the number of protons present in the aromatic region and as predicted by the ^{1}H NMR integration, we obtain eight protons in the aromatic region (Figure 4.31). We observe an isolated cross-peak at 166 ppm and based on previous HSQC experiments, this is most likely due to the imine carbon atom next to the electron withdrawing nitrogen atom. This position agrees with the imine carbon position observed in the HSQC spectrum of pure ligand **1**. This observation suggests that we obtain the same phenomenon observed with complexes **32** and **33** where there is a ^{3}J(^{1}H-^{107,109}Ag) coupling present that affects the imine proton. As observed in previous ^{1}H NMR spectra, the presence of that coupling to silver results in the imine proton appearing as a doublet peak. This could explain the presence of the doublet observed at 9.52 ppm. We note that there are two protons associated with the relatively large doublet located at 7.23 ppm. This brings the total number of assignable peaks in complex **35** to five. The multiplet peak present at 7.01ppm cannot be explained using the proposed structure for complex **35**.
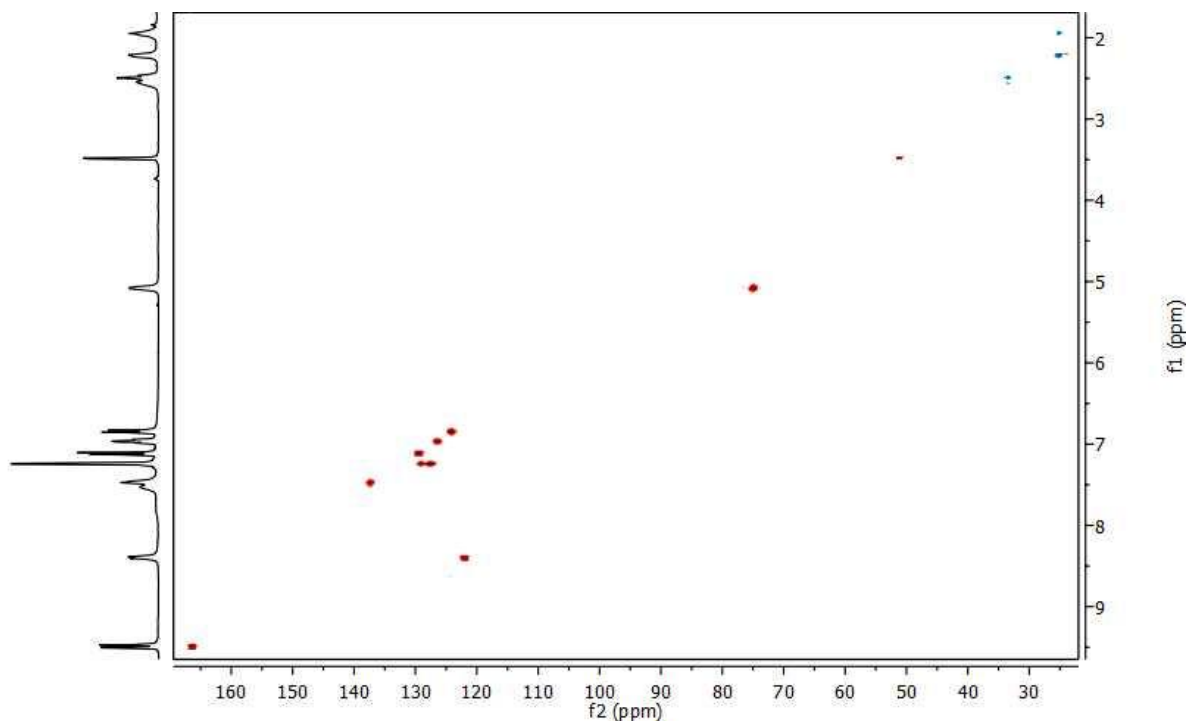
Figure 4.31: 400 MHz HSQC Spectrum of Complex **35** (CDCl₃)

We conducted a COSY experiment to observe the proton coupling present in complex **35** and is shown in Figure 4.32 and 4.33. As observed in complex **33** and **34**, the doublet located downfield at 9.45 ppm exhibits no coupling and can be assigned as the imine proton. Coupling in the aromatic region is similar to what we observe with pure ligand 1 with the exception of one less proton to proton coupling observed in complex **35**. The protons in the cyclohexyl backbone are free to rotate in solution and are slightly inequivalent given their equatorial and axial positions. However, the peaks observed on the ^{1}H NMR show an average signal. We were interested in slowing down the motion of the protons in the backbone making them inequivalent on the NMR time scale resulting in symmetry of the complex to be lost. We should obtain twice the number of peaks observed in the ^{1}H NMR spectrum if the complex becomes non-symmetric. We therefore carried out a variable temperature experiment on complex **35** using deuterated chloroform as our NMR solvent (Figure 4.34). We start to observe the proton peak numbers double at 223 K at it should also be mentioned that we could be freezing out a complex with only three donor atoms bound to the metal center that will also result in double the amount of peaks.

147
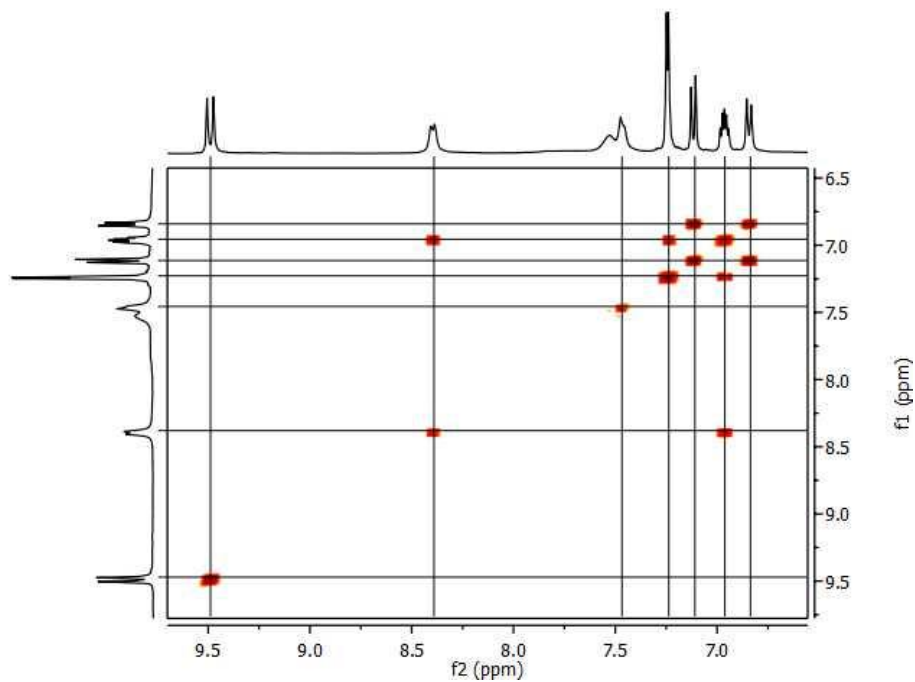
Figure 4.32: 400 MHz Aromatic Region COSY of Complex **35** (CDCl₃)
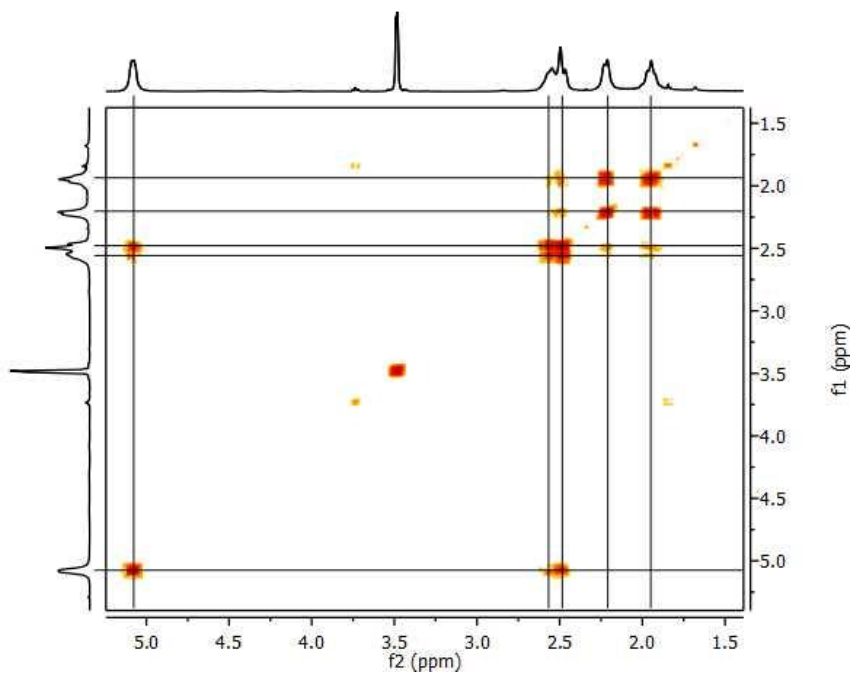
Figure 4.33: 400 MHz Aliphatic Region COSY of Complex **35** (CDCl₃)
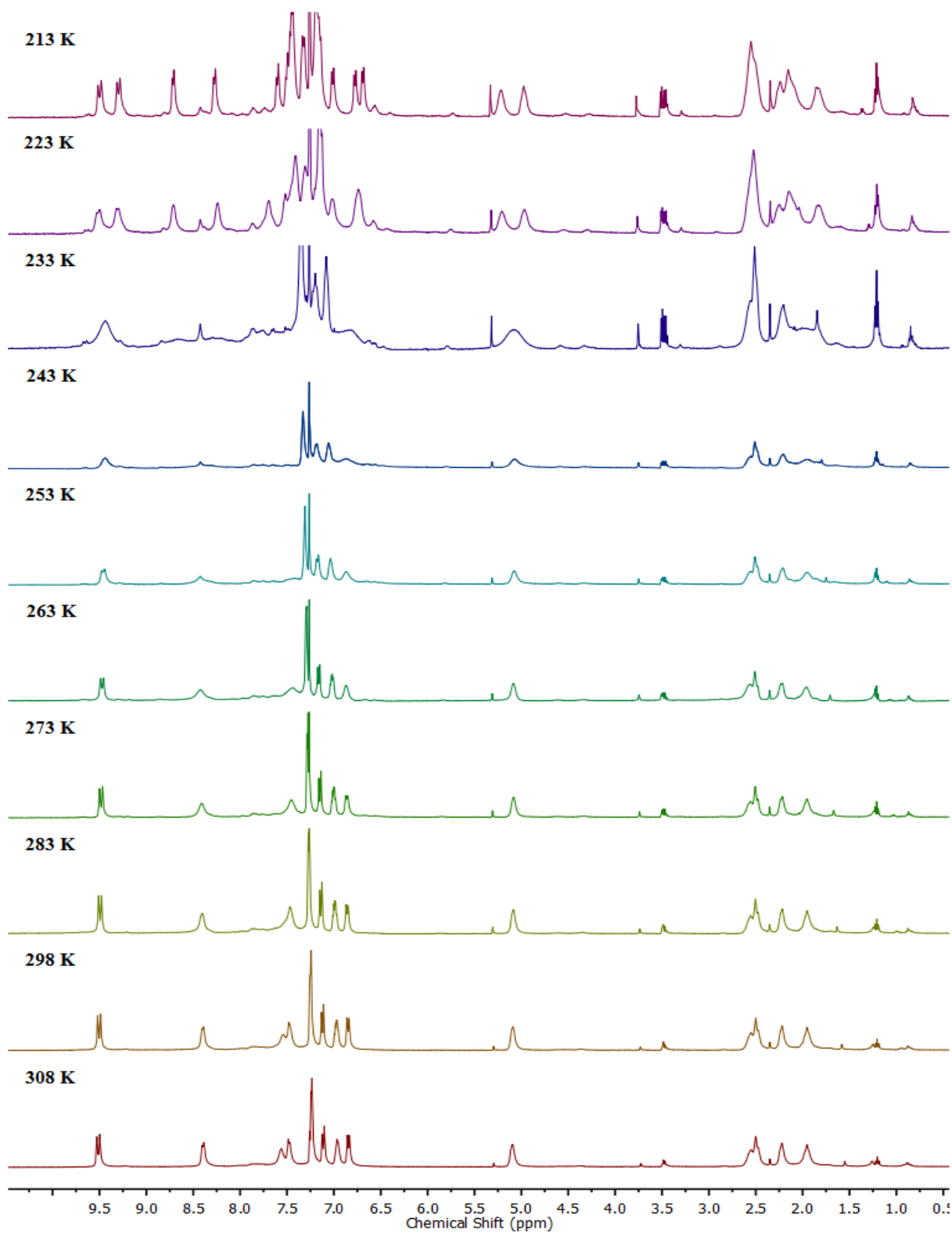
Figure 4.34: Variable Temperature NMR Spectrum of Complex **35** (CDCl$_3$)

149

4.5 Metallation of Ligand 2 with Silver(I)Triflate (Complex 41)
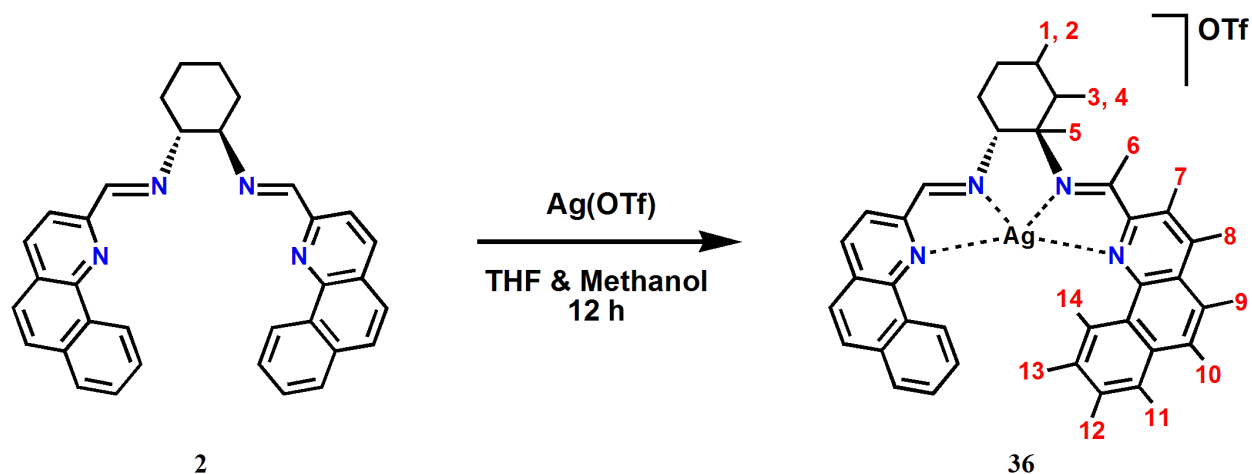
Figure 4.35: Proposed Reaction Scheme of Complex **36**

The same complexation reaction was carried out with ligand **2** and one equivalent of silver(I) triflate to give a solution that also changed color over time from a yellow solution to a red solution, and finally a black solution. After pumping down on the solution with the vacuum line, dark brown colored solids were obtained in 68.2 % yield. The product was stored in the glove box to prevent exposure to water vapor in the atmosphere and wrapped with aluminum foil to prevent the reduction of the silver cation to silver metal. The reaction carried out to produce complex **36** was repeated several times to give the same ^{1}H NMR spectrum shown in Figure 4.36. Analyzing the spectrum is difficult to do because the resonance peaks are not well defined. We observe two sharp doublet peaks at 7.94 ppm and 8.28 ppm, a multiplet at 7.50 ppm, and four broad peaks at 7.18, 7.36, 7.58, and 8.98 ppm. The product cannot be regarded as impure because we obtain a clean ^{1}H NMR spectrum but the peak patterns could not be interpreted to fit our proposed structure of complex **36** shown in Figure 4.35. The ^{1}H NMR spectrum also suggests that there may be some exchange going on solution. In order to get a better idea of the complex formed during this reaction, electro-spray mass spectrometry was conducted on complex **36** (Figure 4.37). We observe the presence of ions corresponding to the formation of a dimmer complex but did not obtain a mass for any of the desired complexes.
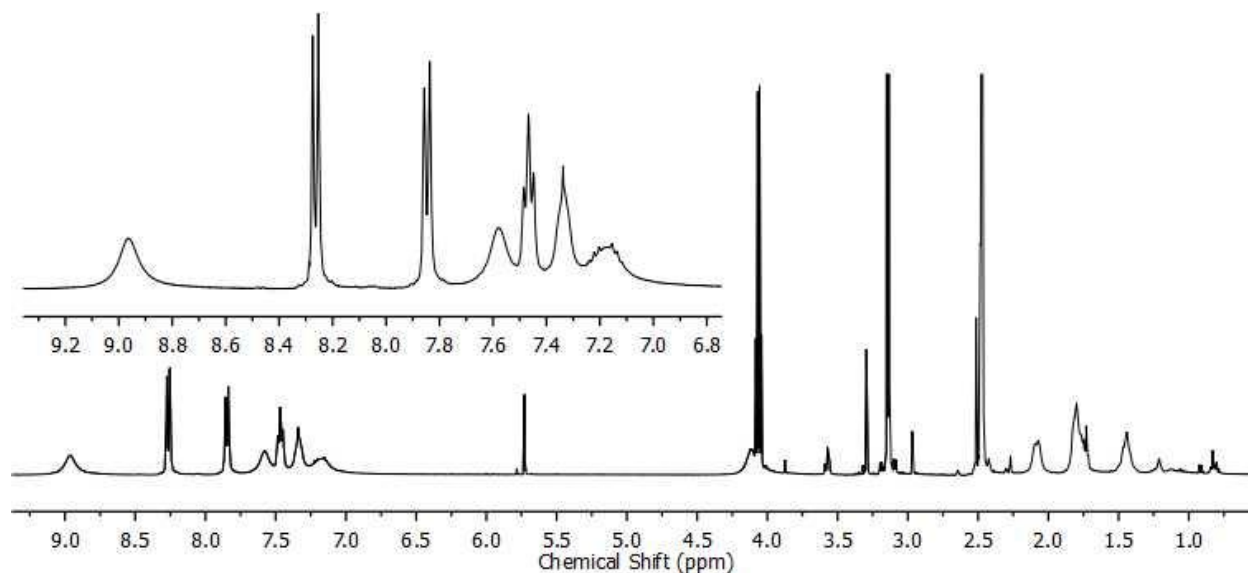
Figure 4.36: 400 MHz ^{1}H NMR Spectrum of Complex **36** (CDCl$_3$)
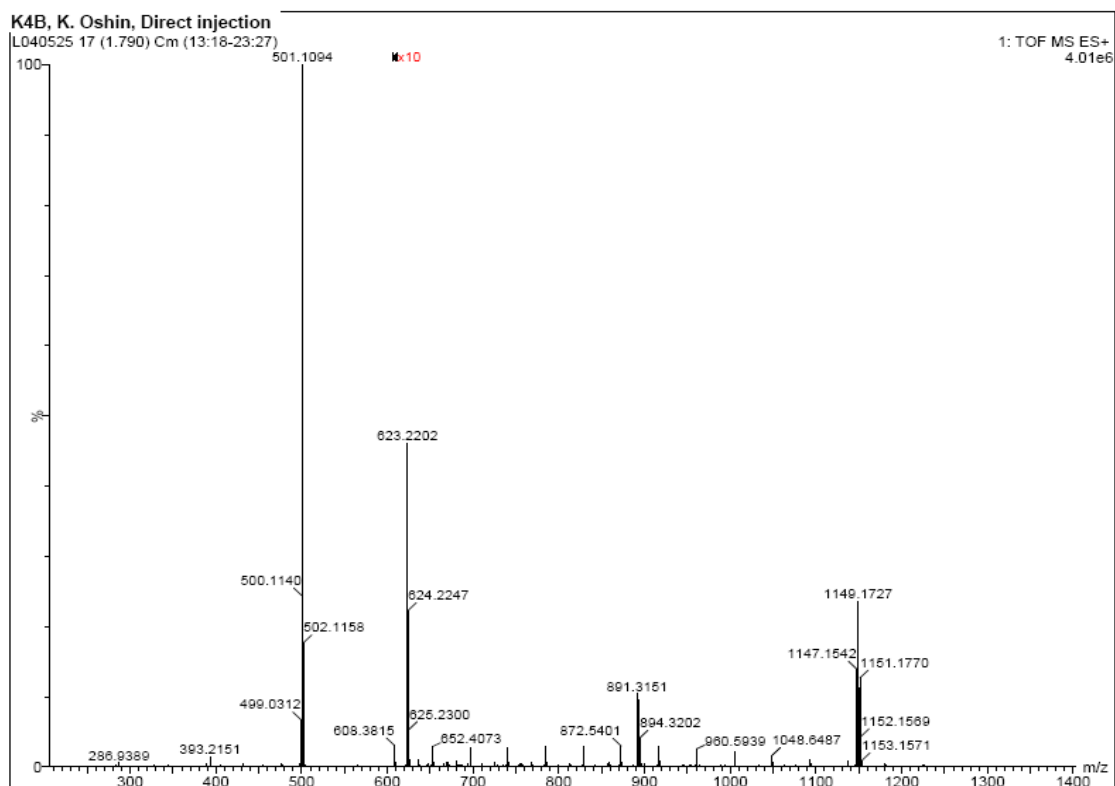
Figure 4.37: Electro-Spray Mass Spectrometry for Complex **36**

151

4.6 Presence of Triflate Counter-ion in Silver(I) Complexes

We wanted to confirm the presence of the coordinated triflate counter-ion to all the silver(I) complexes synthesized and carried out ^{19}F NMR on complex **32**, **33**, **34**, **35**, and **36**. The spectra obtained are shown in Figure 4.38 and confirm the presence of triflate in all complexes.
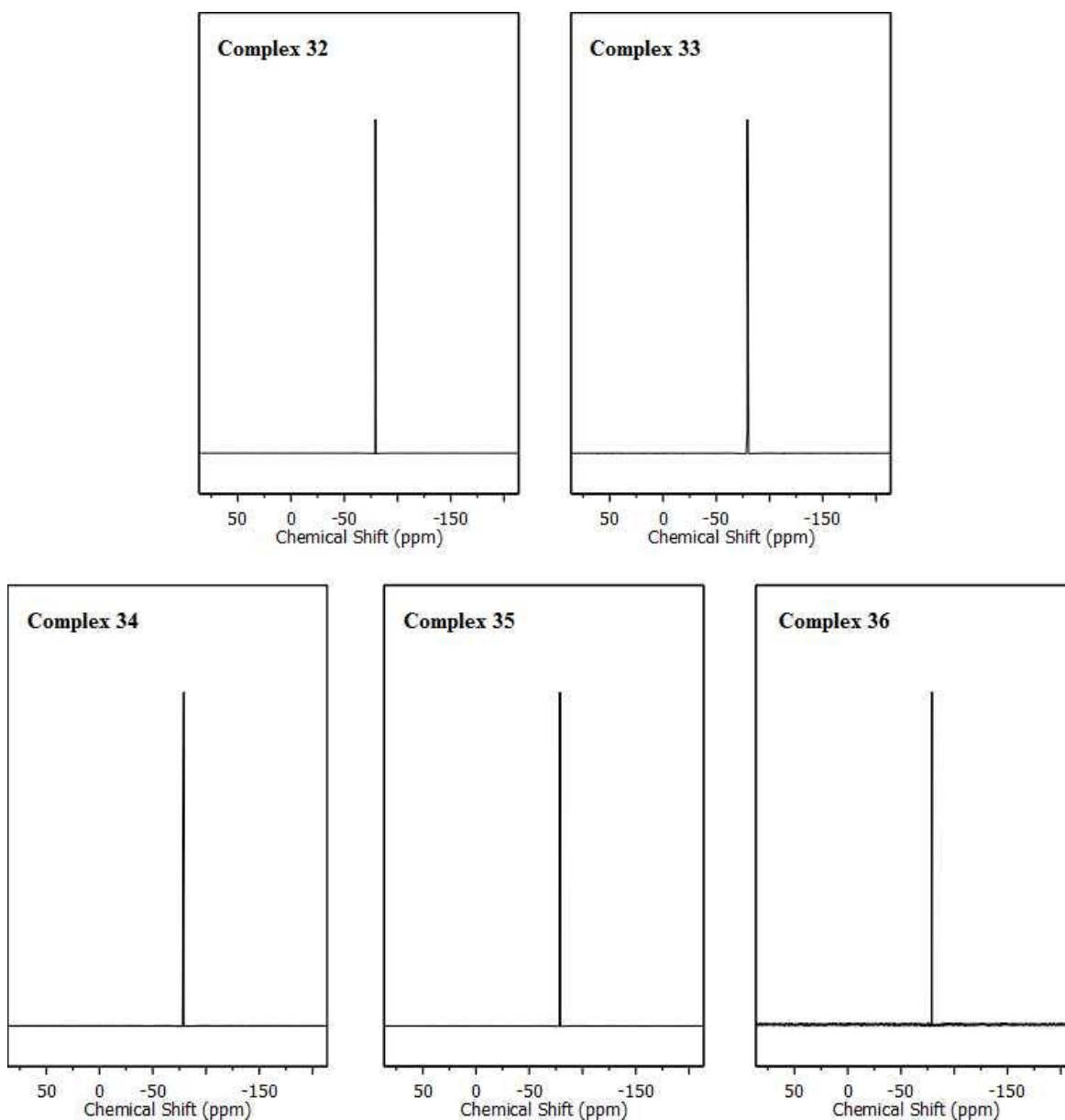
Figure 4.38: 400 MHz ^{19}F NMR Spectrum of Complex **32**, **33**, **34**, **35**, and **36** (CDCl$_3$)

4.7 Ligand to Complex Comparisons
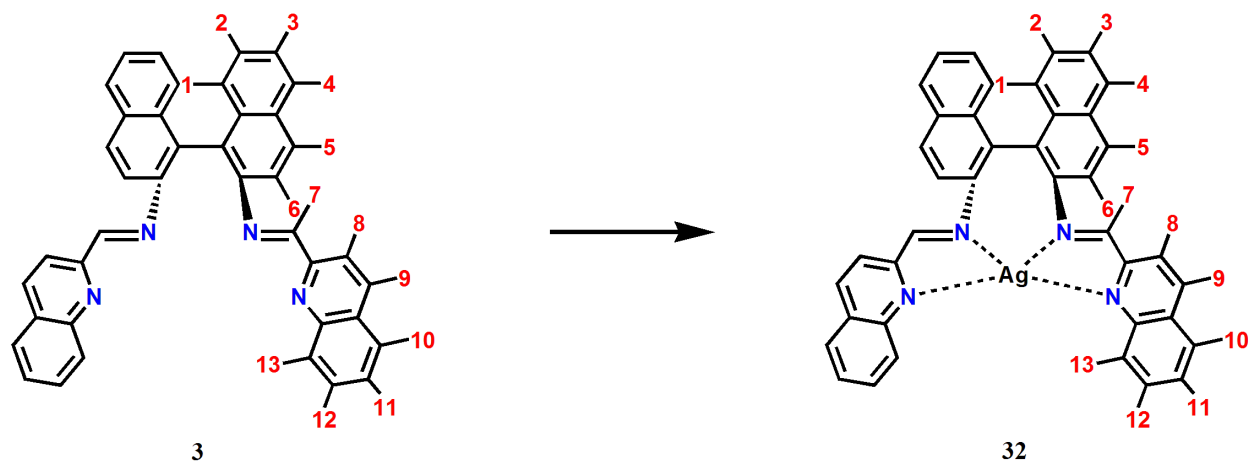
Figure 4.39: Ligand **3** to Complex **32** Comparison

It is obvious that the presence of silver metal in the complexes synthesized in this chapter affect the proton positions as we transition from ligand to complex. A comparison is necessary in order to monitor the effect silver has on the proton resonance signals. A table of ligand and corresponding complex proton positions for the above reaction is shown in Table 4.2. We observe that protons on the binaphthalene backbone (#1 – #6) are shifted upfield after complexation with the exception of proton #6. Many factors may contribute to these shifts such as the electron cloud of the metal center and the anisotropy present in the conjugated phenyl systems of the binaphthalene backbone. Proton #6 is the closest to the metal center on the binaphthalene backbone and its spatial arrangement may explain its upfield shift in the ^{1}H NMR spectrum. The protons on the quinoline side-arm (#8 – #13) show a general shift upfield with the exception of protons #11, #12, and #13. Proton #11 maintains the same peak position of 7.27 ppm and may be attributed to its distance from the metal center as it is the farthest on the quinoline side-arm reducing any shielding or deshielding effects felt by the metal center. The last two protons (#12 and #13) show a comparably large shift upfield and could once again be most likely due to their close positions relative to the silver metal center. There may be shielding experienced by those protons from the metal center resulting in their upfield shift.

#	LIGAND 3 (ppm)	COMPLEX 32 (ppm)
1	7.87	6.43
2	7.61	6.88
3	7.48	6.78
4	7.71	6.41
5	7.54	6.47
6	7.93	7.97
7	8.62	9.35
8	7.50	8.49
9	8.02	8.59
10	7.35	7.82
11	7.27	7.27
12	7.41	6.40
13	7.92	5.88

Table 4.2 Proton Positions for Ligand **3** and Complex **32**
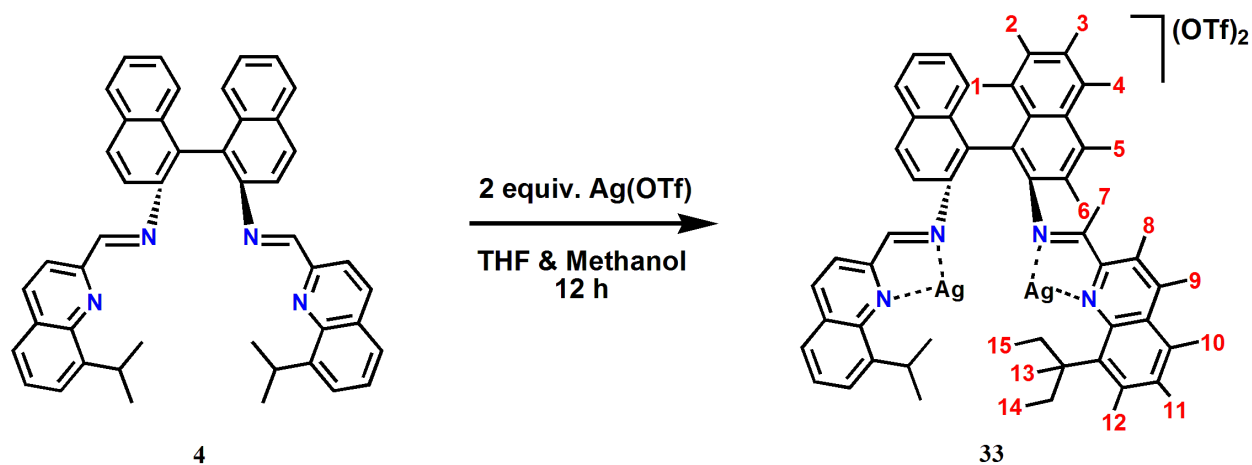
Figure 4.40: Ligand **4** to Complex **33** Comparison

The proton shifts for complex **33** do not follow the trends observed in complex **32** or complex **34**. This may be due to the fact that two metal ions are chelated in the pocket of the ligand changing its physical and chemical properties. It also alters the unique $^3J(^1H\text{-}^{107,109}Ag)$ coupling observed in complex **32** and **34** which will affect the proton positions as observed in the ^1H NMR spectrum obtained for complex **33**. We observe a general downfield proton shift for protons on the binaphthalene backbone, it is opposite of what we observe with complex **32** and **34**. The only exception to this trend is proton #4 which experiences a slight upfield shift. The isopropyl-quinoline side-arm shows a general trend of protons moving downfield with the exception of proton #8 that shifts from 7.90 ppm in the ligand to 7.80 ppm. Once again, various factors contribute to the proton positions with the metal center electron cloud and the anisotropy of the polyaromatic rings contributing to the observed shifts.

#	LIGAND 4 (ppm)	COMPLEX 33 (ppm)
1	7.92	7.93
2	7.39	7.39
3	7.28	7.31
4	7.41	7.23
5	8.00	8.31
6	7.59	8.13
7	8.59	8.92
8	7.90	7.80
9	7.43	8.34
10	7.52	7.62
11	7.54	7.65
12	7.40	7.55
13	4.09	4.01
14	1.08/1.24	0.85/1.36
15	1.08/1.24	0.85/1.36

Table 4.3 Proton Positions for Ligand **4** and Complex **33**
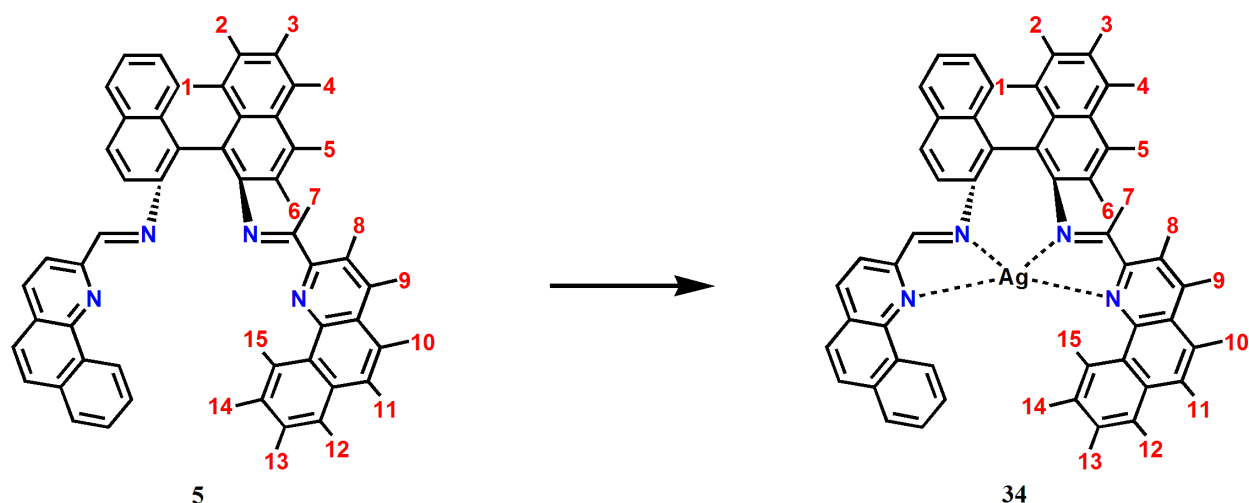
Figure 4.41: Ligand **5** to Complex **34** Comparison

A table of ligand and corresponding complex proton positions for the above reaction is shown in Table 4.4. We are now back to a complex that chelates one metal ion in the pocket of the ligand thereby changing its physical and chemical properties compared to complex **33**. The ^{1}H NMR spectrum obtained for complex **34** shows the presence of the unique $^3J(^1H\text{-}^{107,109}Ag)$ coupling as the imine proton shows up as a doublet peak. This is similar to what we observe with complex **32** and so the proton position trends are similar. Once again, we observe that protons on the binaphthalene backbone (#1 – #6) are shifted upfield after complexation to the silver(I) cation with the exception of proton #6. Many factors may contribute to these shifts such as the electron cloud of the metal center, the anisotropy present in the conjugated phenyl systems of the binaphthalene backbone, and the bond angles and torsion angles present in the complex. Proton #6 is the closest to the metal center on the binaphthalene backbone and its spatial arrangement may explain its upfield shift in the ^{1}H NMR spectrum. The imine proton (#7) experiences a downfield shift similar to both complex **32** and **33**.The protons on the benzoquinoline side-arm (#8 – #15) show a general shift upfield with the exception of protons #8, #9, and #10. Proton #11 is the only peak that is close in position to its ligand counterpart. As observed in complex **32**, proton #11 maintained the same peak position of 7.27 ppm and may this trend attributed to its distance from the metal center as that may affect any shielding or deshielding effects felt by the

156

metal center. Protons #14 shows a comparably large shift upfield and could once again be most likely due to its close proximity to the silver metal center. The observed shit may also be due to the angle of that C–H bond. If the angle is large enough that the proton is held in the electron cloud or coordinating sphere of the metal complex, it may experience shielding from the NMR magnetic moment moving the proton position upfield. The last proton experiences a slight shift upfield which is low in comparison to proton #13 in complex **32** experiencing a shift of 2.1 ppm upfield. The interactions of the benzoquinoline side-arms either through a π-π stacking or σ-π interactions may result in the observed shift. We are pleased to observe a trend in our silver complexes that undergo chelation with the same number of metal salt. It suggests that the proton shifts observed in the ^{1}H NMR spectra are not random events but rather are as a result of the unique interaction of the silver atom with the desired tetradentate ligand.

#	LIGAND 5 (ppm)	COMPLEX 34 (ppm)
1	7.40	6.17
2	7.29	6.38
3	7.43	6.09
4	7.96	6.06
5	8.05	6.53
6	7.52	8.25
7	8.65	9.58
8	7.98	8.78
9	7.76	8.59
10	7.55	7.62
11	7.66	7.56
12	7.71	7.25
13	7.51	6.78
14	7.38	5.40
15	8.79	8.19

Table 4.4 Proton Positions for Ligand **5** and Complex **34**

4.8 NMR Discrimination Experiments with Silver(I) Complexes

Chiral recognition in the coordination of olefins to chiral transition metal fragments is a topic of great interest.[113] Not only because of its involvement in metal promoted enantioselective synthesis[114] but also because it can offer simple procedures for the thermodynamic or kinetic resolution of racemic mixtures or for the analytical determination of relative enantiomeric abundances.[115] Studies on the stereoselectivity and chiral recognition in copper(I) olefin complexes with a chiral diamine show that the chiral olefins preferentially bind one enantiomer to the complex.[116] This preferential binding can be observed in the ^{1}H NMR of the mixture with the bound olefin having a shift in signal positions compared to the unbound olefin. This successful study set the precedent for our study on the enantiomeric selective coordination of racemic chiral olefins using silver(I) complexes.

Although silver-olefin adducts are well established,[115] very few studies on chiral species appear to have been reported in the literature, and these are essentially limited to the use of silver salts, in combination with chiral lanthanide shift reagents, for the NMR discrimination of enantiomeric olefins.[116-7] We form our olefin-coordinated silver(I) species [(N–N–N–N)Ag (olefin)]$^+$ by dissolving our silver complexes (**32**, **33**, or **34**) in the desired NMR solvent and adding three equivalents of the olefin. The olefins of choice were 3-buten-2-ol and 1-penten-3-ol; selected because the metal–olefin bond of hydrocarbon olefins with allylic alcohols are more stable and robust, likely due to a stabilizing intramolecular interaction between the oxygen atom and the metal ion.[118] The olefins were added in excess (three equivalents) to shift the equilibrium to the olefin adduct. Figure 4.44 shows the ^{1}H NMR spectrum of 3-buten-2-ol recorded at 298 K in CDCl$_3$ with the assignments of the various signals. Likewise, Figure 4.46 shows the ^{1}H NMR spectra for 1-penten-3-ol. The olefins exists a racemic mixture of *R*- and *S*- enantiomers as shown below in Figure 4.42.

(*R*)	(*S*)	(*R*)	(*S*)

Figure 4.42: Racemic Mixtures of 3-buten-2-ol and 1-penten-3-ol
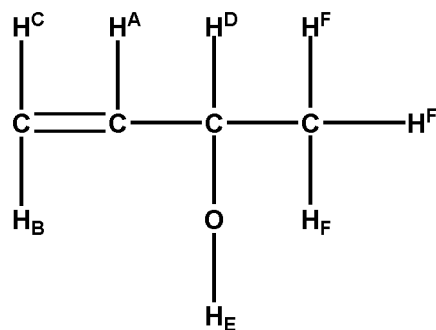
Figure 4.43: Chemical Structure of 3-buten-2-ol
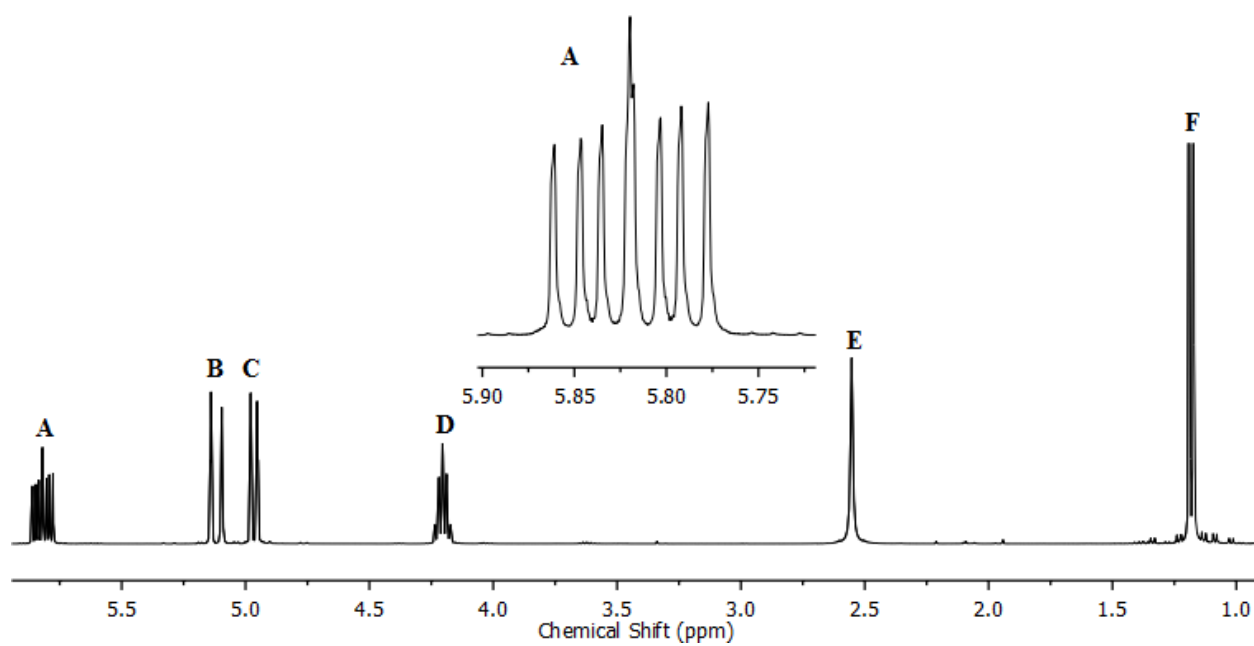
Figure 4.44: 400 MHz ^{1}H NMR Spectrum for 3-buten-2-ol (CDCl$_3$)

159
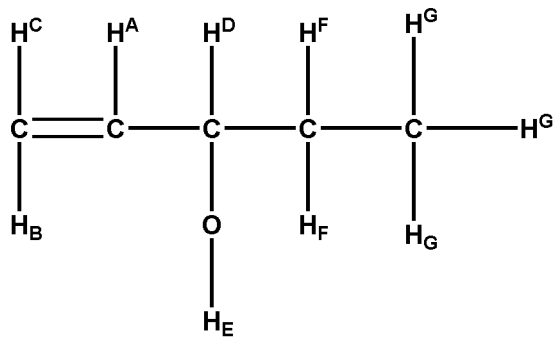
Figure 4.45: Chemical Structure for 1-penten-3-ol
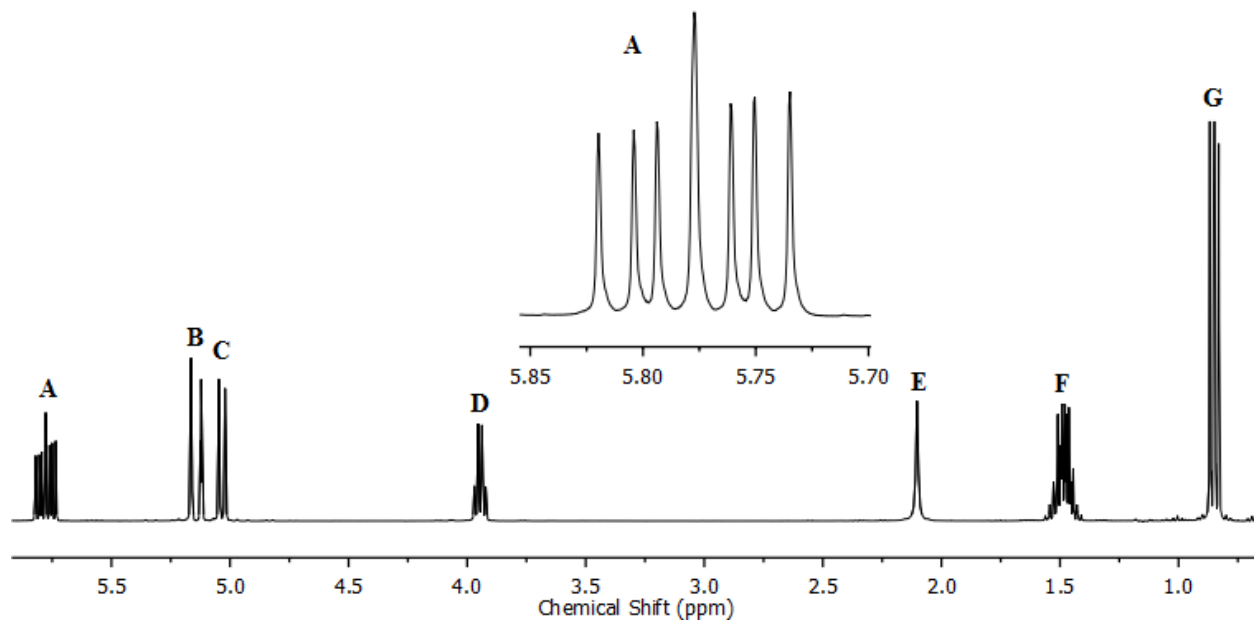
Figure 4.46: 400 MHz ^{1}H NMR Spectrum For 1-penten-3-ol (CDCl$_3$)

160

When the racemic olefin and silver complexes are mixed together, we obtain ^{1}H NMR spectra for the mixture that suggests a preferential binding to one of the enantiomers as one possible scenario that occurs in solution. As observed in Figure 4.47, the ^{1}H NMR for complex **33** and racemic 3-buten-2-ol show a doubling of the proton peak located at 5.90 ppm, corresponding to proton **A** in Figure 4.43. This is not surprising as the protons that should be most affected are the ones directly linked to the olefin double bond, which undergoes the association with the silver metal center. The same effect in noted in the mixture of complex **33** with 1-penten-3-ol shown in Figure 4.48. Here, the effect on proton **A** is not as severe as what we observe with 3-buten-2-ol, but nonetheless, we still observe a doubling of peaks in that region that could suggest the separation of the two olefin enantiomers as the chiral silver complex preferentially bind to only one enantiomer of the olefin with the right face. If this is happening, the unbound olefin will be left in solution but will still be detected in the ^{1}H NMR spectrum with its own distinct proton peak position.
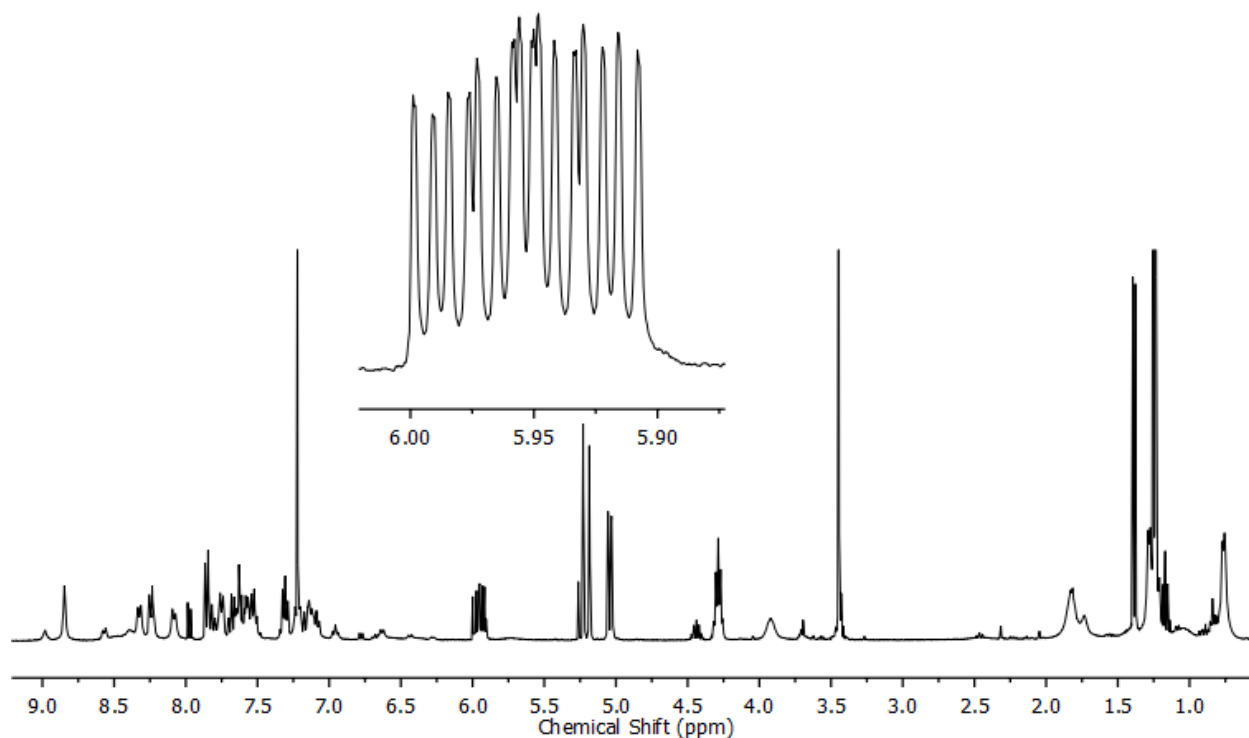
Figure 4.47: 400 MHz ^{1}H NMR Spectrum of Complex **33** with 3-buten-2-ol (CDCl$_3$)

Another scenario to consider is the presence of the following species all together in solution: silver(I) complex bound to the *S* enantiomer of the olefin, unbound silver(I) complex and unbound *S* olefin enantiomer, complex bound to the *R* enantiomer of the olefin, and unbound silver(I) complex and unbound *R* olefin enantiomer. In this set-up, both olefin enantiomers are bound to separate complexes at the same time resulting in the doubling of the proton peak at 5.90 ppm. This process is expected to occur rapidly at room temperature which may translate to averaged signals present in the ^{1}H NMR spectrum. Cooling the mixture further down should slow down this equilibrating process and allow us to see changes in the proton signals for the silver complex and changes in the proton signals for the olefin. Figure 4.49 shows spectrum for the variable temperature experiment conducted on the mixture of complex **33** with 3-buten-2-ol. We do not observe significant changes to the proton peaks corresponding to the silver complex but we do observe separating and coalescing behavior for the olefin peak. Figures 4.50, 4.51 and 4.52 zoom in on the olefin peaks that display the most activity as the temperature drops to 213 K.
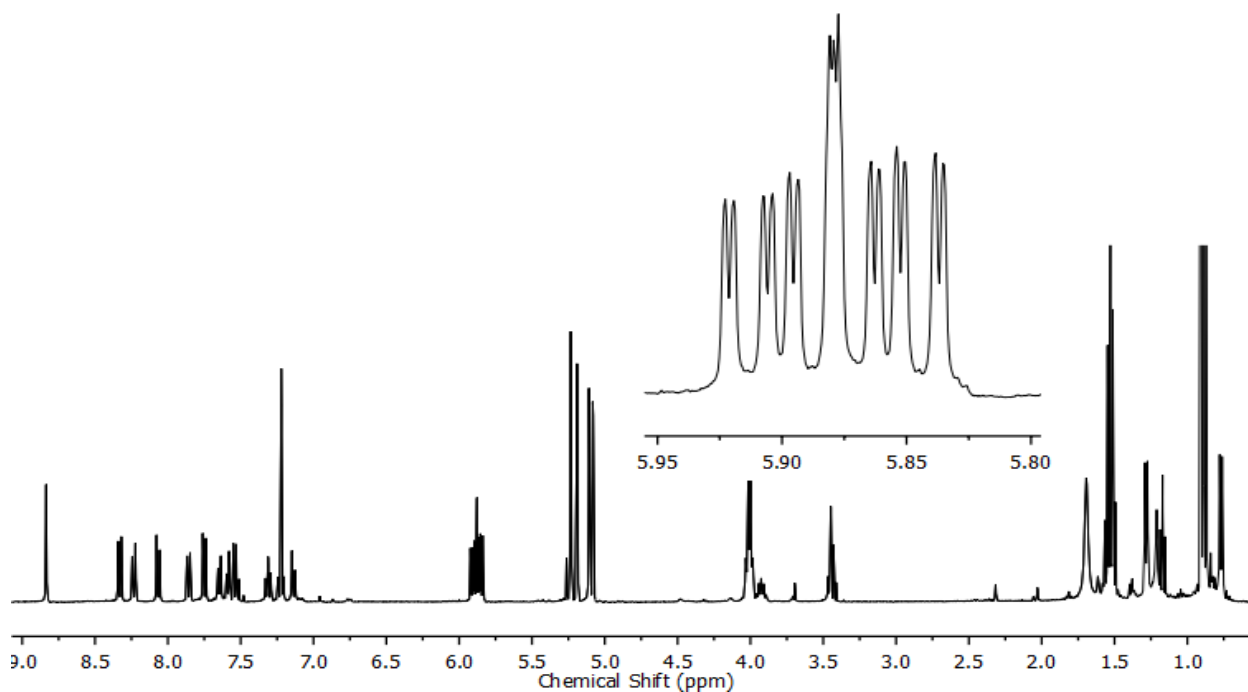
Figure 4.48: 400 MHz ^{1}H NMR Spectrum for Complex **33** with 1-penten-3-ol (CDCl$_3$)

162
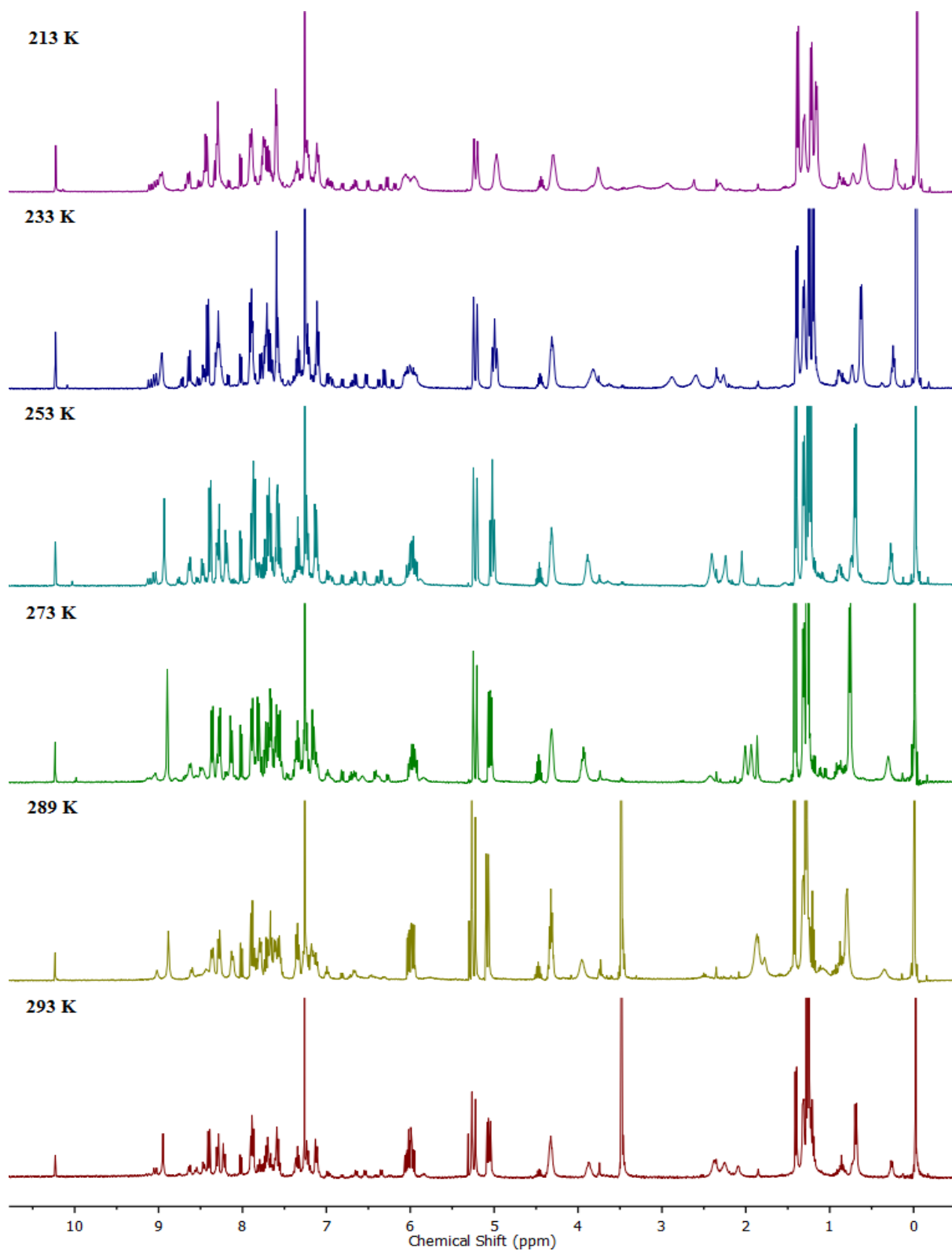
Figure 4.49: Variable Temperature NMR for Complex **33** with 3-buten-2-ol
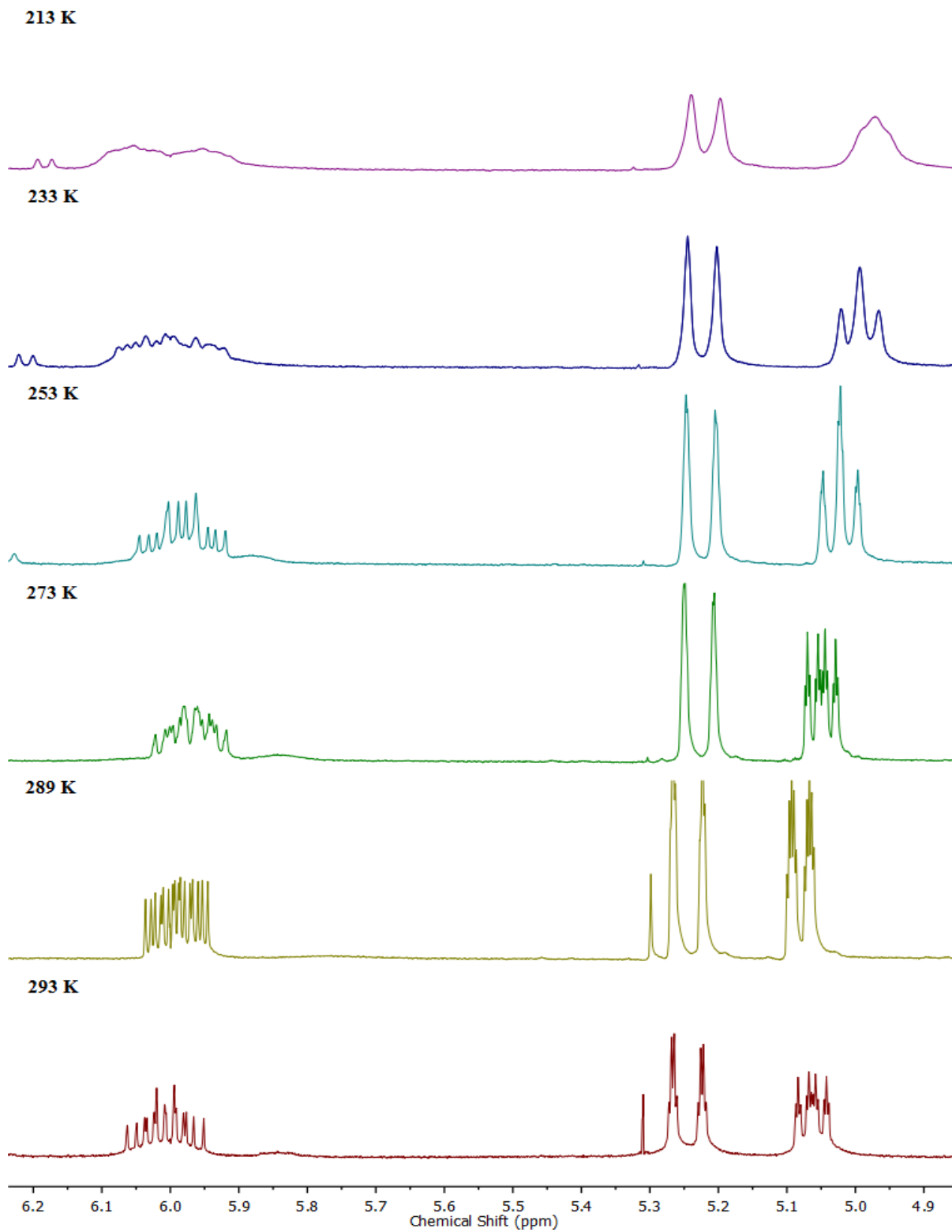
Figure 4.50: Aliphatic Region VT-NMR for Complex **33** with 3-buten-2-ol (CDCl$_3$)
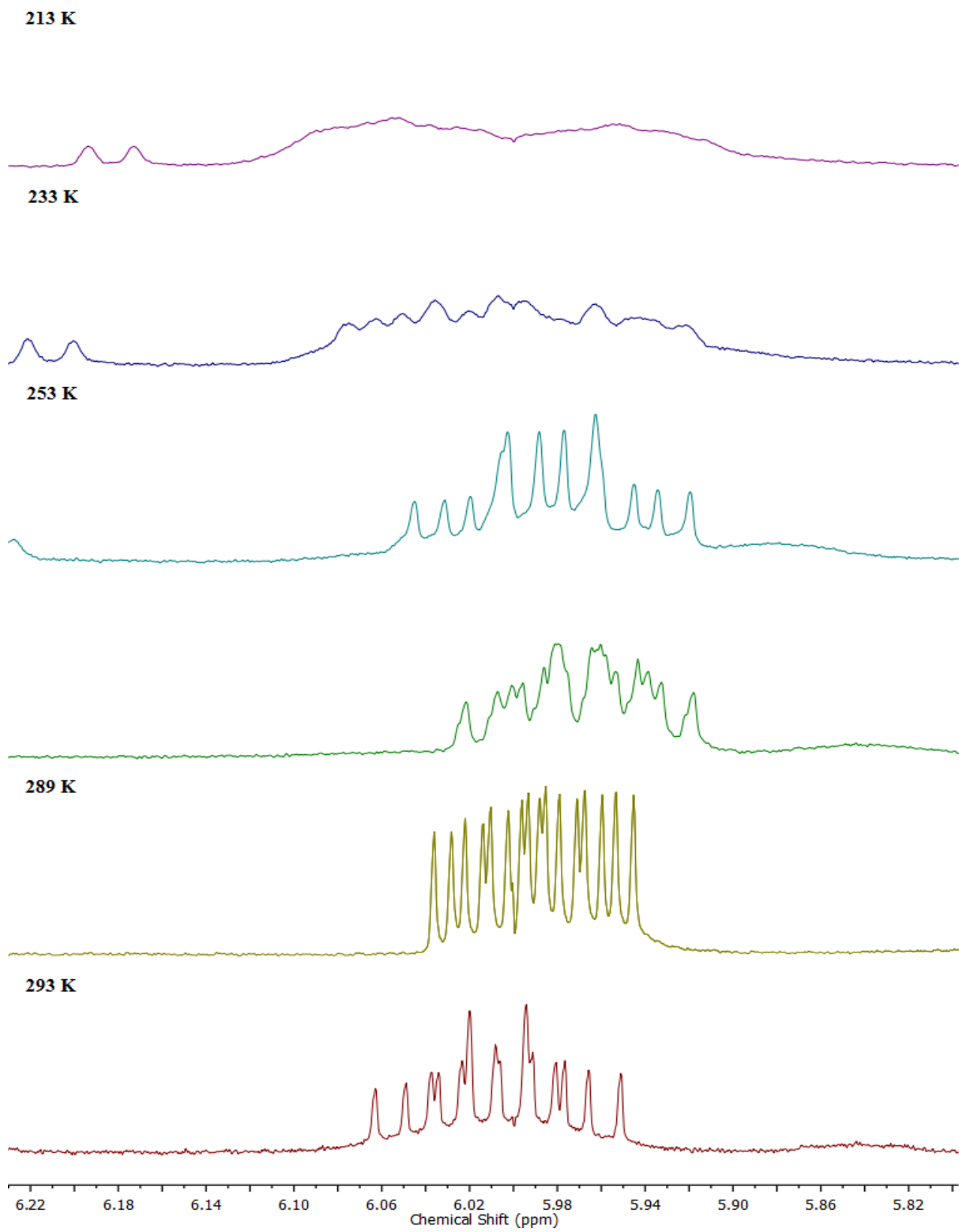
Figure 4.51: VT-NMR of complex **33** with 3-buten-2-ol Focused on 6.00 ppm (CDCl$_3$)
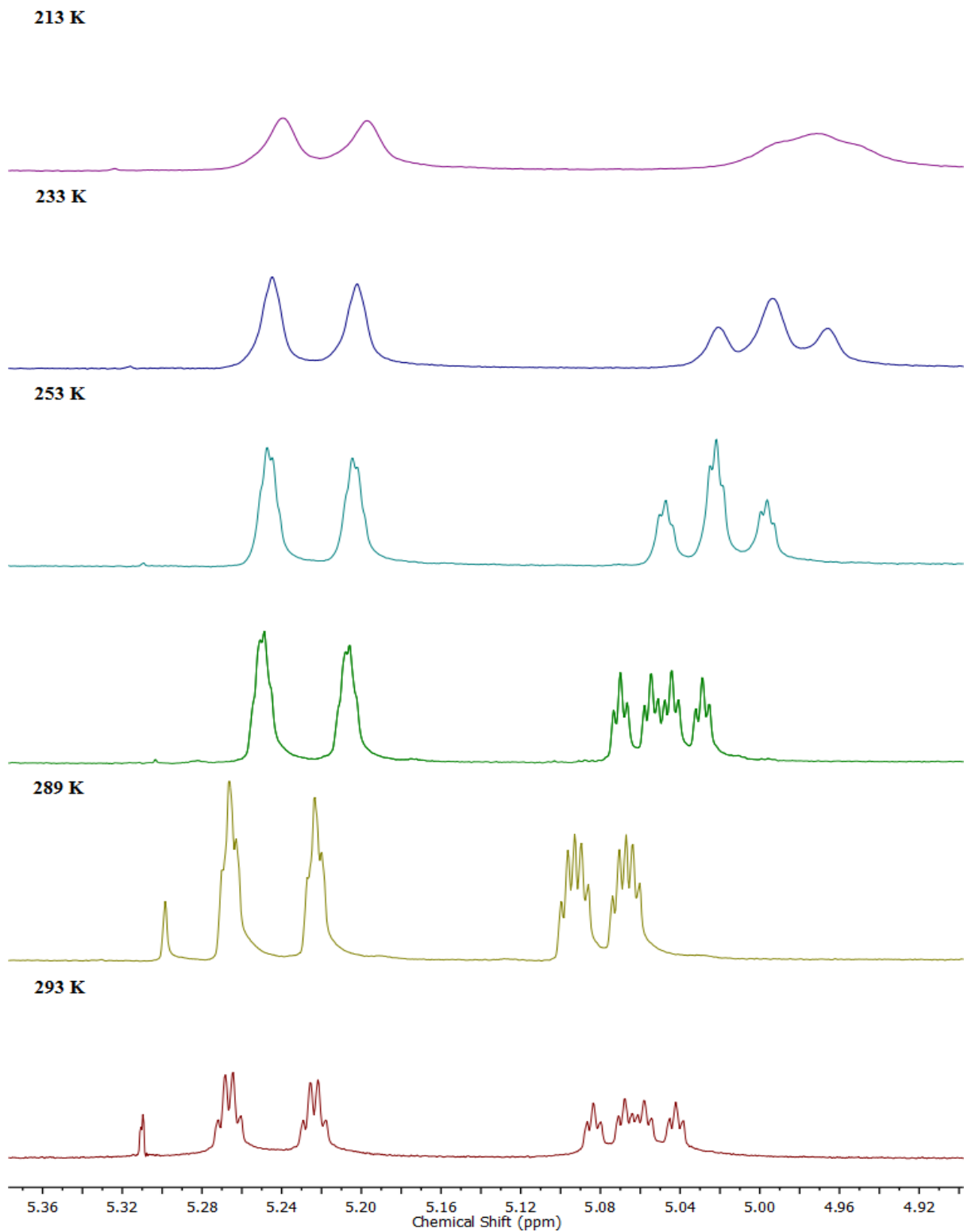
Figure 4.52: VT-NMR Spectrum of Complex **33** with 3-buten-2-ol Focused on 5.04 ppm

In solution, there are various dynamic processes that can occur; nitrogen inversion, olefin exchange, and olefin rotation. We attempted a variable temperature NMR experiment to find the optimum temperature for the association of the olefin with the metal center while minimizing the various dynamic processes that occur at room temperature. The variable temperature experiment of complex **33** with 3-buten-2-ol obtained earlier shows that 289 K gives us the most olefin separation during the cooling process. When we cool the mixture down to 273 K, we observe that proton **C** gets affected to the point that we observe twice the number of protons peaks expected at 5.04 ppm. Once again, we expect the protons that are directly linked to the olefin double bond (protons **A**, **B**, and **C**) to be the most affected during association with the silver(I) metal center. When complex **33** is mixed with 1-penten-3-ol, we obtain the VT- NMR spectrum shown in Figure 4.54 and 4.55. Here, cooling the mixture down to 243 K gave the biggest separation of possible enantiomers. When we move on to a different silver complex and mix complex **34** with 3-buten-2-ol, we obtain the ^{1}H NMR spectrum shown below in Figure 4.53. Once again, we observe the doubling of peaks corresponding to proton A at 5.85 ppm.
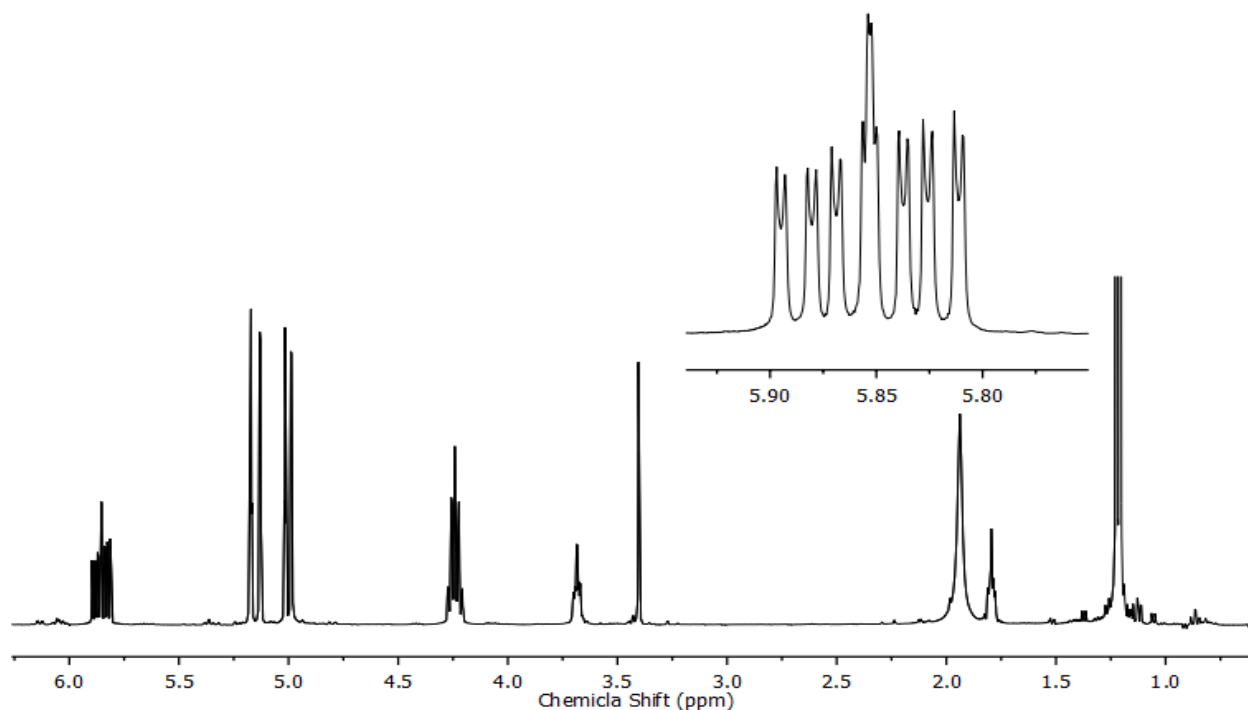
Figure 4.53: 400 MHz ^{1}H NMR Spectrum for Complex **34** with 3-buten-2-ol
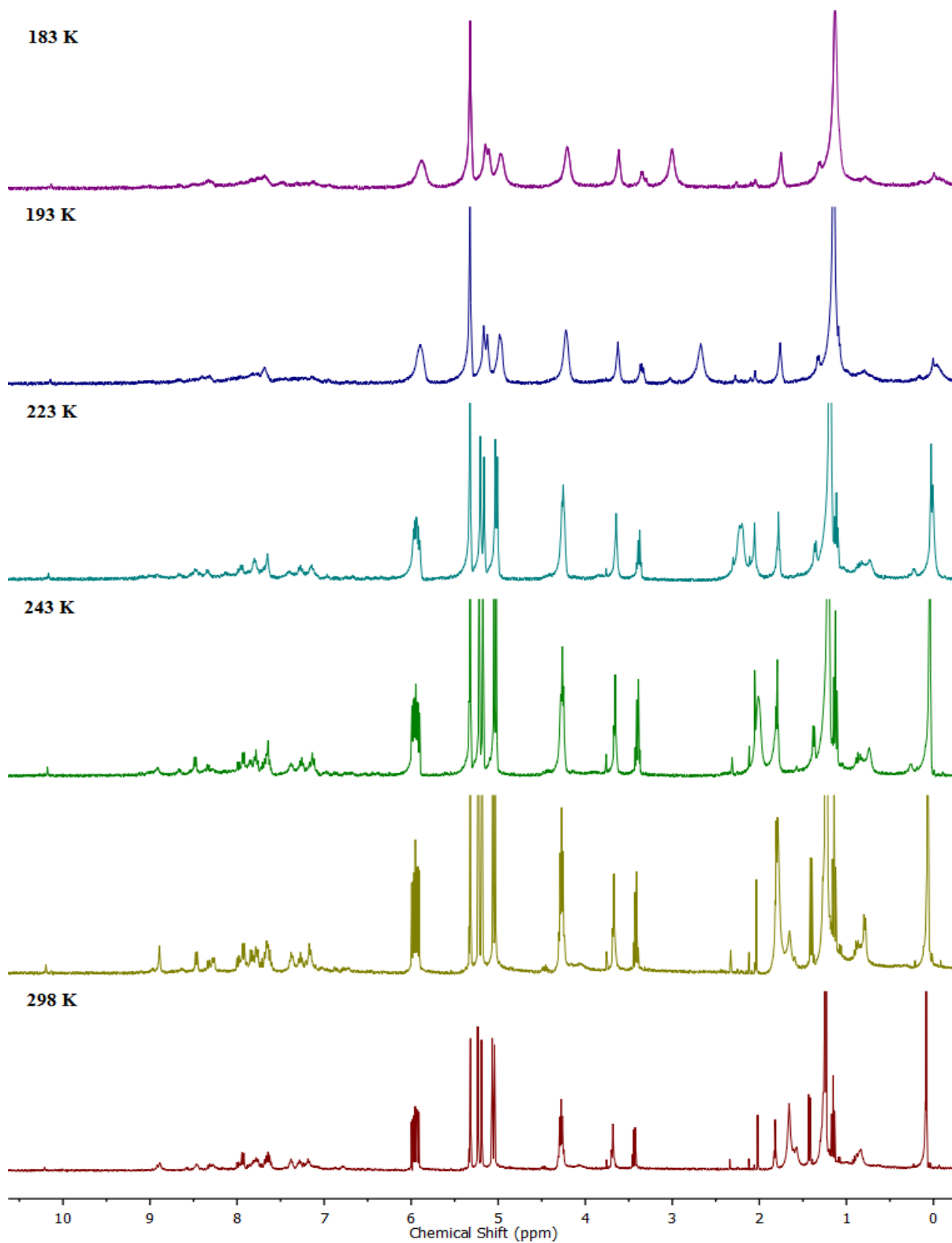
Figure 4.54: 400 MHz VT-NMR Spectrum for Complex **33** with 1-penten-3-ol (CDCl$_3$)
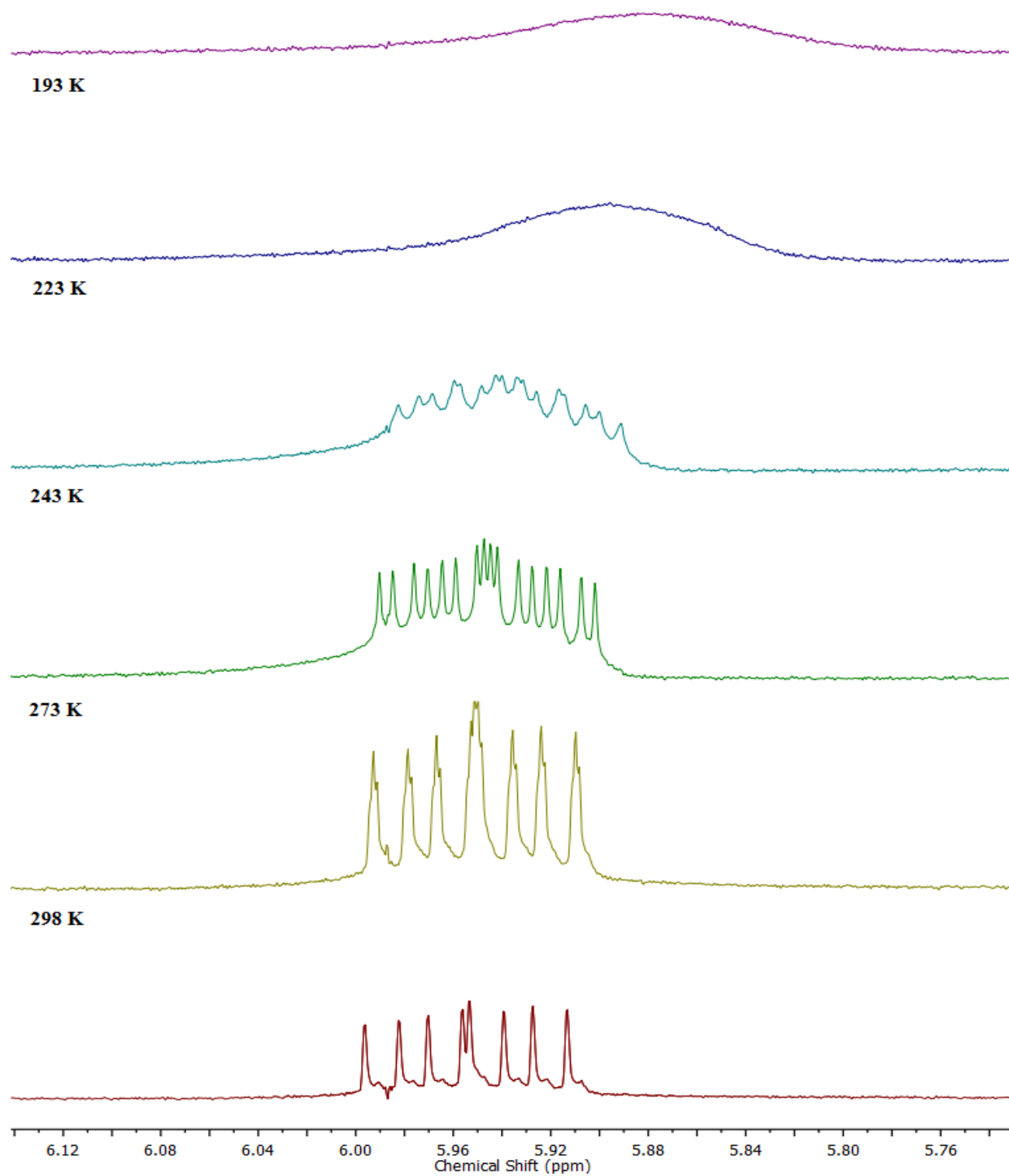
Figure 4.55: 400 MHz VT- NMR Spectrum of complex **33** with 1-penten-3-ol (CDCl$_3$)

In summary, based on literature reports, the enantiomer signals should be well separated from each other if the complex preferentially binds to one olefin over the other. The magnitude of the signal separation results from the balance of the different coordination shifts of the two enantiomers and of their affinities to the chiral metal fragment.[119] The sterics of the ligand used in that study played an important role in the results obtained. The mesityl rings of the diamine ligand that was used are relatively small and had a shielding effect on the coordinated olefin, almost enveloping it from its sides. This resulted to the excellent separation of enantiomers observed with that complex. Our complexes, on the other hand, are much more bulky compared to *N,N'*-bis(mesitylmethyl)-1,2-ethanediamine and do not give well separated enantiomers. Our bulky complexes, may not allow for a strong association to be formed between the olefin and the metal center as shown in figure 4.56. Instead what we could be observing in the ^{1}H NMR spectrum if the olefin "hopping" in and out of the metal pocket with this motion happening so rapidly that we observe average NMRs corresponding to free olefin and bound olefin. This scenario does not eliminate the idea that the silver(I) complex may not preferentially bind to a particular olefin enantiomer and we might be observing both *R* and *S* enantiomers binding and "hopping" out of the pocket to give us averaged NMR signals. If this is what actually happens then would expect to still see averaged signals in a VT experiment as we would have both *R* and *S* bound and frozen to the complex and both *R* and *S* frozen in the NMR solvent.
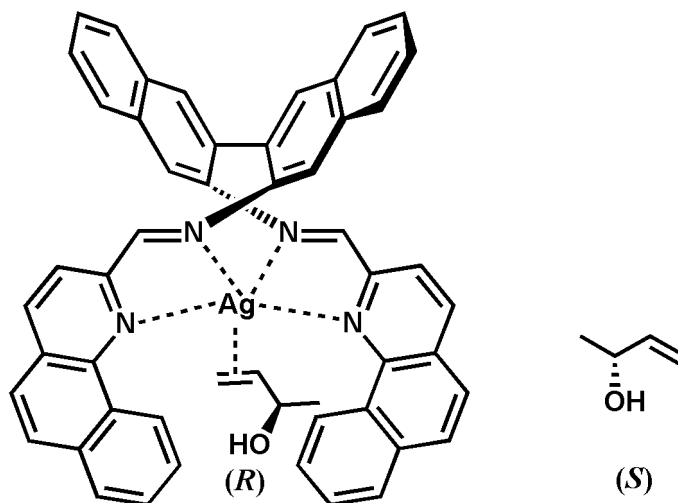
Figure 4.56: Proposed Steric Interaction of Complex **34** with Racemic 3-buten-2-ol

170

The last scenario involves the olefin binding to a dinuclear silver complex and a mononuclear silver complex at the same time to result in double the proton peak numbers observed for the olefin. This is highly unlikely given all the tests carried out on complex **34** which suggest that the silver complex is present as mononuclear specie in solution. Similar NMR discrimination experiments carried out with other silver complexes also display the doubling of peaks in the ^{13}C NMR spectra obtained. They attribute this to the complex preferentially binding to one enantiomer changing its peak position in the ^{13}C NMR compared to the unbound olefin.[120] We carried out a similar ^{13}C NMR experiment on the mixture of complex **33** with 3-buten-2-ol and obtain the spectrum shown in Figure 4.57. We observe that the carbon atoms associated with the olefin double bond show up as two separate peaks in the ^{13}C NMR spectrum which is suggests that the association we observe with our silver(I) complexes if that of preferential binding to one olefin enantiomer over the other (Figure 4.56).
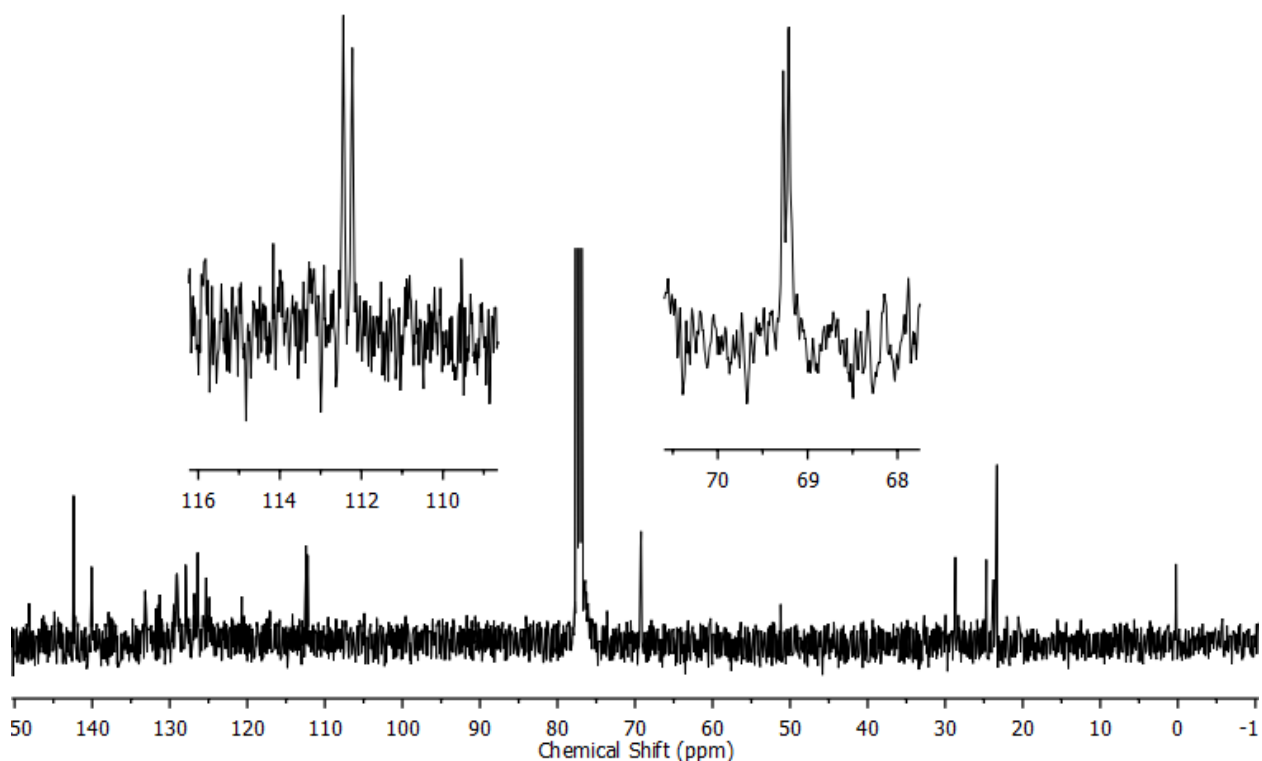
Figure 4.57: 400 MHz ^{13}C NMR Spectrum for Complex **33** with 3-buten-2-ol

CHAPTER 5

Conclusions and Future Work

We have successfully synthesized, characterized, and studied a diverse library of chiral Schiff-base ligands and complexes. The ligands described in this thesis were prepared to serve as building blocks for the design of chiral catalysts. Complete characterization of the ligands **1**, **2**, **3**, **4**, **5**, **11**, and **12** was an important goal for us because we would like to monitor the chemical and physical change as the ligand transitions to a complex and also understand the role the metal center plays in the transition. Characterization of the ligands using 1D NMR experiments proved to be a complicated process because the ligands are polyaromatic systems resulting in coupling network similarities in different parts of the molecule leading to severe overlap of their ^{1}H resonances. To overcome this impediment, we took advantage of various 2D-NMR techniques (COSY, NOESY, ROSEY, HSQC, and HMBC) and were successful in resolving the complete ^{1}H NMR assignments for ligands **1 – 5** as shown in the following figures.
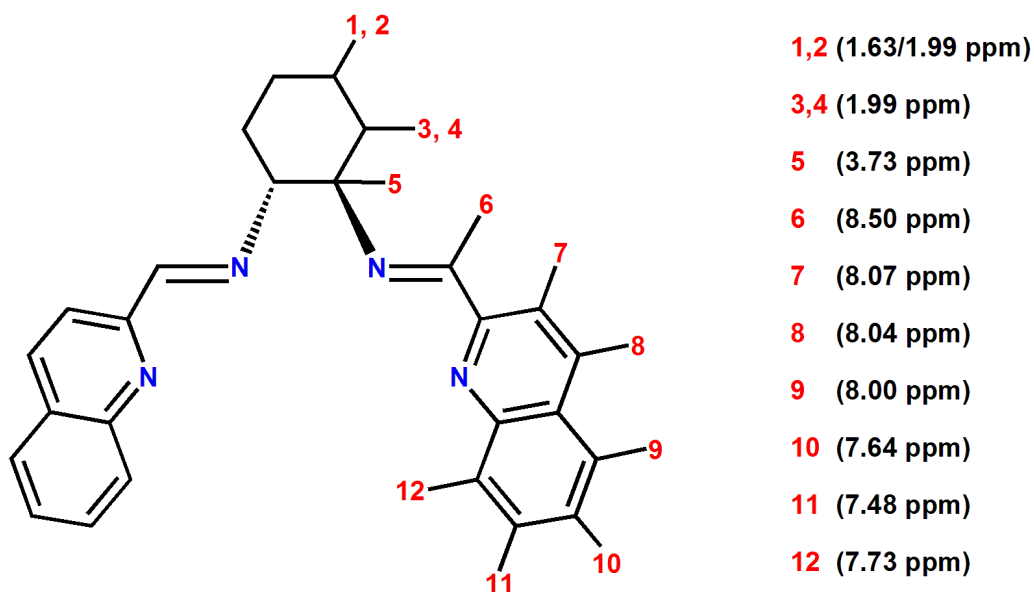
Figure 5.1: Complete ^{1}H NMR Assignment for Ligand **1**
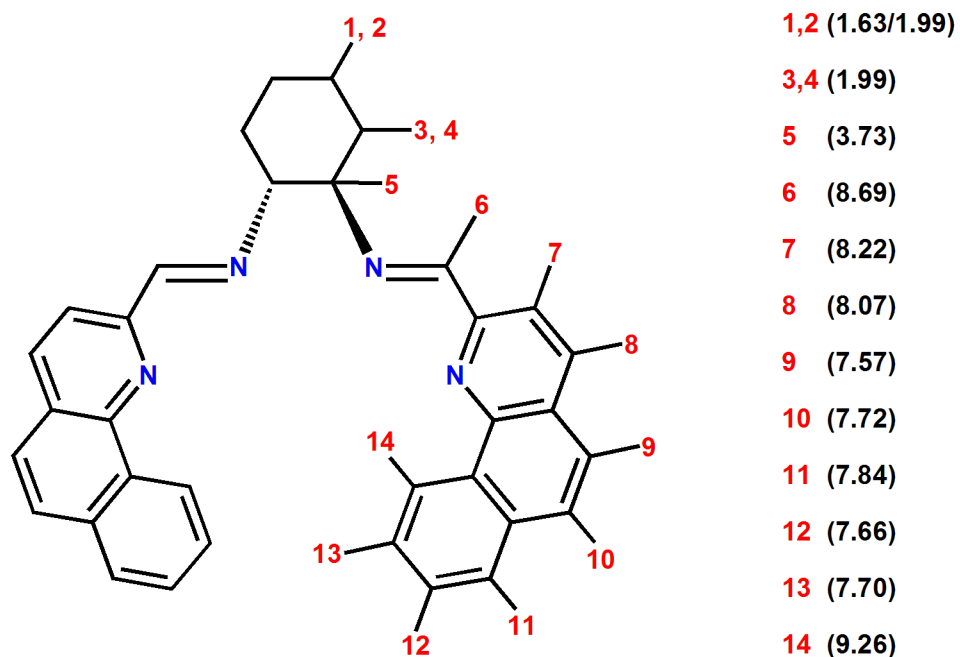
Figure 5.2: Complete ^{1}H NMR Assignment for Ligand **2**

1,2 (1.63/1.99)

3,4 (1.99)

5   (3.73)

6   (8.69)

7   (8.22)

8   (8.07)

9   (7.57)

10 (7.72)

11 (7.84)

12 (7.66)

13 (7.70)

14 (9.26)
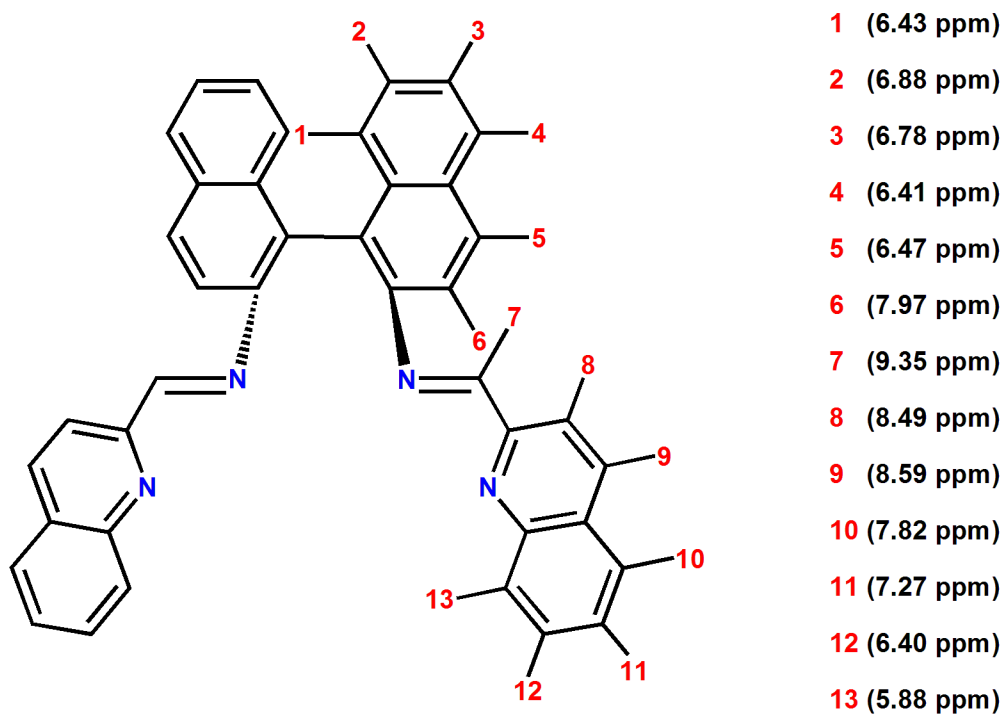
Figure 5.3: Complete ^{1}H NMR Assignment for Ligand **3**

1 (6.43 ppm)

2 (6.88 ppm)

3 (6.78 ppm)

4 (6.41 ppm)

5 (6.47 ppm)

6 (7.97 ppm)

7 (9.35 ppm)

8 (8.49 ppm)

9 (8.59 ppm)

10 (7.82 ppm)

11 (7.27 ppm)

12 (6.40 ppm)

13 (5.88 ppm)
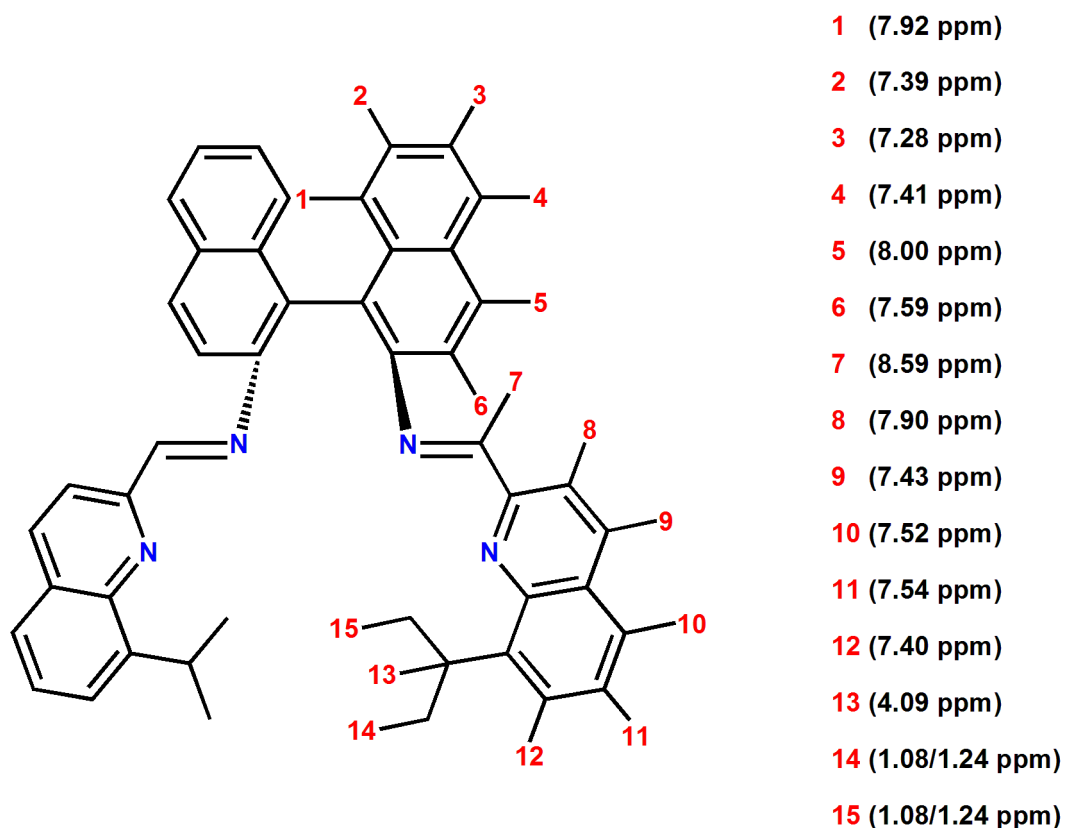
Figure 5.4: Complete ^{1}H NMR Assignment for Ligand **4**

We were successful in the reduction of the ligands that incorporated a cyclohexyl backbone (**1** & **2**) but could not reduce the ligands that had a binaphthalene backbone (**3**, **4**, & **5**). Our desire to reduce the tetradentate ligands was to increase the probability of the ligand completely wrapping around a metal center during complexation reactions. It is clear, from previous work carried out in the Levy group that the formation of a monohelix requires the use of a ligand that is more flexible and less sterically congested upon coordination. To improve flexibility, we chose to reduce the imine bridge of the backbones as this increases the chance of the side-arms completely binding and staying in a locked conformation while making the backbone flexible enough to accommodate bulkier substrates during catalysis reactions. We observed that time played an important role in the reduction reactions with the reduction of ligand **2** taking half the time required to fully reduce ligand **1**. This may be due to the reducing agent attacking the conjugated rings in the bulkier side-arms of ligand **2**.
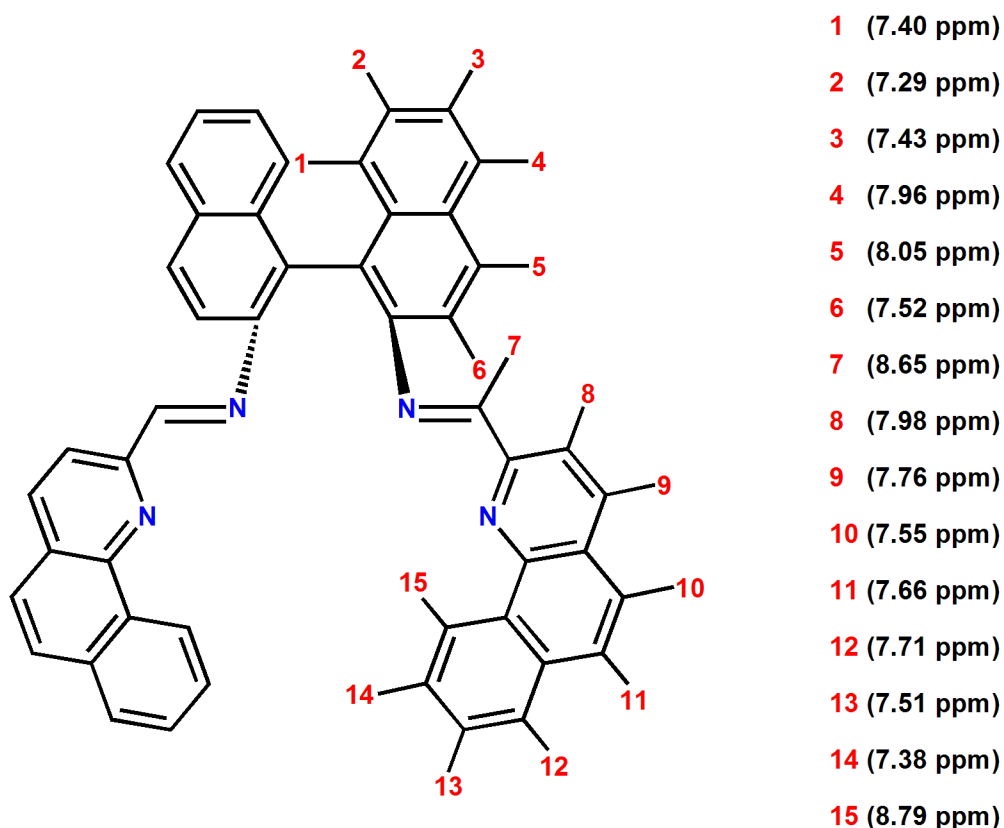
Figure 5.5: Complete ^{1}H NMR Assignment for Ligand **5**

We were able to achieve the partial reduction of ligand **5** using a one-pot reaction of the ligand plus the reducing agent plus a zinc(II) triflate salt to yield complex **13**. A solid state structure was obtained and we observed the formation of a single stranded monohelix. The four nitrogen donor atoms and one triflate ligand bind to the zinc(II) metal center in a distorted square planar geometry. We believe the π-π and σ-π interactions in the complex as a result of the overlapping benzoquinoline side-arms stacking on top of each other improving the stability of the complex and allowing it to stay in a "locked" position. Subsequent chelation reactions with ligands **2**, **5**, and **11** produced a variety of complexes that were characterized with 1D and 2DNMR and electro-spray mass spectrometry. Our goal was to synthesize helical complexes of one hand only so that upon chelation, the overlapping sidearms will produce a conformation that is locked in either the *M* form or *P* form preventing any inter-conversion between the two forms. The following is a brief summary of the different types of helices formed using our ligands.

1.   Reaction of ligand **11** with FeCl$_2$ resulted in the formation of a single stranded monohelix as we desired, complex **18**. We observe that complex **18** is present only as the *M* (left-handed) conformer. The space filling model also suggests that there are π–π and/or σ-π interactions present between the phenyl rings at the ends of the quinoline side-arms. The aromatic rings do not lie directly on top of each other but are slightly offset creating an ideal alignment that fosters a π-π interaction or σ-π interaction.   The reaction FeCl$_2$ produced a fascinating solid state structure with two iron centers and an oxo bridging ligand. We plan to use this complex in future hydroxylation reactions given the success of similar complexes for such catalytic reactions in the literature. The oxidation state of the metal centers remains elusive but information obtained from the ^{1}H NMR and EPR spectra suggest that both iron centers are of the +3 oxidation state
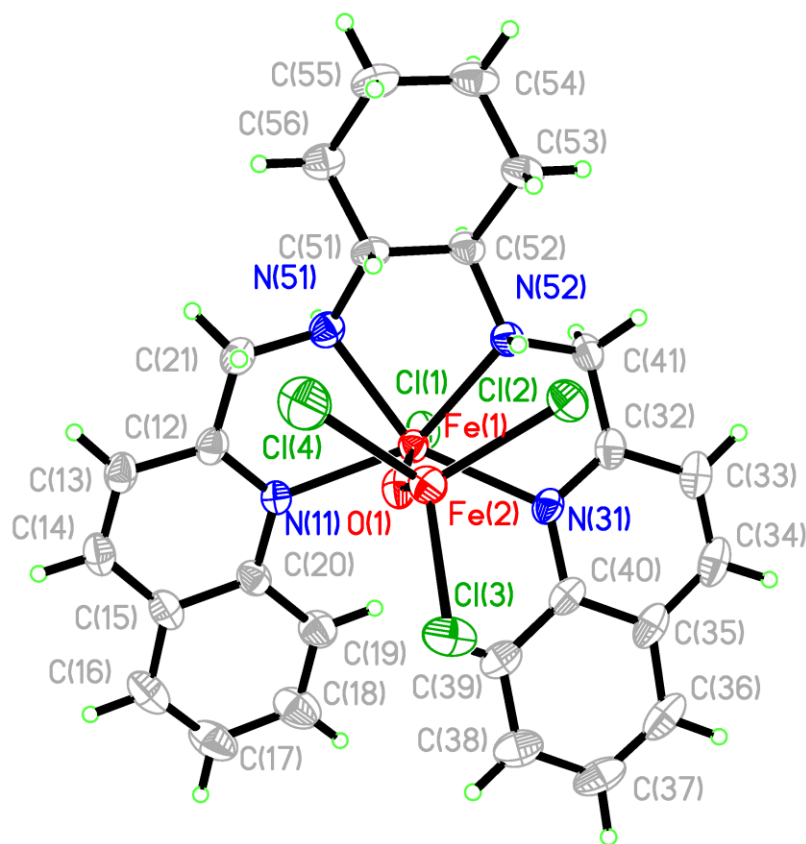
Figure 5.6: Thermal Ellipsoid Crystal Structure for Complex **18**

2.   The reaction of Ligand **11** with RuCl$_2$(COD) also resulted in the formation of a single stranded monohelix, complex **19**. The thermal ellipsoid model for complex **19** displays the presence of two single stranded monohelices and also shows the ruthenium metal center bound in a distorted octahedral fashion. We observe that complex **18** is present in a ratio of 1:1mixture of *M* (left-handed) conformer and *P* (right-handed) conformer that have the same orientation relative to each other. The core difference lies in the orientation of their quinoline side-arms.
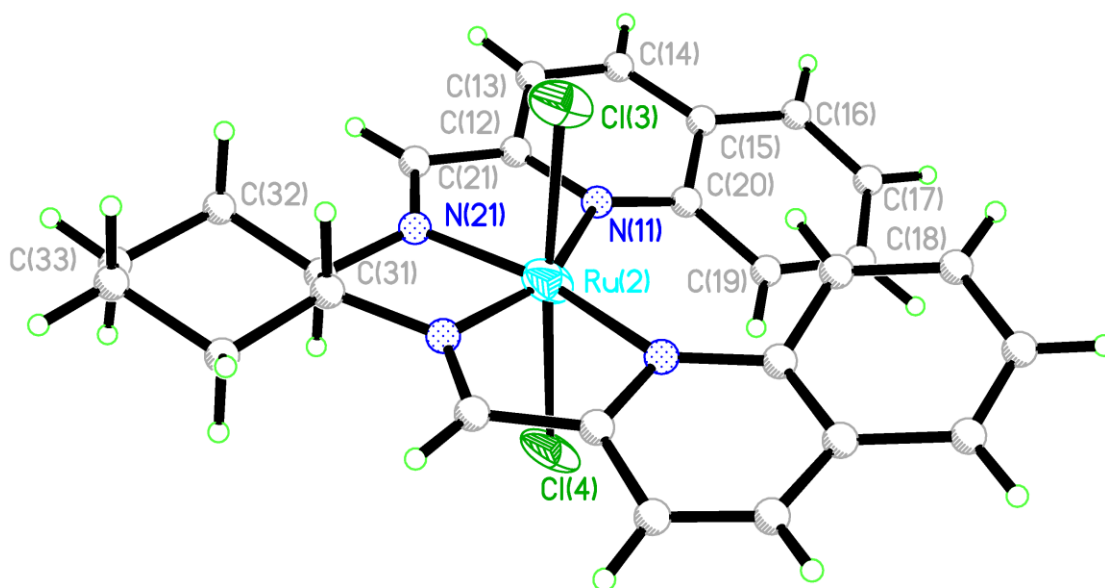
Figure 5.7: Thermal Ellipsoid Crystal *P*-helix Structure for Complex **19**

3.   The reaction of Ligand **5** with Ag(OTf) resulted in the formation of a dinuclear double stranded helicate, complex **34**. The ligands are arranged with the benzoquinoline side-arm of one ligand stacked with the binaphthalene backbone of the second ligand. This orientation suggests that π-π or σ-π interactions played a significant role in the orientation of complex **34** in the solid state. The silver(I) cations do not completely bind to all available nitrogen donor groups resulting in one metal center to have a trigonal planar geometry while the second silver cation is arranged in a bent or angular geometry.

177
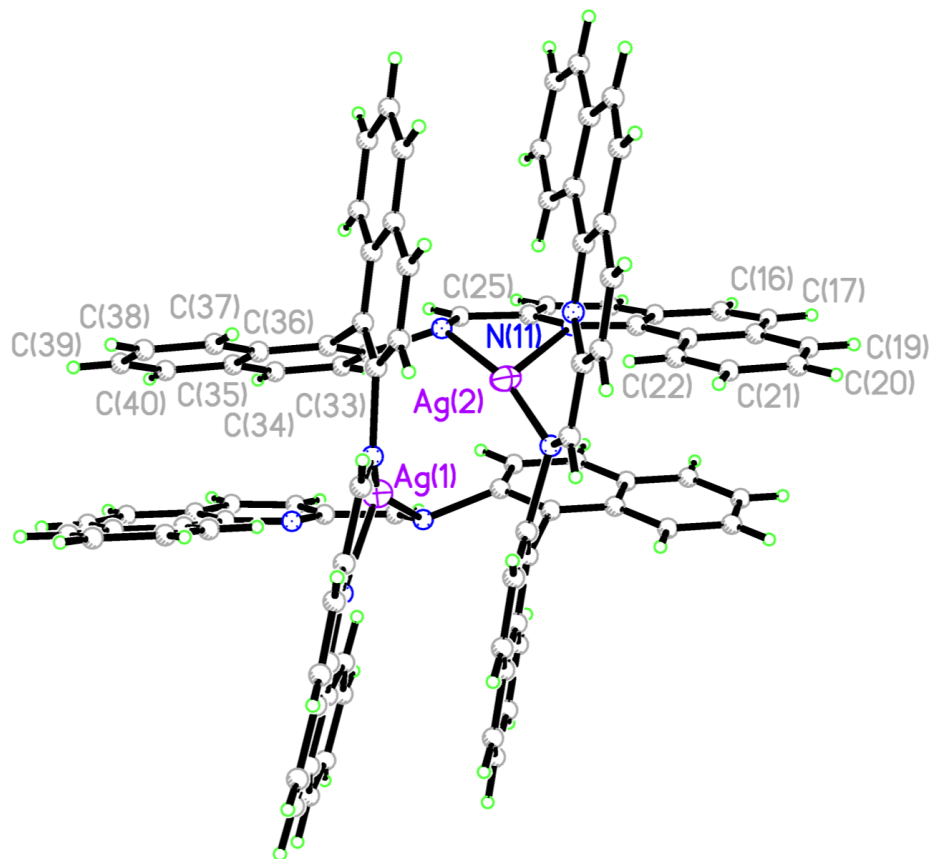
Figure 5.8: Thermal Ellipsoid Crystal *P*-helix Structure for Complex **34**

We carried out some interesting studies using our ligands and silver(I) triflate salts. The complexation reaction with ligands **3**, **4**, and **5** produced products with unusual expanded aromatic region in the ^{1}H NMR spectrum obtained. This may the due to the silver salt acting as an NMR shift reagent as suggested in the literature. We observe that complex **32** and **34** have a unique ^{3}J(^{1}H-^{107,109}Ag) coupling present that causes the distinct imine proton to appear as a doublet in the ^{1}H NMR spectra obtained. We do not observe this coupling in complex **33** because it prefers to react with two equivalent of the silver(I) triflate most likely forming a di-nuclear complex and interfering with the ^{3}J(^{1}H-^{107,109}Ag) coupling that would have otherwise occurred. The combination of all 1D (^{1}H, ^{13}C, HOMODEC) and 2D (COSY, ROSEY, NOESY, HSQC, HMBC) NMR experiments allowed us to navigate the severe proton overlaps observed in polyaromatic systems and obtain the complete ^{1}H NMR assignments for complexes **32**, **33**, & **34**.
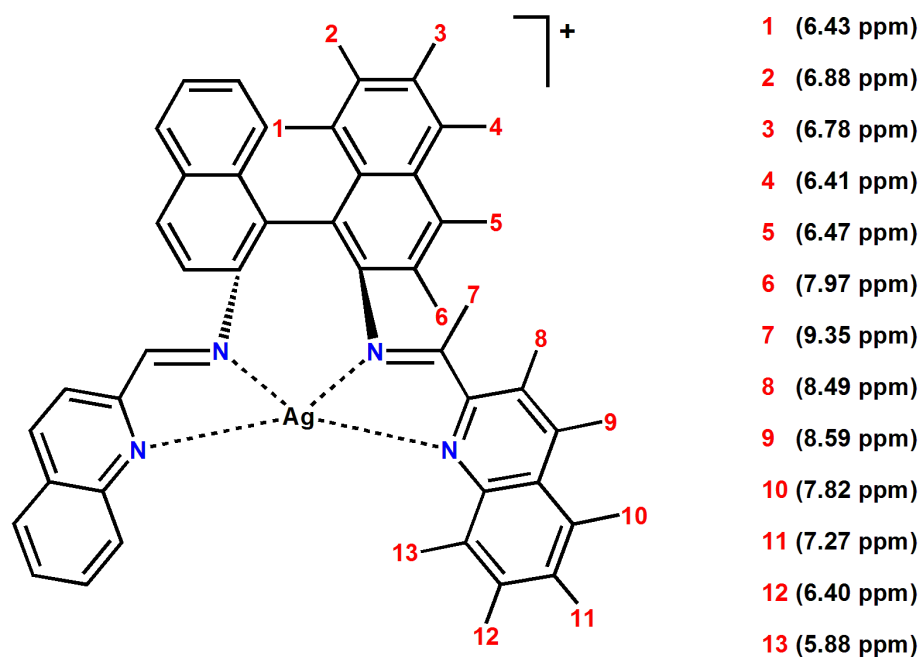
Figure 5.9: Complete ^{1}H NMR Assignment for Complex **32**

1 (6.43 ppm)
2 (6.88 ppm)
3 (6.78 ppm)
4 (6.41 ppm)
5 (6.47 ppm)
6 (7.97 ppm)
7 (9.35 ppm)
8 (8.49 ppm)
9 (8.59 ppm)
10 (7.82 ppm)
11 (7.27 ppm)
12 (6.40 ppm)
13 (5.88 ppm)
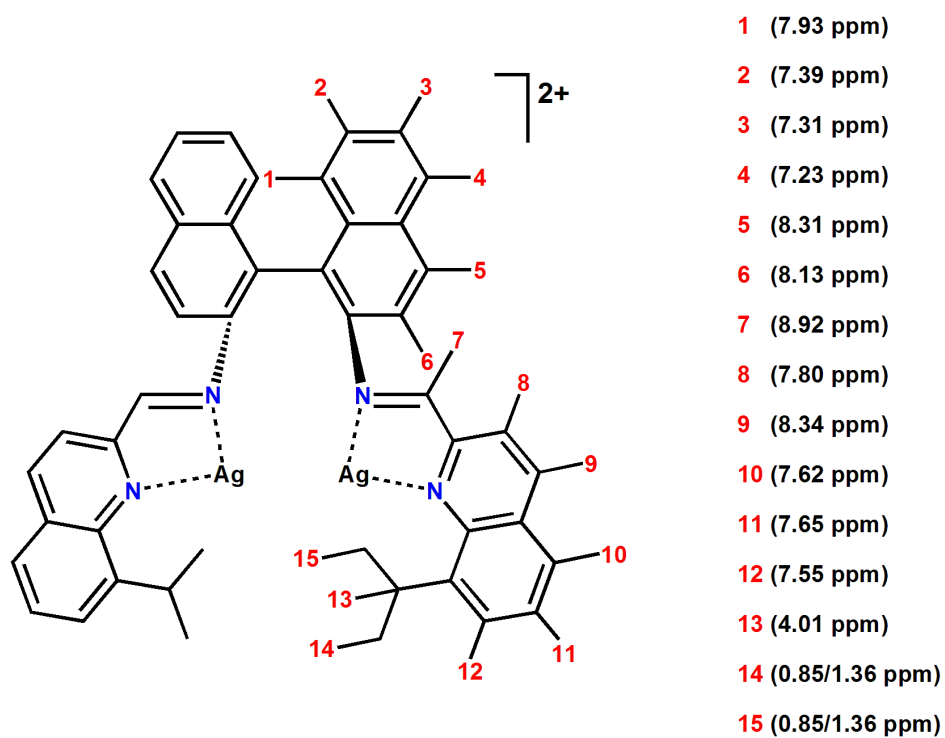
Figure 5.10: Complete ^{1}H NMR Assignment for complex **33**

1 (7.93 ppm)
2 (7.39 ppm)
3 (7.31 ppm)
4 (7.23 ppm)
5 (8.31 ppm)
6 (8.13 ppm)
7 (8.92 ppm)
8 (7.80 ppm)
9 (8.34 ppm)
10 (7.62 ppm)
11 (7.65 ppm)
12 (7.55 ppm)
13 (4.01 ppm)
14 (0.85/1.36 ppm)
15 (0.85/1.36 ppm)

179
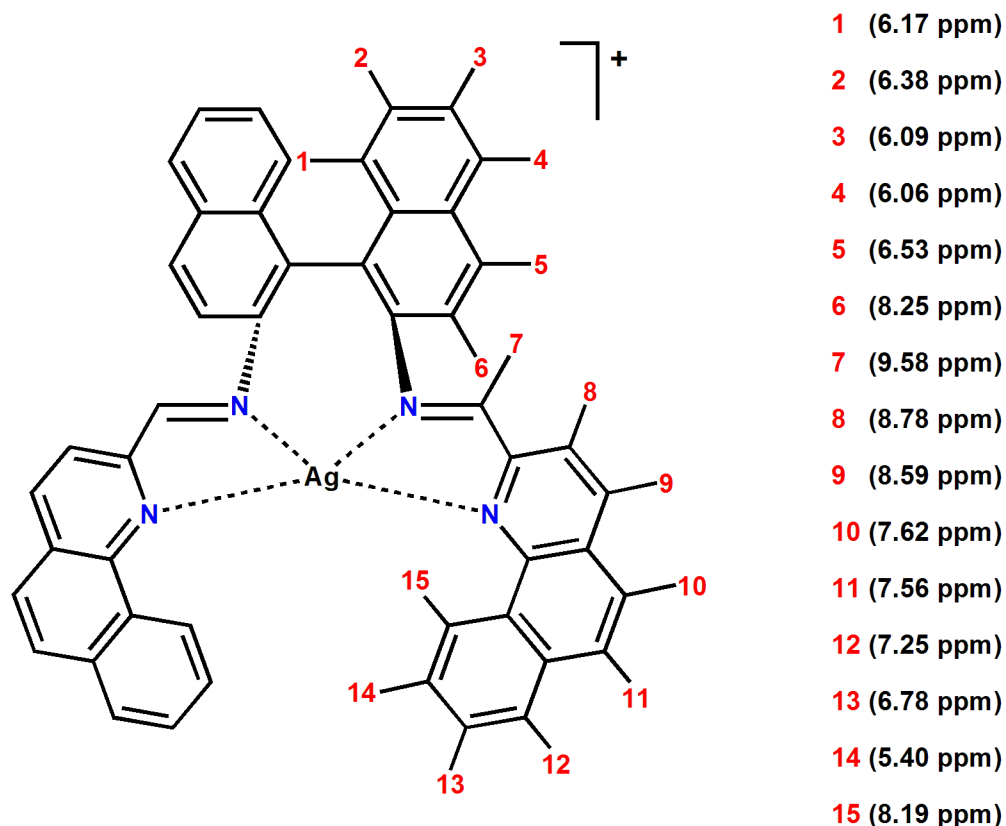
Figure 5.11: Complete[1]H NMR Assignment for Complex **34**

We were able to demonstrate the use of our silver(I) complexes in the chiral recognition of olefins using 3-buten-2-ol and 1-penten-3-ol. We chose allylic alcohols because they are more stable and robust most likely due to a stabilizing intramolecular interaction between the atom and the metal ion. The reactions produced ^{1}H NMR spectra the displayed a slight separation of the olefin peaks most likely due to the preferential binding on the chiral silver(I) complex with a particular face of the chiral olefin. This cannot be postulated as the only scenario as there are many dynamic processes that can be taking place in solution between our complexes and the olefins. Another scenario is the presence of the following species all together in solution: silver(I) complex bound to the *S* enantiomer of the olefin, unbound silver(I) complex and unbound *S* olefin enantiomer, complex bound to the *R* enantiomer of the olefin, and unbound silver(I) complex and unbound *R* olefin enantiomer. The species interchange rapidly at room temperature but slow down with cooling and may be what we observe in the ^{1}H NMR spectra.

6.1 Future Work

The reduction of ligands bearing the binaphthalene backbone still eludes us. As detailed in the thesis, several changes were made to the reaction conditions to increase the likelihood of reducing the imine bond to no avail. The use of other reducing agents apart from LAH and NaBH$_4$ might afford the desired reduced compound. Further one-pot reactions with the ligand, should be attempted with other metal salts to see if this is a viable way to carry out the reduction and complexation of our chiral tetradentate ligands. As detailed in this thesis, thirty-six new complexes were synthesized and characterized. The overriding goal of these complexation reactions is to prepare novel compounds that can be used as catalysts in various asymmetric reactions. Even though single stranded monohelices were not obtained for all metallation reactions, double-stranded, triple-stranded, di-nuclear, and dihelicates complexes still have potential to be used in catalytic processes. For example, mono and dinuclear nickel complexes could potentially be used as catalysts for olefin polymerization reactions. The iron complex obtained (**18**) shows promise, based on literature studies, for use in the area of hydroxylation reactions. The ruthenium complex synthesized (**19**) has potential use in the design of photovoltaic cells. The silver(I) complexes obtained in chapter four show enormous potential for use in the area of chiral recognition and the NMR discrimination of chiral olefins. Attempts should be made to synthesized more complexes with different steric parameters and observe how those factor into the efficiency of the complex in chiral recognition.

EXPERIMENTAL SECTION

General Methods

All reactions were carried out under an inert atmosphere (nitrogen or argon). Solvents used in complexation reactions were pre-dried with calcium hydride, sodium benzophenone ketyl or magnesium alkoxide and degassed prior to transfer via high-vacuum line techniques. Inert gases were passed through 4Å molecular sieves and a Englehard Q5 catalyst bed before use. NMR solvents were also dried over 4Å molecular sieves and kept in the glove box. Air-sensitive NMR samples were placed in a sealed J Young NMR tube. All complexes were stored in a glove box with the ones from silver reaction wrapped with aluminum foil.

Electro-spray mass spectrometry was carried out by the University of Kansas Mass Spectrometry Laboratory, Lawrence, Kansas. Electron Paramagnetic Resonance analyses were carried out by the University of Kansas Molecular Structures Group (MSG), Lawrence, Kansas with microwave frequency, 9.636638 GHz (perpendicular) and 9.392624 GHz (parallel). Microwave power used is 31.70 mW, field sweep rate is 5 mT/s, field modulation frequency is 100 kHz, modulation amplitude, 0.4 mT, conversion time, 8 ms, and a time constant of 81.92 ms. UV-vis spectra were acquired on a Varian Cary 500 spectrometer. Solution samples were placed in a 1 cm pathlength quartz cell. ^{1}H, ^{13}C and all 2D NMR spectra were acquired on either a Varian Unity 400 MHz, or a Mercury 400 MHz spectrometer equipped with a TCI cryprobe. Residual solvent protons were used as the internal standard. Crystallographic data was collected using either a Bruker SMART 1000 CCD or a Bruker-AXS SMART APEX CCD.

(1*R*,2*R*)-*N*,*N*'Bis[(2-quinolyl)methylene]-1,2-cyclohexanediamine (Ligand 1). (*R*,*R*)-6 (0.2 g, 1.8 mmol) and quinoline (0.75 g, 3.6 mmol) were refluxed in ethanol (5 mL) for 3 hours. The yellow precipitate formed was filtered and washed with ethanol (5 mL) to afford Ligand **1** (0.63 g, 73 % yield). ^{1}H NMR (CDCl$_3$, 400 MHz): δ 1.24 (br, 2 H, CH), 1.56 (br, 2 H, CH), 1.97 (br, 2 H, CH), 3.62 (br, 2 H, CH), 7.48 (t, 1 H, *J* = 8.06 Hz, CH), 7.65 (t, 1 H, *J* = 8.06 Hz, CH), 7.74 (d, 1 H, *J* = 8.06 Hz, CH), 8.03 (d, 1 H, *J* = 8.56 Hz, CH), 8.06 (s, 1 H, CH), 8.52 (s, 1 H, CH).

(1*R*,2*R*)-*N*,*N*'Bis[(2-benzoquinolyl)methylene]-1,2-cyclohexanediamine (Ligand 2). (1*R*,2*R*)-1,2-cyclohexanediamine (0.4 g, 3.6 mmol) and benzoquinoline (1.50 g, 7.2 mmol) were refluxed in ethanol (10 mL) for 3 hours. The brownish colored precipitate formed was filtered and washed with ethanol (15 mL) to afford Ligand **2** (1.12 g, 78 % yield). ^{1}H NMR (CDCl$_3$, 400 MHz): δ 1.24 (br, 2 H, CH), 1.56 (br, 2 H, CH), 1.97 (br, 2 H, CH), 3.62 (br, 2 H, CH), 7.59 (d, 6 H, CH), 7.63-7.74 (m, 3 H, CH), 7.82 (d, 2 H, *J* = 8.56 Hz, CH), 8.06 (d, 2 H, *J* = 7.05 Hz, CH), 8.22 (d, 2 H, *J* = 7.55 Hz, CH), 8.69 (s, 1 H, CH), 9.23 (d, 2 H, *J* = 7.55 Hz, CH)

(1*R*)-*N*,*N*'-Bis[(quinoline)methylene]-[1,1'-binaphthalene]-2,2'-diamine (Ligand 3). (*R*)-[1,1'-binapthalene]-2,2'-diamine (1.43 g, 5.0 mmol) and **8** (2.01 g, 10.1 mmol) were refluxed in ethanol (30 mL) in the presence of 3 Å molecular sieves for 2 hours. The brownish- yellow precipitate was filtered and washed twice with ethanol (5 mL) to afford ligand **3** (1.772 g, 55% yield). ^{1}H NMR (CDCl$_3$, 400 MHz): δ 7.32 (t, 2 H, *J* = 8.00 Hz, CH), 7.37 (d, 2 H, *J* = 8.06 Hz, CH), 7.40 (t, 2 H, *J* = 7.05 Hz, CH), 7.52 (t, 2 H, *J* = 7.00 Hz, CH), 7.55 (d, 2 H, *J* = 7.00 Hz,

CH), 7.58 (d, 2 H, *J* = 8.56 Hz, CH), 7.65 (t, 2 H, *J* = 9.06 Hz, CH), 7.75 (d, 2 H, *J* = 8.56 Hz, CH), 7.87 (d, 2 H, *J* = 7.55 Hz, CH), 7.95 (d, 2 H, *J* = 8.06 Hz, CH), 8.06 (d, 2 H, *J* = 8.06 Hz, CH), 8.65 (s, 2 H, CH).

(1*R*)-*N*,*N*'-Bis[(8-isopropyl-2-quioline)methylene]-[1,1'-binaphthalene]-2,2'-diamine

(Ligand 4). (*R*)-[1,1'-binapthalene]-2,2'-diamine (0.72 g, 2.5 mmol) and **8** (1.01 g, 5.1 mmol) were refluxed in ethanol (20 mL) in the presence of 3 Å molecular sieves for 2 hours. The yellow precipitate was filtered and washed twice with ethanol (5 mL) to afford ligand **4** (0.881 g, 57% yield). ^{1}H NMR (CDCl$_3$, 400 MHz): δ 1.11 (d, 6 H, *J* = 6.90 Hz, CH$_3$), 1.27 (d, 6 H, *J* = 6.90 Hz, CH$_3$), 4.12 (sept, 2 H, *J* = 6.9 Hz, CH), 7.28-7.34 (m, 2 H, CH), 7.30-7.58 (m, 12 H, CH), 7.62 (d, 2 H, *J* = 8.5 Hz, CH), 7.91-7.98 (m, 4 H, CH), 8.03 (d, 2 H, *J* = 8.7 Hz, CH), 8.62 (s, 2 H, CH).

(1*R*)-*N*,*N*'-Bis[(2-benzoquinolyl)methylene]-[1,1'-binaphthalene]-2,2'-diamine (Ligand 5). (*R*)-[1,1'-binapthalene]-2,2'-diamine (0.52 g, 1.8 mmol) and **10** (0.75 g, 3.6 mmol) were refluxed in ethanol (25 mL) in the presence of 3 Å molecular sieves for 2 hours. The yellow precipitate was filtered and washed twice with ethanol (5 mL) to afford ligand **5** (1.11 g, 92% yield). ^{1}H NMR (CDCl$_3$, 400 MHz): δ 7.32 (t, 2 H, *J* = 8.00 Hz, CH), 7.35 (d, 2 H, *J* = 8.06 Hz, CH), 7.40 (t, 2 H, *J* = 7.05 Hz, CH), 7.46 (t, 2 H, *J* = 7.00 Hz, CH), 7.55 (t, 2 H, *J* = 7.00 Hz, CH), 7.58 (d, 2 H, *J* = 8.56 Hz, CH), 7.63 (d, 2 H, *J* = 9.06 Hz, CH), 7.72 (d, 2 H, *J* = 8.56 Hz, CH), 7.77 (d, 2

H, J = 7.55 Hz, CH), 7.81 (d, 2 H, J = 8.06 Hz, CH), 8.01 (d, 2 H, J = 8.06 Hz, CH), 8.07 (d, 2

H, J = 8.06 Hz, CH), 8.10 (d, 2 H, J = 8.56 Hz, CH), 8.70 (s, 2 H, CH), 8.80 (d, 2 H, J = 8.06 Hz,

CH).

(1R,2R)-1,2-cyclohexanediamine (R,R-6). Synthesis was carried out using literature

procedures. ^{1}H NMR data collected for the pure material was consistent with literature.

(1R)-N,N'-[1,1'-binaphthalene]-2,2'-diamine (R-7). The procedure for (R)-**7** was followed

using (*rac*)-[1,1'-binapthalene]-2,2'-diamine in place of the *R*-enantiomer to afford (*rac*)-**6**

(0.395 g, 85% yield). ^{1}H NMR spectra were identical to that of compound (R)-**7**.

2-quinolinecarboxaldehyde (8). Synthesis was carried out using literature procedures. ^{1}H NMR

data collected for the pure material was consistent with literature.

8-isopropyl-2-quinolinecarboxaldehyde (9). A solution of 2-methyl-8-isopropyl-quinoline

(23.07 g, 125 mmol) in dioxane (25 ml) was added to a solution of selenium dioxide (13.82 g,

125 mmol) in dioxane (120 mL) and H_2O (7 mL). The reaction was refluxed for 3 h and filtered

after cooling. Solution was concentrated into an oil, redissolved in into diethyl ether (150 mL)

and washed with HCl (4 x 50) The ether phase was dried over $MgSO_4$, filtered and concentrated

to give **9** as a brown oil (20.89 g, 84% yield). ^{1}H NMR (CDCl$_3$, 400 MHz): δ 1.44 (d, 6 H, *J* = 7.00 Hz, CH), 4.49 (sept, 1 H, *J* = 7.06 Hz, CH), 7.62-7.75 (m, 3 H, CH), 8.01 (d, 1 H, *J* = 8.40 Hz, CH), 8.27 (d, 1 H, *J* = 8.40 Hz, CH), 10.25 (s, 1 H, CH).

2-Formylbenzoquinoline (10). A solution of **4** (4.0 g, 20 mmol) in dioxane (4.4 mL) was added to a solution of selenium dioxide (2.28 g, 20 mmol) in dioxane (21 mL) and H$_2$O (1.2 mL). The reaction mixture was refluxed for 26 hours, and after cooling, filtered to remove precipitated selenium. The solution was then concentrated to a red/orange solid. This was redissolved in a 4:1 mixture of hexanes/ethyl acetate (30 mL) and subsequently filtered through a silica gel plug to remove selenium byproduct. Concentration of the solution yielded **10** (1.5 g, 38% yield) as a white solid. ^{1}H NMR (CDCl$_3$, 800 MHz): δ 7.75 (d, 1 H, *J* = 8.56 Hz, CH), 7.78 (t, 1 H, *J* = 7.05 Hz, CH), 7.82 (t, 1 H, *J* = 7.55 Hz, CH), 7.95 (d, 1 H, *J* = 8.56 Hz, CH), 7.96 (d, 1 H, *J* = 8.06 Hz, CH), 8.16 (d, 1 H, *J* = 8.06 Hz, CH), 8.31 (d, 1 H, *J* = 8.06 Hz, CH), 9.43 (d, 1 H, *J* = 8.56 Hz, CH), 10.36 (s, 1 H, CH).

(1*R*,2*R*)-*N*,*N*'Bis[(2-quinolyl)methylene]-1,2-cyclohexanediamine (Ligand 11). Ligand **1** (1.2 g, 1.8 mmol) and sodium borohydride (0.86 g, 2.0 mmol) were dissolved in methanol in a swivel frit apparatus and allowed to mix at room temperature for 12 h to afford Ligand **11** (0.75 g, 73 % yield). ^{1}H NMR (CDCl$_3$, 400 MHz): δ 1.24 (br, 2 H, CH), 1.56 (br, 2 H, CH), 1.97 (br, 2 H, CH), 3.62 (br, 2 H, CH), 4.22 (dd, 2 H, *J* = 8.06 Hz, CH), 7.55 (t, 1 H, *J* = 8.06 Hz, CH), 7.61-

7.73 (m, CH), 7.81 (d, 1 H, J = 8.56 Hz, CH), 8.06 (d, 1 H J = 8.06 Hz, CH), 8.08 (d, 1 H J = 8.06 Hz, CH).

(1*R*,2*R*)-*N*,*N*'Bis[(2-benzoquinolyl)methylene]-1,2-cyclohexanediamine (Ligand 12). Ligand **2** (0.5 g, 0.7 mmol) and sodium borohydride (1.5 g, 0.8 mmol) were dissolved in methanol in a swivel frit apparatus and allowed to mix at room temperature for 6 h to afford the brown colored Ligand **11** (0.53 g, 68 % yield). ^{1}H NMR (CDCl$_3$, 400 MHz): δ 1.24 (br, 2 H, CH), 1.56 (br, 2 H, CH), 1.97 (br, 2 H, CH), 3.62 (br, 2 H, CH), 4.22 (dd, 2 H, J = 8.06 Hz, CH), 7.42-7.68 (m, 3 H, CH), 7.75 (d, 1 H, J = 8.56 Hz, CH), 7.86 (d, 1 H J = 8.06 Hz, CH), 8.04 (d, 1 H J = 8.06 Hz, CH), 9.37 (d, 1 H, J = 8.56 Hz, CH).

Zn(II)triflate-(ligand 5) complex (13). Zinc triflouromethanesulfonate (0.046 g, 0.15 mmol) and ligand **1** (0.1 g, 0.15 mmol) were added to a mixture tetrahydrofuran (10 mL) and ethanol (15 mL) and allowed to mix for 15 h. The resulting red precipitate was obtained complex **13** (0.1 g, 65% yield). ^{1}H NMR (CDCl$_3$, 400 MHz): δ 5.10-5.18 (m, 1 H, CH), 5.66-5.75 (m, 1 H, CH), 6.08-6.19 (m, 1 H, CH), 6.30-6.36 (m, 1 H, CH), 6.40 (d, 1 H, J = 9.16 Hz, CH), 6.87 (t, 1 H, J = 7.60 Hz, CH), 7.03 (d, 1 H, J = 8.24 Hz, CH), 7.05 (d, 1 H, J = 7.14 Hz, CH), 7.12-7.46 (m, 8 H, CH), 7.47-7.59 (m, 3 H, CH), 7.61-7.74 (m, 3 H, CH), 7.92 (d, 1 H, J = 8.61 Hz, CH), 7.99 (d, 1 H, J = 8.24 Hz, CH), 8.08 (d, 1 H, J = 8.42 Hz, CH), 8.21 (d, 1 H, J = 8.42 Hz, CH), 8.24 (d, 1 H, J = 8.06 Hz, CH), 8.32 (d, 1 H, J = 8.24 Hz, CH), 8.39 (d, 1 H, J = 8.06 Hz, CH), 8.46 (d, 1 H, J = 8.79 Hz, CH), 9.74 (s, 1 H, CH

ZnCl$_2$-(ligand 11) complex 14. Zinc chloride (0.04 g, 0.30 mmol) and ligand **11** (0.1 g, 0.15 mmol) were suspended in methylene chloride (15 mL) and ethanol and stirred at room temperature for 6 hours. After concentrating the solution down to 2 mL, the resulting orange precipitate was filtered and washed with toluene (5 mL) to afford complex **14** (0.1 g, 70% yield). ^{1}H NMR (CDCl$_3$, 400 MHz): 1.75 (br, 2 H, J = 8.06 Hz, CH), 1.87 (br, 2 H, J = 6.55 Hz, CH), 2.23 (br, 2 H, J = 6.55 Hz, CH), 2.48 (br,4 H, J = 9.06 Hz, CH), 4.25 (dd, 2 H, J = 8.06 Hz, CH), 7.48-7.93 (m, 4 H, CH), 8.02-8.23 (m, 2 H, CH), 8.50 (s, 2 H, CH).

Zn(OTf)$_2$-(ligand 11) complex 15. Zinc triflate (0.03 g, 0.25 mmol) and ligand **11** (0.13 g, 0.18 mmol) were suspended in methylene chloride (15 mL) and ethanol and stirred at room temperature for 6 hours. After concentrating the solution down to 2 mL, the resulting orange precipitate was filtered and washed with toluene (5 mL) to afford complex **15** (0.12 g, 74% yield). ^{1}H NMR (CDCl$_3$, 400 MHz): 1.75 (br, 2 H, J = 8.06 Hz, CH), 1.87 (br, 2 H, J = 6.55 Hz, CH), 2.23 (br, 2 H, J = 6.55 Hz, CH), 2.48 (br,4 H, J = 9.06 Hz, CH), 4.35 (dd, 2 H, J = 8.06 Hz, CH), 7.25-7.43 (br, 1 H, CH), 7.42-7.60 (br, 2 H, CH), 7.80-7.98 (br, 2 H, CH), 8.42-8.45 (d, 1 H, J = 6.55 Hz, CH), 8.50 (d, 1 H, J = 6.55 Hz, CH).

Ni(II)triflate-(ligand 11) complex 16. Nickel triflate (0.072 g, 0.2 mmol) and ligand **11** (0.1 g, 0.2 mmol) were suspended in a mixture of methylene chloride (15 mL) and ethanol (10 mL) and stirred for 6 hours under gentle heat. After cooling to room temperature, all solvent was removed using the vacuum line and a resulting brown precipitate was obtained complex**16** (0.11 g, 66%

yield). ^{1}H NMR (CDCl$_3$, 400 MHz): δ -5.05 (br, CH), 0-2.5 (br, CH), 3.28 (br, CH), 5.13 (br, CH), 7.74 (br, CH), 13.00 (br, CH), 15.15 (br, CH), 20.05 (br, CH), 22.20 (br, CH), 24.28 (br, CH), 25.03 (br, CH), 26.74 (br, CH), 28.20 (br, CH), 38.75 (br, CH).

NiI$_2$-(ligand 11) complex 17. Nickel iodide (0.055 g, 0.3 mmol) and ligand **11** (0.13 g, 0.3 mmol) were suspended in a mixture of methylene chloride (15 mL) and ethanol (10 mL) and stirred for 6 hours under gentle heat. After cooling to room temperature, all solvent was removed using the vacuum line and a resulting brown precipitate was obtained complex **17** (0.09 g, 76% yield). ^{1}H NMR (CDCl$_3$, 400 MHz): δ -5.05 (br, CH), 0-2.5 (br, CH), 3.28 (br, CH), 5.13 (br, CH), 7.74-8.90 (br, CH), 10.80 (br, CH), 13.25 (br, CH), 14.05 (br, CH), 24.20 (br, CH), 27.34 (br, CH), 37.01 (br, CH).

Fe(II)Cl$_2$-(ligand 11) complex 18. Iron (II) chloride (0.043 g , 0.34 mmol), ligand **11** (0.2 g, 0.34 mmol) were suspended in a mixture of methylene chloride (15 mL) and ethanol (10 mL) and stirred for 6 hours under gentle heat. After cooling to room temperature, all solvent was removed using the vacuum line and a resulting brown precipitate was obtained complex **18** (0.09 g, 37%). ^{1}H NMR (CDCl$_3$, 400 MHz): δ -32.05 (br, CH), -25.05 (br, CH), -19.28 (br, CH), -9.83 (br, CH), 0-10.00 (br, CH), 11.28 (br, CH), 14.25 (br, CH), 24.05 (br, CH), 75.20 (br, CH),

Ru(II)Cl$_2$(COD)-(ligand 11) complex 19. RuCl$_2$(COD) (0.052 g , 0.24 mmol), ligand **11** (0.32 g, 0.40 mmol) and sodium methoxide (0.036 g , 0.067 mmol) were suspended in a mixture of tetrahydrofuran (15 mL) and methanol (10 mL) and stirred for 6 hours.   All solvent was subsequently removed using the vacuum line and a resulting deep blue precipitate was obtained complex **19** (0.09 g, 37%).   ^{1}H NMR (CDCl$_3$, 400 MHz): δ 1.24 (br, 2 H, CH), 1.56 (br, 2 H, CH), 1.97 (br, 2 H, CH), 3.62 (br, 2 H, CH), 4.22 (dd, 2 H, J = 8.06 Hz, CH), 7.55 (t, 1 H, J = 8.06 Hz, CH), 7.61-7.73 (m, CH), 7.81 (d, 1 H, J = 8.56 Hz, CH), 8.06 (d, 1 H J = 8.06 Hz, CH), 8.08 (d, 1 H J = 8.06 Hz, CH).

Ni(II)triflate-(Ligand 2) complex 20. Nickel triflate (0.072 g, 0.2 mmol) and ligand **2** (0.1 g, 0.2 mmol) were suspended in a mixture of tetrahydrofuran (15 mL) and methanol (10 mL) and stirred for 24 hours. The solvent was removed by pumping down on the solution to give the resulting brown precipitate complex **20**. Analysis by ^{1}H NMR resulted in rather complicated spectra, multiple broad peaks were observed indicating the presence of more than one species in solution.

Ni(II)triflate-(Ligand 2) complex 21. Nickel triflate (0.144 g, 0.4 mmol) and ligand **2** (0.1 g, 0.2 mmol) were suspended in a mixture of tetrahydrofuran (25 mL) and methanol (10 mL) and stirred for 24 hours. The solvent was removed by pumping down on the solution to give the resulting brown precipitate complex **21** (0.73 g, 43%). Analysis by ^{1}H NMR resulted in rather

complicated spectra, multiple broad peaks; however, we were still able to obtain a little bit of information from the spectrum. ^{1}H NMR (CDCl$_3$, 400 MHz): δ 8.65 (br, CH), 10.92 (br, CH), -20.02 (br, CH), 32.00 (br, CH), 33.80 (br, CH).

Ni(II)I$_2$-(ligand 2) complex 22. Nickel iodide (0.063 g, 0.2 mmol) and ligand **2** (0.1 g, 0.2 mmol) were suspended in a mixture of toluene (15 mL) and methanol (10 mL) then stirred at for 24 hours. The resulting brown precipitate was filtered and washed with 5 mL of the toluene/ethanol mixture to afford complex **22** (0.09 g, 55% yield). Analysis by ^{1}H NMR resulted in rather complicated spectra, multiple broad peaks were observed indicating the presence of more than one species in solution.

Au(III)chloride-(ligand 5) complex 24. Gold chloride (0.05 g, 0.15 mmol) and ligand **5** (0.1 g, 0.15 mmol) were suspended in tetrahydrofuran (10 mL) and methanol (15 mL) then stirred for 12 hours. The resulting yellow precipitate was filtered and vacuum dried to afford complex **24** (0.1 g, 65% yield). It appears that the ligand decomposed during the reaction producing a ^{1}H NMR spectrum with peaks that cannot be defined.

Hg(II)bromide-(ligand 5) complex 25. Mercury bromide (0.055 g, 0.12 mmol) and ligand **5** (0.1 g, 0.15 mmol) were suspended in tetrahydrofuran (10 mL) and methanol (15 mL) then stirred for 12 hours. The resulting red colored precipitate was filtered and vacuum dried to

afford complex **25** (0.1 g, 65% yield). ^{1}H NMR (CDCl$_3$, 400 MHz): δ 7.31 (t, 2 H, J = 8.00 Hz, CH), 7.30 (d, 2 H, J = 8.06 Hz, CH), 7.42 (t, 2 H, J = 7.05 Hz, CH), 7.46 (d 2 H, J = 7.00 Hz, CH), 7.55 (t, 2 H, J = 7.00 Hz, CH), 7.58 (d, 2 H, J = 8.56 Hz, CH), 7.63 (d, 2 H, J = 9.06 Hz, CH), 7.72 (d, 2 H, J = 8.56 Hz, CH), 7.77 (d, 2 H, J = 7.55 Hz, CH), 7.92 (d, 2 H, J = 8.06 Hz, CH), 8.01 (d, 2 H, J = 8.06 Hz, CH), 8.07 (d, 2 H, J = 8.06 Hz, CH), 8.70 (s, 1 H, CH), 9.05 (d, 2 H, J = 8.06 Hz, CH).

Pd(II)acetate-(ligand 5) complex 26. Palladium acetate (0.475 g, 0.13 mmol) and ligand **5** (0.1 g, 0.15 mmol) were suspended in tetrahydrofuran (10 mL) and methanol (15 mL) then stirred for 12 hours. The resulting bluish-green colored precipitate was filtered and vacuum dried to afford complex **26** (0.09 g, 61% yield). ^{1}H NMR (CDCl$_3$, 400 MHz): δ 7.28 (t, 2 H, J = 8.00 Hz, CH), 7.37 (d, 2 H, J = 8.06 Hz, CH), 7.42 (t, 2 H, J = 7.05 Hz, CH), 7.46 (d 2 H, J = 7.00 Hz, CH), 7.55 (t, 2 H, J = 7.00 Hz, CH), 7.58 (d, 2 H, J = 8.56 Hz, CH), 7.63 (d, 2 H, J = 9.06 Hz, CH), 7.72 (d, 2 H, J = 8.56 Hz, CH), 7.77 (d, 2 H, J = 7.55 Hz, CH), 7.92 (d, 2 H, J = 8.06 Hz, CH), 8.01 (d, 2 H, J = 8.06 Hz, CH), 8.07 (d, 2 H, J = 8.06 Hz, CH), 8.62 (s, 1 H, CH), 8.78 (d, 2 H, J = 8.06 Hz, CH).

Co(II)chloride-(ligand 5) complex 27. Cobalt chloride (0.44 g, 0.21 mmol) and ligand **5** (0.1 g, 0.15 mmol) were suspended in tetrahydrofuran (10 mL) and methanol (15 mL) then stirred for 12 hours. The resulting yellowish colored precipitate was filtered and vacuum dried to afford complex **27** (0.12 g, 68% yield). ^{1}H NMR (CDCl$_3$, 400 MHz): δ 7.28 (t, 2 H, J = 8.00 Hz, CH),

7.37 (d, 2 H, J = 8.06 Hz, CH), 7.42 (t, 2 H, J = 7.05 Hz, CH), 7.46 (d 2 H, J = 7.00 Hz, CH),

7.55 (t, 2 H, J = 7.00 Hz, CH), 7.58 (d, 2 H, J = 8.56 Hz, CH), 7.63 (d, 2 H, J = 9.06 Hz, CH),

7.72 (d, 2 H, J = 8.56 Hz, CH), 7.77 (d, 2 H, J = 7.55 Hz, CH), 7.95 (d, 2 H, J = 8.06 Hz, CH),

8.01 (d, 2 H, J = 8.06 Hz, CH), 8.62 (s, 1 H, CH), 8.77 (d, 2 H, J = 8.06 Hz, CH).

Cu(II)triflate-(ligand 5) complex 28. Copper triflate (0.47 g, 0.15 mmol) and ligand **5** (0.1 g, 0.15 mmol) were suspended in tetrahydrofuran (10 mL) and methanol (15 mL) then stirred for 12 hours. The resulting black colored precipitate was filtered and vacuum dried to afford complex **28.** It appears that the ligand decomposed during the complexation reaction producing a ^{1}H NMR spectrum with peaks that cannot be defined.

Mn(II)chloride-(ligand 5) complex 29. Manganese chloride (0.50g, 0.18 mmol) and ligand **5** (0.1 g, 0.15 mmol) were suspended in tetrahydrofuran (10 mL) and methanol (15 mL) then stirred for 12 hours. The resulting yellowish colored precipitate was filtered and vacuum dried to afford complex **29** (0.19 g, 82% yield). ^{1}H NMR (CDCl$_3$, 400 MHz): δ 7.28 (t, 2 H, J = 8.00 Hz, CH), 7.38 (d, 2 H, J = 8.06 Hz, CH), 7.41 (t, 2 H, J = 7.05 Hz, CH), 7.53 (d 2 H, J = 7.00 Hz, CH), 7.65 (t, 2 H, J = 7.00 Hz, CH), 7.70 (d, 2 H, J = 8.56 Hz, CH), 7.75 (d, 2 H, J = 9.06 Hz, CH), 7.92-8.0 (br, 2 H, CH), 7.77 (d, 2 H, J = 8.05 Hz, CH), 8.62 (s, 1 H, CH), 8.78 (d, 2 H, J = 8.06 Hz, CH).

Cd(II)chloride-(ligand 5) complex 30. Cadmium chloride (0.55 g, 0.19 mmol) and ligand **5** (0.1 g, 0.15 mmol) were suspended in tetrahydrofuran (10 mL) and methanol (15 mL) then stirred for 12 hours. The resulting bright yellow colored precipitate was filtered and vacuum dried to afford complex **30** (0.16 g, 74% yield). ^{1}H NMR (CDCl$_3$, 400 MHz): δ 7.30 (t, 2 H, J = 8.00 Hz, CH), 7.37 (d, 2 H, J = 8.06 Hz, CH), 7.42 (t, 2 H, J = 7.05 Hz, CH), 7.46 (d 2 H, J = 7.00 Hz, CH), 7.55 (t, 2 H, J = 7.00 Hz, CH), 7.63 (d, 2 H, J = 9.06 Hz, CH), 7.72 (d, 2 H, J = 8.56 Hz, CH), 7.77 (d, 2 H, J = 7.55 Hz, CH), 7.95 (d, 2 H, J = 8.06 Hz, CH), 7.98 (d, 2 H, J = 8.06 Hz, CH), 8.61 (s, 1 H, CH), 8.76 (d, 2 H, J = 8.06 Hz, CH).

Au(II)chloride-(ligand 5) complex 31. Gold dimethylchlorosulfide (0.50 g, 0.19 mmol) and ligand **5** (0.1 g, 0.15 mmol) were suspended in tetrahydrofuran (10 mL) and methanol (15 mL) then stirred for 12 hours. The resulting orangish-red colored precipitate was filtered and vacuum dried to afford complex **31** (0.09 g, 54% yield). ^{1}H NMR (CDCl$_3$, 400 MHz): δ 7.26 (br, CH), 7.48 (br, CH), 7.53 (br, CH), 7.60-7.80 (br, CH), 7.90-8.10 (br, CH), 8.68-8.75.

Ag(I)triflate-(ligand 3) complex 32. Silver triflate (0.51 g, 0.22 mmol) and ligand **3** (0.1 g, 0.15 mmol) were suspended in tetrahydrofuran (10 mL) and methanol (15 mL) then stirred for 12 hours. The resulting brown colored precipitate was filtered and vacuum dried to afford complex **32** (0.19g, 84% yield). ^{1}H NMR (CDCl$_3$, 400 MHz): δ 5.88 (d, 1 H, J = 8.40 Hz, CH), 6.37-6.45 (br, 4 H, CH), 6.78 (t, 1 H, J = 7.05 Hz, CH), 6.85 (t, 1 H, J = 7.60 Hz, CH), 7.25 (d, 1 H, J =

194

7.00 Hz, CH), 7.80 (d, 1 H, J = 9.06 Hz, CH), 7.94 (d, 1 H, J = 8.40 Hz, CH), 8.48 (d, 1 H, J =

7.55 Hz, CH), 8.59 (d, 1 H, J = 8.46 Hz, CH), 9.36 (d, 1 H, J = 8.46 Hz, CH)

Ag(I)triflate-(ligand 4) complex 33. Silver triflate (0.54 g, 0.18 mmol) and ligand **4** (0.1 g,

0.15 mmol) were suspended in tetrahydrofuran (10 mL) and methanol (15 mL) then stirred for 12

hours. The resulting brown colored precipitate was filtered and vacuum dried to afford complex

32 (0.15g, 81% yield). ¹H NMR (CDCl₃, 400 MHz): δ 7.15 (d, 1 H, J = 8.20 Hz, CH), 7.25 (t, 1

H, J = 7.05 Hz, CH), 7.31 (t, 1 H, J = 7.60 Hz, CH), 7.48 (d, 1 H, J = 7.00 Hz, CH), 7.55 (d, 1 H,

J = 9.06 Hz, CH), 7.57 (d, 1 H, J = 8.40 Hz, CH), 7.72 (d, 1 H, J = 7.55 Hz, CH), 7.85 (d, 1 H, J

= 8.46 Hz, CH), 8.06 (d, 1 H, J = 8.40 Hz, CH), 8.23 (d, 1 H, CH), 8.25 (d, 2 H, J = 8.40 Hz,

CH), 8.72 (s, 1 H, CH).

Ag(I)triflate-(ligand 5) complex 34. Silver triflate (0.51 g, 0.22 mmol) and ligand **5** (0.1 g,

0.15 mmol) were suspended in tetrahydrofuran (10 mL) and methanol (15 mL) then stirred for 12

hours. The resulting brown colored precipitate was filtered and vacuum dried to afford complex

34 (0.20g, 87% yield). ¹H NMR (CDCl₃, 400 MHz): δ 5.40 (t, 1 H, J = 8.40 Hz, CH), 6.02-6.11

(br, 2 H, CH), 6.18 (d, 1 H, J = 7.05 Hz, CH), 6.38 (t, 1 H, J = 7.60 Hz, CH), 6.52 (d, 1 H, J =

7.00 Hz, CH), 6.78 (d, 1 H, J = 9.06 Hz, CH), 7.24 (d, 1 H, J = 8.40 Hz, CH), 7.58 (d, 1 H, J =

7.55 Hz, CH), 7.62 (d, 1 H, J = 8.46 Hz, CH), 8.18 (d, 2 H, J = 8.46 Hz, CH), 8.22 (d, 1 H, J =

8.46 Hz CH), 8.59 (d, 2 H, J = 8.40 Hz, CH), 8.78 (d, 1 H, J = 8.46 Hz, CH), 9.58 (d, 2 H, J =

8.46 Hz, CH).

Ag(I)triflate-(ligand 1) complex 35. Silver triflate (0.50 g, 0.22 mmol) and ligand **1** (0.1 g, 0.15 mmol) were suspended in tetrahydrofuran (10 mL) and methanol (15 mL) then stirred for 12 hours. The resulting brown colored precipitate was filtered and vacuum dried to afford complex **35** (0.09g, 54% yield). ^{1}H NMR (CDCl$_3$, 400 MHz): δ 6.85 (d, 1 H, J = 8.40 Hz, CH), 6.95-7.00 (m, 1 H, CH), 7.13 (d, 1 H, J = 7.05 Hz, CH), 7.26 (d, 2 H, J = 7.60 Hz, CH), 7.45-7.6 (br, 1 H, CH), 8.40 (d, 1 H, J = 9.06 Hz, CH).

Ag(I)triflate-(ligand 2) complex 36. Silver triflate (0.57 g, 0.23 mmol) and ligand **2** (0.1 g, 0.15 mmol) were suspended in tetrahydrofuran (10 mL) and methanol (15 mL) then stirred for 12 hours. The resulting brown colored precipitate was filtered and vacuum dried to afford complex **36** (0.10g, 69% yield). ^{1}H NMR (CDCl$_3$, 400 MHz): δ 7.32 (br, 1 H, CH), 7.48 (m, 2 H, CH), 7.60 (br, 1 H, CH), 7.88 (d, 1 H, J = 7.60 Hz, CH), 8.28 (d, 1 H, J = 7.00 Hz, CH), 8.98 (br, 1 H, CH).

References

1. Kozlowski, Marisa C.; Walsh, Patrick J. *Fundamentals of Asymmetric Catalysis*. **2009**, 115 – 161.

2. Whitesell, J. K. *Chem. Res.* **1989**, 89, 1581 – 1615.

3. Trost, B. M. *Acc. Chem. Res.* **1996**, 29, 355 – 364.

4. Trost, B M. *Acc. Chem. Res.* **2006**, 39, 747 – 760.

5. Blochl, P. E.; Togni, A. *Organometallics*. **1996**, 15, 4125 – 4132.

6. Johnson, J. S.; Evans, D. A. *Acc. Chem. Res.* **2000**, 33, 325 – 335.

7. Pfaltz, A. P. *Acc. Chem. Res.* **1993**, 26, 339 – 345.

8. Fritschi, H. C.; Leutenegger, U.; Pfaltz, A. *Helv.Chim.Acta*. **1998**, 71, 1553 – 1565.

9. Wiznycia, Alexander V.; Desper, John; Levy, Christopher J. *Can. J. Chem.* **2009**, 87, 224 – 231.

10. Prema, Dipesh; Wiznycia, Alexander V.; Scott, Benjamin M.; Levy, Christopher J. *Dalton Trans*. **2007**, 4788 – 4796.

11. Hathaway, B. J. *Comprehensive Coordination Chemistry*. **1987**, 5, 533 – 774.

12. Evans, D. A.; Rovis, T; Kozlowski, M. C.; Tedrow, J. S. *J. Am. Chem. Soc*. **1999**, 121, 1994 – 1995.

13. Mosca, Lorenzo; Luigi, Fabbrizzi; Amendola, Valeria; Biocchi, Massimo. *Inorganic Chemistry*. **2010**, 49, 997 – 1007.

14. Canard, G; Piguet, C. *Inorganic Chem*. **2007**, 46, 3511 – 3522.

15. Hannon, Michael J.; Alcock, Nathaniel W.; Childs, Laura J. *Dalton Trans*. **2002**, 164 – 169.

16. Fabbrizzi, L. *J. Chem. Edu*. **2008**, 85, 1501 – 1511.

17. Piguet, C.; Bernardinelli, G.; Hopfgartner, G. *Chem. Rev*. **1997**, 97, 2005 – 2062.

18. Amendola, V.; Fabbrizzi, L.; Linati, L.; Mangaano, C. *Eur. J. Chem*. **1999**, 5, 3679 – 3688.

19. Guofu, Zi; Xang, Li; Yadong, Zhang; Qiuwen, Wang. *J. Orgmettalic Chem*. **2007**, 692, 3949 – 3956.

20. Vitagliano, Aldo; Cucciolito, Maria E. *Organometallics*. **2004**, 23, 15 – 17.

21. Masood, M. A.; Enemark, E. K. *Angew. Chem. Int. Ed*. **1998**, 37, 928 – 932.

22. Zhang, X.; Wang, B.; Longmire, J. M. *J. Am. Chem. Soc*. **2003**, 125, 4018 – 4026.

23. Montalti, Marco; Mangano, Carlo Y.; Fernandez, Yuri, D.; Zacchroni, Nelsi. *DaltonTrans*. **2003**, 4340 – 4345.

24. Masoosd, E. J.; Enemark, E J.; Stack, P. *Angew Chem. Int. Ed*. **1998**, 372, 928 – 935.

25. Lippert, Bernhard; Trotscher-Kaus, Gabrielle; Shen, Wei-Zheng. *Dalton Trans*. **2009**, 8023 – 8214.

26. Matthews, R. S.; Jones, D. W.; Bartle, K. D. *Tetrahedron*. **1969**, 25, 2701 – 2714.

27. Strongin, Robert M.; Bhacca, Norman S.; Juneau, Gary P.; Biswapati, Mukherjee. *Organic Letters*. **2000**, 2, 3813 – 3815.

28. Haslinger, Ernst; Schroder, Harald. *Magnetic Resonance in Chemistry*. **1994**, 32, 12 – 15.

29. Harvey, Ronald G.; Bongsup, Cho P. *J. Org. Chem*. **1987**, 52, 5679 – 5684.

30. Liu, Xiaolong.; Penner, Glenn H. *PNMRS*. **2006**, 49, 151 – 167.

31. Taura, Y.; Tanaka, M.; Funakoshi, Sakai K.. *Tetrahedron Lett*. **1989**, 30, 6349 – 6352.

32. Bosnich, B. *Encylopedia of Inorganic Chemistry*. **2005**, 2978 – 2984.

33. Seebach, D.; Planttner, D. A.; Beck, A. K.. *Helv. Chim. Acta*. **1992**, 75, 2171 – 2209.

34. Gothelf, K. V.; Hazzel, R. G.; Jorgensen, G.;. *J. Am. Chem. So*. **1995**, 117, 4435 – 4436.

35. Braun, M. *Angew. Chem. Int. ed. Eng*. **1996**, 35, 519 – 522.

36. Webber, B.; Seebach, D. *tetrahedron*. **1994**, 50, 7473 – 7484.

37. Narasaka, K.; Iwasawa, N. *J. Am. Chem. Soc*. **1989**, 111, 5340 – 5345.

38. Gothelf, K. V.; Jorgenson, K. A. *Chem. Soc.Perkins. Trans*. **1997**, 111 – 116.

39. Hasse, C.; Sarko, C R. *J. Org. Chem*. **1995**, 60, 1777 – 1787.

40. Garcia, J I.; Martinez-Merio, V.; Myoral, J. A.. *J. Org Chem.*. **1998**, 632 – 639.

41. Hathaway, B. J. *Comprehensive Coordination Chemistry*. **1987**, 5, 533 – 774.

42. Evans, D. A.; Rovis, T; Kozlowski, M. C.; Tedrow, J. S. *J. Am. Chem. Soc*. **1999**, 121, 1994 – 1995.

43. Mosca, Lorenzo; Luigi, Fabbrizzi; Amendola, Valeria; Biocchi, Massimo. *Inorganic Chemistry*. **2010**, 49, 997 – 1007.

44. Canard, G; Piguet, C. *Inorganic Chem*. **2007**, 46, 3511 – 3522.

45.   Hannon, Michael J.; Alcock, Nathaniel W.; Childs, Laura J. *Dalton Trans*. **2002**, 164 – 169.

43.   Pritchett, S.; Woodmansee, D. H. *J. Am. Chem. Soc.* **1998**, 34 – 47.

44.   Talahashi, H.; Yoshiba, X. *Tetrahedron.* **1995**, 51, 1203 – 1206.

45.   Corey, E. J.; Sarshar , S. *A. Chem Soc* **1994**, 116 12089 – 12090.

46.   Hathaway, B. J. *Comprehensive Coordination Chemistry*. **1987**, 5, 533 – 774.

47.   Evans, D. A.; Rovis, T; Kozlowski, M. C.; Tedrow, J. S. *J. Am. Chem. Soc*. **1999**, 121, 1994 – 1995.

48.   Mosca, Lorenzo; Luigi, Fabbrizzi; Amendola, Valeria; Biocchi, Massimo. *Inorganic Chemistry*. **2010**, 49, 997 – 1007.

49.   Canard, G; Piguet, C. *Inorganic Chem*. **2007**, 46, 3511 – 3522.

50.   Hannon, Michael J.; Alcock, Nathaniel W.; Childs, Laura J. *Dalton Trans*. **2002**, 164 – 169.

51.   Mosca, Lorenzo; Luigi, Fabbrizzi; Amendola, Valeria; Biocchi, Massimo. *Inorganic Chemistry*. **2010**, 49, 997 – 1007.

52.   Canard, G; Piguet, C. *Inorganic Chem*. **2007**, 46, 3511 – 3522.

53.   Hannon, Michael J.; Alcock, Nathaniel W.; Childs, Laura J. *Dalton Trans*. **2002**, 164 – 169.

54.   Fabbrizzi, L. *J. Chem. Edu*. **2002**, 70, 79 – 91.

55.   Piguet, C.; Bernardinelli, G.; Hopfgartner, G. *Chem. Rev*. **1997**, 97, 2005 – 2062.

56.   Amendola, V.; Fabbrizzi, L.; Linati, L.; Mangaano, C. *Eur. J. Chem.* **1999**, 5, 3679 – 3688.

57.   Guofu, Zi; Xang, Li; Yadong, Zhang; Qiuwen, Wang. *J. Orgmettalic Chem*. **2007**, 692, 3949 – 3956.

58.   Cuajungo, Math P.; Faget, Kyle Y.; Huang, Rudolph E.; Bush, Ashley I. *Annals New York Academy of Sciences*. **2007**, 292 – 304.

55.   Royo, E.; Belancort, J. M. *Organometallicss*. **2000**, 19, 4840 – 4851.

56.   Armistead, L T.; White, P. S. *Organometallics*. **1998**, 17, 216 – 220.

57.   Ichiyanagi T.; Shimizu , M. *J. Org. Chem*. **1997**, 62, 7937 – 7941.

58.   Denmark, S. E.; O'Connor, S. P. *Angew. Chem.. Int. Ed. Engl*. **1998**, 1149 –1151.

59. Evans, D. A.; Campos, K. R.; Tedrow, J. S. *J. Am.Chem. Soc.* **2000**, 7905 – 7920.

60. Barbaro, P.; Currao, A.; Hermann, J. *Organometallics.* **1996**,15, 3534 – 3543..

61. Dipesh, Prema P. *Different coordination modes of bis(imine-pyridine) ligands.* **2007.**

62. Zhang, X.; Wang, B.; Longmire, J. M. *J. Am. Chem. Soc.* **2003**, 125, 4018 – 4026.

63. Montalti, Marco; Mangano, Carlo Y.; Fernandez, Yuri, D.; Zacchroni, Nelsi. *DaltonTrans.* **2003**, 4340 – 4345.

64. Hasse, C.; Sarko, C R. *J. Org. Chem.* **1995**, 60, 1777 – 1787.

65. Garcia, J I.; Martinez-Merio, V.; Myoral, J. A.. *J. Org Chem..* **1998**, 632 – 639.

66. Hathaway, B. J. *Comprehensive Coordination Chemistry.* **1987**, 5, 533 – 774.

67. Evans, D. A.; Rovis, T; Kozlowski, M. C.; Tedrow, J. S. *J. Am. Chem. Soc.* **1999**, 121, 1994 – 1995.

68. Mosca, Lorenzo; Luigi, Fabbrizzi; Amendola, Valeria; Biocchi, Massimo. *Inorganic Chemistry.* **2010**, 49, 997 – 1007.

69. Canard, G; Piguet, C. *Inorganic Chem.* **2007**, 46, 3511 – 3522.

70. Brown, J. M.; Evans, P. *Tetrahedron.* **1998**, 44905 – 4916.

71. Faller, J. W.; Parr, J. *Organometallics.* **2001**, 20, 679 – 699.

72. Babin, J. E.; Whitekar, Kyle Y. *Chem. Absr.* **1994**, 122, 18660.

73. Zhang, W; Math P. *Synlett.* **2006**, 1185 – 1188.

74. Imai, Y.; Kida, W. *J. Org. Chem.* **2000**, 65, 3326 – 3333.

75. Hathaway, B. J. *Comprehensive Coordination Chemistry.* **1987**, 5, 533 – 774.

76. Evans, D. A.; Rovis, T; Kozlowski, M. C.; Tedrow, J. S. *J. Am. Chem. Soc.* **1999**, 121, 1994 – 1995.

77. Mosca, Lorenzo; Luigi, Fabbrizzi; Amendola, Valeria; Biocchi, Massimo. *Inorganic Chemistry.* **2010**, 49, 997 – 1007.

78. Canard, G; Piguet, C. *Inorganic Chem.* **2009**, 44, 2571 – 25284.

79. Hannon, Michael J.; Alcock, Nathaniel W.; Childs, Laura J. *Dalton Trans.* **2002**, 164 – 169.

80. Fabbrizzi, L. *J. Chem. Edu.* **2008**, 85, 1501 – 1511.

81. Piguet, C.; Bernardinelli, G.; Hopfgartner, G. *Chem. Rev.* **1997**, 97, 2005 – 2062.

82. Amendola, V.; Fabbrizzi, L.; Linati, L.; Mangaano, C. *Eur. J. Chem.* **1999**, 5, 3679 – 3688.

82. Schlicting, I.; Berendezen, J. *Science*. **2000**, 287,1615 – 1622.

83. Que, L.; Ho, R. Y.; I. *Chem Rev*. **1996**, 96, 2607 – 2624.

84. Lipscomd, J.; Que, L.; I. *J. Biol. Inorg. Chem*. **1998**, 3, 331 – 336.

85. Siegbahn, P.; Crabtree R. H. *J. Biol. Inorg. Chem*. **2001**, 276, 1945 – 1953.

86. Pritchett, S.; Woodmansee, D. H. *J. Am. Chem. Soc*. **1998**, 34 – 47.

87. Talahashi, H.; Yoshiba, X. *Tetrahedron*. **1995**, 51, 1203 – 1206.

88. Corey, E. J.; Sarshar , S. *A. Chem Soc* **1994**, 116 12089 – 12090.

89. Hathaway, B. J. *Comprehensive Coordination Chemistry*. **1987**, 5, 533 – 774.

90. Evans, D. A.; Rovis, T; Kozlowski, M. C.; Tedrow, J. S. *J. Am. Chem. Soc*. **1999**, 121, 1994 – 1995.

91. Mosca, Lorenzo; Luigi, Fabbrizzi; Amendola, Valeria; Biocchi, Massimo. *Inorganic Chemistry*. **2010**, 49, 997 – 1007.

92. Canard, G; Piguet, C. *Inorganic Chem*. **2007**, 46, 3511 – 3522.

93. Hannon, Michael J.; Alcock, Nathaniel W.; Childs, Laura J. *Dalton Trans*. **2002**, 164 – 169.

94. Mosca, Lorenzo; Luigi, Fabbrizzi; Amendola, Valeria; Biocchi, Massimo. *Inorganic Chemistry*. **2010**, 49, 997 – 1007.

95. Canard, G; Piguet, C. *Inorganic Chem*. **2007**, 46, 3511 – 3522.

96. Hannon, Michael J.; Alcock, Nathaniel W.; Childs, Laura J. *Dalton Trans*. **2002**, 164 – 169.

97. Lubben, M.; Meetsma, A. *Angew Chem. Int. Ed. Engl*. **2005**, 202 – 213.

98. Kojima, T.; Lesing, R A. *J. Am. Chem. Soc*. **1990**, 112, 1154 – 1162.

99. Pritchett, S.; Woodmansee, D. H. *J. Am. Chem. Soc*. **1998**, 34 – 47.

100. Talahashi, H.; Yoshiba, X. *Tetrahedron*. **1995**, 51, 1203 – 1206.

101. Corey, E. J.; Sarshar , S. *A. Chem Soc* **1994**, 116 12089 – 12090.

102 Hathaway, B. J. *Comprehensive Coordination Chemistry*. **1987**, 5, 533 – 774.

103. Evans, D. A.; Rovis, T; Kozlowski, M. C.; Tedrow, J. S. *J. Am. Chem. Soc*. **1999**, 121,

104. Que, L.; Ho, R. Y.; I. *Chem Rev*. **1996**, 96, 2607 – 2624.

105. Lipscomd, J.; Que, L.; I. *J. Biol. Inorg. Chem*. **1998**, 3, 331 – 336.

106. Siegbahn, P.; Crabtree R. H. *J. Biol. Inorg. Chem*. **2001**, 276, 1945 – 1953.

107. Pritchett, S.; Woodmansee, D. H. *J. Am. Chem. Soc.* **1998**, 34 – 47.

108. Talahashi, H.; Yoshiba, X. *Tetrahedron.* **1995**, 51, 1203 – 1206.

109. Corey, E. J.; Sarshar , S. *A. Chem Soc* **1994**, 116 12089 – 12090.

110. Harvey, Ronald G.; Bongsup, Cho P. *J. Org. Chem.* **1987**, 52, 5679 – 5684.

111. Taura, Y.; Tanaka, M.; Funakoshi, Sakai K.. *Tetrahedron Lett*. **1989**, 30, 6349 – 6352.

112. Bosnich, B. *Encylopedia of Inorganic Chemistry*. **2005**, 2978 – 2984.

113. Seebach, D.; Planttner, D. A.; Beck, A. K.. *Helv. Chim. Acta*. **1992**, 75, 2171 – 2209.

114. Gothelf, K. V.; Hazzel, R. G.; Jorgensen, G.;. *J. Am. Chem. So.* **1995**, 117, 4435 – 4436.

115. Braun, M. *Angew. Chem. Int. ed. Eng*. **1996**, 35, 519 – 522.

116. Webber, B.; Seebach, D. *tetrahedron*. **1994**, 50, 7473 – 7484.

117. Narasaka, K.; Iwasawa, N. *J. Am. Chem. Soc*. **1989**, 111, 5340 – 5345.

118. Hasse, C.; Sarko, C R. *J. Org. Chem*. **1995**, 60, 1777 – 1787.

Appendix A - NMR & Mass Spectrometry Data

(Numerical Order)
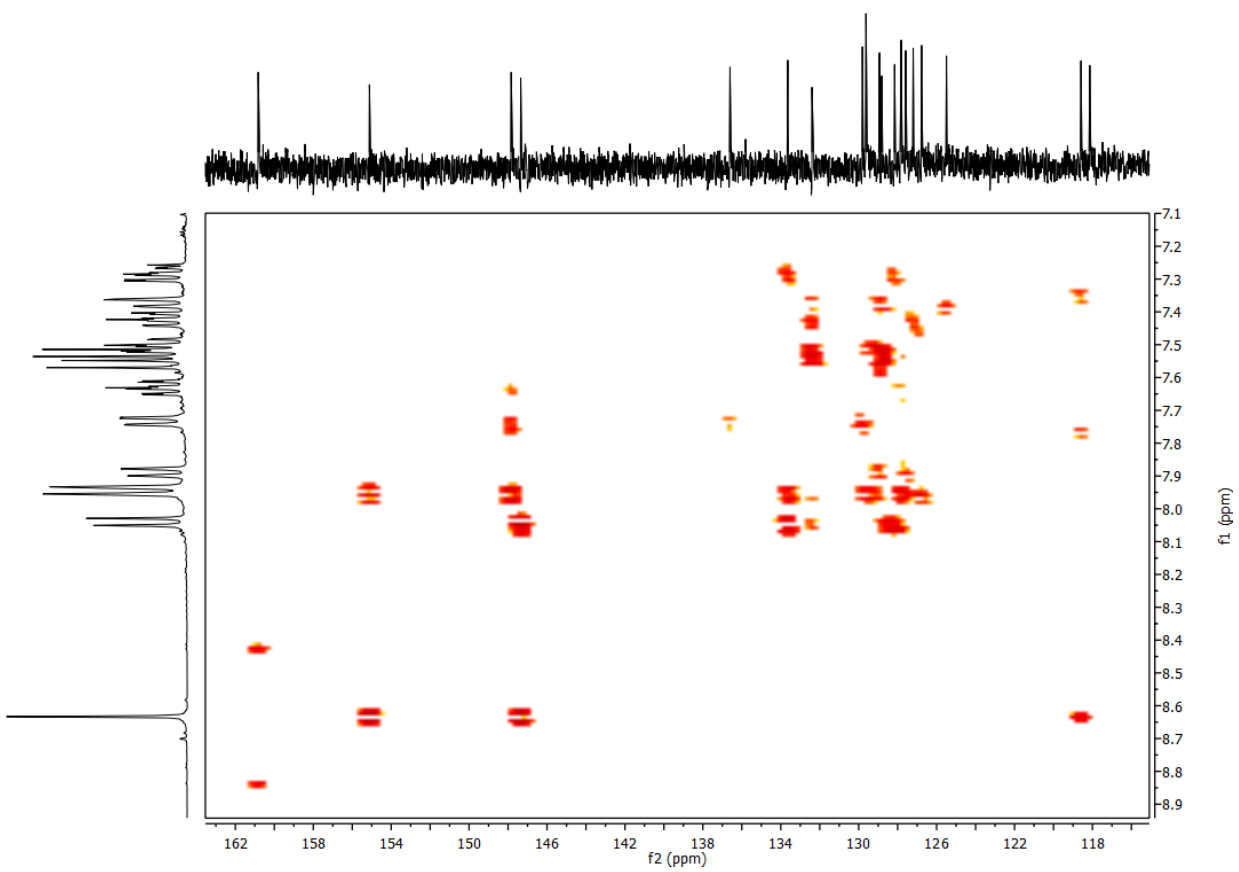
Figure A.1 400 MHz HMBC Spectrum for Ligand **3** (CDCl$_3$)
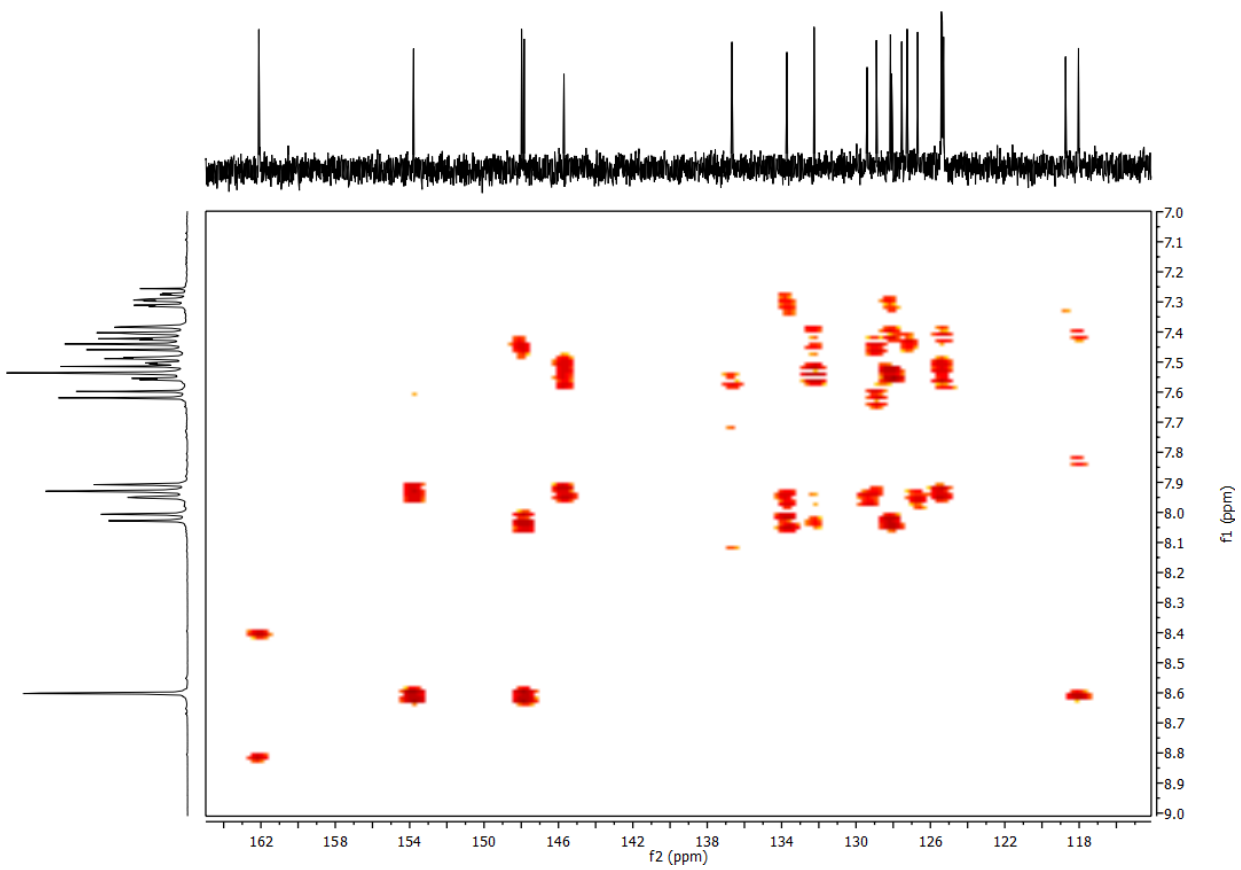
Figure A.2 400 MHz HMBC Aromatic Region Spectrum for Ligand **4** (CDCl$_3$)
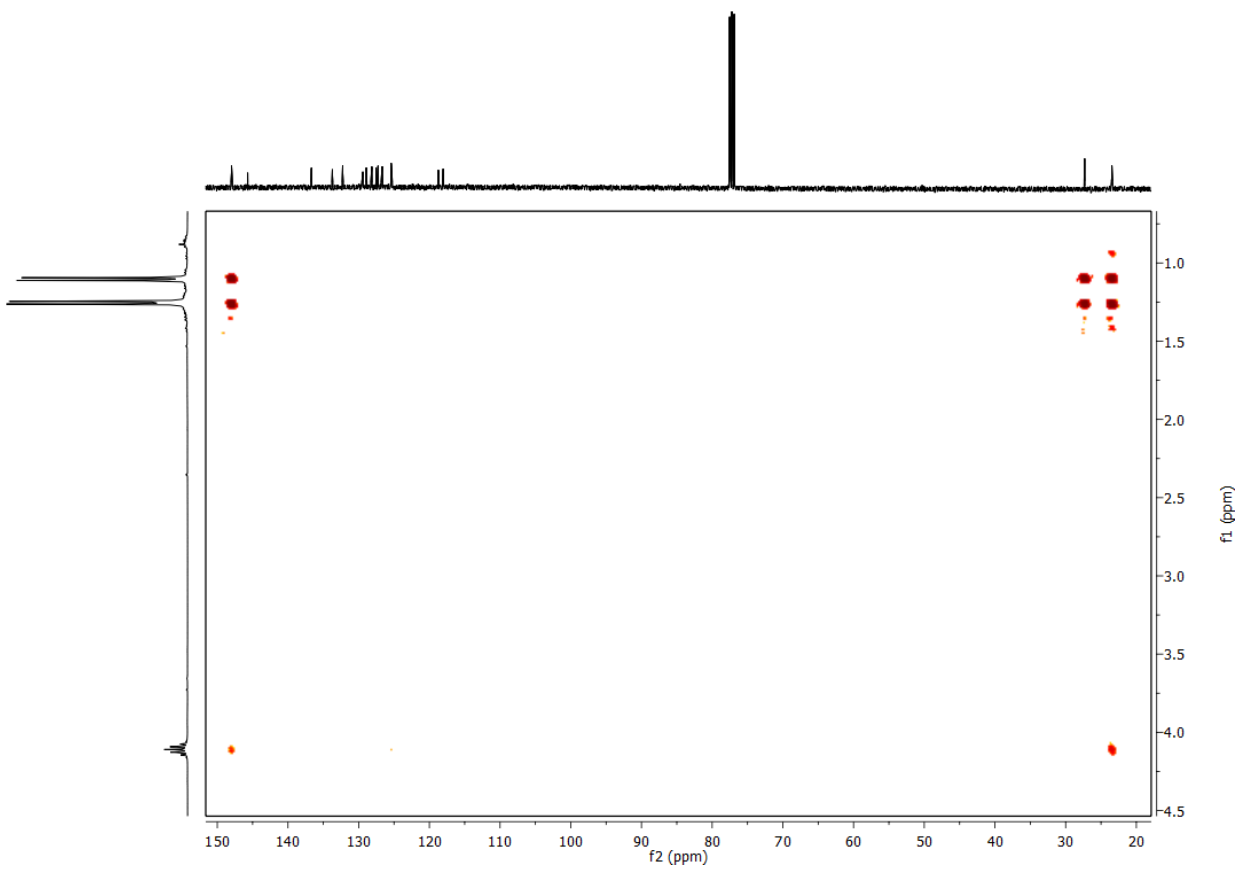
Figure A.3 400 MHz HMBC Aliphatic Region Spectrum for Ligand **4** (CDCl$_3$)
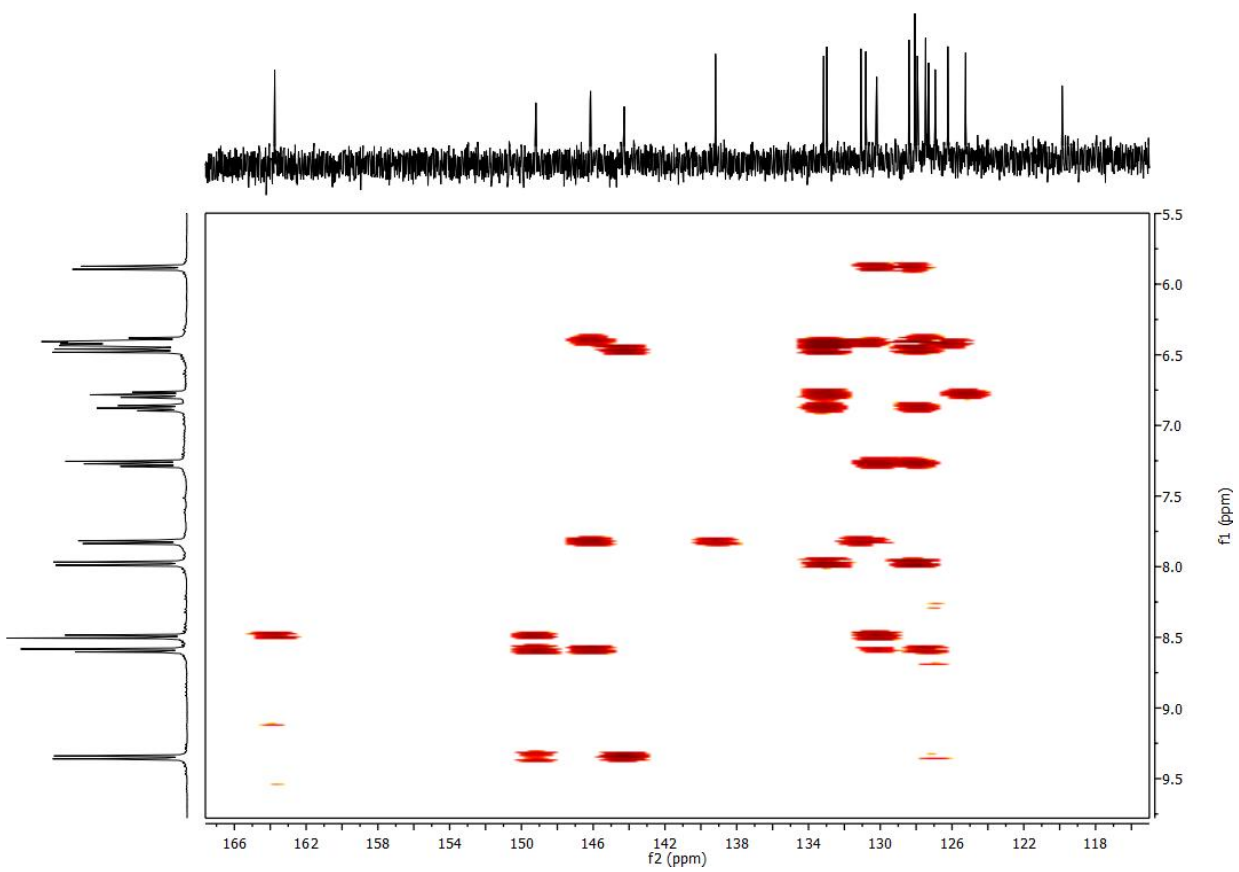
Figure A.4 400 MHz HMBC Spectrum for Complex **32** (CDCl$_3$)
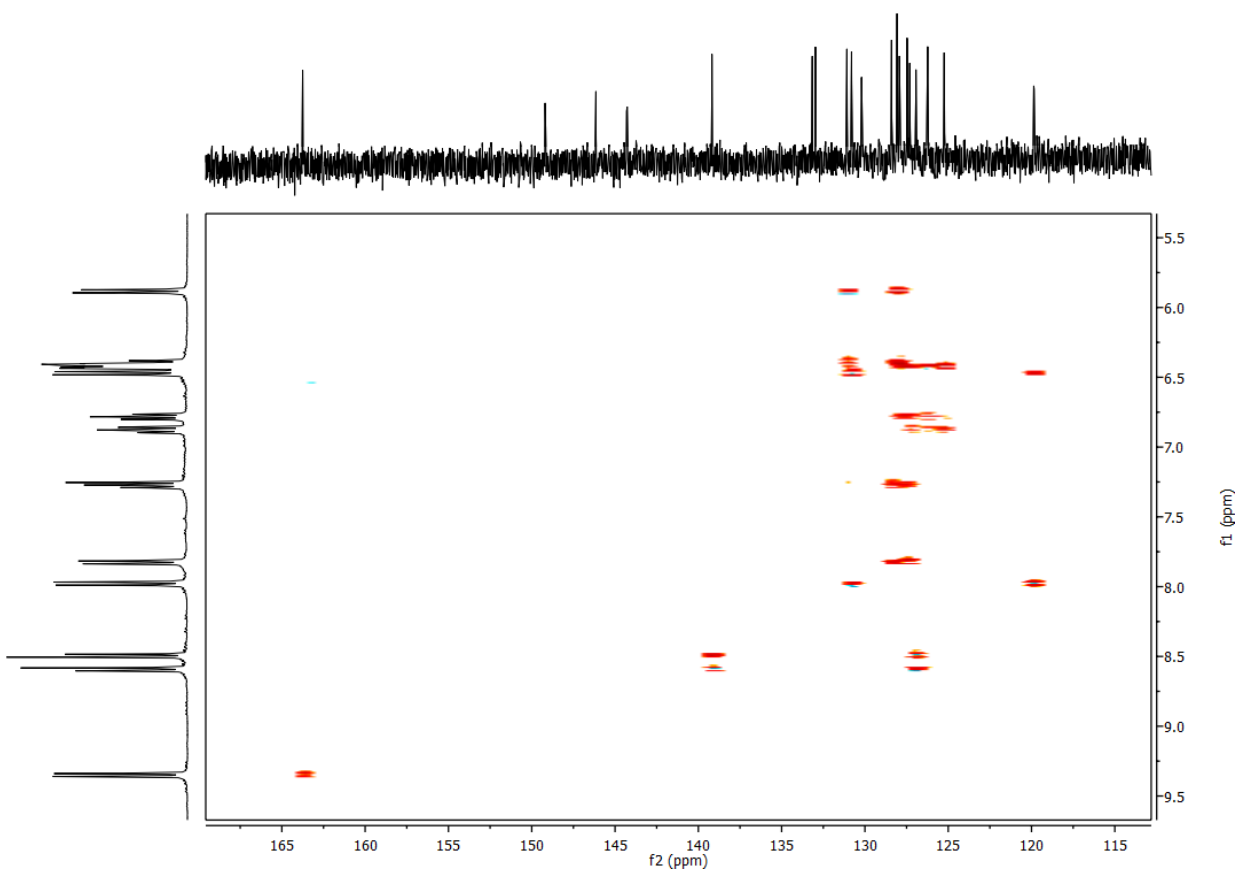
Figure A.5 400 MHz TOXY Spectrum for Complex **32** (CDCl$_3$)
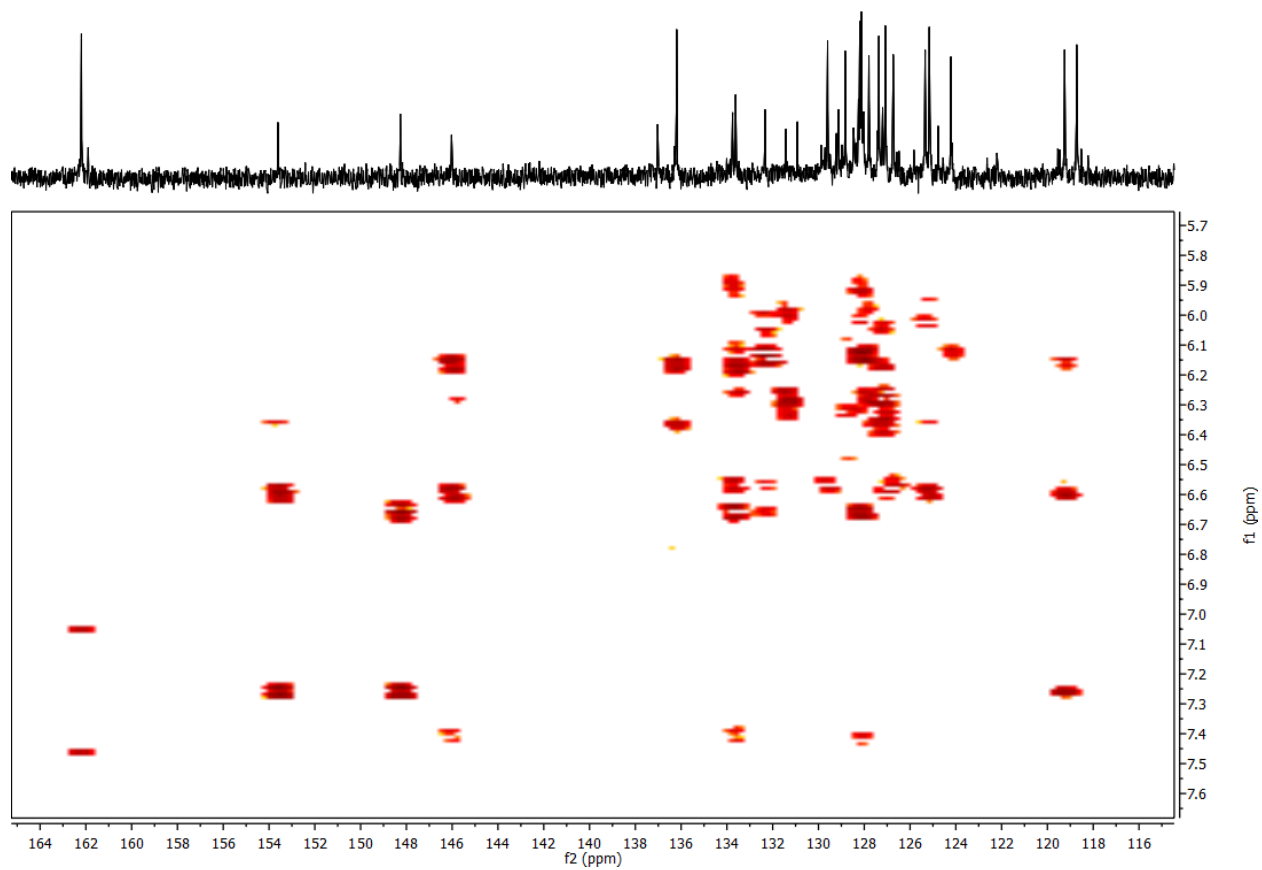
Figure A.6 400 MHz HMBC Spectrum for Complex **34** (CDCl₃)
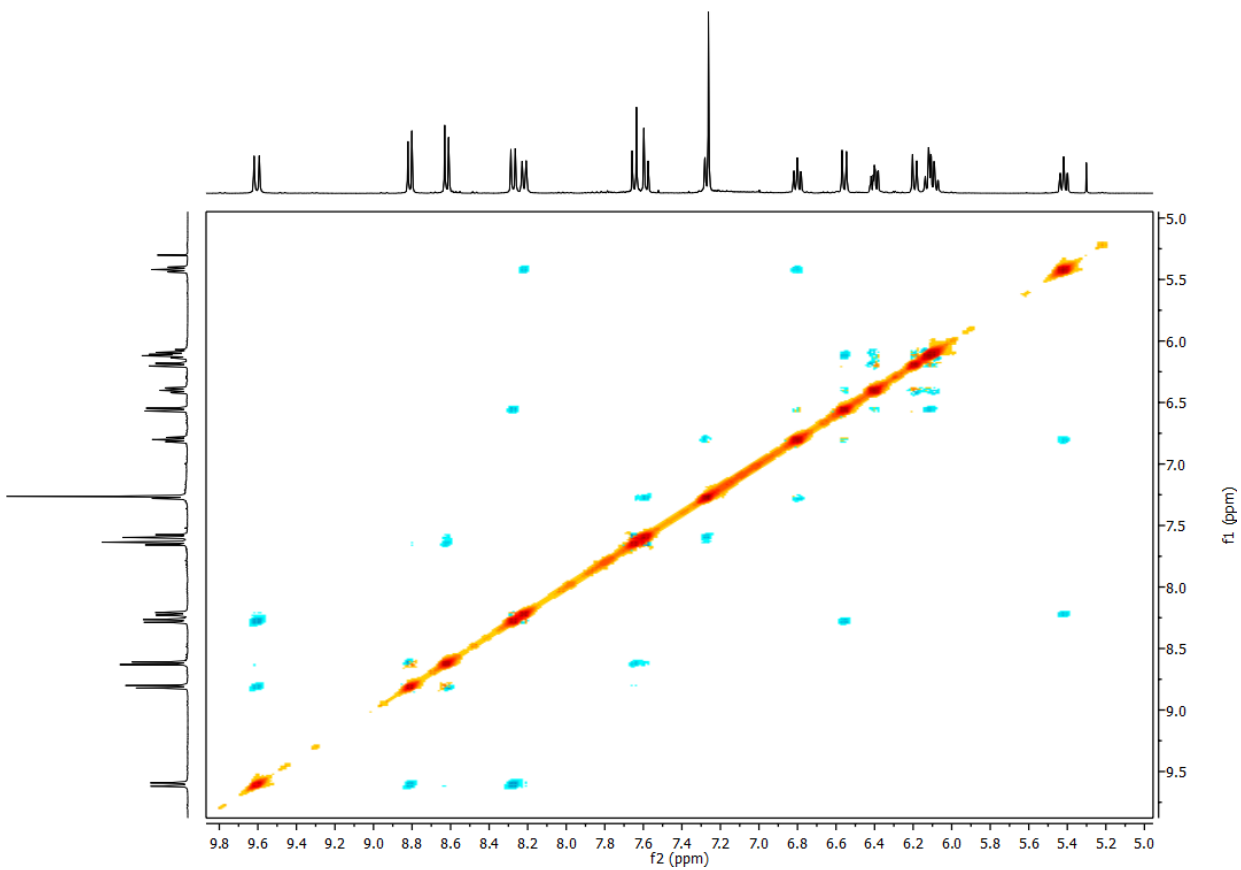
Figure A.7 400 MHz ROSEY Spectrum for Ligand **3** (CDCl$_3$)
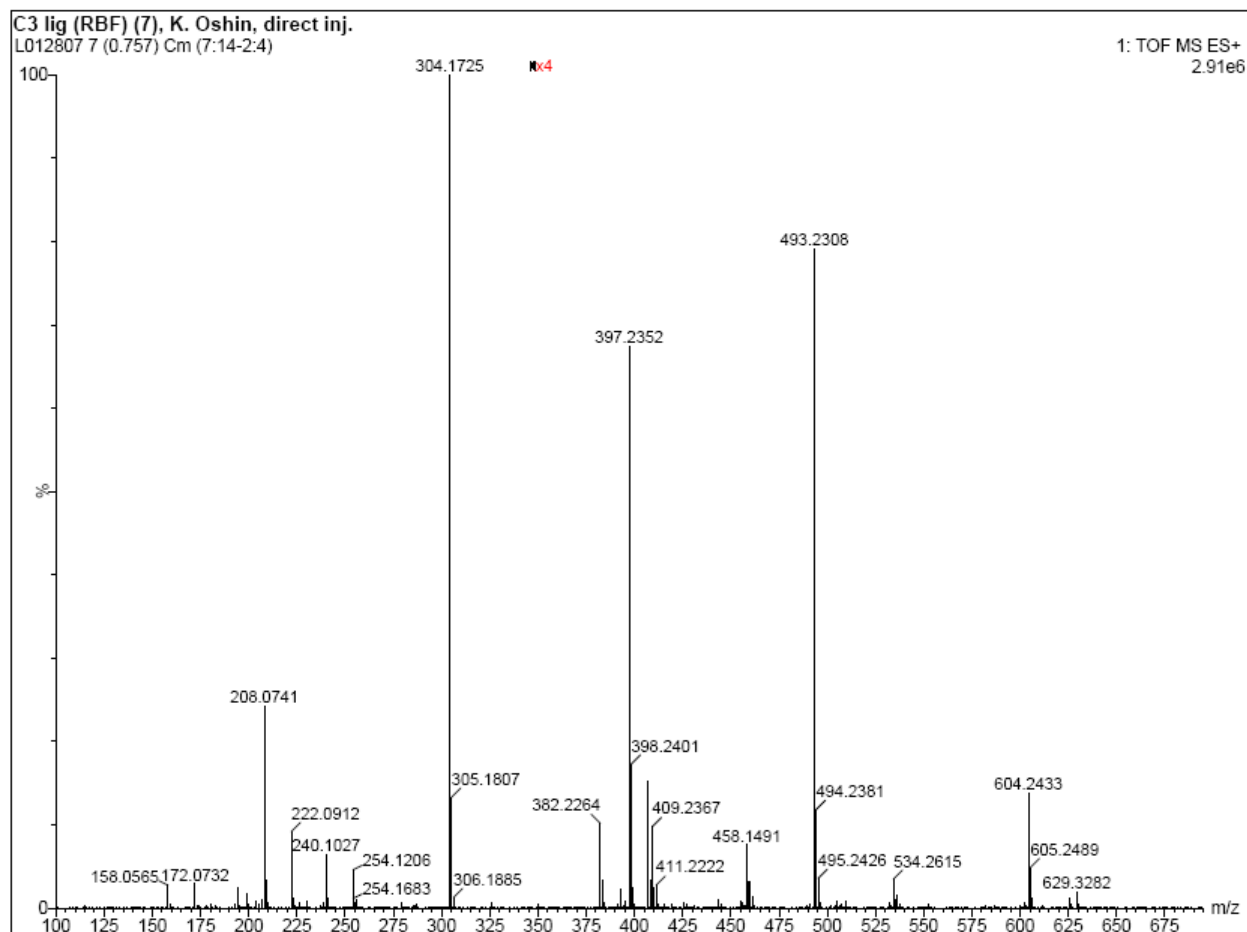
Figure A.8 Electro-Spray Mass Spectrum for Ligand **2** (CH_2Cl_2)
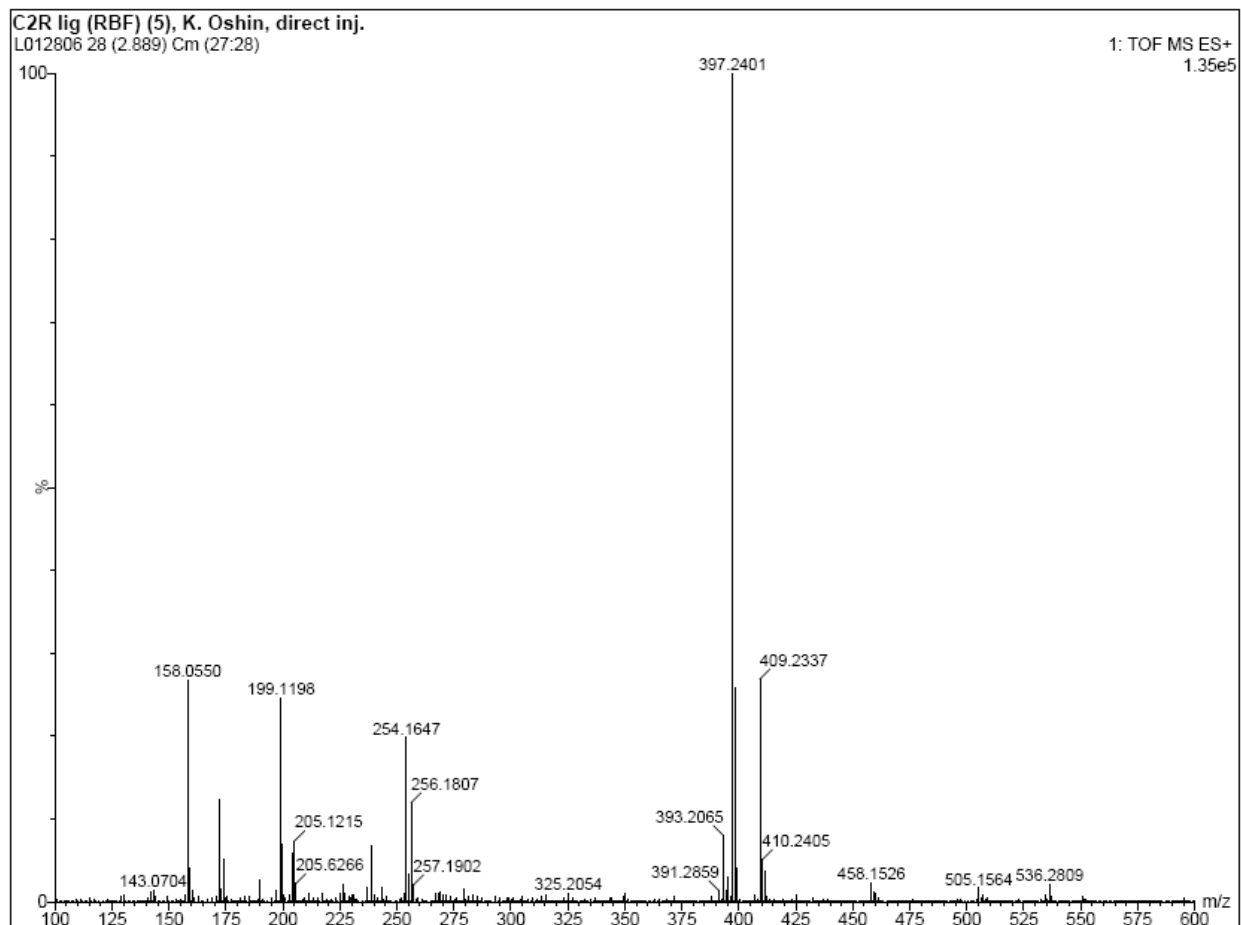
Figure A.9 Electro-Spray Mass Spectrum for Ligand **11** (CH$_2$Cl$_2$)
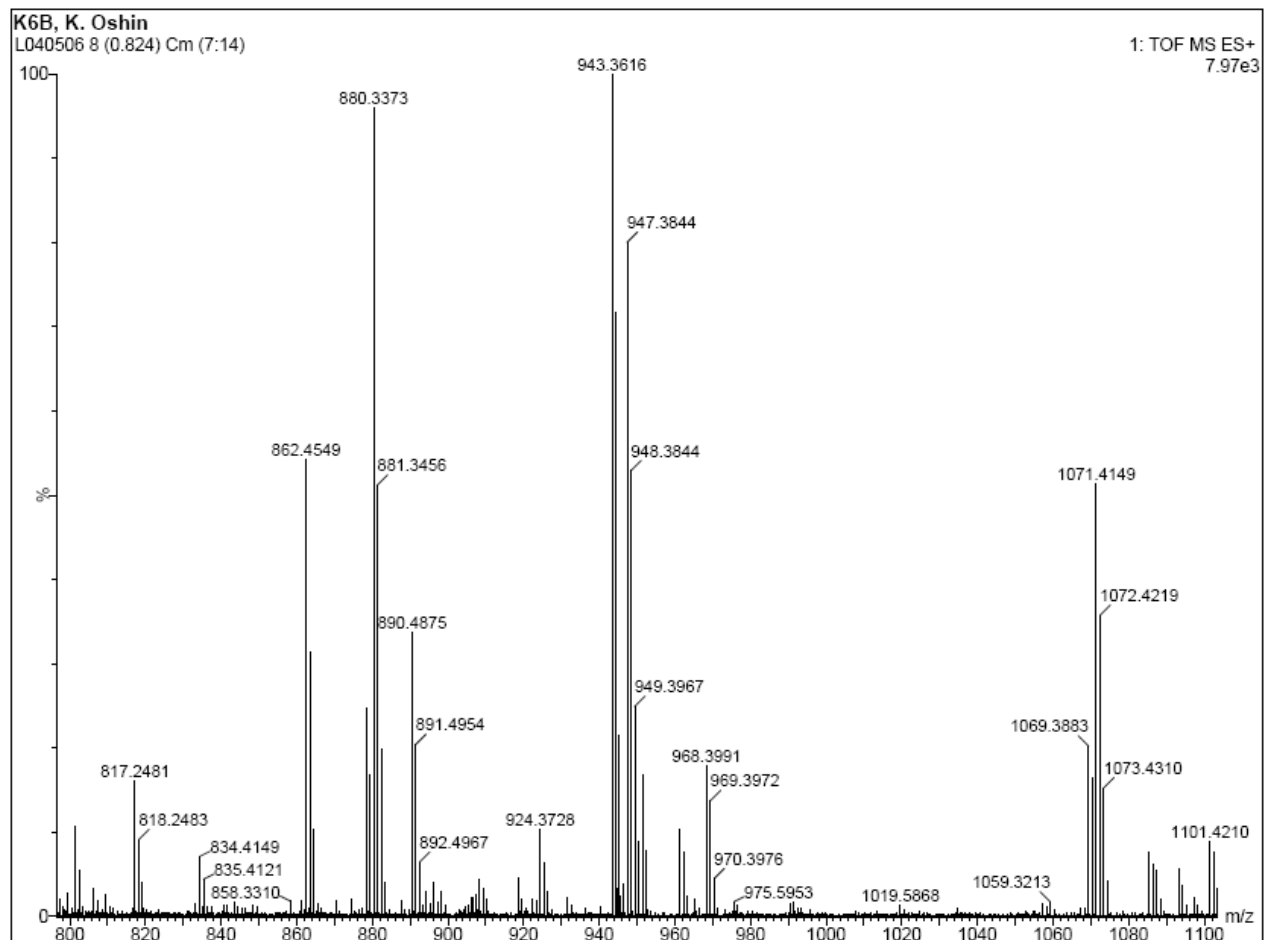
Figure A.10 Electro-Spray Mass Spectrum for Complex **13** (CH$_2$Cl$_2$)
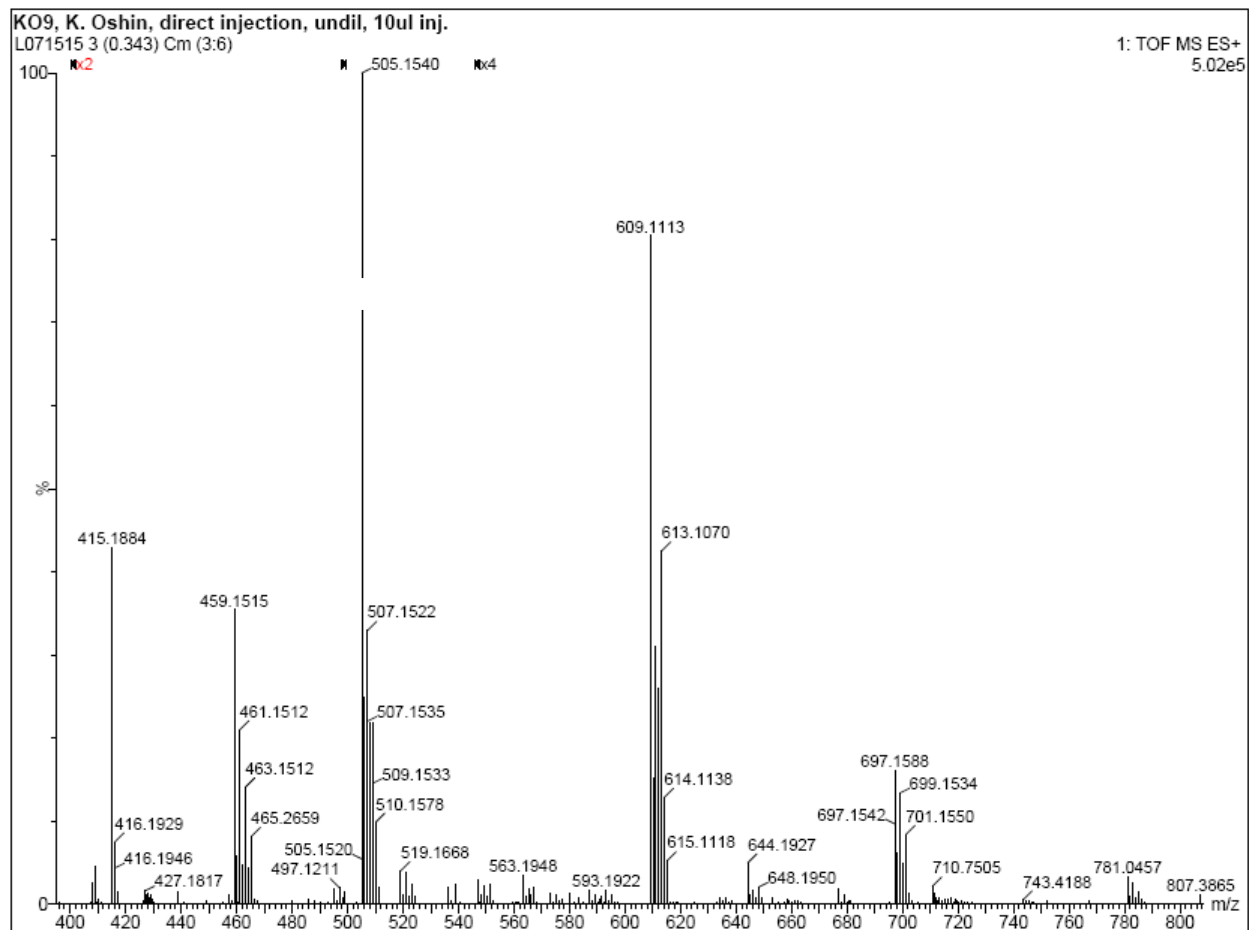
Figure A.11 Electro-Spray Mass Spectrum for Complex **15** (CH_2Cl_2)
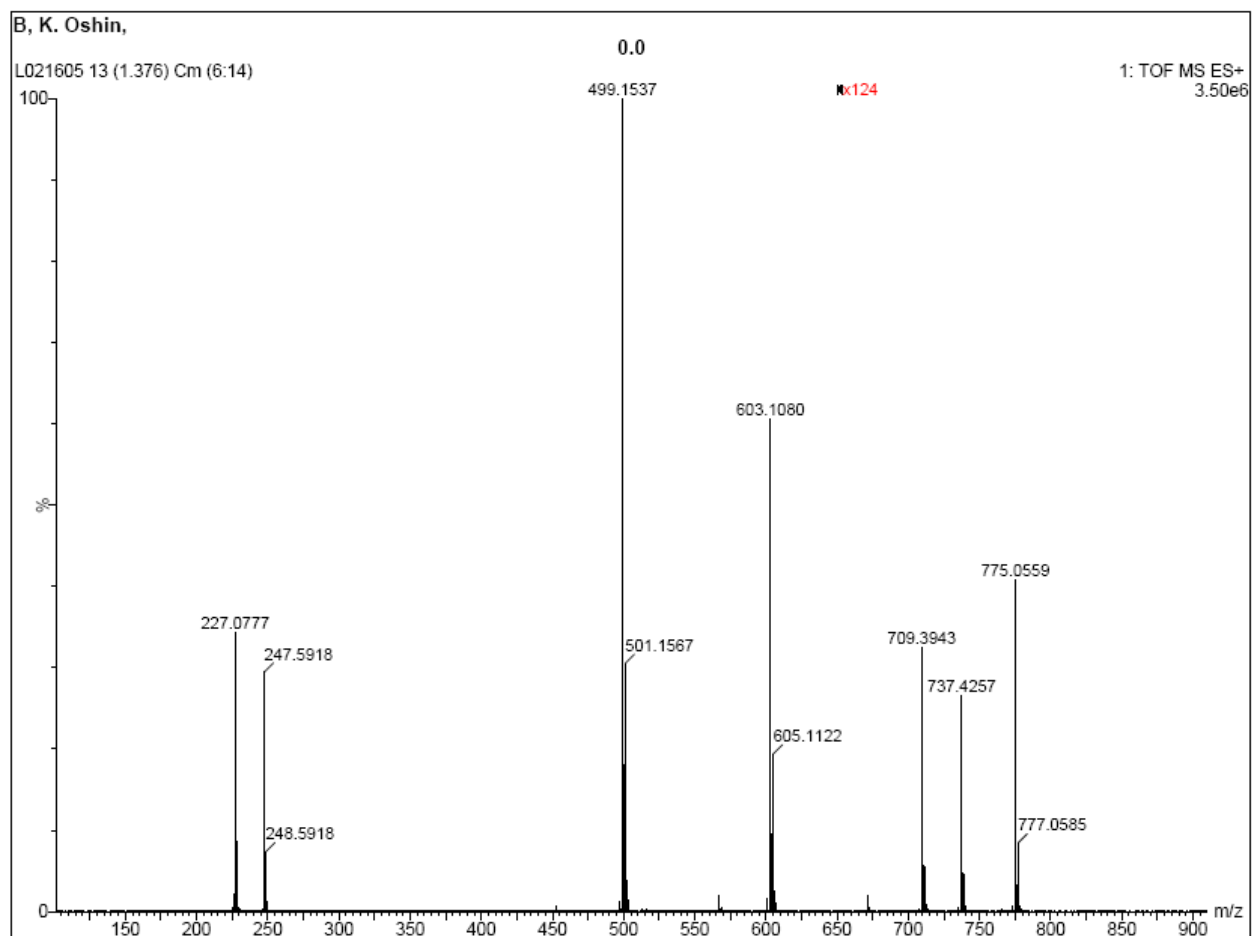
Figure A.12 Electro-Spray Mass Spectrum for Complex **16** (CH$_2$Cl$_2$)
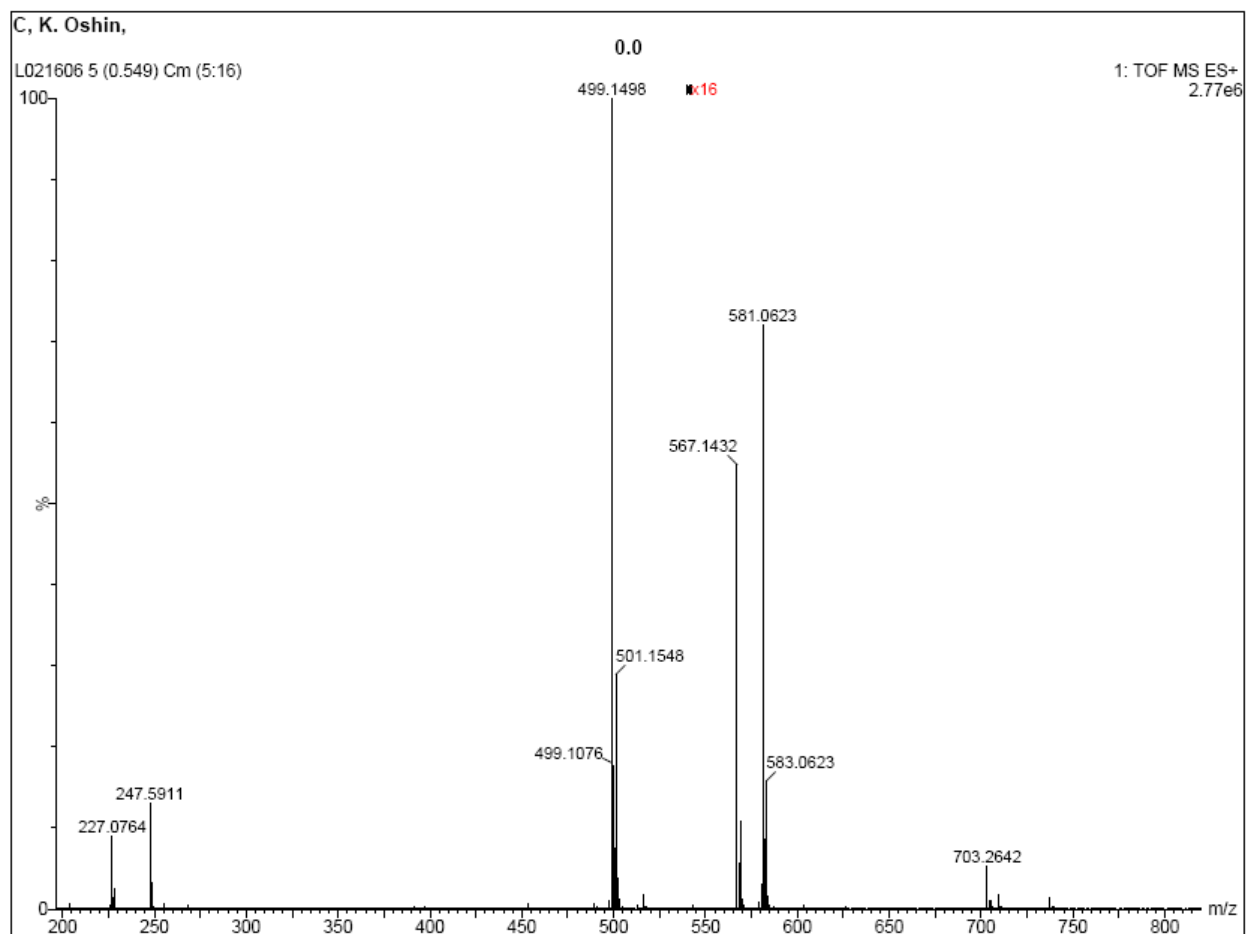
Figure A.13 Electro-Spray Mass Spectrum for Complex **17** (CH_2Cl_2)
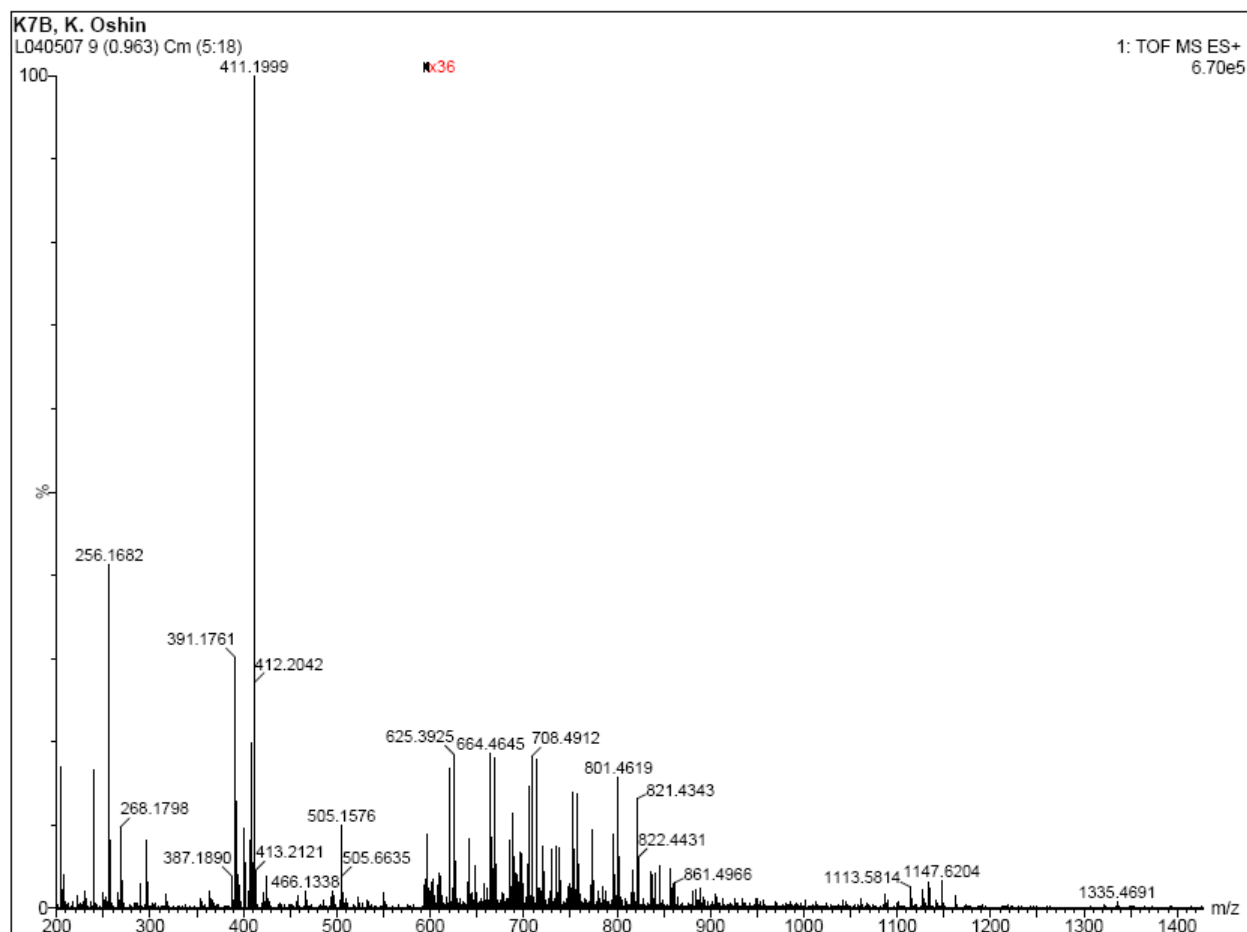
Figure A.14 Full Electro-Spray Mass Spectrum for Complex **18** (CH₂Cl₂)
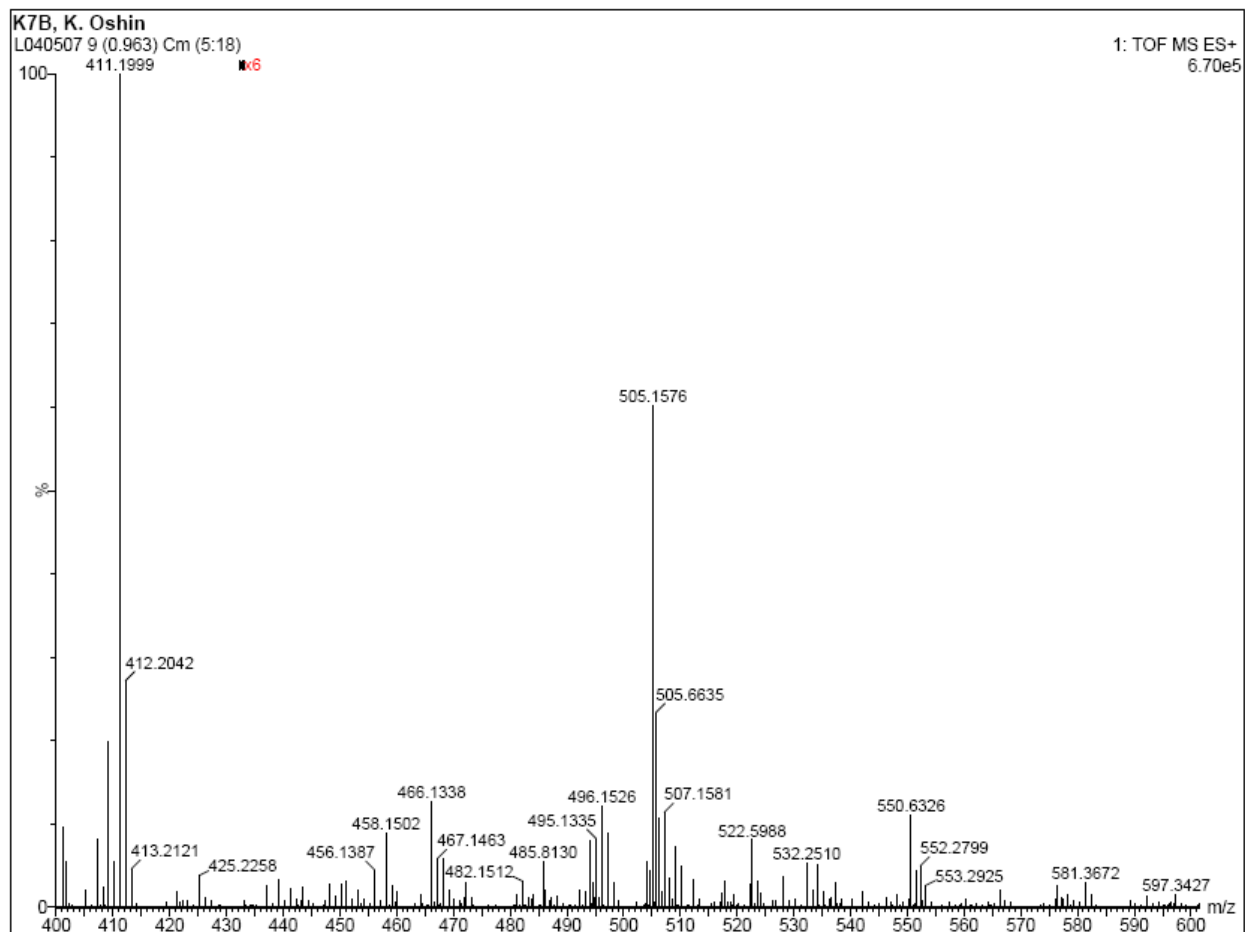
Figure A.15 Electro-Spray Mass Spectrum (Focused View) for Complex **18** (CH$_2$Cl$_2$)
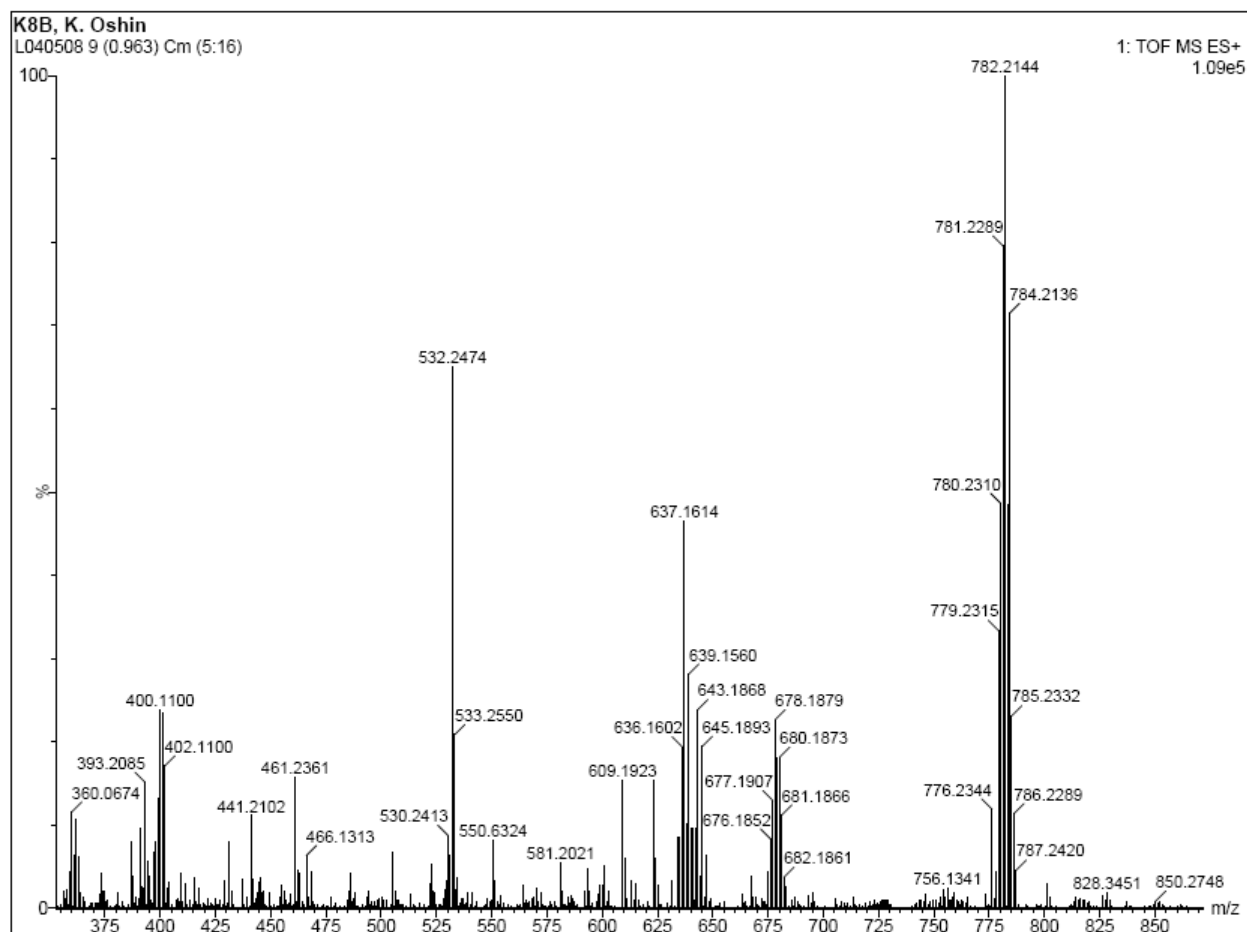
Figure A.16 Electro-Spray Mass Spectrum for Complex **19** (CH_2Cl_2)
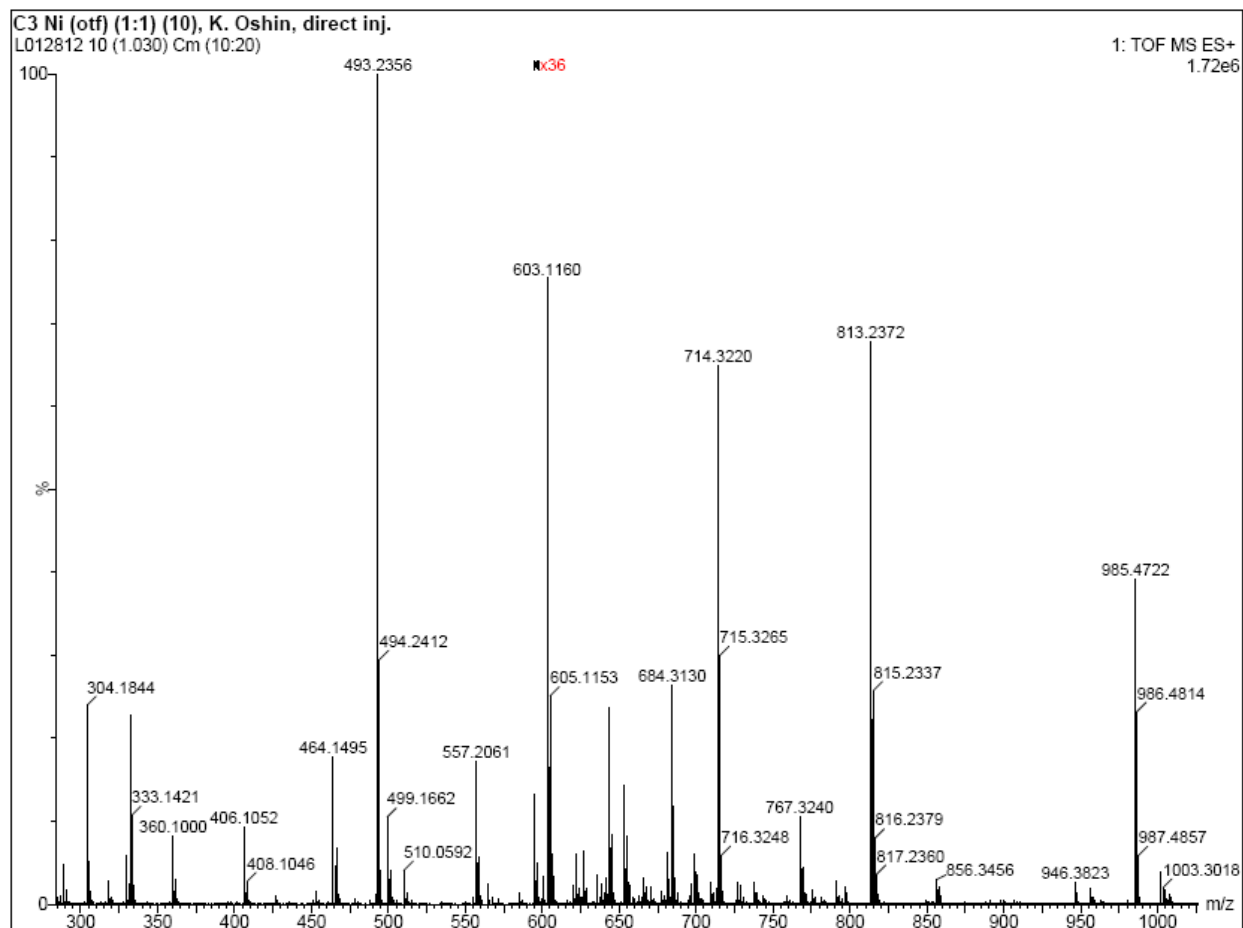
Figure A.17 Electro-Spray Mass Spectrum for Complex **20** (CH$_2$Cl$_2$)
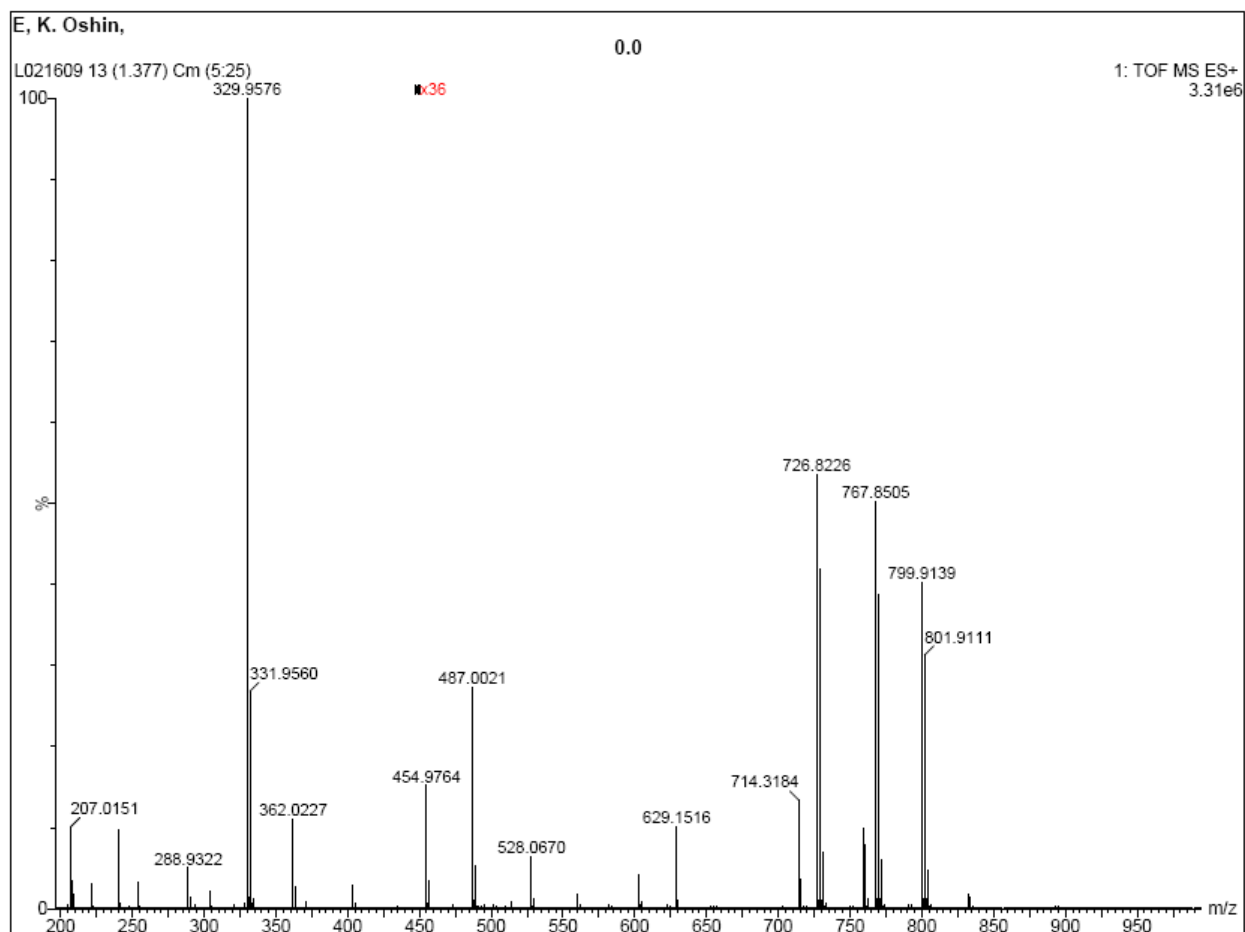
Figure A.18 Electro-Spray Mass Spectrum for Complex **21** (CH_2Cl_2)
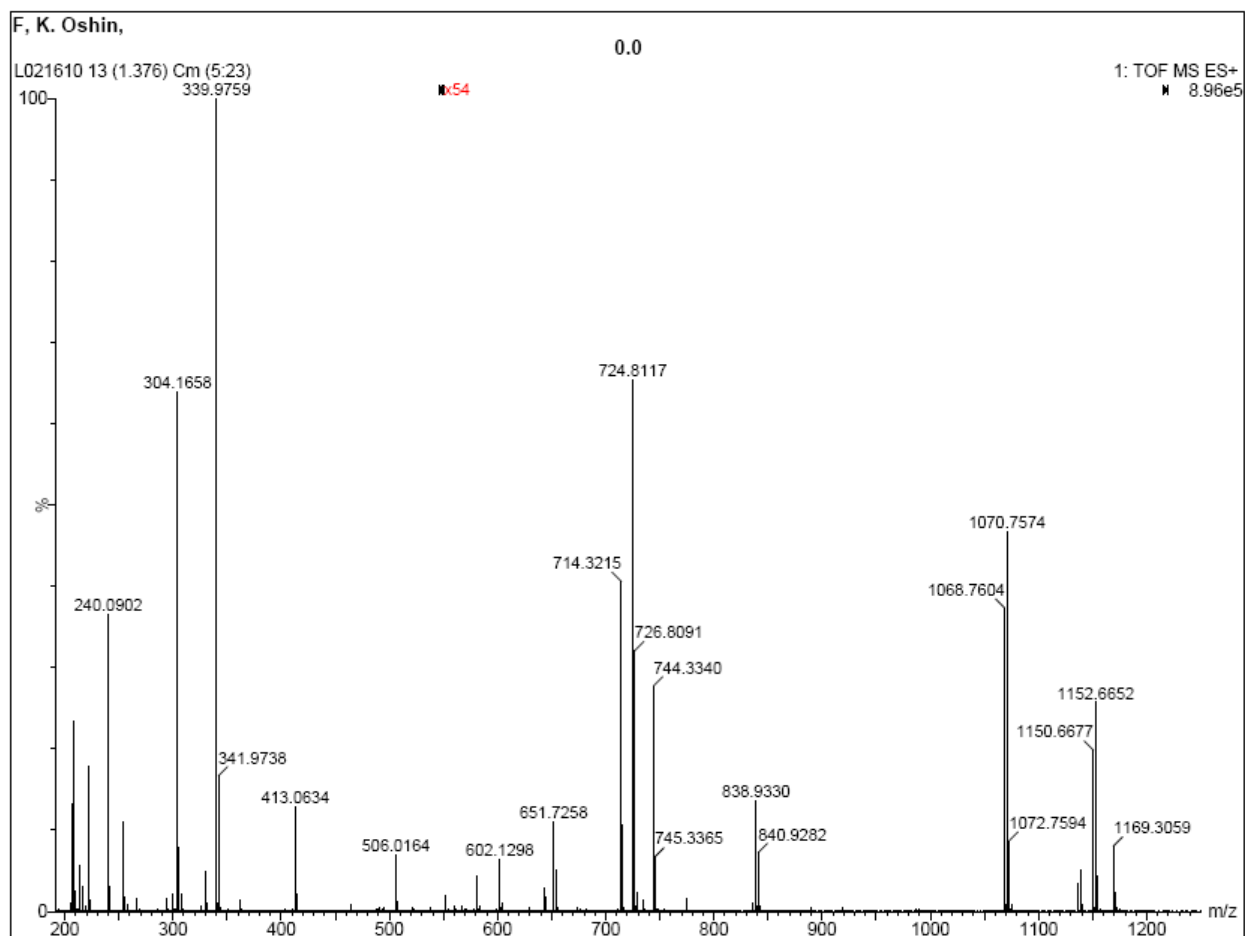
Figure A.19 Electro-Spray Mass Spectrum for Complex **22** (CH$_2$Cl$_2$)
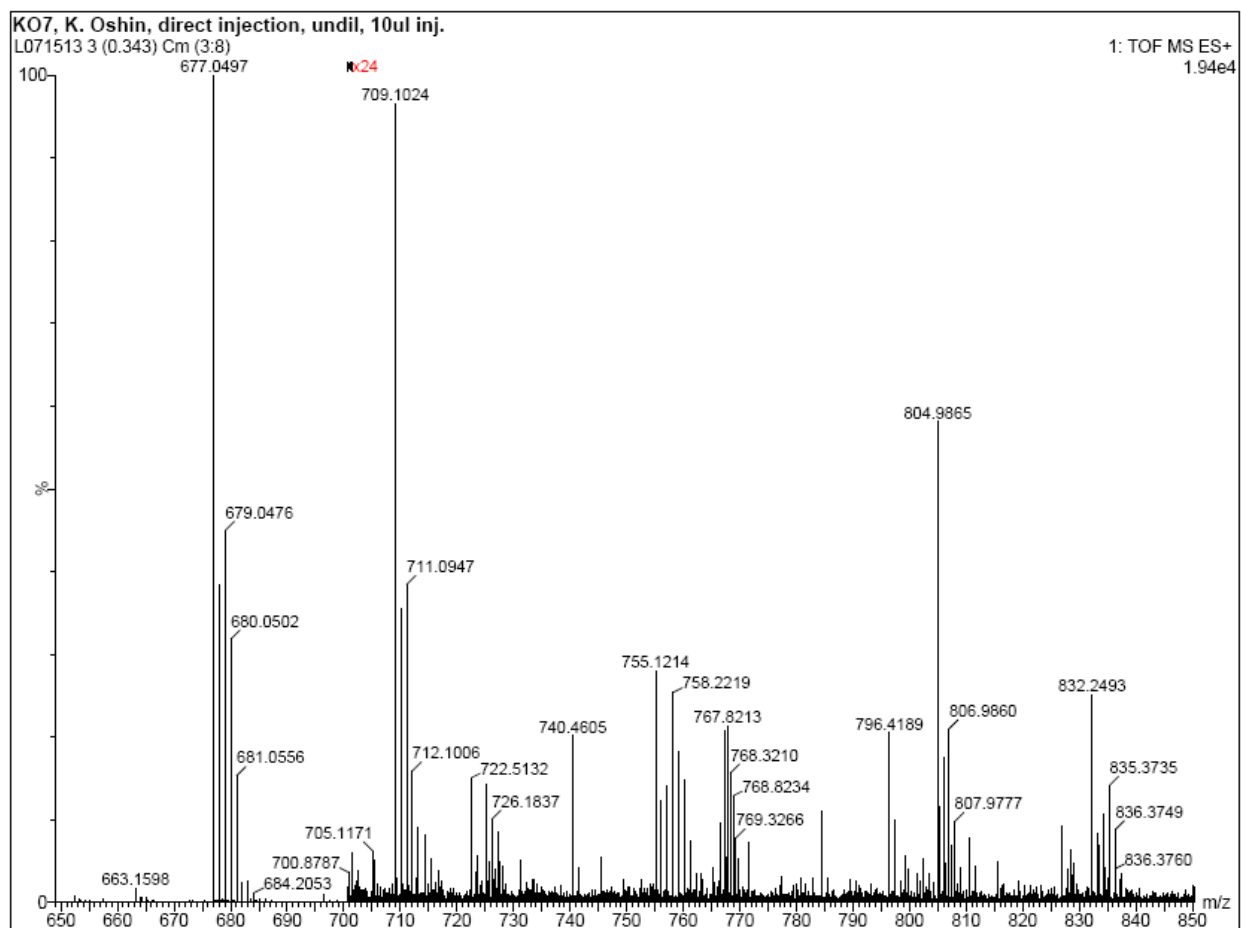
Figure A.20 Electro-Spray Mass Spectrum for Complex **23** (Sand-Brown) (CH$_2$Cl$_2$)
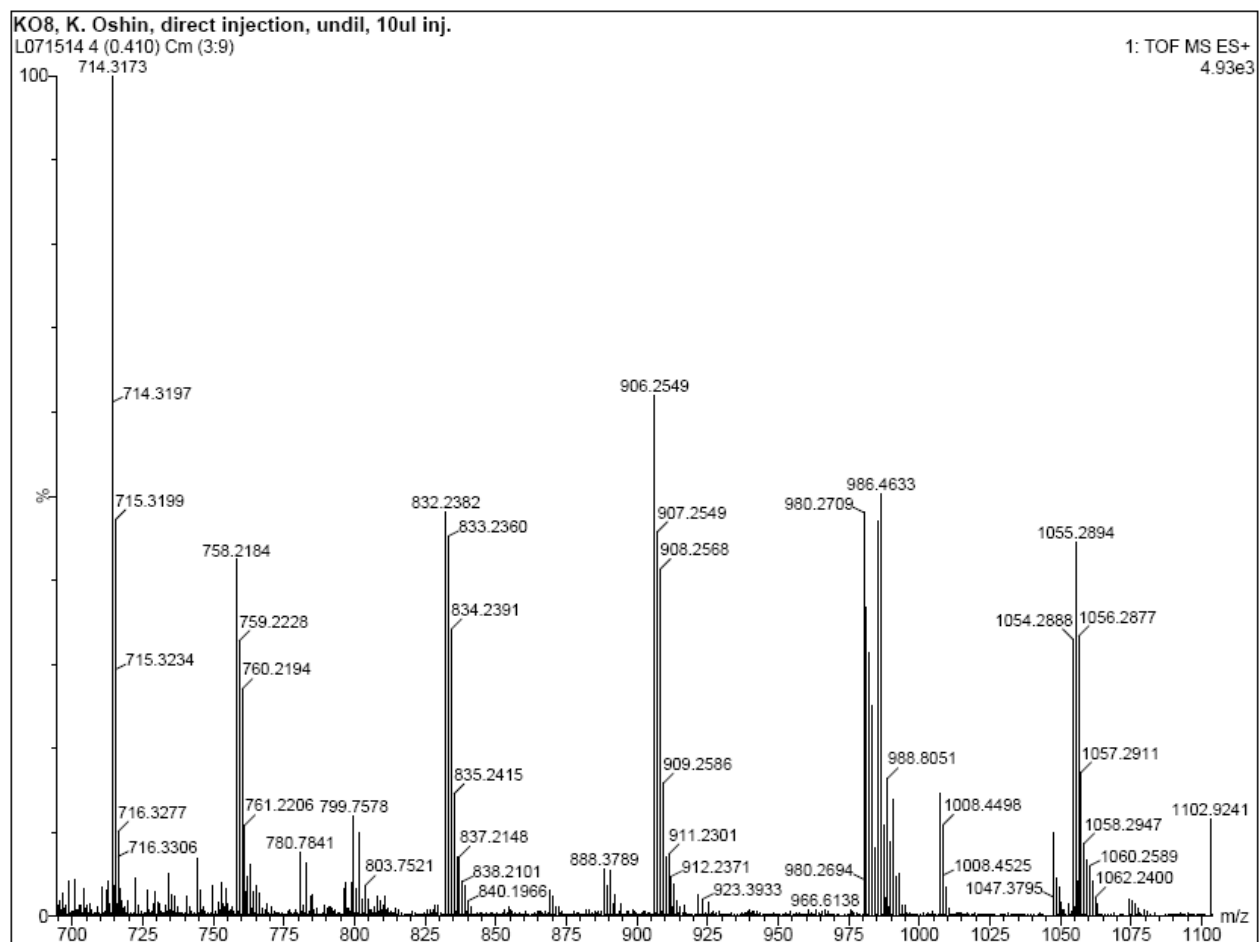
Figure A.21 Electro-Spray Mass Spectrum for Complex **23** (Dark-Green) (CH$_2$Cl$_2$)
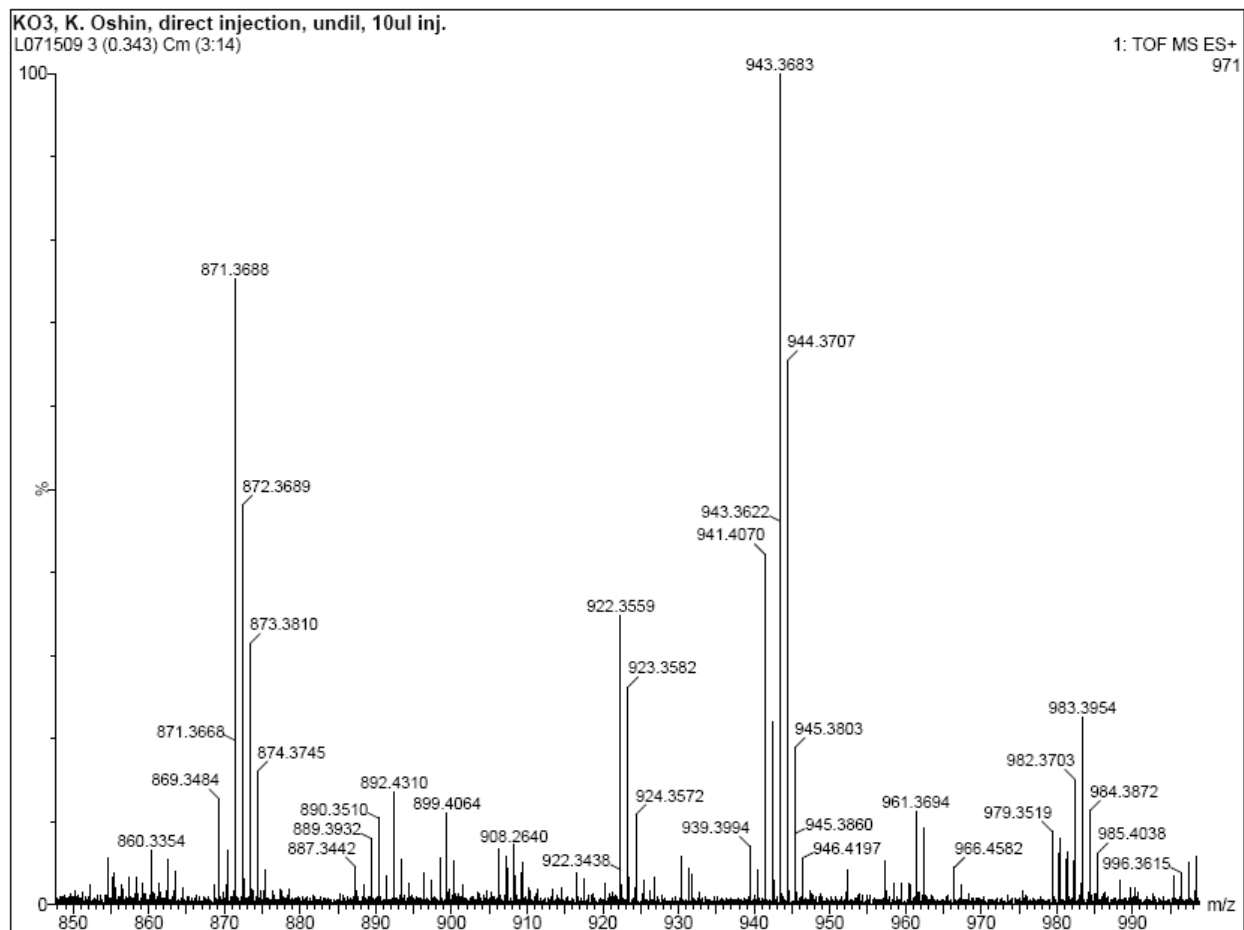
Figure A.22 Electro-Spray Mass Spectrum for Complex **24** (CH_2Cl_2)
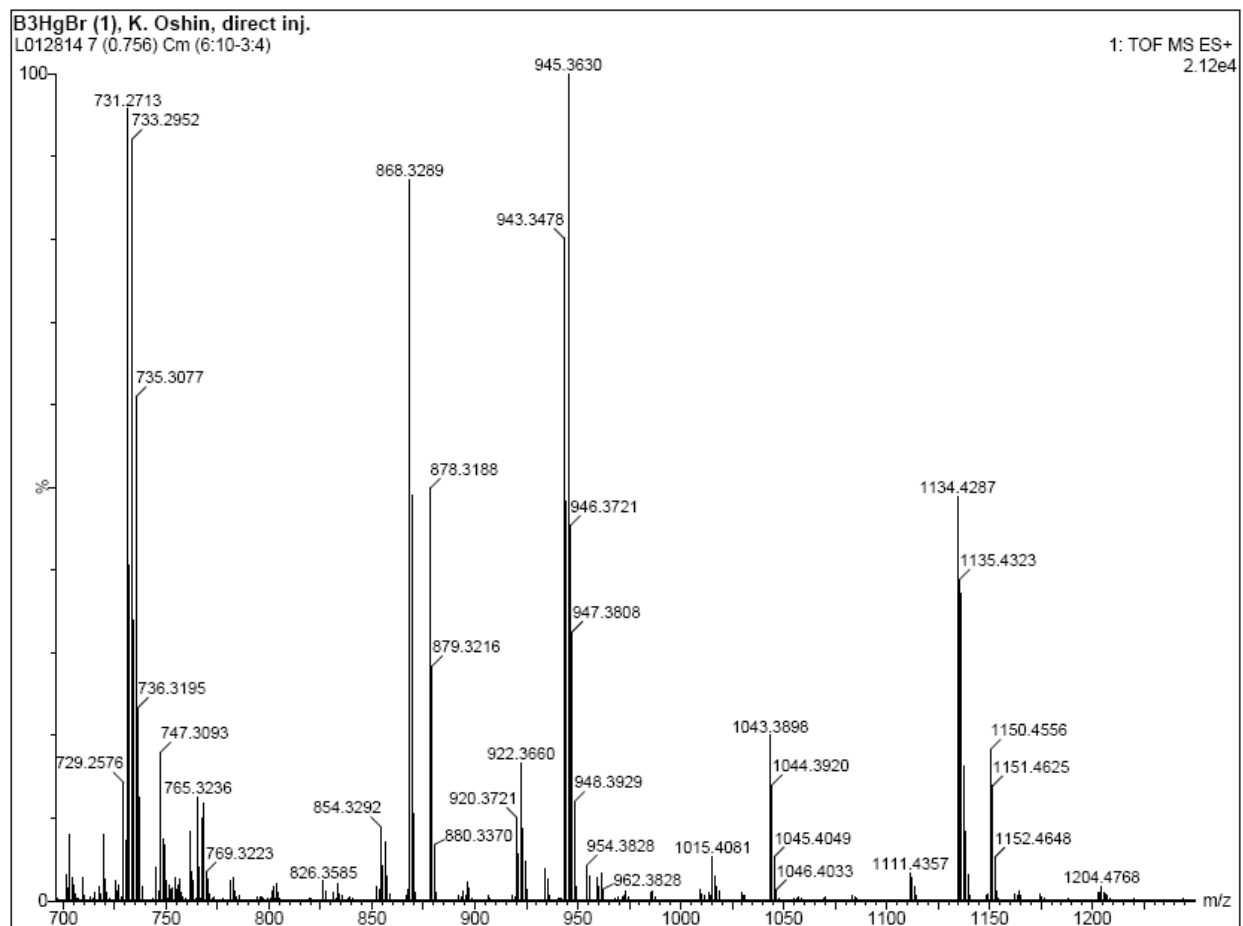
Figure A.23 Electro-Spray Mass Spectrum for Complex **25** (CH_2Cl_2)
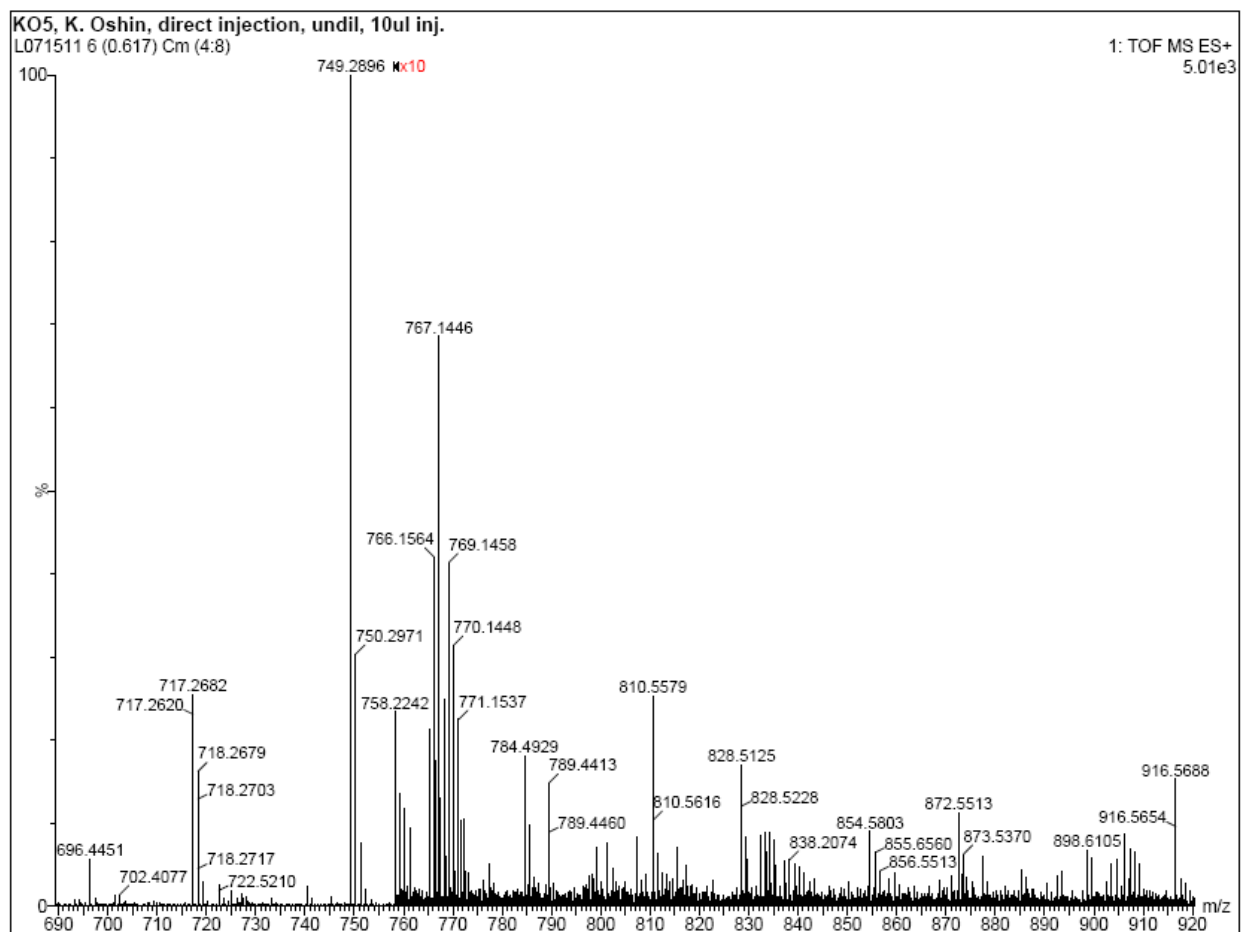
Figure A.24 Electro-Spray Mass Spectrum for Complex **26** (CH$_2$Cl$_2$)
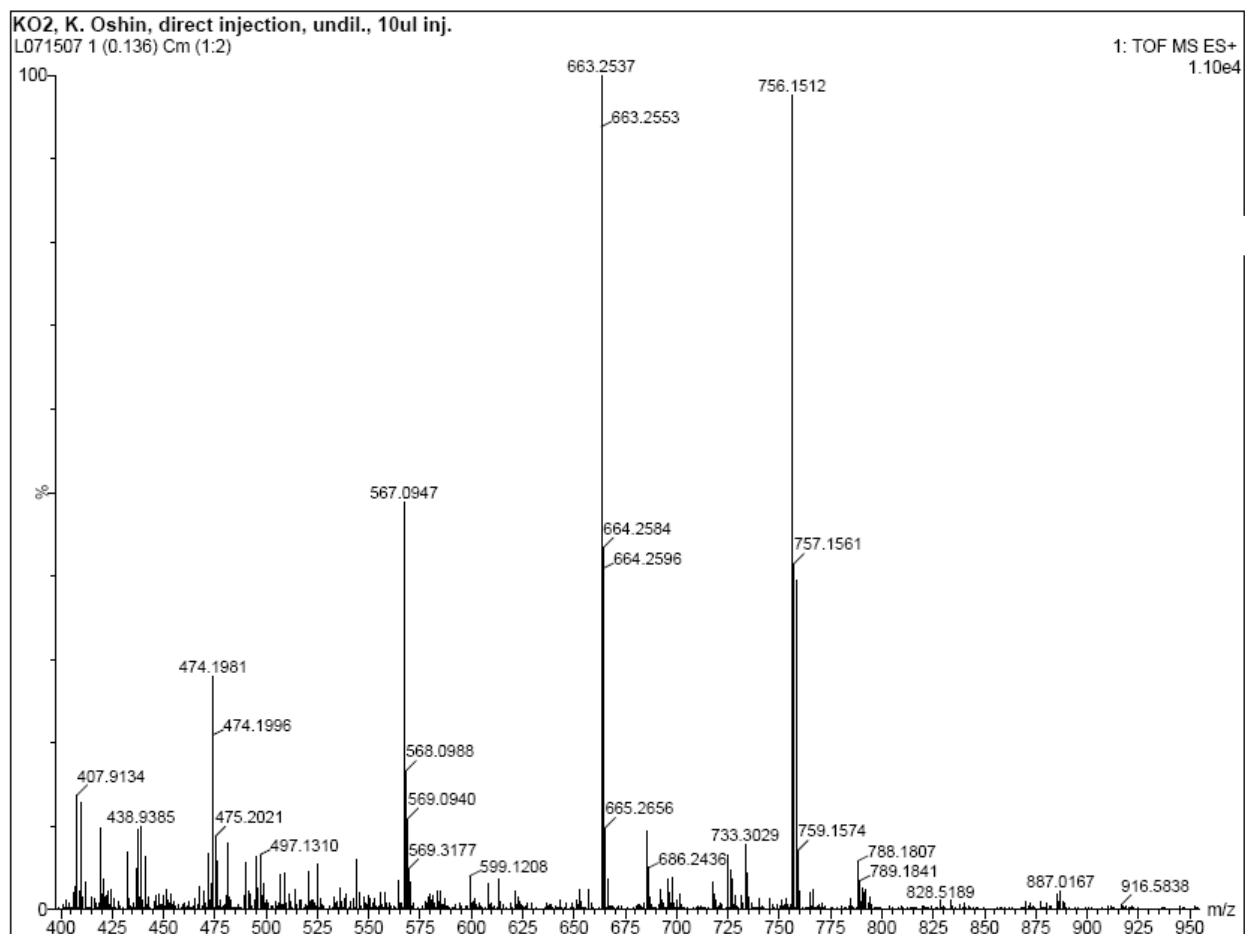
Figure A.25 Electro-Spray Mass Spectrum for Complex **27** (CH$_2$Cl$_2$)
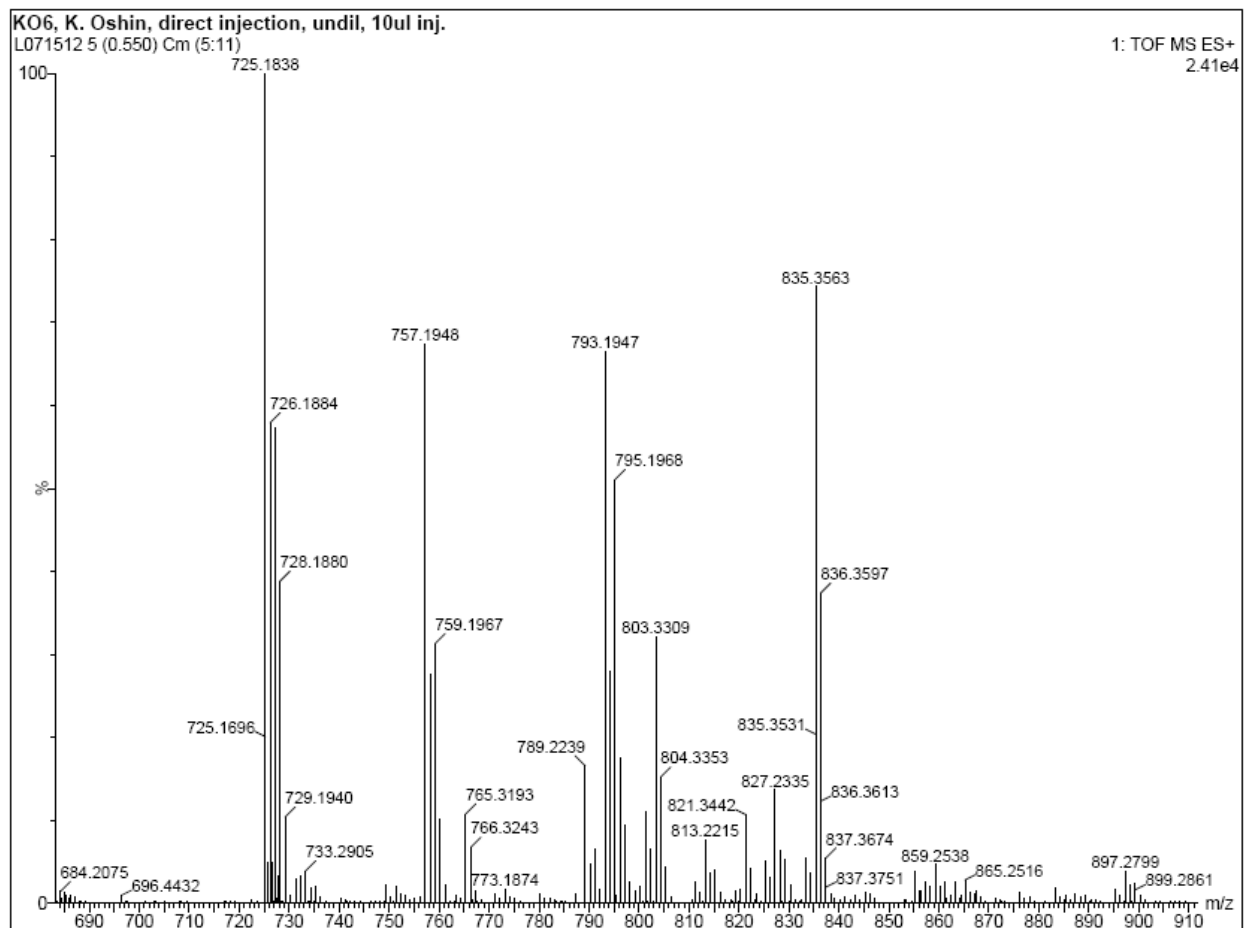
Figure A.26 Electro-Spray Mass Spectrum for Complex **28** (CH$_2$Cl$_2$)
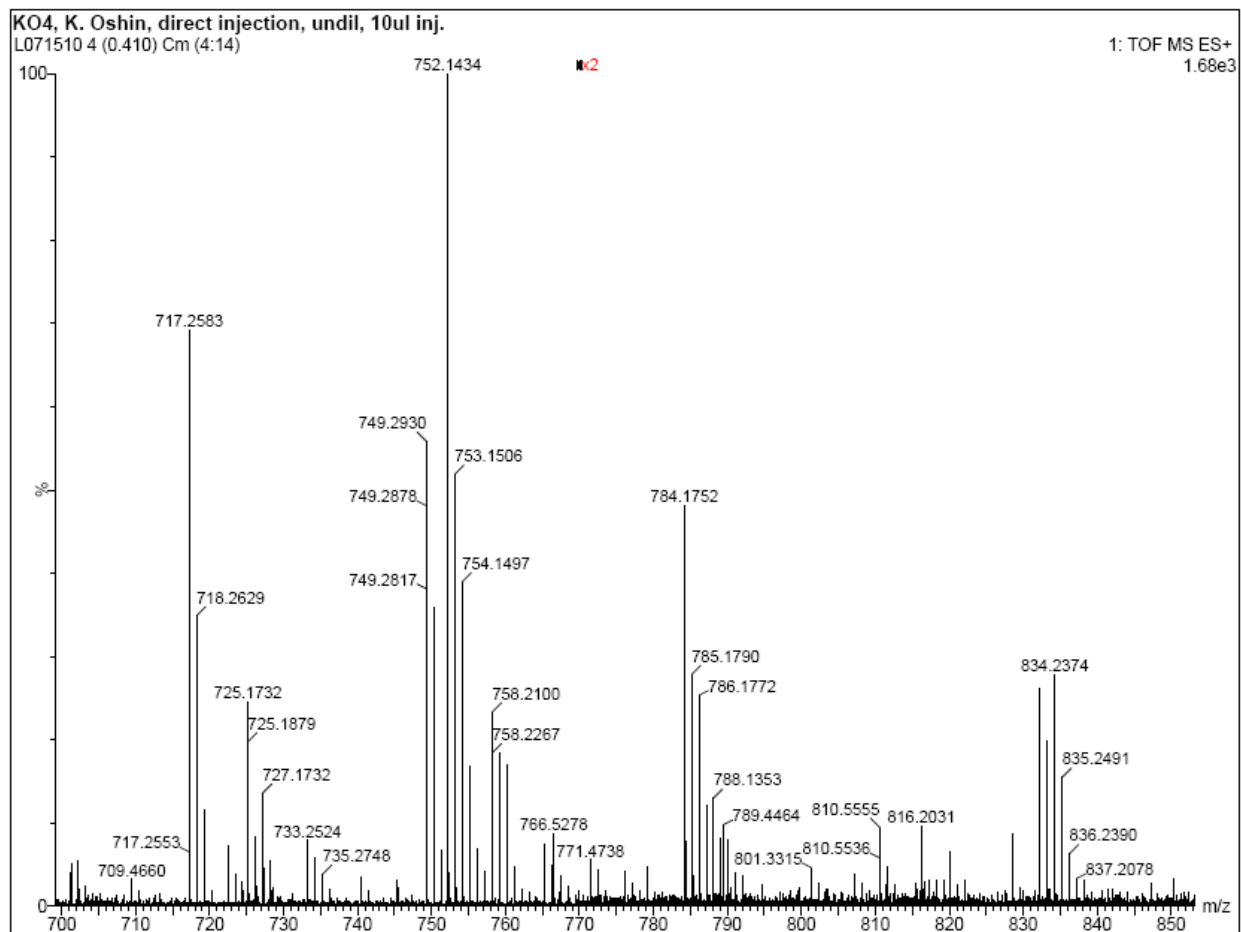
Figure A.27 Electro-Spray Mass Spectrum for Complex **29** (CH$_2$Cl$_2$)
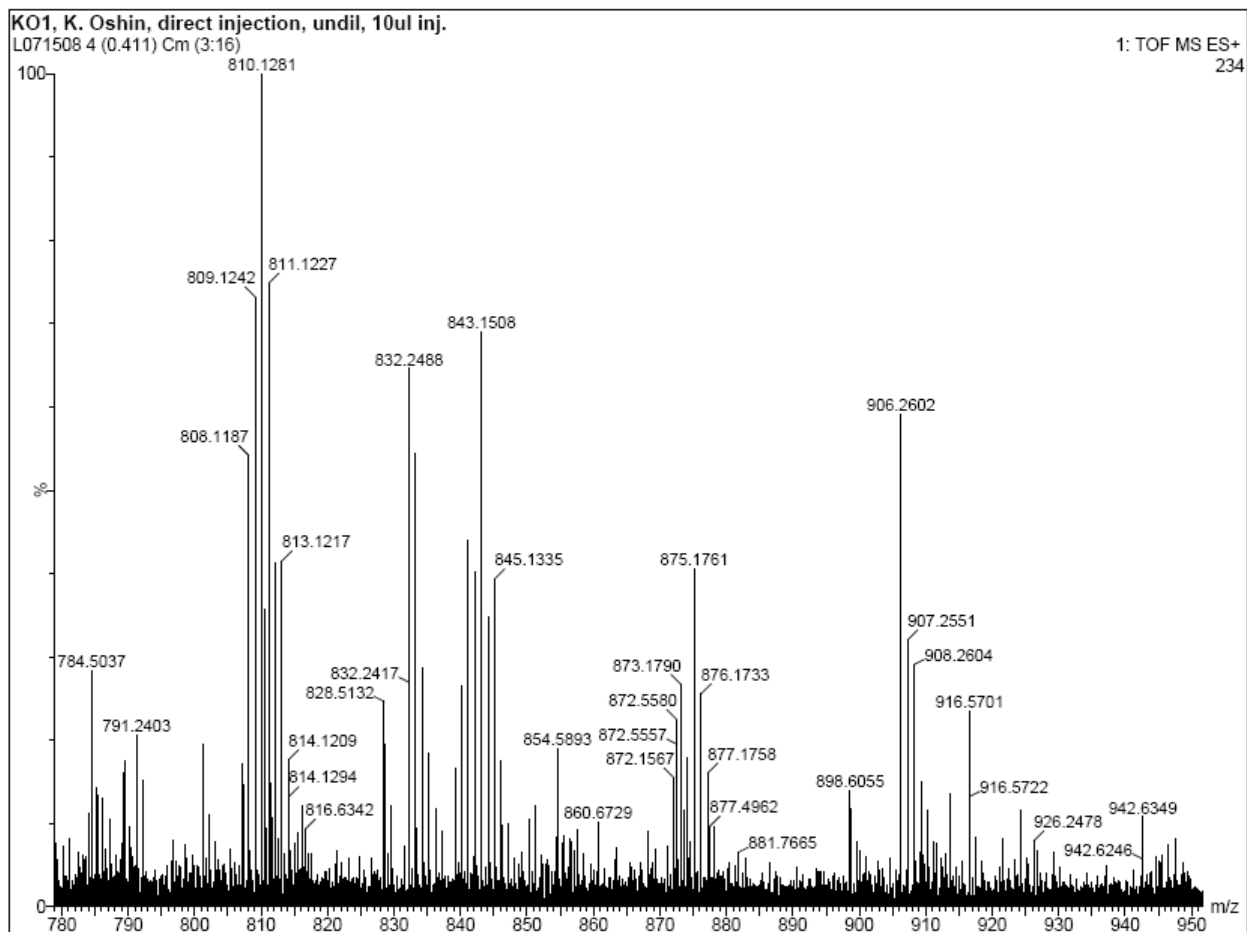
Figure A.28 Electro-Spray Mass Spectrum for Complex **30** (CH$_2$Cl$_2$)
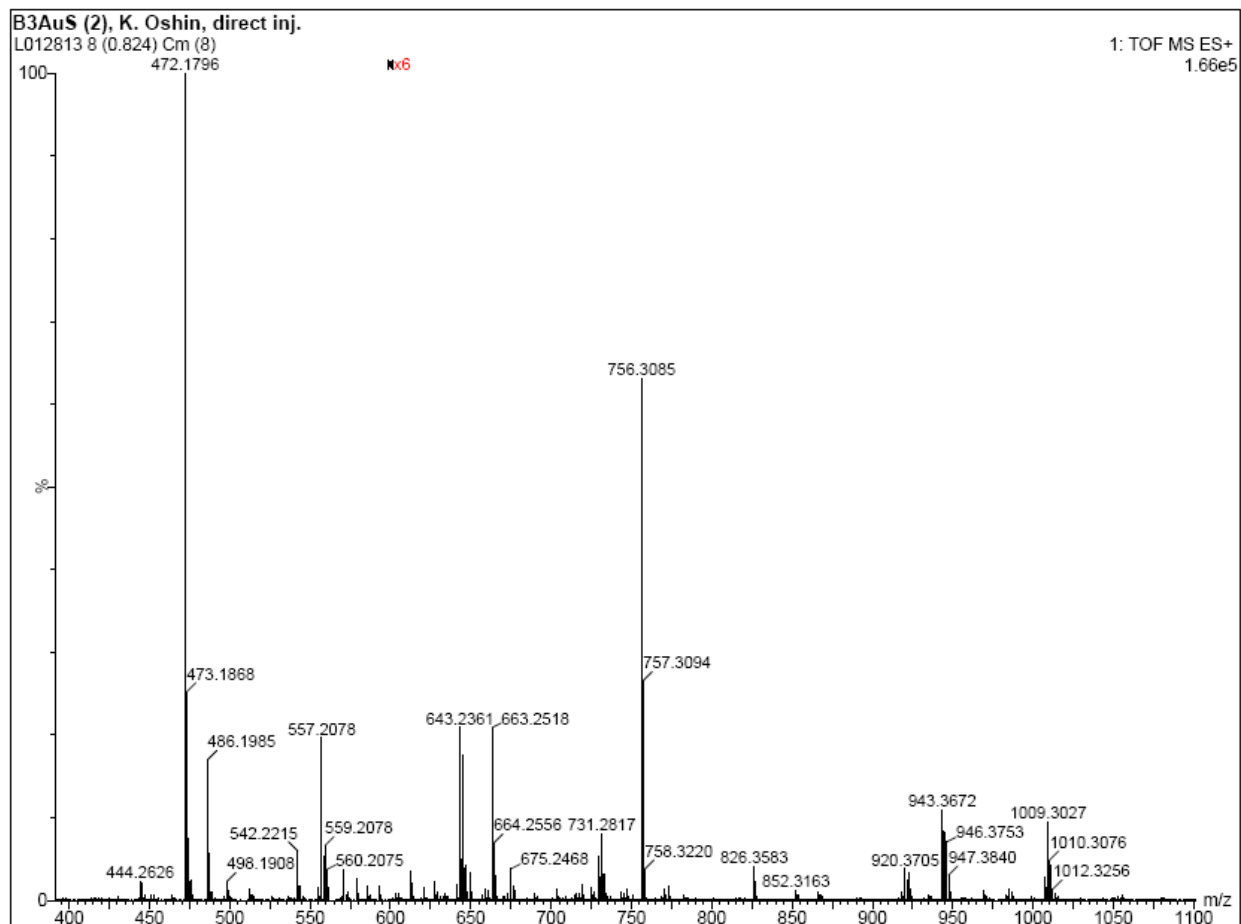
Figure A.29 Electro-Spray Mass Spectrum for Complex **31** (CH$_2$Cl$_2$)
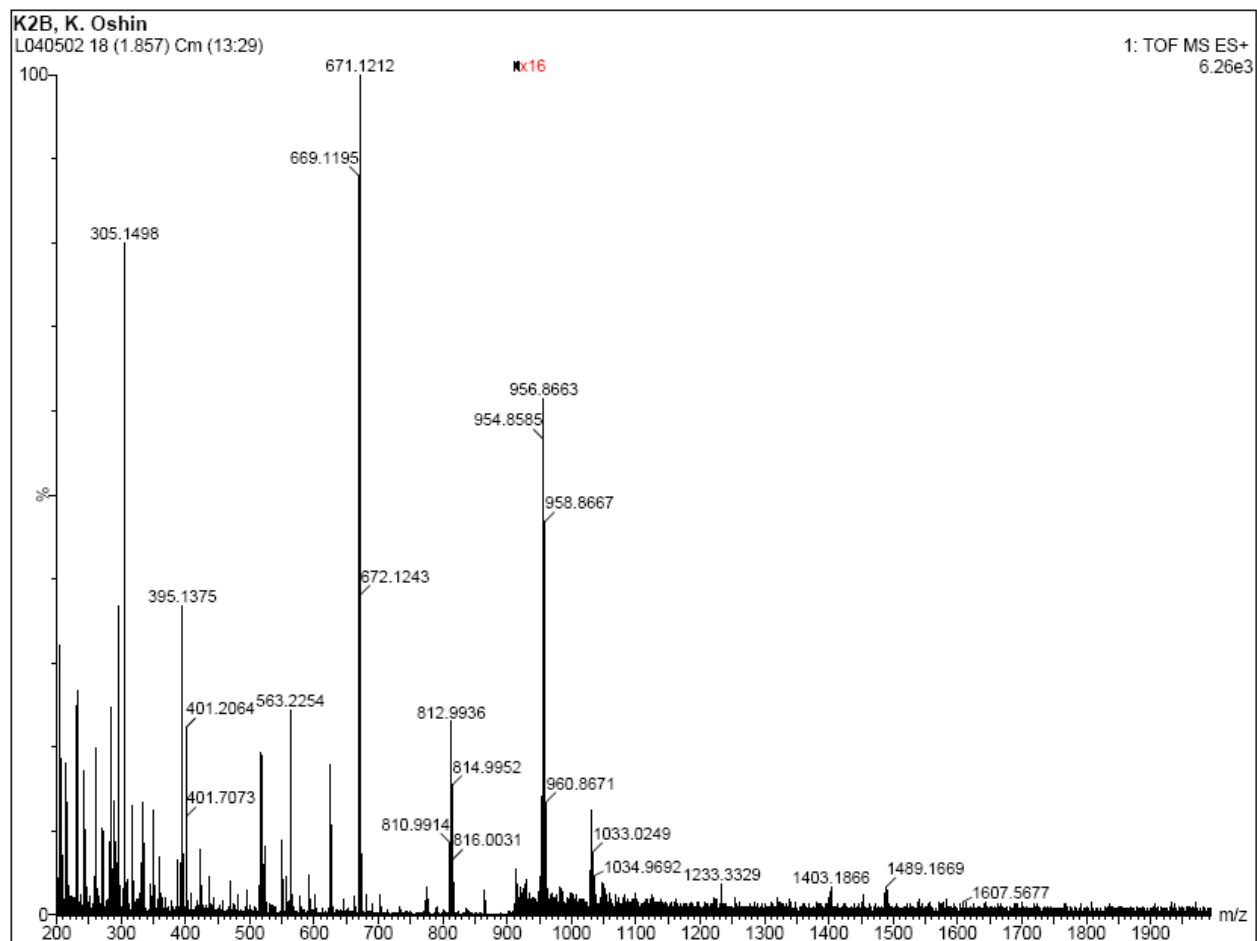
Figure A.30 Electro-Spray Mass Spectrum for Complex **32** (CH$_2$Cl$_2$)
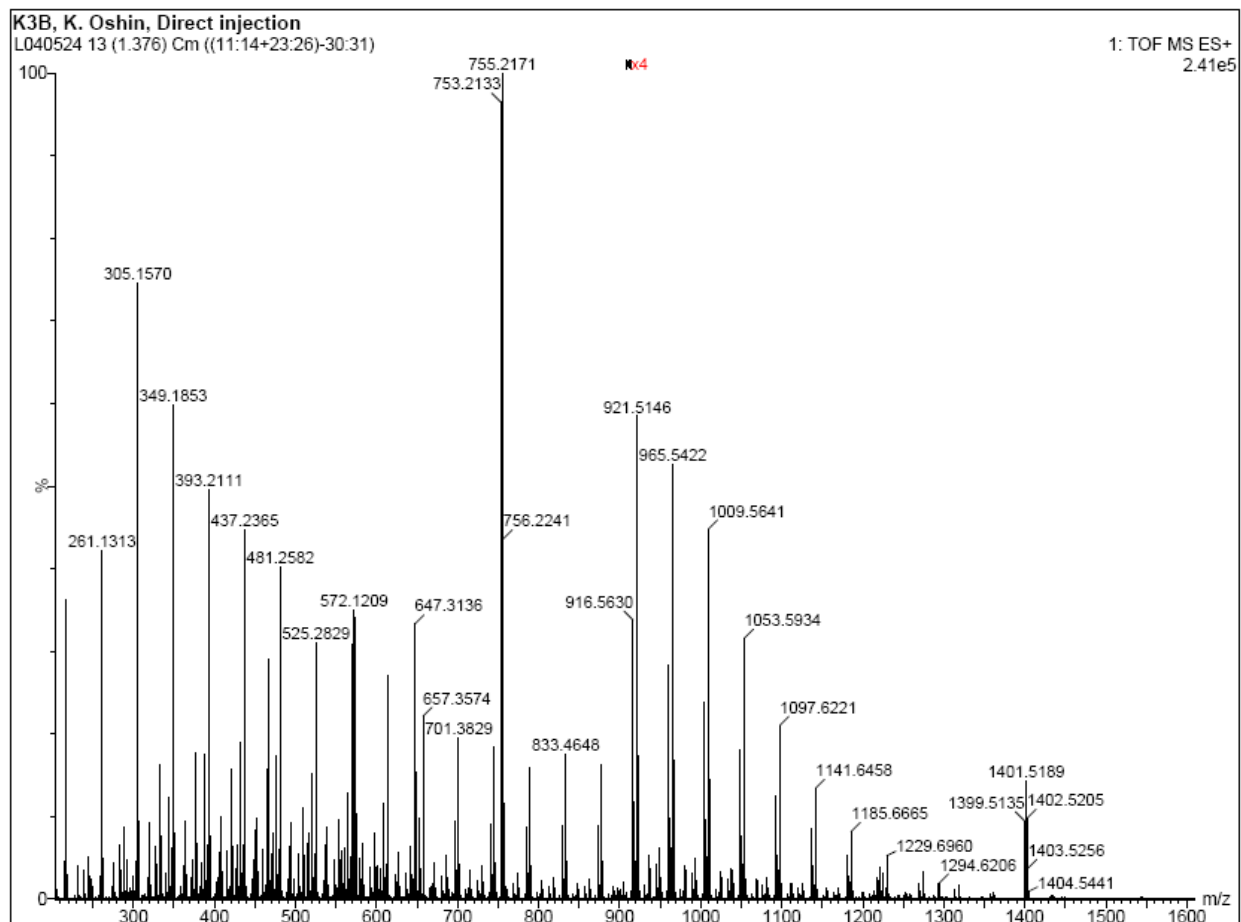
Figure A.31 Electro-Spray Mass Spectrum for Complex **33** (CH₂Cl₂)
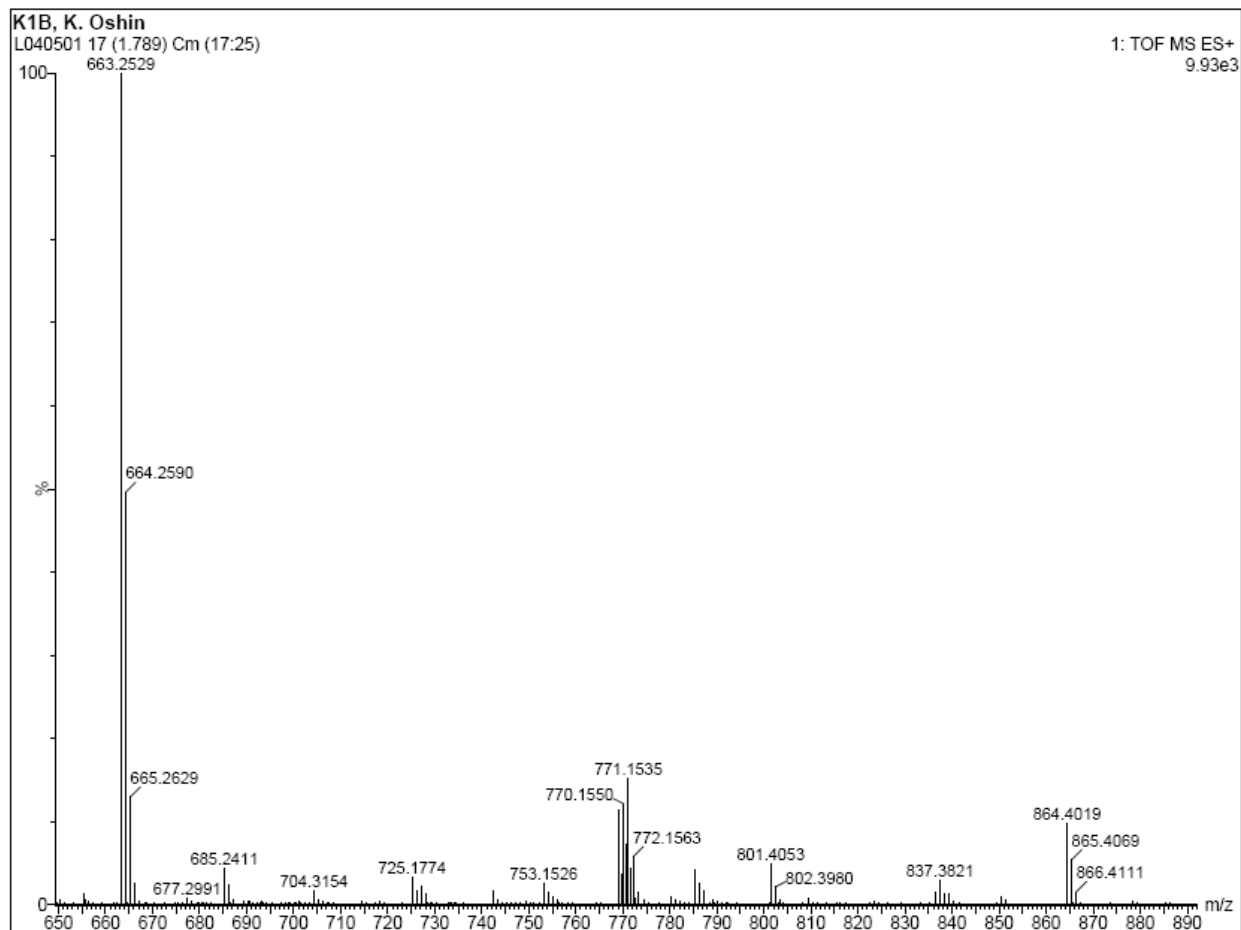
Figure A.32 Electro-Spray Mass Spectrum for Complex **34** (CH_2Cl_2)
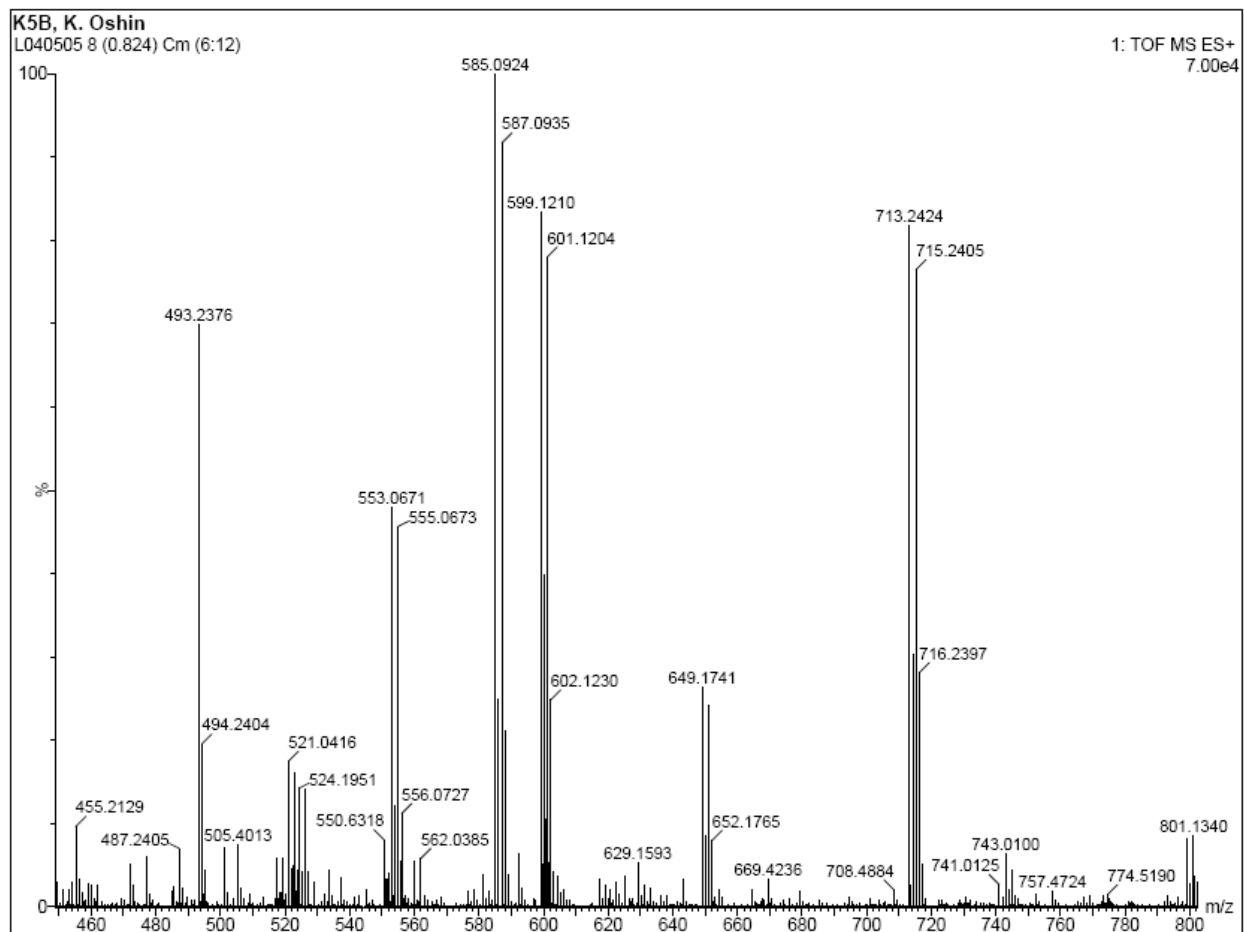
Figure A.33 Electro-Spray Mass Spectrum for Complex **35** (CH$_2$Cl$_2$)
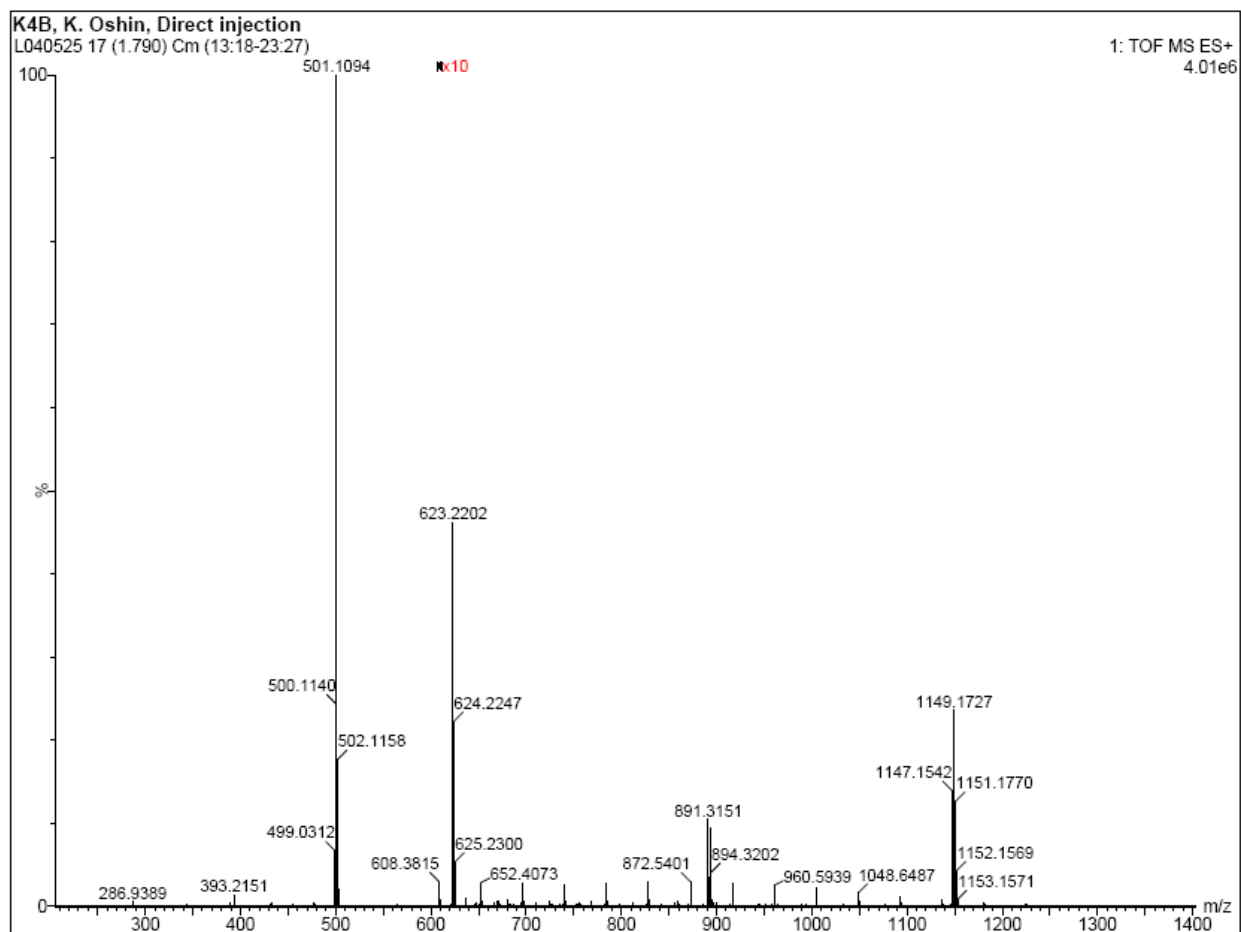
Figure A.34 Electro-Spray Mass Spectrum for Complex **36** (CH$_2$Cl$_2$)

Appendix B - Crystal Data

(Numerical Order)

Table 1. Crystal data and structure refinement for complex **13**.

Identification code   ko1002m

Empirical formula   C103 H70 Cl6 F12 N8 O12 S4 Zn2

Formula weight   2311.35

Temperature   120(2) K

Wavelength   0.71073 Å

Crystal system   Monoclinic

Space group   P2(1)

Unit cell dimensions   a = 11.8410(8) Å α= 90°

                                            b = 23.1233(16) Å β= 94.189(4)°

                                            c = 17.8406(12) Å γ = 90°

Volume   4871.8(6) Å^3

Z   2

Density (calculated)   1.576 g/cm^3

Absorption coefficient   0.834 mm^{-1}

F(000)   2348

Crystal size   0.24 x 0.20 x 0.16 mm^3

Theta range for data collection   1.14 to 31.51°

Index ranges   -17<=h<=17, -34<=k<=34, -26<=l<=26

Reflections collected   134347

Independent reflections   32276 [R(int) = 0.0864]

Completeness to theta = 31.51°   99.9 %

Absorption correction   None

Refinement method   Full-matrix least-squares on F^2

Data / restraints / parameters   32276 / 79 / 1383

Goodness-of-fit on F^2 0.976

Final R indices [I>2sigma(I)]   R1 = 0.0488, wR2 = 0.1018

R indices (all data)   R1 = 0.0845, wR2 = 0.1196

Absolute structure parameter   0.008(5)

Table 2. Atomic coordinates (x 10^4) and equivalent isotropic displacement parameters (Å^2 x 10^3) for complex **13**. U(eq) is defined as one third of the trace of the orthogonalized U^{ij} tensor.

	x	y	z	U(eq)
C(1S)	10062(3)	6041(2)	7211(2)	46(1)
Cl(1)	9242(1)	6673(1)	7088(1)	73(1)
Cl(2)	9183(1)	5438(1)	7364(1)	45(1)
C(2S)	4852(4)	6501(2)	7540(2)	55(1)
Cl(3)	5607(1)	7149(1)	7590(1)	83(1)
Cl(4)	5762(2)	5900(1)	7461(1)	101(1)
C(3A)	1544(13)	7861(4)	6780(7)	41(2)
Cl(5A)	2277(3)	7480(2)	7501(2)	102(1)
Cl(6A)	1889(7)	8615(3)	6785(3)	53(1)
C(3B)	1800(30)	7828(10)	6991(16)	66(8)
Cl(5B)	2733(7)	7726(4)	7780(4)	102(1)
Cl(6B)	1863(17)	8547(6)	6647(7)	53(1)
Zn11	4716(1)	3793(1)	5382(1)	22(1)
S1A1	7150(1)	3580(1)	6237(1)	22(1)
O1A1	5968(2)	3398(2)	6049(2)	25(1)
O1B1	7890(2)	3112(1)	6448(1)	30(1)
O1C1	7533(2)	3995(1)	5705(1)	27(1)
C1A1	6994(3)	3994(2)	7095(2)	27(1)
F1A1	6634(2)	3665(1)	7642(1)	32(1)
F1B1	6217(4)	4419(2)	6971(3)	35(1)
F1C1	7970(2)	4244(1)	7336(1)	35(1)
S1B1	6389(7)	3818(4)	6859(5)	50(2)
O1D1	5880(19)	3568(11)	6165(13)	29(8)
O1E1	6060(40)	4389(15)	7060(40)	60(20)
O1F1	6370(20)	3443(12)	7477(14)	59(9)

C1B1	7863(16)	3891(8)	6656(10)	34(6)
F1D1	8344(15)	3365(9)	6572(12)	50(5)
F1E1	7930(20)	4183(12)	6006(13)	77(8)
F1F1	8451(18)	4169(14)	7206(16)	78(11)
S21	2378(1)	6418(1)	5514(1)	29(1)
O2A1	3378(2)	6234(1)	5954(2)	46(1)
O2B1	1384(2)	6084(1)	5620(1)	46(1)
O2C1	2234(2)	7033(1)	5480(2)	45(1)
C21	2708(4)	6232(2)	4559(2)	51(1)
F2A1	2929(3)	5661(1)	4510(2)	74(1)
F2B1	1888(2)	6351(2)	4056(1)	81(1)
F2C1	3627(2)	6521(1)	4371(1)	66(1)
N111	3872(2)	3179(1)	4711(1)	22(1)
C121	4645(2)	2800(1)	4509(2)	25(1)
C131	4387(3)	2214(1)	4385(2)	29(1)
C141	3306(3)	2029(1)	4480(2)	33(1)
C151	2455(3)	2432(1)	4647(2)	30(1)
C161	1311(3)	2256(2)	4739(2)	35(1)
C171	528(3)	2652(2)	4888(2)	39(1)
C181	776(3)	3252(2)	4920(2)	33(1)
C191	-61(3)	3669(2)	5038(2)	40(1)
C201	163(3)	4246(2)	5018(2)	44(1)
C211	1248(3)	4438(2)	4872(2)	38(1)
C221	2093(3)	4050(2)	4762(2)	29(1)
C231	1902(2)	3449(1)	4811(2)	24(1)
C241	2754(2)	3019(1)	4725(2)	24(1)
C251	5818(2)	3030(1)	4389(2)	25(1)
N311	3558(2)	3991(1)	6232(1)	24(1)
C321	3497(3)	4578(1)	6273(2)	27(1)
C331	2651(3)	4869(2)	6626(2)	36(1)

C341	1776(3)	4555(2)	6876(2)	39(1)
C351	1775(3)	3948(2)	6819(2)	33(1)
C361	833(3)	3611(2)	7028(2)	42(1)
C371	848(3)	3031(2)	6968(2)	39(1)
C381	1840(3)	2727(2)	6759(2)	33(1)
C391	1884(3)	2117(2)	6765(2)	36(1)
C401	2851(3)	1826(2)	6613(2)	37(1)
C411	3830(3)	2138(2)	6467(2)	34(1)
C421	3804(3)	2734(1)	6450(2)	28(1)
C431	2809(2)	3041(1)	6571(2)	26(1)
C441	2737(3)	3672(1)	6541(2)	26(1)
C451	4341(3)	4911(1)	5902(2)	28(1)
C511	4816(2)	4918(1)	3253(2)	22(1)
C521	5403(2)	4588(1)	3838(2)	21(1)
C531	5313(2)	3990(1)	3820(2)	22(1)
N531	5819(2)	3666(1)	4440(1)	23(1)
C541	4693(2)	3710(1)	3216(2)	24(1)
C551	4175(2)	4023(1)	2644(2)	25(1)
C561	4213(2)	4638(1)	2650(2)	24(1)
C571	3667(2)	4974(2)	2055(2)	28(1)
C581	3701(3)	5559(2)	2079(2)	30(1)
C591	4272(3)	5843(1)	2696(2)	30(1)
C601	4825(2)	5539(1)	3263(2)	24(1)
C611	7192(2)	5139(1)	4176(2)	24(1)
C621	6164(2)	4893(1)	4413(2)	22(1)
C631	5902(2)	4967(1)	5142(2)	24(1)
N631	4961(2)	4668(1)	5421(1)	24(1)
C641	6631(3)	5290(1)	5661(2)	28(1)
C651	7601(3)	5519(1)	5443(2)	31(1)
C661	7930(3)	5454(1)	4695(2)	27(1)

C671	8956(3)	5686(1)	4466(2)	33(1)
C681	9245(3)	5612(2)	3745(2)	35(1)
C691	8535(3)	5306(2)	3229(2)	35(1)
C701	7542(2)	5074(1)	3431(2)	27(1)
Zn22	695(1)	2941(1)	9738(1)	20(1)
S32	-1494(1)	2775(1)	8658(1)	22(1)
O3A2	-515(2)	2515(1)	9091(1)	29(1)
O3B2	-1167(2)	3205(1)	8141(1)	32(1)
O3C2	-2406(2)	2900(1)	9114(1)	34(1)
C32	-1944(3)	2147(1)	8090(2)	30(1)
F3A2	-2875(2)	2268(1)	7649(1)	40(1)
F3B2	-2184(2)	1710(1)	8528(1)	50(1)
F3C2	-1146(2)	1979(1)	7657(1)	45(1)
S42	2573(1)	5670(1)	8894(1)	29(1)
O4A2	1632(2)	5335(1)	8589(2)	49(1)
O4B2	3660(2)	5435(1)	8784(2)	56(1)
O4C2	2468(2)	6283(1)	8783(2)	45(1)
C42	2476(3)	5585(2)	9902(2)	44(1)
F4A2	2574(2)	5025(1)	10105(1)	61(1)
F4B2	1529(2)	5788(1)	10136(1)	76(1)
F4C2	3328(3)	5864(1)	10282(1)	76(1)
N112	1343(2)	2341(1)	10506(1)	23(1)
C122	505(3)	1994(1)	10695(2)	25(1)
C132	679(3)	1409(1)	10862(2)	30(1)
C142	1749(3)	1186(1)	10826(2)	30(1)
C152	2663(3)	1547(1)	10681(2)	27(1)
C162	3803(3)	1338(1)	10647(2)	33(1)
C172	4653(3)	1705(2)	10521(2)	32(1)
C182	4462(3)	2318(1)	10469(2)	28(1)
C192	5380(3)	2704(2)	10403(2)	34(1)

C202	5204(3)	3285(2)	10414(2)	35(1)
C212	4121(3)	3514(2)	10503(2)	31(1)
C222	3211(3)	3147(1)	10567(2)	26(1)
C232	3364(2)	2541(1)	10516(2)	23(1)
C242	2436(2)	2137(1)	10561(2)	22(1)
C252	-659(3)	2266(1)	10731(2)	27(1)
N312	1992(2)	3104(1)	8975(1)	20(1)
C322	2115(2)	3682(1)	8914(2)	22(1)
C332	3070(3)	3951(1)	8656(2)	27(1)
C342	3981(3)	3609(2)	8521(2)	31(1)
C352	3899(2)	3004(1)	8582(2)	25(1)
C362	4850(3)	2628(1)	8486(2)	29(1)
C372	4743(3)	2052(1)	8545(2)	28(1)
C382	3666(3)	1785(1)	8643(2)	25(1)
C392	3533(3)	1179(1)	8631(2)	30(1)
C402	2490(3)	928(1)	8687(2)	33(1)
C412	1532(3)	1280(1)	8734(2)	31(1)
C422	1643(3)	1871(1)	8748(2)	27(1)
C432	2702(2)	2137(1)	8733(2)	21(1)
C442	2849(2)	2758(1)	8765(2)	22(1)
C452	1161(2)	4035(1)	9144(2)	23(1)
C512	252(2)	4245(1)	11619(2)	22(1)
C522	-274(2)	3857(1)	11077(2)	22(1)
C532	-175(2)	3267(1)	11184(2)	23(1)
N532	-613(2)	2890(1)	10594(1)	24(1)
C542	423(3)	3044(2)	11830(2)	31(1)
C552	900(3)	3410(2)	12365(2)	29(1)
C562	824(3)	4015(1)	12278(2)	28(1)
C572	1333(3)	4397(2)	12831(2)	31(1)
C582	1287(3)	4983(2)	12722(2)	34(1)

C592	765(3)	5210(2)	12055(2)	31(1)
C602	242(2)	4854(1)	11521(2)	25(1)
C612	-2073(2)	4327(1)	10522(2)	24(1)
C622	-971(2)	4095(1)	10411(2)	20(1)
C632	-583(2)	4109(1)	9708(2)	20(1)
N632	450(2)	3813(1)	9572(1)	20(1)
C642	-1216(3)	4364(1)	9094(2)	24(1)
C652	-2266(2)	4582(1)	9188(2)	25(1)
C662	-2728(2)	4570(1)	9898(2)	23(1)
C672	-3837(2)	4781(1)	10000(2)	28(1)
C682	-4263(3)	4768(1)	10692(2)	32(1)
C692	-3622(3)	4523(1)	11310(2)	31(1)
C702	-2556(2)	4311(1)	11228(2)	25(1)

Table 3. Bond lengths [Å] and angles [°] for complex **13**.

C(1S)-Cl(1)	1.759(4)	C(3B)-Cl(6B)	1.777(14)
C(1S)-Cl(2)	1.774(4)	C(3B)-H(3C)	0.9900
C(1S)-H(1A)	0.9900	C(3B)-H(3D)	0.9900
C(1S)-H(1B)	0.9900	Zn11-O1D1	1.96(2)
C(2S)-Cl(3)	1.743(5)	Zn11-N631	2.044(3)
C(2S)-Cl(4)	1.770(5)	Zn11-O1A1	2.046(3)
C(2S)-H(2A)	0.9900	Zn11-N111	2.067(2)
C(2S)-H(2B)	0.9900	Zn11-N311	2.167(2)
C(3A)-Cl(5A)	1.738(9)	Zn11-N531	2.222(3)
C(3A)-Cl(6A)	1.791(8)	S1A1-O1B1	1.425(2)
C(3A)-H(3A)	0.9900	S1A1-O1C1	1.446(2)
C(3A)-H(3B)	0.9900	S1A1-O1A1	1.476(3)
C(3B)-Cl(5B)	1.740(14)	S1A1-C1A1	1.827(4)

C1A1-F1A1	1.331(4)	C171-H171	0.9500
C1A1-F1C1	1.335(4)	C181-C191	1.409(5)
C1A1-F1B1	1.353(5)	C181-C231	1.435(4)
S1B1-O1F1	1.406(17)	C191-C201	1.362(6)
S1B1-O1E1	1.43(2)	C191-H191	0.9500
S1B1-O1D1	1.456(16)	C201-C211	1.402(5)
S1B1-C1B1	1.82(2)	C201-H201	0.9500
C1B1-F1F1	1.327(18)	C211-C221	1.369(5)
C1B1-F1E1	1.349(18)	C211-H211	0.9500
C1B1-F1D1	1.356(18)	C221-C231	1.412(4)
S21-O2C1	1.431(3)	C221-H221	0.9500
S21-O2B1	1.433(2)	C231-C241	1.432(4)
S21-O2A1	1.436(3)	C251-N531	1.471(4)
S21-C21	1.827(4)	C251-H25A1	0.9900
C21-F2B1	1.301(5)	C251-H25B1	0.9900
C21-F2C1	1.340(4)	N311-C321	1.361(4)
C21-F2A1	1.351(5)	N311-C441	1.367(4)
N111-C121	1.336(4)	C321-C331	1.395(4)
N111-C241	1.376(4)	C321-C451	1.459(4)
C121-C131	1.404(4)	C331-C341	1.367(5)
C121-C251	1.517(4)	C331-H331	0.9500
C131-C141	1.372(5)	C341-C351	1.406(5)
C131-H131	0.9500	C341-H341	0.9500
C141-C151	1.419(5)	C351-C441	1.427(4)
C141-H141	0.9500	C351-C361	1.432(5)
C151-C241	1.407(4)	C361-C371	1.347(5)
C151-C161	1.435(4)	C361-H361	0.9500
C161-C171	1.343(5)	C371-C381	1.441(5)
C161-H161	0.9500	C371-H371	0.9500
C171-C181	1.418(5)	C381-C391	1.411(5)

C381-C431	1.419(4)	C591-H591	0.9500
C391-C401	1.372(5)	C601-H601	0.9500
C391-H391	0.9500	C611-C661	1.426(4)
C401-C411	1.406(5)	C611-C701	1.430(4)
C401-H401	0.9500	C611-C621	1.434(4)
C411-C421	1.377(5)	C621-C631	1.371(4)
C411-H411	0.9500	C631-C641	1.430(4)
C421-C431	1.406(4)	C631-N631	1.431(4)
C421-H421	0.9500	C641-C651	1.348(5)
C431-C441	1.462(4)	C641-H641	0.9500
C451-N631	1.296(4)	C651-C661	1.425(5)
C451-H451	0.9500	C651-H651	0.9500
C511-C561	1.406(4)	C661-C671	1.415(4)
C511-C521	1.432(4)	C671-C681	1.366(5)
C511-C601	1.437(4)	C671-H671	0.9500
C521-C531	1.386(4)	C681-C691	1.394(5)
C521-C621	1.493(4)	C681-H681	0.9500
C531-C541	1.415(4)	C691-C701	1.364(4)
C531-N531	1.431(4)	C691-H691	0.9500
N531-H531	0.82(3)	C701-H701	0.9500
C541-C551	1.360(4)	Zn22-O3A2	2.029(2)
C541-H541	0.9500	Zn22-N632	2.056(2)
C551-C561	1.422(4)	Zn22-N112	2.058(2)
C551-H551	0.9500	Zn22-N312	2.159(2)
C561-C571	1.431(4)	Zn22-N532	2.256(2)
C571-C581	1.355(5)	S32-O3C2	1.428(2)
C571-H571	0.9500	S32-O3B2	1.430(2)
C581-C591	1.411(5)	S32-O3A2	1.473(2)
C581-H581	0.9500	S32-C32	1.828(3)
C591-C601	1.360(4)	C32-F3B2	1.321(4)

C32-F3C2	1.322(4)	C212-H212	0.9500
C32-F3A2	1.337(4)	C222-C232	1.417(4)
S42-O4B2	1.424(3)	C222-H222	0.9500
S42-O4A2	1.431(3)	C232-C242	1.449(4)
S42-O4C2	1.435(2)	C252-N532	1.465(4)
S42-C42	1.821(4)	C252-H25A2	0.9900
C42-F4B2	1.312(5)	C252-H25B2	0.9900
C42-F4C2	1.339(4)	N312-C322	1.348(4)
C42-F4A2	1.347(4)	N312-C442	1.365(4)
N112-C122	1.337(4)	C322-C332	1.399(4)
N112-C242	1.374(4)	C322-C452	1.476(4)
C122-C132	1.398(4)	C332-C342	1.373(4)
C122-C252	1.521(4)	C332-H332	0.9500
C132-C142	1.374(5)	C342-C352	1.409(5)
C132-H132	0.9500	C342-H342	0.9500
C142-C152	1.406(5)	C352-C442	1.426(4)
C142-H142	0.9500	C352-C362	1.443(4)
C152-C242	1.406(4)	C362-C372	1.343(5)
C152-C162	1.439(4)	C362-H362	0.9500
C162-C172	1.347(5)	C372-C382	1.439(4)
C162-H162	0.9500	C372-H372	0.9500
C172-C182	1.438(5)	C382-C392	1.409(4)
C172-H172	0.9500	C382-C432	1.422(4)
C182-C232	1.406(4)	C392-C402	1.375(5)
C182-C192	1.417(5)	C392-H392	0.9500
C192-C202	1.361(5)	C402-C412	1.403(4)
C192-H192	0.9500	C402-H402	0.9500
C202-C212	1.407(5)	C412-C422	1.373(4)
C202-H202	0.9500	C412-H412	0.9500
C212-C222	1.383(4)	C422-C432	1.399(4)

C422-H422	0.9500	C642-C652	1.364(4)
C432-C442	1.447(4)	C642-H642	0.9500
C452-N632	1.283(4)	C652-C662	1.416(4)
C452-H452	0.9500	C652-H652	0.9500
C512-C562	1.417(4)	C662-C672	1.425(4)
C512-C602	1.419(4)	C672-C682	1.367(5)
C512-C522	1.428(4)	C672-H672	0.9500
C522-C532	1.381(4)	C682-C692	1.412(5)
C522-C622	1.500(4)	C682-H682	0.9500
C532-C542	1.407(4)	C692-C702	1.371(4)
C532-N532	1.434(4)	C692-H692	0.9500
N532-H532	0.82(3)	C702-H702	0.9500
C542-C552	1.366(5)		
C542-H542	0.9500	Cl(1)-C(1S)-Cl(2)	110.3(2)
C552-C562	1.410(5)	Cl(1)-C(1S)-H(1A)	109.6
C552-H552	0.9500	Cl(2)-C(1S)-H(1A)	109.6
C562-C572	1.425(4)	Cl(1)-C(1S)-H(1B)	109.6
C572-C582	1.369(5)	Cl(2)-C(1S)-H(1B)	109.6
C572-H572	0.9500	H(1A)-C(1S)-H(1B)	108.1
C582-C592	1.402(5)	Cl(3)-C(2S)-Cl(4)	111.4(3)
C582-H582	0.9500	Cl(3)-C(2S)-H(2A)	109.3
C592-C602	1.373(4)	Cl(4)-C(2S)-H(2A)	109.3
C592-H592	0.9500	Cl(3)-C(2S)-H(2B)	109.3
C602-H602	0.9500	Cl(4)-C(2S)-H(2B)	109.3
C612-C702	1.422(4)	H(2A)-C(2S)-H(2B)	108.0
C612-C662	1.425(4)	Cl(5A)-C(3A)-Cl(6A)	112.8(7)
C612-C622	1.438(4)	Cl(5A)-C(3A)-H(3A)	109.0
C622-C632	1.367(4)	Cl(6A)-C(3A)-H(3A)	109.0
C632-C642	1.410(4)	Cl(5A)-C(3A)-H(3B)	109.0
C632-N632	1.438(4)	Cl(6A)-C(3A)-H(3B)	109.0

H(3A)-C(3A)-H(3B)	107.8	F1A1-C1A1-F1B1	106.6(4)
Cl(5B)-C(3B)-Cl(6B)	111.5(13)	F1C1-C1A1-F1B1	107.5(3)
Cl(5B)-C(3B)-H(3C)	109.3	F1A1-C1A1-S1A1	111.8(2)
Cl(6B)-C(3B)-H(3C)	109.3	F1C1-C1A1-S1A1	111.0(3)
Cl(5B)-C(3B)-H(3D)	109.3	F1B1-C1A1-S1A1	110.7(3)
Cl(6B)-C(3B)-H(3D)	109.3	O1F1-S1B1-O1E1	111(3)
H(3C)-C(3B)-H(3D)	108.0	O1F1-S1B1-O1D1	113.1(19)
O1D1-Zn11-N631	98.5(7)	O1E1-S1B1-O1D1	118(3)
O1D1-Zn11-O1A1	12.9(6)	O1F1-S1B1-C1B1	106.6(12)
N631-Zn11-O1A1	109.08(12)	O1E1-S1B1-C1B1	104.4(16)
O1D1-Zn11-N111	121.1(7)	O1D1-S1B1-C1B1	102.2(11)
N631-Zn11-N111	139.48(9)	S1B1-O1D1-Zn11	136.6(17)
O1A1-Zn11-N111	109.29(12)	F1F1-C1B1-F1E1	110(2)
O1D1-Zn11-N311	90.3(7)	F1F1-C1B1-F1D1	108(2)
N631-Zn11-N311	82.09(10)	F1E1-C1B1-F1D1	108(2)
O1A1-Zn11-N311	98.95(11)	F1F1-C1B1-S1B1	111.0(16)
N111-Zn11-N311	104.25(10)	F1E1-C1B1-S1B1	109.4(14)
O1D1-Zn11-N531	94.7(8)	F1D1-C1B1-S1B1	110.9(13)
N631-Zn11-N531	93.86(10)	O2C1-S21-O2B1	116.40(17)
O1A1-Zn11-N531	86.59(11)	O2C1-S21-O2A1	114.16(16)
N111-Zn11-N531	75.93(9)	O2B1-S21-O2A1	114.84(17)
N311-Zn11-N531	173.96(9)	O2C1-S21-C21	103.12(18)
O1B1-S1A1-O1C1	117.46(16)	O2B1-S21-C21	103.23(16)
O1B1-S1A1-O1A1	113.52(19)	O2A1-S21-C21	102.47(19)
O1C1-S1A1-O1A1	112.21(16)	F2B1-C21-F2C1	107.5(3)
O1B1-S1A1-C1A1	105.93(15)	F2B1-C21-F2A1	107.4(3)
O1C1-S1A1-C1A1	104.90(16)	F2C1-C21-F2A1	107.8(4)
O1A1-S1A1-C1A1	100.72(19)	F2B1-C21-S21	113.2(3)
S1A1-O1A1-Zn11	129.8(2)	F2C1-C21-S21	110.4(3)
F1A1-C1A1-F1C1	109.1(3)	F2A1-C21-S21	110.3(3)

C121-N111-C241	120.5(3)	C121-N111-Zn11	107.11(18)
C241-N111-Zn11	126.82(19)	N111-C121-C131	122.1(3)
N111-C121-C251	117.4(3)	C131-C121-C251	120.5(3)
C141-C131-C121	118.4(3)	C141-C131-H131	120.8
C121-C131-H131	120.8	C131-C141-C151	120.3(3)
C131-C141-H141	119.8	C151-C141-H141	119.8
C241-C151-C141	118.5(3)	C241-C151-C161	119.6(3)
C141-C151-C161	121.9(3)	C171-C161-C151	120.1(3)
C171-C161-H161	120.0	C151-C161-H161	120.0
C161-C171-C181	122.0(3)	C161-C171-H171	119.0
C181-C171-H171	119.0	C191-C181-C171	121.9(3)
C191-C181-C231	118.3(3)	C171-C181-C231	119.7(3)
C201-C191-C181	121.7(3)	C201-C191-H191	119.2
C181-C191-H191	119.2	C191-C201-C211	119.9(3)
C191-C201-H201	120.0	C211-C201-H201	120.0
C221-C211-C201	120.5(4)	C221-C211-H211	119.7
C201-C211-H211	119.7	C211-C221-C231	121.0(3)
C211-C221-H221	119.5	C231-C221-H221	119.5
C221-C231-C241	124.0(3)	C221-C231-C181	118.3(3)
C241-C231-C181	117.6(3)	N111-C241-C151	119.5(3)
N111-C241-C231	120.1(3)	C151-C241-C231	120.4(3)
N531-C251-C121	109.8(2)	N531-C251-H25A1	109.7
C121-C251-H25A1	109.7	N531-C251-H25B1	109.7
C121-C251-H25B1	109.7	H25A1-C251-H25B1	108.2
C321-N311-C441	118.3(3)	C321-N311-Zn11	106.67(19)
C441-N311-Zn11	132.3(2)	N311-C321-C331	123.3(3)
N311-C321-C451	117.4(3)	C331-C321-C451	119.2(3)
C341-C331-C321	118.5(3)	C341-C331-H331	120.8
C321-C331-H331	120.8	C331-C341-C351	120.2(3)
C331-C341-H341	119.9	C351-C341-H341	119.9

C341-C351-C441	118.4(3)	C341-C351-C361	121.4(3)
C441-C351-C361	120.2(3)	C371-C361-C351	120.5(3)
C371-C361-H361	119.8	C351-C361-H361	119.8
C361-C371-C381	121.4(3)	C361-C371-H371	119.3
C381-C371-H371	119.3	C391-C381-C431	118.9(3)
C391-C381-C371	121.0(3)	C431-C381-C371	120.0(3)
C401-C391-C381	121.3(3)	C401-C391-H391	119.4
C381-C391-H391	119.4	C391-C401-C411	119.7(3)
C391-C401-H401	120.1	C411-C401-H401	120.1
C421-C411-C401	120.0(3)	C421-C411-H411	120.0
C401-C411-H411	120.0	C411-C421-C431	121.3(3)
C411-C421-H421	119.3	C431-C421-H421	119.3
C421-C431-C381	118.6(3)	C421-C431-C441	123.1(3)
C381-C431-C441	118.3(3)	N311-C441-C351	120.5(3)
N311-C441-C431	120.8(3)	C351-C441-C431	118.7(3)
N631-C451-C321	120.8(3)	N631-C451-H451	119.6
C321-C451-H451	119.6	C561-C511-C521	120.3(3)
C561-C511-C601	118.3(3)	C521-C511-C601	121.4(3)
C531-C521-C511	118.9(3)	C531-C521-C621	121.9(2)
C511-C521-C621	119.0(3)	C521-C531-C541	120.5(3)
C521-C531-N531	118.6(3)	C541-C531-N531	120.9(3)
C531-N531-C251	118.5(2)	C531-N531-Zn11	106.17(17)
C251-N531-Zn11	100.40(18)	C531-N531-H531	110(2)
C251-N531-H531	113(3)	Zn11-N531-H531	107(2)
C551-C541-C531	120.6(3)	C551-C541-H541	119.7
C531-C541-H541	119.7	C541-C551-C561	121.0(3)
C541-C551-H551	119.5	C561-C551-H551	119.5
C511-C561-C551	118.7(3)	C511-C561-C571	119.6(3)
C551-C561-C571	121.7(3)	C581-C571-C561	120.6(3)
C581-C571-H571	119.7	C561-C571-H571	119.7

C571-C581-C591	120.0(3)	C571-C581-H581	120.0
C591-C581-H581	120.0	C601-C591-C581	121.2(3)
C601-C591-H591	119.4	C581-C591-H591	119.4
C591-C601-C511	120.2(3)	C591-C601-H601	119.9
C511-C601-H601	119.9	C661-C611-C701	116.8(3)
C661-C611-C621	120.4(3)	C701-C611-C621	122.8(3)
C631-C621-C611	119.1(3)	C631-C621-C521	122.9(3)
C611-C621-C521	117.9(3)	C621-C631-C641	120.8(3)
C621-C631-N631	120.4(3)	C641-C631-N631	118.4(3)
C451-N631-C631	120.9(3)	C451-N631-Zn11	111.4(2)
C631-N631-Zn11	125.3(2)	C651-C641-C631	120.3(3)
C651-C641-H641	119.9	C631-C641-H641	119.9
C641-C651-C661	121.8(3)	C641-C651-H651	119.1
C661-C651-H651	119.1	C671-C661-C651	122.0(3)
C671-C661-C611	120.3(3)	C651-C661-C611	117.7(3)
C681-C671-C661	120.3(3)	C681-C671-H671	119.9
C661-C671-H671	119.9	C671-C681-C691	120.3(3)
C671-C681-H681	119.8	C691-C681-H681	119.8
C701-C691-C681	121.1(3)	C701-C691-H691	119.5
C681-C691-H691	119.5	C691-C701-C611	121.2(3)
C691-C701-H701	119.4	C611-C701-H701	119.4
O3A2-Zn22-N632	107.92(9)	O3A2-Zn22-N112	105.34(9)
N632-Zn22-N112	143.08(9)	O3A2-Zn22-N312	103.35(9)
N632-Zn22-N312	80.59(9)	N112-Zn22-N312	106.88(9)
O3A2-Zn22-N532	82.42(9)	N632-Zn22-N532	93.02(9)
N112-Zn22-N532	75.85(9)	N312-Zn22-N532	172.42(9)
O3C2-S32-O3B2	118.54(15)	O3C2-S32-O3A2	112.54(13)
O3B2-S32-O3A2	112.52(13)	O3C2-S32-C32	105.97(14)
O3B2-S32-C32	106.08(14)	O3A2-S32-C32	98.73(14)
S32-O3A2-Zn22	126.55(13)	F3B2-C32-F3C2	108.3(3)

F3B2-C32-F3A2	107.7(3)	F3C2-C32-F3A2	108.2(3)
F3B2-C32-S32	110.3(2)	F3C2-C32-S32	111.4(2)
F3A2-C32-S32	110.7(2)	O4B2-S42-O4A2	115.32(19)
O4B2-S42-O4C2	115.36(18)	O4A2-S42-O4C2	115.20(17)
O4B2-S42-C42	102.52(18)	O4A2-S42-C42	102.31(17)
O4C2-S42-C42	103.34(17)	F4B2-C42-F4C2	107.2(3)
F4B2-C42-F4A2	108.5(3)	F4C2-C42-F4A2	106.2(3)
F4B2-C42-S42	113.1(3)	F4C2-C42-S42	110.4(3)
F4A2-C42-S42	111.0(3)	C122-N112-C242	119.3(2)
C122-N112-Zn22	108.92(19)	C242-N112-Zn22	125.5(2)
N112-C122-C132	122.2(3)	N112-C122-C252	117.1(2)
C132-C122-C252	120.8(3)	C142-C132-C122	118.5(3)
C142-C132-H132	120.8	C122-C132-H132	120.8
C132-C142-C152	120.7(3)	C132-C142-H142	119.7
C152-C142-H142	119.7	C242-C152-C142	117.6(3)
C242-C152-C162	119.3(3)	C142-C152-C162	123.1(3)
C172-C162-C152	120.7(3)	C172-C162-H162	119.6
C152-C162-H162	119.6	C162-C172-C182	121.0(3)
C162-C172-H172	119.5	C182-C172-H172	119.5
C232-C182-C192	119.5(3)	C232-C182-C172	120.0(3)
C192-C182-C172	120.5(3)	C202-C192-C182	120.1(3)
C202-C192-H192	120.0	C182-C192-H192	120.0
C192-C202-C212	121.0(3)	C192-C202-H202	119.5
C212-C202-H202	119.5	C222-C212-C202	120.0(3)
C222-C212-H212	120.0	C202-C212-H212	120.0
C212-C222-C232	119.9(3)	C212-C222-H222	120.1
C232-C222-H222	120.1	C182-C232-C222	119.3(3)
C182-C232-C242	118.4(3)	C222-C232-C242	122.2(3)
N112-C242-C152	120.8(3)	N112-C242-C232	119.4(3)
C152-C242-C232	119.8(3)	N532-C252-C122	110.8(2)

254

N532-C252-H25A2	109.5	C122-C252-H25A2	109.5
N532-C252-H25B2	109.5	C122-C252-H25B2	109.5
H25A2-C252-H25B2	108.1	C322-N312-C442	118.1(2)
C322-N312-Zn22	107.99(18)	C442-N312-Zn22	130.37(19)
N312-C322-C332	124.2(3)	N312-C322-C452	115.9(2)
C332-C322-C452	119.9(3)	C342-C332-C322	117.8(3)
C342-C332-H332	121.1	C322-C332-H332	121.1
C332-C342-C352	119.9(3)	C332-C342-H342	120.0
C352-C342-H342	120.0	C342-C352-C442	118.6(3)
C342-C352-C362	122.1(3)	C442-C352-C362	119.3(3)
C372-C362-C352	120.6(3)	C372-C362-H362	119.7
C352-C362-H362	119.7	C362-C372-C382	121.6(3)
C362-C372-H372	119.2	C382-C372-H372	119.2
C392-C382-C432	118.8(3)	C392-C382-C372	121.6(3)
C432-C382-C372	119.6(3)	C402-C392-C382	121.2(3)
C402-C392-H392	119.4	C382-C392-H392	119.4
C392-C402-C412	119.6(3)	C392-C402-H402	120.2
C412-C402-H402	120.2	C422-C412-C402	120.0(3)
C422-C412-H412	120.0	C402-C412-H412	120.0
C412-C422-C432	121.6(3)	C412-C422-H422	119.2
C432-C422-H422	119.2	C422-C432-C382	118.5(3)
C422-C432-C442	122.8(3)	C382-C432-C442	118.6(3)
N312-C442-C352	120.5(3)	N312-C442-C432	120.1(3)
C352-C442-C432	119.3(3)	N632-C452-C322	119.4(3)
N632-C452-H452	120.3	C322-C452-H452	120.3
C562-C512-C602	118.2(3)	C562-C512-C522	119.0(3)
C602-C512-C522	122.8(3)	C532-C522-C512	119.9(3)
C532-C522-C622	120.5(3)	C512-C522-C622	119.5(3)
C522-C532-C542	120.5(3)	C522-C532-N532	118.5(3)
C542-C532-N532	120.8(3)	C532-N532-C252	119.5(2)

C532-N532-Zn22	103.60(17)	C252-N532-Zn22	101.57(18)
C532-N532-H532	109(2)	C252-N532-H532	116(3)
Zn22-N532-H532	106(2)	C552-C542-C532	120.2(3)
C552-C542-H542	119.9	C532-C542-H542	119.9
C542-C552-C562	121.3(3)	C542-C552-H552	119.4
C562-C552-H552	119.4	C552-C562-C512	119.0(3)
C552-C562-C572	121.3(3)	C512-C562-C572	119.7(3)
C582-C572-C562	120.3(3)	C582-C572-H572	119.8
C562-C572-H572	119.8	C572-C582-C592	120.1(3)
C572-C582-H582	119.9	C592-C582-H582	119.9
C602-C592-C582	120.8(3)	C602-C592-H592	119.6
C582-C592-H592	119.6	C592-C602-C512	120.8(3)
C592-C602-H602	119.6	C512-C602-H602	119.6
C702-C612-C662	118.1(3)	C702-C612-C622	122.7(3)
C662-C612-C622	119.2(3)	C632-C622-C612	119.1(2)
C632-C622-C522	122.2(2)	C612-C622-C522	118.7(2)
C622-C632-C642	121.8(3)	C622-C632-N632	119.4(2)
C642-C632-N632	118.5(3)	C452-N632-C632	120.9(2)
C452-N632-Zn22	112.75(19)	C632-N632-Zn22	123.71(18)
C652-C642-C632	119.8(3)	C652-C642-H642	120.1
C632-C642-H642	120.1	C642-C652-C662	121.1(3)
C642-C652-H652	119.4	C662-C652-H652	119.4
C652-C662-C612	118.9(3)	C652-C662-C672	121.8(3)
C612-C662-C672	119.3(3)	C682-C672-C662	120.8(3)
C682-C672-H672	119.6	C662-C672-H672	119.6
C672-C682-C692	120.1(3)	C672-C682-H682	120.0
C692-C682-H682	120.0	C702-C692-C682	120.4(3)
C702-C692-H692	119.8	C682-C692-H692	119.8

Symmetry transformations used to generate equivalent atoms:

Table 4. Anisotropic displacement parameters ($\mathring{A}^2$ x 10^3) for complex **13**. The anisotropic displacement factor exponent takes the following form: $-2\pi^2[\,h^2\,a^{*2}U^{11} + ... \ + 2\,h\,k\,a^*\,b^*\,U^{12}\,]$

	U^{11}	U^{22}	U^{33}	U^{23}	U^{13}	U^{12}
C(1S)	52(2)	44(2)	42(2)	-2(2)	7(2)	-7(2)
Cl(1)	136(1)	30(1)	51(1)	0(1)	-11(1)	0(1)
Cl(2)	49(1)	33(1)	54(1)	1(1)	4(1)	-1(1)
C(2S)	60(3)	68(3)	38(2)	-10(2)	3(2)	3(2)
Cl(3)	118(1)	90(1)	40(1)	10(1)	-4(1)	-31(1)
Cl(4)	116(1)	124(1)	62(1)	-46(1)	0(1)	45(1)
C(3A)	46(5)	36(4)	43(4)	0(3)	19(3)	8(3)
Cl(5A)	100(2)	149(3)	59(2)	32(2)	21(1)	70(2)
Cl(6A)	60(1)	50(2)	51(2)	-23(1)	22(2)	-14(1)
C(3B)	70(20)	50(13)	80(20)	-8(11)	43(13)	-7(11)
Cl(5B)	100(2)	149(3)	59(2)	32(2)	21(1)	70(2)
Cl(6B)	60(1)	50(2)	51(2)	-23(1)	22(2)	-14(1)
Zn11	24(1)	19(1)	24(1)	1(1)	2(1)	0(1)
S1A1	20(1)	24(1)	23(1)	2(1)	1(1)	2(1)
O1A1	22(1)	25(2)	28(1)	2(1)	0(1)	0(1)
O1B1	28(1)	30(2)	32(1)	0(1)	-2(1)	9(1)
O1C1	22(1)	31(1)	28(1)	7(1)	4(1)	3(1)
C1A1	30(2)	24(2)	27(2)	2(1)	-2(1)	2(2)
F1A1	34(1)	36(1)	26(1)	4(1)	7(1)	2(1)
F1B1	45(2)	30(2)	30(2)	0(1)	3(2)	17(1)
F1C1	36(1)	31(1)	37(1)	-2(1)	-4(1)	-9(1)
S21	28(1)	26(1)	34(1)	-5(1)	5(1)	-5(1)
O2A1	45(2)	42(2)	50(2)	-2(1)	-5(1)	0(1)
O2B1	38(1)	57(2)	45(1)	-3(1)	12(1)	-22(1)
O2C1	49(2)	27(1)	60(2)	-4(1)	8(1)	2(1)

C21	54(3)	54(3)	46(2)	-8(2)	14(2)	-24(2)
F2A1	106(2)	50(2)	71(2)	-27(1)	37(2)	-18(2)
F2B1	83(2)	116(3)	40(1)	10(2)	-15(1)	-37(2)
F2C1	67(2)	77(2)	59(1)	-16(1)	33(1)	-33(1)
N111	24(1)	20(1)	23(1)	3(1)	3(1)	1(1)
C121	27(1)	22(2)	25(1)	2(1)	-1(1)	4(1)
C131	34(2)	20(2)	33(2)	-1(1)	5(1)	5(1)
C141	41(2)	22(2)	37(2)	-2(1)	3(1)	-2(1)
C151	34(2)	30(2)	25(1)	4(1)	1(1)	-8(1)
C161	33(2)	38(2)	34(2)	-2(2)	2(1)	-14(2)
C171	27(2)	55(2)	35(2)	4(2)	3(1)	-13(2)
C181	29(2)	44(2)	25(1)	5(1)	0(1)	-1(2)
C191	21(2)	59(3)	42(2)	9(2)	6(1)	5(2)
C201	35(2)	54(3)	43(2)	13(2)	8(2)	17(2)
C211	42(2)	38(2)	34(2)	11(2)	8(2)	18(2)
C221	26(2)	35(2)	25(1)	5(1)	3(1)	7(1)
C231	23(1)	31(2)	19(1)	4(1)	2(1)	2(1)
C241	22(1)	26(2)	24(1)	1(1)	1(1)	-3(1)
C251	25(1)	18(2)	32(1)	1(1)	4(1)	7(1)
N311	30(1)	23(1)	20(1)	2(1)	4(1)	0(1)
C321	34(2)	23(2)	23(1)	1(1)	4(1)	4(1)
C331	44(2)	29(2)	35(2)	-1(1)	11(1)	8(2)
C341	40(2)	42(2)	37(2)	4(2)	18(2)	11(2)
C351	40(2)	35(2)	26(2)	2(1)	10(1)	1(2)
C361	36(2)	48(2)	44(2)	6(2)	18(2)	3(2)
C371	34(2)	47(2)	37(2)	6(2)	14(1)	-6(2)
C381	33(2)	38(2)	28(2)	5(1)	4(1)	-4(1)
C391	40(2)	38(2)	32(2)	6(2)	5(1)	-14(2)
C401	46(2)	27(2)	37(2)	7(1)	4(2)	-6(2)
C411	39(2)	29(2)	33(2)	9(1)	-1(1)	2(1)

C421	30(2)	25(2)	28(1)	7(1)	-2(1)	-2(1)
C431	28(2)	27(2)	22(1)	6(1)	3(1)	-2(1)
C441	29(2)	30(2)	21(1)	0(1)	3(1)	-2(1)
C451	32(2)	23(2)	28(1)	1(1)	2(1)	2(1)
C511	20(1)	23(2)	22(1)	2(1)	5(1)	2(1)
C521	19(1)	21(1)	24(1)	-1(1)	4(1)	2(1)
C531	20(1)	22(1)	24(1)	3(1)	5(1)	3(1)
N531	21(1)	20(1)	28(1)	1(1)	1(1)	0(1)
C541	21(1)	22(2)	30(1)	-2(1)	6(1)	-2(1)
C551	21(1)	27(2)	26(1)	-3(1)	2(1)	-2(1)
C561	19(1)	26(2)	27(1)	3(1)	6(1)	1(1)
C571	20(1)	38(2)	25(1)	1(1)	2(1)	3(1)
C581	27(2)	34(2)	30(2)	13(1)	0(1)	5(1)
C591	30(2)	23(2)	36(2)	8(1)	8(1)	4(1)
C601	21(1)	25(2)	28(1)	4(1)	6(1)	1(1)
C611	23(1)	15(1)	32(2)	3(1)	0(1)	3(1)
C621	23(1)	17(1)	27(1)	1(1)	1(1)	0(1)
C631	24(1)	17(1)	30(1)	2(1)	1(1)	2(1)
N631	30(1)	20(1)	22(1)	5(1)	0(1)	-2(1)
C641	38(2)	17(1)	28(1)	3(1)	-2(1)	0(1)
C651	32(2)	19(2)	40(2)	-1(1)	-9(1)	2(1)
C661	26(2)	16(1)	40(2)	1(1)	-4(1)	2(1)
C671	23(2)	22(2)	53(2)	-3(1)	-3(1)	-5(1)
C681	25(2)	27(2)	54(2)	1(2)	8(1)	-2(1)
C691	24(2)	36(2)	45(2)	0(2)	8(1)	0(1)
C701	22(1)	23(2)	36(2)	-1(1)	4(1)	-2(1)
Zn22	18(1)	15(1)	27(1)	2(1)	2(1)	1(1)
S32	18(1)	20(1)	28(1)	-1(1)	1(1)	-1(1)
O3A2	23(1)	24(1)	40(1)	-3(1)	-4(1)	2(1)
O3B2	39(1)	24(1)	32(1)	6(1)	3(1)	-3(1)

O3C2	22(1)	41(1)	40(1)	-6(1)	7(1)	0(1)
C32	27(2)	27(2)	37(2)	-5(1)	5(1)	-7(1)
F3A2	27(1)	49(1)	44(1)	-11(1)	-4(1)	-6(1)
F3B2	64(2)	29(1)	56(1)	7(1)	-4(1)	-21(1)
F3C2	36(1)	40(1)	60(1)	-24(1)	13(1)	-3(1)
S42	33(1)	21(1)	34(1)	0(1)	4(1)	-1(1)
O4A2	59(2)	37(2)	48(1)	12(1)	-18(1)	-20(1)
O4B2	47(2)	57(2)	65(2)	2(2)	18(1)	17(1)
O4C2	63(2)	20(1)	53(2)	4(1)	6(1)	6(1)
C42	47(2)	43(2)	40(2)	2(2)	0(2)	-4(2)
F4A2	77(2)	51(2)	52(1)	22(1)	-14(1)	-11(1)
F4B2	77(2)	97(2)	59(2)	7(2)	34(1)	18(2)
F4C2	94(2)	84(2)	46(1)	0(1)	-16(1)	-34(2)
N112	26(1)	16(1)	28(1)	1(1)	2(1)	3(1)
C122	32(2)	16(1)	27(1)	1(1)	4(1)	-1(1)
C132	34(2)	18(1)	38(2)	4(1)	4(1)	-2(1)
C142	43(2)	16(1)	32(2)	3(1)	1(1)	5(1)
C152	35(2)	20(2)	25(1)	-1(1)	-5(1)	8(1)
C162	41(2)	23(2)	33(2)	-2(1)	-4(1)	13(1)
C172	28(2)	33(2)	34(2)	-4(1)	-3(1)	11(1)
C182	28(2)	32(2)	23(1)	-5(1)	-2(1)	3(1)
C192	20(2)	44(2)	38(2)	-10(2)	1(1)	1(1)
C202	25(2)	38(2)	44(2)	-8(2)	3(1)	-5(2)
C212	29(2)	28(2)	38(2)	-8(1)	2(1)	-3(1)
C222	27(2)	22(2)	27(1)	-6(1)	0(1)	5(1)
C232	23(1)	24(2)	21(1)	-4(1)	-1(1)	1(1)
C242	24(1)	19(1)	23(1)	-2(1)	0(1)	5(1)
C252	30(2)	17(1)	36(2)	6(1)	9(1)	-3(1)
N312	21(1)	19(1)	22(1)	-1(1)	1(1)	1(1)
C322	20(1)	19(2)	27(1)	0(1)	2(1)	-3(1)

C332	31(2)	20(2)	31(2)	2(1)	11(1)	-4(1)
C342	29(2)	31(2)	35(2)	1(1)	13(1)	-2(1)
C352	23(1)	27(2)	26(1)	0(1)	7(1)	-1(1)
C362	22(2)	35(2)	33(2)	-3(1)	10(1)	3(1)
C372	21(1)	29(2)	34(2)	-6(1)	7(1)	7(1)
C382	26(2)	24(2)	24(1)	-2(1)	4(1)	4(1)
C392	28(2)	26(2)	38(2)	-4(1)	5(1)	8(1)
C402	36(2)	20(2)	42(2)	-7(1)	2(1)	0(1)
C412	28(2)	24(2)	42(2)	-9(1)	2(1)	0(1)
C422	23(2)	23(2)	34(2)	-6(1)	-1(1)	3(1)
C432	22(1)	19(1)	21(1)	-4(1)	2(1)	3(1)
C442	21(1)	24(1)	21(1)	-1(1)	3(1)	1(1)
C452	26(2)	16(1)	29(1)	0(1)	2(1)	2(1)
C512	15(1)	24(2)	27(1)	0(1)	7(1)	1(1)
C522	19(1)	21(2)	27(1)	1(1)	5(1)	2(1)
C532	20(1)	23(2)	26(1)	2(1)	6(1)	0(1)
N532	20(1)	17(1)	34(1)	4(1)	4(1)	-1(1)
C542	31(2)	27(2)	34(2)	4(1)	7(1)	6(1)
C552	27(2)	35(2)	25(1)	6(1)	2(1)	4(1)
C562	24(2)	34(2)	25(1)	0(1)	7(1)	3(1)
C572	23(2)	43(2)	27(1)	-4(1)	0(1)	0(1)
C582	25(2)	42(2)	34(2)	-12(2)	3(1)	-2(1)
C592	22(2)	31(2)	39(2)	-10(1)	2(1)	-2(1)
C602	21(1)	25(2)	31(1)	-2(1)	3(1)	1(1)
C612	21(1)	16(1)	33(2)	-6(1)	5(1)	-4(1)
C622	19(1)	13(1)	28(1)	-2(1)	1(1)	1(1)
C632	18(1)	14(1)	30(1)	-2(1)	1(1)	-1(1)
N632	20(1)	16(1)	25(1)	1(1)	2(1)	3(1)
C642	28(2)	15(1)	29(1)	0(1)	4(1)	0(1)
C652	22(1)	17(1)	36(2)	-1(1)	-4(1)	3(1)

C662	21(1)	14(1)	35(2)	0(1)	0(1)	-1(1)
C672	21(1)	17(1)	46(2)	-3(1)	-1(1)	1(1)
C682	18(1)	24(2)	53(2)	-8(1)	4(1)	3(1)
C692	28(2)	28(2)	40(2)	-11(1)	11(1)	-6(1)
C702	22(1)	20(1)	34(2)	-5(1)	4(1)	-4(1)

Table 5. Hydrogen coordinates (x 10^4) and isotropic displacement parameters (Å^2 x 10^3) for complex **13**.

	x	y	z	U(eq)
H(1A)	10622	6090	7647	55
H(1B)	10482	5973	6759	55
H(2A)	4292	6511	7100	67
H(2B)	4432	6458	7997	67
H(3A)	721	7816	6827	49
H(3B)	1720	7692	6292	49
H(3C)	1020	7743	7122	79
H(3D)	1991	7555	6592	79
H131	4948	1951	4238	35
H141	3125	1630	4434	40
H161	1107	1860	4695	42
H171	-215	2526	4975	47
H191	-801	3544	5133	49
H201	-415	4518	5103	53
H211	1398	4841	4848	45
H221	2819	4187	4652	34

H25A1	6372	2869	4776	30
H25B1	6043	2910	3889	30
H331	2683	5277	6691	43
H341	1167	4747	7090	47
H361	194	3799	7210	50
H371	190	2817	7067	47
H391	1231	1904	6876	44
H401	2859	1415	6606	44
H411	4510	1939	6381	40
H421	4471	2940	6354	34
H451	4439	5310	6013	33
H531	6440(30)	3800(16)	4572(18)	28
H541	4638	3300	3210	29
H551	3782	3828	2235	29
H571	3278	4785	1640	33
H581	3340	5779	1680	36
H591	4271	6253	2715	36
H601	5218	5739	3668	29
H641	6430	5345	6163	33
H651	8078	5729	5797	37
H671	9445	5894	4815	40
H681	9934	5769	3595	42
H691	8746	5257	2730	42
H701	7074	4866	3069	33
H132	72	1172	10997	36
H142	1872	783	10899	37
H162	3958	938	10714	40
H172	5390	1556	10466	38
H192	6119	2556	10351	41
H202	5822	3540	10361	42

H212	4015	3921	10519	38
H222	2485	3301	10645	31
H25A2	-1196	2084	10350	33
H25B2	-939	2195	11233	33
H332	3087	4357	8577	32
H342	4666	3781	8385	37
H362	5559	2789	8381	35
H372	5395	1814	8520	34
H392	4175	940	8583	36
H402	2418	519	8695	39
H412	805	1109	8755	38
H422	986	2104	8769	32
H452	1074	4424	8977	28
H532	-1190(30)	3034(16)	10390(18)	28
H542	495	2638	11896	37
H552	1290	3254	12803	35
H572	1707	4245	13277	37
H582	1609	5236	13099	40
H592	774	5616	11972	37
H602	-131	5017	11081	30
H642	-911	4383	8616	29
H652	-2694	4746	8770	30
H672	-4285	4933	9583	34
H682	-4991	4924	10757	38
H692	-3930	4504	11787	38
H702	-2133	4150	11650	30

Table 6. Torsion angles [°] for complex **13**.

O1B1-S1A1-O1A1-Zn11	-155.6(2)	O1C1-S1A1-O1A1-Zn11	-19.5(3)
C1A1-S1A1-O1A1-Zn11	91.6(3)	O1D1-Zn11-O1A1-S1A1	-66(4)
N631-Zn11-O1A1-S1A1	-30.3(3)	N111-Zn11-O1A1-S1A1	136.4(3)
N311-Zn11-O1A1-S1A1	-115.0(3)	N531-Zn11-O1A1-S1A1	62.6(3)
O1B1-S1A1-C1A1-F1A1	-55.5(3)	O1C1-S1A1-C1A1-F1A1	179.6(2)
O1A1-S1A1-C1A1-F1A1	63.0(3)	O1B1-S1A1-C1A1-F1C1	66.6(3)
O1C1-S1A1-C1A1-F1C1	-58.3(3)	O1A1-S1A1-C1A1-F1C1	174.9(2)
O1B1-S1A1-C1A1-F1B1	-174.1(3)	O1C1-S1A1-C1A1-F1B1	61.0(4)
O1A1-S1A1-C1A1-F1B1	-55.7(4)	O1F1-S1B1-O1D1-Zn11	128(2)
O1E1-S1B1-O1D1-Zn11	-4(4)	C1B1-S1B1-O1D1-Zn11	-118(2)
N631-Zn11-O1D1-S1B1	32(3)	O1A1-Zn11-O1D1-S1B1	178(6)
N111-Zn11-O1D1-S1B1	-157(2)	N311-Zn11-O1D1-S1B1	-50(3)
N531-Zn11-O1D1-S1B1	126(2)	O1F1-S1B1-C1B1-F1F1	-67(2)
O1E1-S1B1-C1B1-F1F1	50(4)	O1D1-S1B1-C1B1-F1F1	174(2)
O1F1-S1B1-C1B1-F1E1	172(2)	O1E1-S1B1-C1B1-F1E1	-71(4)
O1D1-S1B1-C1B1-F1E1	53(2)	O1F1-S1B1-C1B1-F1D1	53(2)
O1E1-S1B1-C1B1-F1D1	170(4)	O1D1-S1B1-C1B1-F1D1	65.8(19)
O2C1-S21-C21-F2B1	-62.9(3)	O2B1-S21-C21-F2B1	58.7(3)
O2A1-S21-C21-F2B1	178.3(3)	O2C1-S21-C21-F2C1	57.7(3)
O2B1-S21-C21-F2C1	179.3(3)	O2A1-S21-C21-F2C1	61.1(3)
O2C1-S21-C21-F2A1	176.8(3)	O2B1-S21-C21-F2A1	61.6(3)
O2A1-S21-C21-F2A1	58.0(3)	O1D1-Zn11-N111-C121	43.4(9)
N631-Zn11-N111-C121	122.8(2)	O1A1-Zn11-N111-C121	37.6(2)
N311-Zn11-N111-C121	-142.66(19)	N531-Zn11-N111-C121	43.57(18)
O1D1-Zn11-N111-C241	109.9(9)	N631-Zn11-N111-C241	83.9(3)
O1A1-Zn11-N111-C241	115.7(2)	N311-Zn11-N111-C241	10.7(2)
N531-Zn11-N111-C241	-163.1(2)	C241-N111-C121-C131	-7.1(4)
Zn11-N111-C121-C131	148.2(2)	C241-N111-C121-C251	170.8(2)

Zn11-N111-C121-C251	-33.9(3)	N111-C121-C131-C141	-0.4(4)
C251-C121-C131-C141	-178.2(3)	C121-C131-C141-C151	4.4(5)
C131-C141-C151-C241	-1.1(5)	C131-C141-C151-C161	179.0(3)
C241-C151-C161-C171	0.9(5)	C141-C151-C161-C171	-179.2(3)
C151-C161-C171-C181	3.5(5)	C161-C171-C181-C191	176.7(3)
C161-C171-C181-C231	-1.7(5)	C171-C181-C191-C201	-175.6(3)
C231-C181-C191-C201	2.9(5)	C181-C191-C201-C211	0.5(6)
C191-C201-C211-C221	-1.3(5)	C201-C211-C221-C231	-1.4(5)
C211-C221-C231-C241	-178.1(3)	C211-C221-C231-C181	4.7(5)
C191-C181-C231-C221	-5.4(4)	C171-C181-C231-C221	173.1(3)
C191-C181-C231-C241	177.3(3)	C171-C181-C231-C241	-4.3(4)
C121-N111-C241-C151	10.4(4)	Zn11-N111-C241-C151	-139.7(2)
C121-N111-C241-C231	-168.9(3)	Zn11-N111-C241-C231	41.0(3)
C141-C151-C241-N111	-6.3(4)	C161-C151-C241-N111	173.6(3)
C141-C151-C241-C231	173.0(3)	C161-C151-C241-C231	-7.0(4)
C221-C231-C241-N111	10.7(4)	C181-C231-C241-N111	-172.1(3)
C221-C231-C241-C151	-168.6(3)	C181-C231-C241-C151	8.6(4)
N111-C121-C251-N531	-6.8(3)	C131-C121-C251-N531	171.2(3)
O1D1-Zn11-N311-C321	105.9(8)	N631-Zn11-N311-C321	7.32(19)
O1A1-Zn11-N311-C321	115.5(2)	N111-Zn11-N311-C321	-131.84(19)
N531-Zn11-N311-C321	-40.9(10)	O1D1-Zn11-N311-C441	-93.8(8)
N631-Zn11-N311-C441	167.7(3)	O1A1-Zn11-N311-C441	-84.2(3)
N111-Zn11-N311-C441	28.5(3)	N531-Zn11-N311-C441	119.4(9)
C441-N311-C321-C331	1.2(4)	Zn11-N311-C321-C331	164.8(3)
C441-N311-C321-C451	-176.5(2)	Zn11-N311-C321-C451	-12.9(3)
N311-C321-C331-C341	-6.9(5)	C451-C321-C331-C341	170.7(3)
C321-C331-C341-C351	4.0(5)	C331-C341-C351-C441	4.0(5)
C331-C341-C351-C361	-175.6(3)	C341-C351-C361-C371	180.0(3)
C441-C351-C361-C371	0.4(5)	C351-C361-C371-C381	5.6(6)
C361-C371-C381-C391	174.1(3)	C361-C371-C381-C431	-3.4(5)

C431-C381-C391-C401	1.8(5)	C371-C381-C391-C401	-175.8(3)
C381-C391-C401-C411	1.7(5)	C391-C401-C411-C421	-2.4(5)
C401-C411-C421-C431	-0.4(5)	C411-C421-C431-C381	3.8(4)
C411-C421-C431-C441	-178.7(3)	C391-C381-C431-C421	-4.5(4)
C371-C381-C431-C421	173.1(3)	C391-C381-C431-C441	177.9(3)
C371-C381-C431-C441	-4.5(4)	C321-N311-C441-C351	7.2(4)
Zn11-N311-C441-C351	-151.3(2)	C321-N311-C441-C431	-174.8(3)
Zn11-N311-C441-C431	26.7(4)	C341-C351-C441-N311	-9.8(4)
C361-C351-C441-N311	169.8(3)	C341-C351-C441-C431	172.2(3)
C361-C351-C441-C431	-8.2(4)	C421-C431-C441-N311	14.6(4)
C381-C431-C441-N311	-167.9(3)	C421-C431-C441-C351	-167.4(3)
C381-C431-C441-C351	10.1(4)	N311-C321-C451-N631	14.6(4)
C331-C321-C451-N631	-163.2(3)	C561-C511-C521-C531	-3.6(4)
C601-C511-C521-C531	176.4(3)	C561-C511-C521-C621	171.7(3)
C601-C511-C521-C621	-8.3(4)	C511-C521-C531-C541	2.8(4)
C621-C521-C531-C541	-172.3(3)	C511-C521-C531-N531	-174.6(2)
C621-C521-C531-N531	10.3(4)	C521-C531-N531-C251	-174.3(3)
C541-C531-N531-C251	8.3(4)	C521-C531-N531-Zn11	73.9(3)
C541-C531-N531-Zn11	-103.5(3)	C121-C251-N531-C531	-75.6(3)
C121-C251-N531-Zn11	39.4(2)	O1D1-Zn11-N531-C531	-160.1(8)
N631-Zn11-N531-C531	-61.24(19)	O1A1-Zn11-N531-C531	-170.2(2)
N111-Zn11-N531-C531	78.98(19)	N311-Zn11-N531-C531	-13.5(10)
O1D1-Zn11-N531-C251	75.9(7)	N631-Zn11-N531-C251	174.81(17)
O1A1-Zn11-N531-C251	65.89(18)	N111-Zn11-N531-C251	-44.97(17)
N311-Zn11-N531-C251	-137.4(9)	C521-C531-C541-C551	-0.1(4)
N531-C531-C541-C551	177.3(3)	C531-C541-C551-C561	-2.0(4)
C521-C511-C561-C551	1.6(4)	C601-C511-C561-C551	-178.4(3)
C521-C511-C561-C571	-177.6(3)	C601-C511-C561-C571	2.4(4)
C541-C551-C561-C511	1.2(4)	C541-C551-C561-C571	-179.6(3)
C511-C561-C571-C581	-1.8(4)	C551-C561-C571-C581	179.0(3)

C561-C571-C581-C591	-0.3(5)	C571-C581-C591-C601	2.0(5)
C581-C591-C601-C511	-1.3(5)	C561-C511-C601-C591	-0.8(4)
C521-C511-C601-C591	179.2(3)	C661-C611-C621-C631	0.1(4)
C701-C611-C621-C631	178.7(3)	C661-C611-C621-C521	177.7(3)
C701-C611-C621-C521	-3.7(4)	C531-C521-C621-C631	-76.5(4)
C511-C521-C621-C631	108.4(3)	C531-C521-C621-C611	106.0(3)
C511-C521-C621-C611	-69.1(3)	C611-C621-C631-C641	0.9(4)
C521-C621-C631-C641	-176.5(3)	C611-C621-C631-N631	-172.2(3)
C521-C621-C631-N631	10.4(4)	C321-C451-N631-C631	-170.4(3)
C321-C451-N631-Zn11	-7.0(3)	C621-C631-N631-C451	-144.2(3)
C641-C631-N631-C451	42.6(4)	C621-C631-N631-Zn11	54.8(3)
C641-C631-N631-Zn11	-118.5(3)	O1D1-Zn11-N631-C451	-89.5(8)
O1A1-Zn11-N631-C451	-97.1(2)	N111-Zn11-N631-C451	102.4(2)
N311-Zn11-N631-C451	-0.3(2)	N531-Zn11-N631-C451	175.1(2)
O1D1-Zn11-N631-C631	73.0(8)	O1A1-Zn11-N631-C631	65.4(2)
N111-Zn11-N631-C631	-95.1(2)	N311-Zn11-N631-C631	162.2(2)
N531-Zn11-N631-C631	-22.3(2)	C621-C631-C641-C651	-1.3(4)
N631-C631-C641-C651	171.9(3)	C631-C641-C651-C661	0.7(5)
C641-C651-C661-C671	-179.0(3)	C641-C651-C661-C611	0.4(4)
C701-C611-C661-C671	0.0(4)	C621-C611-C661-C671	178.6(3)
C701-C611-C661-C651	-179.5(3)	C621-C611-C661-C651	-0.8(4)
C651-C661-C671-C681	179.6(3)	C611-C661-C671-C681	0.2(5)
C661-C671-C681-C691	-0.2(5)	C671-C681-C691-C701	-0.1(5)
C681-C691-C701-C611	0.3(5)	C661-C611-C701-C691	-0.2(4)
C621-C611-C701-C691	-178.8(3)	O3C2-S32-O3A2-Zn22	-80.8(2)
O3B2-S32-O3A2-Zn22	56.3(2)	C32-S32-O3A2-Zn22	167.80(17)
N632-Zn22-O3A2-S32	-7.84(19)	N112-Zn22-O3A2-S32	155.90(16)
N312-Zn22-O3A2-S32	-92.11(17)	N532-Zn22-O3A2-S32	82.90(17)
O3C2-S32-C32-F3B2	-57.8(3)	O3B2-S32-C32-F3B2	175.4(2)
O3A2-S32-C32-F3B2	58.8(2)	O3C2-S32-C32-F3C2	-178.1(2)

O3B2-S32-C32-F3C2	55.0(3)	O3A2-S32-C32-F3C2	61.6(2)
O3C2-S32-C32-F3A2	61.4(2)	O3B2-S32-C32-F3A2	65.4(2)
O3A2-S32-C32-F3A2	178.0(2)	O4B2-S42-C42-F4B2	178.7(3)
O4A2-S42-C42-F4B2	-61.5(3)	O4C2-S42-C42-F4B2	58.5(3)
O4B2-S42-C42-F4C2	58.5(3)	O4A2-S42-C42-F4C2	178.3(3)
O4C2-S42-C42-F4C2	-61.7(3)	O4B2-S42-C42-F4A2	-59.1(3)
O4A2-S42-C42-F4A2	60.7(3)	O4C2-S42-C42-F4A2	-179.3(3)
O3A2-Zn22-N112-C122	-35.8(2)	N632-Zn22-N112-C122	117.8(2)
N312-Zn22-N112-C122	-145.32(19)	N532-Zn22-N112-C122	42.02(19)
O3A2-Zn22-N112-C242	115.9(2)	N632-Zn22-N112-C242	-90.4(3)
N312-Zn22-N112-C242	6.5(2)	N532-Zn22-N112-C242	-166.2(2)
C242-N112-C122-C132	-7.8(4)	Zn22-N112-C122-C132	146.0(3)
C242-N112-C122-C252	171.5(3)	Zn22-N112-C122-C252	-34.7(3)
N112-C122-C132-C142	-0.3(5)	C252-C122-C132-C142	-179.6(3)
C122-C132-C142-C152	4.8(5)	C132-C142-C152-C242	-1.2(4)
C132-C142-C152-C162	179.1(3)	C242-C152-C162-C172	1.7(4)
C142-C152-C162-C172	-178.7(3)	C152-C162-C172-C182	4.3(5)
C162-C172-C182-C232	-2.9(5)	C162-C172-C182-C192	174.4(3)
C232-C182-C192-C202	2.5(5)	C172-C182-C192-C202	-174.8(3)
C182-C192-C202-C212	1.0(5)	C192-C202-C212-C222	-1.2(5)
C202-C212-C222-C232	-2.3(5)	C192-C182-C232-C222	-5.9(4)
C172-C182-C232-C222	171.4(3)	C192-C182-C232-C242	178.2(3)
C172-C182-C232-C242	-4.4(4)	C212-C222-C232-C182	5.8(4)
C212-C222-C232-C242	-178.5(3)	C122-N112-C242-C152	11.5(4)
Zn22-N112-C242-C152	-137.7(2)	C122-N112-C242-C232	-166.8(3)
Zn22-N112-C242-C232	44.1(3)	C142-C152-C242-N112	-7.0(4)
C162-C152-C242-N112	172.7(3)	C142-C152-C242-C232	171.3(3)
C162-C152-C242-C232	-9.1(4)	C182-C232-C242-N112	-171.4(3)
C222-C232-C242-N112	12.9(4)	C182-C232-C242-C152	10.4(4)
C222-C232-C242-C152	-165.4(3)	N112-C122-C252-N532	-3.9(4)

C132-C122-C252-N532	175.4(3)	O3A2-Zn22-N312-C322	118.39(18)
N632-Zn22-N312-C322	12.06(18)	N112-Zn22-N312-C322	-130.75(18)
N532-Zn22-N312-C322	-20.7(8)	O3A2-Zn22-N312-C442	-83.7(2)
N632-Zn22-N312-C442	170.0(2)	N112-Zn22-N312-C442	27.2(2)
N532-Zn22-N312-C442	137.2(6)	C442-N312-C322-C332	-0.6(4)
Zn22-N312-C322-C332	160.5(2)	C442-N312-C322-C452	179.6(2)
Zn22-N312-C322-C452	-19.3(3)	N312-C322-C332-C342	-6.2(4)
C452-C322-C332-C342	173.6(3)	C322-C332-C342-C352	5.3(5)
C332-C342-C352-C442	1.8(5)	C332-C342-C352-C362	-176.5(3)
C342-C352-C362-C372	-179.7(3)	C442-C352-C362-C372	2.1(4)
C352-C362-C372-C382	5.1(5)	C362-C372-C382-C392	173.7(3)
C362-C372-C382-C432	-4.4(4)	C432-C382-C392-C402	1.5(5)
C372-C382-C392-C402	-176.7(3)	C382-C392-C402-C412	2.0(5)
C392-C402-C412-C422	-2.2(5)	C402-C412-C422-C432	-1.3(5)
C412-C422-C432-C382	4.8(4)	C412-C422-C432-C442	-178.5(3)
C392-C382-C432-C422	-4.8(4)	C372-C382-C432-C422	173.4(3)
C392-C382-C432-C442	178.4(3)	C372-C382-C432-C442	-3.4(4)
C322-N312-C442-C352	8.0(4)	Zn22-N312-C442-C352	-148.1(2)
C322-N312-C442-C432	-172.5(2)	Zn22-N312-C442-C432	31.4(4)
C342-C352-C442-N312	-8.7(4)	C362-C352-C442-N312	169.6(2)
C342-C352-C442-C432	171.9(3)	C362-C352-C442-C432	-9.8(4)
C422-C432-C442-N312	14.3(4)	C382-C432-C442-N312	-169.1(2)
C422-C432-C442-C352	-166.3(3)	C382-C432-C442-C352	10.4(4)
N312-C322-C452-N632	19.7(4)	C332-C322-C452-N632	-160.2(3)
C562-C512-C522-C532	-3.0(4)	C602-C512-C522-C532	176.1(3)
C562-C512-C522-C622	174.5(3)	C602-C512-C522-C622	-6.5(4)
C512-C522-C532-C542	1.2(4)	C622-C522-C532-C542	-176.2(3)
C512-C522-C532-N532	-173.7(2)	C622-C522-C532-N532	8.9(4)
C522-C532-N532-C252	-171.7(3)	C542-C532-N532-C252	13.4(4)
C522-C532-N532-Zn22	76.3(3)	C542-C532-N532-Zn22	-98.5(3)

C122-C252-N532-C532	-77.8(3)	C122-C252-N532-Zn22	35.3(3)
O3A2-Zn22-N532-C532	-169.20(19)	N632-Zn22-N532-C532	-61.52(18)
N112-Zn22-N532-C532	82.81(18)	N312-Zn22-N532-C532	-29.2(8)
O3A2-Zn22-N532-C252	66.32(18)	N632-Zn22-N532-C252	174.01(18)
N112-Zn22-N532-C252	-41.66(18)	N312-Zn22-N532-C252	-153.7(6)
C522-C532-C542-C552	0.9(5)	N532-C532-C542-C552	175.7(3)
C532-C542-C552-C562	-1.1(5)	C542-C552-C562-C512	-0.7(5)
C542-C552-C562-C572	-179.2(3)	C602-C512-C562-C552	-176.4(3)
C522-C512-C562-C552	2.7(4)	C602-C512-C562-C572	2.1(4)
C522-C512-C562-C572	-178.8(3)	C552-C562-C572-C582	177.5(3)
C512-C562-C572-C582	-1.0(5)	C562-C572-C582-C592	-1.8(5)
C572-C582-C592-C602	3.5(5)	C582-C592-C602-C512	-2.3(5)
C562-C512-C602-C592	-0.5(4)	C522-C512-C602-C592	-179.6(3)
C702-C612-C622-C632	177.7(3)	C662-C612-C622-C632	-0.5(4)
C702-C612-C622-C522	-3.6(4)	C662-C612-C622-C522	178.2(3)
C532-C522-C622-C632	-78.0(4)	C512-C522-C622-C632	104.5(3)
C532-C522-C622-C612	103.3(3)	C512-C522-C622-C612	-74.1(3)
C612-C622-C632-C642	2.4(4)	C522-C622-C632-C642	-176.3(3)
C612-C622-C632-N632	-172.1(2)	C522-C622-C632-N632	9.3(4)
C322-C452-N632-C632	-169.9(2)	C322-C452-N632-Zn22	-7.7(3)
C622-C632-N632-C452	-141.1(3)	C642-C632-N632-C452	44.3(4)
C622-C632-N632-Zn22	58.8(3)	C642-C632-N632-Zn22	-115.8(2)
O3A2-Zn22-N632-C452	-103.4(2)	N112-Zn22-N632-C452	103.3(2)
N312-Zn22-N632-C452	-2.32(19)	N532-Zn22-N632-C452	173.6(2)
O3A2-Zn22-N632-C632	58.2(2)	N112-Zn22-N632-C632	-95.1(2)
N312-Zn22-N632-C632	159.3(2)	N532-Zn22-N632-C632	-24.8(2)
C622-C632-C642-C652	-2.8(4)	N632-C632-C642-C652	171.7(3)
C632-C642-C652-C662	1.3(4)	C642-C652-C662-C612	0.5(4)

Symmetry transformations used to generate equivalent atoms:

Table 1. Crystal data and structure refinement for complex **14**.

Identification code   ko0601m

Empirical formula   C27 H30 Cl4 N4 Zn

Formula weight   617.72

Temperature   173(2) K

Wavelength   0.71073 Å

Crystal system   Orthorhombic

Space group   P2(1)2(1)2(1)

Unit cell dimensions   a = 7.8835(5) Å α= 90°

                                                  b = 11.1237(7) Å β= 90°

                                                  c = 32.0002(19) Å γ = 90°

Volume   2806.2(3) Å^3

Z   4

Density (calculated)   1.462 g/cm^3

Absorption coefficient   1.280 mm^{-1}

F(000)   1272

Crystal size   0.30 x 0.25 x 0.20 mm^3

Theta range for data collection   1.94 to 26.39°

Index ranges   -9<=h<=9, -12<=k<=13, -35<=l<=34

Reflections collected   14740

Independent reflections   5063 [R(int) = 0.0414]

Completeness to theta = 26.39°   92.7 %

Absorption correction   Semi-empirical from equivalents

Refinement method   Full-matrix least-squares on F^2

Data / restraints / parameters   5063 / 0 / 331

Goodness-of-fit on F^2 1.035

Final R indices [I>2sigma(I)]   R1 = 0.0333, wR2 = 0.0855

R indices (all data)   R1 = 0.0387, wR2 = 0.0892

Absolute structure parameter   0.039(11)

Table 2. Atomic coordinates (x 10^4) and equivalent isotropic displacement parameters (Å^2 x 10^3) for complex **14**. U(eq) is defined as one third of the trace of the orthogonalized U^{ij} tensor.

	x	y	z	U(eq)
Zn(1)	5328(1)	5758(1)	4352(1)	23(1)
Cl(1)	5022(1)	4036(1)	3983(1)	35(1)
Cl(2)	3114(1)	6747(1)	4639(1)	32(1)
N(11)	6466(3)	4857(2)	4910(1)	22(1)
C(12)	8111(3)	5079(3)	4942(1)	23(1)
C(13)	9152(4)	4513(3)	5236(1)	29(1)
C(14)	8506(4)	3680(3)	5493(1)	29(1)
C(15)	6739(4)	3413(3)	5474(1)	25(1)
C(16)	5964(4)	2568(3)	5738(1)	31(1)
C(17)	4251(4)	2368(3)	5714(1)	31(1)
C(18)	3281(4)	2996(3)	5419(1)	28(1)
C(19)	4006(4)	3794(3)	5152(1)	27(1)
C(20)	5769(3)	4036(3)	5177(1)	22(1)
C(21)	8854(3)	5966(3)	4641(1)	27(1)
N(21)	7551(3)	6744(3)	4464(1)	24(1)
N(31)	5388(4)	6415(3)	2948(1)	34(1)
C(32)	4052(4)	6977(3)	3089(1)	32(1)
C(33)	2807(4)	7483(4)	2823(1)	41(1)
C(34)	3036(5)	7405(4)	2403(1)	51(1)
C(35)	4482(5)	6821(4)	2238(1)	41(1)
C(36)	4827(6)	6719(4)	1811(1)	56(1)
C(37)	6239(7)	6143(4)	1679(1)	58(1)
C(38)	7372(6)	5661(4)	1965(1)	61(1)
C(39)	7076(5)	5755(4)	2381(1)	49(1)
C(40)	5609(5)	6324(3)	2527(1)	37(1)

C(41)	3887(4)	7059(4)	3560(1)	35(1)
N(41)	5469(3)	6816(3)	3780(1)	27(1)
C(51)	8109(4)	7448(3)	4097(1)	22(1)
C(52)	6529(4)	7888(3)	3866(1)	25(1)
C(53)	7026(4)	8614(4)	3486(1)	33(1)
C(54)	8161(4)	9671(3)	3609(1)	37(1)
C(55)	9743(4)	9222(4)	3834(1)	36(1)
C(56)	9275(4)	8473(3)	4214(1)	30(1)
Cl(3)	9877(2)	9741(1)	1644(1)	74(1)
Cl(4)	8259(2)	9128(1)	2422(1)	80(1)
C(1S)	8153(6)	9041(5)	1884(1)	61(1)

Table 3. Bond lengths [Å] and angles [°] for complex **14**.

Zn(1)-N(21)	2.098(3)	Zn(1)-N(41)	2.181(3)
Zn(1)-N(11)	2.235(3)	Zn(1)-Cl(2)	2.2574(8)
Zn(1)-Cl(1)	2.2643(9)	N(11)-C(12)	1.324(4)
N(11)-C(20)	1.365(4)	C(12)-C(13)	1.397(4)
C(12)-C(21)	1.500(4)	C(13)-C(14)	1.340(5)
C(13)-H(13)	0.9500	C(14)-C(15)	1.426(4)
C(14)-H(14)	0.9500	C(15)-C(20)	1.403(4)
C(15)-C(16)	1.404(5)	C(16)-C(17)	1.370(5)
C(16)-H(16)	0.9500	C(17)-C(18)	1.401(5)
C(17)-H(17)	0.9500	C(18)-C(19)	1.360(5)
C(18)-H(18)	0.9500	C(19)-C(20)	1.417(4)
C(19)-H(19)	0.9500	C(21)-N(21)	1.458(4)
C(21)-H(21A)	0.9900	C(21)-H(21B)	0.9900
N(21)-C(51)	1.479(4)	N(21)-H(21)	0.87(3)

274

N(31)-C(32)	1.306(4)	N(31)-C(40)	1.363(5)
C(32)-C(33)	1.417(5)	C(32)-C(41)	1.513(5)
C(33)-C(34)	1.357(6)	C(33)-H(33)	0.9500
C(34)-C(35)	1.415(6)	C(34)-H(34)	0.9500
C(35)-C(40)	1.396(5)	C(35)-C(36)	1.398(6)
C(36)-C(37)	1.352(7)	C(36)-H(36)	0.9500
C(37)-C(38)	1.388(7)	C(37)-H(37)	0.9500
C(38)-C(39)	1.355(6)	C(38)-H(38)	0.9500
C(39)-C(40)	1.398(5)	C(39)-H(39)	0.9500
C(41)-N(41)	1.458(4)	C(41)-H(41A)	0.9900
C(41)-H(41B)	0.9900	N(41)-C(52)	1.482(4)
N(41)-H(41)	0.83(4)	C(51)-C(56)	1.511(5)
C(51)-C(52)	1.528(4)	C(51)-H(51)	1.0000
C(52)-C(53)	1.511(5)	C(52)-H(52)	1.0000
C(53)-C(54)	1.529(5)	C(53)-H(53A)	0.9900
C(53)-H(53B)	0.9900	C(54)-C(55)	1.525(5)
C(54)-H(54A)	0.9900	C(54)-H(54B)	0.9900
C(55)-C(56)	1.519(5)	C(55)-H(55A)	0.9900
C(55)-H(55B)	0.9900	C(56)-H(56A)	0.9900
C(56)-H(56B)	0.9900	Cl(3)-C(1S)	1.744(5)
Cl(4)-C(1S)	1.728(5)	C(1S)-H(1A)	0.9900
C(1S)-H(1B)	0.9900	N(21)-Zn(1)-N(41)	79.51(10)
N(21)-Zn(1)-N(11)	76.31(9)	N(41)-Zn(1)-N(11)	153.20(9)
N(21)-Zn(1)-Cl(2)	108.79(8)	N(41)-Zn(1)-Cl(2)	96.72(8)
N(11)-Zn(1)-Cl(2)	101.84(7)	N(21)-Zn(1)-Cl(1)	128.33(8)
N(41)-Zn(1)-Cl(1)	91.30(8)	N(11)-Zn(1)-Cl(1)	94.65(7)
Cl(2)-Zn(1)-Cl(1)	122.80(3)	C(12)-N(11)-C(20)	118.1(3)
C(12)-N(11)-Zn(1)	111.8(2)	C(20)-N(11)-Zn(1)	129.56(18)
N(11)-C(12)-C(13)	122.9(3)	N(11)-C(12)-C(21)	117.1(3)
C(13)-C(12)-C(21)	120.0(3)	C(14)-C(13)-C(12)	120.1(3)

C(14)-C(13)-H(13)	119.9	C(12)-C(13)-H(13)	119.9
C(13)-C(14)-C(15)	119.2(3)	C(13)-C(14)-H(14)	120.4
C(15)-C(14)-H(14)	120.4	C(20)-C(15)-C(16)	120.1(3)
C(20)-C(15)-C(14)	117.4(3)	C(16)-C(15)-C(14)	122.6(3)
C(17)-C(16)-C(15)	120.3(3)	C(17)-C(16)-H(16)	119.8
C(15)-C(16)-H(16)	119.8	C(16)-C(17)-C(18)	119.6(3)
C(16)-C(17)-H(17)	120.2	C(18)-C(17)-H(17)	120.2
C(19)-C(18)-C(17)	121.3(3)	C(19)-C(18)-H(18)	119.3
C(17)-C(18)-H(18)	119.3	C(18)-C(19)-C(20)	120.1(3)
C(18)-C(19)-H(19)	120.0	C(20)-C(19)-H(19)	120.0
N(11)-C(20)-C(15)	122.3(3)	N(11)-C(20)-C(19)	119.1(3)
C(15)-C(20)-C(19)	118.6(3)	N(21)-C(21)-C(12)	111.4(2)
N(21)-C(21)-H(21A)	109.3	C(12)-C(21)-H(21A)	109.3
N(21)-C(21)-H(21B)	109.3	C(12)-C(21)-H(21B)	109.3
H(21A)-C(21)-H(21B)	108.0	C(21)-N(21)-C(51)	114.4(2)
C(21)-N(21)-Zn(1)	110.11(19)	C(51)-N(21)-Zn(1)	112.97(18)
C(21)-N(21)-H(21)	105(2)	C(51)-N(21)-H(21)	106(2)
Zn(1)-N(21)-H(21)	108(2)	C(32)-N(31)-C(40)	118.7(3)
N(31)-C(32)-C(33)	122.8(3)	N(31)-C(32)-C(41)	116.3(3)
C(33)-C(32)-C(41)	121.0(3)	C(34)-C(33)-C(32)	118.5(4)
C(34)-C(33)-H(33)	120.7	C(32)-C(33)-H(33)	120.7
C(33)-C(34)-C(35)	120.4(3)	C(33)-C(34)-H(34)	119.8
C(35)-C(34)-H(34)	119.8	C(40)-C(35)-C(36)	119.4(4)
C(40)-C(35)-C(34)	116.6(3)	C(36)-C(35)-C(34)	124.0(4)
C(37)-C(36)-C(35)	120.4(4)	C(37)-C(36)-H(36)	119.8
C(35)-C(36)-H(36)	119.8	C(36)-C(37)-C(38)	120.3(4)
C(36)-C(37)-H(37)	119.8	C(38)-C(37)-H(37)	119.8
C(39)-C(38)-C(37)	120.6(4)	C(39)-C(38)-H(38)	119.7
C(37)-C(38)-H(38)	119.7	C(38)-C(39)-C(40)	120.3(4)
C(38)-C(39)-H(39)	119.8	C(40)-C(39)-H(39)	119.8

N(31)-C(40)-C(35)	123.0(4)	N(31)-C(40)-C(39)	118.0(3)
C(35)-C(40)-C(39)	119.0(4)	N(41)-C(41)-C(32)	113.3(3)
N(41)-C(41)-H(41A)	108.9	C(32)-C(41)-H(41A)	108.9
N(41)-C(41)-H(41B)	108.9	C(32)-C(41)-H(41B)	108.9
H(41A)-C(41)-H(41B)	107.7	C(41)-N(41)-C(52)	115.0(3)
C(41)-N(41)-Zn(1)	117.6(2)	C(52)-N(41)-Zn(1)	107.83(19)
C(41)-N(41)-H(41)	103(3)	C(52)-N(41)-H(41)	107(3)
Zn(1)-N(41)-H(41)	105(3)	N(21)-C(51)-C(56)	112.5(3)
N(21)-C(51)-C(52)	108.1(2)	C(56)-C(51)-C(52)	112.0(3)
N(21)-C(51)-H(51)	108.0	C(56)-C(51)-H(51)	108.0
C(52)-C(51)-H(51)	108.0	N(41)-C(52)-C(53)	115.3(3)
N(41)-C(52)-C(51)	107.0(3)	C(53)-C(52)-C(51)	110.4(2)
N(41)-C(52)-H(52)	108.0	C(53)-C(52)-H(52)	108.0
C(51)-C(52)-H(52)	108.0	C(52)-C(53)-C(54)	110.9(3)
C(52)-C(53)-H(53A)	109.4	C(54)-C(53)-H(53A)	109.5
C(52)-C(53)-H(53B)	109.4	C(54)-C(53)-H(53B)	109.4
H(53A)-C(53)-H(53B)	108.0	C(55)-C(54)-C(53)	110.3(3)
C(55)-C(54)-H(54A)	109.6	C(53)-C(54)-H(54A)	109.6
C(55)-C(54)-H(54B)	109.6	C(53)-C(54)-H(54B)	109.6
H(54A)-C(54)-H(54B)	108.1	C(56)-C(55)-C(54)	111.1(3)
C(56)-C(55)-H(55A)	109.4	C(54)-C(55)-H(55A)	109.4
C(56)-C(55)-H(55B)	109.4	C(54)-C(55)-H(55B)	109.4
H(55A)-C(55)-H(55B)	108.0	C(51)-C(56)-C(55)	111.3(3)
C(51)-C(56)-H(56A)	109.4	C(55)-C(56)-H(56A)	109.4
C(51)-C(56)-H(56B)	109.4	C(55)-C(56)-H(56B)	109.4
H(56A)-C(56)-H(56B)	108.0	Cl(4)-C(1S)-Cl(3)	112.1(2)
Cl(4)-C(1S)-H(1A)	109.2	Cl(3)-C(1S)-H(1A)	109.2
Cl(4)-C(1S)-H(1B)	109.2	Cl(3)-C(1S)-H(1B)	109.2

Symmetry transformations used to generate equivalent atoms:

Table 4. Anisotropic displacement parameters ($\mathring{A}^2$ x 10^3) for complex **14**. The anisotropic displacement factor exponent takes the following form: $-2\pi^2[\, h^2\, a^{*2}U^{11} + ... + 2\, h\, k\, a^*\, b^*\, U^{12}\,]$

	U^{11}	U^{22}	U^{33}	U^{23}	U^{13}	U^{12}
Zn(1)	21(1)	25(1)	23(1)	0(1)	1(1)	-1(1)
Cl(1)	50(1)	26(1)	30(1)	-3(1)	-4(1)	-3(1)
Cl(2)	26(1)	42(1)	28(1)	-2(1)	2(1)	9(1)
N(11)	25(1)	20(2)	23(2)	1(1)	-1(1)	2(1)
C(12)	24(1)	20(2)	27(2)	-1(2)	-2(1)	1(1)
C(13)	25(1)	31(2)	31(2)	-1(2)	-3(1)	3(1)
C(14)	28(1)	32(2)	26(2)	3(2)	0(1)	7(1)
C(15)	31(1)	21(2)	23(2)	-4(1)	3(1)	3(1)
C(16)	36(2)	28(2)	29(2)	5(2)	4(1)	3(2)
C(17)	42(2)	24(2)	27(2)	3(2)	7(1)	-6(1)
C(18)	28(1)	27(2)	30(2)	-2(2)	3(1)	-2(1)
C(19)	27(1)	25(2)	28(2)	-2(2)	2(1)	3(1)
C(20)	28(1)	19(2)	19(2)	-3(1)	2(1)	2(1)
C(21)	20(1)	28(2)	33(2)	5(2)	-1(1)	0(1)
N(21)	22(1)	26(2)	25(2)	3(1)	-1(1)	1(1)
N(31)	46(1)	31(2)	27(2)	0(1)	-3(1)	4(2)
C(32)	34(1)	30(2)	32(2)	2(2)	-6(1)	-4(2)
C(33)	39(2)	46(3)	40(2)	2(2)	-11(2)	7(2)
C(34)	59(2)	58(3)	35(2)	15(2)	-20(2)	-4(2)
C(35)	59(2)	34(2)	28(2)	5(2)	-10(2)	-18(2)
C(36)	85(3)	47(3)	35(2)	5(2)	-16(2)	-28(3)
C(37)	100(3)	52(3)	20(2)	-2(2)	9(2)	-26(3)
C(38)	88(3)	59(3)	35(3)	-7(2)	17(2)	4(3)
C(39)	71(2)	46(2)	30(2)	2(2)	7(2)	11(2)
C(40)	57(2)	27(2)	27(2)	0(2)	-5(2)	-5(2)

278

C(41)	29(1)	45(2)	31(2)	1(2)	-4(1)	0(2)
N(41)	29(1)	30(2)	22(2)	-1(1)	-1(1)	-1(1)
C(51)	25(1)	21(2)	20(2)	3(1)	0(1)	-2(1)
C(52)	29(1)	25(2)	22(2)	-2(1)	2(1)	0(1)
C(53)	36(2)	39(2)	24(2)	4(2)	-4(1)	-2(2)
C(54)	43(2)	32(2)	37(2)	10(2)	3(2)	0(2)
C(55)	36(1)	35(2)	38(2)	3(2)	-1(1)	-9(2)
C(56)	30(2)	27(2)	33(2)	4(2)	-1(1)	-5(1)
Cl(3)	79(1)	91(1)	51(1)	-2(1)	6(1)	-18(1)
Cl(4)	106(1)	81(1)	52(1)	10(1)	10(1)	-13(1)
C(1S)	71(2)	58(3)	54(3)	6(2)	-15(2)	-15(3)

Table 5. Hydrogen coordinates (x 10^4) and isotropic displacement parameters (Å^2 x 10^3) for complex **14**.

	x	y	z	U(eq)
H(13)	10319	4719	5253	35
H(14)	9218	3271	5686	35
H(16)	6630	2132	5933	37
H(17)	3725	1807	5897	38
H(18)	2092	2861	5406	34
H(19)	3331	4190	4948	32
H(21A)	9711	6463	4786	32
H(21B)	9432	5527	4412	32
H(21)	7330(40)	7260(30)	4660(11)	29
H(33)	1833	7869	2936	49
H(34)	2220	7745	2220	61

H(36)	4066	7055	1613	67
H(37)	6457	6069	1388	69
H(38)	8363	5262	1869	73
H(39)	7869	5433	2574	59
H(41A)	3489	7875	3635	42
H(41B)	3017	6478	3654	42
H(41)	6010(40)	6390(30)	3612(12)	32
H(51)	8744	6897	3906	26
H(52)	5882	8426	4059	30
H(53A)	5992	8920	3347	39
H(53B)	7637	8092	3286	39
H(54A)	8496	10121	3355	45
H(54B)	7525	10225	3793	45
H(55A)	10432	8731	3640	44
H(55B)	10437	9918	3924	44
H(56A)	10320	8145	4342	36
H(56B)	8708	8990	4423	36
H(1A)	7091	9426	1787	73
H(1B)	8121	8186	1799	73

Table 6. Torsion angles [°] for complex **14**.

N(21)-Zn(1)-N(11)-C(12)	-21.2(2)	N(41)-Zn(1)-N(11)-C(12)	4.9(4)
Cl(2)-Zn(1)-N(11)-C(12)	-128.0(2)	Cl(1)-Zn(1)-N(11)-C(12)	107.1(2)
N(21)-Zn(1)-N(11)-C(20)	167.5(3)	N(41)-Zn(1)-N(11)-C(20)	-166.4(3)
Cl(2)-Zn(1)-N(11)-C(20)	60.7(3)	Cl(1)-Zn(1)-N(11)-C(20)	-64.2(3)
C(20)-N(11)-C(12)-C(13)	-0.1(5)	Zn(1)-N(11)-C(12)-C(13)	-172.5(3)
C(20)-N(11)-C(12)-C(21)	178.8(3)	Zn(1)-N(11)-C(12)-C(21)	6.4(4)

N(11)-C(12)-C(13)-C(14)	1.9(5)	C(21)-C(12)-C(13)-C(14)	-176.9(3)
C(12)-C(13)-C(14)-C(15)	-2.3(5)	C(13)-C(14)-C(15)-C(20)	1.0(5)
C(13)-C(14)-C(15)-C(16)	-178.9(3)	C(20)-C(15)-C(16)-C(17)	-1.7(5)
C(14)-C(15)-C(16)-C(17)	178.2(3)	C(15)-C(16)-C(17)-C(18)	1.3(6)
C(16)-C(17)-C(18)-C(19)	0.6(5)	C(17)-C(18)-C(19)-C(20)	-2.1(5)
C(12)-N(11)-C(20)-C(15)	-1.2(5)	Zn(1)-N(11)-C(20)-C(15)	169.7(2)
C(12)-N(11)-C(20)-C(19)	179.2(3)	Zn(1)-N(11)-C(20)-C(19)	-9.9(4)
C(16)-C(15)-C(20)-N(11)	-179.3(3)	C(14)-C(15)-C(20)-N(11)	0.7(5)
C(16)-C(15)-C(20)-C(19)	0.3(5)	C(14)-C(15)-C(20)-C(19)	-179.7(3)
C(18)-C(19)-C(20)-N(11)	-178.8(3)	C(18)-C(19)-C(20)-C(15)	1.6(5)
N(11)-C(12)-C(21)-N(21)	20.6(4)	C(13)-C(12)-C(21)-N(21)	-160.5(3)
C(12)-C(21)-N(21)-C(51)	-166.8(3)	C(12)-C(21)-N(21)-Zn(1)	-38.3(3)
N(41)-Zn(1)-N(21)-C(21)	-136.8(2)	N(11)-Zn(1)-N(21)-C(21)	31.53(19)
Cl(2)-Zn(1)-N(21)-C(21)	129.59(19)	Cl(1)-Zn(1)-N(21)-C(21)	-53.5(2)
N(41)-Zn(1)-N(21)-C(51)	-7.5(2)	N(11)-Zn(1)-N(21)-C(51)	160.8(2)
Cl(2)-Zn(1)-N(21)-C(51)	-101.1(2)	Cl(1)-Zn(1)-N(21)-C(51)	75.8(2)
C(40)-N(31)-C(32)-C(33)	0.8(5)	C(40)-N(31)-C(32)-C(41)	-179.4(3)
N(31)-C(32)-C(33)-C(34)	-1.6(6)	C(41)-C(32)-C(33)-C(34)	178.6(4)
C(32)-C(33)-C(34)-C(35)	0.5(6)	C(33)-C(34)-C(35)-C(40)	1.1(6)
C(33)-C(34)-C(35)-C(36)	-178.9(4)	C(40)-C(35)-C(36)-C(37)	0.0(6)
C(34)-C(35)-C(36)-C(37)	-179.9(4)	C(35)-C(36)-C(37)-C(38)	-0.8(7)
C(36)-C(37)-C(38)-C(39)	0.3(7)	C(37)-C(38)-C(39)-C(40)	1.0(7)
C(32)-N(31)-C(40)-C(35)	1.0(5)	C(32)-N(31)-C(40)-C(39)	177.9(3)
C(36)-C(35)-C(40)-N(31)	178.1(4)	C(34)-C(35)-C(40)-N(31)	-2.0(5)
C(36)-C(35)-C(40)-C(39)	1.2(5)	C(34)-C(35)-C(40)-C(39)	-178.8(4)
C(38)-C(39)-C(40)-N(31)	-178.8(4)	C(38)-C(39)-C(40)-C(35)	-1.7(6)
N(31)-C(32)-C(41)-N(41)	17.1(5)	C(33)-C(32)-C(41)-N(41)	-163.1(3)
C(32)-C(41)-N(41)-C(52)	91.2(4)	C(32)-C(41)-N(41)-Zn(1)	-140.1(3)
N(21)-Zn(1)-N(41)-C(41)	-154.1(3)	N(11)-Zn(1)-N(41)-C(41)	-179.9(2)
Cl(2)-Zn(1)-N(41)-C(41)	-46.1(3)	Cl(1)-Zn(1)-N(41)-C(41)	77.1(3)

N(21)-Zn(1)-N(41)-C(52)	-22.0(2)	N(11)-Zn(1)-N(41)-C(52)	-47.9(3)
Cl(2)-Zn(1)-N(41)-C(52)	85.90(19)	Cl(1)-Zn(1)-N(41)-C(52)	-150.85(19)
C(21)-N(21)-C(51)-C(56)	-73.8(3)	Zn(1)-N(21)-C(51)-C(56)	159.2(2)
C(21)-N(21)-C(51)-C(52)	162.1(3)	Zn(1)-N(21)-C(51)-C(52)	35.0(3)
C(41)-N(41)-C(52)-C(53)	-57.0(4)	Zn(1)-N(41)-C(52)-C(53)	169.7(2)
C(41)-N(41)-C(52)-C(51)	179.9(3)	Zn(1)-N(41)-C(52)-C(51)	46.5(3)
N(21)-C(51)-C(52)-N(41)	-53.8(3)	C(56)-C(51)-C(52)-N(41)	-178.4(2)
N(21)-C(51)-C(52)-C(53)	-179.9(3)	C(56)-C(51)-C(52)-C(53)	55.5(4)
N(41)-C(52)-C(53)-C(54)	-178.2(3)	C(51)-C(52)-C(53)-C(54)	-56.9(4)
C(52)-C(53)-C(54)-C(55)	57.7(4)	C(53)-C(54)-C(55)-C(56)	-56.3(4)
N(21)-C(51)-C(56)-C(55)	-176.7(3)	C(52)-C(51)-C(56)-C(55)	-54.6(4)

Symmetry transformations used to generate equivalent atoms:

Table 1. Crystal data and structure refinement for complex **18**.

Identification code	ko1001m
Empirical formula	C27 H29 Cl7 Fe2 N4 O
Formula weight	785.39
Temperature	120(2) K
Wavelength	0.71073 Å
Crystal system	Orthorhombic
Space group	P2(1)2(1)2(1)
Unit cell dimensions	a = 10.3489(6) Å α= 90°
	b = 14.3664(8) Å β= 90°
	c = 21.4619(13) Å γ = 90°
Volume	3190.9(3) Å^3
Z	4
Density (calculated)	1.635 g/cm^3
Absorption coefficient	1.525 mm^{-1}
F(000)	1592
Crystal size	0.26 x 0.22 x 0.14 mm^3
Theta range for data collection	2.37 to 31.50°
Index ranges	-14<=h<=15, -20<=k<=20, -30<=l<=31
Reflections collected	79878
Independent reflections	10524 [R(int) = 0.0645]
Completeness to theta = 31.50°	99.4 %
Absorption correction	None
Refinement method	Full-matrix least-squares on F^2
Data / restraints / parameters	10524 / 12 / 389
Goodness-of-fit on F^2	1.039
Final R indices [I>2sigma(I)]	R1 = 0.0505, wR2 = 0.1215
R indices (all data)	R1 = 0.0637, wR2 = 0.1288
Absolute structure parameter	0.024(16)

Table 2.   Atomic coordinates (x 10^4) and equivalent isotropic displacement parameters (Å^2 x 10^3) for complex **18**. U(eq) is defined as one third of the trace of the orthogonalized U^{ij} tensor.

	x	y	z	U(eq)
Fe(1)	7495(1)	6502(1)	1309(1)	23(1)
Cl(1)	6504(1)	6149(1)	350(1)	30(1)
O(1)	7889(2)	6917(2)	2081(1)	30(1)
Fe(2)	8706(1)	6779(1)	2792(1)	27(1)
Cl(2)	9325(1)	5287(1)	2866(1)	33(1)
Cl(3)	7456(1)	7118(1)	3602(1)	41(1)
Cl(4)	10449(1)	7693(1)	2761(1)	62(1)
C(1A)	4482(6)	3057(4)	-37(2)	51(2)
Cl(5A)	5498(9)	4037(5)	45(4)	53(1)
Cl(6A)	5289(12)	2041(6)	208(5)	130(1)
Cl(7A)	4047(3)	2945(2)	-829(1)	59(1)
C(1B)	4982(3)	2888(4)	-316(3)	51(2)
Cl(5B)	5418(9)	4029(5)	-94(4)	53(1)
Cl(6B)	5457(10)	2094(6)	269(5)	130(1)
Cl(7B)	3282(2)	2824(2)	-403(1)	59(1)
N(11)	7139(3)	8004(2)	1081(1)	25(1)
C(12)	8225(3)	8480(2)	1010(2)	27(1)
C(13)	8241(4)	9463(2)	964(2)	31(1)
C(14)	7136(4)	9945(2)	1022(2)	33(1)
C(15)	5945(4)	9468(2)	1093(2)	31(1)
C(16)	4752(5)	9931(3)	1157(2)	43(1)
C(17)	3623(4)	9441(3)	1220(2)	50(1)
C(18)	3661(4)	8462(3)	1214(2)	48(1)
C(19)	4809(3)	7993(3)	1152(2)	35(1)
C(20)	5983(3)	8481(2)	1106(2)	28(1)

C(21)	9472(4)	7955(2)	1005(2)	32(1)
N(31)	6290(3)	5375(2)	1713(1)	26(1)
C(32)	6645(3)	4530(2)	1544(2)	29(1)
C(33)	5879(4)	3728(3)	1664(2)	38(1)
C(34)	4718(4)	3833(3)	1952(2)	39(1)
C(35)	4303(3)	4720(3)	2145(2)	33(1)
C(36)	3098(4)	4888(3)	2429(2)	40(1)
C(37)	2737(4)	5763(4)	2591(2)	42(1)
C(38)	3584(4)	6505(3)	2504(2)	40(1)
C(39)	4770(3)	6384(3)	2234(2)	34(1)
C(40)	5137(3)	5489(3)	2031(2)	28(1)
C(41)	7910(3)	4435(2)	1210(2)	30(1)
C(51)	10351(3)	6346(2)	990(2)	26(1)
N(51)	9249(3)	6968(2)	849(1)	28(1)
C(52)	9862(3)	5347(2)	925(2)	26(1)
N(52)	8688(3)	5270(2)	1322(1)	25(1)
C(53)	10911(3)	4649(3)	1100(2)	32(1)
C(54)	12135(4)	4800(3)	710(2)	37(1)
C(55)	12605(4)	5803(3)	752(2)	36(1)
C(56)	11524(3)	6489(3)	571(2)	32(1)

Table 3. Bond lengths [Å] and angles [°] for complex **18**.

Fe(1)-O(1)	1.807(2)	Fe(1)-N(52)	2.159(3)
Fe(1)-N(51)	2.172(3)	Fe(1)-N(31)	2.221(3)
Fe(1)-N(11)	2.243(3)	Fe(1)-Cl(1)	2.3558(9)
O(1)-Fe(2)	1.756(2)	Fe(2)-Cl(3)	2.2198(10)
Fe(2)-Cl(4)	2.2328(11)	Fe(2)-Cl(2)	2.2427(10)

C(1A)-Cl(6A)	1.762(2)	C(1A)-Cl(7A)	1.766(2)
C(1A)-Cl(5A)	1.766(2)	C(1A)-H(1AA)	1.0000
C(1B)-Cl(6B)	1.765(2)	C(1B)-Cl(5B)	1.766(2)
C(1B)-Cl(7B)	1.771(2)	C(1B)-H(1BA)	1.0000
N(11)-C(12)	1.324(4)	N(11)-C(20)	1.380(4)
C(12)-C(13)	1.416(5)	C(12)-C(21)	1.495(5)
C(13)-C(14)	1.343(5)	C(13)-H(13)	0.9500
C(14)-C(15)	1.419(5)	C(14)-H(14)	0.9500
C(15)-C(16)	1.409(6)	C(15)-C(20)	1.418(5)
C(16)-C(17)	1.371(7)	C(16)-H(16)	0.9500
C(17)-C(18)	1.406(6)	C(17)-H(17)	0.9500
C(18)-C(19)	1.373(5)	C(18)-H(18)	0.9500
C(19)-C(20)	1.407(5)	C(19)-H(19)	0.9500
C(21)-N(51)	1.474(5)	C(21)-H(21A)	0.9900
C(21)-H(21B)	0.9900	N(31)-C(32)	1.318(4)
N(31)-C(40)	1.383(4)	C(32)-C(33)	1.422(5)
C(32)-C(41)	1.499(5)	C(33)-C(34)	1.360(6)
C(33)-H(33)	0.9500	C(34)-C(35)	1.407(6)
C(34)-H(34)	0.9500	C(35)-C(36)	1.409(6)
C(35)-C(40)	1.423(5)	C(36)-C(37)	1.357(7)
C(36)-H(36)	0.9500	C(37)-C(38)	1.393(6)
C(37)-H(37)	0.9500	C(38)-C(39)	1.368(5)
C(38)-H(38)	0.9500	C(39)-C(40)	1.411(5)
C(39)-H(39)	0.9500	C(41)-N(52)	1.465(4)
C(41)-H(41A)	0.9900	C(41)-H(41B)	0.9900
C(51)-N(51)	1.480(4)	C(51)-C(56)	1.525(5)
C(51)-C(52)	1.529(5)	C(51)-H(51A)	1.0000
N(51)-H(51)	0.86(5)	C(52)-N(52)	1.487(4)
C(52)-C(53)	1.524(4)	C(52)-H(52A)	1.0000
N(52)-H(52)	0.85(4)	C(53)-C(54)	1.534(5)

C(53)-H(53A)	0.9900	C(53)-H(53B)	0.9900
C(54)-C(55)	1.524(6)	C(54)-H(54A)	0.9900
C(54)-H(54B)	0.9900	C(55)-C(56)	1.541(5)
C(55)-H(55A)	0.9900	C(55)-H(55B)	0.9900
C(56)-H(56A)	0.9900	C(56)-H(56B)	0.9900
O(1)-Fe(1)-N(52)	97.47(11)	O(1)-Fe(1)-N(51)	97.25(12)
N(52)-Fe(1)-N(51)	77.30(11)	O(1)-Fe(1)-N(31)	90.55(11)
N(52)-Fe(1)-N(31)	73.63(10)	N(51)-Fe(1)-N(31)	150.64(11)
O(1)-Fe(1)-N(11)	85.42(10)	N(52)-Fe(1)-N(11)	152.29(10)
N(51)-Fe(1)-N(11)	75.00(10)	N(31)-Fe(1)-N(11)	134.04(10)
O(1)-Fe(1)-Cl(1)	166.11(8)	N(52)-Fe(1)-Cl(1)	94.75(8)
N(51)-Fe(1)-Cl(1)	91.86(9)	N(31)-Fe(1)-Cl(1)	86.56(8)
N(11)-Fe(1)-Cl(1)	86.84(8)	Fe(2)-O(1)-Fe(1)	150.28(15)
O(1)-Fe(2)-Cl(3)	112.06(9)	O(1)-Fe(2)-Cl(4)	107.22(9)
Cl(3)-Fe(2)-Cl(4)	111.43(5)	O(1)-Fe(2)-Cl(2)	107.85(8)
Cl(3)-Fe(2)-Cl(2)	108.74(4)	Cl(4)-Fe(2)-Cl(2)	109.46(4)
Cl(6A)-C(1A)-Cl(7A)	109.4(2)	Cl(6A)-C(1A)-Cl(5A)	110.3(2)
Cl(7A)-C(1A)-Cl(5A)	108.7(2)	Cl(6A)-C(1A)-H(1AA)	109.5
Cl(7A)-C(1A)-H(1AA)	109.5	Cl(5A)-C(1A)-H(1AA)	109.5
Cl(6B)-C(1B)-Cl(5B)	109.7(2)	Cl(6B)-C(1B)-Cl(7B)	108.6(3)
Cl(5B)-C(1B)-Cl(7B)	109.3(2)	Cl(6B)-C(1B)-H(1BA)	109.8
Cl(5B)-C(1B)-H(1BA)	109.8	Cl(7B)-C(1B)-H(1BA)	109.8
C(12)-N(11)-C(20)	118.9(3)	C(12)-N(11)-Fe(1)	112.5(2)
C(20)-N(11)-Fe(1)	127.7(2)	N(11)-C(12)-C(13)	122.2(3)
N(11)-C(12)-C(21)	118.3(3)	C(13)-C(12)-C(21)	119.5(3)
C(14)-C(13)-C(12)	119.9(3)	C(14)-C(13)-H(13)	120.1
C(12)-C(13)-H(13)	120.1	C(13)-C(14)-C(15)	120.1(3)
C(13)-C(14)-H(14)	120.0	C(15)-C(14)-H(14)	120.0
C(16)-C(15)-C(20)	119.6(4)	C(16)-C(15)-C(14)	123.0(3)

C(20)-C(15)-C(14)	117.4(3)	C(17)-C(16)-C(15)	120.9(4)
C(17)-C(16)-H(16)	119.5	C(15)-C(16)-H(16)	119.5
C(16)-C(17)-C(18)	119.3(4)	C(16)-C(17)-H(17)	120.4
C(18)-C(17)-H(17)	120.4	C(19)-C(18)-C(17)	121.1(4)
C(19)-C(18)-H(18)	119.5	C(17)-C(18)-H(18)	119.5
C(18)-C(19)-C(20)	120.6(4)	C(18)-C(19)-H(19)	119.7
C(20)-C(19)-H(19)	119.7	N(11)-C(20)-C(19)	120.2(3)
N(11)-C(20)-C(15)	121.4(3)	C(19)-C(20)-C(15)	118.4(3)
N(51)-C(21)-C(12)	110.5(3)	N(51)-C(21)-H(21A)	109.5
C(12)-C(21)-H(21A)	109.5	N(51)-C(21)-H(21B)	109.5
C(12)-C(21)-H(21B)	109.5	H(21A)-C(21)-H(21B)	108.1
C(32)-N(31)-C(40)	119.0(3)	C(32)-N(31)-Fe(1)	114.0(2)
C(40)-N(31)-Fe(1)	126.2(2)	N(31)-C(32)-C(33)	122.7(3)
N(31)-C(32)-C(41)	117.4(3)	C(33)-C(32)-C(41)	119.9(3)
C(34)-C(33)-C(32)	119.0(4)	C(34)-C(33)-H(33)	120.5
C(32)-C(33)-H(33)	120.5	C(33)-C(34)-C(35)	120.2(3)
C(33)-C(34)-H(34)	119.9	C(35)-C(34)-H(34)	119.9
C(34)-C(35)-C(36)	123.5(3)	C(34)-C(35)-C(40)	117.9(3)
C(36)-C(35)-C(40)	118.6(4)	C(37)-C(36)-C(35)	120.9(4)
C(37)-C(36)-H(36)	119.6	C(35)-C(36)-H(36)	119.6
C(36)-C(37)-C(38)	120.1(4)	C(36)-C(37)-H(37)	120.0
C(38)-C(37)-H(37)	120.0	C(39)-C(38)-C(37)	121.6(4)
C(39)-C(38)-H(38)	119.2	C(37)-C(38)-H(38)	119.2
C(38)-C(39)-C(40)	119.2(4)	C(38)-C(39)-H(39)	120.4
C(40)-C(39)-H(39)	120.4	N(31)-C(40)-C(39)	119.5(3)
N(31)-C(40)-C(35)	121.0(3)	C(39)-C(40)-C(35)	119.5(3)
N(52)-C(41)-C(32)	109.1(3)	N(52)-C(41)-H(41A)	109.9
C(32)-C(41)-H(41A)	109.9	N(52)-C(41)-H(41B)	109.9
C(32)-C(41)-H(41B)	109.9	H(41A)-C(41)-H(41B)	108.3
N(51)-C(51)-C(56)	114.3(3)	N(51)-C(51)-C(52)	107.1(3)

C(56)-C(51)-C(52)	109.7(3)	N(51)-C(51)-H(51A)	108.5
C(56)-C(51)-H(51A)	108.5	C(52)-C(51)-H(51A)	108.5
C(21)-N(51)-C(51)	114.4(3)	C(21)-N(51)-Fe(1)	108.9(2)
C(51)-N(51)-Fe(1)	111.4(2)	C(21)-N(51)-H(51)	107(3)
C(51)-N(51)-H(51)	111(3)	Fe(1)-N(51)-H(51)	104(3)
N(52)-C(52)-C(53)	113.1(3)	N(52)-C(52)-C(51)	106.7(3)
C(53)-C(52)-C(51)	111.1(3)	N(52)-C(52)-H(52A)	108.6
C(53)-C(52)-H(52A)	108.6	C(51)-C(52)-H(52A)	108.6
C(41)-N(52)-C(52)	114.6(3)	C(41)-N(52)-Fe(1)	110.82(19)
C(52)-N(52)-Fe(1)	113.58(19)	C(41)-N(52)-H(52)	112(3)
C(52)-N(52)-H(52)	104(3)	Fe(1)-N(52)-H(52)	102(3)
C(52)-C(53)-C(54)	111.2(3)	C(52)-C(53)-H(53A)	109.4
C(54)-C(53)-H(53A)	109.4	C(52)-C(53)-H(53B)	109.4
C(54)-C(53)-H(53B)	109.4	H(53A)-C(53)-H(53B)	108.0
C(55)-C(54)-C(53)	111.4(3)	C(55)-C(54)-H(54A)	109.4
C(53)-C(54)-H(54A)	109.4	C(55)-C(54)-H(54B)	109.4
C(53)-C(54)-H(54B)	109.4	H(54A)-C(54)-H(54B)	108.0
C(54)-C(55)-C(56)	111.0(3)	C(54)-C(55)-H(55A)	109.4
C(56)-C(55)-H(55A)	109.4	C(54)-C(55)-H(55B)	109.4
C(56)-C(55)-H(55B)	109.4	H(55A)-C(55)-H(55B)	108.0
C(51)-C(56)-C(55)	110.0(3)	C(51)-C(56)-H(56A)	109.7
C(55)-C(56)-H(56A)	109.7	C(51)-C(56)-H(56B)	109.7
C(55)-C(56)-H(56B)	109.7	H(56A)-C(56)-H(56B)	108.2

Symmetry transformations used to generate equivalent atoms:

Table 4. Anisotropic displacement parameters ($\mathring{A}^2$ x 10^3) for complex **18**. The anisotropic displacement factor exponent takes the following form: $-2\pi^2[\, h^2\, a^{*2}U^{11} + ... \; + 2\, h\, k\, a^*\, b^*\, U^{12}\,]$

	U^{11}	U^{22}	U^{33}	U^{23}	U^{13}	U^{12}
Fe(1)	21(1)	22(1)	26(1)	3(1)	-2(1)	0(1)
Cl(1)	34(1)	28(1)	29(1)	2(1)	-7(1)	0(1)
O(1)	33(1)	24(1)	32(1)	4(1)	-2(1)	-1(1)
Fe(2)	24(1)	28(1)	30(1)	-3(1)	-3(1)	0(1)
Cl(2)	33(1)	31(1)	35(1)	3(1)	-3(1)	5(1)
Cl(3)	37(1)	50(1)	37(1)	-3(1)	3(1)	12(1)
Cl(4)	35(1)	44(1)	106(1)	-25(1)	-2(1)	-14(1)
C(1A)	82(5)	41(3)	30(3)	1(3)	13(3)	23(3)
Cl(5A)	69(1)	45(1)	44(3)	2(1)	-36(2)	7(1)
Cl(6A)	279(4)	59(1)	52(2)	11(1)	-45(2)	26(2)
Cl(7A)	60(1)	45(1)	72(1)	-17(1)	5(1)	-2(1)
C(1B)	82(5)	41(3)	30(3)	1(3)	13(3)	23(3)
Cl(5B)	69(1)	45(1)	44(3)	2(1)	-36(2)	7(1)
Cl(6B)	279(4)	59(1)	52(2)	11(1)	-45(2)	26(2)
Cl(7B)	60(1)	45(1)	72(1)	-17(1)	5(1)	-2(1)
N(11)	27(1)	21(1)	28(1)	2(1)	1(1)	0(1)
C(12)	33(2)	27(1)	21(1)	3(1)	2(1)	-4(1)
C(13)	43(2)	27(2)	24(2)	0(1)	3(1)	-7(1)
C(14)	51(2)	23(1)	25(2)	0(1)	1(2)	-2(1)
C(15)	46(2)	25(2)	23(2)	0(1)	-2(1)	4(1)
C(16)	57(3)	33(2)	38(2)	-4(2)	-6(2)	15(2)
C(17)	39(2)	47(2)	64(3)	-12(2)	-7(2)	16(2)
C(18)	34(2)	48(2)	62(3)	-12(2)	-10(2)	8(2)
C(19)	29(2)	35(2)	41(2)	-2(2)	-4(2)	1(1)
C(20)	32(2)	26(1)	26(2)	3(1)	-2(1)	5(1)

C(21)	31(2)	31(2)	35(2)	2(1)	4(1)	-5(1)
N(31)	22(1)	26(1)	29(1)	3(1)	-2(1)	-5(1)
C(32)	33(2)	26(2)	28(2)	5(1)	-5(1)	-4(1)
C(33)	46(2)	30(2)	39(2)	7(1)	-5(2)	-9(2)
C(34)	41(2)	36(2)	40(2)	11(2)	-7(2)	-17(2)
C(35)	30(2)	44(2)	25(2)	12(1)	-8(1)	-14(1)
C(36)	29(2)	64(3)	27(2)	16(2)	-5(1)	-17(2)
C(37)	23(2)	76(3)	29(2)	4(2)	0(1)	-5(2)
C(38)	29(2)	59(2)	32(2)	-4(2)	0(1)	0(2)
C(39)	28(2)	44(2)	29(2)	0(2)	1(1)	-6(1)
C(40)	23(1)	38(2)	22(2)	5(1)	-3(1)	-7(1)
C(41)	32(2)	21(1)	37(2)	1(1)	-3(1)	1(1)
C(51)	21(1)	35(2)	23(2)	0(1)	-1(1)	2(1)
N(51)	29(1)	30(1)	25(1)	3(1)	1(1)	0(1)
C(52)	24(1)	29(2)	23(2)	3(1)	-2(1)	6(1)
N(52)	24(1)	25(1)	24(1)	2(1)	-3(1)	1(1)
C(53)	27(2)	38(2)	29(2)	0(1)	-1(1)	8(1)
C(54)	33(2)	52(2)	26(2)	1(2)	3(1)	13(2)
C(55)	28(2)	54(2)	28(2)	-1(2)	4(2)	1(2)
C(56)	29(2)	41(2)	26(2)	1(1)	0(1)	2(1)

Table 5. Hydrogen coordinates (x 10^4) and isotropic displacement parameters (Å^2 x 10^3) for complex **18**.

	x	y	z	U(eq)
H(1AA)	3685	3147	220	61
H(1BA)	5412	2724	-718	61

H(13)	9033	9780	892	37
H(14)	7152	10606	1015	39
H(16)	4730	10592	1157	51
H(17)	2824	9759	1267	60
H(18)	2879	8121	1254	57
H(19)	4811	7332	1140	42
H(21A)	10064	8234	694	39
H(21B)	9887	8000	1419	39
H(33)	6175	3128	1544	46
H(34)	4184	3305	2023	47
H(36)	2531	4381	2508	48
H(37)	1905	5869	2764	51
H(38)	3332	7110	2635	48
H(39)	5339	6898	2184	40
H(41A)	8375	3878	1364	36
H(41B)	7758	4357	758	36
H(51A)	10620	6450	1432	32
H(51)	9050(40)	6950(30)	460(20)	34
H(52A)	9608	5238	482	31
H(52)	8990(40)	5280(30)	1690(20)	30
H(53A)	10585	4009	1032	38
H(53B)	11123	4717	1547	38
H(54A)	12824	4377	860	44
H(54B)	11953	4644	269	44
H(55A)	13353	5890	470	44
H(55B)	12894	5935	1183	44
H(56A)	11841	7136	613	38
H(56B)	11275	6389	130	38

Table 6. Torsion angles [°] for complex **18**.

N(52)-Fe(1)-O(1)-Fe(2)	-2.4(3)	N(51)-Fe(1)-O(1)-Fe(2)	-80.5(3)
N(31)-Fe(1)-O(1)-Fe(2)	71.2(3)	N(11)-Fe(1)-O(1)-Fe(2)	-154.7(3)
Cl(1)-Fe(1)-O(1)-Fe(2)	149.0(2)	Fe(1)-O(1)-Fe(2)-Cl(3)	-136.3(3)
Fe(1)-O(1)-Fe(2)-Cl(4)	101.2(3)	Fe(1)-O(1)-Fe(2)-Cl(2)	-16.6(3)
O(1)-Fe(1)-N(11)-C(12)	75.8(2)	N(52)-Fe(1)-N(11)-C(12)	-21.6(4)
N(51)-Fe(1)-N(11)-C(12)	-23.0(2)	N(31)-Fe(1)-N(11)-C(12)	162.1(2)
Cl(1)-Fe(1)-N(11)-C(12)	-115.7(2)	O(1)-Fe(1)-N(11)-C(20)	-93.3(3)
N(52)-Fe(1)-N(11)-C(20)	169.3(3)	N(51)-Fe(1)-N(11)-C(20)	167.9(3)
N(31)-Fe(1)-N(11)-C(20)	-7.0(3)	Cl(1)-Fe(1)-N(11)-C(20)	75.1(3)
C(20)-N(11)-C(12)-C(13)	0.6(5)	Fe(1)-N(11)-C(12)-C(13)	-169.6(3)
C(20)-N(11)-C(12)-C(21)	178.1(3)	Fe(1)-N(11)-C(12)-C(21)	7.9(4)
N(11)-C(12)-C(13)-C(14)	3.2(5)	C(21)-C(12)-C(13)-C(14)	-174.3(3)
C(12)-C(13)-C(14)-C(15)	-3.6(5)	C(13)-C(14)-C(15)-C(16)	179.9(4)
C(13)-C(14)-C(15)-C(20)	0.5(5)	C(20)-C(15)-C(16)-C(17)	-1.2(6)
C(14)-C(15)-C(16)-C(17)	179.5(4)	C(15)-C(16)-C(17)-C(18)	-0.6(7)
C(16)-C(17)-C(18)-C(19)	0.5(7)	C(17)-C(18)-C(19)-C(20)	1.4(7)
C(12)-N(11)-C(20)-C(19)	177.1(3)	Fe(1)-N(11)-C(20)-C(19)	-14.4(5)
C(12)-N(11)-C(20)-C(15)	-3.7(5)	Fe(1)-N(11)-C(20)-C(15)	164.8(2)
C(18)-C(19)-C(20)-N(11)	176.0(4)	C(18)-C(19)-C(20)-C(15)	-3.2(6)
C(16)-C(15)-C(20)-N(11)	-176.1(3)	C(14)-C(15)-C(20)-N(11)	3.2(5)
C(16)-C(15)-C(20)-C(19)	3.1(5)	C(14)-C(15)-C(20)-C(19)	-177.6(3)
N(11)-C(12)-C(21)-N(51)	21.1(4)	C(13)-C(12)-C(21)-N(51)	-161.3(3)
O(1)-Fe(1)-N(31)-C(32)	-122.4(2)	N(52)-Fe(1)-N(31)-C(32)	-24.8(2)
N(51)-Fe(1)-N(31)-C(32)	-16.5(4)	N(11)-Fe(1)-N(31)-C(32)	153.4(2)
Cl(1)-Fe(1)-N(31)-C(32)	71.2(2)	O(1)-Fe(1)-N(31)-C(40)	68.1(3)
N(52)-Fe(1)-N(31)-C(40)	165.7(3)	N(51)-Fe(1)-N(31)-C(40)	174.0(2)
N(11)-Fe(1)-N(31)-C(40)	-16.1(3)	Cl(1)-Fe(1)-N(31)-C(40)	-98.3(3)
C(40)-N(31)-C(32)-C(33)	1.1(5)	Fe(1)-N(31)-C(32)-C(33)	-169.2(3)

C(40)-N(31)-C(32)-C(41)	-179.0(3)	Fe(1)-N(31)-C(32)-C(41)	10.7(4)
N(31)-C(32)-C(33)-C(34)	1.6(6)	C(41)-C(32)-C(33)-C(34)	-178.2(3)
C(32)-C(33)-C(34)-C(35)	-2.0(6)	C(33)-C(34)-C(35)-C(36)	178.0(4)
C(33)-C(34)-C(35)-C(40)	-0.3(5)	C(34)-C(35)-C(36)-C(37)	-178.3(4)
C(40)-C(35)-C(36)-C(37)	0.0(5)	C(35)-C(36)-C(37)-C(38)	-3.0(6)
C(36)-C(37)-C(38)-C(39)	2.5(6)	C(37)-C(38)-C(39)-C(40)	0.9(6)
C(32)-N(31)-C(40)-C(39)	177.8(3)	Fe(1)-N(31)-C(40)-C(39)	-13.2(4)
C(32)-N(31)-C(40)-C(35)	-3.5(5)	Fe(1)-N(31)-C(40)-C(35)	165.5(2)
C(38)-C(39)-C(40)-N(31)	174.9(3)	C(38)-C(39)-C(40)-C(35)	-3.9(5)
C(34)-C(35)-C(40)-N(31)	3.1(5)	C(36)-C(35)-C(40)-N(31)	-175.3(3)
C(34)-C(35)-C(40)-C(39)	-178.2(3)	C(36)-C(35)-C(40)-C(39)	3.4(5)
N(31)-C(32)-C(41)-N(52)	18.4(4)	C(33)-C(32)-C(41)-N(52)	-161.7(3)
C(12)-C(21)-N(51)-C(51)	-164.9(3)	C(12)-C(21)-N(51)-Fe(1)	-39.5(3)
C(56)-C(51)-N(51)-C(21)	-69.4(4)	C(52)-C(51)-N(51)-C(21)	168.9(3)
C(56)-C(51)-N(51)-Fe(1)	166.4(2)	C(52)-C(51)-N(51)-Fe(1)	44.7(3)
O(1)-Fe(1)-N(51)-C(21)	-50.2(2)	N(52)-Fe(1)-N(51)-C(21)	-146.3(2)
N(31)-Fe(1)-N(51)-C(21)	-154.4(2)	N(11)-Fe(1)-N(51)-C(21)	33.1(2)
Cl(1)-Fe(1)-N(51)-C(21)	119.3(2)	O(1)-Fe(1)-N(51)-C(51)	77.0(2)
N(52)-Fe(1)-N(51)-C(51)	-19.1(2)	N(31)-Fe(1)-N(51)-C(51)	-27.3(4)
N(11)-Fe(1)-N(51)-C(51)	160.2(2)	Cl(1)-Fe(1)-N(51)-C(51)	-113.5(2)
N(51)-C(51)-C(52)-N(52)	-52.8(3)	C(56)-C(51)-C(52)-N(52)	-177.4(2)
N(51)-C(51)-C(52)-C(53)	-176.6(3)	C(56)-C(51)-C(52)-C(53)	58.8(4)
C(32)-C(41)-N(52)-C(52)	-169.2(3)	C(32)-C(41)-N(52)-Fe(1)	-39.1(3)
C(53)-C(52)-N(52)-C(41)	-71.1(4)	C(51)-C(52)-N(52)-C(41)	166.4(3)
C(53)-C(52)-N(52)-Fe(1)	160.1(2)	C(51)-C(52)-N(52)-Fe(1)	37.6(3)
O(1)-Fe(1)-N(52)-C(41)	122.5(2)	N(51)-Fe(1)-N(52)-C(41)	-141.7(2)
N(31)-Fe(1)-N(52)-C(41)	34.1(2)	N(11)-Fe(1)-N(52)-C(41)	-143.1(2)
Cl(1)-Fe(1)-N(52)-C(41)	-50.9(2)	O(1)-Fe(1)-N(52)-C(52)	-106.8(2)
N(51)-Fe(1)-N(52)-C(52)	-11.0(2)	N(31)-Fe(1)-N(52)-C(52)	164.8(2)
N(11)-Fe(1)-N(52)-C(52)	-12.4(4)	Cl(1)-Fe(1)-N(52)-C(52)	79.8(2)

N(52)-C(52)-C(53)-C(54)	-176.0(3)	C(51)-C(52)-C(53)-C(54)	-56.0(4)
C(52)-C(53)-C(54)-C(55)	53.8(4)	C(53)-C(54)-C(55)-C(56)	-54.6(4)
N(51)-C(51)-C(56)-C(55)	-179.4(3)	C(52)-C(51)-C(56)-C(55)	-59.2(4)
C(54)-C(55)-C(56)-C(51)	57.6(4)		

Symmetry transformations used to generate equivalent atoms:

Table 1. Crystal data and structure refinement for complex **19**.

Identification code	ko1003m
Empirical formula	C26 H24 Cl2 N4 O4.25 Ru
Formula weight	632.46
Temperature	120(2) K
Wavelength	0.71073 Å
Crystal system	Monoclinic
Space group	C2
Unit cell dimensions	a = 27.302(4) Å $\quad$ α= 90°
	b = 27.200(3) Å $\quad$ β= 96.713(8)°
	c = 8.6518(9) Å $\quad$ γ = 90°
Volume	6381.0(13) Å^3
Z	8
Density (calculated)	1.317 g/cm^3
Absorption coefficient	0.693 mm^{-1}
F(000)	2560
Crystal size	0.22 x 0.14 x 0.08 mm^3
Theta range for data collection	2.37 to 29.05°
Index ranges	-37<=h<=36, -36<=k<=37, -11<=l<=11
Reflections collected	56716
Independent reflections	8638 [R(int) = 0.3565]
Completeness to theta = 29.05°	99.3 %
Absorption correction	Semi-empirical from equivalents
Refinement method	Full-matrix least-squares on F^2
Data / restraints / parameters	8638 / 207 / 324
Goodness-of-fit on F^2	1.157
Final R indices [I>2sigma(I)]	R1 = 0.1193, wR2 = 0.2280
R indices (all data)	R1 = 0.2855, wR2 = 0.2959
Absolute structure parameter	0.06(16)

Table 2. Atomic coordinates (x 10^4) and equivalent isotropic displacement parameters (Å^2 x 10^3) for complex **19**. U(eq) is defined as one third of the trace of the orthogonalized U^{ij} tensor.

	x	y	z	U(eq)
O(1W)	470(20)	6870(20)	11890(70)	320(20)
O(2W)	4270(20)	5240(20)	6760(70)	290(30)
O(3W)	392(16)	8865(17)	7170(60)	237(18)
O(4W)	4609(15)	5401(15)	-1880(50)	211(16)
O(5W)	4225(18)	6966(17)	1740(60)	280(20)
O(6W)	4560(20)	3040(20)	11080(60)	310(20)
O(7W)	4340(30)	3710(30)	1060(80)	370(30)
O(8W)	0	3120(30)	5000	310(40)
O(9W)	290(20)	2730(20)	6380(70)	330(30)
Ru(1)	2319(1)	3144(1)	9388(3)	36(1)
Cl(1)	2795(4)	3385(3)	11794(10)	44(2)
Cl(2)	1783(3)	2868(4)	7200(11)	48(3)
Ru(2)	2325(1)	5514(1)	4428(3)	38(1)
Cl(3)	2807(4)	5265(3)	6772(10)	42(2)
Cl(4)	1804(4)	5811(3)	2224(8)	45(2)
N111	2166(7)	2447(5)	10420(20)	31(6)
C121	2414(8)	2084(5)	9770(20)	31(6)
C131	2361(9)	1576(6)	10170(30)	43(7)
C141	2032(7)	1442(5)	11120(20)	30(5)
C151	1767(7)	1807(6)	11820(20)	27(5)
C161	1430(8)	1695(7)	12920(20)	43(6)
C171	1220(8)	2061(7)	13650(20)	37(5)
C181	1311(10)	2568(8)	13360(30)	64(9)
C191	1653(10)	2696(7)	12350(30)	52(9)
C201	1883(10)	2317(6)	11580(30)	47(9)

C211	2779(8)	2241(6)	8800(20)	37(6)
N211	2809(6)	2706(5)	8650(20)	25(5)
C311	3069(7)	2976(6)	7480(30)	50(6)
C321	3575(8)	2765(9)	7360(30)	44(7)
C331	3836(9)	3061(8)	6110(30)	87(9)
N112	1814(6)	3757(6)	9710(30)	38(7)
C122	2034(7)	4183(5)	9360(30)	29(6)
C132	1826(9)	4652(7)	9730(30)	57(8)
C142	1438(8)	4679(7)	10500(30)	56(7)
C152	1156(9)	4256(7)	10660(40)	70(10)
C162	714(8)	4242(8)	11390(30)	64(8)
C172	454(9)	3823(9)	11510(40)	84(10)
C182	614(9)	3375(9)	10890(40)	69(9)
C192	1066(8)	3368(7)	10300(30)	51(9)
C202	1367(7)	3786(6)	10270(30)	40(7)
C212	2468(8)	4128(7)	8620(30)	41(7)
N212	2618(7)	3680(7)	8410(30)	31(6)
C312	3111(9)	3522(7)	7920(30)	56(7)
C322	3350(9)	3823(7)	6710(30)	58(7)
C332	3848(9)	3602(10)	6420(40)	102(12)
N113	1856(7)	4871(6)	4620(30)	42(7)
C123	2083(10)	4465(7)	4130(40)	80(12)
C133	1936(9)	3983(7)	4530(30)	62(9)
C143	1530(9)	3926(7)	5170(30)	74(9)
C153	1249(9)	4326(7)	5560(40)	67(9)
C163	803(10)	4295(10)	6250(40)	95(12)
C173	517(10)	4695(10)	6360(40)	89(11)
C183	651(10)	5172(10)	5880(40)	95(13)
C193	1093(8)	5220(7)	5220(30)	53(9)
C203	1396(7)	4812(7)	5050(30)	54(9)

C213	2530(9)	4524(8)	3460(40)	57(9)
N213	2639(9)	4985(9)	3360(40)	63(10)
C313	2969(8)	5138(8)	2420(30)	72(9)
C323	3323(11)	4720(9)	2000(40)	84(11)
C333	3709(9)	4957(8)	1060(30)	71(9)
N114	2225(7)	6230(6)	5480(20)	39(7)
C124	2521(8)	6556(6)	4820(30)	35(7)
C134	2464(9)	7076(6)	5000(30)	39(6)
C144	2181(8)	7246(6)	6020(30)	48(7)
C154	1875(9)	6929(6)	6740(30)	46(7)
C164	1547(9)	7084(8)	7810(30)	59(8)
C174	1332(10)	6743(8)	8640(30)	67(8)
C184	1393(9)	6225(7)	8470(20)	43(6)
C194	1687(8)	6048(6)	7370(20)	28(6)
C204	1895(8)	6402(5)	6430(20)	23(6)
C214	2878(9)	6353(7)	3920(30)	51(8)
N214	2865(7)	5876(6)	3830(20)	43(6)
C314	3243(8)	5569(8)	3220(30)	58(6)
C324	3602(8)	5803(7)	2220(30)	59(9)
C334	3981(8)	5394(10)	1830(30)	91(10)

Table 3. Bond lengths [Å] and angles [°] for complex **19**.

O(2W)-O(4W)#1	1.48(6)	O(3W)-O(7W)#2	1.68(7)
O(4W)-O(2W)#3	1.48(6)	O(7W)-O(3W)#4	1.68(7)
O(8W)-O(9W)#5	1.73(6)	O(8W)-O(9W)	1.73(6)
Ru(1)-N212	1.912(19)	Ru(1)-N211	1.950(16)
Ru(1)-N111	2.155(14)	Ru(1)-N112	2.204(15)

Ru(1)-Cl(2)	2.376(10)	Ru(1)-Cl(1)	2.413(10)
Ru(2)-N214	1.894(19)	Ru(2)-N213	1.96(3)
Ru(2)-N114	2.180(15)	Ru(2)-N113	2.185(16)
Ru(2)-Cl(4)	2.381(9)	Ru(2)-Cl(3)	2.383(9)
N111-C121	1.355(14)	N111-C201	1.383(14)
C121-C131	1.436(15)	C121-C211	1.441(16)
C131-C141	1.332(17)	C131-H131	0.9500
C141-C151	1.407(17)	C141-H141	0.9500
C151-C161	1.431(17)	C151-C201	1.444(15)
C161-C171	1.35(2)	C161-H161	0.9500
C171-C181	1.428(19)	C171-H171	0.9500
C181-C191	1.397(16)	C181-H181	0.9500
C191-C201	1.417(16)	C191-H191	0.9500
C211-N211	1.275(14)	C211-H211	0.9500
N211-C311	1.50(2)	C311-C321	1.511(16)
C311-C312	1.533(16)	C311-H311	1.0000
C321-C331	1.586(17)	C321-H32A1	0.9900
C321-H32B1	0.9900	C331-C332	1.497(18)
C331-H33A1	0.9900	C331-H33B1	0.9900
N112-C122	1.355(14)	N112-C202	1.368(14)
C122-C212	1.419(16)	C122-C132	1.447(15)
C132-C142	1.314(18)	C132-H132	0.9500
C142-C152	1.401(18)	C142-H142	0.9500
C152-C162	1.423(18)	C152-C202	1.457(16)
C162-C172	1.35(2)	C162-H162	0.9500
C172-C182	1.423(19)	C172-H172	0.9500
C182-C192	1.387(16)	C182-H182	0.9500
C192-C202	1.404(17)	C192-H192	0.9500
C212-N212	1.306(14)	C212-H212	0.9500
N212-C312	1.52(2)	C312-C322	1.531(16)

C312-H312	1.0000	C322-C332	1.536(17)
C322-H32A2	0.9900	C322-H32B2	0.9900
C332-H33A2	0.9900	C332-H33B2	0.9900
N113-C123	1.359(15)	N113-C203	1.361(15)
C123-C213	1.420(17)	C123-C133	1.427(16)
C133-C143	1.305(18)	C133-H133	0.9500
C143-C153	1.393(18)	C143-H143	0.9500
C153-C163	1.418(18)	C153-C203	1.465(16)
C163-C173	1.35(2)	C163-H163	0.9500
C173-C183	1.422(19)	C173-H173	0.9500
C183-C193	1.402(17)	C183-H183	0.9500
C193-C203	1.402(17)	C193-H193	0.9500
C213-N213	1.295(15)	C213-H213	0.9500
N213-C313	1.35(3)	C313-C314	1.518(17)
C313-C323	1.560(18)	C313-H313	1.0000
C323-C333	1.543(18)	C323-H32A3	0.9900
C323-H32B3	0.9900	C333-C334	1.513(18)
C333-H33A3	0.9900	C333-H33B3	0.9900
N114-C124	1.369(14)	N114-C204	1.372(14)
C124-C214	1.430(16)	C124-C134	1.434(15)
C134-C144	1.316(18)	C134-H134	0.9500
C144-C154	1.399(18)	C144-H144	0.9500
C154-C164	1.428(17)	C154-C204	1.459(15)
C164-C174	1.35(2)	C164-H164	0.9500
C174-C184	1.429(19)	C174-H174	0.9500
C184-C194	1.401(15)	C184-H184	0.9500
C194-C204	1.420(16)	C194-H194	0.9500
C214-N214	1.299(15)	C214-H214	0.9500
N214-C314	1.47(2)	C314-C324	1.521(16)
C314-H314	1.0000	C324-C334	1.583(17)

C324-H32A4	0.9900	C324-H32B4	0.9900
C334-H33A4	0.9900	C334-H33B4	0.9900
O(9W)#5-O(8W)-O(9W)	103(7)	N212-Ru(1)-N211	88.8(6)
N212-Ru(1)-N111	164.8(6)	N211-Ru(1)-N111	76.8(5)
N212-Ru(1)-N112	77.5(6)	N211-Ru(1)-N112	165.1(6)
N111-Ru(1)-N112	117.3(6)	N212-Ru(1)-Cl(2)	98.3(8)
N211-Ru(1)-Cl(2)	86.0(6)	N111-Ru(1)-Cl(2)	85.4(7)
N112-Ru(1)-Cl(2)	90.2(7)	N212-Ru(1)-Cl(1)	87.6(8)
N211-Ru(1)-Cl(1)	97.3(6)	N111-Ru(1)-Cl(1)	89.6(6)
N112-Ru(1)-Cl(1)	88.0(7)	Cl(2)-Ru(1)-Cl(1)	173.3(3)
N214-Ru(2)-N213	81.7(8)	N214-Ru(2)-N114	77.8(6)
N213-Ru(2)-N114	159.3(7)	N214-Ru(2)-N113	156.7(6)
N213-Ru(2)-N113	75.0(7)	N114-Ru(2)-N113	125.5(6)
N214-Ru(2)-Cl(4)	91.0(7)	N213-Ru(2)-Cl(4)	97.2(10)
N114-Ru(2)-Cl(4)	86.5(7)	N113-Ru(2)-Cl(4)	91.9(7)
N214-Ru(2)-Cl(3)	90.5(7)	N213-Ru(2)-Cl(3)	87.8(10)
N114-Ru(2)-Cl(3)	89.0(7)	N113-Ru(2)-Cl(3)	88.7(7)
Cl(4)-Ru(2)-Cl(3)	174.9(3)	C121-N111-C201	117.3(13)
C121-N111-Ru(1)	110.0(9)	C201-N111-Ru(1)	132.7(10)
N111-C121-C131	122.3(13)	N111-C121-C211	115.7(12)
C131-C121-C211	121.6(14)	C141-C131-C121	120.4(15)
C141-C131-H131	119.8	C121-C131-H131	119.8
C131-C141-C151	119.2(14)	C131-C141-H141	120.4
C151-C141-H141	120.4	C141-C151-C161	122.6(13)
C141-C151-C201	118.9(13)	C161-C151-C201	118.0(14)
C171-C161-C151	120.0(15)	C171-C161-H161	120.0
C151-C161-H161	120.0	C161-C171-C181	122.6(15)
C161-C171-H171	118.7	C181-C171-H171	118.7
C191-C181-C171	119.6(17)	C191-C181-H181	120.2

C171-C181-H181	120.2	C181-C191-C201	118.7(16)
C181-C191-H191	120.6	C201-C191-H191	120.6
N111-C201-C191	118.3(13)	N111-C201-C151	120.2(13)
C191-C201-C151	121.0(13)	N211-C211-C121	114.3(14)
N211-C211-H211	122.9	C121-C211-H211	122.9
C211-N211-C311	126.6(15)	C211-N211-Ru(1)	121.2(12)
C311-N211-Ru(1)	108.6(10)	N211-C311-C321	111.7(15)
N211-C311-C312	109.6(15)	C321-C311-C312	110.0(17)
N211-C311-H311	108.5	C321-C311-H311	108.5
C312-C311-H311	108.5	C311-C321-C331	109.9(14)
C311-C321-H32A1	109.7	C331-C321-H32A1	109.7
C311-C321-H32B1	109.7	C331-C321-H32B1	109.7
H32A1-C321-H32B1	108.2	C332-C331-C321	112.3(19)
C332-C331-H33A1	109.1	C321-C331-H33A1	109.1
C332-C331-H33B1	109.1	C321-C331-H33B1	109.1
H33A1-C331-H33B1	107.9	C122-N112-C202	117.8(13)
C122-N112-Ru(1)	108.6(9)	C202-N112-Ru(1)	133.4(11)
N112-C122-C212	115.2(12)	N112-C122-C132	120.6(14)
C212-C122-C132	124.3(14)	C142-C132-C122	121.4(17)
C142-C132-H132	119.3	C122-C132-H132	119.3
C132-C142-C152	119.4(16)	C132-C142-H142	120.3
C152-C142-H142	120.3	C142-C152-C162	124.8(16)
C142-C152-C202	117.4(15)	C162-C152-C202	117.1(16)
C172-C162-C152	122.5(17)	C172-C162-H162	118.7
C152-C162-H162	118.7	C162-C172-C182	120.2(18)
C162-C172-H172	119.9	C182-C172-H172	119.9
C192-C182-C172	118.4(18)	C192-C182-H182	120.8
C172-C182-H182	120.8	C182-C192-C202	123.0(16)
C182-C192-H192	118.5	C202-C192-H192	118.5
N112-C202-C192	120.6(14)	N112-C202-C152	121.7(14)

C192-C202-C152	117.2(14)	N212-C212-C122	116.9(15)
N212-C212-H212	121.6	C122-C212-H212	121.6
C212-N212-C312	127.2(17)	C212-N212-Ru(1)	119.7(12)
C312-N212-Ru(1)	110.2(12)	N212-C312-C322	120.1(18)
N212-C312-C311	107.4(16)	C322-C312-C311	112.0(14)
N212-C312-H312	105.4	C322-C312-H312	105.4
C311-C312-H312	105.4	C312-C322-C332	111.0(14)
C312-C322-H32A2	109.4	C332-C322-H32A2	109.4
C312-C322-H32B2	109.4	C332-C322-H32B2	109.4
H32A2-C322-H32B2	108.0	C331-C332-C322	114.3(16)
C331-C332-H33A2	108.7	C322-C332-H33A2	108.7
C331-C332-H33B2	108.7	C322-C332-H33B2	108.7
H33A2-C332-H33B2	107.6	C123-N113-C203	117.3(15)
C123-N113-Ru(2)	109.6(11)	C203-N113-Ru(2)	133.1(12)
N113-C123-C213	118.7(15)	N113-C123-C133	121.4(16)
C213-C123-C133	118.8(17)	C143-C133-C123	119.2(17)
C143-C133-H133	120.4	C123-C133-H133	120.4
C133-C143-C153	122.0(17)	C133-C143-H143	119.0
C153-C143-H143	119.0	C143-C153-C163	125.4(17)
C143-C153-C203	117.0(15)	C163-C153-C203	117.2(16)
C173-C163-C153	121.0(19)	C173-C163-H163	119.5
C153-C163-H163	119.5	C163-C173-C183	123.0(19)
C163-C173-H173	118.5	C183-C173-H173	118.5
C193-C183-C173	117.8(19)	C193-C183-H183	121.1
C173-C183-H183	121.1	C183-C193-C203	120.9(17)
C183-C193-H193	119.5	C203-C193-H193	119.5
N113-C203-C193	120.6(15)	N113-C203-C153	118.9(15)
C193-C203-C153	119.9(14)	N213-C213-C123	110.5(16)
N213-C213-H213	124.7	C123-C213-H213	124.7
C213-N213-C313	121(2)	C213-N213-Ru(2)	124.4(15)

C313-N213-Ru(2)	114.8(17)	N213-C313-C314	107(2)
N213-C313-C323	113(2)	C314-C313-C323	113(2)
N213-C313-H313	108.1	C314-C313-H313	108.1
C323-C313-H313	108.1	C333-C323-C313	107.3(15)
C333-C323-H32A3	110.3	C313-C323-H32A3	110.3
C333-C323-H32B3	110.3	C313-C323-H32B3	110.3
H32A3-C323-H32B3	108.5	C334-C333-C323	115(2)
C334-C333-H33A3	108.4	C323-C333-H33A3	108.4
C334-C333-H33B3	108.4	C323-C333-H33B3	108.4
H33A3-C333-H33B3	107.5	C124-N114-C204	119.4(13)
C124-N114-Ru(2)	107.2(9)	C204-N114-Ru(2)	132.6(11)
N114-C124-C214	116.8(12)	N114-C124-C134	121.0(14)
C214-C124-C134	122.2(14)	C144-C134-C124	120.0(15)
C144-C134-H134	120.0	C124-C134-H134	120.6(15)
C134-C144-H144	119.7	C154-C144-H144	119.7
C144-C154-C164	124.3(15)	C144-C154-C204	119.1(13)
C164-C154-C204	116.6(14)	C174-C164-C154	119.3(16)
C174-C164-H164	120.4	C154-C164-H164	120.4
C164-C174-C184	123.9(17)	C164-C174-H174	118.0
C194-C184-C174	119.6(16)	C194-C184-H184	120.2
C174-C184-H184	120.2	C184-C194-C204	117.1(14)
C184-C194-H194	121.5	C204-C194-H194	121.5
N114-C204-C194	116.5(13)	N114-C204-C154	119.1(13)
C194-C204-C154	122.3(13)	N214-C214-C124	113.7(15)
N214-C214-H214	123.2	C124-C214-H214	123.2
C214-N214-C314	121.4(13)	C314-N214-Ru(2)	113.8(13)
N214-C314-C313	106.0(16)	N214-C314-C324	119.5(18)
C313-C314-C324	112.2(14)	N214-C314-H314	106.1
C324-C314-H314	106.1	C314-C324-C334	107.9(14)
C314-C324-H32A4	110.1	C334-C324-H32A4	110.1

C314-C324-H32B4	110.1	C334-C324-H32B4	110.1
H32A4-C324-H32B4	108.4	C333-C334-C324	110.3(14)
C333-C334-H33A4	109.6	C324-C334-H33A4	109.6
C333-C334-H33B4	109.6	C324-C334-H33B4	109.6
H33A4-C334-H33B4	108.1		

<div align="center">

Symmetry transformations used to generate equivalent atoms:

#1 x,y,z+1   #2 -x+1/2,y+1/2,-z+1   #3 x,y,z-1   #4 -x+1/2,y-1/2,-z+1   #5 -x,y,-z+1

</div>

Table 4. Anisotropic displacement parameters (Å^2 x 10^3) for complex **19**. The anisotropic displacement factor exponent takes the following form: $-2\pi^2[\,h^2\,a^{*2}U^{11} + ... + 2\,h\,k\,a^*\,b^*\,U^{12}\,]$

	U^{11}	U^{22}	U^{33}	U^{23}	U^{13}	U^{12}
Ru(1)	55(2)	25(2)	30(2)	1(1)	9(1)	4(2)
Cl(1)	64(6)	28(5)	40(6)	-9(4)	13(5)	-6(5)
Ru(2)	62(2)	27(2)	24(2)	-1(1)	8(1)	1(2)
Cl(3)	66(6)	28(5)	30(5)	0(4)	-2(5)	-4(5)
Cl(4)	88(5)	33(3)	15(2)	2(2)	8(3)	-7(3)

Table 5. Hydrogen coordinates (x 10^4) and isotropic displacement parameters (Å^2 x 10^3) for complex **19**.

	x	y	z	U(eq)
H131	2561	1334	9765	51
H141	1977	1104	11312	37

H161	1355	1362	13128	52
H171	1003	1979	14396	44
H181	1139	2816	13854	77
H191	1731	3031	12191	63
H211	2980	2018	8314	44
H311	2868	2947	6443	60
H32A1	3545	2414	7060	53
H32B1	3777	2785	8389	53
H33A1	4177	2939	6109	105
H33B1	3657	3000	5064	105
H132	1972	4946	9415	68
H142	1350	4982	10933	67
H162	598	4538	11797	77
H172	163	3828	12019	101
H182	416	3087	10870	83
H192	1177	3067	9910	62
H212	2640	4405	8288	50
H312	3350	3535	8890	68
H32A2	3398	4165	7087	69
H32B2	3127	3830	5725	69
H33A2	3965	3772	5522	122
H33B2	4091	3667	7342	122
H133	2132	3706	4337	75
H143	1422	3603	5380	88
H163	705	3989	6638	113
H173	212	4656	6772	107
H183	448	5449	6014	114
H193	1188	5534	4873	64
H213	2723	4261	3132	68
H313	2782	5260	1428	86

H32A3	3487	4565	2954	101
H32B3	3135	4464	1363	101
H33A3	3954	4704	864	85
H33B3	3542	5064	40	85
H134	2629	7298	4393	47
H144	2186	7586	6259	57
H164	1480	7423	7942	71
H174	1127	6854	9388	80
H184	1236	6002	9097	52
H194	1744	5706	7250	33
H214	3103	6548	3424	61
H314	3449	5430	4154	70
H32A4	3780	6078	2793	71
H32B4	3422	5935	1252	71
H33A4	4207	5532	1129	109
H33B4	4181	5286	2802	109

Table 6. Torsion angles [°] for complex **19**.

N212-Ru(1)-N111-C121	-30(4)	N211-Ru(1)-N111-C121	-11.8(17)
N112-Ru(1)-N111-C121	163.0(17)	Cl(2)-Ru(1)-N111-C121	75.1(17)
Cl(1)-Ru(1)-N111-C121	-109.4(17)	N212-Ru(1)-N111-C201	149(3)
N211-Ru(1)-N111-C201	167(3)	N112-Ru(1)-N111-C201	-18(3)
Cl(2)-Ru(1)-N111-C201	-106(3)	Cl(1)-Ru(1)-N111-C201	69(3)
C201-N111-C121-C131	5(4)	Ru(1)-N111-C121-C131	-177(2)
C201-N111-C121-C211	-168(2)	Ru(1)-N111-C121-C211	11(3)
N111-C121-C131-C141	5(4)	C211-C121-C131-C141	178(2)
C121-C131-C141-C151	-5(4)	C131-C141-C151-C161	-176(2)

C131-C141-C151-C201	-4(3)	C141-C151-C161-C171	174(2)
C201-C151-C161-C171	2(4)	C151-C161-C171-C181	1(4)
C161-C171-C181-C191	-4(4)	C171-C181-C191-C201	3(5)
C121-N111-C201-C191	175(3)	Ru(1)-N111-C201-C191	-4(5)
C121-N111-C201-C151	-14(4)	Ru(1)-N111-C201-C151	167.4(18)
C181-C191-C201-N111	171(3)	C181-C191-C201-C151	0(5)
C141-C151-C201-N111	14(4)	C161-C151-C201-N111	-174(2)
C141-C151-C201-C191	-175(3)	C161-C151-C201-C191	-3(4)
N111-C121-C211-N211	-2(3)	C131-C121-C211-N211	-174(2)
C121-C211-N211-C311	-166(2)	C121-C211-N211-Ru(1)	-10(3)
N212-Ru(1)-N211-C211	-172(2)	N111-Ru(1)-N211-C211	12.5(19)
N112-Ru(1)-N211-C211	-149(3)	Cl(2)-Ru(1)-N211-C211	-73.8(19)
Cl(1)-Ru(1)-N211-C211	100.3(19)	N212-Ru(1)-N211-C311	-12.4(15)
N111-Ru(1)-N211-C311	172.3(16)	N112-Ru(1)-N211-C311	10(4)
Cl(2)-Ru(1)-N211-C311	86.0(14)	Cl(1)-Ru(1)-N211-C311	-99.8(14)
C211-N211-C311-C321	-46(3)	Ru(1)-N211-C311-C321	155.8(16)
C211-N211-C311-C312	-168(2)	Ru(1)-N211-C311-C312	34(2)
N211-C311-C321-C331	180(2)	C312-C311-C321-C331	-58(3)
C311-C321-C331-C332	54(3)	N212-Ru(1)-N112-C122	-12.5(17)
N211-Ru(1)-N112-C122	-36(4)	N111-Ru(1)-N112-C122	164.0(16)
Cl(2)-Ru(1)-N112-C122	-111.0(17)	Cl(1)-Ru(1)-N112-C122	75.4(17)
N212-Ru(1)-N112-C202	173(3)	N211-Ru(1)-N112-C202	149(3)
N111-Ru(1)-N112-C202	-11(3)	Cl(2)-Ru(1)-N112-C202	74(3)
Cl(1)-Ru(1)-N112-C202	-99(2)	C202-N112-C122-C212	-173(2)
Ru(1)-N112-C122-C212	12(3)	C202-N112-C122-C132	6(4)
Ru(1)-N112-C122-C132	-169(2)	N112-C122-C132-C142	4(4)
C212-C122-C132-C142	-176(3)	C122-C132-C142-C152	-14(4)
C132-C142-C152-C162	-177(3)	C132-C142-C152-C202	13(4)
C142-C152-C162-C172	180(3)	C202-C152-C162-C172	-10(5)
C152-C162-C172-C182	-1(5)	C162-C172-C182-C192	7(5)

C172-C182-C192-C202	-2(5)	C122-N112-C202-C192	165(3)
Ru(1)-N112-C202-C192	-21(4)	C122-N112-C202-C152	-7(4)
Ru(1)-N112-C202-C152	167(2)	C182-C192-C202-N112	179(3)
C182-C192-C202-C152	-9(4)	C142-C152-C202-N112	-2(4)
C162-C152-C202-N112	-173(3)	C142-C152-C202-C192	-175(3)
C162-C152-C202-C192	14(4)	N112-C122-C212-N212	-3(4)
C132-C122-C212-N212	178(3)	C122-C212-N212-C312	-168(2)
C122-C212-N212-Ru(1)	-10(4)	N211-Ru(1)-N212-C212	-174(2)
N111-Ru(1)-N212-C212	-156(3)	N112-Ru(1)-N212-C212	12(2)
Cl(2)-Ru(1)-N212-C212	101(2)	Cl(1)-Ru(1)-N212-C212	-76(2)
N211-Ru(1)-N212-C312	-11.7(17)	N111-Ru(1)-N212-C312	6(4)
N112-Ru(1)-N212-C312	174.1(19)	Cl(2)-Ru(1)-N212-C312	-97.5(16)
Cl(1)-Ru(1)-N212-C312	85.6(16)	C212-N212-C312-C322	-38(4)
Ru(1)-N212-C312-C322	161.9(18)	C212-N212-C312-C311	-167(3)
Ru(1)-N212-C312-C311	32(2)	N211-C311-C312-N212	-43(3)
C321-C311-C312-N212	-166.1(19)	N211-C311-C312-C322	-177(2)
C321-C311-C312-C322	60(3)	N212-C312-C322-C332	179(2)
C311-C312-C322-C332	-54(3)	C321-C331-C332-C322	-49(4)
C312-C322-C332-C331	49(3)	N214-Ru(2)-N113-C123	10(4)
N213-Ru(2)-N113-C123	9(2)	N114-Ru(2)-N113-C123	-167(2)
Cl(4)-Ru(2)-N113-C123	106(2)	Cl(3)-Ru(2)-N113-C123	-79(2)
N214-Ru(2)-N113-C203	-167(3)	N213-Ru(2)-N113-C203	-167(3)
N114-Ru(2)-N113-C203	17(3)	Cl(4)-Ru(2)-N113-C203	-70(3)
Cl(3)-Ru(2)-N113-C203	105(3)	C203-N113-C123-C213	171(3)
Ru(2)-N113-C123-C213	-6(4)	C203-N113-C123-C133	-21(5)
Ru(2)-N113-C123-C133	162(3)	N113-C123-C133-C143	11(6)
C213-C123-C133-C143	179(3)	C123-C133-C143-C153	-4(5)
C133-C143-C153-C163	180(3)	C133-C143-C153-C203	7(5)
C143-C153-C163-C173	-169(3)	C203-C153-C163-C173	3(5)
C153-C163-C173-C183	-4(6)	C163-C173-C183-C193	3(6)

C173-C183-C193-C203	-1(5)	C123-N113-C203-C193	-165(3)
Ru(2)-N113-C203-C193	12(4)	C123-N113-C203-C153	24(4)
Ru(2)-N113-C203-C153	-160(2)	C183-C193-C203-N113	-170(3)
C183-C193-C203-C153	1(5)	C143-C153-C203-N113	-17(4)
C163-C153-C203-N113	170(3)	C143-C153-C203-C193	171(3)
C163-C153-C203-C193	-2(5)	N113-C123-C213-N213	-3(5)
C133-C123-C213-N213	-171(3)	C123-C213-N213-C313	-163(3)
C123-C213-N213-Ru(2)	14(5)	N214-Ru(2)-N213-C213	167(3)
N114-Ru(2)-N213-C213	157(3)	N113-Ru(2)-N213-C213	-13(3)
Cl(4)-Ru(2)-N213-C213	-103(3)	Cl(3)-Ru(2)-N213-C213	76(3)
N214-Ru(2)-N213-C313	-17(3)	N114-Ru(2)-N213-C313	-26(5)
N113-Ru(2)-N213-C313	163(3)	Cl(4)-Ru(2)-N213-C313	73(3)
Cl(3)-Ru(2)-N213-C313	-108(3)	C213-N213-C313-C314	-145(3)
Ru(2)-N213-C313-C314	38(3)	C213-N213-C313-C323	-21(5)
Ru(2)-N213-C313-C323	162(2)	N213-C313-C323-C333	-174(3)
C314-C313-C323-C333	-53(3)	C313-C323-C333-C334	53(3)
N214-Ru(2)-N114-C124	14.4(18)	N213-Ru(2)-N114-C124	24(4)
N113-Ru(2)-N114-C124	-167.2(17)	Cl(4)-Ru(2)-N114-C124	-77.4(18)
Cl(3)-Ru(2)-N114-C124	105.1(18)	N214-Ru(2)-N114-C204	-176(3)
N213-Ru(2)-N114-C204	-166(3)	N113-Ru(2)-N114-C204	3(3)
Cl(4)-Ru(2)-N114-C204	93(2)	Cl(3)-Ru(2)-N114-C204	-85(2)
C204-N114-C124-C214	176(2)	Ru(2)-N114-C124-C214	-12(3)
C204-N114-C124-C134	-5(4)	Ru(2)-N114-C124-C134	166(2)
N114-C124-C134-C144	11(4)	C214-C124-C134-C144	-170(3)
C124-C134-C144-C154	-10(4)	C134-C144-C154-C164	-178(3)
C134-C144-C154-C204	4(4)	C144-C154-C164-C174	-169(3)
C204-C154-C164-C174	10(4)	C154-C164-C174-C184	-3(4)
C164-C174-C184-C194	-1(4)	C174-C184-C194-C204	-2(4)
C124-N114-C204-C194	-165(2)	Ru(2)-N114-C204-C194	26(4)
C124-N114-C204-C154	-1(4)	Ru(2)-N114-C204-C154	-170.3(19)

C184-C194-C204-N114	173(2)	C184-C194-C204-C154	10(4)
C144-C154-C204-N114	2(4)	C164-C154-C204-N114	-176(2)
C144-C154-C204-C194	165(2)	C164-C154-C204-C194	-13(4)
N114-C124-C214-N214	1(4)	C134-C124-C214-N214	-178(2)
C124-C214-N214-C314	-169(2)	C124-C214-N214-Ru(2)	14(3)
N213-Ru(2)-N214-C214	167(2)	N114-Ru(2)-N214-C214	-16(2)
N113-Ru(2)-N214-C214	167(2)	Cl(4)-Ru(2)-N214-C214	70(2)
Cl(3)-Ru(2)-N214-C214	-105(2)	N213-Ru(2)-N214-C314	-10.4(19)
N114-Ru(2)-N214-C314	166.2(18)	N113-Ru(2)-N214-C314	-11(3)
Cl(4)-Ru(2)-N214-C314	-107.6(16)	Cl(3)-Ru(2)-N214-C314	77.3(16)
C214-N214-C314-C313	-145(3)	Ru(2)-N214-C314-C313	32(2)
C214-N214-C314-C324	-18(4)	Ru(2)-N214-C314-C324	159.9(17)
N213-C313-C314-N214	-44(3)	C323-C313-C314-N214	-168(2)
N213-C313-C314-C324	-176(2)	C323-C313-C314-C324	60(3)
N214-C314-C324-C334	177(2)	C313-C314-C324-C334	-58(3)
C323-C333-C334-C324	-56(3)	C314-C324-C334-C333	56(3)

Symmetry transformations used to generate equivalent atoms:

#1 x,y,z+1 #2 -x+1/2,y+1/2,-z+1 #3 x,y,z-1 #4 -x+1/2,y-1/2,-z+1 #5 -x,y,-z+1

Table 1. Crystal data and structure refinement for complex **23**.

Identification code	ko0801m
Empirical formula	C35 H30 Cl2 I2 N4 Ni
Formula weight	890.04
Temperature	120(2) K
Wavelength	0.71073 Å
Crystal system	Monoclinic
Space group	P2(1)
Unit cell dimensions	a = 10.3835(8) Å $\quad$ α= 90°
	b = 24.3333(18) Å $\quad$ β= 104.843(2)°
	c = 13.5638(9) Å $\quad$ γ = 90°
Volume	3312.7(4) Å^3
Z	4
Density (calculated)	1.785 Mg/m^3
Absorption coefficient	2.643 mm^{-1}
F(000)	1744
Crystal size	0.20 x 0.15 x 0.10 mm^3
Theta range for data collection	2.03 to 32.14°
Index ranges	-15<=h<=15, -35<=k<=36, -17<=l<=20
Reflections collected	43378
Independent reflections	21618 [R(int) = 0.0310]
Completeness to theta = 32.14°	97.9 %
Absorption correction	None
Refinement method	Full-matrix least-squares on F^2
Data / restraints / parameters	21618 / 1 / 793
Goodness-of-fit on F^2	1.061
Final R indices [I>2sigma(I)]	R1 = 0.0364, wR2 = 0.0776
R indices (all data)	R1 = 0.0469, wR2 = 0.0826
Absolute structure parameter	0.017(13)

Table 2. Atomic coordinates (x 10^4) and equivalent isotropic displacement parameters (Å^2 x 10^3) for complex **23**. U(eq) is defined as one third of the trace of the orthogonalized U^{ij} tensor.

	x	y	z	U(eq)
Cl11	1971(2)	5183(1)	7652(1)	79(1)
Cl21	3407(2)	4137(1)	7896(1)	66(1)
C1S1	2314(6)	4569(3)	8330(4)	55(1)
Ni11	8463(1)	3155(1)	7507(1)	25(1)
I11	6025(1)	3110(1)	6302(1)	33(1)
I21	10187(1)	3468(1)	9216(1)	36(1)
N111	8232(3)	2330(1)	8104(2)	26(1)
C121	8848(4)	1976(2)	7606(3)	31(1)
C131	8895(5)	1407(2)	7751(3)	37(1)
C141	8299(5)	1199(2)	8465(3)	38(1)
C151	7701(5)	1545(2)	9013(3)	36(1)
C161	7144(6)	1331(2)	9797(4)	51(1)
C171	6562(7)	1663(2)	10339(5)	59(2)
C181	6421(5)	2243(2)	10147(4)	42(1)
C191	5719(6)	2576(2)	10679(4)	47(1)
C201	5532(5)	3125(2)	10473(3)	40(1)
C211	6044(4)	3357(2)	9708(3)	35(1)
C221	6724(4)	3040(2)	9172(3)	29(1)
C231	6946(4)	2479(2)	9371(3)	30(1)
C241	7648(4)	2121(2)	8816(3)	30(1)
C251	9451(4)	2212(2)	6827(3)	32(1)
N251	9346(3)	2723(1)	6663(2)	27(1)
N311	7740(3)	5145(2)	6666(2)	29(1)
C321	7896(4)	4639(2)	7040(3)	30(1)
C331	7313(5)	4457(2)	7814(3)	32(1)

314

C341	6574(4)	4823(2)	8207(3)	31(1)
C351	6367(4)	5355(2)	7828(3)	33(1)
C361	5578(6)	5751(2)	8165(4)	48(1)
C371	5380(7)	6254(2)	7741(5)	62(2)
C381	5963(5)	6420(2)	6938(4)	45(1)
C391	5708(6)	6940(2)	6467(5)	57(2)
C401	6217(5)	7073(2)	5680(5)	57(2)
C411	7005(5)	6695(2)	5298(4)	44(1)
C421	7286(5)	6189(2)	5746(3)	37(1)
C431	6771(4)	6042(2)	6577(3)	35(1)
C441	6984(4)	5501(2)	7036(3)	28(1)
C451	8803(4)	4313(2)	6588(3)	29(1)
N451	9114(3)	3812(1)	6738(2)	28(1)
C511	9783(3)	3019(2)	5869(2)	28(1)
C521	10863(4)	2735(2)	5486(3)	34(1)
C531	11293(4)	3101(2)	4705(3)	40(1)
C541	11731(4)	3656(2)	5145(3)	37(1)
C551	10633(4)	3947(2)	5524(3)	33(1)
C561	10197(3)	3590(2)	6302(2)	29(1)
Cl32	1666(2)	4303(1)	2338(1)	84(1)
Cl42	3199(2)	3290(1)	2532(2)	98(1)
C2S2	2707(8)	3874(3)	1811(5)	76(2)
Ni22	6587(1)	5267(1)	2521(1)	25(1)
I32	4909(1)	4897(1)	832(1)	34(1)
I42	8999(1)	5392(1)	3735(1)	35(1)
N112	6695(4)	6084(1)	1881(2)	29(1)
C122	6018(5)	6428(2)	2347(3)	34(1)
C132	5966(5)	6995(2)	2220(4)	41(1)
C142	6615(5)	7228(2)	1570(4)	45(1)
C152	7298(5)	6883(2)	1025(4)	43(1)

C162	7901(8)	7113(3)	292(5)	67(2)
C172	8527(8)	6794(3)	-223(6)	81(2)
C182	8647(6)	6209(3)	-68(4)	49(1)
C192	9337(6)	5881(3)	-613(4)	55(1)
C202	9534(5)	5333(2)	-421(3)	43(1)
C212	9028(5)	5089(2)	328(3)	40(1)
C222	8320(5)	5399(2)	851(3)	37(1)
C232	8095(4)	5957(2)	677(3)	32(1)
C242	7353(4)	6310(2)	1217(3)	31(1)
C252	5219(4)	6173(2)	2960(3)	35(1)
N252	5295(3)	5656(2)	3075(2)	29(1)
N312	7350(3)	3273(1)	3312(2)	28(1)
C322	7221(4)	3790(2)	2987(3)	27(1)
C332	7813(5)	3986(2)	2230(3)	31(1)
C342	8563(5)	3628(2)	1821(3)	34(1)
C352	8727(5)	3087(2)	2158(3)	35(1)
C362	9584(6)	2707(2)	1826(4)	50(1)
C372	9789(7)	2202(3)	2232(4)	58(2)
C382	9104(5)	2008(2)	2965(4)	43(1)
C392	9326(6)	1480(2)	3370(4)	50(1)
C402	8720(6)	1309(2)	4107(4)	48(1)
C412	7892(5)	1667(2)	4454(3)	40(1)
C422	7647(5)	2189(2)	4069(3)	36(1)
C432	8263(4)	2370(2)	3312(3)	31(1)
C442	8076(4)	2922(2)	2912(3)	30(1)
C452	6465(4)	4122(2)	3554(3)	29(1)
N452	6198(3)	4630(1)	3453(2)	27(1)
C512	4536(3)	5316(2)	3612(2)	30(1)
C522	3819(4)	5623(2)	4293(3)	38(1)
C532	3130(4)	5213(2)	4856(3)	43(1)

C542	4121(4)	4804(2)	5457(3)	41(1)
C552	4843(4)	4489(2)	4778(3)	33(1)
C562	5523(3)	4887(2)	4199(2)	28(1)

Table 3. Bond lengths [Å] and angles [°] for complex **23**.

Cl11-C1S1	1.744(7)	Cl21-C1S1	1.755(7)
C1S1-H1A1	0.9900	C1S1-H1B1	0.9900
Ni11-N251	1.947(3)	Ni11-N451	2.112(3)
Ni11-N111	2.202(4)	Ni11-I11	2.6402(6)
Ni11-I21	2.6516(5)	N111-C121	1.352(6)
N111-C241	1.362(6)	C121-C131	1.398(6)
C121-C251	1.476(6)	C131-C141	1.373(7)
C131-H131	0.9500	C141-C151	1.372(7)
C141-H141	0.9500	C151-C241	1.424(6)
C151-C161	1.433(7)	C161-C171	1.336(8)
C161-H161	0.9500	C171-C181	1.436(8)
C171-H171	0.9500	C181-C191	1.407(8)
C181-C231	1.425(6)	C191-C201	1.368(8)
C191-H191	0.9500	C201-C211	1.400(7)
C201-H201	0.9500	C211-C221	1.373(6)
C211-H211	0.9500	C221-C231	1.399(6)
C221-H221	0.9500	C231-C241	1.462(7)
C251-N251	1.264(6)	C251-H251	0.9500
N251-C511	1.460(5)	N311-C321	1.325(6)
N311-C441	1.349(6)	C321-C331	1.412(6)
C321-C451	1.479(6)	C331-C341	1.370(7)
C331-H331	0.9500	C341-C351	1.389(6)

C341-H341	0.9500	C351-C361	1.415(7)
C351-C441	1.428(6)	C361-C371	1.347(8)
C361-H361	0.9500	C371-C381	1.432(8)
C371-H371	0.9500	C381-C391	1.412(8)
C381-C431	1.414(7)	C391-C401	1.346(9)
C391-H391	0.9500	C401-C411	1.415(9)
C401-H401	0.9500	C411-C421	1.371(7)
C411-H411	0.9500	C421-C431	1.411(7)
C421-H421	0.9500	C431-C441	1.450(6)
C451-N451	1.265(5)	C451-H451	0.9500
N451-C561	1.498(5)	C511-C521	1.518(5)
C511-C561	1.527(5)	C511-H511	1.0000
C521-C531	1.535(6)	C521-H52A1	0.9900
C521-H52B1	0.9900	C531-C541	1.498(6)
C531-H53A1	0.9900	C531-H53B1	0.9900
C541-C551	1.539(6)	C541-H54A1	0.9900
C541-H54B1	0.9900	C551-C561	1.523(5)
C551-H55A1	0.9900	C551-H55B1	0.9900
C561-H561	1.0000	Cl32-C2S2	1.779(9)
Cl42-C2S2	1.726(9)	C2S2-H2A2	0.9900
C2S2-H2B2	0.9900	Ni22-N252	1.944(3)
Ni22-N452	2.104(3)	Ni22-N112	2.183(3)
Ni22-I42	2.6386(6)	Ni22-I32	2.6549(5)
N112-C122	1.349(6)	N112-C242	1.376(6)
C122-C132	1.391(6)	C122-C252	1.455(7)
C132-C142	1.362(8)	C132-H132	0.9500
C142-C152	1.423(8)	C142-H142	0.9500
C152-C242	1.417(7)	C152-C162	1.419(8)
C162-C172	1.322(10)	C162-H162	0.9500
C172-C182	1.439(9)	C172-H172	0.9500

C182-C192	1.403(9)	C182-C232	1.422(7)
C192-C202	1.364(8)	C192-H192	0.9500
C202-C212	1.391(7)	C202-H202	0.9500
C212-C222	1.373(7)	C212-H212	0.9500
C222-C232	1.386(7)	C222-H222	0.9500
C232-C242	1.469(7)	C252-N252	1.266(6)
C252-H252	0.9500	N252-C512	1.460(5)
N312-C322	1.329(6)	N312-C442	1.342(6)
C322-C332	1.407(6)	C322-C452	1.473(6)
C332-C342	1.377(7)	C332-H332	0.9500
C342-C352	1.388(7)	C342-H342	0.9500
C352-C442	1.421(6)	C352-C362	1.433(7)
C362-C372	1.342(8)	C362-H362	0.9500
C372-C382	1.442(8)	C372-H372	0.9500
C382-C392	1.393(7)	C382-C432	1.403(7)
C392-C402	1.376(8)	C392-H392	0.9500
C402-C412	1.388(8)	C402-H402	0.9500
C412-C422	1.373(7)	C412-H412	0.9500
C422-C432	1.413(6)	C422-H422	0.9500
C432-C442	1.443(6)	C452-N452	1.268(5)
C452-H452	0.9500	N452-C562	1.507(5)
C512-C522	1.522(5)	C512-C562	1.535(5)
C512-H512	1.0000	C522-C532	1.539(7)
C522-H52A2	0.9900	C522-H52B2	0.9900
C532-C542	1.512(7)	C532-H53A2	0.9900
C532-H53B2	0.9900	C542-C552	1.533(6)
C542-H54A2	0.9900	C542-H54B2	0.9900
C552-C562	1.528(5)	C552-H55A2	0.9900
C552-H55B2	0.9900	C562-H562	1.0000

Cl11-C1S1-Cl21	113.5(3)	Cl11-C1S1-H1A1	108.9
Cl21-C1S1-H1A1	108.9	Cl11-C1S1-H1B1	108.9
Cl21-C1S1-H1B1	108.9	H1A1-C1S1-H1B1	107.7
N251-Ni11-N451	81.94(14)	N251-Ni11-N111	80.60(14)
N451-Ni11-N111	162.01(14)	N251-Ni11-I11	97.77(9)
N451-Ni11-I11	95.92(8)	N111-Ni11-I11	90.71(8)
N251-Ni11-I21	110.78(9)	N451-Ni11-I21	89.12(8)
N111-Ni11-I21	93.02(8)	I11-Ni11-I21	151.44(2)
C121-N111-C241	118.0(4)	C121-N111-Ni11	106.6(3)
C241-N111-Ni11	135.4(3)	N111-C121-C131	124.4(4)
N111-C121-C251	116.9(4)	C131-C121-C251	118.6(4)
C141-C131-C121	117.2(4)	C141-C131-H131	121.4
C121-C131-H131	121.4	C151-C141-C131	120.3(4)
C151-C141-H141	119.9	C131-C141-H141	119.9
C141-C151-C241	120.2(4)	C141-C151-C161	120.2(4)
C241-C151-C161	119.6(4)	C171-C161-C151	120.9(5)
C171-C161-H161	119.6	C151-C161-H161	119.6
C161-C171-C181	122.3(5)	C161-C171-H171	118.8
C181-C171-H171	118.8	C191-C181-C231	119.5(5)
C191-C181-C171	121.1(5)	C231-C181-C171	119.3(5)
C201-C191-C181	121.6(5)	C201-C191-H191	119.2
C181-C191-H191	119.2	C191-C201-C211	118.9(5)
C191-C201-H201	120.5	C211-C201-H201	120.5
C221-C211-C201	120.6(5)	C221-C211-H211	119.7
C201-C211-H211	119.7	C211-C221-C231	121.9(4)
C211-C221-H221	119.1	C231-C221-H221	119.1
C221-C231-C181	117.4(4)	C221-C231-C241	124.1(4)
C181-C231-C241	118.5(4)	N111-C241-C151	119.8(4)
N111-C241-C231	120.9(4)	C151-C241-C231	119.3(4)
N251-C251-C121	118.4(4)	N251-C251-H251	120.8

C121-C251-H251	120.8	C251-N251-C511	125.8(3)
C251-N251-Ni11	117.4(3)	C511-N251-Ni11	116.7(2)
C321-N311-C441	118.7(4)	N311-C321-C331	122.9(4)
N311-C321-C451	111.6(4)	C331-C321-C451	125.4(4)
C341-C331-C321	118.4(4)	C341-C331-H331	120.8
C321-C331-H331	120.8	C331-C341-C351	120.7(4)
C331-C341-H341	119.7	C351-C341-H341	119.7
C341-C351-C361	124.2(4)	C341-C351-C441	117.0(4)
C361-C351-C441	118.8(4)	C371-C361-C351	121.3(5)
C371-C361-H361	119.4	C351-C361-H361	119.4
C361-C371-C381	122.2(5)	C361-C371-H371	118.9
C381-C371-H371	118.9	C391-C381-C431	119.0(5)
C391-C381-C371	122.0(5)	C431-C381-C371	119.0(5)
C401-C391-C381	120.5(6)	C401-C391-H391	119.7
C381-C391-H391	119.7	C391-C401-C411	121.1(5)
C391-C401-H401	119.5	C411-C401-H401	119.5
C421-C411-C401	119.9(5)	C421-C411-H411	120.1
C401-C411-H411	120.1	C411-C421-C431	120.0(5)
C411-C421-H421	120.0	C431-C421-H421	120.0
C421-C431-C381	119.5(4)	C421-C431-C441	121.7(4)
C381-C431-C441	118.7(4)	N311-C441-C351	122.4(4)
N311-C441-C431	117.6(4)	C351-C441-C431	120.0(4)
N451-C451-C321	127.9(4)	N451-C451-H451	116.0
C321-C451-H451	116.0	C451-N451-C561	118.1(3)
C451-N451-Ni11	135.1(3)	C561-N451-Ni11	106.8(2)
N251-C511-C521	115.1(3)	N251-C511-C561	105.9(3)
C521-C511-C561	112.7(3)	N251-C511-H511	107.6
C521-C511-H511	107.6	C561-C511-H511	107.6
C511-C521-C531	110.0(4)	C511-C521-H52A1	109.7
C531-C521-H52A1	109.7	C511-C521-H52B1	109.7

C531-C521-H52B1	109.7	H52A1-C521-H52B1	108.2
C541-C531-C521	111.2(3)	C541-C531-H53A1	109.4
C521-C531-H53A1	109.4	C541-C531-H53B1	109.4
C521-C531-H53B1	109.4	H53A1-C531-H53B1	108.0
C531-C541-C551	111.9(3)	C531-C541-H54A1	109.2
C551-C541-H54A1	109.2	C531-C541-H54B1	109.2
C551-C541-H54B1	109.2	H54A1-C541-H54B1	107.9
C561-C551-C541	110.2(3)	C561-C551-H55A1	109.6
C541-C551-H55A1	109.6	C561-C551-H55B1	109.6
C541-C551-H55B1	109.6	H55A1-C551-H55B1	108.1
N451-C561-C551	117.0(3)	N451-C561-C511	108.3(3)
C551-C561-C511	110.9(3)	N451-C561-H561	106.7
C551-C561-H561	106.7	C511-C561-H561	106.7
Cl42-C2S2-Cl32	112.2(4)	Cl42-C2S2-H2A2	109.2
Cl32-C2S2-H2A2	109.2	Cl42-C2S2-H2B2	109.2
Cl32-C2S2-H2B2	109.2	H2A2-C2S2-H2B2	107.9
N252-Ni22-N452	82.43(14)	N252-Ni22-N112	79.72(15)
N452-Ni22-N112	161.27(14)	N252-Ni22-I42	109.94(9)
N452-Ni22-I42	90.42(8)	N112-Ni22-I42	90.34(9)
N252-Ni22-I32	97.66(9)	N452-Ni22-I32	94.79(8)
N112-Ni22-I32	93.18(8)	I42-Ni22-I32	152.36(2)
C122-N112-C242	117.7(4)	C122-N112-Ni22	107.0(3)
C242-N112-Ni22	135.1(3)	N112-C122-C132	124.4(5)
N112-C122-C252	116.5(4)	C132-C122-C252	118.9(5)
C142-C132-C122	118.8(5)	C142-C132-H132	120.6
C122-C132-H132	120.6	C132-C142-C152	119.1(5)
C132-C142-H142	120.4	C152-C142-H142	120.4
C242-C152-C162	120.9(5)	C242-C152-C142	119.1(5)
C162-C152-C142	120.0(5)	C172-C162-C152	120.1(6)
C172-C162-H162	119.9	C152-C162-H162	119.9

C162-C172-C182	122.7(6)	C162-C172-H172	118.6
C182-C172-H172	118.6	C192-C182-C232	118.8(5)
C192-C182-C172	121.5(5)	C232-C182-C172	119.7(6)
C202-C192-C182	121.8(5)	C202-C192-H192	119.1
C182-C192-H192	119.1	C192-C202-C212	119.4(5)
C192-C202-H202	120.3	C212-C202-H202	120.3
C222-C212-C202	119.7(5)	C222-C212-H212	120.2
C202-C212-H212	120.2	C212-C222-C232	122.7(4)
C212-C222-H222	118.7	C232-C222-H222	118.7
C222-C232-C182	117.5(5)	C222-C232-C242	125.0(4)
C182-C232-C242	117.4(4)	N112-C242-C152	120.6(4)
N112-C242-C232	120.3(4)	C152-C242-C232	119.0(4)
N252-C252-C122	117.8(4)	N252-C252-H252	121.1
C122-C252-H252	121.1	C252-N252-C512	126.9(4)
C252-N252-Ni22	117.6(3)	C512-N252-Ni22	115.5(3)
C322-N312-C442	119.2(4)	N312-C322-C332	122.4(4)
N312-C322-C452	111.5(4)	C332-C322-C452	125.9(4)
C342-C332-C322	118.6(4)	C342-C332-H332	120.7
C322-C332-H332	120.7	C332-C342-C352	120.1(4)
C332-C342-H342	120.0	C352-C342-H342	120.0
C342-C352-C442	117.7(4)	C342-C352-C362	122.8(5)
C442-C352-C362	119.4(4)	C372-C362-C352	120.5(5)
C372-C362-H362	119.7	C352-C362-H362	119.7
C362-C372-C382	121.9(5)	C362-C372-H372	119.0
C382-C372-H372	119.0	C392-C382-C432	120.1(5)
C392-C382-C372	120.8(5)	C432-C382-C372	119.0(5)
C402-C392-C382	120.4(5)	C402-C392-H392	119.8
C382-C392-H392	119.8	C392-C402-C412	119.6(5)
C392-C402-H402	120.2	C412-C402-H402	120.2
C422-C412-C402	121.5(5)	C422-C412-H412	119.2

C402-C412-H412	119.2	C412-C422-C432	119.4(5)
C412-C422-H422	120.3	C432-C422-H422	120.3
C382-C432-C422	119.0(4)	C382-C432-C442	119.6(4)
C422-C432-C442	121.4(4)	N312-C442-C352	122.1(4)
N312-C442-C432	118.4(4)	C352-C442-C432	119.4(4)
N452-C452-C322	127.5(4)	N452-C452-H452	116.3
C322-C452-H452	116.3	C452-N452-C562	117.2(3)
C452-N452-Ni22	135.6(3)	C562-N452-Ni22	107.0(2)
N252-C512-C522	115.8(4)	N252-C512-C562	105.7(3)
C522-C512-C562	112.6(3)	N252-C512-H512	107.5
C522-C512-H512	107.5	C562-C512-H512	107.5
C512-C522-C532	110.2(4)	C512-C522-H52A2	109.6
C532-C522-H52A2	109.6	C512-C522-H52B2	109.6
C532-C522-H52B2	109.6	H52A2-C522-H52B2	108.1
C542-C532-C522	110.8(3)	C542-C532-H53A2	109.5
C522-C532-H53A2	109.5	C542-C532-H53B2	109.5
C522-C532-H53B2	109.5	H53A2-C532-H53B2	108.1
C532-C542-C552	112.1(3)	C532-C542-H54A2	109.2
C552-C542-H54A2	109.2	C532-C542-H54B2	109.2
C552-C542-H54B2	109.2	H54A2-C542-H54B2	107.9
C562-C552-C542	110.7(4)	C562-C552-H55A2	109.5
C542-C552-H55A2	109.5	C562-C552-H55B2	109.5
C542-C552-H55B2	109.5	H55A2-C552-H55B2	108.1
N452-C562-C552	116.0(3)	N452-C562-C512	107.3(3)
C552-C562-C512	111.3(3)	N452-C562-H562	107.3
C552-C562-H562	107.3	C512-C562-H562	107.3

Symmetry transformations used to generate equivalent atoms:

Table 4. Anisotropic displacement parameters ($\mathring{A}^2$ x 10^3) for complex **23**. The anisotropic displacement factor exponent takes the following form: $-2\pi^2[\,h^2a*^2U^{11} + ... + 2\,h\,k\,a*\,b*\,U^{12}\,]$

	U^{11}	U^{22}	U^{33}	U^{23}	U^{13}	U^{12}
Cl11	86(1)	80(1)	71(1)	18(1)	19(1)	-15(1)
Cl21	45(1)	88(1)	57(1)	3(1)	1(1)	-13(1)
C1S1	58(3)	67(4)	38(2)	1(2)	7(2)	-18(3)
Ni11	29(1)	24(1)	24(1)	-2(1)	9(1)	-1(1)
I11	32(1)	34(1)	32(1)	2(1)	5(1)	-3(1)
I21	40(1)	40(1)	26(1)	0(1)	5(1)	-7(1)
N111	27(2)	26(2)	25(1)	-2(1)	5(1)	-1(1)
C121	34(2)	26(2)	32(2)	-5(1)	8(1)	3(2)
C131	43(2)	27(2)	37(2)	-6(2)	7(2)	5(2)
C141	46(3)	22(2)	44(2)	-1(2)	6(2)	-4(2)
C151	40(2)	24(2)	42(2)	5(2)	7(2)	-3(2)
C161	69(4)	26(2)	69(3)	8(2)	36(3)	0(2)
C171	89(4)	30(3)	73(3)	13(2)	49(3)	-2(3)
C181	52(3)	34(3)	46(2)	6(2)	26(2)	-5(2)
C191	57(3)	49(3)	45(3)	1(2)	32(2)	-8(2)
C201	43(2)	43(3)	41(2)	-4(2)	20(2)	2(2)
C211	39(2)	31(2)	38(2)	1(2)	14(2)	2(2)
C221	34(2)	26(2)	30(2)	4(1)	11(2)	-1(2)
C231	33(2)	28(2)	29(2)	0(1)	8(2)	-2(2)
C241	34(2)	24(2)	29(2)	2(1)	5(2)	-5(2)
C251	35(2)	32(2)	29(2)	-6(1)	9(1)	3(2)
N251	28(2)	29(2)	25(1)	-4(1)	7(1)	-1(1)
N311	31(2)	26(2)	30(2)	0(1)	9(1)	-1(1)
C321	30(2)	30(2)	29(2)	-1(1)	8(1)	-3(2)
C331	38(2)	27(2)	33(2)	2(2)	10(2)	-1(2)

C341	37(2)	33(2)	24(2)	0(2)	14(1)	-3(2)
C351	31(2)	35(2)	33(2)	-3(2)	10(2)	1(2)
C361	60(3)	39(3)	60(3)	-1(2)	41(2)	4(2)
C371	81(4)	33(3)	88(4)	3(3)	53(3)	11(3)
C381	45(3)	34(3)	59(3)	5(2)	19(2)	4(2)
C391	50(3)	32(3)	85(4)	14(3)	13(3)	3(2)
C401	43(3)	39(3)	79(4)	23(3)	-2(2)	-4(2)
C411	45(2)	35(2)	47(2)	11(2)	2(2)	-12(2)
C421	36(2)	34(2)	40(2)	5(2)	7(2)	-7(2)
C431	36(2)	25(2)	42(2)	0(2)	6(2)	-2(2)
C441	28(2)	29(2)	27(2)	0(1)	7(1)	-3(2)
C451	31(2)	30(2)	27(2)	0(1)	10(1)	-1(2)
N451	31(2)	29(2)	24(1)	-2(1)	10(1)	-1(1)
C511	30(2)	30(2)	26(2)	-4(1)	10(1)	-2(1)
C521	35(2)	40(2)	30(2)	-5(2)	12(1)	1(2)
C531	39(2)	53(3)	32(2)	-5(2)	18(1)	0(2)
C541	33(2)	46(3)	38(2)	-4(2)	18(1)	-1(2)
C551	35(2)	35(2)	33(2)	-1(2)	16(1)	-2(2)
C561	27(2)	34(2)	26(1)	-2(1)	9(1)	0(1)
Cl32	55(1)	116(2)	71(1)	0(1)	-2(1)	-29(1)
Cl42	107(2)	115(2)	79(1)	27(1)	37(1)	1(1)
C2S2	80(5)	97(6)	52(3)	-10(3)	18(3)	-35(4)
Ni22	28(1)	25(1)	23(1)	-1(1)	8(1)	1(1)
I32	38(1)	35(1)	27(1)	-5(1)	4(1)	-1(1)
I42	29(1)	46(1)	30(1)	2(1)	6(1)	-5(1)
N112	35(2)	24(2)	27(2)	0(1)	4(1)	-4(1)
C122	38(2)	29(2)	32(2)	0(2)	2(2)	1(2)
C132	46(3)	25(2)	48(2)	-5(2)	8(2)	2(2)
C142	51(3)	19(2)	60(3)	0(2)	5(2)	-1(2)
C152	44(3)	31(2)	52(3)	2(2)	12(2)	-8(2)

326

C162	84(5)	35(3)	91(4)	18(3)	40(4)	-7(3)
C172	103(6)	58(4)	106(5)	29(4)	72(5)	-4(4)
C182	50(3)	47(3)	54(3)	7(2)	24(2)	-10(2)
C192	58(3)	63(4)	50(3)	14(3)	29(2)	-2(3)
C202	39(2)	55(3)	39(2)	-8(2)	20(2)	-8(2)
C212	49(3)	38(3)	38(2)	-2(2)	19(2)	-5(2)
C222	44(2)	43(3)	29(2)	2(2)	17(2)	-7(2)
C232	32(2)	34(2)	30(2)	5(2)	8(2)	-7(2)
C242	32(2)	26(2)	34(2)	1(2)	6(2)	-3(2)
C252	41(2)	32(2)	32(2)	-3(2)	9(2)	7(2)
N252	29(2)	34(2)	24(1)	-4(1)	5(1)	3(1)
N312	32(2)	25(2)	28(1)	0(1)	10(1)	-4(1)
C322	30(2)	26(2)	29(2)	-1(1)	11(1)	-2(2)
C332	40(2)	23(2)	34(2)	4(2)	18(2)	1(2)
C342	39(2)	29(2)	37(2)	2(2)	15(2)	-2(2)
C352	46(2)	29(2)	30(2)	0(2)	12(2)	-1(2)
C362	77(4)	37(3)	46(2)	6(2)	36(2)	11(2)
C372	88(4)	42(3)	58(3)	4(2)	41(3)	19(3)
C382	52(3)	31(2)	46(2)	1(2)	15(2)	5(2)
C392	57(3)	36(3)	59(3)	5(2)	16(2)	8(2)
C402	59(3)	24(2)	55(3)	9(2)	5(2)	-1(2)
C412	46(2)	35(2)	40(2)	8(2)	11(2)	-12(2)
C422	37(2)	33(2)	36(2)	0(2)	8(2)	-8(2)
C432	38(2)	28(2)	27(2)	2(1)	6(1)	-5(2)
C442	36(2)	26(2)	26(2)	1(1)	4(1)	-2(2)
C452	32(2)	29(2)	28(2)	3(1)	10(1)	2(2)
N452	24(1)	32(2)	24(1)	-1(1)	6(1)	-1(1)
C512	26(2)	37(2)	26(2)	-3(1)	8(1)	2(1)
C522	37(2)	44(3)	35(2)	-8(2)	13(2)	8(2)
C532	36(2)	56(3)	42(2)	-11(2)	20(2)	2(2)

C542	40(2)	55(3)	32(2)	-7(2)	18(1)	-12(2)
C552	37(2)	37(2)	29(2)	1(1)	15(1)	1(2)
C562	27(2)	32(2)	26(1)	-1(1)	9(1)	0(1)

Table 5. Hydrogen coordinates (x 10^4) and isotropic displacement parameters (Å^2 x 10^3) for complex **23**.

	x	y	z	U(eq)
H1A1	1467	4370	8278	66
H1B1	2707	4654	9059	66
H131	9321	1173	7370	44
H141	8301	814	8582	46
H161	7188	947	9933	62
H171	6230	1509	10869	70
H191	5366	2417	11193	56
H201	5063	3345	10843	48
H211	5919	3738	9557	42
H221	7054	3206	8652	35
H251	9907	1985	6457	39
H331	7430	4089	8057	39
H341	6199	4712	8745	37
H361	5181	5660	8702	58
H371	4834	6508	7981	74
H391	5172	7198	6707	68
H401	6044	7426	5377	68
H411	7339	6792	4731	53

H421	7828	5937	5498	44
H451	9199	4503	6129	35
H511	8990	3064	5274	34
H52A1	10524	2380	5165	41
H52B1	11640	2658	6067	41
H53A1	12034	2922	4492	48
H53B1	10538	3144	4094	48
H54A1	11975	3885	4618	45
H54B1	12533	3614	5720	45
H55A1	10972	4303	5839	40
H55B1	9860	4022	4939	40
H561	10998	3539	6888	34
H2A2	2220	3766	1112	91
H2B2	3506	4083	1766	91
H132	5486	7217	2581	49
H142	6611	7615	1482	54
H162	7856	7498	172	80
H172	8912	6957	-716	97
H192	9675	6045	-1131	65
H202	10012	5120	-796	51
H212	9173	4709	476	48
H222	7969	5225	1353	45
H252	4659	6387	3264	42
H332	7697	4357	2006	37
H342	8969	3751	1307	41
H362	10011	2814	1314	59
H372	10404	1965	2032	70
H392	9900	1237	3136	61
H402	8867	947	4378	57
H412	7485	1547	4969	48

H422	7068	2427	4310	43
H452	6139	3932	4054	35
H512	3846	5115	3085	36
H52A2	3147	5873	3873	45
H52B2	4468	5847	4796	45
H53A2	2710	5416	5325	52
H53B2	2420	5015	4355	52
H54A2	3649	4539	5794	49
H54B2	4785	5000	5996	49
H55A2	5519	4242	5206	40
H55B2	4195	4260	4286	40
H562	6221	5089	4717	33

Table 6. Torsion angles [°] for complex **23**.

N251-Ni11-N111-C121	2.0(3)	N451-Ni11-N111-C121	-12.1(5)
I11-Ni11-N111-C121	99.8(2)	I21-Ni11-N111-C121	-108.6(2)
N251-Ni11-N111-C241	-178.3(4)	N451-Ni11-N111-C241	167.7(4)
I11-Ni11-N111-C241	-80.5(4)	I21-Ni11-N111-C241	71.2(4)
C241-N111-C121-C131	1.9(6)	Ni11-N111-C121-C131	-178.3(4)
C241-N111-C121-C251	178.9(3)	Ni11-N111-C121-C251	-1.3(4)
N111-C121-C131-C141	-1.6(7)	C251-C121-C131-C141	-178.6(4)
C121-C131-C141-C151	-0.6(7)	C131-C141-C151-C241	2.4(7)
C131-C141-C151-C161	-176.6(5)	C141-C151-C161-C171	179.8(6)
C241-C151-C161-C171	0.7(9)	C151-C161-C171-C181	2.2(11)
C161-C171-C181-C191	175.3(6)	C161-C171-C181-C231	-1.6(10)
C231-C181-C191-C201	-0.4(8)	C171-C181-C191-C201	-177.3(6)
C181-C191-C201-C211	0.6(8)	C191-C201-C211-C221	-0.1(7)

C201-C211-C221-C231	-0.6(7)	C211-C221-C231-C181	0.9(6)
C211-C221-C231-C241	179.2(4)	C191-C181-C231-C221	-0.4(7)
C171-C181-C231-C221	176.6(5)	C191-C181-C231-C241	-178.8(4)
C171-C181-C231-C241	-1.8(7)	C121-N111-C241-C151	0.0(6)
Ni11-N111-C241-C151	-179.7(3)	C121-N111-C241-C231	-179.0(4)
Ni11-N111-C241-C231	1.3(6)	C141-C151-C241-N111	-2.2(6)
C161-C151-C241-N111	176.9(4)	C141-C151-C241-C231	176.9(4)
C161-C151-C241-C231	-4.0(7)	C221-C231-C241-N111	5.2(6)
C181-C231-C241-N111	-176.5(4)	C221-C231-C241-C151	-173.8(4)
C181-C231-C241-C151	4.5(6)	N111-C121-C251-N251	-0.8(5)
C131-C121-C251-N251	176.4(4)	C121-C251-N251-C511	-174.7(3)
C121-C251-N251-Ni11	2.8(5)	N451-Ni11-N251-C251	173.0(3)
N111-Ni11-N251-C251	-2.6(3)	I11-Ni11-N251-C251	-92.1(3)
I21-Ni11-N251-C251	87.0(3)	N451-Ni11-N251-C511	-9.3(2)
N111-Ni11-N251-C511	175.1(2)	I11-Ni11-N251-C511	85.6(2)
I21-Ni11-N251-C511	-95.2(2)	C441-N311-C321-C331	-0.4(6)
C441-N311-C321-C451	-177.2(3)	N311-C321-C331-C341	-1.3(6)
C451-C321-C331-C341	175.1(4)	C321-C331-C341-C351	2.2(6)
C331-C341-C351-C361	177.6(4)	C331-C341-C351-C441	-1.5(6)
C341-C351-C361-C371	-177.7(6)	C441-C351-C361-C371	1.4(8)
C351-C361-C371-C381	-0.8(10)	C361-C371-C381-C391	177.4(6)
C361-C371-C381-C431	0.2(10)	C431-C381-C391-C401	0.6(8)
C371-C381-C391-C401	-176.6(6)	C381-C391-C401-C411	0.7(8)
C391-C401-C411-C421	-1.6(8)	C401-C411-C421-C431	1.1(7)
C411-C421-C431-C381	0.2(6)	C411-C421-C431-C441	176.6(4)
C391-C381-C431-C421	-1.0(7)	C371-C381-C431-C421	176.2(5)
C391-C381-C431-C441	-177.5(5)	C371-C381-C431-C441	-0.2(7)
C321-N311-C441-C351	1.1(6)	C321-N311-C441-C431	-176.8(4)
C341-C351-C441-N311	-0.2(6)	C361-C351-C441-N311	-179.3(4)
C341-C351-C441-C431	177.7(4)	C361-C351-C441-C431	-1.5(6)

C421-C431-C441-N311	2.5(6)	C381-C431-C441-N311	178.8(4)
C421-C431-C441-C351	-175.5(4)	C381-C431-C441-C351	0.9(6)
N311-C321-C451-N451	-176.3(4)	C331-C321-C451-N451	6.9(7)
C321-C451-N451-C561	-171.9(3)	C321-C451-N451-Ni11	7.8(6)
N251-Ni11-N451-C451	161.9(4)	N111-Ni11-N451-C451	176.0(4)
I11-Ni11-N451-C451	64.9(4)	I21-Ni11-N451-C451	-87.0(4)
N251-Ni11-N451-C561	-18.4(2)	N111-Ni11-N451-C561	-4.3(5)
I11-Ni11-N451-C561	-115.41(19)	I21-Ni11-N451-C561	92.8(2)
C251-N251-C511-C521	-23.3(5)	Ni11-N251-C511-C521	159.3(2)
C251-N251-C511-C561	-148.5(4)	Ni11-N251-C511-C561	34.0(3)
N251-C511-C521-C531	-176.6(3)	C561-C511-C521-C531	-54.9(4)
C511-C521-C531-C541	55.7(4)	C521-C531-C541-C551	-57.3(5)
C531-C541-C551-C561	56.5(4)	C451-N451-C561-C551	-12.8(5)
Ni11-N451-C561-C551	167.4(2)	C451-N451-C561-C511	-139.0(3)
Ni11-N451-C561-C511	41.2(3)	C541-C551-C561-N451	-179.2(3)
C541-C551-C561-C511	-54.3(4)	N251-C511-C561-N451	-48.5(3)
C521-C511-C561-N451	-175.1(3)	N251-C511-C561-C551	-178.1(3)
C521-C511-C561-C551	55.2(4)	N252-Ni22-N112-C122	10.6(3)
N452-Ni22-N112-C122	-7.3(5)	I42-Ni22-N112-C122	-99.6(3)
I32-Ni22-N112-C122	107.8(3)	N252-Ni22-N112-C242	-175.6(4)
N452-Ni22-N112-C242	166.5(3)	I42-Ni22-N112-C242	74.2(4)
I32-Ni22-N112-C242	-78.4(4)	C242-N112-C122-C132	-1.6(6)
Ni22-N112-C122-C132	173.4(4)	C242-N112-C122-C252	173.8(3)
Ni22-N112-C122-C252	-11.2(4)	N112-C122-C132-C142	1.3(7)
C252-C122-C132-C142	-173.9(4)	C122-C132-C142-C152	1.4(7)
C132-C142-C152-C242	-3.7(7)	C132-C142-C152-C162	175.6(5)
C242-C152-C162-C172	0.0(11)	C142-C152-C162-C172	-179.3(7)
C152-C162-C172-C182	-0.9(13)	C162-C172-C182-C192	-178.9(7)
C162-C172-C182-C232	-0.9(12)	C232-C182-C192-C202	-2.6(9)
C172-C182-C192-C202	175.4(6)	C182-C192-C202-C212	0.7(8)

C192-C202-C212-C222	1.1(7)	C202-C212-C222-C232	-1.0(7)
C212-C222-C232-C182	-0.9(7)	C212-C222-C232-C242	-179.5(4)
C192-C182-C232-C222	2.6(7)	C172-C182-C232-C222	-175.4(6)
C192-C182-C232-C242	-178.6(5)	C172-C182-C232-C242	3.3(8)
C122-N112-C242-C152	-0.9(6)	Ni22-N112-C242-C152	-174.2(3)
C122-N112-C242-C232	-179.2(4)	Ni22-N112-C242-C232	7.5(6)
C162-C152-C242-N112	-175.9(5)	C142-C152-C242-N112	3.5(7)
C162-C152-C242-C232	2.5(7)	C142-C152-C242-C232	-178.1(4)
C222-C232-C242-N112	-7.1(6)	C182-C232-C242-N112	174.3(4)
C222-C232-C242-C152	174.5(4)	C182-C232-C242-C152	-4.1(6)
N112-C122-C252-N252	5.2(6)	C132-C122-C252-N252	-179.1(4)
C122-C252-N252-C512	-176.7(3)	C122-C252-N252-Ni22	5.3(5)
N452-Ni22-N252-C252	165.5(3)	N112-Ni22-N252-C252	-8.8(3)
I42-Ni22-N252-C252	77.8(3)	I32-Ni22-N252-C252	-100.6(3)
N452-Ni22-N252-C512	-12.8(2)	N112-Ni22-N252-C512	172.9(2)
I42-Ni22-N252-C512	-100.5(2)	I32-Ni22-N252-C512	81.1(2)
C442-N312-C322-C332	0.5(6)	C442-N312-C322-C452	-176.4(3)
N312-C322-C332-C342	-0.7(6)	C452-C322-C332-C342	175.7(4)
C322-C332-C342-C352	-0.2(7)	C332-C342-C352-C442	1.3(6)
C332-C342-C352-C362	-174.6(5)	C342-C352-C362-C372	174.8(6)
C442-C352-C362-C372	-1.0(8)	C352-C362-C372-C382	3.9(10)
C362-C372-C382-C392	179.5(6)	C362-C372-C382-C432	-4.1(9)
C432-C382-C392-C402	0.3(8)	C372-C382-C392-C402	176.7(5)
C382-C392-C402-C412	-0.6(8)	C392-C402-C412-C422	0.8(8)
C402-C412-C422-C432	-0.8(7)	C392-C382-C432-C422	-0.3(7)
C372-C382-C432-C422	-176.7(5)	C392-C382-C432-C442	177.9(5)
C372-C382-C432-C442	1.5(7)	C412-C422-C432-C382	0.5(6)
C412-C422-C432-C442	-177.6(4)	C322-N312-C442-C352	0.6(6)
C322-N312-C442-C432	176.8(4)	C342-C352-C442-N312	-1.5(6)
C362-C352-C442-N312	174.5(4)	C342-C352-C442-C432	-177.6(4)

C362-C352-C442-C432	-1.6(6)	C382-C432-C442-N312	-175.0(4)
C422-C432-C442-N312	3.1(6)	C382-C432-C442-C352	1.3(6)
C422-C432-C442-C352	179.4(4)	N312-C322-C452-N452	178.0(4)
C332-C322-C452-N452	1.2(7)	C322-C452-N452-C562	-174.0(3)
C322-C452-N452-Ni22	0.5(6)	N252-Ni22-N452-C452	168.7(4)
N112-Ni22-N452-C452	-173.6(4)	I42-Ni22-N452-C452	-81.3(4)
I32-Ni22-N452-C452	71.6(4)	N252-Ni22-N452-C562	-16.4(2)
N112-Ni22-N452-C562	1.4(5)	I42-Ni22-N452-C562	93.66(19)
I32-Ni22-N452-C562	-113.51(19)	C252-N252-C512-C522	-14.5(5)
Ni22-N252-C512-C522	163.6(2)	C252-N252-C512-C562	-139.9(4)
Ni22-N252-C512-C562	38.2(3)	N252-C512-C522-C532	-176.8(3)
C562-C512-C522-C532	-55.0(4)	C512-C522-C532-C542	56.0(4)
C522-C532-C542-C552	-57.2(5)	C532-C542-C552-C562	55.8(4)
C452-N452-C562-C552	-18.5(4)	Ni22-N452-C562-C552	165.5(2)
C452-N452-C562-C512	-143.5(3)	Ni22-N452-C562-C512	40.5(3)
C542-C552-C562-N452	-176.3(3)	C542-C552-C562-C512	-53.3(4)
N252-C512-C562-N452	-50.5(4)	C522-C512-C562-N452	-177.9(3)
N252-C512-C562-C552	-178.4(3)	C522-C512-C562-C552	54.2(4)

Symmetry transformations used to generate equivalent atoms:

Table 1. Crystal data and structure refinement for complex **34**.

Identification code	ko0901m
Empirical formula	C96 H60 Ag2 N8 O14
Formula weight	1765.26
Temperature	120(2) K
Wavelength	0.71073 Å
Crystal system	Monoclinic
Space group	P2(1)
Unit cell dimensions	a = 12.8987(7) Å α= 90°
	b = 25.1827(17) Å β= 90.563(3)°
	c = 15.0524(8) Å γ = 90°
Volume	4889.1(5) Å^3
Z	2
Density (calculated)	1.199 g/cm^3
Absorption coefficient	0.461 mm^{-1}
F(000)	1796
Crystal size	0.30 x 0.25 x 0.15 mm^3
Theta range for data collection	0.81 to 28.28°
Index ranges	-17<=h<=17, -31<=k<=33, -15<=l<=20
Reflections collected	76040
Independent reflections	22910 [R(int) = 0.1162]
Completeness to theta = 28.28°	99.9 %
Absorption correction	None
Refinement method	Full-matrix least-squares on F^2
Data / restraints / parameters	22910 / 117 / 228
Goodness-of-fit on F^2	1.714
Final R indices [I>2sigma(I)]	R1 = 0.1911, wR2 = 0.4823
R indices (all data)	R1 = 0.2844, wR2 = 0.5225
Absolute structure parameter	0.15(11)

Table 2. Atomic coordinates (x 10^4) and equivalent isotropic displacement parameters (Å^2 x 10^3) complex **34**. U(eq) is defined as one third of the trace of the orthogonalized U^{ij} tensor.

	x	y	z	U(eq)
Ag(1)	3206(1)	4547(1)	1230(1)	58(1)
Ag(2)	2599(1)	4488(1)	3428(1)	80(1)
N111	2286(8)	5216(4)	4583(7)	83(5)
C121	1760(9)	5610(4)	4167(7)	83(5)
C131	1697(12)	6132(4)	4480(9)	94(6)
C141	2184(13)	6244(4)	5273(10)	98(6)
C151	2698(11)	5851(4)	5731(8)	111(6)
C161	3158(15)	5962(5)	6582(9)	136(8)
C171	3658(14)	5584(6)	7038(8)	138(8)
C181	3794(11)	5057(5)	6695(8)	118(6)
C191	4388(13)	4678(6)	7160(9)	98(7)
C201	4557(14)	4181(6)	6822(11)	104(7)
C211	4135(14)	4052(5)	5989(11)	122(8)
C221	3559(11)	4416(4)	5519(9)	130(8)
C231	3361(9)	4925(4)	5849(7)	104(6)
C241	2764(8)	5330(4)	5371(7)	88(5)
C251	1265(11)	5479(5)	3307(8)	78(6)
N251	1370(13)	5014(6)	3005(8)	88(6)
C311	841(10)	4534(4)	1565(6)	54(4)
C321	1167(10)	4998(5)	1981(7)	63(5)
C331	1057(12)	5483(5)	1549(9)	64(5)
C341	621(13)	5503(4)	701(9)	94(6)
C351	295(9)	5039(4)	286(6)	81(5)
C361	405(7)	4554(4)	717(6)	62(4)
C371	79(12)	4089(4)	302(8)	77(5)

C381	-357(13)	4110(6)	-546(9)	87(6)
C391	-467(13)	4594(7)	-977(7)	92(6)
C401	-141(13)	5059(6)	-562(7)	87(6)
N112	4309(8)	3903(4)	285(6)	95(6)
C122	3954(9)	3421(4)	534(8)	103(6)
C132	4382(12)	2938(4)	263(11)	121(7)
C142	5201(13)	2959(4)	-311(12)	123(7)
C152	5565(10)	3439(4)	-603(10)	118(6)
C162	6384(12)	3460(5)	-1239(11)	123(7)
C172	6745(11)	3925(6)	-1532(10)	122(7)
C182	6364(9)	4424(5)	-1211(8)	99(6)
C192	6808(11)	4907(6)	-1483(10)	108(7)
C202	6479(13)	5383(5)	-1152(12)	113(7)
C212	5688(14)	5388(4)	-523(13)	114(7)
C222	5246(11)	4922(4)	-241(10)	98(6)
C232	5555(8)	4428(4)	-572(7)	103(6)
C242	5121(8)	3921(4)	-287(6)	97(6)
C252	3087(10)	3412(5)	1166(9)	88(6)
N252	2738(10)	3850(6)	1444(9)	64(5)
C312	879(10)	4060(5)	2128(9)	68(5)
C322	1624(9)	3667(6)	2022(10)	65(5)
C332	1510(10)	3180(5)	2445(11)	83(6)
C342	651(11)	3086(4)	2973(11)	86(6)
C352	-94(9)	3479(4)	3078(8)	85(5)
C362	20(8)	3966(4)	2655(7)	69(5)
C372	-725(10)	4359(4)	2761(10)	77(5)
C382	-1584(10)	4266(6)	3288(11)	88(6)
C392	-1698(10)	3779(7)	3711(11)	91(6)
C402	-953(11)	3385(5)	3606(11)	93(6)
N113	2889(7)	5268(3)	-25(5)	48(3)

337

C123	3000(8)	5750(4)	363(6)	78(5)
C133	2599(11)	6223(3)	15(7)	98(6)
C143	2079(11)	6194(3)	-783(8)	98(6)
C153	1978(8)	5716(3)	-1214(6)	85(5)
C163	1484(11)	5691(4)	-2070(7)	80(5)
C173	1382(10)	5229(4)	-2500(6)	80(6)
C183	1724(8)	4735(4)	-2122(6)	72(5)
C193	1540(11)	4250(4)	-2559(7)	93(6)
C203	1825(12)	3776(4)	-2188(9)	99(6)
C213	2301(12)	3775(3)	-1349(9)	90(6)
C223	2483(9)	4242(3)	-904(7)	61(5)
C233	2213(6)	4735(3)	-1269(5)	59(4)
C243	2376(6)	5243(3)	-819(5)	54(4)
C253	3542(11)	5765(5)	1230(7)	87(6)
N253	3857(12)	5332(5)	1563(7)	107(7)
C313	4695(18)	5140(7)	3154(13)	120(7)
C323	4004(18)	5461(8)	2687(12)	101(7)
C333	3741(16)	5958(8)	3018(13)	96(6)
C343	4169(16)	6133(6)	3817(13)	108(7)
C353	4860(13)	5811(6)	4284(10)	119(7)
C363	5123(13)	5315(6)	3952(11)	124(7)
C373	5815(17)	4993(7)	4419(15)	122(8)
C383	6243(18)	5169(9)	5218(15)	123(8)
C393	5979(19)	5665(10)	5550(13)	130(8)
C403	5288(19)	5987(8)	5083(12)	123(8)
N114	2302(7)	3648(4)	4548(7)	87(5)
C124	3057(8)	3303(5)	4319(8)	103(6)
C134	3066(10)	2765(5)	4546(10)	120(7)
C144	2262(11)	2581(4)	5053(11)	120(7)
C154	1498(9)	2921(4)	5324(9)	104(6)

C164	690(11)	2735(4)	5893(10)	99(6)
C174	-59(10)	3062(5)	6165(9)	97(6)
C184	-119(8)	3606(4)	5884(7)	86(5)
C194	-956(8)	3931(5)	6129(9)	91(6)
C204	-1042(9)	4443(5)	5835(10)	90(6)
C214	-281(10)	4645(4)	5271(10)	76(5)
C224	540(8)	4335(4)	5017(8)	73(5)
C234	658(7)	3812(3)	5313(6)	74(5)
C244	1510(7)	3463(3)	5054(6)	86(5)
C254	3897(9)	3511(6)	3758(11)	98(7)
N254	3857(10)	3991(6)	3517(12)	114(8)
C314	5144(13)	4641(7)	2595(12)	88(6)
C324	4810(14)	4122(8)	2728(13)	106(7)
C334	5314(17)	3704(6)	2313(16)	110(7)
C344	6152(17)	3804(5)	1764(15)	119(7)
C354	6486(12)	4323(5)	1630(10)	105(6)
C364	5982(11)	4741(5)	2046(10)	95(6)
C374	6315(17)	5260(5)	1912(15)	109(7)
C384	7153(18)	5360(7)	1363(17)	128(8)
C394	7658(15)	4941(9)	948(15)	129(8)
C404	7324(14)	4423(8)	1081(14)	113(7)
O(11)	4169(8)	1992(4)	2411(7)	25(2)
O(12)	1891(9)	7091(4)	2238(7)	35(2)
O(13)	8019(12)	2702(6)	1171(10)	58(4)
O(14)	-3738(11)	2636(5)	4631(9)	50(3)
O(15)	-1601(11)	2154(5)	2783(9)	49(3)
O(16)	-1398(12)	5731(6)	-2750(10)	59(4)
O(17)	4542(19)	1730(8)	-1308(16)	98(6)
O(18)	-251(18)	6558(8)	6332(15)	94(6)
O(19)	7940(20)	6662(11)	2480(20)	129(9)

339

O(20)	-740(40)	6485(18)	-1020(30)	206(17)
O(21)	-1450(20)	6409(9)	-96(17)	109(7)
O(22)	3909(19)	2711(8)	-2336(16)	99(6)
O(23)	6121(14)	3567(7)	5674(12)	71(4)
O(24)	-1430(30)	7560(14)	200(30)	162(12)

Table 3. Bond lengths [Å] and angles [°] for complex **34**.

Ag(1)-N252	1.885(14)	Ag(1)-N253	2.204(13)
Ag(1)-N112	2.594(10)	Ag(2)-N254	2.051(16)
Ag(2)-N251	2.157(15)	Ag(2)-N111	2.562(10)
N111-C121	1.3517	N111-C241	1.3622
C121-C131	1.3986	C121-C251	1.4758
C131-C141	1.3727	C131-H131	0.9500
C141-C151	1.3719	C141-H141	0.9500
C151-C241	1.4242	C151-C161	1.4334
C161-C171	1.3360	C161-H161	0.9500
C171-C181	1.4356	C171-H171	0.9500
C181-C191	1.4068	C181-C231	1.4247
C191-C201	1.3677	C191-H191	0.9500
C201-C211	1.4000	C201-H201	0.9500
C211-C221	1.3734	C211-H211	0.9500
C221-C231	1.3996	C221-H221	0.9500
C231-C241	1.4622	C251-N251	1.2642
C251-H25A1	0.9500	N251-C321	1.562(14)
C311-C321	1.3900	C311-C361	1.3900
C311-C312	1.463(15)	C321-C331	1.3900
C331-C341	1.3900	C331-H331	0.9500

C341-C351	1.3900	C341-H341	0.9500
C351-C361	1.3900	C351-C401	1.3900
C361-C371	1.3900	C371-C381	1.3900
C371-H371	0.9500	C381-C391	1.3900
C381-H381	0.9500	C391-C401	1.3900
C391-H391	0.9500	C401-H401	0.9500
N112-C122	1.3516	N112-C242	1.3623
C122-C132	1.3985	C122-C252	1.4757
C132-C142	1.3728	C132-H132	0.9500
C142-C152	1.3717	C142-H142	0.9500
C152-C242	1.4246	C152-C162	1.4334
C162-C172	1.3363	C162-H162	0.9500
C172-C182	1.4360	C172-H172	0.9500
C182-C192	1.4067	C182-C232	1.4246
C192-C202	1.3681	C192-H192	0.9500
C202-C212	1.4000	C202-H202	0.9500
C212-C222	1.3739	C212-H212	0.9500
C222-C232	1.3991	C222-H222	0.9500
C232-C242	1.4619	C252-N252	1.2639
C252-H25B2	0.9500	N252-C322	1.750(15)
C312-C322	1.3900	C312-C362	1.3900
C322-C332	1.3900	C332-C342	1.3900
C332-H332	0.9500	C342-C352	1.3900
C342-H342	0.9500	C352-C362	1.3900
C352-C402	1.3900	C362-C372	1.3900
C372-C382	1.3900	C372-H372	0.9500
C382-C392	1.3900	C382-H382	0.9500
C392-C402	1.3900	C392-H392	0.9500
C402-H402	0.9500	N113-C123	1.3517
N113-C243	1.3624	C123-C133	1.3984

C123-C253	1.4759	C133-C143	1.3725
C133-H133	0.9500	C143-C153	1.3718
C143-H143	0.9500	C153-C243	1.4243
C153-C163	1.4334	C163-C173	1.3364
C163-H163	0.9500	C173-C183	1.4352
C173-H173	0.9500	C183-C193	1.4071
C183-C233	1.4246	C193-C203	1.3679
C193-H193	0.9500	C203-C213	1.3999
C203-H203	0.9500	C213-C223	1.3735
C213-H213	0.9500	C223-C233	1.3993
C223-H223	0.9500	C233-C243	1.4621
C253-N253	1.2638	C253-H25C3	0.9500
N253-C323	1.731(19)	C313-C323	1.3900
C313-C363	1.3900	C313-C314	1.62(2)
C323-C333	1.3900	C333-C343	1.3900
C333-H333	0.9500	C343-C353	1.3900
C343-H343	0.9500	C353-C363	1.3900
C353-C403	1.3900	C363-C373	1.3900
C373-C383	1.3900	C373-H373	0.9500
C383-C393	1.3900	C383-H383	0.9500
C393-C403	1.3900	C393-H393	0.9500
C403-H403	0.9500	N114-C124	1.3518
N114-C244	1.3622	C124-C134	1.3985
C124-C254	1.4759	C134-C144	1.3727
C134-H134	0.9500	C144-C154	1.3717
C144-H144	0.9500	C154-C244	1.4244
C154-C164	1.4332	C164-C174	1.3362
C164-H164	0.9500	C174-C184	1.4357
C174-H174	0.9500	C184-C194	1.4068
C184-C234	1.4245	C194-C204	1.3680

C194-H194	0.9500	C204-C214	1.4000
C204-H204	0.9500	C214-C224	1.3736
C214-H214	0.9500	C224-C234	1.3992
C224-H224	0.9500	C234-C244	1.4621
C254-N254	1.2641	C254-H25D4	0.9500
N254-C324	1.749(17)	C314-C324	1.3900
C314-C364	1.3900	C324-C334	1.3900
C334-C344	1.3900	C334-H334	0.9500
C344-C354	1.3900	C344-H344	0.9500
C354-C364	1.3900	C354-C404	1.3900
C364-C374	1.3900	C374-C384	1.3900
C374-H374	0.9500	C384-C394	1.3900
C384-H384	0.9500	C394-C404	1.3900
C394-H394	0.9500	C404-H404	0.9500
O(20)-O(21)	1.68(6)		
N252-Ag(1)-N253	156.8(5)	N252-Ag(1)-N112	71.9(4)
N253-Ag(1)-N112	118.4(5)	N254-Ag(2)-N251	166.4(6)
N254-Ag(2)-N111	121.4(6)	N251-Ag(2)-N111	68.9(3)
C121-N111-C241	118.0	C121-N111-Ag(2)	107.0(3)
C241-N111-Ag(2)	132.0(3)	N111-C121-C131	124.4
N111-C121-C251	116.9	C131-C121-C251	118.6
C141-C131-C121	117.2	C141-C131-H131	121.4
C121-C131-H131	121.4	C151-C141-C131	120.3
C151-C141-H141	119.8	C131-C141-H141	119.8
C141-C151-C241	120.2	C141-C151-C161	120.2
C241-C151-C161	119.6	C171-C161-C151	120.9
C171-C161-H161	119.6	C151-C161-H161	119.6
C161-C171-C181	122.3	C161-C171-H171	118.8
C181-C171-H171	118.8	C191-C181-C231	119.5

C191-C181-C171	121.2	C231-C181-C171	119.3
C201-C191-C181	121.6	C201-C191-H191	119.2
C181-C191-H191	119.2	C191-C201-C211	118.9
C191-C201-H201	120.5	C211-C201-H201	120.5
C221-C211-C201	120.6	C221-C211-H211	119.7
C201-C211-H211	119.7	C211-C221-C231	121.9
C211-C221-H221	119.1	C231-C221-H221	119.1
C221-C231-C181	117.4	C221-C231-C241	124.1
C181-C231-C241	118.5	N111-C241-C151	119.8
N111-C241-C231	120.9	C151-C241-C231	119.3
N251-C251-C121	118.4	N251-C251-H25A1	120.8
C121-C251-H25A1	120.8	C251-N251-C321	111.1(9)
C251-N251-Ag(2)	123.0(3)	C321-N251-Ag(2)	113.0(10)
C321-C311-C361	120.0	C321-C311-C312	114.7(8)
C361-C311-C312	124.9(8)	C311-C321-C331	120.0
C311-C321-N251	120.8(9)	C331-C321-N251	117.1(9)
C341-C331-C321	120.0	C341-C331-H331	120.0
C321-C331-H331	120.0	C331-C341-C351	120.0
C331-C341-H341	120.0	C351-C341-H341	120.0
C361-C351-C341	120.0	C361-C351-C401	120.0
C341-C351-C401	120.0	C351-C361-C371	120.0
C351-C361-C311	120.0	C371-C361-C311	120.0
C381-C371-C361	120.0	C381-C371-H371	120.0
C361-C371-H371	120.0	C371-C381-C391	120.0
C371-C381-H381	120.0	C391-C381-H381	120.0
C401-C391-C381	120.0	C401-C391-H391	120.0
C381-C391-H391	120.0	C391-C401-C351	120.0
C391-C401-H401	120.0	C351-C401-H401	120.0
C122-N112-C242	118.0	C122-N112-Ag(1)	102.7(3)
C242-N112-Ag(1)	139.1(3)	N112-C122-C132	124.4

N112-C122-C252	116.9	C132-C122-C252	118.6
C142-C132-C122	117.2	C142-C132-H132	121.4
C122-C132-H132	121.4	C152-C142-C132	120.3
C152-C142-H142	119.9	C132-C142-H142	119.9
C142-C152-C242	120.2	C142-C152-C162	120.2
C242-C152-C162	119.6	C172-C162-C152	120.9
C172-C162-H162	119.6	C152-C162-H162	119.6
C162-C172-C182	122.3	C162-C172-H172	118.8
C182-C172-H172	118.8	C192-C182-C232	119.5
C192-C182-C172	121.1	C232-C182-C172	119.3
C202-C192-C182	121.6	C202-C192-H192	119.2
C182-C192-H192	119.2	C192-C202-C212	118.9
C192-C202-H202	120.5	C212-C202-H202	120.5
C222-C212-C202	120.6	C222-C212-H212	119.7
C202-C212-H212	119.7	C212-C222-C232	121.9
C212-C222-H222	119.0	C232-C222-H222	119.0
C222-C232-C182	117.4	C222-C232-C242	124.1
C182-C232-C242	118.5	N112-C242-C152	119.8
N112-C242-C232	120.9	C152-C242-C232	119.3
N252-C252-C122	118.4	N252-C252-H25B2	120.8
C122-C252-H25B2	120.8	C252-N252-C322	103.3(8)
C252-N252-Ag(1)	129.8(3)	C322-N252-Ag(1)	126.6(9)
C322-C312-C362	120.0	C322-C312-C311	122.3(8)
C362-C312-C311	116.5(8)	C312-C322-C332	120.0
C312-C322-N252	116.1(8)	C332-C322-N252	123.5(8)
C322-C332-C342	120.0	C322-C332-H332	120.0
C342-C332-H332	120.0	C352-C342-C332	120.0
C352-C342-H342	120.0	C332-C342-H342	120.0
C362-C352-C342	120.0	C362-C352-C402	120.0
C342-C352-C402	120.0	C372-C362-C352	120.0

C372-C362-C312	120.0	C352-C362-C312	120.0
C362-C372-C382	120.0	C362-C372-H372	120.0
C382-C372-H372	120.0	C372-C382-C392	120.0
C372-C382-H382	120.0	C392-C382-H382	120.0
C402-C392-C382	120.0	C402-C392-H392	120.0
C382-C392-H392	120.0	C392-C402-C352	120.0
C392-C402-H402	120.0	C352-C402-H402	120.0
C123-N113-C243	118.0	N113-C123-C133	124.4
N113-C123-C253	116.9	C133-C123-C253	118.6
C143-C133-C123	117.2	C143-C133-H133	121.4
C123-C133-H133	121.4	C153-C143-C133	120.3
C153-C143-H143	119.9	C133-C143-H143	119.9
C143-C153-C243	120.2	C143-C153-C163	120.2
C243-C153-C163	119.6	C173-C163-C153	120.9
C173-C163-H163	119.6	C153-C163-H163	119.6
C163-C173-C183	122.3	C163-C173-H173	118.8
C183-C173-H173	118.8	C193-C183-C233	119.5
C193-C183-C173	121.1	C233-C183-C173	119.3
C203-C193-C183	121.6	C203-C193-H193	119.2
C183-C193-H193	119.2	C193-C203-C213	118.9
C193-C203-H203	120.5	C213-C203-H203	120.5
C223-C213-C203	120.6	C223-C213-H213	119.7
C203-C213-H213	119.7	C213-C223-C233	121.9
C213-C223-H223	119.1	C233-C223-H223	119.0
C223-C233-C183	117.4	C223-C233-C243	124.1
C183-C233-C243	118.5	N113-C243-C153	119.8
N113-C243-C233	120.9	C153-C243-C233	119.3
N253-C253-C123	118.4	N253-C253-H25C3	120.8
C123-C253-H25C3	120.8	C253-N253-C323	104.9(9)
C253-N253-Ag(1)	124.2(3)	C323-N253-Ag(1)	115.3(11)

C323-C313-C363	120.0	C323-C313-C314	114.8(12)
C363-C313-C314	123.6(12)	C333-C323-C313	120.0
C333-C323-N253	119.6(12)	C313-C323-N253	116.7(12)
C323-C333-C343	120.0	C323-C333-H333	120.0
C343-C333-H333	120.0	C353-C343-C333	120.0
C353-C343-H343	120.0	C333-C343-H343	120.0
C343-C353-C363	120.0	C343-C353-C403	120.0
C363-C353-C403	120.0	C373-C363-C353	120.0
C373-C363-C313	120.0	C353-C363-C313	120.0
C363-C373-C383	120.0	C363-C373-H373	120.0
C383-C373-H373	120.0	C373-C383-C393	120.0
C373-C383-H383	120.0	C393-C383-H383	120.0
C383-C393-C403	120.0	C383-C393-H393	120.0
C403-C393-H393	120.0	C393-C403-C353	120.0
C393-C403-H403	120.0	C353-C403-H403	120.0
C124-N114-C244	118.0	N114-C124-C134	124.4
N114-C124-C254	116.9	C134-C124-C254	118.6
C144-C134-C124	117.2	C144-C134-H134	121.4
C124-C134-H134	121.4	C154-C144-C134	120.3
C154-C144-H144	119.9	C134-C144-H144	119.9
C144-C154-C244	120.2	C144-C154-C164	120.2
C244-C154-C164	119.6	C174-C164-C154	120.9
C174-C164-H164	119.6	C154-C164-H164	119.6
C164-C174-C184	122.3	C164-C174-H174	118.9
C184-C174-H174	118.9	C194-C184-C234	119.5
C194-C184-C174	121.1	C234-C184-C174	119.3
C204-C194-C184	121.6	C204-C194-H194	119.2
C184-C194-H194	119.2	C194-C204-C214	118.9
C194-C204-H204	120.5	C214-C204-H204	120.5
C224-C214-C204	120.6	C224-C214-H214	119.7

C204-C214-H214	119.7	C214-C224-C234	121.9
C214-C224-H224	119.1	C234-C224-H224	119.1
C224-C234-C184	117.4	C224-C234-C244	124.1
C184-C234-C244	118.5	N114-C244-C154	119.8
N114-C244-C234	120.9	C154-C244-C234	119.3
N254-C254-C124	118.4	N254-C254-H25D4	120.8
C124-C254-H25D4	120.8	C254-N254-C324	110.4(10)
C254-N254-Ag(2)	129.2(3)	C324-N254-Ag(2)	113.6(11)
C324-C314-C364	120.0	C324-C314-C313	122.7(12)
C364-C314-C313	116.8(12)	C334-C324-C314	120.0
C334-C324-N254	119.8(12)	C314-C324-N254	119.8(12)
C324-C334-C344	120.0	C324-C334-H334	120.0
C344-C334-H334	120.0	C334-C344-C354	120.0
C334-C344-H344	120.0	C354-C344-H344	120.0
C344-C354-C364	120.0	C344-C354-C404	120.0
C364-C354-C404	120.0	C374-C364-C354	120.0
C374-C364-C314	120.0	C354-C364-C314	120.0
C364-C374-C384	120.0	C364-C374-H374	120.0
C384-C374-H374	120.0	C394-C384-C374	120.0
C394-C384-H384	120.0	C374-C384-H384	120.0
C384-C394-C404	120.0	C384-C394-H394	120.0
C404-C394-H394	120.0	C394-C404-C354	120.0
C394-C404-H404	120.0	C354-C404-H404	120.0

Symmetry transformations used to generate equivalent atoms:

Table 4. Anisotropic displacement parameters ($\mathring{A}^2$ x 10^3) for complex **34**. The anisotropic displacement factor exponent takes the following form: $-2\pi^2[\,h^2\,a^{*2}U^{11} + ... + 2\,h\,k\,a^*\,b^*\,U^{12}\,]$

	U^{11}	U^{22}	U^{33}	U^{23}	U^{13}	U^{12}
Ag(1)	32(1)	108(1)	36(1)	-2(1)	3(1)	-1(1)
Ag(2)	26(1)	177(2)	37(1)	-26(1)	6(1)	-12(1)

Table 5. Hydrogen coordinates (x 10^4) and isotropic displacement parameters ($\mathring{A}^2$ x 10^3) for complex **34**.

	x	y	z	U(eq)
H131	1332	6398	4157	113
H141	2165	6594	5505	117
H161	3107	6310	6825	163
H171	3933	5667	7609	166
H191	4678	4768	7722	117
H201	4955	3929	7147	125
H211	4248	3708	5748	146
H221	3286	4320	4952	156
H25A1	878	5738	2987	94
H331	1280	5801	1833	77
H341	546	5835	406	113
H371	154	3758	597	93
H381	-580	3792	-830	105
H391	-765	4608	-1557	110

H401	-216	5391	-857	105
H132	4116	2608	468	146
H142	5518	2640	-506	147
H162	6675	3139	-1454	148
H172	7271	3925	-1969	146
H192	7349	4902	-1906	130
H202	6783	5706	-1347	136
H212	5454	5717	-288	137
H222	4715	4935	191	117
H25B2	2798	3086	1360	106
H332	2019	2911	2373	100
H342	573	2753	3262	103
H372	-647	4692	2472	92
H382	-2093	4534	3360	106
H392	-2285	3715	4072	109
H402	-1031	3053	3895	111
H133	2682	6551	320	117
H143	1788	6505	-1039	117
H163	1225	6007	-2336	95
H173	1073	5228	-3075	97
H193	1210	4252	-3126	112
H203	1701	3452	-2495	119
H213	2501	3447	-1084	108
H223	2801	4231	-333	73
H25C3	3652	6092	1532	105
H333	3268	6177	2699	115
H343	3989	6472	4044	129
H373	5995	4654	4193	147
H383	6715	4949	5537	148
H393	6272	5785	6096	156

H403	5108	6326	5310	148
H134	3606	2535	4358	144
H144	2236	2217	5216	143
H164	687	2375	6078	118
H174	-569	2930	6558	116
H194	-1474	3791	6507	109
H204	-1610	4658	6011	108
H214	-334	5000	5062	92
H224	1043	4480	4628	88
H25D4	4454	3289	3582	118
H334	5086	3350	2404	132
H344	6497	3518	1480	143
H374	5970	5545	2196	131
H384	7381	5714	1272	153
H394	8230	5010	573	155
H404	7669	4137	798	136

Table 6. Torsion angles [°] for complex **34**.

N254-Ag(2)-N111-C121	151.6(5)	N251-Ag(2)-N111-C121	-18.5(6)
N254-Ag(2)-N111-C241	-7.8(7)	N251-Ag(2)-N111-C241	-178.0
C241-N111-C121-C131	1.9	Ag(2)-N111-C121-C131	-160.9(5)
C241-N111-C121-C251	178.9	Ag(2)-N111-C121-C251	16.1(5)
N111-C121-C131-C141	-1.6	C251-C121-C131-C141	-178.6
C121-C131-C141-C151	-0.6	C131-C141-C151-C241	2.4
C131-C141-C151-C161	-176.6	C141-C151-C161-C171	179.8
C241-C151-C161-C171	0.7	C151-C161-C171-C181	2.2
C161-C171-C181-C191	175.3	C161-C171-C181-C231	-1.6

C231-C181-C191-C201	-0.4	C171-C181-C191-C201	-177.3
C181-C191-C201-C211	0.6	C191-C201-C211-C221	-0.1
C201-C211-C221-C231	-0.6	C211-C221-C231-C181	0.9
C211-C221-C231-C241	179.2	C191-C181-C231-C221	-0.4
C171-C181-C231-C221	176.6	C191-C181-C231-C241	-178.8
C171-C181-C231-C241	-1.8	C121-N111-C241-C151	0.0
Ag(2)-N111-C241-C151	157.7(6)	C121-N111-C241-C231	-179.0
Ag(2)-N111-C241-C231	-21.3(6)	C141-C151-C241-N111	-2.1
C161-C151-C241-N111	176.9	C141-C151-C241-C231	176.9
C161-C151-C241-C231	-4.0	C221-C231-C241-N111	5.2
C181-C231-C241-N111	-176.5	C221-C231-C241-C151	-173.8
C181-C231-C241-C151	4.5	N111-C121-C251-N251	-0.8
C131-C121-C251-N251	176.4	C121-C251-N251-C321	-159.3(11)
C121-C251-N251-Ag(2)	-20.7(6)	N254-Ag(2)-N251-C251	-120(2)
N111-Ag(2)-N251-C251	21.3(6)	N254-Ag(2)-N251-C321	18(3)
N111-Ag(2)-N251-C321	159.2(10)	C361-C311-C321-C331	0.0
C312-C311-C321-C331	-172.7(12)	C361-C311-C321-N251	163.0(12)
C312-C311-C321-N251	-9.7(12)	C251-N251-C321-C311	-154.7(6)
Ag(2)-N251-C321-C311	62.4(13)	C251-N251-C321-C331	8.8(12)
Ag(2)-N251-C321-C331	-134.1(8)	C311-C321-C331-C341	0.0
N251-C321-C331-C341	-163.6(12)	C321-C331-C341-C351	0.0
C331-C341-C351-C361	0.0	C331-C341-C351-C401	180.0
C341-C351-C361-C371	180.0	C401-C351-C361-C371	0.0
C341-C351-C361-C311	0.0	C401-C351-C361-C311	180.0
C321-C311-C361-C351	0.0	C312-C311-C361-C351	172.0(13)
C321-C311-C361-C371	180.0	C312-C311-C361-C371	-8.0(13)
C351-C361-C371-C381	0.0	C311-C361-C371-C381	180.0
C361-C371-C381-C391	0.0	C371-C381-C391-C401	0.0
C381-C391-C401-C351	0.0	C361-C351-C401-C391	0.0
C341-C351-C401-C391	180.0	N252-Ag(1)-N112-C122	-3.8(6)

N253-Ag(1)-N112-C122	153.5(4)	N252-Ag(1)-N112-C242	-178.0
N253-Ag(1)-N112-C242	-20.7(6)	C242-N112-C122-C132	1.9
Ag(1)-N112-C122-C132	-173.8(4)	C242-N112-C122-C252	178.9
Ag(1)-N112-C122-C252	3.2(4)	N112-C122-C132-C142	-1.6
C252-C122-C132-C142	-178.6	C122-C132-C142-C152	-0.6
C132-C142-C152-C242	2.4	C132-C142-C152-C162	-176.7
C142-C152-C162-C172	179.8	C242-C152-C162-C172	0.7
C152-C162-C172-C182	2.2	C162-C172-C182-C192	175.3
C162-C172-C182-C232	-1.6	C232-C182-C192-C202	-0.4
C172-C182-C192-C202	-177.3	C182-C192-C202-C212	0.6
C192-C202-C212-C222	-0.1	C202-C212-C222-C232	-0.6
C212-C222-C232-C182	0.8	C212-C222-C232-C242	179.2
C192-C182-C232-C222	-0.4	C172-C182-C232-C222	176.6
C192-C182-C232-C242	-178.8	C172-C182-C232-C242	-1.8
C122-N112-C242-C152	0.0	Ag(1)-N112-C242-C152	173.6(7)
C122-N112-C242-C232	-179.0	Ag(1)-N112-C242-C232	-5.4(7)
C142-C152-C242-N112	-2.2	C162-C152-C242-N112	176.9
C142-C152-C242-C232	176.9	C162-C152-C242-C232	-4.0
C222-C232-C242-N112	5.2	C182-C232-C242-N112	-176.5
C222-C232-C242-C152	-173.8	C182-C232-C242-C152	4.5
N112-C122-C252-N252	-0.8	C132-C122-C252-N252	176.4
C122-C252-N252-C322	171.3(9)	C122-C252-N252-Ag(1)	-4.1(8)
N253-Ag(1)-N252-C252	-116.0(14)	N112-Ag(1)-N252-C252	4.4(8)
N253-Ag(1)-N252-C322	70(2)	N112-Ag(1)-N252-C322	-170.0(12)
C321-C311-C312-C322	-106.8(8)	C361-C311-C312-C322	80.9(11)
C321-C311-C312-C362	85.7(9)	C361-C311-C312-C362	-86.7(11)
C362-C312-C322-C332	0.0	C311-C312-C322-C332	-167.2(13)
C362-C312-C322-N252	-173.4(11)	C311-C312-C322-N252	19.5(11)
C252-N252-C322-C312	-157.4(6)	Ag(1)-N252-C322-C312	18.2(15)
C252-N252-C322-C332	29.5(11)	Ag(1)-N252-C322-C332	-154.9(10)

C312-C322-C332-C342	0.0	N252-C322-C332-C342	172.8(12)
C322-C332-C342-C352	0.0	C332-C342-C352-C362	0.0
C332-C342-C352-C402	180.0	C342-C352-C362-C372	180.0
C402-C352-C362-C372	0.0	C342-C352-C362-C312	0.0
C402-C352-C362-C312	180.0	C322-C312-C362-C372	180.0
C311-C312-C362-C372	-12.1(12)	C322-C312-C362-C352	0.0
C311-C312-C362-C352	167.9(12)	C352-C362-C372-C382	0.0
C312-C362-C372-C382	180.0	C362-C372-C382-C392	0.0
C372-C382-C392-C402	0.0	C382-C392-C402-C352	0.0
C362-C352-C402-C392	0.0	C342-C352-C402-C392	180.0
C243-N113-C123-C133	1.9	C243-N113-C123-C253	178.9
N113-C123-C133-C143	-1.6	C253-C123-C133-C143	-178.6
C123-C133-C143-C153	-0.6	C133-C143-C153-C243	2.4
C133-C143-C153-C163	-176.6	C143-C153-C163-C173	179.8
C243-C153-C163-C173	0.7	C153-C163-C173-C183	2.2
C163-C173-C183-C193	175.3	C163-C173-C183-C233	-1.6
C233-C183-C193-C203	-0.4	C173-C183-C193-C203	-177.3
C183-C193-C203-C213	0.6	C193-C203-C213-C223	-0.1
C203-C213-C223-C233	-0.6	C213-C223-C233-C183	0.8
C213-C223-C233-C243	179.2	C193-C183-C233-C223	-0.3
C173-C183-C233-C223	176.6	C193-C183-C233-C243	-178.8
C173-C183-C233-C243	-1.8	C123-N113-C243-C153	0.0
C123-N113-C243-C233	-179.0	C143-C153-C243-N113	-2.2
C163-C153-C243-N113	176.9	C143-C153-C243-C233	176.9
C163-C153-C243-C233	-4.0	C223-C233-C243-N113	5.2
C183-C233-C243-N113	-176.4	C223-C233-C243-C153	-173.8
C183-C233-C243-C153	4.5	N113-C123-C253-N253	-0.8
C133-C123-C253-N253	176.4	C123-C253-N253-C323	-159.0(11)
C123-C253-N253-Ag(1)	-23.3(5)	N252-Ag(1)-N253-C253	-140.2(12)
N112-Ag(1)-N253-C253	108.5(6)	N252-Ag(1)-N253-C323	-8(2)

N112-Ag(1)-N253-C323	-119.8(11)	C363-C313-C323-C333	0.0
C314-C313-C323-C333	-166.1(18)	C363-C313-C323-N253	158.3(16)
C314-C313-C323-N253	-7.9(13)	C253-N253-C323-C333	2.4(14)
Ag(1)-N253-C323-C333	-137.9(10)	C253-N253-C323-C313	-156.0(7)
Ag(1)-N253-C323-C313	63.7(13)	C313-C323-C333-C343	0.0
N253-C323-C333-C343	-157.6(16)	C323-C333-C343-C353	0.0
C333-C343-C353-C363	0.0	C333-C343-C353-C403	180.0
C343-C353-C363-C373	180.0	C403-C353-C363-C373	0.0
C343-C353-C363-C313	0.0	C403-C353-C363-C313	180.0
C323-C313-C363-C373	180.0	C314-C313-C363-C373	-15.2(19)
C323-C313-C363-C353	0.0	C314-C313-C363-C353	164.8(19)
C353-C363-C373-C383	0.0	C313-C363-C373-C383	180.0
C363-C373-C383-C393	0.0	C373-C383-C393-C403	0.0
C383-C393-C403-C353	0.0	C343-C353-C403-C393	180.0
C363-C353-C403-C393	0.0	C244-N114-C124-C134	1.9
C244-N114-C124-C254	178.9	N114-C124-C134-C144	-1.6
C254-C124-C134-C144	-178.6	C124-C134-C144-C154	-0.6
C134-C144-C154-C244	2.5	C134-C144-C154-C164	-176.6
C144-C154-C164-C174	179.8	C244-C154-C164-C174	0.7
C154-C164-C174-C184	2.2	C164-C174-C184-C194	175.3
C164-C174-C184-C234	-1.6	C234-C184-C194-C204	-0.3
C174-C184-C194-C204	-177.3	C184-C194-C204-C214	0.6
C194-C204-C214-C224	-0.1	C204-C214-C224-C234	-0.7
C214-C224-C234-C184	0.9	C214-C224-C234-C244	179.2
C194-C184-C234-C224	-0.4	C174-C184-C234-C224	176.6
C194-C184-C234-C244	-178.8	C174-C184-C234-C244	-1.8
C124-N114-C244-C154	0.0	C124-N114-C244-C234	-179.0
C144-C154-C244-N114	-2.2	C164-C154-C244-N114	176.9
C144-C154-C244-C234	176.9	C164-C154-C244-C234	-4.0
C224-C234-C244-N114	5.3	C184-C234-C244-N114	-176.5

C224-C234-C244-C154	-173.8	C184-C234-C244-C154	4.5
N114-C124-C254-N254	-0.8	C134-C124-C254-N254	176.4
C124-C254-N254-C324	-171.0(12)	C124-C254-N254-Ag(2)	-22.2(7)
N251-Ag(2)-N254-C254	-118(2)	N111-Ag(2)-N254-C254	104.7(8)
N251-Ag(2)-N254-C324	30(3)	N111-Ag(2)-N254-C324	-107.3(12)
C323-C313-C314-C324	-104.9(12)	C363-C313-C314-C324	89.6(16)
C323-C313-C314-C364	83.1(13)	C363-C313-C314-C364	-82.4(16)
C364-C314-C324-C334	0.0	C313-C314-C324-C334	-171.7(17)
C364-C314-C324-N254	172.6(15)	C313-C314-C324-N254	0.8(16)
C254-N254-C324-C334	14.3(14)	Ag(2)-N254-C324-C334	-139.7(11)
C254-N254-C324-C314	-158.3(8)	Ag(2)-N254-C324-C314	47.7(16)
C314-C324-C334-C344	0.0	N254-C324-C334-C344	-172.6(15)
C324-C334-C344-C354	0.0	C334-C344-C354-C364	0.0
C334-C344-C354-C404	180.0	C344-C354-C364-C374	180.0
C404-C354-C364-C374	0.0	C344-C354-C364-C314	0.0
C404-C354-C364-C314	180.0	C324-C314-C364-C374	180.0
C313-C314-C364-C374	-7.8(17)	C324-C314-C364-C354	0.0
C313-C314-C364-C354	172.2(17)	C354-C364-C374-C384	0.0
C314-C364-C374-C384	180.0	C364-C374-C384-C394	0.0
C374-C384-C394-C404	0.0	C384-C394-C404-C354	0.0
C344-C354-C404-C394	180.0	C364-C354-C404-C394	0.0

Symmetry transformations used to generate equivalent atoms: